

General Disclaimer

One or more of the Following Statements may affect this Document

- This document has been reproduced from the best copy furnished by the organizational source. It is being released in the interest of making available as much information as possible.
- This document may contain data, which exceeds the sheet parameters. It was furnished in this condition by the organizational source and is the best copy available.
- This document may contain tone-on-tone or color graphs, charts and/or pictures, which have been reproduced in black and white.
- This document is paginated as submitted by the original source.
- Portions of this document are not fully legible due to the historical nature of some of the material. However, it is the best reproduction available from the original submission.

NATIONAL AERONAUTICS AND SPACE ADMINISTRATION

Technical Memorandum 33-792

*Advanced Multilateration Theory, Software
Development, and Data Processing:
The MICRODOT System*

(NASA-CP-148839) ADVANCED MULTILATERATION
THEORY, SOFTWARE DEVELOPMENT, AND DATA
PROCESSING: THE MICRODOT SYSTEM (Jet
Propulsion Lab.) 459 p HC \$12.00 CSCI 09G

N76-33586

Unclas
G3/42 07969



JET PROPULSION LABORATORY
CALIFORNIA INSTITUTE OF TECHNOLOGY
PASADENA, CALIFORNIA

July 4, 1976

PREFACE

The work described in this report was performed by the Mission Analysis Division of the Jet Propulsion Laboratory during the period 1974-1976. Primary software support was provided by Computer Sciences Corporation (CSC), Applied Technology Division, San Francisco Operations, under the auspices of the Jet Propulsion Laboratory's Science and Engineering Computing Section. It is the hope of the authors that effort expended herein will be the foundation for numerous flight experiments by which the long list of possible applications related to the field of multilateration will be tested and the derived benefits passed on to the general public.

ACKNOWLEDGMENTS

A work such as this always relies on the generous contributions and suggestions of many people. The authors of this report wish to thank all of these contributors. Special emphasis is placed on the discussions held with L. Knopoff relative to the solid Earth tide models and those with G. J. Bierman and D. G. Carta on a host of statistical matters and review of milestone documents which were fundamental to the development of the proper filtering algorithms. The authors also wish to thank R. K. Hylkema for his assistance in the area of tropospheric calibration. Thanks are due to Y. S. Park for software generation related to ionospheric calibration and square root filtering. Similarly A. Tam is acknowledged for her assistance in software development related to the solid Earth tides. The authors appreciate the effort of P. M. Muller in communicating with NASA Wallops relative to present and future MICRODOT development. Finally, the foundations of previous work undertaken by other co-workers, such as the contribution of R. Jaffe to Appendix A18, are not taken for granted (see Section 11).

ABSTRACT

The main body of this report consists of a summary overview wherein the process of geometric parameter estimation to accuracies of one centimeter, i.e., multilateration, is defined and applications listed. In this summary a brief functional explanation of the theory is presented. Next, various multilateration systems are described in order of increasing system complexity. Expected systems accuracy is discussed from a general point of view and a summary of the errors is listed.

An outline of the design of a software processing system for multilateration, herein called MICRODOT, is presented next. The links of this software, which can be used for multilateration data simulations or operational data reduction, are examined on an individual basis. Functional flow diagrams are presented to aid in understanding the software capability. MICRODOT capability is described with respect to vehicle configurations, interstation coordinate reduction, geophysical parameter estimation, and orbit determination.

Numerical results obtained from MICRODOT via data simulations are displayed both for hypothetical and real world vehicle/station configurations such as used in the GEOS-3 Project. These simulations show the inherent power of the multilateration procedure.

The rest of this work is comprised of twenty-two appendices which detail all of the theory contained in the MICRODOT software. These appendices deal with data compression and synchronization, minimum variance estimation of parameters, Earth and ocean tide modeling, atmospheric data calibrations, geometric orbit determination, operational data requirements, and so forth.

The presentation of the advanced concepts, software and operational requirements presented herein comprise an in-depth look at multilateration and at the future applications to which such systems must of necessity be applied.

CONTENTS

PREFACE	iii
ACKNOWLEDGEMENTS	iv
ABSTRACT	v
1. INTRODUCTION	1
2. APPLICATIONS OF THE MICRODOT PROCESSING SYSTEM	3
2.1 PRELIMINARY REMARKS	3
2.2 SPECIFIC APPLICATIONS	3
3. THE MULTILATERATION PROCESS	5
3.1 FUNCTIONAL EXPLANATION OF THE THEORY	5
3.2 IMPORTANT QUALIFYING REMARKS	6
3.3 ADVANCED CONCEPTS	8
4. MULTILATERATION SYSTEMS	10
4.1 SYSTEM A - MULTIBASELINE SYSTEM	10
4.2 SYSTEM B - HYBRID MULTILATERATION SYSTEM	10
4.3 SYSTEM C - SINGLE AIRPLANE SYSTEM	10
4.4 SYSTEM D - UPRATED TWO-AIRPLANE SYSTEM	13
4.5 SYSTEM E - MINIMUM COST SINGLE SATELLITE SYSTEM	15
4.6 SYSTEM F - UPRATED SINGLE SATELLITE SYSTEM	15
4.7 SYSTEM G - MODERATE COST SATELLITE/AIRPLANE SYSTEM	17
4.8 SYSTEM H - TWO SATELLITE SYSTEM	17
4.9 SYSTEM I - UPRATED TWO SATELLITE SYSTEM	17
4.10 SYSTEM J - COMBINED SYSTEMS	20
5. EXPECTED SYSTEM ACCURACIES	21
5.1 HARDWARE ERROR SOURCES	22
5.2 ATMOSPHERIC ERROR SOURCES	23

PRECEDING PAGE BLANK NOT FILMED

CONTENTS (contd)

5.3	EARTH/OCEAN TIDAL ERRORS	23
5.4	SUMMARY OF ERRORS	26
6.	SOFTWARE DESIGN	28
6.1	REAL TIME OPERATIONS LINK	28
6.2	EDITOR LINK	31
6.3	PREPROCESSOR/SYNCHRONIZER LINK	33
6.4	COORDINATE TRANSFORMATION LINK	35
6.5	MULTILATERATION EQUATION SOLVING LINK	35
6.6	GEODETIC COORDINATE ESTIMATION LINK	40
6.7	MULTILATERATION SIMULATION LINK	42
6.8	GEOMETRIC ORBIT DETERMINATION LINK	42
7.	SOFTWARE CAPABILITY	48
7.1	VEHICLE CONFIGURATIONS	48
7.2	INTERSTATION COORDINATE REDUCTION	48
7.3	GEOPHYSICAL PARAMETER ESTIMATION	48
7.4	ORBIT DETERMINATION CAPABILITY	48
8.	INITIAL SOFTWARE DATA SIMULATION AND VERIFICATION	52
8.1	INTRODUCTION	52
8.2	CONTINENTAL USA CONFIGURATION	53
8.3	SYSTEM H SIMULATION WITH PERFECT DATA	56
8.4	SYSTEM H SIMULATION WITH NOISY DATA	60
8.5	SYSTEM I SIMULATION WITH PERFECT DATA	63
8.6	GEOS-3 BERMUDA TRIANGLE CONFIGURATION	63
8.7	GEOS-3 COORDINATE ESTIMATION	67
8.8	GEOS-3/ATS-6 COORDINATE ESTIMATION	71
9.	A GUIDE TO THE APPENDICES CONTAINED IN THIS REPORT	72

CONTENTS (contd)

10.	REFERENCES	74
11.	BIBLIOGRAPHY OF JET PROPULSION LABORATORY MULTILATERATION EFFORT.....	75

APPENDICES

A1.	MULTILATERATION DATA COMPRESSION	83
A1.1	INTRODUCTION	84
A1.2	DATA COMPRESSION FUNCTION.....	84
A1.3	POLYNOMIAL FITTING PROCEDURE.....	86
A1.4	REFERENCES.....	91
A2.	EXPLICIT MATRIX SOLUTION FOR OBTAINING MINIMUM VARIANCE ESTIMATES OF PARAMETERS CONTAINED IN A LARGE SET OF NONLINEAR EQUATIONS	93
A2.1	INTRODUCTION AND SUMMARY	94
A2.2	GROSS COMPUTATIONAL FLOW DIAGRAM	96
A2.3	OUTLINE OF SOLUTION OF MULTILATERATION EQUATIONS	96
A2.4	EXPLICIT DEVELOPMENT OF A SINGLE MULTILATERATION EQUATION AT A FIXED TIME	105
A2.5	EXPLICIT DEVELOPMENT OF MULTILATERATION EQUATIONS AT A FIXED TIME (GROUPING BY TIME)	110
A2.6	EXPLICIT DEVELOPMENT OF MULTILATERATION EQUATIONS FOR A SEQUENCE OF TIMES (GROUPING BY BATCH)	112
A2.7	DEVELOPMENT OF WEIGHTING MATRIX	114
A2.8	COVARIANCE MATRIX OF TO-BE-SOLVED-FOR PARAMETERS	117
A2.9	FITTING COEFFICIENT COVARIANCE	118
A2.10	COVARIANCE OF FITTING COEFFICIENTS WITH INTERROGATION TIMES	124
A2.11	SEQUENTIAL BATCH PROCESSING TECHNIQUE ...	125
A2.12	REFERENCES	127

CONTENTS (contd)

A3.	EXPLICIT ANALYTICAL MODEL FOR EARTH TIDE STATION COORDINATE DEFLECTIONS	129
A3.1	INTRODUCTION	130
A3.2	EXPLICIT DEVELOPMENT OF TIDAL POTENTIAL	131
A3.3	EFFECT OF TIDAL POTENTIALS	135
A3.4	COMPUTATION OF DEFORMATIONS	136
A3.5	TRANSFORMATION OF COORDINATES	140
A3.6	TRANSFORMATION OF VARIATIONS	147
A3.7	REFERENCES	149
A4.	GROUND STATION DEFLECTIONS DUE TO OCEAN TIDES	151
A4.1	INTRODUCTION	152
A4.2	OCEAN SURFACE EQUATIONS	153
A4.3	INTEGRATION LIMITS OVER THE OCEAN SURFACE	160
A4.4	NUMERICAL DEVELOPMENT OF LOADING POTENTIAL	162
A4.5	CALIBRATION VIA GRAVIMETER DATA	164
A4.6	INVESTIGATION OF SINGULARITY POINT	165
A4.7	REFERENCES	168
A5.	GENERALIZED TROPOSPHERIC CALIBRATION AND ERROR ANALYSIS	171
A5.1	INTRODUCTION	172
A5.2	ERROR BUDGET ANALYSIS	172
A5.3	TROPOSPHERIC RANGE CORRECTION DERIVATION	179
A5.4	DEVELOPMENT OF ANALYTIC EXPRESSIONS FOR TROPOSPHERIC RANGE CORRECTIONS	183
A5.5	THE REFRACTIVE INDEX AS A FUNCTION OF ALTITUDE	185
A5.6	DETERMINATION OF THE RANGE CORRECTION...	187
A5.7	COMPUTATIONAL ALGORITHM	204

CONTENTS (contd)

A5.8	COVARIANCE MATRIX	211
A5.9	REFERENCES	217
A6.	IONOSPHERIC CALIBRATION AND ERROR ANALYSIS	219
A6.1	INTRODUCTION	220
A6.2	ERROR BUDGET ANALYSIS	220
A6.3	THE IONOSPHERIC RANGE CORRECTION	224
A6.4	COMPUTATIONAL ALGORITHM	232
A6.5	COVARIANCE MATRIX	241
A6.6	REFERENCES	243
A7.	COORDINATE TRANSFORMATIONS AND COVARIANCE MAPPINGS FOR HIGH PRECISION ORBITAL STATE ESTIMATION	245
A7.1	INTRODUCTION	246
A7.2	TRANSFORMATION FROM GEODETIC TO GEOMETRIC COORDINATES	248
A7.3	TRANSFORMATION FROM TOPOCENTRIC TO GEOGRAPHIC FRAME INCLUDING EARTH/OCEAN TIDE EFFECTS	251
A7.4	STATION POSITIONS/VELOCITIES AND COVARIANCES IN GEOMETRIC FRAME	253
A7.5	TRANSFORMATION OF ANY GEOGRAPHIC POSITION AND VELOCITY VECTOR INTO THE TRUE SIDEREAL SYSTEM (TOD) AND DEVELOPMENT OF ERROR DIFFERENTIAL OF THE TRANSFORMATION	255
A7.6	TRANSFORMATION OF ANY TRUE OF DATE POSITION AND VELOCITY VECTOR INTO THE MEAN OF DATE (MOD) SYSTEM AND DEVELOP- MENT OF THE ERROR DIFFERENTIAL OF THE TRANSFORMATION	261
A7.7	TRANSFORMATION OF ANY MEAN OF DATE POSITION AND VELOCITY VECTOR INTO THE MEAN OF EPOCH (MOE) SYSTEM AND DEVELOPMENT OF THE ERROR DIFFERENTIAL OF THE TRANSFORMATION	265
A7.8	COMPOUND COORDINATE ROTATIONS AND COVARIANCE TRANSFORMATIONS	267
A7.9	REFERENCES	269

CONTENTS (contd)

A8.	SHORT AND LONG-ARC ORBIT DETERMINATION USING MULTILATERATION	271
A8.1	INTRODUCTION	272
A8.2	TRILATERATION EQUATIONS	273
A8.3	DEVELOPMENT OF ORBIT DETERMINATION FUNCTIONS	275
A8.4	ESTIMATION EQUATIONS WITH NO CORRELATION	277
A8.5	EXTENSION OF MATRIX SYSTEM FOR ADDITIONAL STATIONS	279
A8.6	ESTIMATION EQUATIONS WITH CORRELATION ...	279
A8.7	A NEW APPROACH TO REPETITIVE SHORT-ARC ORBIT DETERMINATION	284
A8.8	OUTLINE OF ORBIT DETERMINATION ESTIMATION PROCEDURE FOR LONG-ARC PROPAGATION	285
A8.9	USE OF VARIATIONAL EQUATIONS FOR PARTIAL DERIVATIVE GENERATION	288
A8.10	REFERENCES	289
A9.	FAST ALGORITHM FOR COMPLETE NUTATION AND NUTATION RATE CALCULATIONS	291
A9.1	INTRODUCTION	292
A9.2	NUTATION AND NUTATION RATE ALGORITHM	293
A9.3	REFERENCES	305
A10.	PRECESSION ALGORITHM	307
A10.1	INTRODUCTION	308
A10.2	PRECESSION AND PRECESSION RATE ALGORITHM	309
A10.3	REFERENCES	312
A11.	AUTOMATIC GENERATION OF MULTILATERATION FUNCTIONS FOR SST AND RANGE ONLY DATA TYPES WITH IDENTICAL ALGEBRAIC STRUCTURES	313
A11.1	INTRODUCTION AND OUTLINE	314
A11.2	ANALYSIS	319

CONTENTS (contd)

A11.3	CONSTRUCTION OF MULTILATERATION FUNCTIONS	324
A11.4	EXPLICIT FORMULA FOR RESULTANT OF TWO QUADRATIC EQUATIONS	326
A11.5	QUADRATIC RESOLVENTS IN MULTILATERATION	327
A11.6	REFERENCES	329
A12.	OBTAINING SLANT RANGE BETWEEN STATION AND SATELLITE OR SATELLITE-TO-SATELLITE FROM TURNAROUND TIMING PULSES	331
A12.1	INTRODUCTION	332
A12.2	TIMING CONSIDERATIONS FOR TWO-SATELLITE RANGING WITH AND WITHOUT AN SST LINK	333
A12.3	COMPUTATIONAL ALGORITHM	338
A12.4	REFERENCES	340
A13.	CENTER OF MASS CORRECTIONS	341
A13.1	INTRODUCTION	342
A13.2	ATTITUDE DETERMINATION	342
A13.3	LASER SLANT RANGE CORRECTION	342
A13.4	RADIO FREQUENCY ANTENNA SLANT RANGE CORRECTION	345
A13.5	RADIO FREQUENCY SATELLITE-TO-SATELLITE RANGE CORRECTION	349
A13.6	REFERENCES	349
A14.	ESTIMATION OF GEOGRAPHIC COORDINATES FROM MULTILATERATION CONSTRAINTS: THE N-DIMENSIONAL CASE	351
A14.1	INTRODUCTION	352
A14.2	COMPUTATION OF BASELINE DISTANCE AND COVARIANCE	352
A14.3	SOLUTION OF EQUATIONS IN GEOGRAPHIC BASIS	356
A14.4	REDUCTION OF SOLUTION TO THE ONE- DIMENSIONAL CASE	361
A14.5	REFERENCES	364

CONTENTS (contd)

A15.	DATA STREAM DEFINITION FOR CALIBRATION	365
A15.1	INTRODUCTION	366
A15.2	MEASUREMENT DATA TYPE	366
A15.3	ATMOSPHERIC DATA TYPE (TROPOSPHERE)	366
A15.4	ATMOSPHERIC DATA TYPE (IONOSPHERE)	368
A15.5	EARTH/OCEAN DATA TYPE	368
A15.6	VEHICLE DATA TYPE	368
A15.7	TOTAL NUMBER OF DATA STREAMS	369
A15.8	REFERENCE	369
A16.	PARTIAL DERIVATIVES OF ESTIMATED PARAMETERS WITH RESPECT TO NON-ESTIMATED PARAMETERS	371
A16.1	INTRODUCTION	372
A16.2	THE MULTILATERATION FUNCTION	372
A16.3	PARTIAL DERIVATIVE COMPUTATION	373
A17.	ANALYTIC PARTIAL DERIVATIVE GENERATION	375
A17.1	INTRODUCTION	376
A17.2	METHOD OF DERIVATION	376
A17.3	DERIVATION OF PARTIAL DERIVATIVES OF THE BASIS UNIT VECTORS WITH RESPECT TO THE GEOGRAPHIC CARTESIAN COORDINATES OF THE THREE BASIS STATIONS	377
A17.4	MACHINE IMPLEMENTATION OF THE FORMULAS FOR THE PARTIAL DERIVATIVES	382
A18.	SIGNAL STRENGTH FLUCTUATIONS IN A LASER RANGING SYSTEM DUE TO OPTICAL INTERFERENCE BETWEEN THE MANY REFLECTORS ON A VEHICLE	383
A18.1	INTRODUCTION	384
A18.2	DERIVATION OF THE PROBABILITY DENSITY OF THE RECEIVED POWER	385
A18.3	ANALYSIS	386
A18.4	PROBABILITY DISTRIBUTION OF THE DYNAMIC RANGE	391

CONTENTS (contd)

A18.5	PROBABILITY THAT THE DYNAMIC RANGE OF THE SEQUENCE OF M-PULSES WILL BE $\leq k$	393
A18.6	CONCLUSIONS	394
A18.7	REFERENCES	396
A19.	LASER PULSE SHAPE DEGRADATION BY MULTIPLE REFLECTION FROM CORNER REFLECTORS MOUNTED ON A SATELLITE	397
A19.1	INTRODUCTION	398
A19.2	ANALYSIS	398
A19.3	TYPICAL RESULTS	401
A20.	ABERRATION AND FRESNEL DIFFRACTION	405
A20.1	INTRODUCTION	406
A20.2	ANALYSIS	407
A20.3	TYPICAL RESULTS	410
A21.	MULTIBASELINE: A THREE-DIMENSIONAL PRECISION GEODETIC MEASUREMENT SYSTEM NOT USING AIRPLANES OR DATA SYNCHRONIZATION	415
A21.1	INTRODUCTION	416
A21.2	THE MULTIBASELINE CONCEPT	420
A21.3	MULTIBASELINE NUMERICAL RESULTS	424
A21.4	STATIC MULTILATERATION EQUIVALENCE	428
A21.5	HYBRID MULTILATERATION	430
A21.6	HYBRID MULTILATERATION NUMERICAL RESULTS	431
A21.7	DETERMINATION OF THE OUT-OF-PLANE COORDINATE FOR FLAT TOPOGRAPHY	431
A21.8	NETWORK DENSIFICATION	434
A21.9	CONCLUSIONS	435
A21.10	REFERENCES	436
A22.	APPLICATIONS OF MULTILATERATION	437
A22.1	INTRODUCTION	438
A22.2	DISCUSSION	439

TABLES

1.	Applications of multilateration systems	4
2.	Hardware parameters (S-band)	22
3.	Atmospheric parameters	24
4.	Earth/ocean tide parameters	25
5.	Bias error contributions (cm)	26
6.	MICRODOT capability relative to vehicle configuration	49
7.	MICRODOT capability relative to coordinate reduction	49
8.	MICRODOT capability relative to geophysical parameter estimation	50
9.	MICRODOT capability relative to orbit determination	50
10.	Adopted station locations for USA data simulation	53
11.	Orbital parameters for USA data simulation	54
12.	Assumed and converged station coordinates	59
13.	MICRODOT convergence with one centimeter noise and 150 meter coordinate offset	61
14.	Station coordinate covariance matrix (1 cm noise)	62
15.	C-band primary station constellation	66
16.	C-band (ATS-6) stations	66
17.	Orbital parameters for GEOS-3 and ATS-6 spacecraft	67
18.	GEOS-3/MICRODOT convergence with one centimeter noise and one meter coordinate offset	69
19.	GEOS-3 station coordinate standard deviations (1 cm noise). . .	70
20.	GEOS-3/ATS-6 station coordinate standard deviations (1 cm noise)	71
A2.1	Existing error sources	94
A4.1	Harmonic coefficients	156
A5.1	Atmospheric parameters	176
A5.2	Pertinent partial derivatives	177

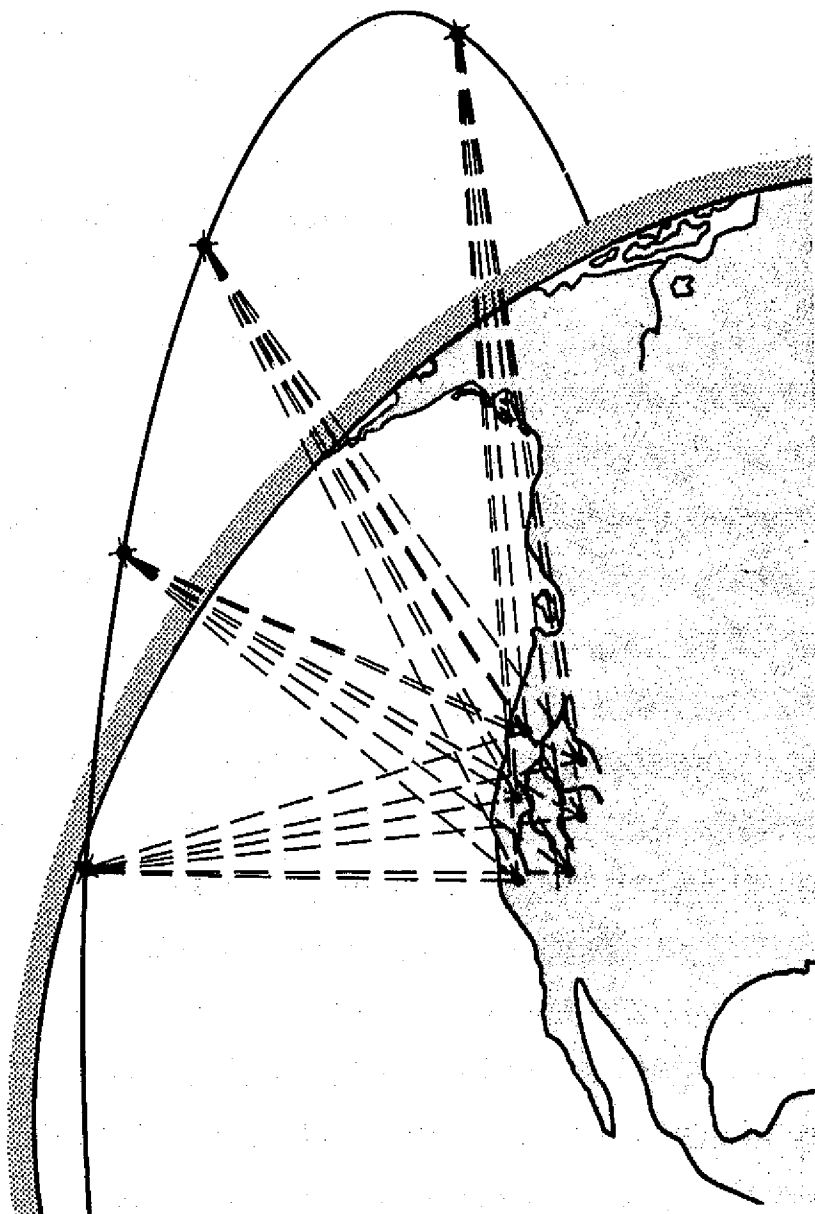
A6.1	Atmospheric parameters (F-layer)	221
A6.2	Worst case pertinent partial derivatives	222
A14.1	Multilateration invariants	354
A21.1	Adopted station coordinates	424
A21.2	Solution of multibaseline equations for non-optimum configurations	426
A21.3	Standard deviation of Z_4 (cm) as a function of decreasing Z_4 (meters) for various geodolite accuracies σ (mm)	427
A21.4	Hybrid multilateration	432

FIGURES

1.	Multilateration geometric coordinate system (bars indicate specified coordinates)	7
2.	Multibaseline system	11
3.	Airplane system	12
4.	Two-airplane systems	14
5.	Single satellite system	16
6.	Airplane-satellite system	18
7.	Two-satellite system	19
8.	The MICRODOT link structure	29
9.	Real time operations link	30
10.	Editor link	32
11.	Preprocessor/synchronizer link	34
12.	Coordinate transformation link	36
13.	Multilateration equation solving link	37
14.	Geodetic coordinate estimation link	41
15.	Multilateration simulation link	43
16.	Geometric orbit determination link	44

17.	MICRODOT processing system	46
18.	Orbital ground trace for USA data simulation	55
19.	Data compression intervals	57
20.	Equation convergence with perfect data	58
21.	Data compression interval for SST	64
22.	SST equation convergence with perfect data	65
23.	CEOS-3 ground trace over C-band station constellation	68
A1.1	Data compression function	85
A1.2	Data compression results	87
A2.1	Overall Flow Diagram	97
A3.1	Pertinent geometry	131
A3.2	Greenwich and geometric coordinate system	140
A3.3	Oblate spheroidal model for station coordinates	140
A4.1	Geometry for development of potential	153
A4.2	Difference in equipotential surfaces	159
A4.3	Subdivision of land/sea surfaces	160
A4.4	Sea water Mascon	162
A5.1	Plot of exact versus analytic range correction residuals	178
A5.2	Geometry considered	201
A5.3	Temperature profile versus altitude	202
A5.4	The U. S. extension to the I. C. A. O. standard atmosphere	203
A6.1	Geometry of the system	239
A6.2a	Cross-section through the X-Z plane of figure A6.1	239
A6.2b	Cross-section through the X-Y plane of figure A6.1	240
A6.3	Transformation from the Sun oriented to the geographical coordinate system	240

A7.1	Coordinate systems	247
A7.2	Geographic and geometric coordinate systems	248
A8.1	Geographic coordinate basis	276
A10.1	Coordinate rotations induced by the precession of the equinox	308
A11.1	Topocentric multilateration coordinate system using or not using SST data types	315
A12.1	Geometry of the system	332
A13.1	Laser retroreflector geometry	343
A13.2	Radio ranging geometry	346
A14.1	3 stations	353
A14.2	4 stations	353
A14.3	5 stations	353
A18.1	Probability distribution of dynamic range	395
A19.1	Reflectors mounted on spherical satellite	399
A19.2	Pulse shapes	403
A20.1	The idealized configuration for the optical system consisting of a corner reflector and a beam spreading lens	412
A20.2	The mathematical model simulating Figure A20.1	412
A20.3	Frauenhofer and Fresnel diffraction	413
A21.1	Multibaseline system	417
A21.2	Arbitrarily scattered benchmarks	421
A21.3	Geodolite determined baselines in a geometrically defined basis	422
A21.4	Addition of extra stations	422
A21.5	Simulation terrain for Hollister experiment	425



MULTILATERATION:

- A GEOMETRIC METHOD TO DETERMINE GEOGRAPHIC INTERSTATION POSITIONS INDEPENDENT OF SATELLITE COORDINATES
- A GEOMETRIC METHOD OF ORBIT DETERMINATION
- A GEOMETRIC METHOD OF GEOPHYSICAL PARAMETER ESTIMATION

1. INTRODUCTION

Multilateration: the process of parameter estimation based on strict geometric laws is introduced in this volume from the point of view of advanced software processing systems. The main objective of this volume is to acquaint the reader as to the power of the multilateration technique and to describe the MICRODOT (Multilateration Interstation Coordinate Reduction and Orbit Determination Operational Trilateration) software presently developed at the Jet Propulsion Laboratory under Task N-16 for Tracking Station and Location Improvement in support of GEOS-3.

In order to make clear what specific problems might be solved with a software system such as MICRODOT, the specific applications on which such a software system might have scientific impact are introduced first. If these problems are of interest to the reader then it follows that an explanation of the Multilateration process also should be of concern to the reader.

The theory introduced in the main body of this volume is presented functionally with all derivations placed in detailed Appendices. The intent of this section is to make the reader aware of why without accurately knowing the position of the spacecraft or vehicle, or the location of the group of stations (constellation) participating in the experiment it is possible to a) locate the vehicle, and b) compute the interstation distances, to extreme precision.

Various multilateration systems are then introduced to illustrate the complexity to which such geometric foundations can be expanded in order to estimate geophysical parameters of interest to the applications presently to be mentioned.

The section on expected system accuracy attempts to identify in some detail hardware, atmospheric, Earth/ocean, and miscellaneous error sources. Having identified these error sources, some preliminary estimates on the approximate estimation power of both microwave and laser based multilateration systems are presented.

Next, from a functional point of view, a detailed description of the MICRODOT processing system is presented. Starting from a crude block diagram, the link structure and rationale behind the software design is developed

on a link-by-link basis; a link herein implying a computer in-core set of words and instructions. Flow diagrams of a functional nature are presented for each link and subsequently the links are all assembled into one final diagram describing the MICRODOT system in its complete structure. Detailed program operation and flow will be presented in the second volume of this report.

The next section recaps program capability and the options presently available on the MICRODOT system. Obviously this section is of temporary nature, since the MICRODOT program will continue to grow. However, the total program options are indicated.

Numerical simulations obtained via MICRODOT of a two-satellite system with a station constellation contained within the continental United States of America with and without satellite-to-satellite tracking are presented in the next section. Included in this section is a real world simulation of the interstation coordinate estimation capability which is afforded by the GEOS-3 satellite.

Finally a guide to the appendices contained in this report is presented in order to clarify their interrelationship.

2. APPLICATIONS OF THE MICRODOT PROCESSING SYSTEM

2.1 PRELIMINARY REMARKS

Recent advances in hardware systems are giving rise to observable data types of increasing accuracy such as range and range-rate from ground station to spacecraft. An illustration of such hardware is provided by two-color laser geodolites currently in operation by the University of Washington which are capable of obtaining the distance between two ground benchmarks within 2-3 tenths of a millimeter over 5 to 10 kilometer baselines. Satellite laser hardware such as used by the Wallops Island system has reached operational accuracies of 4 centimeters. Radio ranging systems have also improved over the past decade. Hence it seems that achievement of subcentimeter hardware measurement systems capable of operating from ground to either satellites or airplanes are almost within reach. This is not to say that lower accuracy measurement systems do not have applications. Many applications, such as surveying land areas, monitoring ocean coastal land erosion, etc. certainly need not have such high precision. It is safe then to assume that hardware measurement systems possessing data type measurement accuracies of σ centimeters do indeed exist, and ask what applications can be undertaken by a software processing system such as MICRODOT which can transform the data types to interstation ground coordinates and vehicle positions to, say, within 2σ . In other words precision simulations with the MICRODOT processing system have demonstrated that geometric degradation in some but not all the multilateration estimated parameters can vary by a factor of two or at most three for favorable geometric configurations.

2.2 SPECIFIC APPLICATIONS

Assuming that the hardware/software system is in hand, a tentative list of applications can be delineated as in Table 1.

Most of the applications which will be mentioned are self-explanatory. No attempt to define these areas of earth science will be undertaken herein since the main thrust of this report is to describe the software which might be used in experiments related to these areas.

Table 1. Applications of Multilateration Systems
 Low \equiv 1-2 meter, Medium \equiv 100-10 cm, High \equiv 1-0.1 cm

Application	Accuracy Requirements
• Practical Earth Surveying	Low
• Coastal and River Erosion Monitoring	Low
• Gravity Anomaly Determination	Medium-to-High
• Measurement and Calibration of Physical Constants	Medium-to-High
• Precision Geometric Orbit Determination Over Long and Short Arcs	High
• Continental Drift Determination	High
• Solid Earth Tide Modeling Improvement	High
• Ocean Earth Tide Modeling Improvement	High
• Rapid Fault and Tectonic Plate Monitoring	High
• Earthquake/Volcano Modeling Improvement	High
• Satellite Altimeter Calibration	High

In essence, the use of multilateration theory in conjunction with the desired hardware system and the MICRODOT processing system will provide science with a valuable tool for investigation of the previously mentioned areas. This tool can be used in conjunction with real data or with the realistic data simulation link within the MICRODOT program which can simulate an experiment prior to actual in-field operation.

3. THE MULTILATERATION PROCESS

Multilateration is defined to mean the process of taking simultaneous measurements of the slant range between an ensemble of ground stations and a flying/orbiting vehicle and the reduction of these measurements into meaningful information. If more than two vehicles are aloft, the act of measuring the distance between the vehicles is also considered as a multilateration process. The objective of multilateration systems, which use the simultaneous data type concept, is to solve for the three-dimensional interstation coordinates plus the vehicle position and velocities. To accomplish this objective using only geometric relationships in lieu of dynamic relationships, the concept of simultaneity of the data types needs to be invoked. This can be accomplished by interpolating the data types against some standard clock.

3.1 FUNCTIONAL EXPLANATION OF THE THEORY

Without belaboring the equations peculiar to the multilateration process, perhaps the easiest way to understand the technique is to use the equations functionally and note that in a specified rectangular coordinate system the equation of a sphere is given by:

$$(x - X_i)^2 + (y - Y_i)^2 + (z - Z_i)^2 = \rho_i^2, \quad (1)$$

where x, y, z are the vehicle positions, X_i, Y_i, Z_i are the station coordinates, and ρ_i are the distances from a station i to the vehicle. Hence, each station, upon measuring the slant range, ρ_i , permits one equation of the previous form to be written. It is evident that if three stations measure the slant ranges at the same time, then the coordinates of the vehicle are identical in the three resulting sphere equations and by direct algebra the vehicle coordinates relative to an adopted origin can be expressed as:

$$\begin{aligned} x &= x(X_i, Y_i, Z_i, \rho_i), \\ y &= y(X_i, Y_i, Z_i, \rho_i), \\ z &= z(X_i, Y_i, Z_i, \rho_i), \quad i = 1, 2, 3. \end{aligned} \quad (2)$$

The process of assuming the station coordinates to be known and insertion of the slant ranges into the three previous equations to obtain a state estimate is called Trilateration. In general then, with three stations a vehicle can be trilaterated to obtain its position at the epoch time of the synchronized measurements. Furthermore, if the slant range rate is known then by differentiation of the previous equations, the velocity \dot{x} , \dot{y} , \dot{z} of the vehicle can also be determined.

Suppose that a fourth station is added to the system such as to provide another spherical relationship of the form:

$$(x - X_4)^2 + (y - Y_4)^2 + (z - Z_4)^2 = \rho_4^2. \quad (3)$$

Now since Eqs. (2) determine the vehicle position, as long as ρ_1, \dots, ρ_4 are measured at the same time, a direct substitution of these equations in Eq. (3) yields a relationship strictly in terms of the interstation coordinates and data:

$$M \equiv M(X_i, Y_i, Z_i, \rho_i) = 0, \quad i = 1, 2, 3, 4. \quad (4)$$

The function M is called the multilateration function (M - function) of the station ensemble. Note that the vehicle position has been eliminated completely from the M -function. Hence using four stations a single equation of the form (4) can be generated wherein, if one desires, the station coordinates can now be treated as unknowns. If Eq. (4) is written at i distinct times where at each time a simultaneous set of four ranges (called a strike) is supplied to these equations, then by continuing this process, more and more equations are added while the number of unknowns is not enlarged. Soon, the algebraic system saturates and a unique solution for the coordinates of the stations becomes possible. The solution of the deterministic or overdetermined system is obtained by numerical methods (see Appendix A2). If the data is not synchronized then high accuracy interpolation and data compression are used to overcome this difficulty (Appendix A1).

3.2 IMPORTANT QUALIFYING REMARKS

The previous discussion would seem to indicate that given four stations and simultaneous range data measurements, all the station coordinates X_i , Y_i , Z_i can be determined. This is false, and almost obviously so. The physics of

the problem demands that the origin of the coordinate system be specified. Hence X_1 , Y_1 , Z_1 need to be a set of specified numbers. These numbers pin down the translational movement of the origin relative to another basis of referral. By additional reasoning it also becomes obvious that the X-axis of the coordinate must be fixed. To accomplish this Y_2 , Z_2 can be specified as numbers. Finally the fundamental plane of the coordinate system needs to be defined. This can be accomplished by setting Z_3 to a fixed number. These last two constraints use up the rotational freedom inherent in the symmetry of the equations. A geometric illustration of the coordinate system is given in Figure 1.

As can be seen from the Figure, station 1 is placed at the origin, station 2 defines the X-axis and station 3 defines the X, Y plane. The coordinates with overhead bars cannot be solved for or estimated. This is tantamount to saying that only the relative three-dimensional interstation coordinates can be obtained via the multilateration procedure. Estimation of geographic coordinates is discussed in Appendix A14.

Another important point relative to multilateration is concerned with the fundamental degeneracy of the algebraic equations which occurs if all four stations are in a plane. It has been shown [1] that if this is the case then a four station multilateration system becomes singular. Unfortunately, the proof of this fact is stated in a very misleading manner in many references, e.g., [1], [2], etc. It can be shown that the planar degeneracy or singularity alluded to

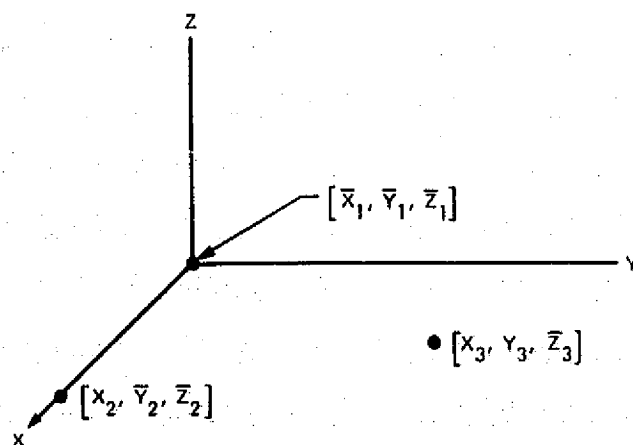


Figure 1. Multilateration Geometric Coordinate System
(Bars Indicate Specified Coordinates)

herein can be removed in a general manner by adding two additional stations. Hence as discussed in [1] a six station system is non-degenerate even if all the stations lie in the plane (or nearly in a plane). This however does not imply that six stations are required to have a non-degenerate multilateration system [3]. Specifically, by permitting one (or more) of the stations to be portable, an M-function can be derived for a system of four stations. The M-function is certainly well defined. By moving one of the stations, new data can then be processed with the newly positioned station and combined with the old data. This is really a five station system. Proceeding as before the portable station can be moved again and new data processed. As far as the multilateration equations are concerned, it appears that data from six independent stations has been accepted whereas in reality only four stations have been used. This movable four station system is non-degenerate, and works as well as a six station system. The system is obviously less expensive to implement, but requires a longer time before estimation of the station coordinates can be attempted.

Finally, for numerical stability of the generalized equations the vehicle undergoing multilateration must be displaced significantly from pass to pass with respect to the altitude above the stations. Obviously with an airplane this presents no adverse system constraint. With satellites, multilateration can be performed with a satellite in an elliptic orbit or two satellites at different altitudes can be used. Actually, enough strength in the solution is achieved in the real world due to the orbital perturbations and plane phasing if only one satellite in a circular orbit is used in the system configuration.

3.3 ADVANCED CONCEPTS

The previous discussion was restricted to what can be called simple multilateration systems or the process of an ensemble of ground stations viewing a vehicle at a common simultaneous time. More advanced multilateration systems can have one cluster of stations viewing vehicle A while a different cluster views vehicle B as the vehicles track each other. This is referred to as vehicle-to-vehicle multilateration.* As is probably obvious, simple and advanced multilateration systems can be codified to add power to the combined estimation

*Denoted herein as SST (satellite-to-satellite) or AAT (airplane-to-airplane) tracking.

procedure. Advanced multilateration systems also suffer from degenerate configurations and actually require additional stations to function at full mathematical strength, e.g., three stations fixed in one cluster will break this degeneracy.

Apart from the simple and advanced systems, hybrid multilateration systems are also of importance. These hybrid systems make use of station baseline information as obtained from the process of direct measurement such as obtained via the use of ground based instruments, e.g., geodolites in conjunction with either/or simple and advanced multilateration systems. If a sufficient number of accurate baselines are available, the mathematical stability of the solutions is greatly enhanced (see Appendix A21 and A22).

Finally, there is the multibaseline system. This is a static multilateration technique by which means baselines measured at different times with, say, two-color or three-color geodolites are combined to yield the interstation three-dimensional position coordinates. The static technique over short baselines indicates that with even slight elevation changes of about 50 meters, the three dimensional coordinates can be recovered to accuracies below 1 centimeter via the power of the two-color geodolite hardware.

At the present time, even more powerful hardware systems are being developed to use in conjunction with existing software packages such as MICRODOT.

4. MULTILATERATION SYSTEMS

As is evident, the previous section described the multilateration procedure and slowly introduced the concept of various systems using the foundations of geometry to obtain the estimated parameters which are desired for applications such as those previously mentioned. To further fix these systems firmly, an extensive but not all inclusive list will be discussed in more detail starting with the least complicated systems.

4.1 SYSTEM A - MULTIBASELINE SYSTEM

This three-dimensional coordinate estimation system [5] requires only the use of a single two-color geodolite and an array of retroreflectors scattered about the periphery of the geodolite emplacement. The virtually self-calibrating hardware is then aimed within minutes to each of the reflectors, and the baselines are measured to extreme precision (1 tenth of a millimeter standard deviations are within the realm of possibility; 2-3 tenths of a millimeter are currently being achieved over baselines of 10 km). The system is illustrated in Figure 2 and fully discussed in Appendix A21.

4.2 SYSTEM B - HYBRID MULTILATERATION SYSTEM

By augmenting the multibaseline system with a helicopter or balloon which carries a retroreflector array some speed in data reduction can be achieved as long as four of the ground stations can range to the hovering vehicle simultaneously with hardware units of high precision [6]. The range measuring instruments used for vehicle ranging can have less precision than the two-color geodolites used in the pure multibaseline system. Specifically range measurements of 1-2 centimeters combined with the high precision baselines should suffice.

4.3 SYSTEM C - SINGLE AIRPLANE SYSTEM

Operation of this system requires an airplane to make subsequent passes over a local area at different altitudes with the portable station placed at different ground positions for different passes (Figure 3).

SYSTEM A

- ONE MOVABLE TWO-COLOR GEODOLITE

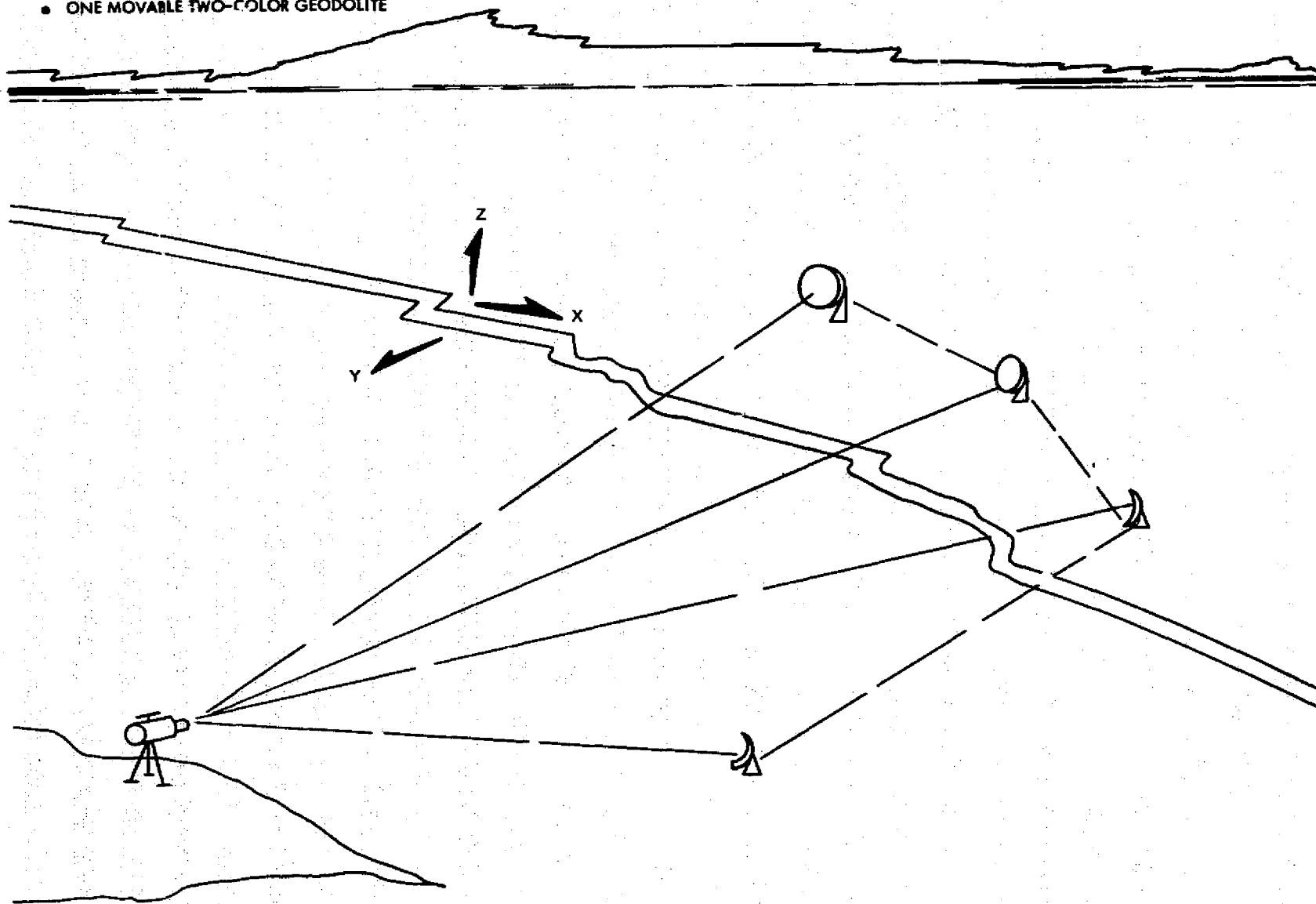


Figure 2. Multibaseline System

SYSTEM C

FIXED STATIONS
PORTABLE STATIONS
AIRPLANE

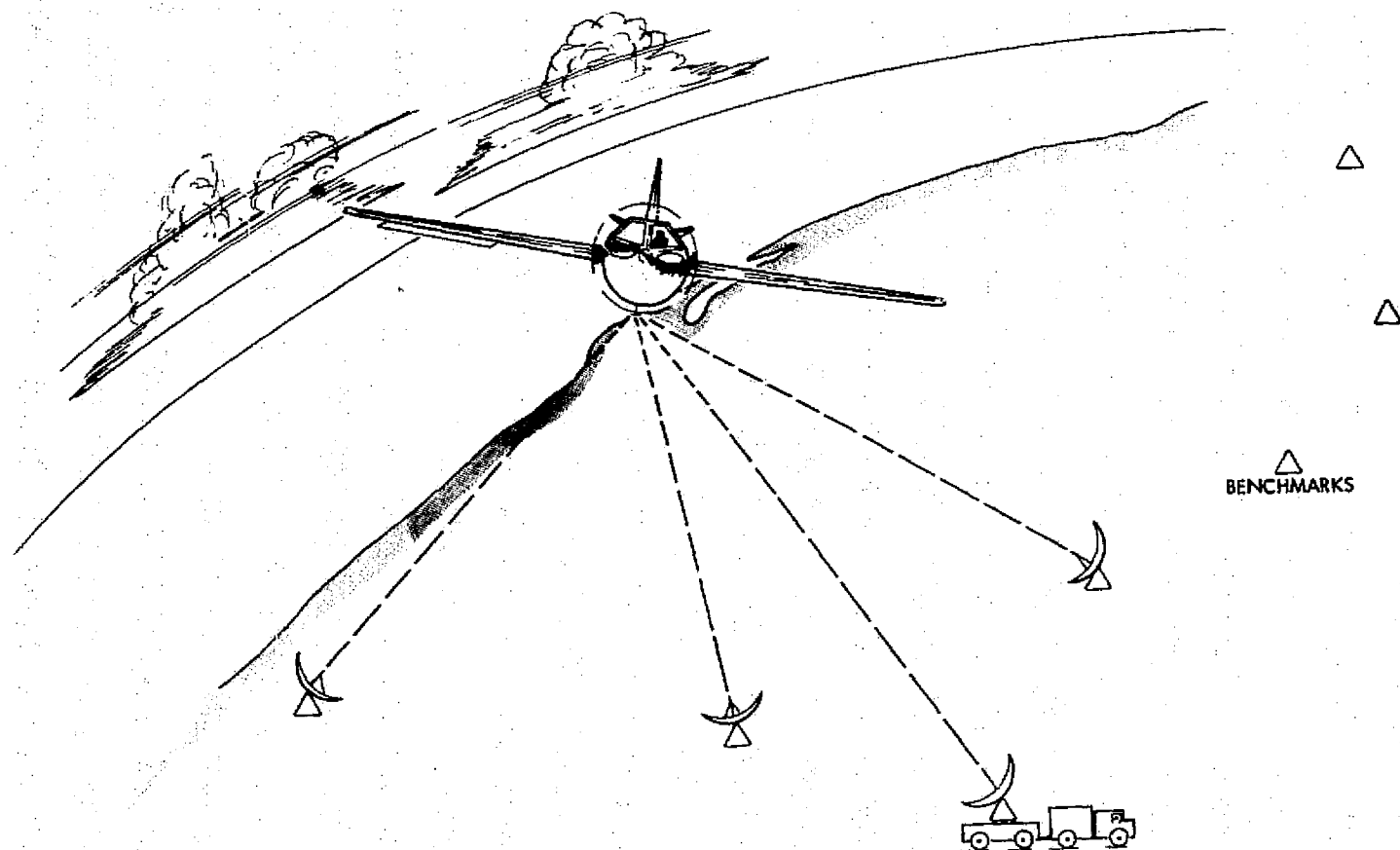


Figure 3. Airplane System

Expected accuracy of this system in station coordinate estimation will be equal (approximately) to the data type accuracy. Expected delay time from experiment initiation to interstation coordinate estimation would be about eight hours (movement of portable station and data processing time considered).

The disadvantage of this system is the accuracy degradation of interstation coordinate determination which occurs if the airplane leaves the area of common visibility of the initial three stations. This system should not be used for extending station coordinate grids over wide ground areas because each time a pivotal benchmark is used the station errors will propagate; some conditioning can be done here, but there are better systems available for station network definition. A second disadvantage is that real time station monitoring will only be possible in 8-10 hour intervals.

The main application of this system would be to accurately and precisely monitor ground movement across local geodetic faults. Obviously base-lines could be introduced to yield more accurate solutions.

4.4 SYSTEM D - UPRATED TWO-AIRPLANE SYSTEM

Figure 4 depicts an uprated two airplane system with a vehicle-to-vehicle datalink. Operation of System D requires that the two airplanes be in common view and that independent station clusters see each airplane. The airplanes would be at different altitudes. Once a ground area of much wider extent than surveyed in System C is sufficiently well monitored, the portable stations can be moved. Expected station coordinate estimation accuracy would be the same as System C.

After the two airplanes are aloft this system provides direct real time station coordinate monitoring (no delay time of any appreciable duration). However a disadvantage of System D is the lack of ability of the system to estimate station coordinates once line-of-sight is lost between the airplanes. It should be noted that error growth in mapping the station network in the viewing area is constrained due to the vehicle-to-vehicle data type. Furthermore the number of stations in this system would permit a System C type operation without having to move the portable station.

Application of System D would be in the areas of real time fault monitoring and station network propagation over wide local areas.

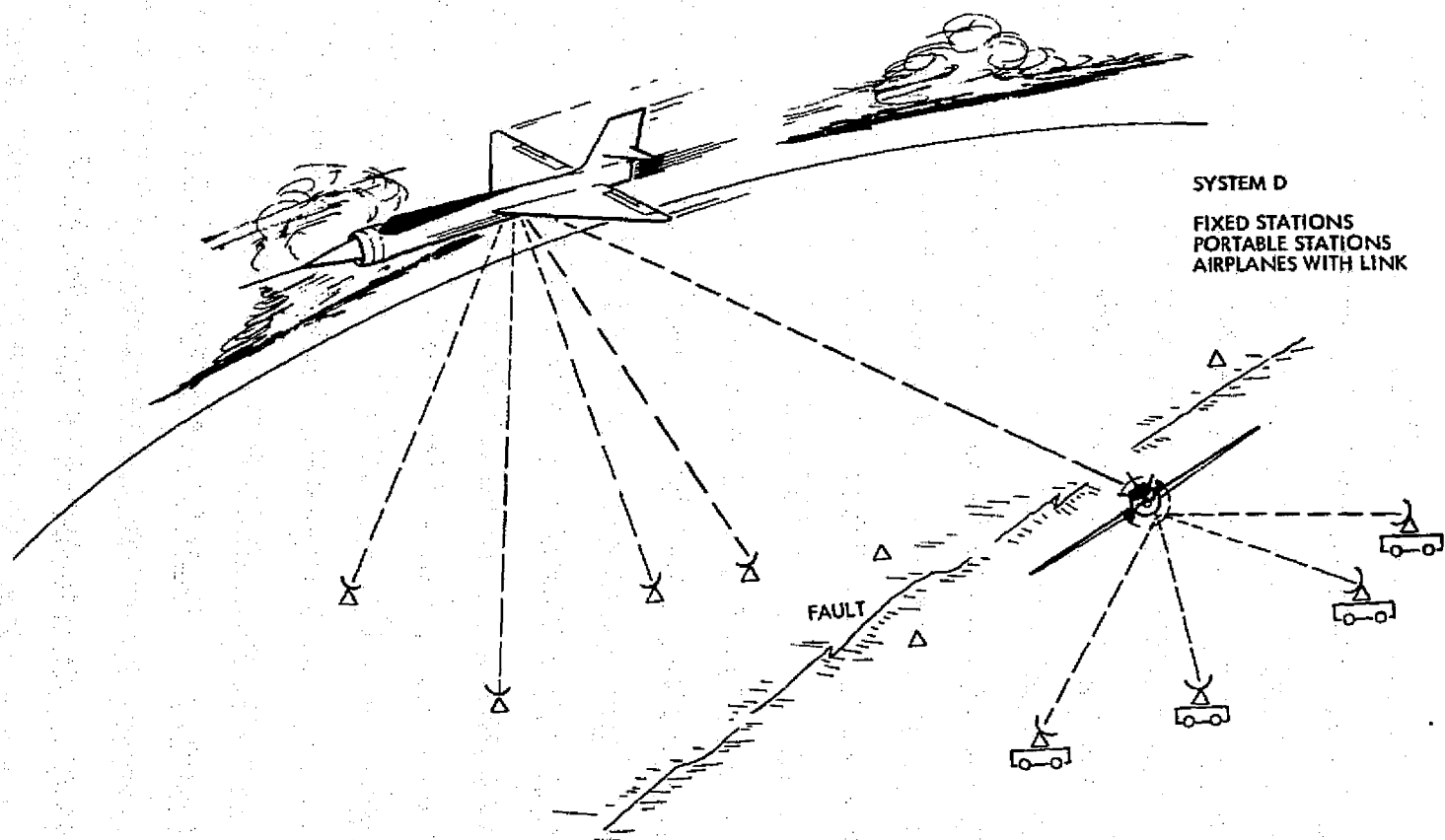


Figure 4. Two-Airplane Systems

4.5 SYSTEM E - MINIMUM COST SINGLE SATELLITE SYSTEM

Figure 5 illustrates the next cost plateau, namely a single satellite system with the following subsystems: a) three fixed stations, b) one portable station, c) one satellite.

Operation of this system requires the satellite to be in a circular orbit (this will provide sufficient altitude change), and to make passes over continental (intercontinental) land masses with the portable station placed at different ground positions per pass. For example, in Figure 5, station 4 would be moved from its initial position on, say, pass 1 to position 4X on pass X, etc. In essence this system is similar to system C with a satellite replacing the airplane.

Expected accuracy of coordinate estimation will be nearly equal to the data type accuracy. The satellite state, i. e., position and velocity in the topocentric coordinate frame discussed in Figure 1 will also be estimated to comparable accuracies. The satellite state in the inertial system will be obtained to accuracies degraded by the errors inherent in the coordinate transformation peculiar to the topocentric/inertial frame of reference (see Section 5).

Expected delay times from satellite injection to interstation coordinate estimation and orbit determination would be of the order of a day or two (movement of portable station, pass phasing and data processing time considered).

System E disadvantages are: a) long delay times and b) the necessity of moving one station. The advantages are that only four stations are required and that station coordinate errors do not propagate relative to the adopted origin of the coordinate system. Note that the portable station could be placed on a different continent than the fixed stations.

Applications of System E would be in the areas of tectonic plate motion, and physical constants estimation, i. e., calibration of dynamic versus geometric orbit determination residuals, etc.

4.6 SYSTEM F - IMPROVED SINGLE SATELLITE SYSTEM

This system is the same as system E except that two stations are added to the system thereby overcoming the phasing constraints previously discussed.

SYSTEM E

3 FIXED STATIONS
1 PORTABLE STATION
1 SATELLITE IN ELLIPTIC ORBIT

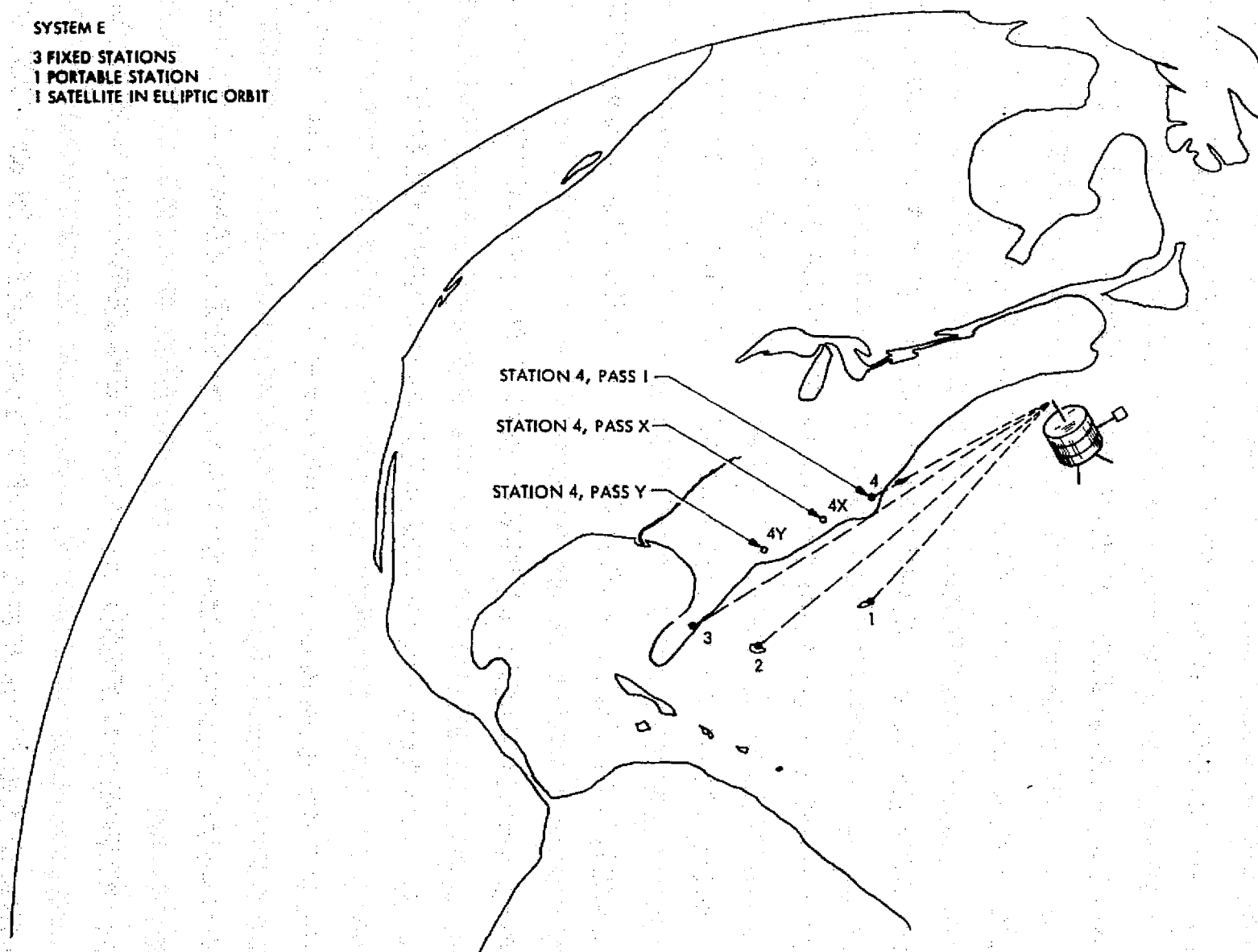


Figure 5. Single Satellite System

4.7 SYSTEM G - MODERATE COST SATELLITE/AIRPLANE SYSTEM

A moderate cost satellite/airplane system is illustrated in Figure 6. The subsystems might be: four fixed stations for the satellite, four portable stations for the airplane, one airplane, and one satellite with vehicle-to-vehicle link.

Operation of System G is similar to System D (two airplane system). The stations peculiar to the airplane cluster are moved periodically in order to permit complete mapping of continental land masses.

Expected delay times from satellite injection to coordinate estimation and geometric orbit determination would occur due to vehicle-to-vehicle viewing window constraints. This system does not require an elliptic orbit because of the wide separation in vehicle altitudes.

Applications of System G are similar to those of System E, however local fault movements could also be monitored by the stations in the airplane cluster.

4.8 SYSTEM H - TWO SATELLITE SYSTEM

An extension of system F would require: six stations (fixed and portable), and two or more satellites.

In system H the vehicle-to-vehicle link is not used. The satellites can be placed in circular orbits of varying altitude. Operation here proceeds by having the station system multilaterate the orbit of each satellite separately on subsequent passes.

Expected delay times from injection to parameter estimation will also occur due to viewing window constraints but on the average will be half as long as for single satellite systems. This system can be used for nearly all other previously mentioned applications.

4.9 SYSTEM I - UPRATED TWO SATELLITE SYSTEM

An uprated version of System G is shown in Figure 7. The subsystems are: six or more stations, two satellites, with vehicle-to-vehicle link, and a possible satellite-to-airplane link.

SYSTEM G

FIXED STATIONS
AIRPLANES
SATELLITES
WITH VEHICLE-TO-VEHICLE LINK

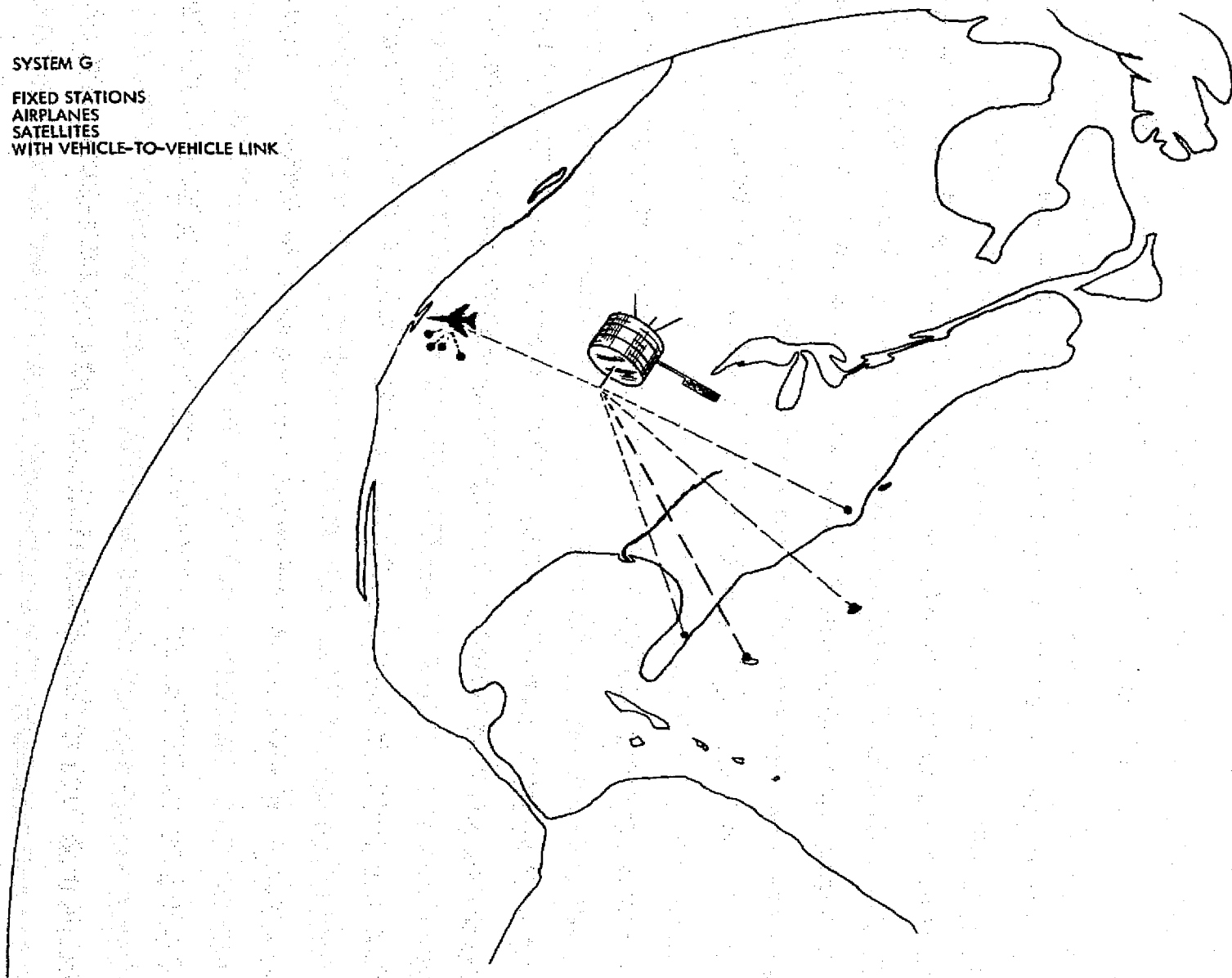


Figure 6. Airplane - Satellite System

SYSTEM I

6 FIXED STATIONS
2 SATELLITES IN CIRCULAR ORBITS
WITH SATELLITE-TO-SATELLITE LINK

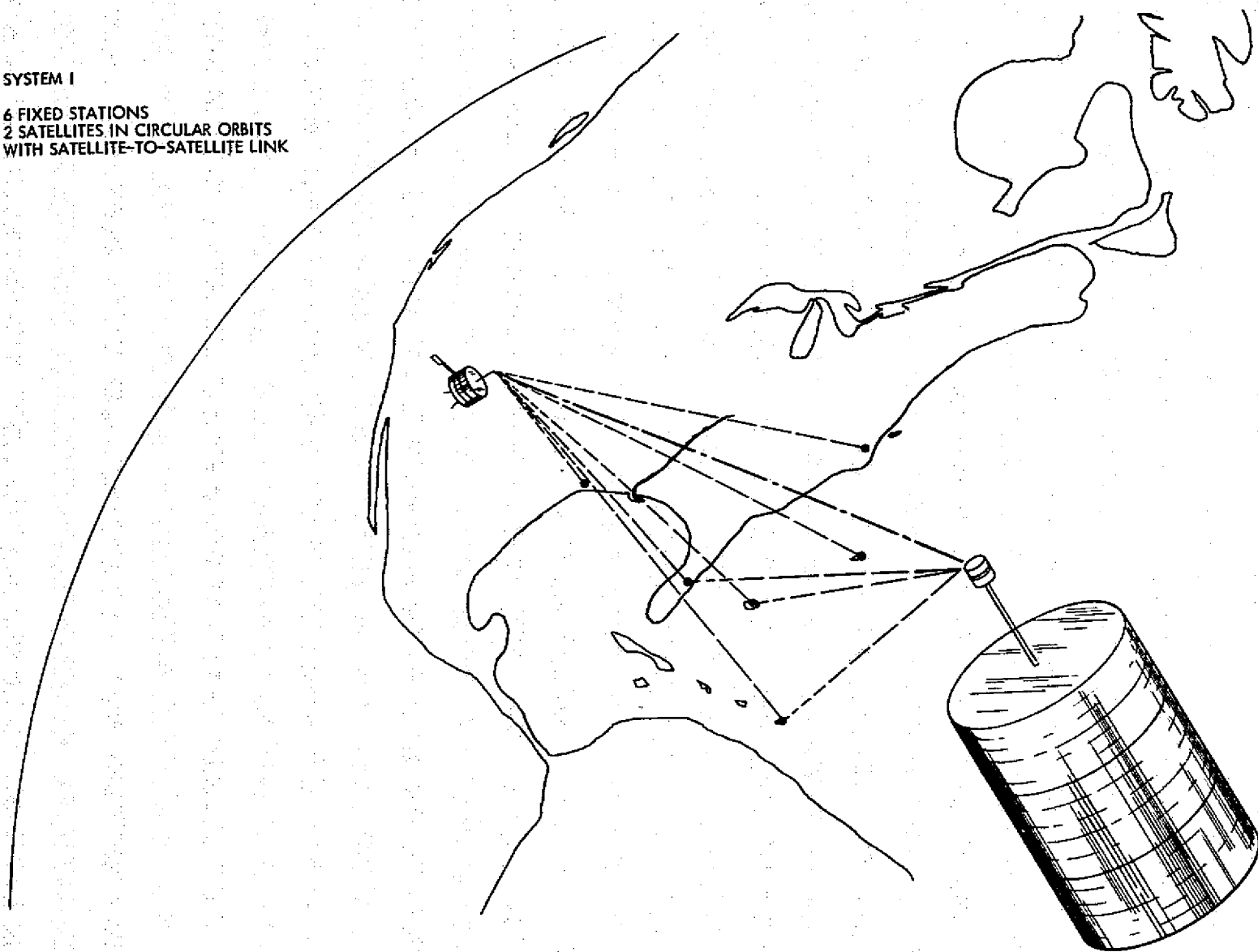


Figure 7. Two-Satellite System

System I uses the satellite-to-satellite link to enhance the accuracy of estimated parameters. The system can function using both low and synchronous altitude satellites. Addition of one portable station on each continent provides for complete global coverage and station network determination.

4.10 SYSTEM J - COMBINED SYSTEMS

As may be evident quite a number of different multilateration systems can be defined. The previous list is by no means exhaustive either as to combinations of system components or as to data type combinations. Certainly the use of range-rate and range-difference (interferometric) data can be an important consideration to enhance overall parameter estimation capability. The same can be said for multilateration systems which combine short baseline data, e.g., as obtained from the USGS with slant range measurements, etc. Hardware can be placed on the ground or flown on the satellite or airplane, e.g., a laser can be fired from the satellite to ground-based retroreflectors. Geometric determination of space probe state can be carried out with surprising accuracy. The possibilities here seem almost without end. The reader is directed to Appendix A22 for an additional overview.

5. EXPECTED SYSTEM ACCURACIES

Multilateration systems are possessed of a unique advantage, namely, estimates of the parameters can be obtained from the solution without the use of Newtonian dynamics, but rather by means of strict geometric laws. Perhaps this statement should be clarified slightly because dynamic laws are used in the atmospheric calibration and Earth/ocean tide models. However the dynamic modeling errors occasioned by these two models are of second order compared to the errors induced in the solution via the dynamic equations of motion of classical orbit determination procedures. The implication here is that the total error budget of a multilateration system will of necessity be less than that of a classic orbit determination system using the Newtonian constants and models of motion. It is true that the Newtonian or physical constants peculiar to classical orbit determination schemes can be estimated along with the station and orbital parameters, i. e., fit to a dynamic model in some mean sense with respect to the center of the Earth — wherever that point is located. By the same token, physical parameters in a multilateration scheme can also be estimated but always with fewer modeling constants and with only a subset of the same models which are used in the dynamic orbital procedure. It is for this reason that comparisons between multilaterated geometrically determined parameters and the same dynamically determined parameters yield residuals which can be used to estimate the dynamic constants to refined levels of accuracy.

For multilateration systems the explicit list of error generating sources is: a) hardware equipment, b) atmospheric parameters and turbulence, c) earth tide constants, d) ocean tide constants, e) multiple reflection errors (laser system), and if a satellite system is used and only if the state of the satellite is desired in the inertial coordinate system, an additional error source is f) the transformation model and constants from the topocentric to the inertial coordinate system.

These error sources will be examined in detail presently and realistic random and bias errors are listed. When possible, the standard deviations on variables which are required for input are purposely made large, e.g., right ascension of the Moon. This permits simple analytic ephemeris models to be used in the tidal models.

5.1 HARDWARE ERROR SOURCES

The hardware errors are listed in Table 2

Table 2 values, except for the speed of light which is used in the light time leg extraction process are system dependent. For radio systems using accurate clocks (Cesium or Rubidium standards) a rough estimate in the derived pseudo observable slant range standard deviation is 1 to 5 meters depending whether S or C band data is used. Data types for satellite-to-satellite tracking obtained via X-band would be more accurate. Bias like errors of about 1/2 meter are realistic. Laser system standard deviations presently attainable are about 4 to 15 cm with bias like errors of 2-3 cm. Advanced laser systems as

Table 2. Hardware Parameters (S-Band)
(Boxed Parameters Denote Bias-like Error Sources)

Definition	Symbol	Value	Units	Error
Turnaround Time Observable	τ		sec	$<10^{-9}$
Bias in Observable	$\Delta\tau$	$\approx 10^{-5}$	sec	10^{-7}
Signal Emit Clock Time	t		sec	10^{-11}
Station Clock Bias Relative to Master Clock	Δt	$\approx 10^{-6}$	sec	10^{-8}
Satellite/Airplane Transponder Delay Time	Δ	$\approx 10^{-6}$	sec	10^{-9}
Satellite/Airplane Transponder Relay Bias	$\Delta(\Delta)$		sec	10^{-9}
Speed of Light	c	$2.99792458 \cdot 10^{10}$	cm/sec	40.0
Master Clock Time (Rubidium)	t^*		sec	$<10^{-12}$

described in [1] could function in the 2-3 centimeter random error range with 1 centimeter bias errors. It should be noted that multiple reflection errors have been roughly estimated to have 4 to 5 cm random errors and possible 1 cm bias contributions.

The hardware induced random errors will of course be reduced by the square root of the number of processed data points up to the bias limit error. Hence with careful data filtering, the estimates adopted herein for the random standard deviation will be 1/4 meter for radio systems and 1-2 centimeters for laser systems.

5.2 ATMOSPHERIC ERROR SOURCES

Atmospheric constants used to compute the effects of delay and turbulence are examined in Table 3. Analysis of the appropriate partial derivatives and sum of the squares for the random errors yields a standard deviation of about 1.3 centimeters with an additional bias error of about 0.25 centimeter. It is evident that the calibration model developed for multilateration studies is totally adequate for radio ranging systems but has increasing importance as the 1 cm threshold accuracy is approached. It should be kept in mind that for radio ranging, ionospheric effects degrade the accuracy of the calibration (see Appendix A6).

5.3 EARTH/OCEAN TIDAL ERRORS

Table 4 lists the relevant parameters of the Earth/Ocean tide model.

It should be noticed that Moon/Sun coordinates, sidereal time and local gravity errors are purposely taken large to permit computation via simple analytic models. The Moon/Sun lag angles (deformations of ground positions, at least theoretically, lag the Moon and Sun) as can be seen are quite uncertain. A rough estimate of the accuracy of prediction of station coordinate motions occasioned by the Moon and Sun are about 3 cm using the Earth tide model. Incorporation of the ocean model should cut this uncertainty down to about 1 cm. Use of gravimeter readings would also cut down these estimates, however it seems unrealistic to assume that bias errors would ever be below the 1 cm threshold.

Table 3. Atmospheric Parameters

Definition	Symbol	Value	Units	Error σ *
Universal Gas Constant	\bar{R}	$8.3142 \cdot 10^4$	$\text{mbar cm}^3 (\text{°K})^{-1}$	$0.0002 \cdot 10^4$
Molecular Weight of Air	M	28.966	g	0.003
Vertical Temperature Lapse Rate	α	6.8	°K/km	0.5
Inversion Layer Attitude	h_0	depending on season and time of day	m	50
Tropopause Altitude	h_1	11000	m	1000
1st Refractivity Constant	K_1			
Microwave:		77.624	°K (mbar)^{-1}	0.1
Laser: (Ruby)		80.34	°K (mbar)^{-1}	0.01
2nd Refractivity Constant	K_2			
Microwave:		12.92	°K (mbar)^{-1}	9.0
Laser: (Ruby)		-11.3		
3rd Refractivity Constant	K_3			
Microwave:		0.3719	$(\text{°K})^2 (\text{mbar})^{-1}$	0.003
Laser:		0.0		
Zenith Angle	z		deg	0.1
Ground Temperature	T_0		°K	0.1
Water Vapor Scale Height	h_w	2	km	0.1
Surface Gravity	g_R	978.0495 at sealevel, equator	cm sec^{-2}	0.25×10^{-3}
Water Vapor Constants of Eq. (30):	k_1	7.567		0.001
	k_2	2066.92	°K	1.0
	k_3	33.45	°K	0.01
	e_1	6.11	mbar	0.01
Ground air mass density at Station 1	ρ_0	1.5×10^{-3}	gm/cm^3	$2.5 \cdot 10^{-5}$
Temperature of Inversion layer	T^*		°K	1°
Dew Point Temperature of H_2O	t		°K	1°
Lower Station Altitude	H_0		cm	100
Upper Station Altitude	H_1		cm	1000

(Boxed Parameters Denote Bias-like Error Sources)

(*Errors Taken Purposely Large)

Table 4. Earth/Ocean Tide Parameters

Definition	Symbol	Value	Units	Error σ^*
Geocentric Coordinates of Topocentric Origin, Axis, and Plane	$X_1 \ Y_1 \ Z_1$ $Y_2 \ Z_2$ Z_3		m	2
Local Sidereal Time	Θ		rads	$1 \cdot 10^{-3}$
Right Ascension/Declination of the Moon	$\alpha_{\text{C}}, \delta_{\text{C}}$		rads	$2.5 \cdot 10^{-4}$
Right Ascension/Declination of the Sun	$\alpha_{\text{O}}, \delta_{\text{O}}$		rads	$2.5 \cdot 10^{-4}$
Moon Distance	R_{C}		Earth Radii	0.1
Sun Distance	R_{O}		Earth Radii	1.0
Moon/Earth Mass	$(M_{\text{C}}/M_{\text{E}})^{-1}$	81.301		$1 \cdot 10^{-3}$
Sun/Earth Mass	$M_{\text{O}}/M_{\text{E}}$	$3.329456 \cdot 10^5$		0.4
Earth Gravitational Constant	GM_{E}	398601.2	$\text{km}^3 \text{sec}^{-2}$	0.4
Mean Equatorial Earth Radius	a_{e}	6378.160	km	$5.0 \cdot 10^{-3}$
Mean Earth Flattening	f	1/298.25		$5.0 \cdot 10^{-7}$
Moon/Sun Phase Angles	$\psi'_{\text{C}}, \psi'_{\text{O}}$	$\approx 3^\circ$		3°
Local Gravity	g	≈ 978.0	cm sec^2	$1.0 \cdot 10^{-2}$
Love Number	h	0.60		0.1
Shida Number	l	0.075		$5.0 \cdot 10^{-3}$
Load Love Number	h'	-0.4		0.1
Sea Water Density	σ	≈ 1	gm cm^3	$1.0 \cdot 10^{-4}$

(Boxed Parameters Denote Bias-like Error Sources)

(*Errors Taken Purposely Large)

5.4 SUMMARY OF ERRORS

In summary, the random error sources present no specific problems, however the system bias errors create a budget of uncertainty below which statistical improvement becomes dubious. Before continuing this discussion a recap of expected accuracies (bias errors) are as follows.

The figures in Table 5 assume high quality hardware systems and are intended to serve as worst case bias error budgets. To improve these budgets two paths are available. The first involves solving for the bias errors (if numerically possible). The second path is to assume that some degree of cancellation will occur due to the large number of bias error sources. Hence, with some degree of certainty:

$$\sigma_{\text{Microwave}} = \sqrt{\sum \sigma^2} \cong 26 \text{ cm},$$

$$\sigma_{\text{Laser}} = \sqrt{\sum \sigma^2} \cong 2 \text{ cm}.$$

These estimates have been made relative to a local topocentric system and express the ultimate accuracies that might be achieved in estimation of interstation and satellite/airplane positions in the topocentric

Table 5. Bias Error Contributions (cm)

Source	Microwave	Laser
Hardware	25	1
Atmosphere		
Troposphere	1	1
Ionosphere		
Single frequency	4	0
Dual frequency	0.5	0
Earth/Ocean Tide	1	1
Multiple Reflection		1
Total	≈ 31.5	≈ 4

system (Figure 1). If a transformation of coordinates to an inertial frame is performed, such as to obtain orbital elements at some epoch, then the rotational, and translational error budgets would degrade the satellite coordinates by at least 1/2 meter.

6. SOFTWARE DESIGN

For efficient data reduction and parameter estimation the design of operational software needs to be modular. The easiest way to implement the proper software design is by the construction of modular links which in the end comprise and define the complete software package. Usually only one link of the software system will be executed at a given time. There is nothing to preclude hooking all the links into one contiguous software package driven by proper input command controls, however for operational post flight data reduction this is not a necessity. The links are of course totally compatible and structured interfaces are implied. With this preliminary understanding of the software link structure, attention is drawn to Figure 8. As can be seen the MICRODOT processing system is composed of eight independent links. A preliminary overview of each of these links follows.

6.1 REAL TIME OPERATIONS LINK

The Real Time Operations Link would be the control center for real time data processing. Actually the word link here is not really applicable since the structure of such a nerve center would involve many additional support functions which would need to be delineated in much more detail. This link however would be responsible for acquisition of real data from all vehicles participating in a given experiment and for the gathering of all additional data required for atmospheric (Appendices A5 and A6) and tidal calibrations (Appendices A3 and A4). The software feedback would result in the real time displays of, e.g., ground fault movements. No in depth design of such a link has been undertaken since it actually constitutes an independent project at the multi-million dollar level. The link does however indicate how the software package could be used in real time to display and monitor geodetic and other parameters of experimental interest. Figure 9 displays this link in more detail.

The hypothetical structure of such a link might be as follows. Entering at the upper left hand corner of the link, i. e., at the real time operations entry point a file would yield the satellite orbital elements at some epoch or raw radio data for radio trilateration. These known vehicle states could then be used to compute station acquisition alert and pointing angles which would in turn be transmitted to the station constellation participating in a given

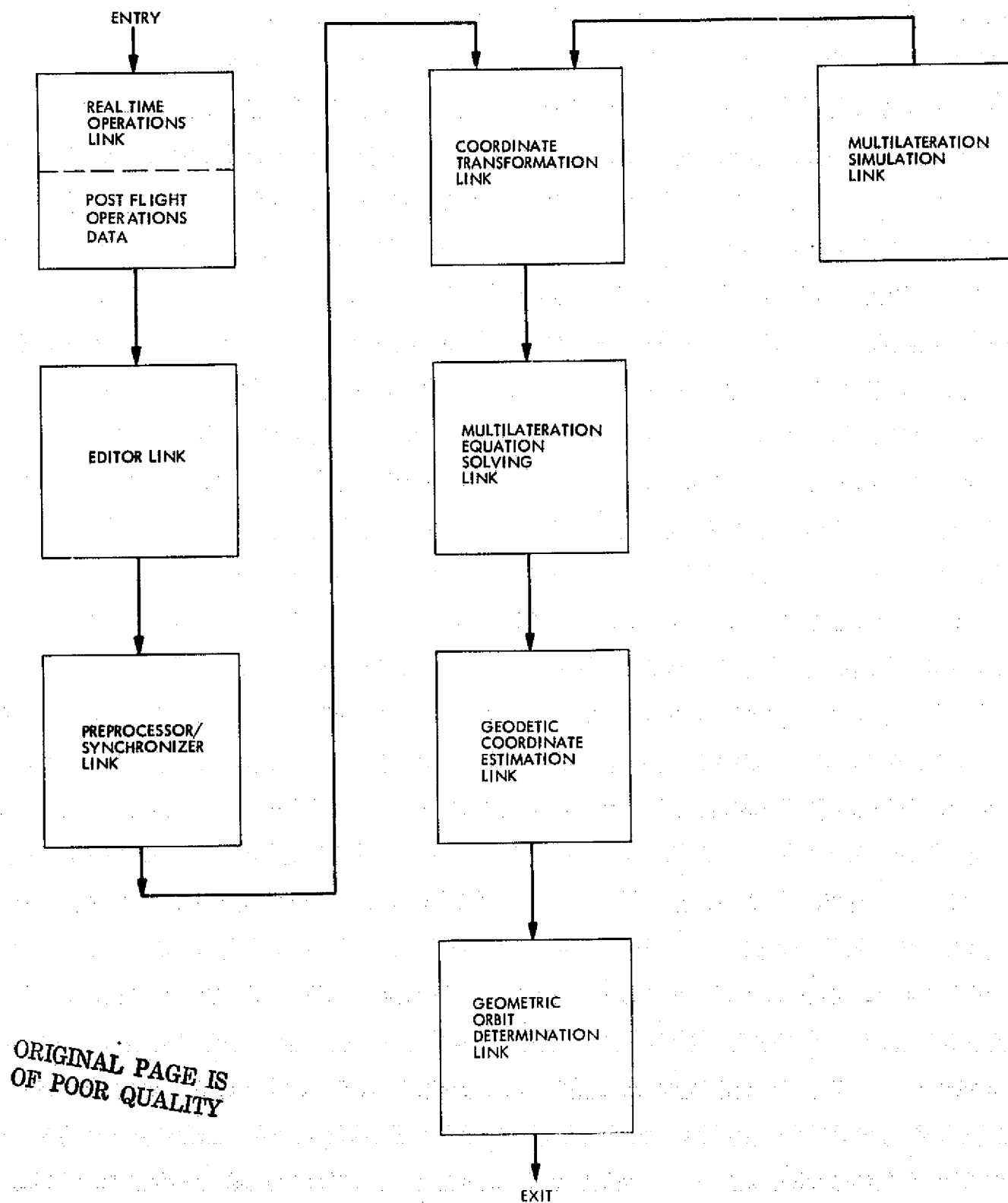


Figure 8. The MICRODOT Link Structure

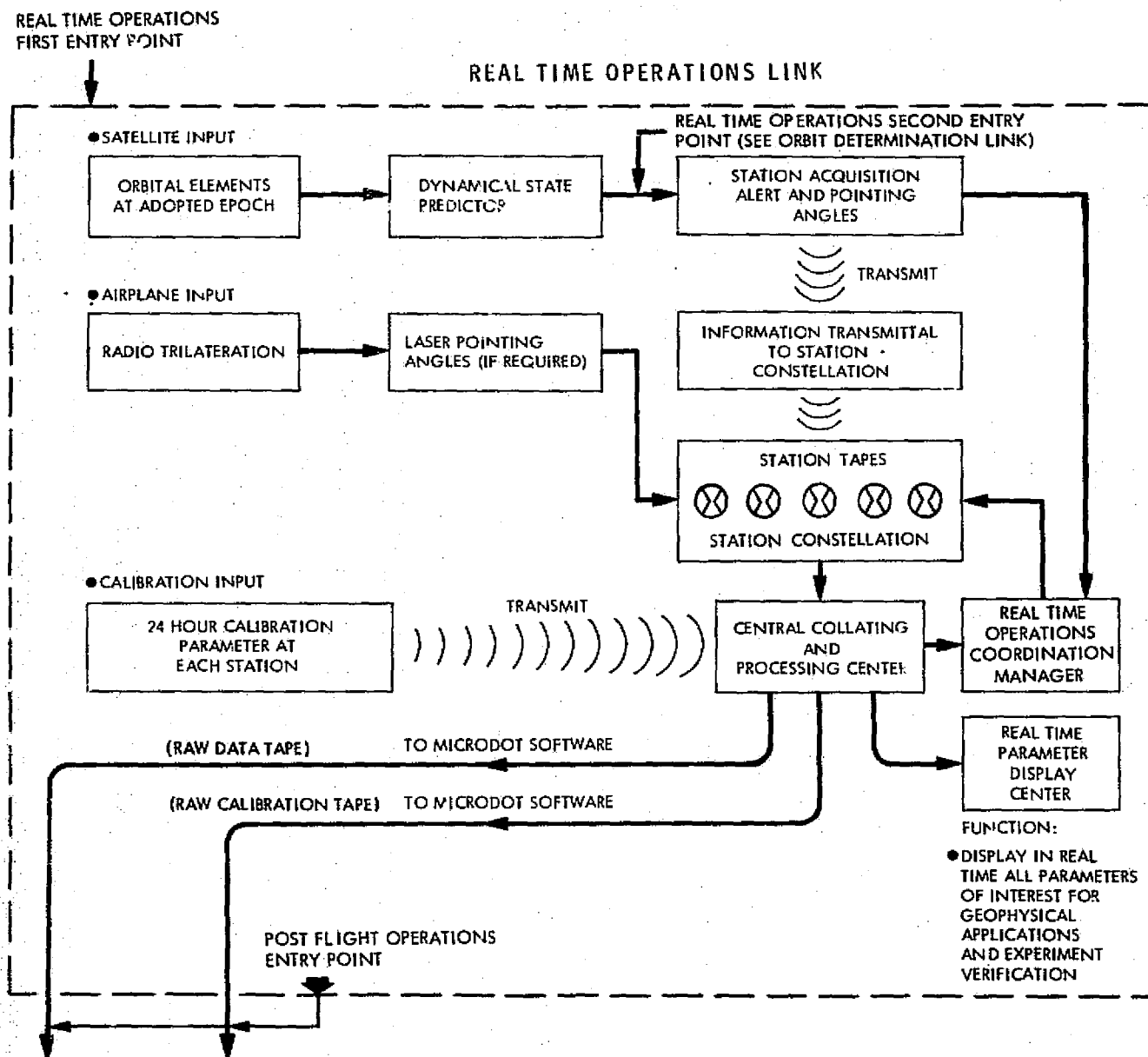


Figure 9. Real Time Operations Link

experiment. The pointing angle predictions are necessary especially for laser systems in order to ensure retroreflector feedback. The individual station tapes would then be cabled into a central collating and processing center and reduced to two different tapes or files. The first of these tapes is the raw data tape which contains a simple data type versus time history for the experiment participating vehicles as monitored at all the ground stations. The second tape is the raw calibration data tape which is a continuous histogram of atmospheric and assorted parameters required for data type calibration (Appendix A15). These tapes will be discussed in more detail in the next software link. Once the Real Time Operations Link is functioning, multilateration feedback to this link is supplied at the second real time operations entry point. The feedback now yields the vehicle state prediction and the desired real time parameter displays, i.e., the link, once placed in operation is self-perpetrating through the actions of the real time coordination/operation manager and the real time parameter display center.

For post flight operations the two necessary data tapes or data streams would be supplied at the post flight operations entry point thereby circumventing the entire previous link and force subsequent exiting from this link into the software Editor Link.

6.2 EDITOR LINK

The first of the two previously discussed data tapes, i.e., data stream 1 (Appendix A15) which contains data types such as range versus universal time, range-rate versus time, vehicle-to-vehicle range versus time etc. is now fed into Editor 1. Basically this editor (Figure 10) determines the station overlap windows which are the overriding multilateration system constraint (note that simultaneous measurements are required for multilateration operation). Hence after format conversion the editor sorts for common visibility windows and writes a new tape with all time tagged overlap periods. This tape is used to interrogate the raw calibration tape, i.e., data stream 2 (Appendix A15). Data stream 2 has station atmospheric parameters versus universal time, e.g., pressure, temperature, etc. and other related parameters such as vehicle attitude etc. which will be required for data calibration. If these

EDITOR LINK

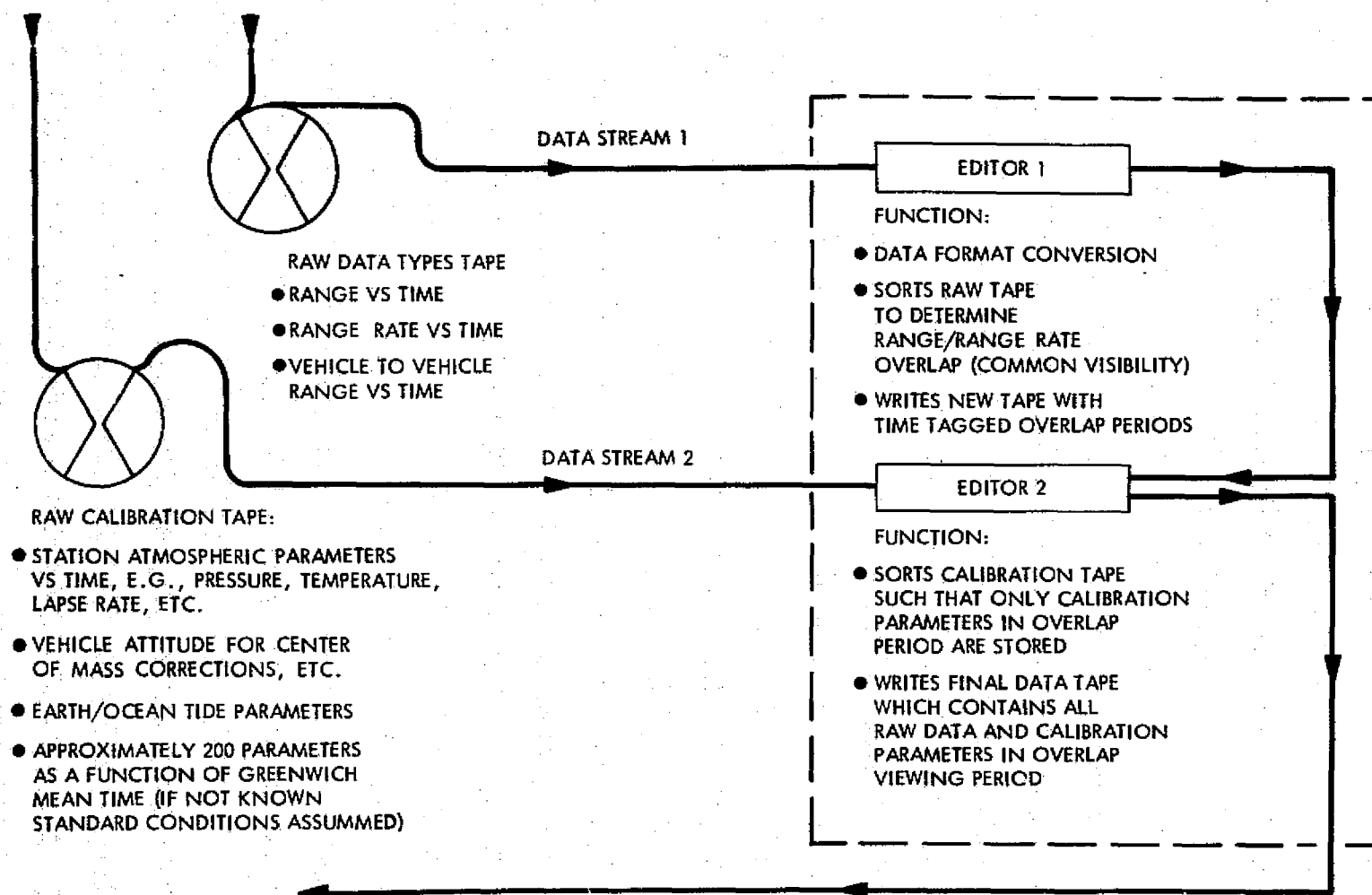


Figure 10. Editor Link

parameters are not known some standard values are assumed, e.g., constant pressure or vehicle attitude throughout the day. Editor 2 sorts the calibration tape such that only calibration parameters in the overlap periods determined via Editor 1 processing are retained, and proceeds to write a final data tape which contains only the parameters peculiar to the overlap periods. This tape is known as the collated data tape. It is this tape that is fed to the Preprocessor/Synchronizer Link.

6.3 PREPROCESSOR/SYNCHRONIZER LINK

Figure 11 displays the Preprocessor/Synchronizer Link. The basic function of this link is to smooth the data and obtain interpolating functions which permit simultaneous data to be recovered as pseudo observables. Hence, the collated data tape is fed to this link and any data or time (clock) biases which are known are removed. Any additional constants are also picked up at this point, e.g., tidal model constants, etc. A quick blunder point removal is performed and a preliminary synchronization module is entered. In this module, a short fit of the data is performed (typically a minute) and the polynomial is differentiated to obtain the range-rate (if this data type is not available). It is now possible to exit this module ignoring all other corrections and perform a trilateration of the vehicle, with assumed a priori station locations. Having obtained the vehicle position and velocity at a convenient epoch via the trilateration procedure permits a reference trajectory to be computed over a long arc, and from this trajectory to obtain reference observables as opposed to the true observables. The reference and the true observables are differenced and the difference data is compressed over the long arc (Appendix A1). The reference trajectory can be computed as accurately as desired in order to permit the interpolation formulas to have the desired range of validity. Furthermore at this point the vehicle zenith angles required for atmospheric calibration can be determined at least to a first approximation. Hence, the preliminary synchronization module can be re-entered and the atmospheric, light time and center of mass corrections (Appendices A5, A6, A13, A14) applied to the true observables. The data can now be refit and the process repeated as required. The final fitting is accomplished in the data compression module using a square root formulation [4,8]. The interpolating coefficients and their covariance,

ORIGINAL PAGE IS
OF POOR QUALITY

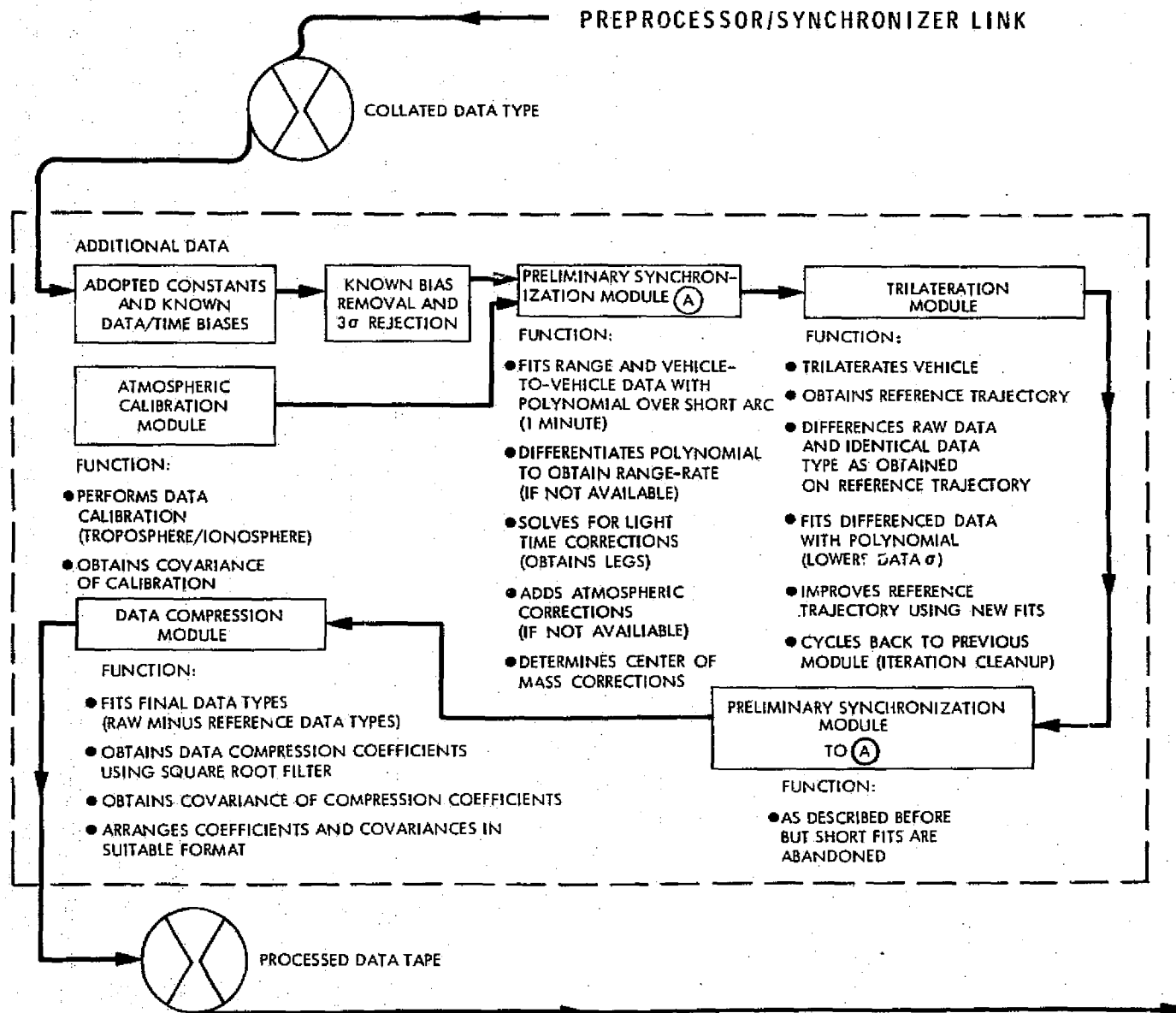


Figure 11. Preprocessor/Synchronizer Link

including atmospheric correlations, data and clock jitter are then output over the common overlap period for the entire station constellation participating in the experiment. This processed data tape is fed to the Coordinate Transformation Link.

6.4 COORDINATE TRANSFORMATION LINK

The coordinate transformation link (Figure 12) is only used once at the beginning of each experiment. The only functions of this link are to retrieve the geodetic a priori station coordinates (and/or any other parameters whose value is to be estimated) and to construct the corresponding parameter covariance matrix in the standard geographic coordinate basis (Appendix A7). This operation is followed by the coordinate transformation of these parameters into the multilateration geometric basis depicted in Figure 1. The covariance matrix is also transformed into this basis with due regard for any translational and rotational errors induced in the process. Coordinate scaling is also performed in order to achieve better numerical stability in the equations. In this process all partial derivatives are extracted analytically and the properly structured a priori covariance matrix is fed into the Multilateration Equation Solving Link. As will be presently discussed the multilateration equation solving link determines the new covariance matrix of the estimated parameters in the geometric basis. Hence after processing a batch of data it is not necessary to utilize the coordinate transformation link when a new batch of data is to be processed, since the old a priori matrix is already in the proper coordinate basis.

6.5 MULTILATERATION EQUATION SOLVING LINK

With the processed data tape and the proper a priori matrix of the estimated parameters, the next link of the software can be called forth (Figure 13). Logic flags consistent with the previous links are activated to determine which parameters will be estimated and which parameters will be treated in a statistical consider mode. Arrays of the link are expanded or contracted internally via variable dimensioning. The flow now proceeds to the multilateration function module. In this module the multilateration functions are generated in one continuous sweeping process for all possible data types

COORDINATE TRANSFORMATION LINK

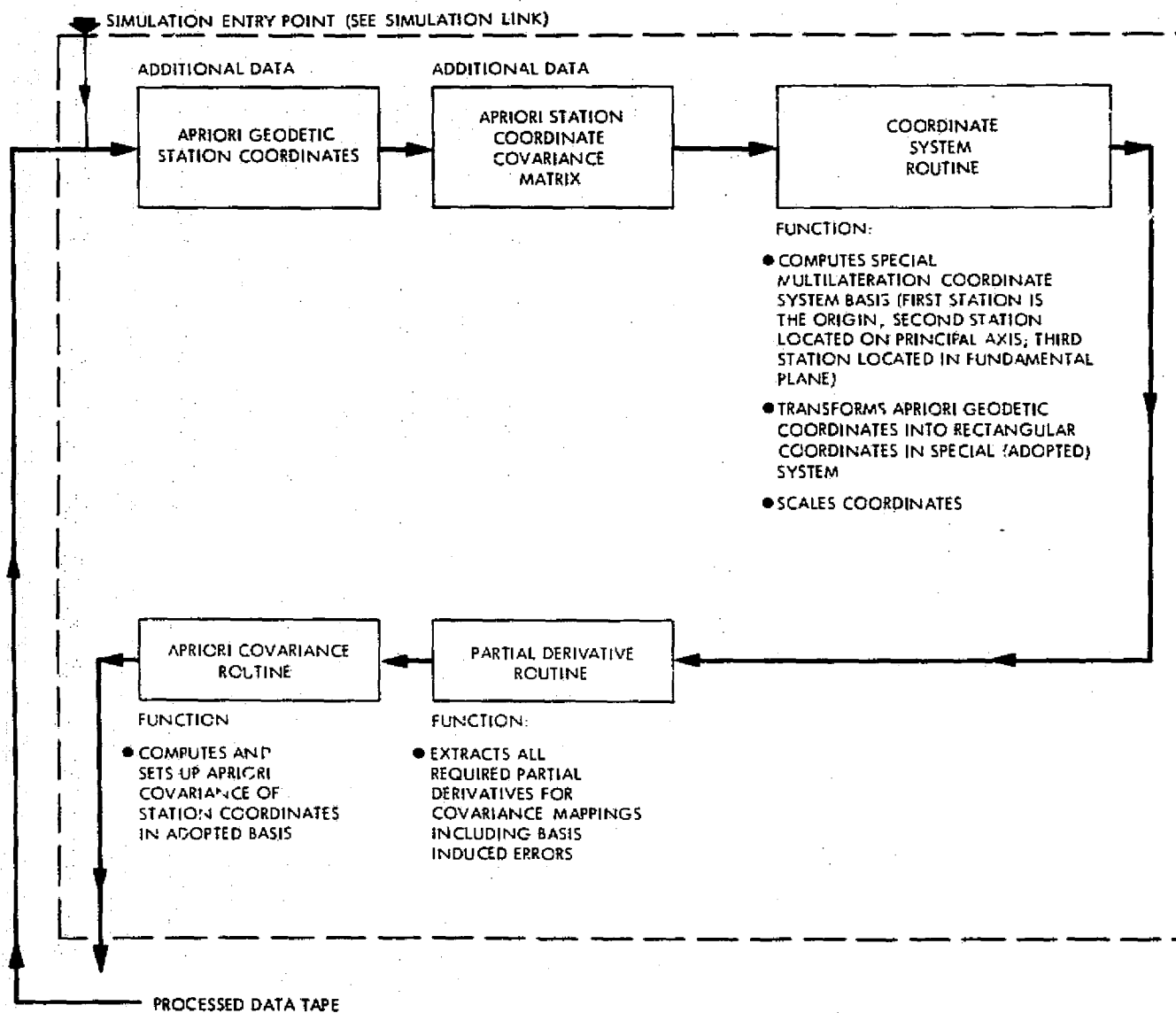


Figure 12. Coordinate Transformation Link

MULTILATERATION EQUATION SOLVER LINK

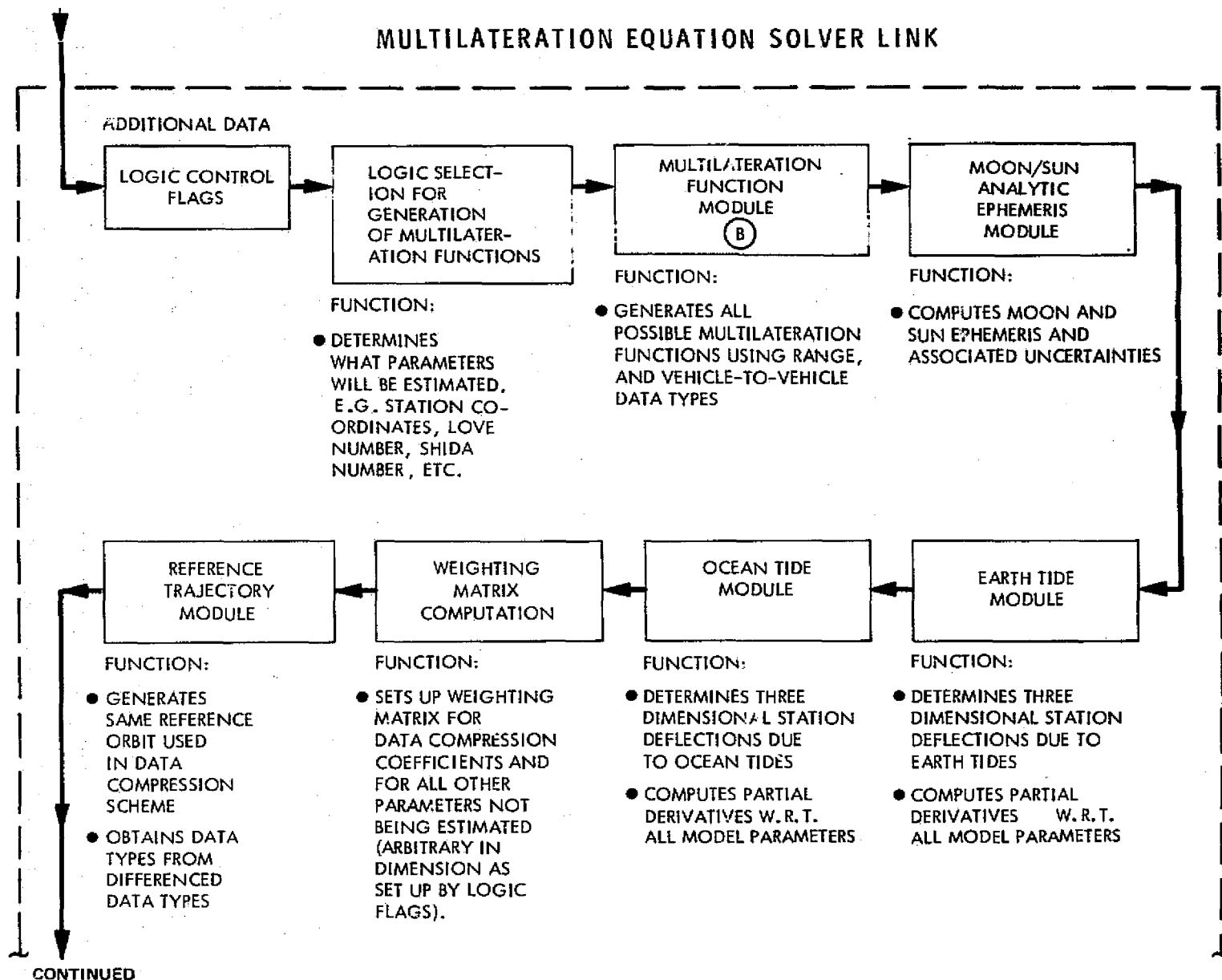
ORIGINAL PAGE IS
OF POOR QUALITY

Figure 13. Multilateration Equation Solving Link (Sheet 1 of 2)

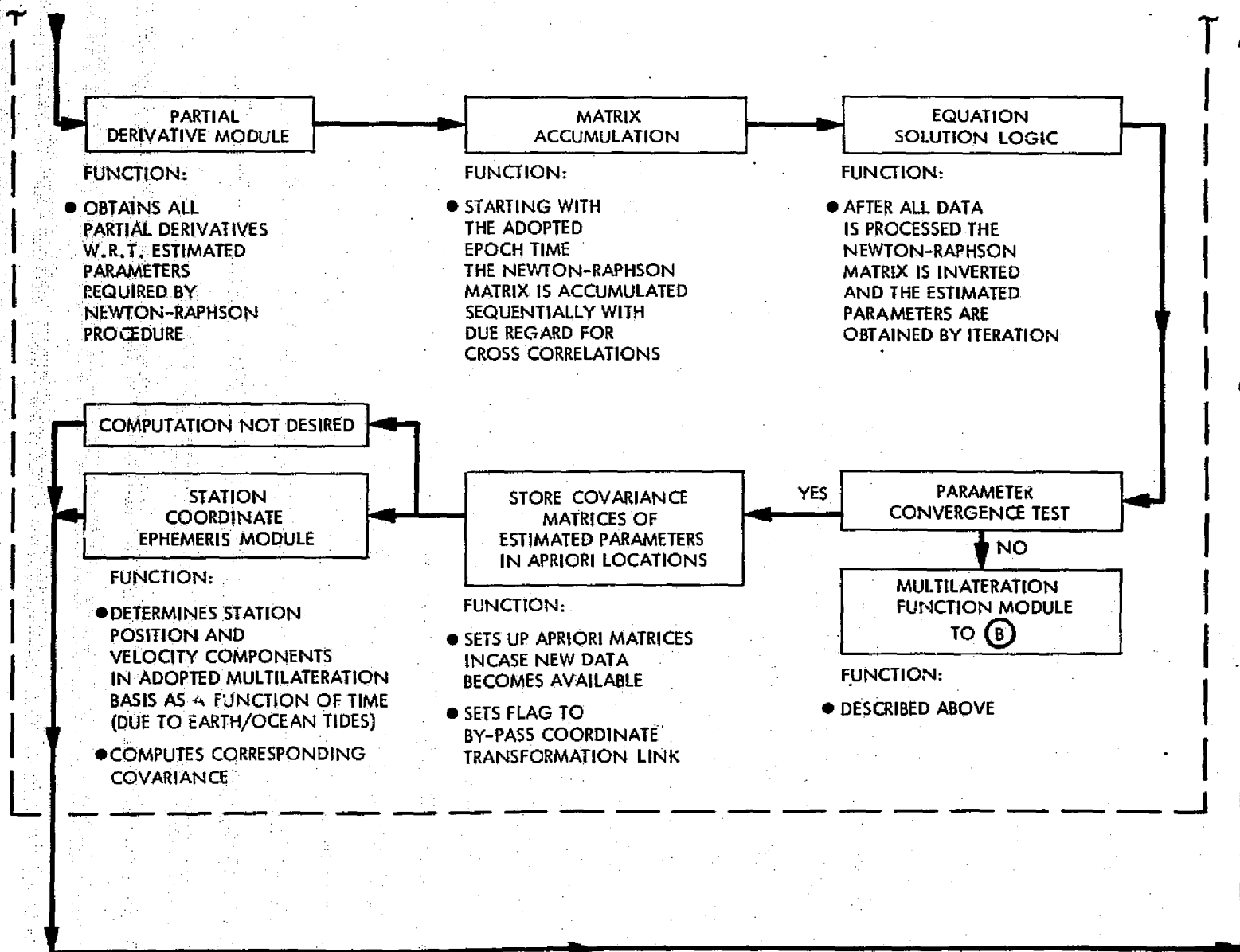


Figure 13. Multilateration Equation Solving Link (Sheet 2 of 2)

over the fitting interval wherein the data compression coefficients are valid (Appendix A11). As will be presently discussed this interval can be determined in the Multilateration Simulation Link. The generation of the multilateration functions is complicated by the Earth deformation occasioned by the solid and ocean tides (Appendices A3, A4, A2). These tides, which over long baselines can cause 20 to 30 cm variations within a period of 12 to 18 hours, need to be modeled in order to correctly combine sequential batches of data. To accomplish this an analytic ephemeris module for the Moon/Sun position is called forth and the Earth tide routine is interrogated at the same time as the relevant multilateration function. This tide routine determines the complete three-dimensional deflections due to the solid Earth tides and computes all the analytic partial derivatives required for covariance determination of the tidal parameters. In a similar manner the ocean tide deflections perturbing the multilateration functions can also be taken into account. These tides can cause about 4 cm positional perturbations. An option is available to by-pass these calculations if low precision computation is to be performed. The next computation involves the multilateration function weighting matrix (Appendix A2). This matrix has three main components. Specifically the weighting component of the data compression coefficients (both auto and cross correlations), the weighting component of the non-estimated or consider parameters, and the weighting component of the clock jitter in the master clock. Note that atmospheric and hardware related errors have been absorbed into the data compression coefficients (Appendices A1, A2). Hence according to the selection flags the matrix is constructed internally. The construction of the multilateration functions also involves the re-generation of the reference trajectory; one should recall that in the preprocessor/synchronizer link a data difference rather than a data absolute function was used to fit the data. At this point, therefore, the absolute data types, e.g., slant ranges, can be recovered.

For a given batch of data the multilateration functions (M-vector) and the appropriate weighting matrix inclusive of all cross correlations are now available in core. This permits initiation of the Newton iteration (Appendix A2). The analytic partial derivatives of the multilateration functions with respect to the estimated parameters are now extracted. The inverse of the weight matrix is postmultiplied by this matrix and premultiplied by its transpose.

If more data is available (other data compression batches) the previously described procedure is repeated from the beginning and the Newton-Raphson matrix for the first iteration is accumulated sequentially till all data is exhausted (Appendix A2). When this process is complete, the a priori covariance is added to the accumulated information matrix and the matrix is inverted. The Newton-Raphson correction is added to the initial estimates of the estimated parameters and tested for convergence. The procedure is repeated until the estimated parameter convergence is achieved.

It should be noted that if the Earth/ocean tide option is activated, it is not possible to solve for the station coordinates, but only for constants in the tidal model. Hence if this option has been selected, and the absolute interstation coordinates are desired at specified times, the station coordinate ephemeris module must be interrogated to yield the instantaneous interstation coordinates as a function of time, i. e., to yield a station ephemeris. The multilateration equation solving link not only computes the covariance matrix of the estimated parameters but it also outputs the matrix of partial derivatives of the estimated parameters with respect to the consider parameters (Appendix A16). If desired the output from this link could be fed to Geodetic Coordinate Estimation Link.

6.6 GEODETIC COORDINATE ESTIMATION LINK

For certain geophysical applications, the ability to determine so called absolute geodetic coordinates, i. e., latitude, longitude and elevation above the geoid is an important consideration. This is the function of the Geodetic Coordinate Estimation Link (Figure 14). Since the previous link has determined the interstation coordinates to high precision, it follows that these coordinates can be used to determine the interstation baselines or distances along with their related covariance. Hence, by recalling the a priori geodetic coordinates and obtaining the appropriate partial derivatives of a redundant system of equations involving the a priori equations plus the interstation distance equations, improved estimates of the geodetic coordinates can be obtained (Appendix A14). This is accomplished by a weighted least squares procedure in the Geodetic Equation Solver Module. Again, if desired the tide induced time variations of the absolute coordinates can be determined. These absolute coordinates can now be fed to the Geometric Orbit Determination Link, if the process of orbit parameter estimation is of consideration. Since the

GEODETIC COORDINATE ESTIMATION LINK

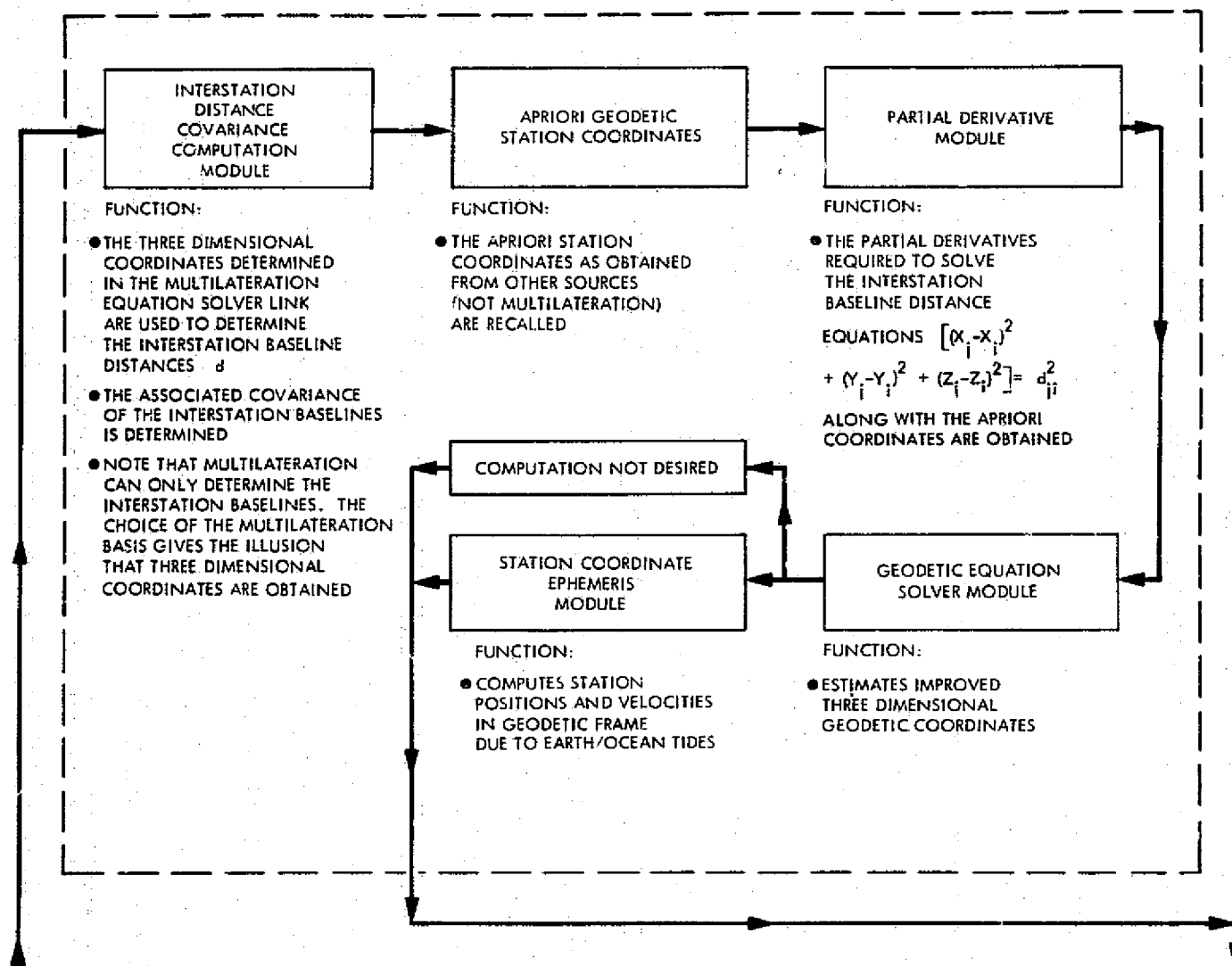


Figure 14. Geodetic Coordinate Estimation Link

process of orbit determination is actually a derived option of the multilateration process this link will be discussed after the Multilateration Simulation Link.

6.7 MULTILATERATION SIMULATION LINK

Simulation of data for a large software package such as MICRODOT is of importance not only for purposes of software verification and checkout but also for proposed experiment verification and interpolation formula duration of validity assessment. These are the functions of the Multilateration Simulation Link (Figure 15). In brief, this link is given a set of reference elements or parameters from which data can be generated for an assumed set of station coordinates. This data, if desired, can then be corrupted with noise and generated with realistic perturbations added to the elements in order to investigate the degree of the interpolating formula required to fit data over a specified duration (Appendix A1). From the point at which the data is generated, the simulator proceeds to handle and compress the data in the same manner as the previously described Preprocessor/Synchronizer Link. The process of obtaining the reference orbit via trilateration, fitting the difference of the observables from reference observables generated via the reference orbit, etc., and obtaining the associated covariances is practically the same and needs no further elaboration at this point. Obviously, this link permits software operation to be exercised without the first three links described herein. The output from this link therefore, yields a smoothed collated data tape which can be input directly into the Multilateration Equation Solving Link of the MICRODOT system.

6.8 GEOMETRIC ORBIT DETERMINATION LINK

The Geometric Orbit Determination Module (Figure 16) receives a file of either the interstation coordinates or the geodetic station coordinates (after improvement by the Geodetic Coordinate Estimation Link). It also accepts the smoothed collated data compression tape. With these two inputs the link can now operate in two distinct modes. First, it can perform a weighted least squares trilateration using all stations viewing the vehicle plus the vehicle-to-vehicle data in the geometric or adopted multilateration frame (Appendix A8). This mode of operation has distinct advantages for altimeter calibration and

MULTILATERATION SIMULATION LINK

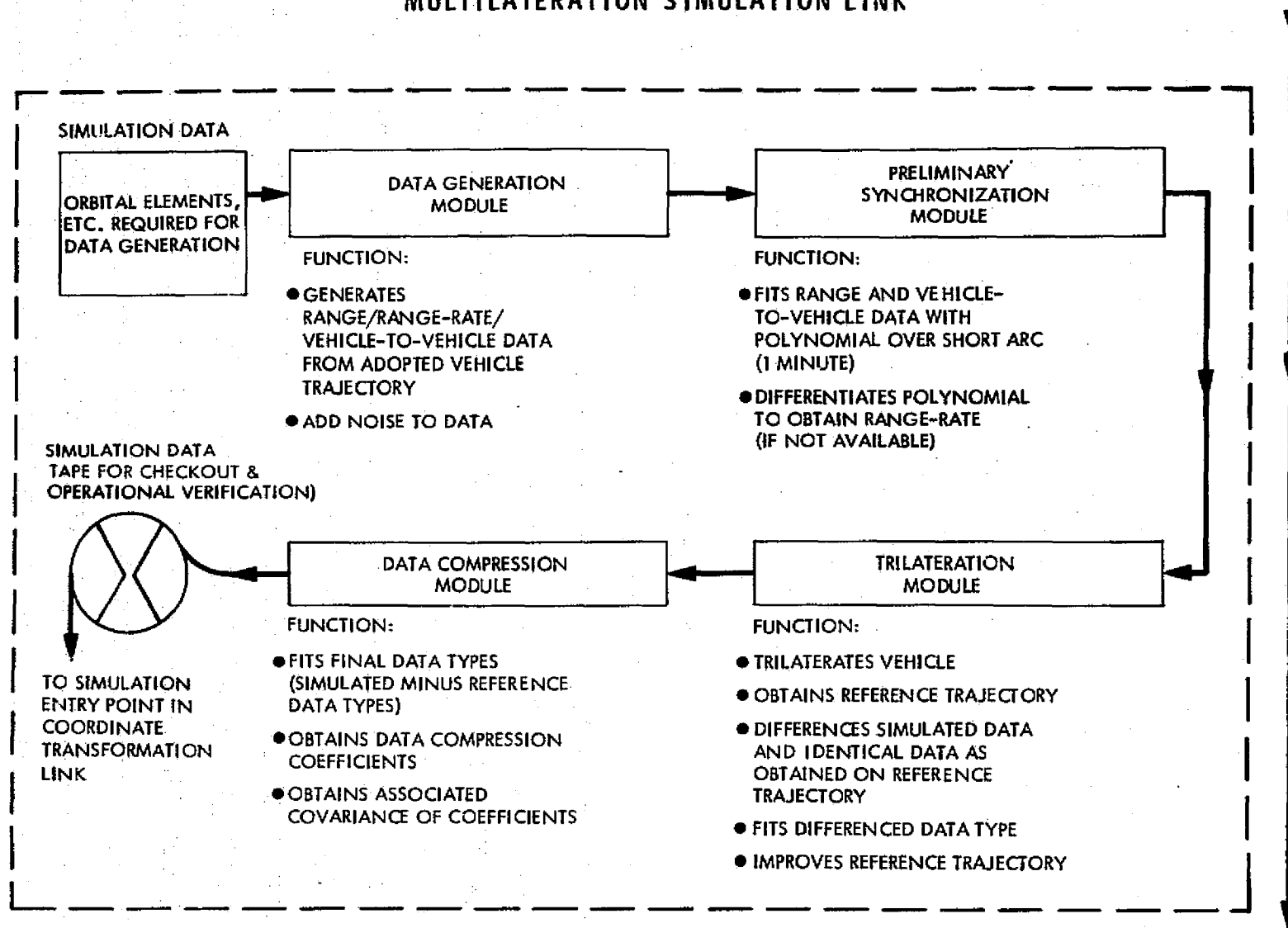


Figure 15. Multilateration Simulation Link

GEOMETRIC ORBIT DETERMINATION LINK

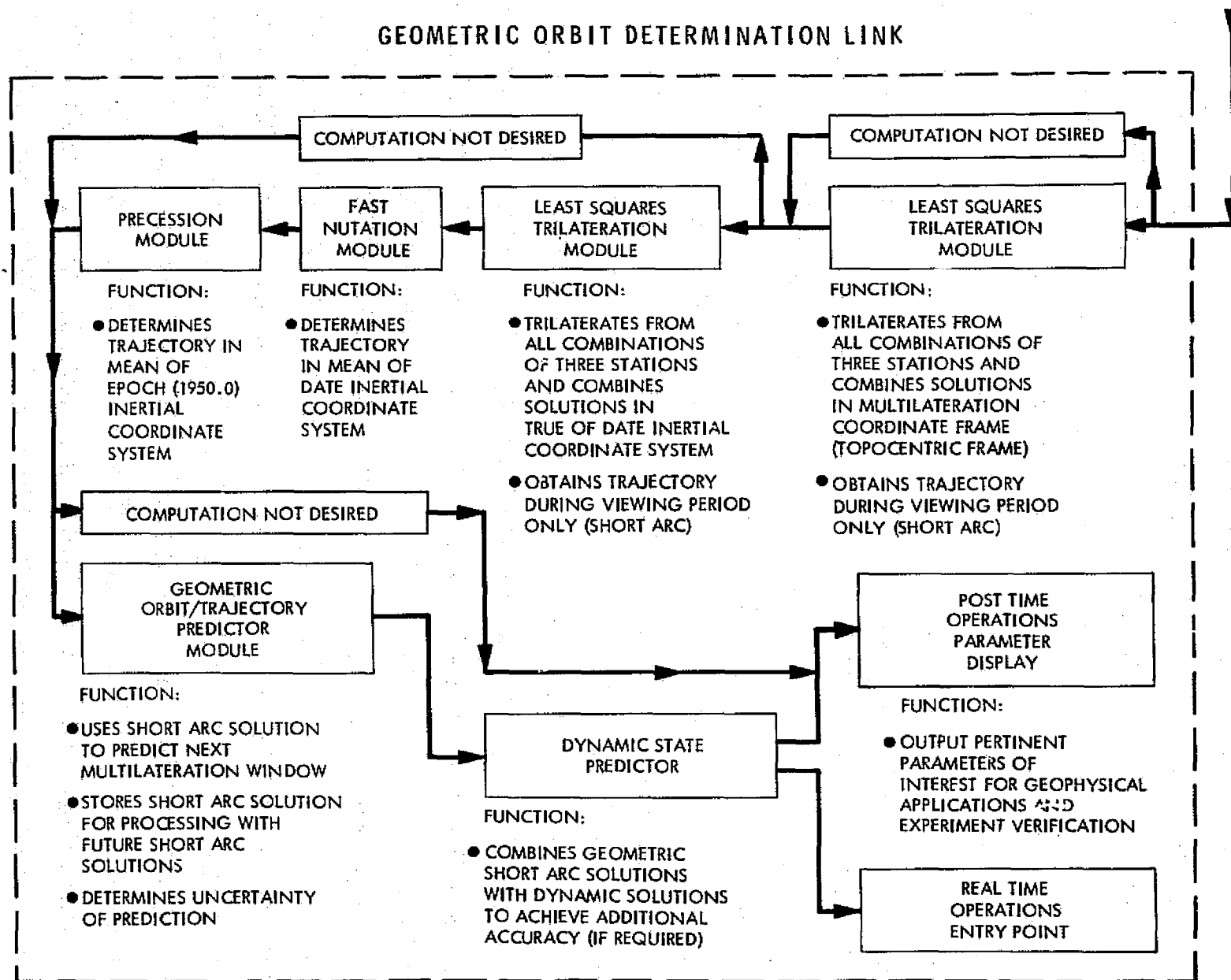
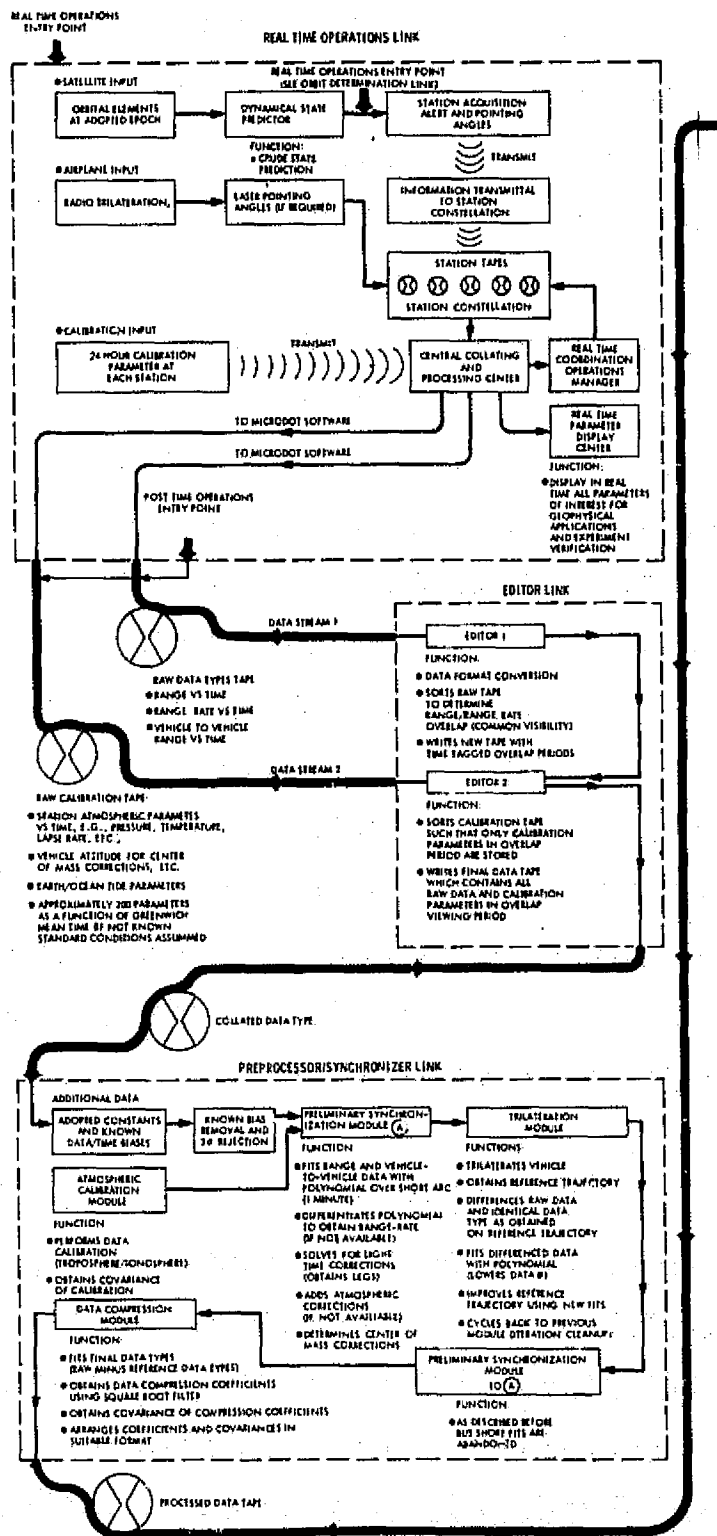


Figure 16. Geometric Orbit Determination Link

other applications wherein only relative distances or coordinates are of importance. Note that in the geometric frame the vehicle positions can be determined to centimeter level accuracy relative to the adopted frame. The second mode of operation uses the same weighted least squares trilateration module but performs the trilateration in the Earth centered geographic system. From this point a fast nutation module and a precession module can quickly place the vehicle in the desired equator and equinox system and compute orbit elements if it is so desired (Appendices A9, A10). The fast nutation module is the complete Woolard expansion but coded with all multiple angles expanded such that each nutation computation requires only eight trigonometric evaluations, the rest of the computation being reduced to a sequence of multiplications. This module permits a short arc prediction of the next viewing window to be performed by means of either a geometric predictor module or a dynamic state predictor. The prediction would be fed to the Software Real Time Operations Entry Point (see Figure 9). If post flight analysis is being undertaken, the output from this link would just be displayed in a suitable format. The software cycle is now complete (see Figure 17).

As an aside, an area which has only been investigated briefly should be mentioned. This area concerns the Geometric Orbit/Trajectory Predictor Module. Obviously over a short viewing arc, a set of mean elements can be obtained via trilateration by the process of jumping out of the adopted geometric multilateration frame into an inertial frame. Another procedure would be to assume the functional form of the equations of motion (the general perturbation or series form) as they are presently tabulated and rotate the resulting coordinates into the geometric frame. One can now forget about dynamics and assume that a series expansion is available in the multilateration frame which represents the orbit to at least a fair approximation. To this series a limited number of polynomial or trigonometric terms can be added to yield a generalized model for the motion of the satellite. The high precision trilateration mode is now used to obtain the necessary constants of the assumed model, in the geometric basis. Details of the orbit determination procedure are given in Appendix A8.

ORIGINAL PAGE IS
OF POOR QUALITY



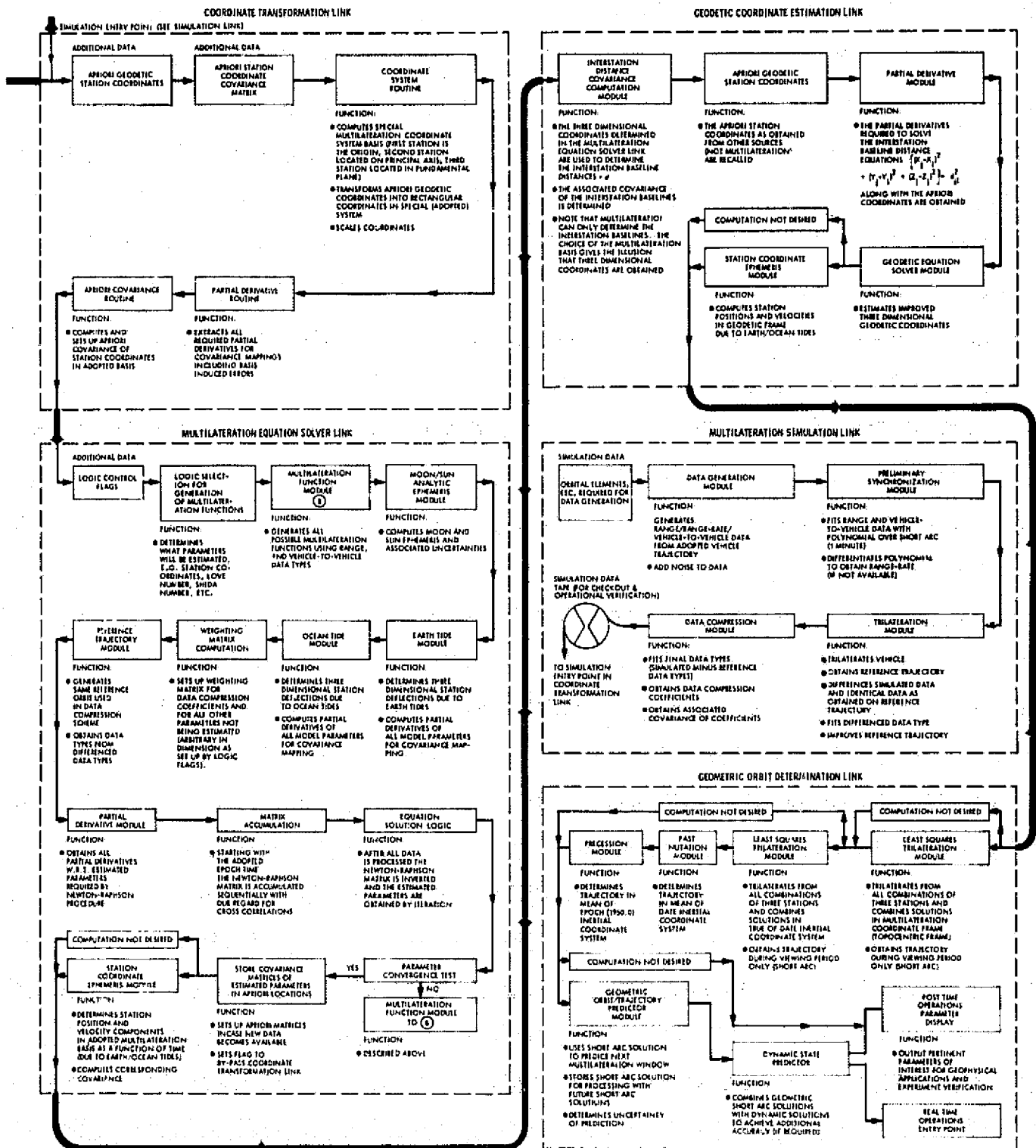


Figure 17. MICRODOT Processing System

7. SOFTWARE CAPABILITY

It is perhaps of value to outline briefly the software capability of the MICRODOT system. This is not to say that all specifically listed options are in operation, since some options are not currently considered necessary to meet present contractual commitments. However the design of the MICRODOT system is complete to the point where all listed options (of those currently not in operation) can be added more or less by just plugging in the proper leads. Two asterisks mark completed options; one asterisk marks near completion; the initials AC denote Analysis Complete.

7.1 VEHICLE CONFIGURATIONS

The present software package can handle various system configurations. These are listed in Table 6.

7.2 INTERSTATION COORDINATE REDUCTION

For interstation Coordinate Reduction the following options exist; see Table 7.

7.3 GEOPHYSICAL PARAMETER ESTIMATION

Geophysical parameter estimation options are listed in Table 8.

7.4 ORBIT DETERMINATION CAPABILITY

The orbit determination options are listed in Table 9.

Table 6. MICRODOT Capability Relative to Vehicle Configuration

System Letter	Designation
A	Multibaseline System (AC)
B	Hybrid Multilateration System (*)
C	Single Airplane System (Simulated) (**)
D	Upated Two Airplane System (Simulated) (**)
E	Minimum Cost Single Satellite System (**)
F	Upated Single Satellite System (**)
G	Moderate Cost Satellite/Airplane System (Simulated) (**)
H	Two-Satellite System (**)
I	Upated Two-Satellite System (**)
J	Combined Systems (AC for various modes)

Table 7. MICRODOT Capability Relative to Coordinate Reduction

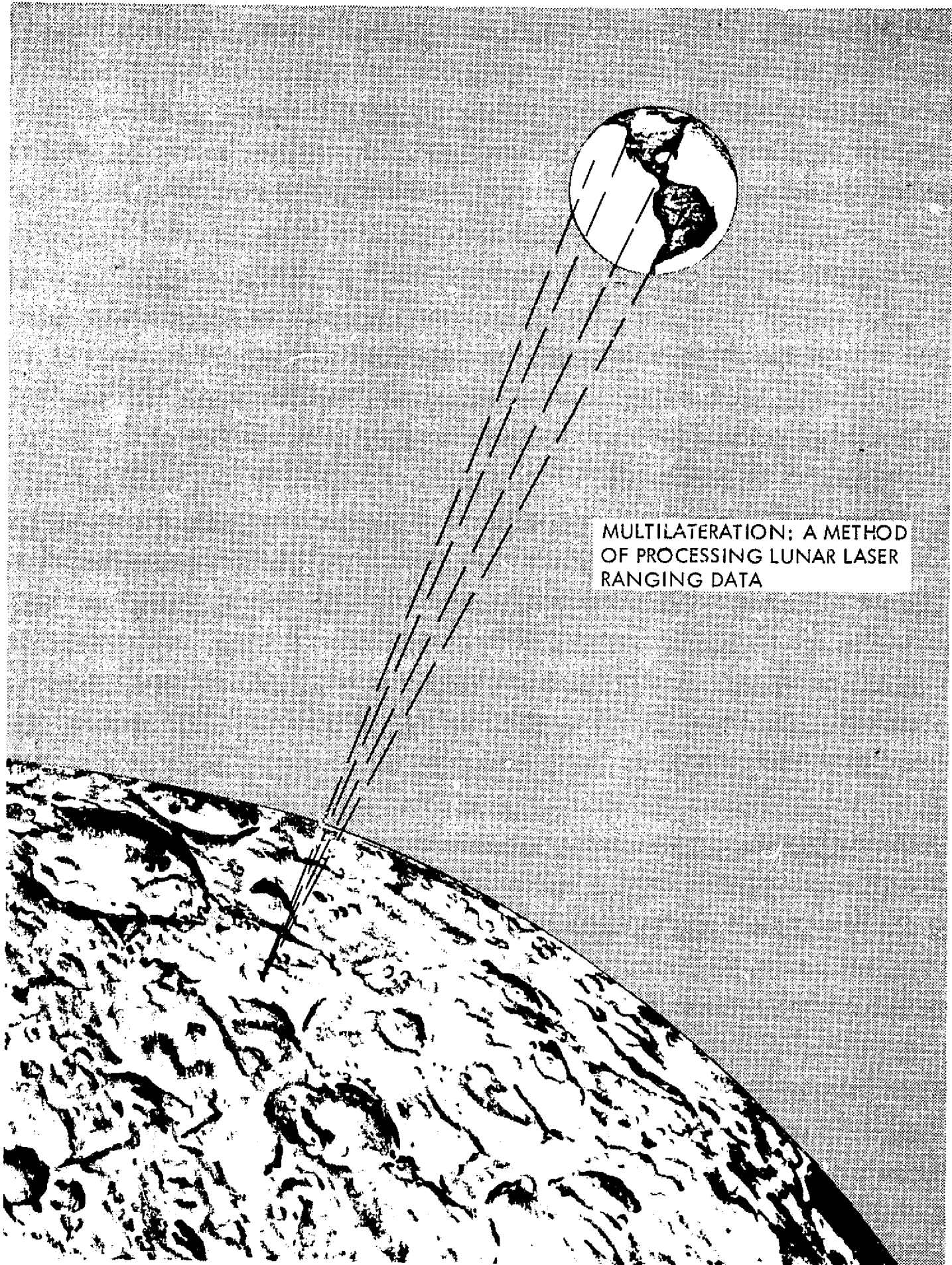
Option Letter	Option
K	Estimate All Station Constellation Interstation Coordinates in the Geometric Frame (**)
L	Fix as Consider Parameters a Subset of the Station Constellation Interstation Coordinates in the Geometric Frame (**)
M	Estimate All Station Constellation Interstation Coordinates in Geographic Frame (AC)
N	Fix as Consider Parameters a Subset of the Station Constellation Interstation Coordinates in the Geographic Frame (AC)
O	Compute Partial Derivatives of Estimated with Respect to Consider Parameters (**) (Option O will be fixed by option K or M)

**Table 8. MICRODOT Capability Relative to Geophysical
Parameter Estimation**

Option Letter	Option
P	Estimate Love and Shida Numbers (*)
Q	Estimate Geometric Flattening and Earth Radius (*)
R	Estimate Assorted Parameters (*)
S	Compute Partial Derivatives of Estimated with Respect to Consider Parameters (**)

Table 9. MICRODOT Capability Relative to Orbit Determination

Option Letter	Option
T	Perform State Estimation in Geographic Frame(*)
U	Perform State Estimation in Geometric Frame (*). Trilateration Option (**)
V	Perform State Estimation Transformation Into Inertial Frame(*)



MULTILATERATION: A METHOD
OF PROCESSING LUNAR LASER
RANGING DATA

ORIGINAL PAGE IS
OF POOR QUALITY

8. INITIAL SOFTWARE DATA SIMULATION AND VERIFICATION

8.1 INTRODUCTION

The purpose of this section is twofold: first, to demonstrate the proper operation of the MICRODOT processing system; and second, to verify that the real world orbital/station configuration currently in use for the GEOS-3 experiment can be used for multilateration data reduction.

The first of these objectives can be met by first generating a set of simulated range measurements using a dynamic model, then reducing those simulated range measurements in the MICRODOT equation solving link using a geometric method. If the elements of the solution vector are sufficiently close to their counterparts used to generate the simulated range measurements, the objective is met. To this end a two-satellite system operating in conjunction with a net of ground stations positioned throughout the continental United States was adopted. Use of the dynamic equations of motion and sets of orbital parameters thus permits the generation of simulated data. This simulated data is generated using a realistic model that includes the second zonal harmonic, which causes the well known drift of the orbital plane, and medium and high frequency orbital element fluctuations such as might be produced by Moon/Sun and mascon perturbations (Appendix A1). Each data point can then be corrupted with an assumed level of hardware noise. The simulated data is then differenced, smoothed and compressed via polynomials over a specified interval in exactly the same manner that actual data would be treated. This compressed data is then fed into the MICRODOT equation solving link and by a geometric scheme, quite distinct from the dynamic scheme used to generate the data, the interstation coordinates which were assumed to generate the data are recovered. This procedure can be carried out with and without noise. Without noise, the coordinates initially assumed to generate the range data must of necessity be recovered with almost perfect precision if the chain of equations used in the process is functioning correctly. After satisfying tests of this kind the second objective can be undertaken.

In essence, this second objective is central to this entire work since GEOS-3 provides the first true multilateration experiment using real data. As will be seen, the results of the GEOS-3 data simulation are

excellent and point out the great importance of performing realistic simulations. In brief, for the first time it became apparent that the old concepts which were originally introduced in [1] and [2] were not fully investigated and in many cases were actually misleading. The data simulation of the GEOS-3 configuration, using a non-multilateration-dedicated satellite and an arbitrarily fixed station net clearly demonstrates that multilateration can be carried out in the real world using a single circular orbit. This is a clear and most important system advantage over the old concepts where it was postulated that two satellites at different altitudes would be required to provide equation stability. The GEOS-3 solution for the interstation coordinates is strong and numerically stable and indicates that the reduction of real data will yield positive results depending only on the accuracy of the data types to be processed.

8.2 CONTINENTAL USA CONFIGURATION

In order to verify software operation a hypothetical station/orbital geometry was adopted for data simulation. The station locations were taken about the continental United States of America as per Table 10.

Table 10. Adopted Station Locations for
USA Data Simulation

Station Identification	Latitude (Geodetic) (Deg.)	Longitude (East) (Deg.)	Elevation (Meters)
Goldstone (1)*	34.0	243.0	0.0
Cape Kennedy (2)*	28.0	278.0	0.0
Spokane (3)*	47.0	245.0	0.0
Denver (4)	38.0	261.0	0.0
Houston (5)	30.0	264.0	0.0
Washington (D. C.) (6)	40.0	283.0	0.0

*Stations (1), (2) and (3) were used here to define the geometric basis used in multilateration data reduction (Appendix A7).

It was next assumed that these stations could range to satellites placed at two different altitudes. The satellite elements are specified in Table 11. The parameters required to generate the geographic Earth fixed rectangular coordinates using the formulas in Appendix A7 are also displayed.

As can be seen from Figure 18 the station/orbital geometry trace indicates good coverage of the continental USA with a ground trace intersection near Denver. The satellite passes do not occur at the same time over Denver.

This specific geometry gave rise to three data compression intervals on the high orbit and two on the low orbit, a data compression interval being the duration wherein the range difference data could be adequately fit by

Table 11. Orbital Parameters for USA Data Simulation

Orbital Elements	Orbit Designation	
	High	Low
Semimajor Axis, a , (Earth Radii)	1.785	1.473
Eccentricity, e	0.0	0.0
Inclination, i , (Deg.)	50.0	50.0
Longitude of Node, Ω , (Deg.)	143.12750	45.12753
Argument of Perigee, ω , (Deg.)	0.0	0.0
Time of Perifocal Passage, T , (Date)	1976 July 4, 0 hrs	1976 July 4, 0 hrs
Flattening, f , = $1/298.3$ Equatorial Radius, a_e , = 6378.15 km		
Second Harmonic, J_2 , = 1082.28×10^{-6} Sidereal Rate, $\dot{\theta}$, = 4.3752695×10^{-3} rad/min.		

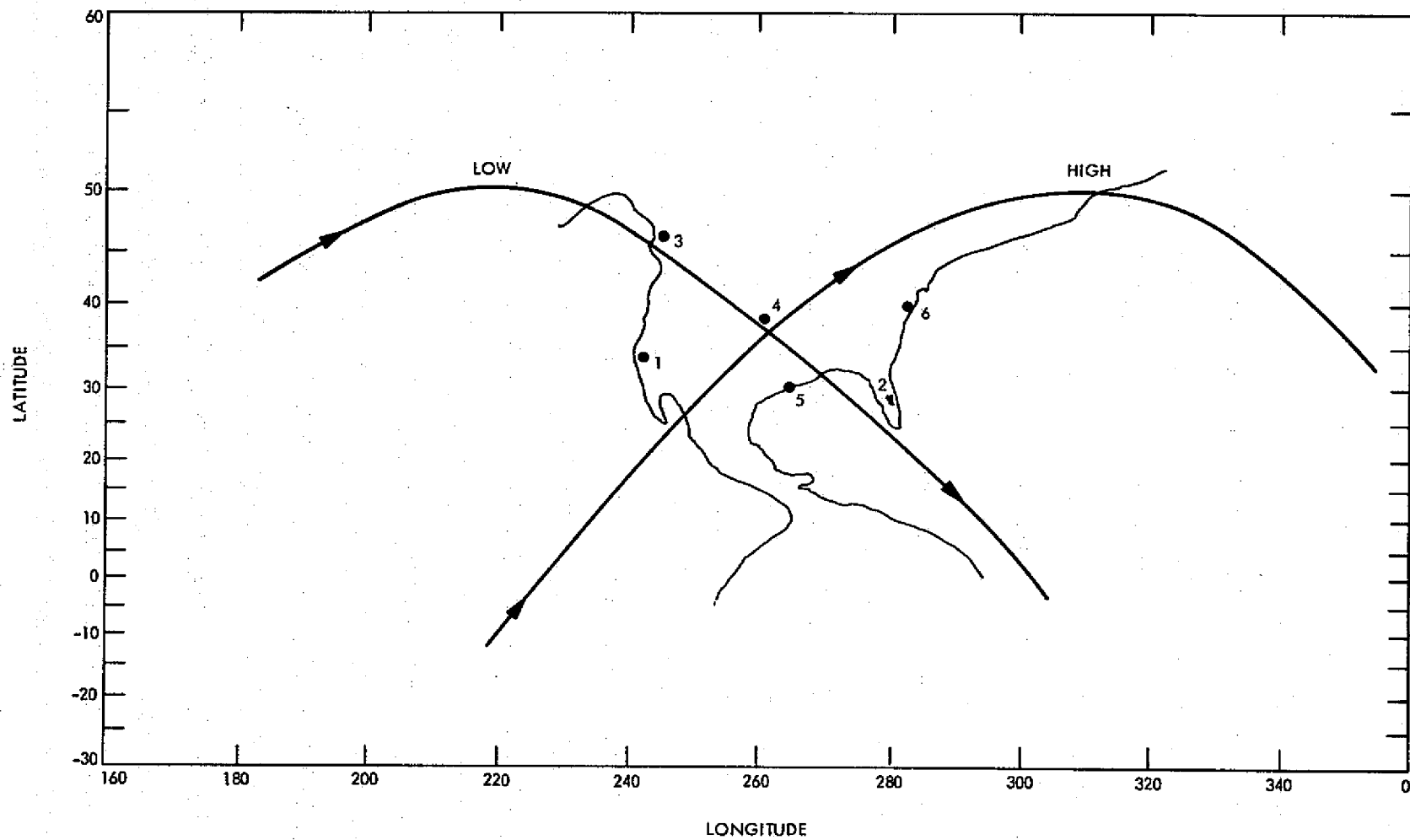


Figure 18. Orbital Ground Trace for USA Data Simulation

a polynomial of degree 4 (see Appendix A1). The approximate (15 minute) intervals are displayed in Figure 19. Figure 19 time limits were generated using the CYCLOPS program [7] with a minimum station elevation of 5°. When the orbit/station configuration is fed into the MICRODOT simulation link, the compression intervals are selected as indicated.

The previous tables and displays completely fix the geometry of the test case for the USA continental configuration. The next two sections discuss the perfect and noisy data simulations for a two-satellite configuration (H-System). Note that the data generated in the simulation link of the MICRODOT package uses dynamic equations to generate the data from an assumed set of station coordinates. The equation solving link of MICRODOT will then recover the assumed coordinates using only geometric equations. The process is thus closed from the point of view of software verification.*

8.3 SYSTEM H SIMULATION WITH PERFECT DATA

In order to test software computational accuracy, simulation data without any noise was generated for the case discussed in the previous section. The modeling error occasioned by the data compression scheme, i. e., the standard deviation of the interpolating polynomials was determined to be less than 1×10^{-8} centimeters or 1×10^{-17} earth radii. Hence, as far as the data compression coefficients are concerned (only the compression coefficients are used in the MICRODOT equation solving link), the coefficients themselves were virtually perfect (see Appendix A1).

These specific data types (the coefficients) were fed into the equation solving link and a Newton-Raphson iteration was initiated with the station coordinates displaced by about 150 meters from the values assumed to generate the data. The RMS of the multilateration functions was then plotted as a function of the iteration number. The results are displayed in Figure 20. As can be seen the RMS of the M-functions drops to about 1×10^{-6} millimeters by the fifth iteration. The RMS of the station coordinates (current minus true) is seen to drop to 2.6×10^{-9} meters for the same iteration number.

*The point is made that the same algorithms are not solved in reverse; a different algorithm recovers the answer.

HIGH ORBIT

- 1 - GOLDSTONE
- 2 - CAPE KENNEDY
- 3 - SPOKANE
- 4 - DENVER
- 5 - HOUSTON
- 6 - WASHINGTON, D.C.

LOW ORBIT

- 1 - GOLDSTONE
- 2 - CAPE KENNEDY
- 3 - SPOKANE
- 4 - DENVER
- 5 - HOUSTON
- 6 - WASHINGTON, D.C.

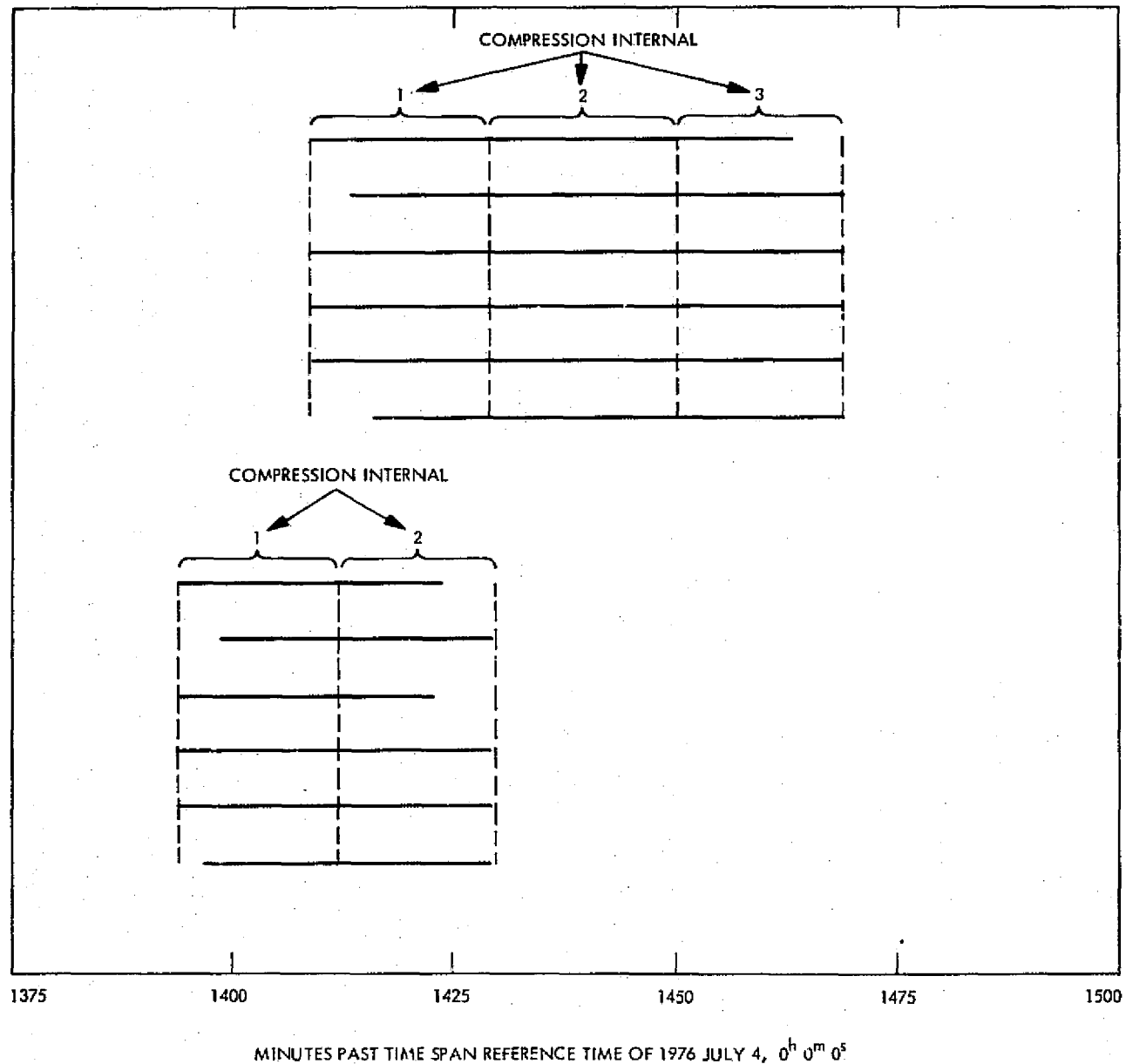


Figure 19. Data Compression Intervals

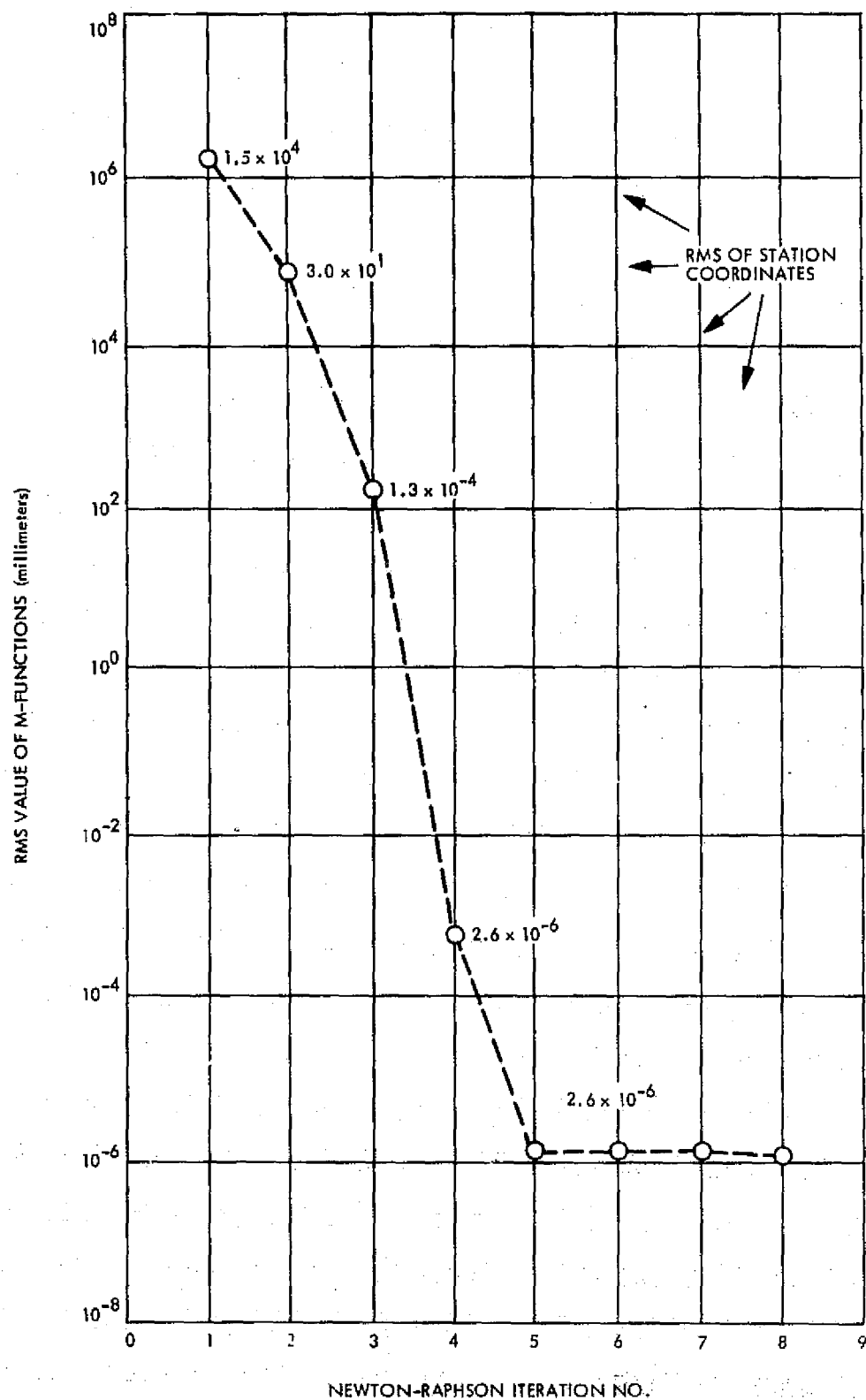


Figure 20. Equation Convergence with Perfect Data

Table 12 displays the double precision rectangular station coordinates (in the adopted geometric basis) as computed from the geodetic coordinates listed in Table 10 and the geoid parameters listed in Table 11. These coordinates are listed under the "True Value" column in Table 12. The residuals between the true values and the converged values are also listed. As can be seen the residuals are all about 10^{-5} millimeters. The results indicate almost perfect recovery of the assumed coordinates.

Table 12. Assumed and Converged Station Coordinates

Coordinate Identification	True Value (km)	Converged Minus True Residual (km) (Iteration No. 5)
Kennedy		
X_2	$+ .335142111527658156 \times 10^4$	$- .36557424 \times 10^{-11}$
Spokane		
X_3	$+ .149870671601874396 \times 10^3$	$- .12549961 \times 10^{-11}$
Y_3	$+ .144245140109117559 \times 10^4$	$+ .24655833 \times 10^{-11}$
Denver		
X_4	$+ .154129206606698051 \times 10^4$	$- .24691360 \times 10^{-11}$
Y_4	$+ .606283665209710953 \times 10^3$	$+ .15543122 \times 10^{-11}$
Z_4	$+ .247524820376550245 \times 10^3$	$+ .15920598 \times 10^{-12}$
Houston		
X_5	$+ .200151549885615644 \times 10^4$	$- .20694557 \times 10^{-11}$
Y_5	$- .198670538086832010 \times 10^3$	$- .19850788 \times 10^{-12}$
Z_5	$+ .195808069168132696 \times 10^3$	$+ .96767039 \times 10^{-12}$
Washington (D. C.)		
X_6	$+ .325503532657255369 \times 10^4$	$- .57056582 \times 10^{-11}$
Y_6	$+ .140208714968781340 \times 10^4$	$+ .35011993 \times 10^{-11}$
Z_6	$- .718139378331780918 \times 10^1$	$- .12987597 \times 10^{-11}$

8.4 SYSTEM H SIMULATION WITH NOISY DATA

The next logical step in MICRODOT certification is the generation of results involving noisy data. To this end, 1 centimeter noise was added to each value of the range data type generated in the simulation link. This data was then compressed to yield the coefficients in each compression interval. For brevity the number of compression intervals used in the multilateration passes of Figure 19 will be denoted by T_N^* . Table 13 presents the pertinent results. It is important to note that as more data is added to the simulation, the root-mean-square of the coordinates decreases (as it should). For the data simulation displayed the final $RMS_C \cong 2.2$ millimeters.

The covariance matrix of the solved-for coordinates of the final iteration is displayed in Table 14. From the covariance matrix the corresponding station coordinate standard deviations can be extracted; in centimeters they are:

$$\begin{array}{lll} \sigma_{X_2} = 1.21, & \sigma_{Y_4} = 0.501, & \sigma_{Z_5} = 0.340 \\ \sigma_{X_3} = 0.857, & \sigma_{Z_4} = 0.0277, & \sigma_{X_6} = 1.52, \\ \sigma_{Y_3} = 0.981, & \sigma_{X_5} = 0.713, & \sigma_{Y_6} = 0.937 \\ \sigma_{X_4} = 0.716, & \sigma_{Y_5} = 0.218, & \sigma_{Z_6} = 0.660. \end{array}$$

As can be seen, the 1 cm noisy data maps over into station uncertainties with worst case scale factor of about 1.5 (for the amount of data processed). A quick examination of the covariance matrix off-diagonal elements shows that the correlation coefficients, ρ , vary all the way from near zero to near unity, i. e.,

$$\rho_{Y_5 Z_6} = 0.044, \rho_{X_2 Z_6} = 0.223, \rho_{X_2 X_6} = 0.854,$$

and thus should never be neglected.

Table 13. MICRODOT Convergence with One Centimeter Noise
and 150 Meter Coordinate Offset

$N \equiv$ Number of Range Points Per T_N^* $T_N^* \equiv$ Number of Data Compression Intervals $RMS_C^2 \equiv \Sigma (\text{Iterant Coordinate Minus True Coordinate})^2 / I$ $RMS_M^2 \equiv \Sigma (\text{Iterant M-Function Minus True M-Function})^2 / M$ $I \equiv$ Number of Solved-for Station Coordinates $M \equiv$ Number of M-Functions				
Iteration	RMS _M (Meters)		RMS _C (Meters)	
	$T_N^* = 5; N = 60$	$T_N^* = 25; N = 120$	$T_N^* = 5; N = 60$	$T_N^* = 25; N = 120$
1	1793.0	1912.0	12.1	0.265
2	49.4	15.8	0.027	0.0022
3	0.216	0.0986	0.016	0.0022
4	0.091	0.0994	0.0156	0.0022
5	0.091	0.0995	0.0156	0.0022

The intent of this section is to display numerical results for purposes of verification and for this reason further discussions of the USA configuration will not be undertaken.

Table 14. Station Coordinate Covariance Matrix (1 cm noise)

X_2	X_3	Y_3	X_4	Y_4	Z_4	X_5	Y_5	Z_5	X_6	Y_6	Z_6
1.47	0.325	-0.711	0.771	-0.348	-0.196	0.828	0.0607	-0.372	1.57	-0.620	0.178
	0.734	-0.526	0.395	-0.248	0.0915	0.112	0.0122	-0.136	0.939	-0.467	0.532
		0.962	-0.492	-0.454	-0.0448	-0.355	-0.0650	0.218	-1.10	0.852	0.379
			0.513	-0.256	-0.0561	0.424	0.0236	-0.211	1.04	-0.444	-0.265
				-0.251	-0.0216	-0.182	-0.0168	0.102	-0.543	0.419	-0.183
					0.0769	-0.125	-0.00305	0.0406	-0.0873	-0.0463	0.0851
						0.508	0.0188	-0.198	0.817	-0.305	0.0410
							0.0474	-0.0272	0.0632	0.0649	0.00633
								0.116	-0.451	0.193	-0.0887
									2.30	-1.01	0.665
										0.878	-0.345
											0.436

8.5 SYSTEM I SIMULATION WITH PERFECT DATA

Tests of the operation of the MICRODOT software using two satellites connected with a satellite-to-satellite tracking (SST) link will be summarized in this section. For the first of these tests all data type noise was turned off and the continental configuration introduced in Section 8.2 was adapted for purposes of simulation. To permit larger satellite-to-satellite tracking windows the time of perifocal passage for the low satellite was increased by 22^m30^s . The resulting viewing window for this configuration is displayed in Figure 21.

MICRODOT allows the user to declare any subset of station coordinate to be estimated. To test this logic only the coordinates of stations 4 and 6 were included in the unknown station coordinate vector. Next data was generated via the simulation link and a Newton-Raphson procedure was initiated. The results are displayed in Figure 22. As can be seen the RMS of the M-functions drops to about 1×10^{-7} millimeters by the fourth iteration. The RMS of the station coordinates drops to about 1×10^{-5} . The initial coordinates were offset by 150 meters. Similar results were obtained by Carta [9].

8.6 GEOS-3 BERMUDA TRIANGLE CONFIGURATION

In support of the GEOS-3 effort, the station constellation in the vicinity of the Bermuda Triangle was selected for additional data simulation. The station coordinates for this simulation are displayed in Table 15. Additional stations which track the ATS-6 are displayed in Table 16. The GEOS-3 experiment was planned not only to permit simple multilateration data reduction (H system) but also stressed the availability of satellite-to-satellite data (I system) to aid in sought for parameter estimation. Both of these cases will be treated but in separate sections. Note the internal MICRODOT code in Tables 15 and 16. The multilateration basis origin was Kennedy (1), the X-axis was taken as Antigua (2) while the X-Y plane was fixed by Wallops (8). The remaining numbers denote the additional stations selected for the simulations.

Table 17 displays the assumed orbital parameters of the GEOS-3 and ATS-6 spacecraft from which simulation data was generated. A constant 5° elevation mask was used for each station. The ground trace orbital pass

HIGH ORBIT

- 1 - GOLDSTONE
- 2 - CAPE KENNEDY
- 3 - SPOKANE
- 4 - DENVER
- 5 - HOUSTON
- 6 - WASHINGTON, D.C.

LOW ORBIT

- 1 - GOLDSTONE
- 2 - CAPE KENNEDY
- 3 - SPOKANE
- 4 - DENVER
- 5 - HOUSTON
- 6 - WASHINGTON, D.C.

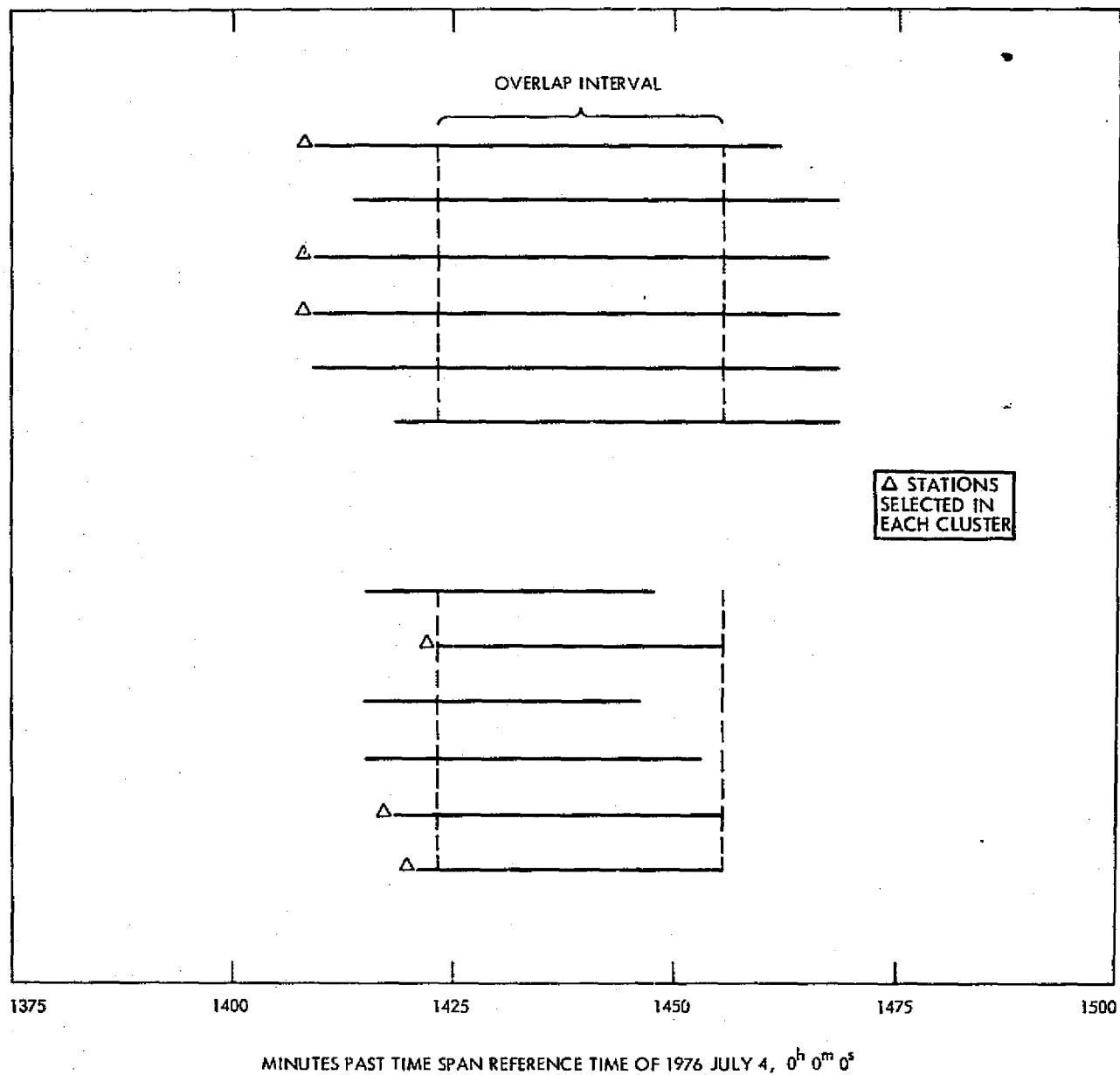


Figure 21. Data Compression Interval for SST

ORIGINAL PAGE IS
OF POOR QUALITY

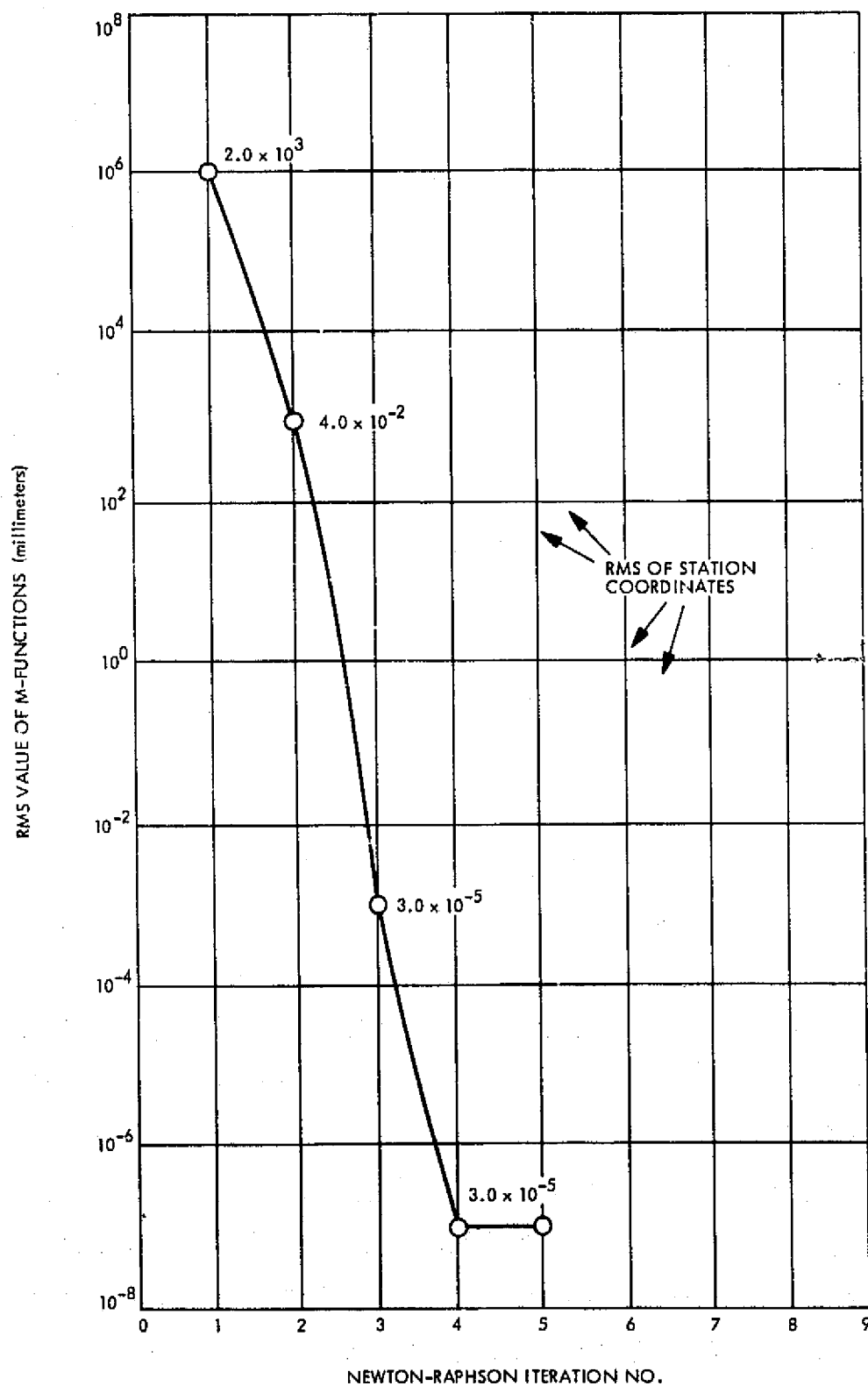


Figure 22. SST Equation Convergence with Perfect Data

Table 15. C-Band Primary Station Constellation

(a_e = 6378155m, 1/f = 298.255)

Code	Station Identification	Geodetic Latitude	East Longitude	Elevation (meters)
1	ETRC AK (Cape Kennedy) 4041	28°28 ^m 53.944 ^s	279°25 ^m 24.400 ^s	- 33.41
2	ETRANT (Antigua) 4061	17°08 ^m 37.156 ^s	298°12 ^m 27.192 ^s	- 19.88
3	ETRGRT (Grand Turk) 4081	21°27 ^m 45.370 ^s	288°52 ^m 4.940 ^s	- 29.17
4	ETRGB8 (Grand Bahama) 4083	26°38 ^m 10.393 ^s	281°43 ^m 56.190 ^s	- 39.18
5	WSH123 (Halloman, N.M.) 4144	32°54 ^m 5.338 ^s	253°54 ^m 2.902 ^s	+1230.07
	WSG218 (Green River, Utah) 4148	38°58 ^m 44.047 ^s	249°53 ^m 14.711 ^s	+1299.89
6	EGLA21 (Eglin, Florida) 4340	30°25 ^m 17.978 ^s	273°12 ^m 7.047 ^s	- 16.93
	NELHAR (Ely, Nevada) 4610	39°18 ^m 30.363 ^s	244°54 ^m 48.376 ^s	+2792.29
7	NBER34 (Bermuda) 4740	32°20 ^m 53.303 ^s	295°20 ^m 47.437 ^s	- 32.34
8	NWAL49 (Wallops, Virg.) 4841	37°56 ^m 38.892 ^s	284°32 ^m 8.760 ^s	- 33.70
	AECM35 (Tonopah, Nevada) 4964	37°45 ^m 41.872 ^s	243°14 ^m 21.858 ^s	+1680.32

Table 16. C-Band (ATS-6) Stations

(a_e = 6377563.4m, 1/f = 299.375)

Code	Station Identification	Geodetic Latitude	East Longitude	Elevation (meters)
10	ATSROS (Rosman) 85	35°11 ^m 55.68 ^s	277°07 ^m 27.45 ^s	+888.0
11	ATSMAD (Madrid) 85	40°27 ^m 23.85 ^s	353°49 ^m 58.23 ^s	+785.1
12	ATSMOJ (Mojave) ATS	35°19 ^m 48.00 ^s	243°06 ^m 3.00 ^s	+929.0

Table 17. Orbital Parameters for GEOS-3 and ATS-6 Spacecraft

Orbit Elements	Orbit Designation	
	GEOS-3	ATS-6
Semimajor axis, a , (Earth radii)	1.131149	6.6106687
Eccentricity, e	0.00049988	0.0
Inclination, i , (deg)	115.0559	0.0
Longitude of node, Ω , (deg)	282.6302	0.0
Argument of perigee, ω , (deg)	238.6468	154.00
Time of perifocal passage, T , (date)	1975 April 26, 23 ^h , 35 ^m , 7 ^s	1975 April 26, 23 ^h , 35 ^m , 7 ^s
Flattening, f , = $1/298.3$ Equatorial radius, a_e = 6378.15 km Second harmonic, J_2 , = 1082.28×10^{-6} Sidereal rate, $\dot{\theta}$, = 4.3752695×10^{-3}		

geometry is shown in Figure 23. Note that six orbital passes of data were generated. The range data corresponding to these passes was then passed through the data compression simulation link of MICRODOT with 1 centimeter noise to generate the data compression coefficients.

8.7 GEOS-3 COORDINATE ESTIMATION

Table 18 displays the convergence of the pertinent parameters. As can be seen, after two iterations interstation coordinate convergence is achieved with a resulting RMS_C bias of about 3 centimeters. This bias can be lowered

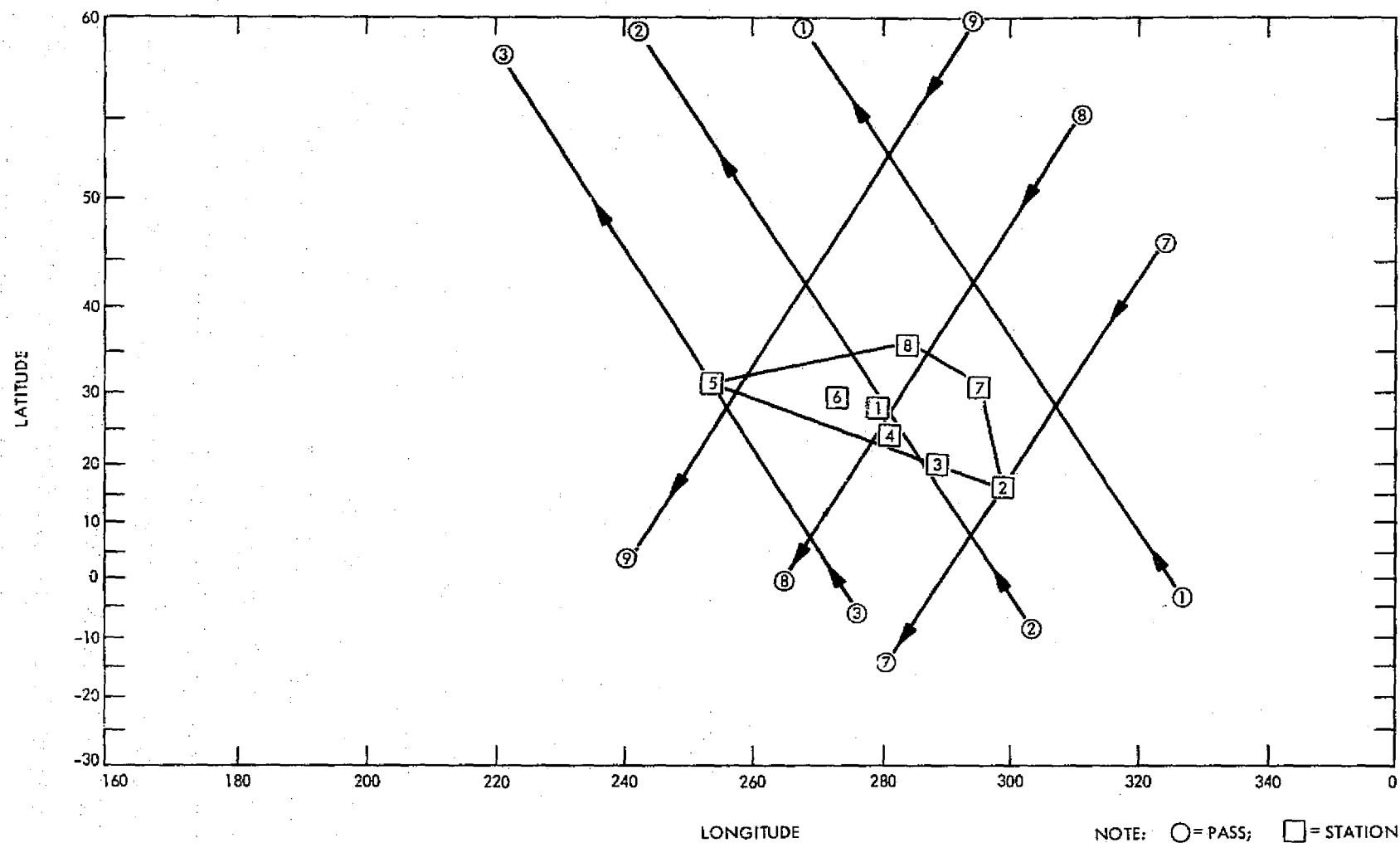


Figure 23. GEOS-3 Ground Trace Over C-band Station Constellation

Table 18. GEOS-3/MICRODOT Convergence with One Centimeter Noise and One Meter Coordinate Offset

$N \equiv \text{Number of Range Points Per } T_N^*$ $T_N^* \equiv \text{Number of Data Compression Intervals}$ $RMS_C^2 \equiv \Sigma (\text{Iterant Coordinate Minus True Coordinate})^2 / I$ $RMS_M^2 \equiv \Sigma (\text{Iterant M-Function Minus True M-Function})^2 / M$ $I \equiv \text{Number of Station Coordinates}$ $M \equiv \text{Number of M-Functions}$		
Iteration	RMS _M (Meters)	RMS _C (Meters)
	$T_N^* = 6; N = 30 - 60$ (5 Data Points Per Minute)	
1	390.8	0.163
2	4.24	0.0321
3	0.950	0.0321
4	0.950	0.0321

by use of additional data (see Table 13) if it is so desired. Hence using 6 passes of data with an assumed noise of 1 cm only a 1 to 3 cm degradation from the fundamental data type to the estimated parameters occurs. Certainly the 1 centimeter noise is unrealistic for C-Band stations, however this accuracy level was adopted to demonstrate the inherent estimation power of the MICRODOT processing system. Optimization of station placement was, of course, not possible with the adopted constellation.

The standard deviations of the X, Y, and Z coordinates are collected in Table 19. It is evident from results that Halloman is the only culprit station; but this is due to its extreme westerly displacement in the overall station constellation. It is emphasized that the above rather dramatic results have been obtained via multilateration using only the GEOS-3 satellite, i. e., with only one satellite in a circular orbit about the Earth. A few cross terms are included to show the strong correlations. This realistic simulation in which the data was filtered, smoothed and compressed in the identical manner in which real data would be processed indicates the viability of the GEOS-3 experiment and the ability of the MICRODOT system to reduce the raw data.

Table 19. GEOS-3 Station Coordinate Standard Deviations
(1 cm noise)

Station	σ_X	σ_Y	σ_Z
Kennedy (K)	-	-	-
Antigua (A)	2.89	-	-
Grand Turk (GT)	1.60	0.70	2.30
Grand Bahama (GB)	0.45	0.30	0.98
Halloman (H)	13.38	3.38	16.49
Eglin (E)	1.40	0.54	2.56
Bermuda (B)	2.45	1.90	4.31
Wallops (W)	2.58	2.18	-
$\rho_{X_H, X_E} = 0.83, \quad \rho_{Y_{GT}, Y_{GB}} = 0.86, \quad \rho_{Z_{GT}, Y_{GB}} = -0.36$ $\rho_{X_B, Y_W} = 0.20$			

8.8 GEOS-3/ATS-6 COORDINATE ESTIMATION

The next question of importance, after verification of the GEOS-3-only multilateration data reduction, deals with the additional improvement afforded by the introduction of the satellite (GEOS-3)-to-satellite (ATS-6) tracking data. To this end 1 centimeter noise was again assumed in all the raw data. For equation stability, the coordinates of the ATS-6 cluster, i. e., Rosman, Madrid and Mojave were held fixed and the same data rate of the previous simulation was adopted. The root-mean-square of the bias in the coordinates dropped to 1 centimeter in two iterations. The standard deviations of the station constellation and a few of the cross terms are displayed in Table 20. A comparison of Tables 19 and 20 shows the additional improvement afforded by this mode of operation. As can be seen even the coordinates of Halloman have been obtained to surprising accuracy while all other coordinates are near or below the 1 centimeter accuracy threshold. The cross terms are large and indicate that they can not be neglected in the calculations. This simulation again demonstrates the viability of the GEOS-3/ATS-6/MICRODOT data reduction experiment.

Table 20. GEOS-3/ATS-6 Station Coordinate Standard Deviations
(1 cm noise)

Station	σ_X	σ_Y	σ_Z
Kennedy (K)	-	-	-
Antiqua (A)	0.97	-	-
Grand Turk (GT)	0.51	0.28	0.80
Grand Bahama (GB)	0.23	0.18	0.46
Halloman (H)	2.89	1.38	1.50
Eglin (E)	0.29	0.29	0.68
Bermuda (B)	0.59	1.13	0.79
Wallops (W)	0.50	0.92	-
$\rho_{X_H, X_E} = 0.04, \quad \rho_{Y_{GT}, Y_{GB}} = 0.38, \quad \rho_{Z_{GT}, Y_{GB}} = -0.18$ $\rho_{X_B, Y_W} = -0.57$			

9.0 A GUIDE TO THE APPENDICES CONTAINED IN THIS REPORT

As is evident, no two readers will have the same background or interest and therefore the organization of any given report will always be non-optimum from their respective viewpoints. Perhaps it would have been useful to change the numbering on certain of the Appendices to follow, however lack of funding precluded this operation. The Appendices are listed more or less in the order of development.

If a reader wanted a continuous development, it might be useful to proceed as follows (the emphasis here is placed on real or post time data processing).

First Appendix A12 and A13 would be read in order to gain an understanding of the manner in which raw time pulse data is transformed into the actual slant range data types so commonly used in multilateration. The necessary corrections to refer data to a common center of mass such that accuracies of 1-2 centimeters can be achieved should also be of interest.

The manner in which the atmospheric calibration is incorporated into the raw observables should probably be addressed next (Appendices A5 and A6), at least in a general sense, to identify and understand the pertinent parameters used to perform the calibration. This might be followed by Appendix 15 wherein the measurement frequency of the atmospheric and other related parameters required to achieve high levels of data calibration accuracy are specified. Appendices A18, A19 and A20 also relate to data measurement problems and thus an understanding of these areas would be of direct benefit.

An entry into Appendix A8, but only into section A8.2, would then be necessary for the reader who is not acquainted with the theory of trilateration, i. e., the process of determining the position and velocity of a satellite by strictly geometric means.

At this point the reader has the background necessary to enter Appendix A1 wherein the general subject of data compression is discussed. Now all the raw data has been corrected, calibrated and compressed into compact matrices of low dimension and the second level of understanding can begin.

If the concept of multilateration functions is not well in hand, then Appendix A11 is suggested as the next step. The solution of the multilateration functions is discussed in detail in Appendix A2; however prior to a full understanding of this appendix, some knowledge of the Earth/ocean tide models described in Appendices A3 and A4 will be required (unless the reader sets all tidal considerations apart in the reading of Appendix A2). Appendices A16 and A17 which detail partial derivative generation are supplementary.

The transformation of coordinates from the adopted geometric frame to either the geographic or inertial frame is treated in Appendix A7. This material should be well understood at this stage (perhaps A7.3, which describes the transformation from geometric to geodetic coordinates, could be read in parallel with Appendix A3). Appendix A7 has the companion Appendices A9 and A10 which deal with high precision algorithms for precession and nutation.

With the previous background Appendix A8 which deals with precision orbit determination should be read.

Finally the reader wishing to examine other facets of geometric parameter estimation, e. g., high precision ground baseline determination, interplanetary probe trajectory estimation, etc., can read Appendices A21 and A22. These last two appendices actually stand on their own and need little technical background from the rest of this report for a general understanding of the subject matter.

10.0 REFERENCES

- [1] Escobal, P.R., et al, 3-D Multilateration: A Precision Geodetic Measurement System, JPL TM 33-605, March 15, 1973.
- [2] Blaha, G., Investigations of Critical Configurations for Fundamental Range Networks, Universal Microfilms, Ann Arbor Michigan, 1971.
- [3] Escobal, P.R., "A New Approach to Four Station Multilateration", JPL IOM 391.6-437 May 3, 1974.*
- [4] Bierman, G.J., "Polynomial Fitting for Data Compression", JPL EM 391-636, March 27, 1975.*
- [5] Escobal, P.R., "Multibaseline: A Three-Dimensional Precision Geodetic Measurement System Not Using Airplanes or Data Synchronization", JPL EM 391-705, November 14, 1975.*
- [6] Escobal, P.R., Hybrid Multilateration: Some Numerical Results, JPL EM 391-707, December 2, 1975.*
- [7] Escobal, P.R., and Gallagher, J.F., "Cyclops Mission Analysis Program; Versions 1 and 2", JPL EM 391-633, March 12, 1975.*
- [8] Bierman, G. J., "Fixed Memory Least Squares Filtering", JPL EM 391-595, September 13, 1974.*
- [9] Carta, D. G., "On Multilateration with Clusters of Three Stations Coupled by Satellite-to-Satellite Data", JPL IOM 391.2-609, April 15, 1975.*

*JPL internal document.

11.0 BIBLIOGRAPHY OF JET PROPULSION LABORATORY
MULTILATERATION EFFORT

- [B1] Escobal, P.R., Methods of Orbit Determination, John Wiley and Sons (First Edition); Krieger Publications (Second Edition); New York, 1965 and 1976.
- [B2] Escobal, P.R., Lange, D.M., and Johnson, R.H., "Trilateration Measurement and Position Prediction", Hughes Aircraft Co., DBR, 1-383-2, December 1971.
- [B3] Escobal, P.R., "Reduction of the Laser Ranging Equations to a Tractable Form", JPL TM 391-290, 22 February 1972.*
- [B4] Escobal, P.R., "A Number of Important Considerations for 3-D Laser Ranging Experiments", JPL TM 391-293, 29 February 1972.*
- [B5] Escobal, P.R., "Discussion of the Four Station Laser Ranging Geometry Equations", JPL TM 391-296, 7 March 1972.*
- [B6] Escobal, P.R., "Theory of Multilateration Station Coordinate Determination Independent of Orbital Ephemeris", JPL TM 391-304, 21 March 1972.*
- [B7] Escobal, P.R., "Coordinate Systems for Ranging Experiments", TM 391-306, 24 March 1972.*
- [B8] Escobal, P.R., and Knopoff, L., "Earthquake Prediction and Multilateration", IOM 391.5-70, 11 August 1972.*
- [B9] Escobal, P.R., K.M. Ong, and von Roos, O.H., "Multilateration With VLBI", JPL EM 391-395, 5 September 1972.*
- [B10] Escobal, P.R., "Hybrid Multilateration: A Method for Determination of Three Dimensional Station Coordinates Using Lasers or VLBI", JPL TM 391-375, 16 October 1972.*
- [B11] Escobal, P.R., "Solution of Range (Laser) and Range Difference (VLBI) Equations in A Geographic Coordinate System", JPL TM 391-386, 16 November 1972.*
- [B12] Escobal, P.R., "Singularities in Multilateration Equations Occasioned by Orbital Selection", JPL TM 391-392, 4 December 1972.*
- [B13] Escobal, P.R., "Dual Trilateration with Vehicle-to-Vehicle Tracking: An Inexpensive Multilateration System", JPL TM 391-393, 4 December 1972.*
- [B14] Escobal, P. R., et al., 3-D Multilateration: A Precision Geodetic Measurement System, JPL TM 33-605, 15 March 1973.

*JPL internal document.

- [B15] Escobal, P.R., "Explicit Development of Dual Trilateration System Equations and Their Solution", JPL TM 391-430, 28 March 1973.*
- [B16] Escobal, P.R., "Obtaining Clock Offsets Via Multilateration", JPL IOM 391.5-124, 3 April 1973.*
- [B17] Escobal, P.R., "Subroutine for RILS Error Mapping", JPL IOM 391.5-127, 10 April 1973.*
- [B18] Escobal, P.R., "Calibration of Spaceborne Altimeters Via Multilateration", JPL IOM 391.6-153, 27 July 1973.*
- [B19] Escobal, P.R., "Simplified and Generalized Coordinate Systems for Multilateration Plus the Generalized Multilateration Solution", JPL IOM 391.5-174, 20 November 1973.*
- [B20] Escobal, P.R., "Earthquake Prediction: A Brief Summary of Knowledge", JPL IOM 391.5-181, 30 November 1973.*
- [B21] Escobal, P.R., "The Random and Bias Errors Occasioned by Fitting Range Data by a Polynomial Approximation", JPL IOM 391.6-415, 12 March 1974.*
- [B22] Escobal, P.R., "Numerical Computation of Standard Deviation and Bias in Fitting Process by Polynomials", JPL IOM 391.6-419, 22 March 1974.*
- [B23] Escobal, P.R., "Automatic Generation of Multilateration Functions for SST and Range Only Data Types with Identical Algebraic Structures", JPL IOM 391.6-426, 4 April 1974.*
- [B24] Escobal, P.R., "Design of Sliding Polynomial Filter for Multilateration Studies", JPL IOM 391.6-434, 16 April 1974.*
- [B25] Escobal, P.R., "Batch and Sequential Solution of Multilateration Functions", JPL IOM 391.6-435, 16 April 1974.*
- [B26] Escobal, P.R., "A New Approach to Four Station Multilateration", JPL IOM 391.6-437, 3 May 1974.*
- [B27] Escobal, P.R., "Explicit Matrix Solution for Obtaining Minimum Variance Estimates of Parameters Contained in a Large Set of Non-linear Equations", JPL EM 391-601, 6 January 1975.*
- [B28] Escobal, P.R., "Fast Nutation Algorithm for Complete Nutation and Nutation Rate Calculations", JPL EM 391-615, 21 January 1975.*
- [B29] Escobal, P.R., "Explicit Analytic Model for Earth Tide Station Coordinate Deflections", JPL EM 391-624, 12 February 1975.*
- [B30] Escobal, P.R., "Basic Explanation, Workable System and Threshold Accuracy of Multilateration", JPL EM 391-623, 12 February 1975.*

*JPL internal document.

- [B31] Escobal, P.R., and von Roos, O.H., "Ground Station Deflections Due to Ocean Tide", JPL EM 391-629, 3 March 1975.*
- [B32] Escobal, P.R., "A Discussion on the Aries Constraint in the LIBRA System", JPL EM 391-641, 24 April 1975.*
- [B33] Escobal, P.R., "Identification of Data Streams Required for Precision Multilateration and Orbit Determination", JPL IOM 391.6-562, 24 April 1975.*
- [B34] Escobal, P.R., "The MICRODOT Processing System: A Summary Overview", JPL IOM 391.6-615, 16 September 1975.*
- [B35] Escobal, P.R., "Precession Algorithm", JPL EM 391-739, 6 May 1976.*
- [B36] Escobal, P.R., "Estimation of Geographic Coordinates from Multilateration Constraints: The N-Dimensional Case", JPL EM 391-691, 1 October 1975.*
- [B37] Escobal, P.R., "Multibaseline: A Three-Dimensional Precision Geodetic Measurement System Not Using Airplanes or Data Synchronization", JPL EM 391-705, 14 November 1975.*
- [B38] Escobal, P.R., "Short and Long-Arc Orbit Determination Using Multilateration", JPL EM 391-736, 23 April 1976.*
- [B39] Escobal, P.R., "Hybrid Multilateration: Some Numerical Results", JPL EM 391-707, 2 December 1975.*
- [B40] Escobal, P.R., "Coordinate and Covariance Transformations for High Precision Orbital State Estimation", JPL EM 391-748, 29 May 1976.*
- [B41] Fliegel, H.F., "Laser Ranging to an Artificial Satellite: Degeneracy in the Solutions", JPL TM 391-228, 1 September 1971.*
- [B42] Fliegel, H.F., and von Roos, O.H., "Dick Jaffe Vindicated and Triumphant: or, A Workable Proposal for 3-D Laser Ranging to a Satellite", JPL TM 391-279, 21 January 1972.*
- [B43] Fliegel, H.F., "A Workable 3-D Laser Proposal (A Precis of TM 391-279)", JPL IOM 391.5-22, 11 February 1972.*
- [B44] Fliegel, H.F., "Geodetic Laser Ranging by K.M. Ong's Collinear Technique: Simple Formulas for Error Estimation, and a Proposal", JPL TM 391-308, 28 March 1972.*
- [B45] Fliegel, H.F., "Fliegel's Fallacy", JPL TM 391-311, 7 April 1972.*
- [B46] Fliegel, H.F., "What Everyone Should Know about Tectonics", JPL IOM 391.5-47, 28 April 1972.*

* JPL internal document.

- [B47] Fliegel, H.F., "A Workable 3-Station Laser Ranging System: A Second-Order Approach to Multilateration", JPL TM 391-357, 18 August 1972.*
- [B48] Fliegel, H.F., "Of Spheres and Circles and Rings and Things", JPL TM 391-367, 8 September 1972.*
- [B49] Fliegel, H.F., "Laser Geodesy by 3 Stations Not in a Straight Line", JPL TM 391-379, 25 October 1972.*
- [B50] Fliegel, H.F., "Who First Discovered the Six Station Case?", JPL IOM 391.5-103, 10 January 1973.*
- [B51] Fliegel, H.F., "Avoiding Singularities in Coplanar Multilateration", JPL IOM 391.5-123, 29 March 1973.*
- [B52] Fliegel, H.F., "A First Look at the Proposed LIBRA System for Airborne Radar Geodesy", JPL IOM 391.5-185, 3 January 1974.*
- [B53] Fliegel, H.F., "Effect of Jerk (The Geometrical Kind) on LIBRA", JPL IOM 391.5-445, 10 July 1975.*
- [B54] Jaffe, R.M., "Formulation of the Laser Ranging Equations in Matrix Notation", JPL TM 391-231, 20 September 1971.*
- [B55] Jaffe, R.M., "Some Preliminary Geometrical Considerations Relating to Laser Ranging Systems", JPL TM 391-188, 5 May 1971.*
- [B56] Jaffe, R.M., "Signal Strength Fluctuation in a Laser Ranging System Due to Optical Interference Between the Many Reflectors on the Satellite", JPL TM 391-218, 28 July 1971.*
- [B57] Jaffe, R.M., "Velocity Aberration Effects when Ranging to a Retro-reflecting Satellite", JPL TM 391-355, 17 August 1972.*
- [B58] Jaffe, R.M., "Summary/Status Report on the Retroreflecting Satellite for the 3-D Laser System", JPL TM 391-369, 20 September 1972.*
- [B59] Ong, K.M., "Station Location Determination by Laser Ranging Assuming Knowledge of the Ephemeris of the Satellite - Mathematical Formulation", JPL TM 391-236, 27 September 1971.*
- [B60] Ong, K.M., "A Reciprocal Triangulation System for Laser Ranging", JPL TM 391-255, 30 November 1971.*
- [B61] Ong, K.M., "A Three-Dimensional Laser Ranging System for the Determination of Station Locations", paper presented to Fall Annual Meeting, American Geophysical Union, San Francisco, December 1971.
- [B62] Ong, K.M., "A Laser Ranging System for Short Baselines", JPL TM 391-292, 28 February 1972.*

*JPL internal document.

- [B63] Ong, K.M., "Laser Ranging Systems for Coplanar and Near Coplanar Station Configurations", JPL TM 391-297, 7 March 1972.*
- [B64] Ong, K.M., "Linearization of the 6-Station Laser Ranging Equations", JPL TM 391-315, 18 April 1972.*
- [B65] Ong, K.M., "Solution of Laser Ranging Equations by the Newton-Raphson Method", JPL TM 391-319, 24 April 1972.*
- [B66] Ong, K.M., "Optimum Vehicle Trajectory for the 3-Station Laser Ranging System", JPL TM 391-349, 4 August 1972.*
- [B67] Ong, K.M., and Escobal, P.R., "Analysis of a 6-Station Multilateration System", paper presented to the Fall Annual Meeting, American Geophysical Union, San Francisco, December 1972.
- [B68] Ong, K.M., "Numerical Solution and Error Analysis of Range Difference Multilateration", JPL EM 391-501, 28 September 1973.*
- [B69] Ong, K.M., "3-D Multilateration for Measurement of Earth Crustal Deformation and Network Densification", paper presented at the International Symposium on Earth's Gravitational Field and Secular Variations in Position, held in Sydney, Australia, November 1973.
- [B70] Ong, K.M., and Escobal, P.R., "Multilateration: A Nondegenerate Method of Obtaining Station Coordinates and Satellite Ephemerides", J. Astron. Sci. 21, pp 206-229, March 1974.
- [B71] Ong, K.M., "Multilateration for Infinite and Vanishing Satellite Altitudes", JPL EM 391-648, 16 May 1975.*
- [B72] Ong, K.M., "Quasar Multilateration and the Coplanar, Infinite Vehicle Altitude Degeneracy Revisited", JPL IOM 391.5-454, 5 August 1975.*
- [B73] Ong, K.M., "Range-Only vs. Range Difference Multilateration", JPL EM 391-699, 31 October 1975.*
- [B74] Ong, K.M., "Are Formalisms Based on Interstation Lengths and on the 3-Dimensional Relative Station Coordinates Equivalent Descriptions of Multilateration?", JPL EM 391-706, 21 November 1975.*
- [B75] Ong, K.M., and von Roos, O.H., "The Improvement in A Priori 3-Dimensional Station Coordinates Via Accurately Determined Integration Lengths", JPL EM 391-710, 8 December 1975.*
- [B76] von Roos, O.H., "Laser Pulse Shape Degradation by Multiple Reflection from Corner Reflectors Mounted on a Satellite", JPL TM 391-219, 30 July 1971.*
- [B77] von Roos, O.H., "More Geometrical Considerations Relating to Laser Ranging Systems", JPL TM 391-213, 20 July 1971.*

*JPL internal document.

- [B78] von Roos, O.H., "Satellite Ranging Via a Laser Ranging System Without the A Priori Knowledge of the Satellites Orbital Parameters", JPL TM 391-222, 3 August 1971.*
- [B79] von Roos, O.H., "3-D Laser Ranging. Simultaneous Range Determination of a Satellite to the 1 cm Accuracy Level with only Rudimentary Knowledge of the Satellite's Orbit and without the Necessity of Pulse Synchronization", JPL TM 391-305, 22 March 1972.*
- [B80] von Roos, O.H., "Multilateration with VLBI. Preliminary Investigation", JPL TM 391-364, 1 September 1972.*
- [B81] von Roos, O.H., "Fresnel Diffraction Pattern of a Circular Aperture: A Preliminary Estimate of the Influence of Beam Widening by Lenses", JPL TM 391-364, 1 September 1972.*
- [B82] von Roos, O.H., "The Timing and Synchronization Requirements for a VLBI Multilateration System", JPL TM 391-382, 31 October 1972.*
- [B83] von Roos, O.H., "Formulation of a Multilateration Problem when the Range Between 2 Satellites is Known", JPL TM 391-510, 29 October 1973.*
- [B84] von Roos, O.H., "Time Dependent Station Coordinates in Multilateration Techniques", JPL TM 391-522, 20 December 1973.*
- [B85] von Roos, O.H., and Lass, H., "A Note on the Determination of Inertial Station Coordinates by Means of Range Measurements", JPL TM 391-529, 20 December 1973.*
- [B86] von Roos, O.H., and Lass, H., "An Example Whereby Station Coordinates and the Motion of a Satellite can be Determined from Range Measurements Only", JPL TM 391-532, 29 January 1974.*
- [B87] von Roos, O.H., "Error Propagation in Ever Enlarged Multilateration Network", JPL TM 391-538, 12 February 1974.*
- [B88] von Roos, O.H., "Error Analysis of Geodetic Systems", JPL TM 391-542, 21 February 1974.*
- [B89] von Roos, O.H., "New Aspects of Multilateration", JPL TM 391-554, 2 April 1974.*
- [B90] von Roos, O.H., "Selection of Stations in a Multilateration Net: (The Rules)", JPL TM 391-557, 3 April 1974.*
- [B91] von Roos, O.H., "The Collapse of SST Data to Ordinary Multilateration when the SST Link Becomes Zero", JPL TM 391-567, 29 May 1974.*
- [B92] von Roos, O.H., "Rules for Establishing a Viable Multilateration Network", JPL TM 391-568, 3 June 1974.*

* JPL internal document.

C. 2

- [B93] von Roos, O.H., "Tropospheric Range Corrections", JPL TM 391-589, 15 August 1974.*
- [B94] von Roos, O.H., Escobal, P.R., Gallagher, J.F., and Hylkema, R.K., "Generalized Tropospheric Calibration and Error Analysis", JPL TM 391-637, 28 March 1975.*
- [B95] von Roos, O.H., and Lass, H., "Some Remarks on the Use of Least Square Estimation for Model Dependent Parameters", JPL TM 391-643, 6 May 1975.*
- [B96] von Roos, O.H., "Station Location Improvement via Multilateration", JPL TM 391-662, 1 July 1975.*
- [B97] von Roos, O.H., "Analysis of a Passive Multilateration System with One Active Station", JPL TM 391-674, 5 August 1975.*

*JPL internal document.

A1. Multilateration Data Compression



Abstract

A data compression scheme is developed in this Appendix. Specifically, large sets of data points (range) are reduced into compact coefficient arrays of small dimension. The errors occasioned by hardware, modeling, atmospheric and clock jitter are considered in the compression scheme. A square root fitting routine is available to perform the compression and determine the coefficients' auto and cross correlations.

PRECEDING PAGE BLANK NOT FILMED

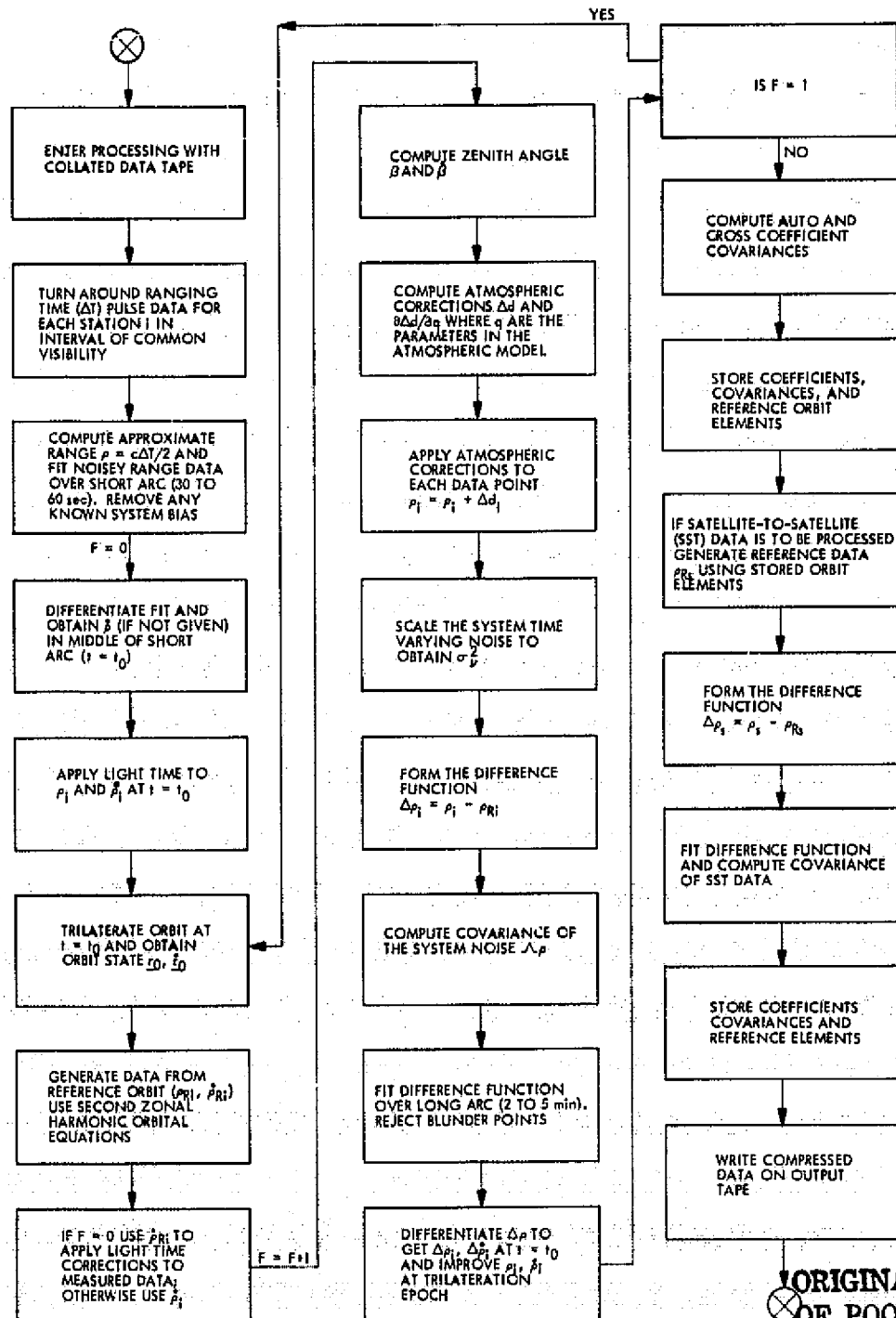
A1.1 INTRODUCTION

The process of multilateration requires the use of accurate interpolation formulas in order to ensure data synchronization for a set of ground stations and vehicle-to-vehicle configurations. This process of interpolation should be possessed of various beneficial characteristics. These characteristics are 1) simplicity in implementation, 2) extension of the duration (timewise) of fit validity, 3) simplicity of extraction of statistical properties of the interpolation formulas, and 4) restriction of covariance matrices to low order arrays. The scheme developed herein attempts to meet these objectives [1.3].

A1.2 DATA COMPRESSION FUNCTION

Figure A1.1 depicts the chain of computations in the data compression function currently adopted for the MICRODOT data preprocessor. In essence this function takes noisy data i. e., either slant range or satellite-to-satellite range (or turn around time pulses) and replaces a large set of data points with a smaller subset of coefficients. These coefficients can be used at a later stage to reconstruct smoothed, calibrated data. The carrying of large matrices of cross correlated data is thus circumvented. Note that the atmospheric equations correlate the data not only from time point to time point at each station, but also between stations. Simulation tests indicated that the fitting of data to noise levels of 1 cm required the use of a reference orbit with second zonal harmonic modeling. The reference orbit is of course adopted as known and thus its effect does not corrupt the compression scheme outlined herein.

The data compression function was tested for a set of adopted orbital elements ($a = 7228$ km, $e = 0$, $i = 115^\circ$). Data was generated from these elements plus perturbations which included: J_2 secular and long period terms (period of $\dot{\omega}$ and $\dot{\Omega}$), short period terms (period, P , of the orbit) of the form $A \sin(2\pi/P)t$, and terms of the form $B \sin(80\pi/P)t$. The amplitude of B was taken to be 3 meters and this variation has a period of about 5 minutes. The latter very high frequency variation is the most severe. Finally 1 cm noise was added to the slant range, the data was compressed, and the standard deviation of the fit was computed as:



ORIGINAL PAGE IS
OF POOR QUALITY

Figure A1.1 Data Compression Function

$$\sigma_f^2 = \frac{1}{N-M} \sum^N [\rho - \text{FIT}(t)]^2$$

where M refers to the degree of the fit and N is the number of points processed. The results are displayed in Figure A1.2. As can be seen a 7th degree polynomial can fit the data within the 1 cm range for about three minutes. Since covisibility periods at the adopted altitudes are only about 5 minutes, half the data arc, say 150 points can be replaced by eight coefficients and an 8 by 8 covariance matrix. Furthermore the compressed data is smoothed and calibrated.

The reader interested in the details of the light time or atmospheric corrections, etc. is directed to other Appendices of this report.

A1.3 POLYNOMIAL FITTING PROCEDURE

Let it be assumed that k raw measurements of the form d_k are taken from a given ground station at times t_k . Let it also be assumed that atmospheric calibration equations of the form

$$\Delta d_k = \Delta d(\omega_1, \dots, \omega_r, \beta, t_k - t_0) \quad (1)$$

are also available such that for specified calibration constants, ω , zenith angle, β , and time t_k the correction Δd_k can be computed. Obviously then, the noisy measurement d_N relates to the true measurement d_T by

$$d_N = d_T + \Delta d_T + \delta d, \quad (2)$$

where δd is the hardware related error. Other error sources are the time jitter δt and epoch error δt_0 . Hence by direct differentiation of the correction Δd_T

ORIGINAL PAGE IS
OF POOR QUALITY

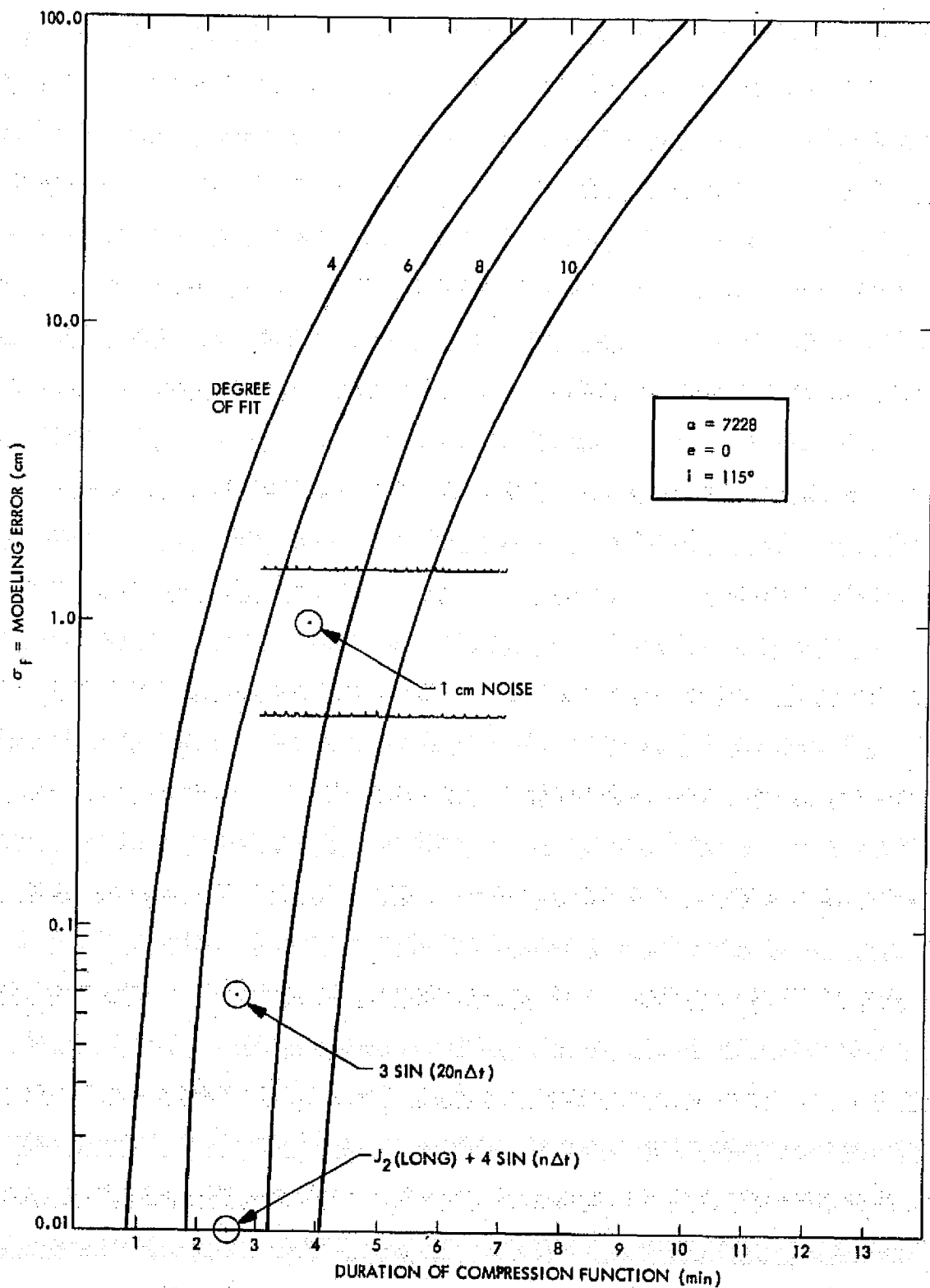


Figure A1.2. Data Compression Results

$$\Delta d_T = \Delta d_N + \frac{\partial \Delta d}{\partial \omega} \delta \omega + \frac{\partial \Delta d}{\partial \beta} \delta \beta + \frac{\partial \Delta d}{\partial \beta} \dot{\beta} \delta t + \frac{\partial \Delta d}{\partial \beta} \dot{\beta}_o \delta t_o$$

so that the calibrated data, d can be written as:

$$d \equiv d_N - \Delta d_N = d_T + \frac{\partial \Delta d}{\partial \omega} \delta \omega + \frac{\partial \Delta d}{\partial \beta} \delta \beta + \frac{\partial \Delta d}{\partial \beta} \dot{\beta} \delta t + \frac{\partial \Delta d}{\partial \beta} \dot{\beta}_o \delta t_o + \delta d. \quad (3)$$

Hence what is desired is to represent d as defined by Eq. (3) in the form

$$d = A_T c + K_1 \delta t + K_2 \delta t_o + K_e \delta \omega + K_4 \delta \beta + \delta d,$$

where the K matrices are obtained by equating the coefficients of Eq. (3), and A is the polynomial fitting matrix associated with the vector c of fitting coefficients. More exactly since t is jittering $A(t_N)$ is only an approximation to A_T and

$$A_T = A + \frac{\partial A}{\partial t} \delta t = A + \dot{A} \delta t$$

$$d = A c + K_1 \delta t + K_2 \delta t_o + K_3 \delta \omega + K_4 \delta \beta + \dot{A} \delta t + \delta d$$

or

$$d = A c + K_1^* \delta t + K_2^* \delta t_o + K_3 \delta \omega + K_4 \delta \beta + \delta d, \quad (4)$$

where all coefficient matrices are defined by Eq. (5).

Note that the error in d due to errors in A can be approximated as $\dot{A} \delta t$ (See [1.1]). So that any estimate of \dot{A} will suffice to model this error, i.e., \dot{A} from the reference orbit. With this understanding and noting that

$$K_1^* = \frac{\partial \Delta d}{\partial \beta} \dot{\beta} + \dot{d}$$

$$K_2^* = \frac{\partial \Delta d}{\partial \beta_o} \dot{\beta}_o + \dot{d}_o$$

(5)

$$K_3 = \frac{\partial \Delta d}{\partial \omega}$$

$$K_4 = \frac{\partial \Delta d}{\partial \beta},$$

it is now desired to fit d with a polynomial such as:

$$f(t) = \sum_0^M c_j \left(\frac{t - t_o}{T} \right)^j,$$

where T is the duration of the fitting interval. In matrix form

$$f(t) = \left[1, \frac{t - t_o}{T}, \dots, \left(\frac{t - t_o}{T} \right)^M \right] c,$$

where $c = [c_o, c_1, \dots, c_M]^T$. It is now possible to assume that d is represented by Eq. (4) with the addition of a modeling error, ϵ , where

$$A \equiv \begin{bmatrix} 1 & (t_1 - t_o)/T & \dots & [(t_1 - t_o)/T]^M \\ \vdots & \vdots & & \vdots \\ 1 & (t_k - t_o)/T & \dots & [(t_k - t_o)/T]^M \end{bmatrix}$$

and where ϵ is taken as a random vector, with zero mean and covariance $\sigma_\epsilon^2 I$. Herein ϵ denotes the modeling error which might be occasioned by fitting perfect data by the polynomial. As suggested by Bierman [1.2] the random time contributions can be scaled such that

$$d = Ac + K_2^* \delta t_0 + K_3 \delta \omega + v, \quad (6)$$

where the noise v is taken as

$$v = K_1^* \delta t + K_4 \delta \beta + \epsilon + \delta d$$

with the approximation:

$$\sigma_v^2 = \sigma_\epsilon^2 + \sigma_d^2 + K_1^{*2} \sigma_t^2 + K_4^{*2} \sigma_\beta^2.$$

The weighted least squares solution to Eq. (6) is obtained directly by computing:

$$\Lambda_d = K_2^* K_2^{*T} \sigma_{t_0}^2 + K_3 \Lambda_\omega K_3^T + I \sigma_v^2 \quad (7)$$

and extraction of the square root of Λ_d (See [1.2]). The standard solution would be

$$\hat{c} = [A^T \Lambda_d^{-1} A]^{-1} A^T \Lambda_d^{-1} d \quad (8)$$

while the covariance of \hat{c} is given by

$$\Lambda_{\hat{c}} = [A^T \Lambda_d^{-1} A]^{-1}. \quad (9)$$

Furthermore for any two stations i and j :

$$\Lambda_{\hat{c}_i \hat{c}_j} = [A_i^T \Lambda_i^{-1} A_i]^{-1} A_i^T \Lambda_i^{-1} K_3 \Lambda_\omega K_3^T \Lambda_{d_j}^{-1} A_j [A_j^T \Lambda_{d_j}^{-1} A_j]^{-1}$$

The actual computation of the coefficients and covariances is performed via square root filtering as outlined in [1.2]. Note that for satellite-to-satellite data compression, the K_3 and K_4 matrices would be set equal to zero.

A1.4 REFERENCES

- [1.1] Escobal, P.R., "Explicit Matrix Solution for obtaining Minimum Variance Estimates of Parameters Contained in a Large Set of Non-Linear Equations," JPL EM-391-601, 6 January 1975.*
- [1.2] Bierman, G.J., "Polynomial Fitting for Data Compression," JPL EM 391-636, 27 March 1975.*
- [1.3] Escobal, P.R., "Multilateration Data Compression," JPL EM 391, 28 April 1976.*

*JPL internal document.

A2. Explicit Matrix Solution for Obtaining Minimum Variance Estimates of Parameters Contained in a Large Set of Nonlinear Equations

Abstract

A system of nonlinear algebraic equations, namely,

$$M(\xi, t, c, \bar{\xi}) = 0,$$

where ξ is the vector of to-be-solved-for parameters, t is time, c are data coefficients, and $\bar{\xi}$ are modeling constants, is solved herein using a minimum variance criterion. The a priori uncertainty in ξ used in solving the Newton-Raphson equations is included along with all statistical cross correlations. The solution of the equations is performed sequentially over the entire range of t so that inversion of the normal equation matrices is required only at each iteration step. A side investigation yields formulas for the covariance of polynomial fitting data compression coefficients including uncertainties in the data measurements, clock times, and atmospheric calibration parameters. The techniques are used in this multilateration study but may be useful elsewhere.

PRECEDING PAGE BLANK NOT FILMED

A2.1 INTRODUCTION AND SUMMARY

A procedure for solving a set of nonlinear equations, herein called multilateration functions, is established [2.4]. Solution of these equations permits a set of to-be-solved-for parameters to be obtained in a minimum variance sense. The solution as developed herein is accomplished in three operations, namely, data presmoothing, batch processing and sequential batch processing. Specifically, a) data types are presmoothed for purposes of obtaining the data types as explicit functions of time recorded at an ensemble of ground stations. These functions are interrogated at a master clock time and are forced to yield synchronized measurements for all data gathering stations; b) since the synchronized data types become correlated via the fitting procedure, a discrete batch of pseudo data valid over a fitting interval of specified duration is processed with all possible cross correlations; c) the discrete batches of pseudo data are then accumulated sequentially for all the fitting intervals of the entire data gathering operation. This is possible because two different data fitting intervals are assumed to be uncorrelated.*

The explicit list of error sources peculiar to the multilateration functions are listed in Table A2.1.

Table A2.1. Existing Error Sources

Error Sources	Symbol
Atmospheric calibration uncertainty	$\delta\omega$
Data type hardware uncertainty	δd
Station clock jitter	δt
Master clock jitter	δt^*
A priori to-be-solved-for uncertainty	$\delta \tilde{\xi}_q$
Modeling constants uncertainty	$\delta \tilde{\xi}$

* A discussion of this implication will be undertaken shortly.

The first three error sources are mapped into the covariance peculiar to the smoothing polynomial coefficients such that the multilateration functions, hereafter referred to as M-functions, only sense the errors in the fitting coefficients, master clock reading, a priori values, and modeling constants. The modeling constants uncertainty arises from the assumed model for the to-be-solved-for parameters, i.e., in the Earth/ocean tidal model which is explicitly included in the solution. The analysis developed herein is exact, including all cross correlations within a fitting interval of specified duration.

For purposes of program efficiency however, a minor assumption is made. Specifically, even though the analysis in each fitting interval is exact, it is realized that weak cross correlations will exist from fitting interval to fitting interval due to two sources. These are:

- 1) The atmospheric calibration model constants which are the same in each adopted fitting interval,
- 2) The Earth/ocean model constants which are the same in each fitting interval.

Hence, the atmospheric calibration constants tend to cross correlate the fitting coefficients, while the other source tends to correlate the system of equations whose minimum variance solution is sought.

Since the analysis performed herein includes all error sources in each fitting interval, an exact solution is certainly possible, the only limit being the storage available on the computing hardware. However, since the omission of these weak correlations tends to yield answers at a great saving in computing efficiency, these correlations are ignored on a fitting interval-to-fitting interval basis but are included in each fitting interval. These distinctions are of academic interest for present applications (GEOS-3) where accuracy requirements on the to-be-solved-for parameters are not as stringent as the ultimate confidence levels to be attained by the software currently under development. However, it was felt that the development of the current software should have the capability of sub-centimeter to-be-solved-for parameter determination.

In this light, the careful inclusion and distinction of the error sources is of paramount importance.

Since the analysis performed herein is rather lengthy a functional flow diagram is presented first to assist the reader in maintaining perspective throughout the analysis. The reader lacking sufficient background should consult [2. 1, 2. 2, 2. 3].

A2.2 GROSS COMPUTATIONAL FLOW DIAGRAM

The main purpose of the flow diagram (Fig. A2.1) presented herein is to show the input parameters, the manner in which the equations are partitioned and the recursive way in which the covariances are updated. It is hoped that the diagram will also aid in making clear that each iteration of the Newton procedure is accomplished once all available data over the entire mission duration is accumulated sequentially into the matrix of normal equations which define the to-be-solved-for system. If real time processing were desired the software package would be much more expensive to operate since many more matrix inversion operations would be required.

Since the nomenclature, etc., are defined in the main text, the reader may wish to briefly scan the diagram and then refer back to it in more detail once the appropriate section in this Appendix is reached.

A2.3 OUTLINE OF SOLUTION OF MULTILATERATION EQUATIONS

The basic form of the general multilateration function can be represented as:

$$M(\xi_T, d_T) = 0, \quad (1)$$

where ξ represents the vector of to-be-solved for parameters, d represents the synchronized data types and the subscript T denotes error free parameters. In more detail:

$$\xi_T = [\xi_{T1}, \xi_{T2}, \dots, \xi_{Tl}]$$
$$d_T = [\rho_{T1}, \rho_{T2}, \dots, \rho_{Tm}, s_T]$$

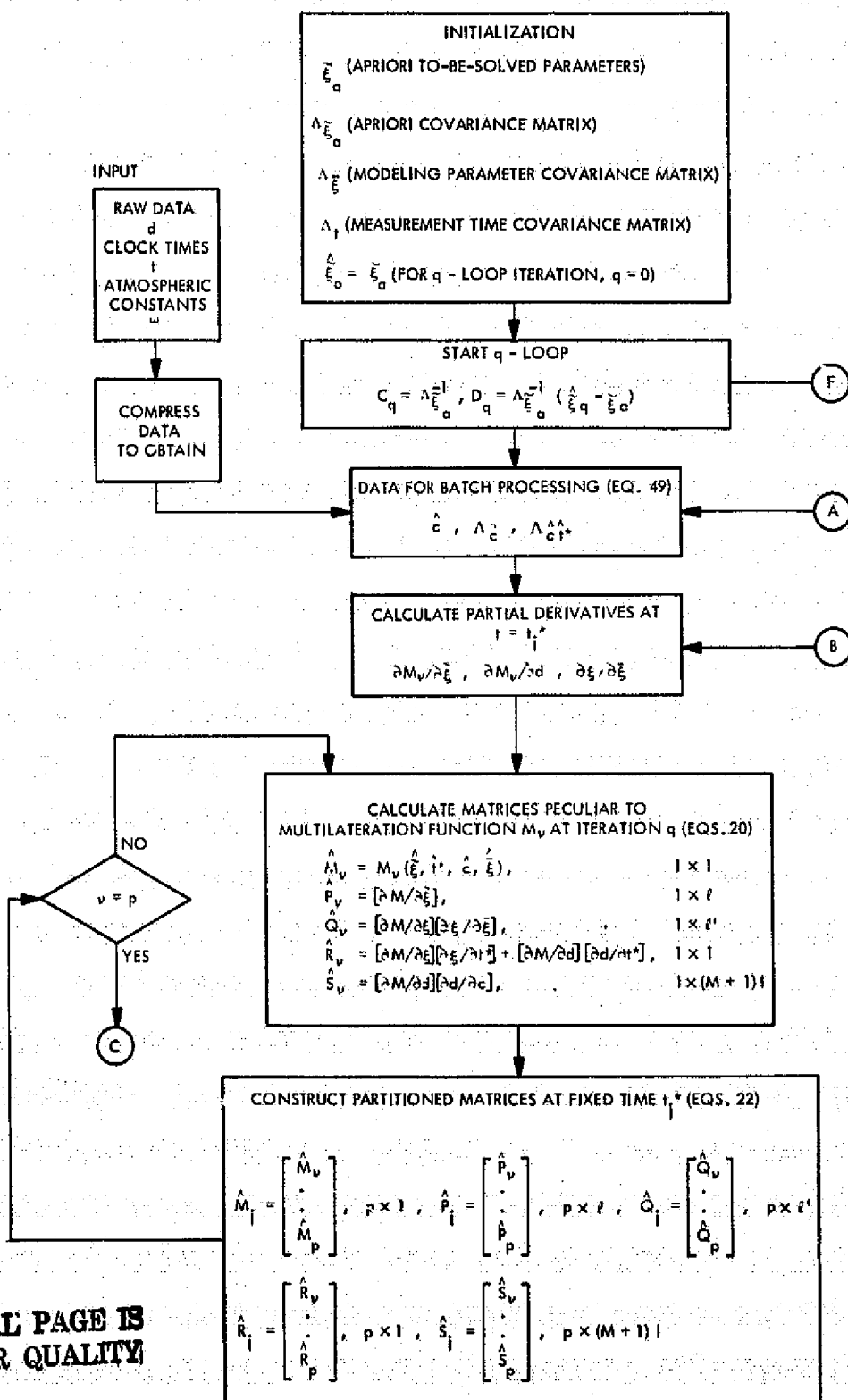


Fig. A2.1. Overall Flow Diagram (Sheet 1 of 3)

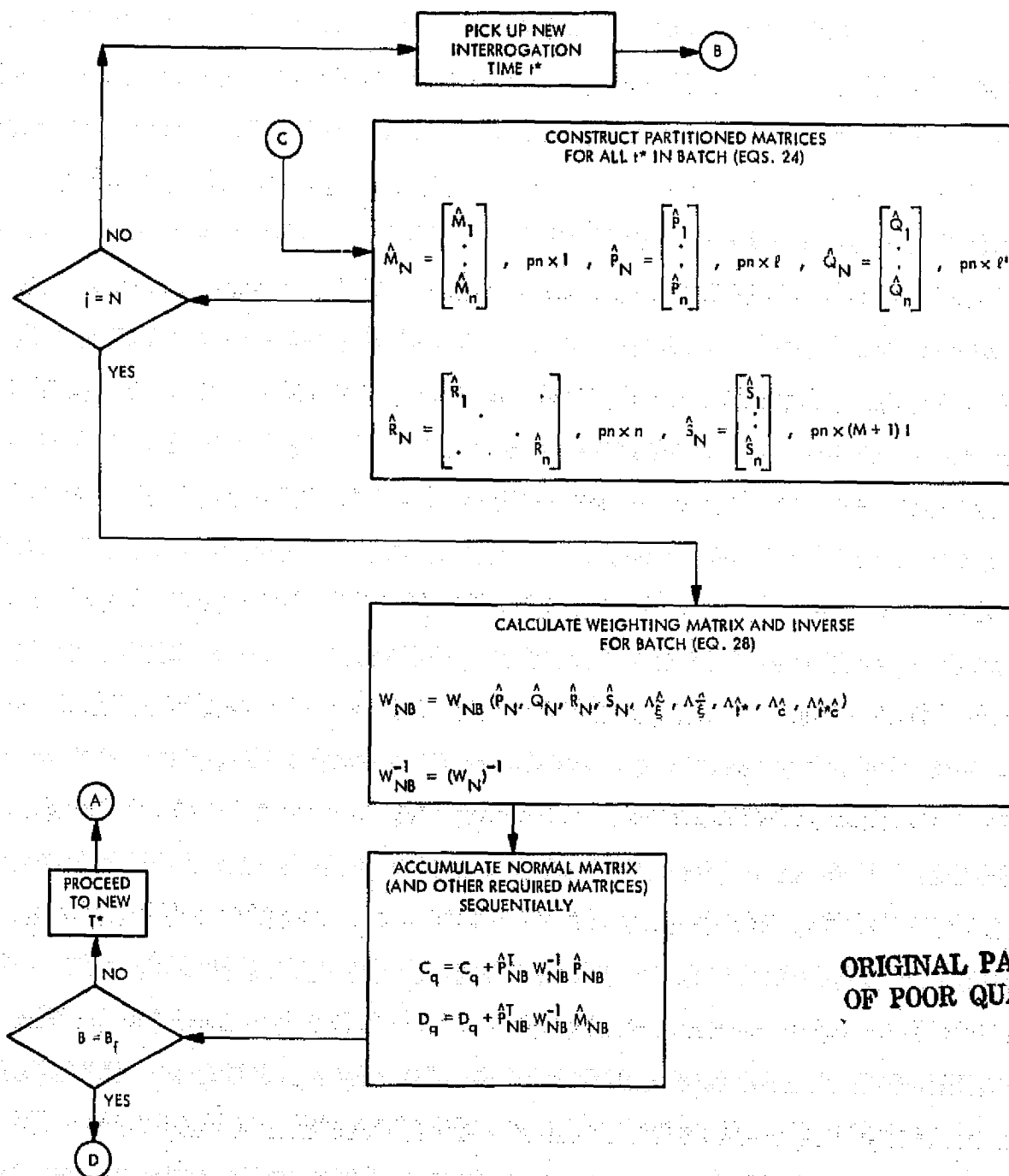


Fig. A2.1. Overall Flow Diagram (Sheet 2 of 3)

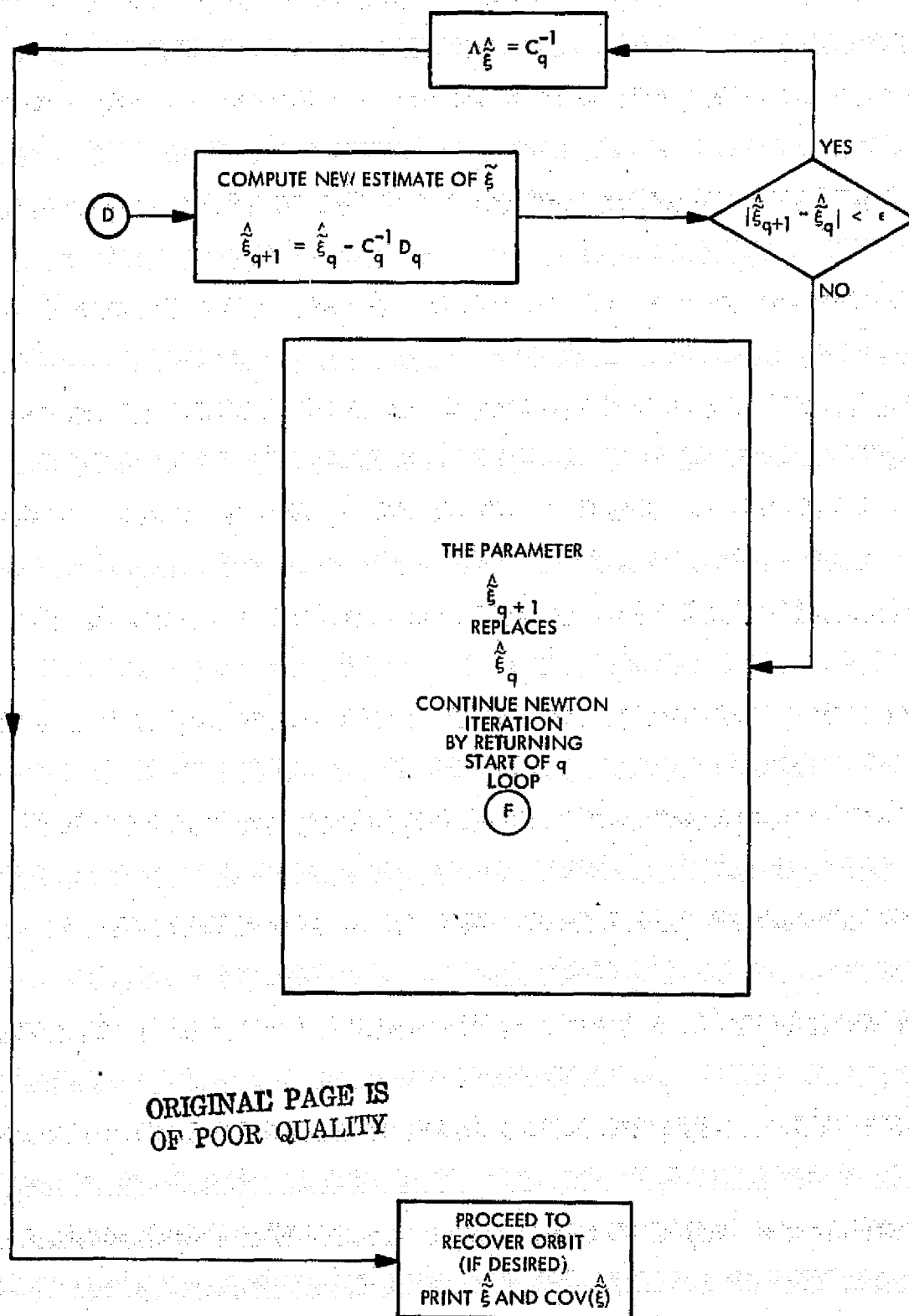


Fig. A2.1. Overall Flow Diagram (Sheet 3 of 3)

with ρ defined as the slant ranges from station i , and s defined as the vehicle-to-vehicle slant range. Equation (1) is an exact relationship which is satisfied with the variable d if it is understood that the subscript T denotes that the variable d is possessed of no statistical uncertainty or any other error.

However, for purposes of multilateration the data must be synchronized. To accomplish this the data is fit by polynomials at each station of the form*

$$d_T = B_T c_T, \quad (2)$$

where the computed data vector d_T is theoretically defined in terms of the exact matrix

$$B_T \equiv \begin{bmatrix} b_1 \\ b_2 \\ \vdots \\ b_j \\ \vdots \\ b_n \end{bmatrix}_T = \begin{bmatrix} 1, (t_1^* - t_0^*), (t_1^* - t_0^*)^2, \dots, (t_1^* - t_0^*)^M \\ \cdot \\ \cdot \\ \cdot \\ 1, (t_n^* - t_0^*), (t_n^* - t_0^*)^2, \dots, (t_n^* - t_0^*)^M \end{bmatrix}_T \quad (3)$$

and

$$c_T = \begin{bmatrix} c_{T0} \\ c_{T1} \\ \vdots \\ c_{TM} \end{bmatrix}, \quad (4)$$

*It is assumed that some mean value coefficients can be found which permit the true data to be represented by a finite polynomial.

with the understanding that t_j^* represents the interrogation time j out of n interrogations referenced to some master clock. The structure of the problem forces Eq. (1) to be written at time t_j^* as:

$$M_j \left\{ \xi_T(\tilde{\xi}_T, \bar{\xi}_T, t_{Tj}^*), b_j(t_{Tj}^*), c(t_T, d_T, \omega_T) \right\} = 0. \quad (5)$$

This equation will be carefully explained in the following discussion: the first term ξ_T represents the parameters inherent in M_j expressed in terms of a set of to-be-solved-for variables, $\tilde{\xi}$, a set of constants, $\bar{\xi}_T$, and master clock time, t_T^* . For example, if ξ represents a station coordinate, then due to Earth tides, etc., ξ would be represented as a time varying parameter which will be represented at each station as:

$$\xi = \tilde{\xi} + f_{\tilde{\xi}}(\tilde{\xi}_k, \bar{\xi}_0, \bar{\xi}_1, \dots, \bar{\xi}_\ell, t_T^* - t_{T0}^*), \quad k = 1, 2, \dots, K,$$

where f is a tidal function[†] specified by a set of constants $\bar{\xi}$ and time t^* . Obviously if $f = 0$, the to-be-solved-for parameters are equal to ξ ($\xi = \tilde{\xi}$). The row vector b_j of dimension $1 \times (M + 1)$, is a function of the interrogation time t_j^* . Finally the coefficients of the fit, c , (required for data type synchronization) are functions of all the data measurements, d , the associated measurement times $t \neq t^*$, and the atmospheric calibration constants, ω , acting over the fitting interval of duration T^* . Hence Eq. (5) can be solved for $\tilde{\xi} \xrightarrow{d} 1 \times \ell$ with $\bar{\xi}_0, \bar{\xi}_1, \dots, \bar{\xi}_\ell$, assumed to be known, or a solution for $\tilde{\xi}$ and some of the $\bar{\xi}$ can be attempted. In the first case $\bar{\xi}$ will have input or specified uncertainties; in the second case the uncertainties of $\tilde{\xi}$ and those $\bar{\xi}$ which are solved for will be determined upon solution of the equations.

[†] As developed in Appendix A3, e.g., the X coordinate of a station in a topocentric coordinate system can be modeled by the tidal function f , namely:

$$X = \tilde{X}_0 + f_X(\tilde{X}_0, \tilde{Y}_0, \tilde{Z}_0, \tilde{h}, \bar{\ell}, \bar{g}, \dots, t_T^* - t_{T0}^*),$$

where, h, ℓ , and g are constants. If, say, X_0, Y_0, Z_0 and h are to be solved for, an overhead tilde is implied on these variables, whereas the overhead bar implies that these variables will not be determined but will be modeled.

In recapitulation, the explicit error sources of the nonlinear problem are identified as:

$$\begin{aligned} t_N^* &= t_T^* + \beta^* \\ \bar{\xi}_N &= \bar{\xi}_T + \mu^* \\ c_N &= c_T + c^*, \end{aligned} \quad (6)$$

where the errors in d , t , ω are assimilated into c , and β^* , μ^* , c^* are the noise and uncertainty associated with the t , $\bar{\xi}$ and c variables. Now since Eq. (5) is only valid for the true values of the parameters, the question is asked as to how M_j actually differs from zero when noisy or uncertain variables are introduced into the equation. Hence by formal differentiation:

$$\begin{aligned} \delta M_j &= \frac{\partial M_j}{\partial \bar{\xi}} \frac{\partial \bar{\xi}}{\partial \bar{\xi}} (\bar{\xi}_T - \bar{\xi}_N) + \frac{\partial M_j}{\partial \bar{\xi}} \frac{\partial \bar{\xi}}{\partial t^*} (t_{Tj}^* - t_{Nj}^*) \\ &+ \frac{\partial M_j}{\partial d} \frac{\partial d}{\partial t^*} (t_{Tj}^* - t_{Nj}^*) + \frac{\partial M_j}{\partial d} \frac{\partial d}{\partial c} (c_T - c_N). \end{aligned} \quad (7)$$

The previous equation is now rewritten as:

$$\delta M_j = E_{1j} \delta \bar{\xi} + E_{2j} \delta t^* + E_{3j} \delta c \quad (8)$$

with

$$E_{1j} = \frac{\partial M_j}{\partial \bar{\xi}} \frac{\partial \bar{\xi}}{\partial \bar{\xi}}$$

$$E_{2j} = \frac{\partial M_j}{\partial \bar{\xi}} \frac{\partial \bar{\xi}}{\partial t^*} + \frac{\partial M_j}{\partial d} \frac{\partial d}{\partial t^*}$$

$$E_{3j} = \frac{\partial M_j}{\partial d} \frac{\partial d}{\partial c},$$

where

$$\bar{\xi}_T \equiv \bar{\xi}_N + \delta\bar{\xi}, \quad t_T^* \equiv t_N^* + \delta t^*, \quad c_T = c_N + \delta c.$$

For purposes of error analysis let it be assumed that estimates of $\bar{\xi} = \frac{\Delta}{\xi}$, $t^* = \hat{t}^*$, $c = \hat{c}$ are available (obviously for t^* , \hat{t}^* is just the reading of the master clock at interrogation time t^*). The partial derivative matrices E_1 , E_2 , E_3 can now be evaluated with sufficient accuracy using $\frac{\Delta}{\xi}$, \hat{t}^* , and \hat{c} , call them \hat{E}_1 , \hat{E}_2 , \hat{E}_3 so that:

$$\delta M_j = \hat{E}_{1j} \delta \frac{\Delta}{\xi} + \hat{E}_{2j} \delta t^* + \hat{E}_{3j} \delta \hat{c}. \quad (9)$$

Hence Eq. (5) now reads

$$M_j(\tilde{\xi}_T, \frac{\Delta}{\xi}, \hat{b}_j, \hat{c}) = -\hat{E}_{1j} \delta \frac{\Delta}{\xi} - \hat{E}_{2j} \delta t^* - \hat{E}_{3j} \delta \hat{c}, \quad (10)$$

Since a priori estimates ξ_a are introduced to solve Eq. (10) with the understanding that $E \begin{bmatrix} \delta \tilde{\xi}_a & \delta \tilde{\xi}_a^T \end{bmatrix} = \Lambda \tilde{\xi}_a$ is a known matrix, it follows that the complete system of equations whose solution via iteration is sought can be written as:

$$T(\tilde{\xi}_T) \equiv \begin{bmatrix} \tilde{\xi}_T - \tilde{\xi}_a \\ M(\tilde{\xi}_T, \frac{\Delta}{\xi}, \hat{b}_j, \hat{c}) \end{bmatrix} = \begin{bmatrix} \eta \\ v_j \end{bmatrix}, \quad (11)$$

where η and v_j are the uncertainties in the a priori and M-functions. From Eq. (10) the uncertainty v_j is given by:

$$v_j = -\hat{E}_{1j} \delta \frac{\Delta}{\xi} - \hat{E}_{2j} \delta t^* - \hat{E}_{3j} \delta \hat{c},$$

however to avoid cumbersome notation, e. g., \hat{E}_{1j} stands for the appropriate partial derivative evaluated at time j with estimate $\frac{\Delta}{\xi}$ on the q^{th} iteration step, v_j is rewritten as:

$$v_j = \hat{Q}_j \delta \frac{\Delta}{\xi} + \hat{R}_j \delta t^* + \hat{S}_j \delta \hat{c}. \quad (12)$$

To condition the system of equations $T(\tilde{\xi}_T)$, i. e., to uncouple the equations statistically let Eqs. (11) be multiplied by the matrix V^{-1} where $VV^T = W$ is the covariance matrix of the error sources. To this end the new function F is constructed as

$$F \equiv V^{-1} T(\tilde{\xi}_T) = V^{-1} \begin{bmatrix} \eta \\ v_j \end{bmatrix} = u, \quad (13)$$

and since the resulting system has uncorrelated components, i. e., $E(uu^T) = U$ where U is the identity matrix, F can be set equal to zero to solve the overdetermined set of equations by the method of least squares. In essence this will yield the minimum variance solution by solution of:

$$F(\tilde{\xi}_q) + \left. \frac{\partial F}{\partial \tilde{\xi}} \right|_{\tilde{\xi}=\tilde{\xi}_q} (\tilde{\xi}_{q+1} - \tilde{\xi}_q) = 0. \quad (14)$$

The standard least squares iteration to the solution of the linear system defined by Eq. (14) is now given by:

$$\hat{\xi}_{q+1} = \hat{\xi}_q - \left\{ \left[\frac{\partial F}{\partial \tilde{\xi}} \right]^T \left[\frac{\partial F}{\partial \tilde{\xi}} \right] \right\}^{-1} \left[\frac{\partial F}{\partial \tilde{\xi}} \right]^T F(\hat{\xi}_q) \quad (15)$$

or since

$$\frac{\partial F}{\partial \tilde{\xi}} = V^{-1} \frac{\partial T}{\partial \tilde{\xi}} (\hat{\xi}_q)$$

$$\hat{\xi}_{q+1} = \hat{\xi}_q - \left\{ \left[\frac{\partial T}{\partial \tilde{\xi}} \right]^T W^{-1} \left[\frac{\partial T}{\partial \tilde{\xi}} \right] \right\}^{-1} \left[\frac{\partial T}{\partial \tilde{\xi}} \right]^T W^{-1} T(\hat{\xi}_q). \quad (16)$$

Noting the partitioning of T and extracting $\partial T / \partial \tilde{\xi}$, namely:

$$\frac{\partial T}{\partial \tilde{\xi}} = \begin{bmatrix} U \\ \frac{\partial M}{\partial \tilde{\xi}} \end{bmatrix} \quad (17)$$

then W takes the form

$$W = \begin{bmatrix} W_a & 0 \\ 0 & W_v \end{bmatrix}, \quad (18)$$

where

$$W_a = \Lambda_{\tilde{\xi}_a}$$

$$W_v = \text{cov} \begin{pmatrix} v_q & v_q^T \end{pmatrix} = Q_q \Lambda_{\tilde{\xi}} Q_q^T + R_q \Lambda_{t^*} R_q^T + S_q \Lambda_{\tilde{\xi}} S_q^T \\ + R_q \Lambda_{t^*} \Lambda_{\tilde{\xi}} S_q^T + S_q \Lambda_{\tilde{\xi}} \Lambda_{t^*} R_q^T.$$

The final form of the Newton-Raphson equations is now obtained by explicitly multiplying out Eq. (14) and using the definition $P = \partial M / \partial \tilde{\xi}$ to yield:

$$\hat{\tilde{\xi}}_{q+1} = \hat{\tilde{\xi}}_q - \left[W_a^{-1} + P_q^T W_v^{-1} P_q \right]^{-1} \left[W_a^{-1} (\hat{\tilde{\xi}}_q - \tilde{\xi}_a) + P_q^T W_v^{-1} \hat{M}_q \right]. \quad (19)$$

A2.4 EXPLICIT DEVELOPMENT OF A SINGLE MULTILATERATION EQUATION AT A FIXED TIME

It has been shown that the generalized multilateration function, after linearization and approximation of the pertinent partial derivatives by estimates ($\hat{\cdot}$) has the following form:

$$P_q^* (\hat{\xi}_{q+1} - \hat{\xi}_q) = -M_q^* \quad , \quad (20)$$

where

$$\hat{P}_q^* \equiv W_a^{-1} + \hat{P}_q^T W_v^{-1} \hat{P}_q$$

$$\hat{M}_q^* \equiv W_a^{-1} (\hat{\xi}_q - \xi_a) + \hat{P}_q^T W_v^{-1} \hat{M}_q$$

$$\hat{M}_q = M_q(\tilde{\xi}_1, \tilde{\xi}_2, \dots, \tilde{\xi}_\ell, \hat{\xi}_1, \hat{\xi}_2, \dots, \hat{\xi}_\ell, \hat{t}^*, \hat{c}) \xrightarrow{d} 1 \times 1 \quad ,$$

with the understanding that a decision has been made as to which parameters will be solved for, $\tilde{\xi}$ (with overhead tilde), and which parameters are being modeled, $\hat{\xi}$ (with overhead bar). The noise v is expressed in matrix notation as:

$$v_q = \hat{Q}_q \delta \hat{\xi} + \hat{R}_q \delta \hat{t}^* + \hat{S}_q \delta \hat{c} \xrightarrow{d} 1 \times 1 \quad .$$

The matrix P is therefore given by:

$$\hat{P}_q = \left[\frac{\partial M}{\partial \tilde{\xi}_1}, \frac{\partial M}{\partial \tilde{\xi}_2}, \dots, \frac{\partial M}{\partial \tilde{\xi}_\ell} \right] \xrightarrow{d} 1 \times \ell \quad .$$

The matrix Q and its error $\delta \hat{\xi}$ are given by noticing that

$$M = M \left\{ \xi_1 (\bar{\xi}_1, \bar{\xi}_2, \dots, \bar{\xi}_\ell, t^*), \xi_2 (\bar{\xi}_1, \bar{\xi}_2, \dots, \bar{\xi}_\ell, t^*) \dots, d(t^*) \right\}$$

so that $\hat{Q} \equiv [\partial M / \partial \bar{\xi}_1, \dots, \partial M / \partial \bar{\xi}_\ell]$ can be obtained as

$$\hat{Q}_q = \left[\frac{\partial M}{\partial \xi_1}, \frac{\partial M}{\partial \xi_2}, \dots, \frac{\partial M}{\partial \xi_{\ell}} \right] \begin{bmatrix} \frac{\partial \xi_1}{\partial \xi_1} & \frac{\partial \xi_1}{\partial \xi_2} & \dots & \frac{\partial \xi_1}{\partial \xi_{\ell'}} \\ \frac{\partial \xi_2}{\partial \xi_1} & \frac{\partial \xi_2}{\partial \xi_2} & & \vdots \\ \vdots & \vdots & & \frac{\partial \xi_{\ell}}{\partial \xi_{\ell'}} \end{bmatrix} \xrightarrow{d} 1 \times \ell'$$

with

$$\delta \bar{\xi} = \left[\delta \bar{\xi}_1, \delta \bar{\xi}_2, \dots, \delta \bar{\xi}_{\ell} \right]^T \xrightarrow{d} \ell' \times 1.$$

Similarly the R matrix and δt^* are obtained as

$$\hat{R}_q = \left[\frac{\partial M}{\partial \xi_1}, \frac{\partial M}{\partial \xi_2}, \dots, \frac{\partial M}{\partial \xi_{\ell}} \right] \begin{bmatrix} \frac{\partial \xi_1}{\partial t^*} \\ \frac{\partial \xi_2}{\partial t^*} \\ \vdots \\ \frac{\partial \xi_{\ell}}{\partial t^*} \end{bmatrix} + \left[\frac{\partial M}{\partial d_1}, \frac{\partial M}{\partial d_2}, \dots, \frac{\partial M}{\partial d_I} \right]$$

$$\times \begin{bmatrix} c_{11} + 2c_{21}t^* + \dots + (M-1)c_{M1}t^{*(M-1)} \\ c_{12} + 2c_{22}t^* + \dots + (M-1)c_{M2}t^{*(M-1)} \\ \vdots \\ c_{1I} + 2c_{2I}t^* + \dots + (M-1)c_{MI}t^{*(M-1)} \end{bmatrix} \xrightarrow{d} 1 \times 1$$

$$\delta t^* = \left[\delta t^* \right] \xrightarrow{d} 1 \times 1.$$

Finally the S matrix can be formed as

$$\hat{S}_q = \left[\frac{\partial M}{\partial d_1} \frac{\partial d_1}{\partial c_{01}}, \frac{\partial M}{\partial d_1} \frac{\partial d_1}{\partial c_{11}}, \dots, \frac{\partial M}{\partial d_1} \frac{\partial d_1}{\partial c_{M1}}, \frac{\partial M}{\partial d_2} \frac{\partial d_2}{\partial c_{02}}, \frac{\partial M}{\partial d_2} \frac{\partial d_2}{\partial c_{12}}, \dots, \right. \\ \left. \frac{\partial M}{\partial d_2} \frac{\partial d_2}{\partial c_{M2}}, \dots, \frac{\partial M}{\partial d_I} \frac{\partial d_I}{\partial c_{MI}} \right] \xrightarrow{d} 1 \times (M+1)I$$

$$\delta \hat{c} = \left[\delta c_{01}, \delta c_{11}, \dots, \delta c_{M1}, \delta c_{02}, \delta c_{12}, \dots, \delta c_{M2}, \dots, \right. \\ \left. \delta c_{MI} \right]^T \xrightarrow{d} (M+1)I \times 1,$$

where in the previous matrices:

$l \equiv$ specified length of to-be-solved-for vector,

$l' \equiv$ specified length of not to-be-solved-for parameters
contained in M - function

$M \equiv$ degree of polynomial fit,

$I \equiv$ number of data types contained in multilateration function.

An example at this point is useful. Suppose an M-function of the following form exists:

$$M = M(X_1, Y_1, Z_1, X_2, Y_2, Z_2, X_3, Y_3, Z_3, X_4, Y_4, Z_4, \\ a_e, h, k, \alpha_c, \delta_c, R_c, g_1, g_2, g_3, g_4, \hat{c}, t^*)$$

The to-be-solved-for parameter vector is selected as:

$$\tilde{\xi} = [X_2, X_3, Y_3, Z_4, h] \equiv [\tilde{\xi}_1, \tilde{\xi}_2, \dots, \tilde{\xi}_5]$$

This implies that

$$\bar{\xi} = (X_1, Y_1, Z_1, Y_2, Z_2, Z_3, X_4, Y_4, a_e, k, \alpha_c, \delta_c, R_c, g_1, g_2, g_3, g_4) \\ \equiv [\bar{\xi}_1, \bar{\xi}_2, \dots, \bar{\xi}_{17}],$$

where for concreteness X, Y, Z are the station coordinates, a_e is the radius of the Earth, h is the Earth Love number, k , etc., are some other constants, α, δ, R are the right-ascension, declination and radial distance of the Moon, and g_1, \dots, g_4 are local gravity values at the stations, i.e., the relevant Earth tide parameters. The parameters in $\bar{\xi}$ are uncertain and thus give rise to the uncertainty vector v . Since the explicit substitution of the Earth tide model is not performed M actually looks like

$$M = M(X_1, Y_1, Z_1, \dots, X_4, Y_4, Z_4, d)$$

or

$$M = M(\xi_1, \xi_2, \dots, \xi_{12}, d),$$

where one must actually bear in mind that ξ_i are actually given by:

$$\xi_i = \tilde{\xi}_i + f_{\xi}(\tilde{\xi}_j, \bar{\xi}, t^*).$$

With this understanding, the appropriate partials can now be constructed to yield the P and Q matrices. Similarly since the polynomial fits are not explicitly substituted in M

$$M = M(\xi, d_1, d_2, d_3, d_4),$$

where

$$d_i = c_{0i} + c_{1i}t^* + \dots + c_{Mi}t^{*M}.$$

Hence using the chain rule, the R and S matrices are easily obtained as listed previously.

A2.5 EXPLICIT DEVELOPMENT OF MULTILATERATION EQUATIONS AT A FIXED TIME (GROUPING BY TIME)

Since in general there will be p multilateration functions in action at a fixed time, t_j^* , Eq. (20) must be augmented to represent the complete system of equations. Hence if v represents an arbitrary M -function then:

$$\left[W_a^{-1} + \begin{bmatrix} \hat{P}_{vq} \\ \vdots \\ \hat{P}_{pq} \end{bmatrix}^T W^{-1} \begin{bmatrix} \hat{P}_{vq} \\ \vdots \\ \hat{P}_{pq} \end{bmatrix} \right] (\hat{\xi}_{q+1} - \hat{\xi}_a) = -W_a^{-1} (\hat{\xi}_q - \xi_a) - \begin{bmatrix} \hat{P}_{vq} \\ \vdots \\ \hat{P}_{pq} \end{bmatrix} W^{-1} \begin{bmatrix} M_{vq} \\ \vdots \\ M_{pq} \end{bmatrix} \quad (21)$$

defines the linearized system whose solution is sought. This system can be compacted by constructing the following matrices internally in the computer:

$$\hat{P} \equiv \begin{bmatrix} \hat{P}_{vq} \\ \hat{P}_{(v+1)q} \\ \vdots \\ \hat{P}_{pq} \end{bmatrix} \xrightarrow{d} p \times l, \quad \hat{M} \equiv \begin{bmatrix} \hat{M}_{vq} \\ \hat{M}_{(v+1)q} \\ \vdots \\ \hat{M}_{pq} \end{bmatrix} \xrightarrow{d} p \times 1, \quad v \equiv \begin{bmatrix} v_{vq} \\ v_{(v+1)q} \\ \vdots \\ v_{pq} \end{bmatrix} \xrightarrow{d} p \times 1, \quad (22)$$

where the number of columns of P expand to account for all new station coordinates augmented to the system by M_{v+1} , M_{v+2} , \dots , M_p and where the matrices defining Q , R , and S are constructed as:

$$\hat{Q} \equiv \begin{bmatrix} \hat{Q}_{vq} \\ \hat{Q}_{(v+1)q} \\ \vdots \\ \hat{Q}_{pq} \end{bmatrix} \xrightarrow{d} p \times l', \quad \hat{R} \equiv \begin{bmatrix} \hat{R}_{vq} \\ \hat{R}_{(v+1)q} \\ \vdots \\ \hat{R}_{pq} \end{bmatrix} \xrightarrow{d} p \times 1, \quad \hat{S} \equiv \begin{bmatrix} \hat{S}_{vq} \\ \hat{S}_{(v+1)q} \\ \vdots \\ \hat{S}_{pq} \end{bmatrix} \xrightarrow{d} p \times (M+1)I$$

with the necessary understanding that I is redefined to mean all the stations in the p multilateration functions, and ℓ' is also redefined to mean the complete list of error sources in the modeling constants peculiar to all p M-functions. This will have the effect of expanding the number of columns in \hat{Q} and \hat{S} , i.e., placing zeros wherever M_v, M_{v+1}, \dots, M_p are lacking in a particular parameter out of the entire list of parameters.

For example if

$$M_v = M_v(\tilde{\xi}_1, \dots, \tilde{\xi}_{12}, \bar{\xi}_1, \dots, \bar{\xi}_{17}, c_{01}, \dots, c_{M4}, t^*)$$

$$M_{v+1} = M_{v+1}(\tilde{\xi}_1, \dots, \tilde{\xi}_9, \tilde{\xi}_{13}, \tilde{\xi}_{14}, \tilde{\xi}_{15}, \bar{\xi}_1, \dots, \bar{\xi}_{18},$$

$$c_{01}, \dots, c_{M3}, c_{05}, \dots, c_{M5}, t^*)$$

that is, M_{v+1} introduces a new station $\tilde{\xi}_{13}, \tilde{\xi}_{14}, \tilde{\xi}_{15}$ with new c_{05}, \dots, c_{M5} and a new modeling constant $\bar{\xi}_{18}$ over and above the parameters contained in M_v , then

$$\hat{P} = \begin{bmatrix} \hat{P}_v \\ \hat{P}_{v+1} \end{bmatrix} = \begin{bmatrix} \frac{\partial M_v}{\partial \tilde{\xi}_1}, \frac{\partial M_v}{\partial \tilde{\xi}_2}, \dots, \frac{\partial M_v}{\partial \tilde{\xi}_{15}} \\ \frac{\partial M_{v+1}}{\partial \tilde{\xi}_1}, \dots, \frac{\partial M_{v+1}}{\partial \tilde{\xi}_{15}} \end{bmatrix},$$

where as is obvious $\partial M_v / \partial \tilde{\xi}_{13} = 0$, etc. Similarly

$$\hat{Q} = \begin{bmatrix} \hat{Q}_v \\ \hat{Q}_{v+1} \end{bmatrix} = \begin{bmatrix} \frac{\partial M_v}{\partial \bar{\xi}_1}, \dots, \frac{\partial M_v}{\partial \bar{\xi}_{18}} \\ \frac{\partial M_{v+1}}{\partial \bar{\xi}_1}, \dots, \frac{\partial M_{v+1}}{\partial \bar{\xi}_{18}} \end{bmatrix},$$

and so forth.

Hence accumulation of these matrices, permits v to be written in the following manner:

$$v = \hat{Q} \delta \hat{\xi} + \hat{R} \delta t^* + \hat{S} \delta \hat{c},$$

so that the new system, Eqs. (21) which replaces Eqs. (20), can be written as:

$$\left[\hat{W}_a^{-1} + \hat{P}^T \hat{W}^{-1} \hat{P} \right] (\hat{\xi}_{q+1} - \hat{\xi}_q) = -\hat{W}_a^{-1} (\hat{\xi}_q - \hat{\xi}_a) - \hat{P}^T \hat{W}^{-1} M \quad (23)$$

This equation represents the system of all multilateration equations in action at fixed time t_j^* . Note that $W = \text{cov}(v v^T)$.

A2.6 EXPLICIT DEVELOPMENT OF MULTILATERATION EQUATIONS FOR A SEQUENCE OF TIMES (GROUPING BY BATCH)

To solve the M-functions, the subsystem of equations defined by Eq. (23) must be written at t_n distinct times, where $n > \ell$, i.e., where the number of interrogations is sufficiently large to permit a deterministic or overdetermined solution. To this end the following new matrices will now be constructed:

$$\hat{P}_N \equiv \begin{bmatrix} \hat{P}_1 \\ \hat{P}_2 \\ \vdots \\ \hat{P}_j \\ \vdots \\ \hat{P}_n \end{bmatrix} \xrightarrow{d} pn \times \ell, \quad \hat{M}_N \equiv \begin{bmatrix} \hat{M}_1 \\ \hat{M}_2 \\ \vdots \\ \hat{M}_j \\ \vdots \\ \hat{M}_n \end{bmatrix} \rightarrow pn \times 1, \quad v_N \equiv \begin{bmatrix} v_1 \\ v_2 \\ \vdots \\ v_j \\ \vdots \\ v_n \end{bmatrix} \xrightarrow{d} pn \times 1, \quad (24)$$

where

$$\hat{Q}_N \equiv \begin{bmatrix} \hat{Q}_1 \\ \vdots \\ \hat{Q}_n \end{bmatrix} \xrightarrow{d} pn \times \ell', \quad \hat{R}_N \equiv \begin{bmatrix} \hat{R}_1 & 0 & 0 & \cdots \\ & \hat{R}_2 & 0 & \cdots \\ & & \ddots & \vdots \\ \text{SYM} & & & \hat{R}_n \end{bmatrix} \xrightarrow{d} pn \times n$$

$$\hat{S}_N = \begin{bmatrix} \hat{S}_1 \\ \vdots \\ \hat{S}_n \end{bmatrix} \xrightarrow{d} pn \times (M+1)I, \quad \delta t_N^* = \begin{bmatrix} \delta t_1^* \\ \vdots \\ \delta t_n^* \end{bmatrix} \xrightarrow{d} n \times 1$$

so that:

$$v_N \equiv \hat{Q}_N \delta \hat{\xi} + \hat{R}_N \delta t_N^* + \hat{S}_N \delta \hat{c}.$$

The complete batch system to be solved is then written as:

$$\left[W_a^{-1} + \hat{P}_N^T W_N^{-1} \hat{P}_N \right] (\hat{\xi}_{q+1} - \hat{\xi}_q) = -W_a^{-1} (\hat{\xi}_q - \xi_a) - \hat{P}_N^T W_N^{-1} \hat{M}_N \quad (25)$$

whose solution by virtue of Eq. (16) is the estimate $\hat{\xi}_{q+1}$ where

$$\hat{\xi}_{q+1} = \hat{\xi}_q - \left[W_a^{-1} + \hat{P}_N^T W_N^{-1} \hat{P}_N \right]^{-1} \left[W_a^{-1} (\hat{\xi}_q - \xi_a) + \hat{P}_N^T W_N^{-1} \hat{M}_N \right] \quad (26)$$

with W taken as

$$W_N = \text{cov} \left(v_N v_N^T \right) \xrightarrow{d} pn \times pn. \quad (27)$$

Examination of Eq. (27) shows that the dimension of W_N becomes a problem if n is large, i.e., inversion of W_N must be performed to properly weight the system. This problem will be discussed presently. However, at this point the explicit form of W_N will be developed.

A2.7 DEVELOPMENT OF WEIGHTING MATRIX

Equation (18) displayed the expression for the weighting matrix W . The expression for W_N written in terms of the newly constructed matrices P_N , M_N , etc. is therefore given by:

$$W_N = W_N^* = Q_N \Lambda_{\xi}^{\Delta} Q_N^T + R_N \Lambda_{t*}^{\Delta} R_N^T + S_N \Lambda_c^{\Delta} S^T + R_N \Lambda_{t*c}^{\Delta} S_N^T + S_N \Lambda_{ct*}^{\Delta} R_N^T, \quad (28)$$

where it is evident that four terms are omitted due to the fact that

$$\Lambda_{\xi c}^{\Delta} = 0, \quad \Lambda_{t*\xi}^{\Delta} = 0,$$

namely, that the station coordinate modeling parameters $\bar{\xi}$ are not correlated with the polynomial fitting coefficients, and that the master clock times have no relationship to the $\bar{\xi}$. These assumptions are obviously true. Hence five covariances need to be defined from a structural point of view. It will be assumed herein that at step q , the covariances will be known, i.e., for $q = 0$ and at initiation of multilateration:

$$\Lambda_{\xi a}^{\Delta} = \begin{bmatrix} \sigma_{\xi_1}^2 & & 0 \\ & \ddots & \\ 0 & & \sigma_{\xi_l}^2 \end{bmatrix}, \quad \Lambda_{t*}^{\Delta} = \begin{bmatrix} \sigma_{t_1}^2 & & 0 \\ & \ddots & \\ 0 & & \sigma_{t_n}^2 \end{bmatrix} = U \sigma_{t*}^2,$$

and so forth. Obviously if data has already been processed via multilateration, and new data is input, the full available a priori covariances will be utilized.

The structure of the four square covariance matrices is as follows.
The to-be-solved for covariance matrix is given by:

$$\Lambda_{\xi}^{\Lambda} = \begin{bmatrix} \sigma_{\xi_1}^2 & \sigma_{\xi_1 \xi_2}^2 & \dots & \sigma_{\xi_1 \xi_l}^2 \\ & \sigma_{\xi_2}^2 & & \vdots \\ & & \ddots & \vdots \\ \text{SYM} & & & \sigma_{\xi_l}^2 \end{bmatrix}_q \xrightarrow{d} l \times l. \quad (29)$$

Similarly, the interrogation time covariance matrix can be specified as:

$$\Lambda_t^{\Lambda*} = \begin{bmatrix} \sigma_{t_1}^2 & 0 \\ & \ddots \\ 0 & \sigma_{t_n}^2 \end{bmatrix} = U \sigma_t^2 \xrightarrow{d} n \times n. \quad (30)$$

The covariance matrix for \hat{c} is obtained by noticing that:

$$\delta \hat{c} = \begin{bmatrix} \delta c_{01}, \delta c_{11}, \dots, \delta c_{M1} \mid \delta c_{02}, \dots, \delta c_{M2} \mid \dots \mid \delta c_{0I}, \dots, \delta c_{MI} \end{bmatrix} \quad (31)$$

and taking expected values of $\delta \hat{c} \delta \hat{c}^T$ which yields

$$\Lambda_{\hat{c}}^{\Lambda} = \begin{bmatrix} \Lambda_{c_1}^{\Lambda} & \Lambda_{c_1 c_2}^{\Lambda} & \dots & \dots \\ & \Lambda_{c_2}^{\Lambda} & & \vdots \\ & & \ddots & \vdots \\ \text{SYM} & & & \Lambda_{c_I}^{\Lambda} \end{bmatrix} \xrightarrow{d} (M+1)I \times (M+1)I \quad (32)$$

where $\Lambda_{C_i}^A$, $i = 1, 2, \dots, I$ are square matrices of dimension $(M + 1) \times (M + 1)$ which are obtained from the fitting polynomials.

In analogous form the covariance for $\bar{\xi}^A$ is obtained by noticing that

$$\delta \bar{\xi}^A = \begin{bmatrix} \delta \bar{\xi}_{11}^A, \dots, \delta \bar{\xi}_{s_1 1}^A & \delta \bar{\xi}_{s_1 2}^A, \dots, \delta \bar{\xi}_{s_2 2}^A & \dots & \delta \bar{\xi}_{s_{I-1} I}^A, \dots, \delta \bar{\xi}_{s_I I}^A \\ \delta \bar{\xi}_{s_{I+1}}^A, \delta \bar{\xi}_{s_{I+2}}^A, \dots, \delta \bar{\xi}_{\ell'}^A \end{bmatrix}^T, \quad (33)$$

namely, that the modeling $\bar{\xi}$ common to station 1 are grouped together, e.g., X_1, Y_1, Z_1, g_1 , followed by station 2, etc., until the last station I, after which all the constants common to all stations are listed, e.g., α_c, δ_c , etc. Hence, taking expected values of $\delta \bar{\xi} \delta \bar{\xi}^T$ yields:

$$\Lambda_{\bar{\xi}}^A = \begin{bmatrix} \Lambda_{s1} & 0 & 0 & \dots & 0 \\ & \Lambda_{s2} & & & \vdots \\ & & \ddots & & \vdots \\ & & & \Lambda_{sI} & \vdots \\ \text{SYM} & & & & \Lambda_K \end{bmatrix} \xrightarrow{d} \ell' \times \ell' \quad (34)$$

Finally, the cross covariance dimensions are:

$$\Lambda_{t^*c}^A \xrightarrow{d} n \times (M + 1) I.$$

The cross covariance is discussed later and as will be seen only exists under certain circumstances.

A2.8 COVARIANCE MATRIX OF TO-BE-SOLVED-FOR PARAMETERS

The structure of the covariance matrix of the to-be-solved-for parameters, $\Lambda_{\hat{\xi}}$ has been previously defined. The actual computation proceeds as follows. Let Eq. (11) be written in terms of the estimate $\hat{\xi}$ as:

$$T(\hat{\xi}) = \begin{bmatrix} \eta \\ v_j \end{bmatrix} \equiv e \quad . \quad (35)$$

Using the notation T to denote the true (errorless) solution, let Eq. (35) be expanded:

$$T(\hat{\xi}) = T(\tilde{\xi}_T) + \frac{\partial T}{\partial \tilde{\xi}} (\tilde{\xi}_T - \hat{\xi}) \quad .$$

Since by definition $T(\tilde{\xi}_T) \equiv 0$, it follows that

$$\frac{\partial T}{\partial \tilde{\xi}} (\tilde{\xi}_T - \hat{\xi}) = e \quad . \quad (36)$$

Squaring up and solving Eqs. (36) yields

$$\tilde{\xi}_T - \hat{\xi} = \left\{ \left[\frac{\partial T}{\partial \tilde{\xi}} \right]^T W^{-1} \left[\frac{\partial T}{\partial \tilde{\xi}} \right] \right\}^{-1} \left[\frac{\partial T}{\partial \tilde{\xi}} \right]^T W^{-1} e \quad ,$$

from which $E \left\{ (\tilde{\xi}_T - \hat{\xi}) (\tilde{\xi}_T - \hat{\xi})^T \right\} = \text{cov}(\hat{\xi}) \equiv \Lambda_{\hat{\xi}}$ can be computed as:

$$\Lambda_{\hat{\xi}} = \left\{ \left[\frac{\partial T}{\partial \tilde{\xi}} \right]^T W^{-1} \left[\frac{\partial T}{\partial \tilde{\xi}} \right] \right\}^{-1} \left[\frac{\partial T}{\partial \tilde{\xi}} \right]^T W^{-1} e e^T W^{-1} \left[\frac{\partial T}{\partial \tilde{\xi}} \right] \left\{ \left[\frac{\partial T}{\partial \tilde{\xi}} \right]^T W^{-1} \left[\frac{\partial T}{\partial \tilde{\xi}} \right] \right\}^{-1} \quad .$$

However since $e e^T = W$ it is evident that:

$$\Lambda_{\xi}^{\Delta} = \left\{ \left[\frac{\partial T}{\partial \xi} \right]^T W^{-1} \left[\frac{\partial T}{\partial \xi} \right] \right\}^{-1} \quad (37)$$

Furthermore since by Eq. (17)

$$\frac{\partial T}{\partial \xi} = \begin{bmatrix} U \\ \frac{\partial M}{\partial \xi} \end{bmatrix} ,$$

a further computation yields:

$$\Lambda_{\xi}^{\Delta} = \left[W_a^{-1} + P_q^T W_v^{-1} P_q \right]^{-1} , \quad (38)$$

which is nothing more than the fundamental matrix of the Newton-Raphson equations (Eqs. 19).

A2.9 FITTING COEFFICIENT COVARIANCE

The coefficients c_0, c_1, \dots, c_M of the fitting process are obtained by solution of the system

$$Ac = d + \Delta d , \quad (39)$$

where

$$A \equiv \begin{bmatrix} 1, t_1 - t_0, (t_1 - t_0)^2, \dots, (t_1 - t_0)^M \\ 1, t_2 - t_0, (t_2 - t_0)^2, \dots, (t_2 - t_0)^M \\ \vdots \\ 1, t_k - t_0, (t_k - t_0)^2, \dots, (t_k - t_0)^M \end{bmatrix}$$

$$c \equiv \begin{bmatrix} c_0 \\ c_1 \\ . \\ . \\ c_{M+1} \end{bmatrix}, \quad d \equiv \begin{bmatrix} d_1 \\ d_2 \\ . \\ . \\ d_k \end{bmatrix}, \quad \Delta d \equiv \begin{bmatrix} \Delta d_1 \\ \Delta d_2 \\ . \\ . \\ \Delta d_k \end{bmatrix}$$

with

$t_i \equiv$ station clock times,

$d_i \equiv$ uncalibrated data type,

$\Delta d_i \equiv$ atmospheric calibration for each t_i ,

$k =$ number of data points.

Equation (39) is valid if error free data were available. However, since only estimates of t , d , and Δd are available, namely, \hat{t} , \hat{d} , $\hat{\Delta d}$ substitution of these estimates into Eq. (39) yield

$$\left(\hat{A} + \frac{\partial A}{\partial t} \delta t \right) c = \hat{d} + \delta \hat{d} + \Delta d + \frac{\partial \Delta d}{\partial \omega} \delta \omega + \frac{\partial \Delta d}{\partial t} \delta t, \quad (40)$$

where it is assumed that an atmospheric calibration model is available which permits a calibration Δd_i to be computed at each t_i from a set of constants $\omega_1, \omega_2, \dots, \omega_R$ which have estimated uncertainties, namely,

$$\Delta d_i = \Delta d(t_i, \omega_1, \dots, \omega_R).$$

In terms of the random errors δt , δd and uncertainty $\delta \omega$, Eq. (40) is rewritten as:

$$\hat{A}c = \hat{d} + \Delta \hat{d} + \left[\frac{\partial \Delta d}{\partial t} - \frac{\partial A}{\partial t} c \right] \delta t + \frac{\partial \Delta d}{\partial \omega} \delta \omega + \delta d$$

or as

$$\hat{A}c = \hat{d} + \Delta\hat{d} + [D - T] \delta t + K\delta\omega + \delta d \quad (41)$$

where

$$D \equiv \frac{\partial \Delta d}{\partial t} = \begin{bmatrix} \frac{\partial \Delta d}{\partial t_1} & 0 & 0 & \dots \\ & \frac{\partial \Delta d}{\partial t_2} & 0 & \dots \\ \text{SYM} & & \ddots & \vdots \\ & & & \frac{\partial \Delta d}{\partial t_k} \end{bmatrix}, \quad K \equiv \frac{\partial \Delta d}{\partial \omega} = \begin{bmatrix} \frac{\partial \Delta d_1}{\partial \omega_1} & \frac{\partial \Delta d_1}{\partial \omega_2} & \dots & \frac{\partial \Delta d_1}{\partial \omega_R} \\ \frac{\partial \Delta d_2}{\partial \omega_1} & \frac{\partial \Delta d_2}{\partial \omega_2} & \dots & \vdots \\ \vdots & & \ddots & \\ \frac{\partial \Delta d_k}{\partial \omega_1} & \dots & & \frac{\partial \Delta d_k}{\partial \omega_R} \end{bmatrix},$$

where $D \xrightarrow{d} k \times k$, $K \xrightarrow{d} k \times R$.

The structure of T now needs to be defined. The quantity $\partial A / \partial t$ is not a matrix, but a tensor; however, the i^{th} component is a matrix, namely,

$$\frac{\partial A}{\partial t_i} = \begin{bmatrix} & & 0 \\ 0, 1, 2(t_i - t_0), \dots, M(t_i - t_0)^{M-1} \\ & & 0 \end{bmatrix} \xrightarrow{d} k \times (M+1).$$

The notation implies that for each t_i , $\partial A / \partial t_i$ is the zero matrix except for the row containing t_i .

A formal computation now yields

$$\frac{\partial A}{\partial t_i} c = \begin{bmatrix} & & 0 \\ c_1 + 2c_2(t_i - t_0) + \dots + Mc_M(t_i - t_0)^{M-1} \\ & & 0 \end{bmatrix} \xrightarrow{d} k \times 1.$$

so that

$$T \equiv \left[\frac{\partial A}{\partial t_1} c, \frac{\partial A}{\partial t_2} c, \dots, \frac{\partial A}{\partial t_k} c \right] \quad (42)$$

or by redefinition:

$$T \equiv \begin{bmatrix} \left\{ c_1 + 2c_2(t_1 - t_0) + \dots + Mc_M(t_1 - t_0)^{M-1} \right\} & 0 & 0 & 0 & \dots & \dots & \dots \\ 0 & \left\{ c_1 + 2c_2(t_2 - t_0) + \dots + Mc_M(t_2 - t_0)^{M-1} \right\} & 0 & \dots & \dots & \dots \\ \text{SYM} & & & & & & \\ & & & & & & \end{bmatrix} \quad (43)$$

$$z = \begin{bmatrix} d_1 & & & 0 \\ & d_2 & & \\ & & \ddots & \\ 0 & & & d_k \end{bmatrix} \xrightarrow{d \rightarrow k \times k.}$$

Equation (41) can now be written as

$$\hat{A}c = \hat{d} + \Delta \hat{d} + \beta \quad (44)$$

where the associated uncertainty is grouped as

$$\beta = \tilde{K} \delta t + \tilde{K} \delta \omega + \delta d.$$

with $\tilde{K} \equiv D - T$.

The covariance of β is obtained directly as:

$$W_\beta = \text{cov } \beta = \tilde{K} \Lambda_t \tilde{K}^T + K \Lambda_\omega K^T + \Lambda_d \quad (45)$$

and using minimum variance weighting

$$\hat{c} = \left[\hat{A}^T W_{\beta}^{-1} \hat{A} \right]^{-1} \hat{A}^T W_{\beta}^{-1} [\hat{d} + \Delta \hat{d}]. \quad (46)$$

The covariance of \hat{c} is now directly obtained by noticing that Eq. (44) can be written as

$$\hat{A}^T W_{\beta}^{-1} \hat{A} c = \hat{A}^T W_{\beta}^{-1} [\hat{d} + \Delta \hat{d}] + \hat{A}^T W_{\beta}^{-1} \beta$$

which upon subtraction of Eq. (46) in the form

$$\hat{A}^T W_{\beta}^{-1} \hat{A} \hat{c} = \hat{A}^T W_{\beta}^{-1} [\hat{d} + \Delta \hat{d}]$$

yields

$$\hat{A}^T W_{\beta}^{-1} \hat{A} [c - \hat{c}] = \hat{A}^T W_{\beta}^{-1} \beta \quad (47)$$

or

$$\delta \hat{c} = \left[\hat{A}^T W_{\beta}^{-1} \hat{A} \right]^{-1} \hat{A}^T W_{\beta}^{-1} \beta \quad (48)$$

Hence

$$\text{cov} \begin{pmatrix} \hat{c} & \hat{c}^T \end{pmatrix} = \left[\hat{A}^T W_{\beta}^{-1} \hat{A} \right]^{-1} \hat{A}^T W_{\beta}^{-1} \text{cov}(\beta \beta^T) W_{\beta}^{-1} \hat{A} \left[\hat{A}^T W_{\beta}^{-1} \hat{A} \right]^{-T}$$

or

$$\Lambda_{\hat{c}} = \left[\hat{A}^T W_{\beta}^{-1} \hat{A} \right]^{-1}. \quad (49)$$

The explicit form of the data time and data covariances is given by,

$$\Lambda_t = U\sigma_t^2, \quad \Lambda_d = U\sigma_d^2$$

while the covariance in the modeling constants of the atmosphere Λ_ω is constructed from the respective variances as

$$\Lambda_\omega \equiv \begin{bmatrix} \sigma_{\omega_1}^2 & & & 0 \\ & \sigma_{\omega_2}^2 & & \\ & & \ddots & \\ 0 & & & \sigma_{\omega_R}^2 \end{bmatrix}, \quad (50)$$

and σ_t , σ_d are the standard deviations in the station time and data respectively. Note that between two separate stations with coefficients c_i , c_j the atmospheric model correlates the coefficients as:

$$\Lambda_{\hat{c}_i \hat{c}_j} = \left[\hat{A}_i^T W_{\beta_i}^{-1} \hat{A}_i \right]^{-1} \hat{A}_i W_{\beta_i}^{-1} \Lambda_K W_{\beta_j}^{-1} \hat{A}_j \left[\hat{A}_j^T W_{\beta_j}^{-1} \hat{A}_j \right]^{-1},$$

where

$$\Lambda_K = K \Lambda_\omega K^T.$$

A2.10 COVARIANCE OF FITTING COEFFICIENTS WITH INTERROGATION TIMES

Equation (28) contained the covariance Λ_{ct}^* . This covariance will be zero if an independent master clock is used to define the interrogation times. If, however, a station clock is used as the master clock and the interrogation time is taken to be a subset of the station time t then $\Lambda_{ct}^* \neq 0$. In this case

$$\Lambda_{ct}^* = E[\delta c(t_j - \hat{t}_j)^T] = E[\delta c \delta t_j^{*T}].$$

Hence using Eq. (48) and omitting all correlations associated with W and d

$$\begin{aligned} \Lambda_{ct}^* &= \left[\hat{A}^T W_\beta^{-1} \hat{A} \right]^{-1} \hat{A}^T W_\beta^{-1} \tilde{K} E \left(\delta t \delta t_j^{*T} \right) \\ &= \left[\hat{A}^T W_\beta^{-1} \hat{A} \right]^{-1} \hat{A}^T W_\beta^{-1} \tilde{K} \Lambda_{tt}^*, \end{aligned} \quad (51)$$

where

$$\Lambda_{tt}^* = \begin{bmatrix} \delta t_1 \\ \delta t_2 \\ \vdots \\ \delta t_k \end{bmatrix} \begin{bmatrix} \delta t_1^* & \dots & \delta t_n^* \end{bmatrix} = \begin{bmatrix} \delta_i^j & & 0 \\ & \delta_i^j & \\ 0 & & \delta_i^j \end{bmatrix} \sigma_t^2 \xrightarrow{d} k \times n,$$

where $\delta_i^j = 0$, $i \neq j$; $\delta_i^j = 1$, $i = j$.

A2.11 SEQUENTIAL BATCH PROCESSING TECHNIQUE

The system of equations defining the batch solution, B, are given by relationship (25), which contains the matrices:

$$C \equiv \hat{P}_N^T W_N \hat{P}_N, \quad D \equiv P_N W_N^{-1} \hat{M}_N. \quad (52)$$

The subscript B will now be introduced to denote a batch of pn equations valid in interval T^* . Hence for a subsequent batch valid in the next T^* interval (next fitting span) the C and D matrices are partitioned (expanded) as:

$$\begin{bmatrix} \hat{P}_{NB} \\ \text{---} \\ \hat{P}_{N(B+1)} \end{bmatrix}^T \begin{bmatrix} W_{NB}^{-1} & \text{---} \\ \text{---} & W_{N(B+1)}^{-1} \end{bmatrix} \begin{bmatrix} \hat{P}_{NB} \\ \text{---} \\ \hat{P}_{N(B+1)} \end{bmatrix}, \quad \begin{bmatrix} \hat{P}_{NB} \\ \text{---} \\ \hat{P}_{N(B+1)} \end{bmatrix}^T \begin{bmatrix} W_{NB}^{-1} & \text{---} \\ \text{---} & W_{N(B+1)}^{-1} \end{bmatrix} \begin{bmatrix} \hat{M}_{NB} \\ \text{---} \\ \hat{M}_{N(B+1)} \end{bmatrix}. \quad (53)$$

It is evident that upon multiplication of the partitioned matrices

$$\begin{aligned} C_{B+1} &\equiv \hat{P}_{NB}^T W_{NB}^{-1} \hat{P}_{NB} \\ &+ \hat{P}_{N(B+1)}^T W_{N(B+1)}^{-1} \hat{P}_{N(B+1)} = C_B + \hat{P}_{N(B+1)}^T W_{N(B+1)}^{-1} \hat{P}_{N(B+1)} \end{aligned} \quad (54)$$

$$\begin{aligned} D_{B+1} &\equiv \hat{P}_{NB}^T W_{NB}^{-1} \hat{M}_{NB} \\ &+ \hat{P}_{N(B+1)}^T W_{N(B+1)}^{-1} \hat{M}_{N(B+1)} = D_B + \hat{P}_{N(B+1)}^T W_{N(B+1)}^{-1} \hat{M}_{N(B+1)}. \end{aligned}$$

In essence then C_{B+1} and D_{B+1} can be computed recursively from the initial values C_B and D_B . The matrix C_{B+1} obviously will be singular until sufficient batch data are processed such that a deterministic system of equations is available. Once sufficient data is processed such that system (54) is overdetermined, then an inversion of C becomes possible and the solution for $\Delta \hat{\xi}_q$, the correction to the to-be-solved for parameters, can be obtained.* This will require inversion of an $\ell \times \ell$ matrix. There is really no point however in performing this inversion until all the available data has been accumulated in C . At the final accumulation ($B = B_f$) the inversion yields $\Delta \hat{\xi}_q$ and

$$\hat{\xi}_{q+1} = \hat{\xi}_q + \Delta \hat{\xi}_q \quad (55)$$

along with

$$\Lambda_{\hat{\xi}} = \left[W_a^{-1} + C_{B+1} \right]^{-1} \quad (56)$$

A return is now made to the first data batch and the accumulation procedure repeated to obtain the $q+1$ correction. This process is continued until

$$\Delta \hat{\xi}_{q+1} < \epsilon$$

where ϵ is a specified tolerance. Note that in the flow diagram (Figure A2.1)

$$C_q = \Lambda_{\hat{\xi}}^{-1} + C_{B+1} \quad (57)$$

$$D_q = \Lambda_{\hat{\xi}}^{-1} + D_{B+1}$$

namely the a priori covariances are loaded into C and D .

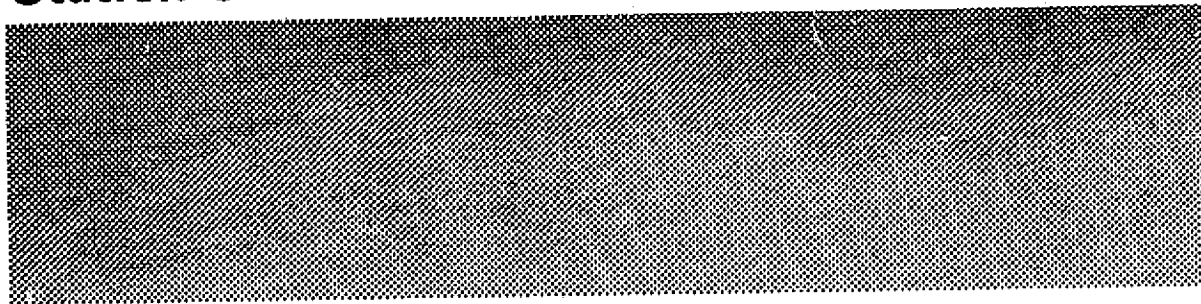
*Obviously, inclusion of the a priori estimates will always permit inversion, but as long as C_B is rank deficient maximum improvement will not be possible.

A2.12 REFERENCES

- [2.1] Bierman, G.J., "Computational Aspects of Discrete Sequential Estimation," JPL TM 900-661, May 1974.*
- [2.2] Gura, I.A., "An Algebraic Approach to Optimal State Estimation," HAC, SSD 70072R, March 1967.
- [2.3] Bierman, G.J., Personal Communication.
- [2.4] Escobal, P.R., "Explicit Matrix Solution for Obtaining Minimum Variance Estimates of Parameters Contained in a Large Set of Nonlinear Equations," JPL EM 391-601, 6 January 1975.*

*JPL internal document.

A3. Explicit Analytical Model for Earth Tide Station Coordinate Deflections



Abstract

An analytic model for the three-dimensional movement of ground stations due to Moon/Sun gravitational forces is developed. Explicit expressions for radial, latitudinal and longitudinal displacements are presented. These expressions will permit modeling of the Earth tide effects to accuracy levels which are of fundamental importance in multilateration studies. The equations peculiar to the model are transformed into a topocentric system such that the time variation of three dimensional interstation coordinates can be computed. The manner in which analytic equations not containing the tidal model transform into equations possessing the model is discussed from a Newton-Raphson point of view. The effect of ocean loading is briefly discussed and modifications to the model are outlined. The partial derivatives of all model parameters, though not presented herein, have been programmed; they are important for an exact error analysis of the model, i.e., to extract the covariance matrix of the model.

PRECEDING PAGE BLANK NOT FILMED

A3.1 INTRODUCTION

The accurate determination of interstation coordinate distances for geophysical applications presents a problem when accuracies of centimeter level are desired with stations located on baselines of increasing extension. This problem is occasioned by the plasticity of the Earth. Accelerations due to the Moon and Sun acting on the surface of the Earth tend to raise and lower the surface point under investigation so that the relative location of two points separated by intercontinental distances can have three-dimensional displacements relative to each other of about 30 centimeters.

In this appendix, equilibrium theory is used to obtain a method wherein the amplitude variation can be computed to within 3 centimeters. Needless to say, for future work in the area of earthquake prediction this accuracy level is not sufficient. To reach the second plateau where accuracies of 1 centimeter are required, the ocean tide effects must be analyzed [3.1, 3.7] (Appendix A4).

To accomplish the difficult task of determining the ocean tide deformations, equilibrium theory can be used to develop the shape of the sea envelope engendered by the gravitational, centripetal and Moon/Sun potentials. The ocean surface can then be subdivided into a finite number of sea water mascons and the potential at a given ground station can be obtained by numerical integration over the ocean regions of the entire Earth. Elastic theory can then be used to predict the deflection occasioned at the station by the loading sea water potential (see Appendix A4). Further accuracy requires the use of a gravimeter (in the simplest terms, a spring with a weight attached) at each station of interest and perhaps a tiltmeter. By taking observations of the gravity variations for a period of one month, a set of constants for each station can be obtained which will be valid for an extended period (years). These constants can then be used to model the station fluctuations to the millimeter level. Since the instruments used to obtain the local gravity also sense the perturbing effects of the Moon and Sun, the segregation of the ground fluctuations caused by these bodies must be analyzed separately. Bearing this in mind, the equilibrium model is developed herein and adopted for the GEOS-3 project, with provision for inclusion of the ocean tide model (Appendix A4), if time permits.

This level of sophistication is necessary for the GEOS-3 project due to the wide baselines under consideration and because the error committed in the omission of the model is too great if the laser accuracy is of the order of 15 to 20 cm. Obviously, as soon as laser hardware is constructed as outlined in [3.5], these corrections will be of absolute necessity.

A3.2 EXPLICIT DEVELOPMENT OF THE TIDAL POTENTIAL

Consider Figure A3.1 which depicts the Moon and Sun in a geocentric inertial coordinate system with an Earth ground station located at point P_s .

From the two spherical triangles peculiar to the figure, it follows that the elongation ψ of the Moon and Sun is given by:

$$\begin{aligned}\cos \psi_{\odot} &= \sin \delta_{\odot} \sin \beta + \cos \delta_{\odot} \cos \beta \cos (HA_{\odot} + \zeta_{\odot}) \\ \cos \psi_{\ominus} &= \sin \delta_{\ominus} \sin \beta + \cos \delta_{\ominus} \cos \beta \cos (HA_{\ominus} + \zeta_{\ominus})\end{aligned}\quad (1)$$

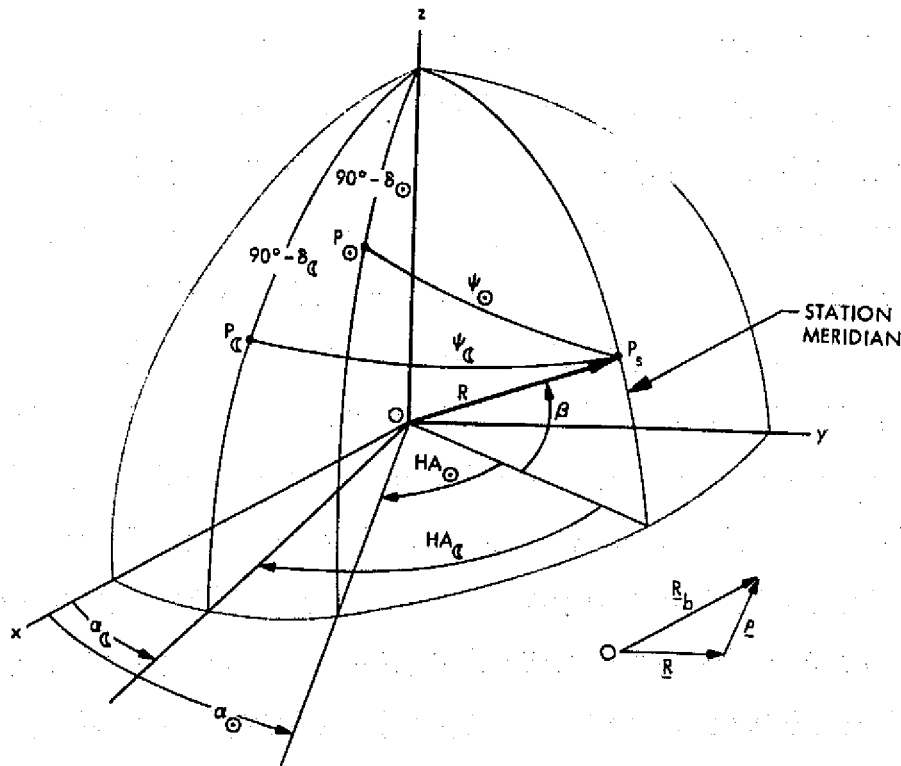


Figure A3.1. Pertinent Geometry

where

$\zeta \equiv$ phase angle

$\delta \equiv$ declination of the Moon (\odot) or Sun (\odot)

$\beta \equiv$ reduced latitude of the Earth station

HA \equiv hour angle of the Moon or Sun.

The hour angle of the Moon and Sun can be determined by computing the station true local sidereal time, θ , and right ascension of the Moon and Sun so that

$$HA = \theta - \alpha, \quad (2)$$

where α is the right ascension of the Moon or Sun. Hence, at universal time t , knowing α and δ along with the reduced station latitude, β , permits the elongation angle ψ to be determined. The reduced latitude [3.4] is defined by:

$$\beta = \phi' + \sin^{-1} \left\{ \frac{H}{R} \sin(\phi - \phi') \right\},$$

where H is the station elevation measured normal to and above the adopted ellipsoid, R is the distance from the center of the Earth to the station, ϕ is the geodetic latitude and ϕ' is the geocentric latitude. The angle β , as will be presently seen, plays an important part in the derivation of the tidal potential.

To determine the disturbing or tidal potential consider the acceleration \underline{a}_b of a specific celestial body, b , acting at point P_s . From [3.4]:

$$\underline{a}_b = k_b^2 \left(\frac{\underline{p}}{\rho^3} - \frac{\underline{R}_b}{R_b^3} \right),$$

where $k_b^2 = Gm_b$ with G being the universal gravitational constant, m_b , the mass of the body and:

\underline{p} = vector position between body b and the point at P_s ,

\underline{R}_b = vector position between body b and the origin O .

Now since $\underline{\rho} = \underline{R}_b - \underline{R}$, where \underline{R} is the position vector of P_s relative to O ,

$$k_b^2 \frac{\underline{\rho}}{\rho^3} = -\nabla \left(\frac{k_b^2}{\rho} + C_1 \right),$$

where C_1 is a constant. Furthermore since \underline{R}_b is not a function of \underline{R} it is possible to construct the expression

$$k_b^2 \frac{\underline{R} \cdot \underline{R}_b}{R_b^3} + C_2$$

and note that:

$$k_b^2 \frac{\underline{R}_b}{R_b^3} = \nabla \left(\frac{k_b^2 \underline{R} \cdot \underline{R}_b}{R_b^3} + C_2 \right).$$

Obviously

$$k_b^2 \left(\frac{\underline{\rho}}{\rho^3} - \frac{\underline{R}_b}{R_b^3} \right) = \nabla k_b^2 \left(\frac{1}{\rho} - \frac{\underline{R} \cdot \underline{R}_b}{R_b^3} + C \right) \equiv \nabla \Phi_b,$$

where Φ_b is the disturbing potential of the body under consideration. It should be noted in accordance with Figure A3.1 that $\underline{R} \cdot \underline{R}_b = RR_b \cos \psi_b$, so that:

$$\Phi_b = k_b^2 \left(\frac{1}{\rho_b} - \frac{R \cos \psi_b}{R_b^2} + C_b \right), \quad (3)$$

where the subscript b represents the Moon or Sun, ρ_b is the slant range from the station to the Moon or Sun, R_b is the distance from the Earth to the Moon or Sun, R is the distance from the center of the Earth to the station, and C_b is a

constant. Obviously $\nabla\Phi_b$ yields the components of acceleration sensed at the station due to body b.

If C_b is taken to make Φ_b vanish at O then *

$$\Phi_b = k_b^2 \left(\frac{1}{\rho_b} - \frac{1}{R_b} - \frac{R \cos \psi_b}{R_b^2} \right). \quad (4)$$

Since the slant range can be written via the law of cosines as:

$$\frac{1}{\rho_b} = \frac{1}{R_b} \left[1 - 2 \frac{R}{R_b} \cos \psi_b + \frac{R^2}{R_b^2} \right]^{-1/2}$$

and since the last two terms in the bracket are $\ll 1$ expansion via the binomial theorem yields

$$\frac{1}{\rho_b} = \frac{1}{R_b} \left[P_0(\cos \psi_b) + \frac{R}{R_b} P_1(\cos \psi_b) + \frac{R^2}{R_b^2} P_2(\cos \psi_b) + \dots \right],$$

where $P_n(\cos \psi_b)$ are the Legendre polynomials:

$$\left. \begin{aligned} P_0(\cos \psi_b) &= 1 \\ P_1(\cos \psi_b) &= \cos \psi_b \\ P_2(\cos \psi_b) &= \frac{3}{2}(\cos^2 \psi_b - \frac{1}{3}) \\ P_3(\cos \psi_b) &= \frac{1}{2}(5 \cos^2 \psi_b - 3 \cos \psi_b) \\ &\vdots \\ P_n \end{aligned} \right\} \quad (5)$$

*Only then are the simple expressions, Eqs (7), valid as explained in [3.3].

Hence

$$\frac{1}{\rho_b} = \frac{1}{R_b} + \frac{R}{R_b^2} \cos \psi_b + \frac{R^2}{R_b^2} P_2(\cos \psi_b) + \frac{R^3}{R_b^3} P_3(\cos \psi_b) + \dots$$

and

$$\Phi_b = k_b^2 \frac{R^2}{R_b^3} \left[P_2(\cos \psi_b) + \frac{R}{R_b} P_3(\cos \psi_b) + \dots \right].$$

Now since $k_b^2 = Gm_b$, adopting a set of units for R , say Earth radii, the combined potential for the Moon and Sun will be:

$$\begin{aligned} \Phi_T = \frac{k_{\odot}^2}{R_{\odot}^3} R^2 \left[P_2(\cos \psi_{\odot}) + \frac{R}{R_{\odot}} P_3(\cos \psi_{\odot}) + \dots \right] \\ + \frac{k_{\oplus}^2}{R_{\oplus}^3} R^2 \left[P_2(\cos \psi_{\oplus}) + \frac{R}{R_{\oplus}} P_3(\cos \psi_{\oplus}) + \dots \right], \end{aligned} \quad (6)$$

where terms of order R^4/R_b^5 are negligible.

A3.3 EFFECT OF TIDAL POTENTIALS

The Earth considered as a plastic body yields to the tide-raising potentials. Love in 1911 [3.2] demonstrated that to determine the amount of Earth yielding it is possible to neglect dynamic effects and use equilibrium theory. Hence for an increase in potential at any point, the increased surface elevation (radially) will be proportional to the disturbing (tidal) potential scaled by the local gravity at the point. Takeuchi [3.3] performs a rather detailed computation and obtains:

$$\Delta R = \frac{h}{g} \Phi_T, \quad B = \frac{\ell}{gR} \frac{\partial \Phi_T}{\partial \beta}, \quad \Delta \lambda = \frac{\ell}{gR \cos \beta} \frac{\partial \Phi_T}{\partial \lambda} \quad (7)$$

(in the notation adopted herein) for the plastic deformation of the Earth in the radius, latitude and longitude coordinates where h and ℓ are numerical factors called the Love and Shida numbers, respectively. Observations of the tidal tilts of the Earth's surface, the Chandler period, etc., can be used to determine these numbers. Presently, to use Eq. (7):

$$h = 0.60, \quad \sigma_h = 0.1$$

$$\ell = 0.075, \quad \sigma_\ell = 0.005$$

with g_0 obtained from the International Gravity Formula (modified 1968) in gals as [3.6]:

$$g_0 = 978.0264 (1 + 0.00530244 \sin^2 \phi' + 0.00001196 \sin^2 2\phi'), \quad \sigma_g = 0.1 \text{ mgal}$$

and g obtained via the Bouguer anomaly as:

$$g = g_0 + (200\pi G\rho - 0.3086 \times 10^{-3})H$$

where H is the height in meters, G is the universal gravitational constant and ρ is the mean density of the mass anomaly above sea level (mountains, etc.).

A3.4 COMPUTATION OF DEFORMATIONS

Given the universal time, the true sidereal time is computed and the right ascensions, declinations and distance of the Moon and Sun are obtained. Equation (6) is now written as:

$$\Phi_T = \frac{k_C^2 R_C^2}{R_C^3} \left[P_{2C} + \frac{R}{R_C} P_{3C} \right] + \frac{k_\odot^2 R_\odot^2}{R_\odot^3} \left[P_{2\odot} + \frac{R}{R_\odot} P_{3\odot} \right] \quad (8)$$

so that the two appropriate partials for the calculation of the Earth deformations are:

$$\frac{\partial \Phi_T}{\partial \beta} = \left\{ \frac{k_C^2 R^2}{R_C^3} \left[+3 \cos \psi_C - \frac{R}{R_C} \left(\frac{3}{2} - \frac{15}{2} \cos^2 \psi_C \right) \right] \right\} \frac{\partial(\cos \psi_C)}{\partial \beta} \\ + \left\{ \frac{k_\odot^2 R^2}{R_\odot^3} \left[+3 \cos \psi_\odot - \frac{R}{R_\odot} \left(\frac{3}{2} - \frac{15}{2} \cos^2 \psi_\odot \right) \right] \right\} \frac{\partial(\sin \psi_\odot)}{\partial \beta}$$

or defining the brackets by G_C and G_\odot

$$\frac{\partial \Phi_T}{\partial \beta} = G_C \frac{\partial(\cos \psi_C)}{\partial \beta} + G_\odot \frac{\partial(\sin \psi_\odot)}{\partial \beta},$$

with a similar expression holding for $\partial \Phi_T / \partial \lambda$.

Note that $\cos \psi$ is obtained from Eq. (1) as

$$\cos \psi_b = \sin \delta_b \sin \beta + \cos \delta_b \cos \beta \cos (\theta - \alpha_b)$$

with

$$\theta = \theta_g + \lambda$$

where θ_g is taken as the true Greenwich sidereal time at the given Universal time. Hence

$$\frac{\partial(\cos \psi_b)}{\partial \beta} = + \sin \delta_b \cos \beta - \cos \delta_b \sin \beta \cos (\theta - \alpha_b) \equiv G'$$

$$\frac{\partial(\cos \psi_b)}{\partial \lambda} = - \cos \delta_b \cos \beta \sin (\theta - \alpha_b) \equiv G''$$

and the explicit partial derivatives become

$$\frac{\partial \Phi_T}{\partial \beta} = G_C G'_C + G_O G'_O, \quad \frac{\partial \Phi}{\partial \lambda} = G_C G''_C + G_O G''_O \quad (9)$$

so that

$$\Delta R = \frac{h}{g} \Phi_T, \quad \Delta \beta = \frac{\ell}{gR} (G_C G'_C + G_O G'_O), \quad \Delta \lambda = \frac{\ell}{gR \cos \beta} (G_C G''_C + G_O G''_O) \quad (10)$$

are the closed expressions for the radial, latitudinal and longitudinal plastic deformation of the Earth at a given station.

The rectangular deflections are obtained by differentiation of

$$\begin{aligned} X_G &= R \cos \beta \cos \lambda \\ Y_G &= R \cos \beta \sin \lambda \\ Z_G &= R \sin \beta \end{aligned} \quad (11)$$

as

$$\begin{aligned} \Delta X_G &= \Delta R \cos \beta \cos \lambda - \Delta \beta R \sin \beta \cos \lambda - \Delta \lambda R \cos \beta \sin \lambda \\ \Delta Y_G &= \Delta R \cos \beta \sin \lambda - \Delta \beta R \sin \beta \sin \lambda + \Delta \lambda R \cos \beta \cos \lambda \\ \Delta Z_G &= \Delta R \sin \beta + \Delta \beta R \cos \beta, \end{aligned} \quad (12)$$

where if β is not available (usually geodetic coordinates ϕ are given), the computation of geocentric coordinates proceeds from the standard formula

$$\beta = \tan^{-1} \left[(1 - f)^2 \tan \phi \right] + \sin^{-1} \left\{ \frac{H}{R} \sin \left\{ \phi - \tan^{-1} \left[(1 - f)^2 \tan \phi \right] \right\} \right\}, \quad (13)$$

where the flattening of the station meridian is given by

$$f = \frac{a - b}{a}$$

with a being the equatorial and b the polar Earth radius. Obviously the meridian deformation is

$$\Delta f = \frac{b}{a^2} \Delta a - \frac{\Delta b}{a},$$

where Δa is the radial deflection of the meridian equatorial radius, namely from Eq. (10)

$$\Delta a = \frac{h}{g} \Phi_T (\beta = 0^\circ, \lambda = \lambda)$$

and Δb is the polar deflection, i.e.,

$$\Delta b = \frac{h}{g} \Phi_T (\beta = 90^\circ, \lambda = 0).$$

The expressions for ψ , Eq. (1) are

$$\cos \psi_0 \equiv \cos \delta_b \cos(\theta - \alpha_b)$$

$$\cos \psi_{90} \equiv \sin \delta_b$$

with the understanding that δ and α have implied \textcircled{C} and \textcircled{O} subscripts. Having the value of Δf , Eq. (13), with f' replacing f ($f' = f + \Delta f$) now yields the correct value of β . Note that

$$\phi' = \tan^{-1} \left[(1 - f')^2 \tan \phi \right] \quad (14)$$

$$\beta = \phi' + \sin^{-1} \left[\frac{H}{R} \sin(\phi - \phi') \right]$$

where f' is now taken as the mean flattening of the adopted ellipsoid.

A3.5 TRANSFORMATION OF COORDINATES

In this Section much reference will be made to the following Figures.

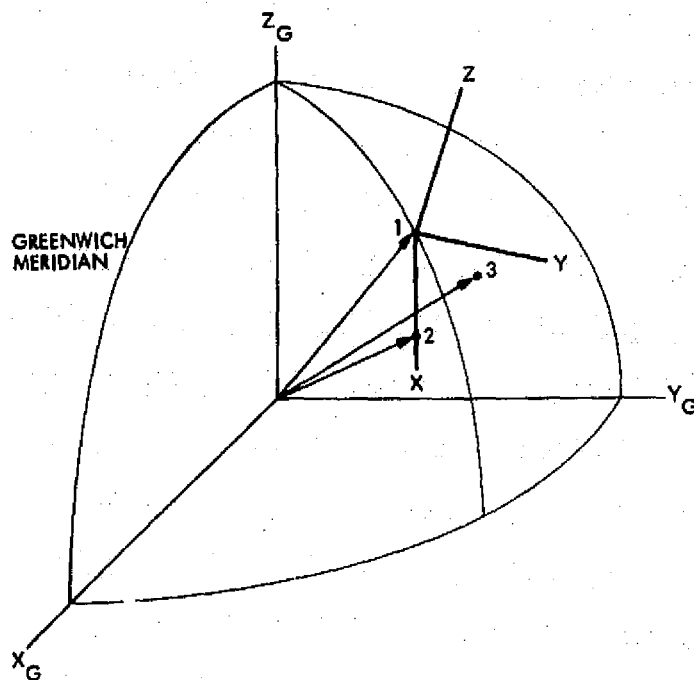


Figure A3.2. Greenwich and Geometric Coordinate System

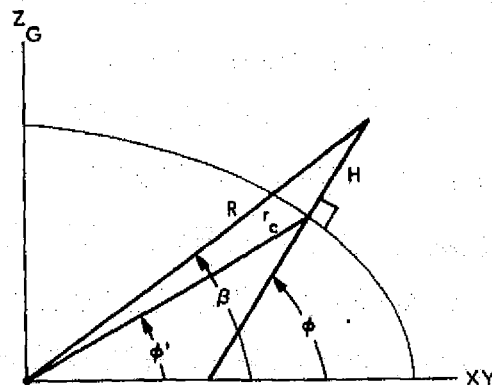


Figure A3.3. Oblate Spheroidal Model for Station Coordinates

The previous formulas for the station coordinate deflections are derived relative to the Earth-fixed Greenwich geographical coordinate system (Figure A3.2). To obtain the deflections in the adopted geometric coordinate system the following procedure needs to be followed. In the geometric coordinate system, the origin is defined to be at ϕ_1, λ_1, H_1 where ϕ is the geodetic latitude, λ is the East longitude of the station and H is the elevation above and measured normal to the adopted geoid. Equation (14) permits the origin to be specified as:

$$\phi_1', \lambda_1', H_1$$

Now from [3.4] the radial distance from the center of the Earth to the surface of the geoid is given by (See Fig. A3.3):

$$r_c^2 = a_e^2 [1 - (2f' - f'^2)] / [1 - (2f' - f'^2) \cos^2 \phi']$$

and by the law of cosines:

$$R = [r_c^2 + H^2 + 2r_c H \cos(\phi - \phi')]^{1/2} \quad (15)$$

Obviously, the values of ϕ_1, λ_1, H_1 can be transformed to ϕ_1', λ_1', R_1 by use of Eqs. (13) and (14) under the assumption that the values ϕ_1, λ_1, H_1 which denote the origin have no initial tidal effects. Specifically it is assumed that, in the coordinates of the origin, the periodic tidal variations occasioned by Moon, Sun and ocean tides have averaged out over the semi-infinite period used to determine the numerical values of these coordinates. By the same reasoning the coordinates ϕ_2', λ_2', R_2 which define the principal or X axis of the geometric system can also be obtained, along with ϕ_3', λ_3', R_3 (which fix the fundamental plane of the geometric system). Schematically, the input values ϕ_i, λ_i, H_i in which the tidal effects are averaged out, are transformed at universal time $t = t_0$ to ϕ_i', λ_i', R_i via the adopted oblate spheroidal model

wherein the fluctuation of the meridian ellipticity due to the Earth tides is taken into account at any given universal time.*

The time varying Earth fixed station coordinates relative to Greenwich can now be written (Eqs. 11 and 12) as

$$\underline{R}_{Gi} = \begin{bmatrix} R \cos \beta \cos \lambda \\ R \cos \beta \sin \lambda \\ R \sin \beta \end{bmatrix}_i + \begin{bmatrix} \Delta X_G \\ \Delta Y_G \\ \Delta Z_G \end{bmatrix}_i \quad i = 1, 2, 3, \quad (16)$$

where β is the reduced latitude [3.4] given by

$$\beta = \phi' + \sin^{-1} \left[\frac{H}{R} \sin(\phi - \phi') \right].$$

The following unit vectors (based on the a priori values of the station coordinates at $t = t_0$) are now introduced (overhead \wedge)

$$\begin{aligned} \underline{\wedge}_x &= (\underline{R}_{G2} - \underline{R}_{G1}) / |\underline{R}_{G2} - \underline{R}_{G1}| \\ \underline{\wedge}_s &= (\underline{R}_{G3} - \underline{R}_{G1}) / |\underline{R}_{G3} - \underline{R}_{G1}|. \end{aligned} \quad (17)$$

Crossing $\underline{\wedge}_x$ into $\underline{\wedge}_s$ yields the z direction of the geometric system, namely:

$$\underline{\wedge}_z = \pm \underline{\wedge}_x \times \underline{\wedge}_s / [1 - (\underline{\wedge}_x \cdot \underline{\wedge}_s)^2]^{1/2}, \quad (18)$$

where the sign of $\underline{\wedge}_z$ is taken such that $\underline{R}_{G1} \cdot \underline{\wedge}_z > 0$.

Finally, crossing $\underline{\wedge}_z$ into $\underline{\wedge}_x$ yields

$$\underline{\wedge}_y = \underline{\wedge}_z \times \underline{\wedge}_x. \quad (19)$$

*The assumption that the station undulations are averaged out at a given point on the Earth's surface seems justified; however at any fixed time the meridians of two distant stations will undergo plastic deformation.

Hence at adopted universal time t_0 for which the solution to the station coordinates will be carried out the geometric coordinate system basis is defined as:

$$\hat{x}_0, \hat{y}_0, \hat{z}_0$$

as computed by formulas (16), (17), (18) and (19). The generalized transformation for any additional station is now given by:

$$\begin{aligned} X_i &= (\underline{R}_{Gi} - \underline{R}_{G1}) \cdot \hat{x}_0 \\ Y_i &= (\underline{R}_{Gi} - \underline{R}_{G1}) \cdot \hat{y}_0, \quad i = 4, 5, 6, \dots, I. \\ Z_i &= (\underline{R}_{Gi} - \underline{R}_{G1}) \cdot \hat{z}_0 \end{aligned} \quad (20)$$

Equation (20) depicts the station coordinates as functions of time. Hence at time t_0 , i. e., at the adopted epoch at which the multilateration solution will be undertaken,

$$\begin{aligned} X_{0i} &\equiv (\underline{R}_{G0i} - \underline{R}_{G01}) \cdot \hat{x}_0 \\ Y_{0i} &\equiv (\underline{R}_{G0i} - \underline{R}_{G01}) \cdot \hat{y}_0 \\ Z_{0i} &\equiv (\underline{R}_{G0i} - \underline{R}_{G01}) \cdot \hat{z}_0 \end{aligned} \quad (21)$$

are the constant to-be-solved-for parameters, so that the instantaneous time varying coordinates are:

$$\begin{aligned} X_i &= X_{0i} + (\Delta \underline{R}_{Gi} - \Delta \underline{R}_{G1}) \cdot \hat{x}_0 \\ Y_i &= Y_{0i} + (\Delta \underline{R}_{Gi} - \Delta \underline{R}_{G1}) \cdot \hat{y}_0 \\ Z_i &= Z_{0i} + (\Delta \underline{R}_{Gi} - \Delta \underline{R}_{G1}) \cdot \hat{z}_0 \end{aligned} \quad (22)$$

Note that the basis $\hat{x}_0, \hat{y}_0, \hat{z}_0$ permits \underline{R}_G or $\Delta \underline{R}_G$ to be written as:

$$\underline{R}_{Gi} = X_i \hat{x}_0 + Y_i \hat{y}_0 + Z_i \hat{z}_0 + \underline{R}_{G1}.$$

Now from Eq. (11)

$$\begin{aligned} \cos \beta \cos \lambda &= X_G/R, & \sin \beta \cos \lambda &= X_G Z_G / \left[(X_G^2 + Y_G^2)^{1/2} R \right] \\ \cos \beta \sin \lambda &= Y_G/R, & \sin \beta \sin \lambda &= Y_G Z_G / \left[(X_G^2 + Y_G^2)^{1/2} R \right] \\ \sin \beta &= Z_G/R, & R^2 &= X_G^2 + Y_G^2 + Z_G^2 \end{aligned} \quad (23)$$

Substitution of these relationships into Eq. (12) yields

$$\begin{aligned} \Delta X_G &= \Delta R X_G/R_G - \Delta \beta X_G Z_G / \left[X_G^2 + Y_G^2 \right]^{1/2} - \Delta \lambda Y_G \\ \Delta Y_G &= \Delta R Y_G/R_G - \Delta \beta Y_G Z_G / \left[X_G^2 + Y_G^2 \right]^{1/2} + \Delta \lambda X_G \\ \Delta Z_G &= \Delta R Z_G/R_G - \Delta \beta \left[1 - (Z_G/R_G)^2 \right]^{1/2}, \end{aligned} \quad (24)$$

where as functions of $X_G, Y_G, Z_G, \Delta R, \Delta \beta$, and $\Delta \lambda$ are given for each body $b = \mathbb{C}/\odot$ as:

$$\left. \begin{aligned} \Delta R &= \frac{h}{g} \Phi_T(R_G) \\ \Delta \beta &= -\frac{\ell}{g R_G} \left[G_{\mathbb{C}}(\psi_{\mathbb{C}}, R_G) G'_{\mathbb{C}}(\alpha_{\mathbb{C}}, \delta_{\mathbb{C}}, X_G, Y_G, Z_G) \right. \\ &\quad \left. + G_{\odot}(\psi_{\odot}, R_G) G'_{\odot}(\alpha_{\odot}, \delta_{\odot}, X_G, Y_G, Z_G) \right] \\ \Delta \lambda &= \frac{\ell}{g R_G} \left[G_{\mathbb{C}}(\psi_{\mathbb{C}}, R_G) G''_{\mathbb{C}}(\alpha_{\mathbb{C}}, \delta_{\mathbb{C}}, X_G, Y_G, Z_G) \right. \\ &\quad \left. + G_{\odot}(\psi_{\odot}, R_G) G''_{\odot}(\alpha_{\odot}, \delta_{\odot}, X_G, Y_G, Z_G) \right] / \left[1 - (Z_G/R_G)^2 \right]^{1/2} \end{aligned} \right\} \quad (25)$$

with

$$\begin{aligned}\cos \psi_{C/\odot} &= \frac{Z_G \sin \delta_{C/\odot}}{R_G} + \left[1 - (Z_G/R_G)^2\right]^{1/2} \cos \delta_{C/\odot} \cos \left(\theta_g - \alpha_{C/\odot} + \tan^{-1} \frac{Y_G}{X_G}\right) \\ X_G &= \hat{x}_x X + \hat{y}_x Y + \hat{z}_x Z + X_{G1} \\ Y_G &= \hat{x}_y X + \hat{y}_y Y + \hat{z}_y Z + Y_{G1} \\ Z_G &= \hat{x}_z X + \hat{y}_z Y + \hat{z}_z Z + Z_{G1}\end{aligned}\quad (26)$$

and where the quadrant of the arctangent is determined by an examination of the numerator and denominator.

Hence in functional notation

$$\Delta \underline{R}_G = \Delta \underline{R}_G(X_0, Y_0, Z_0, \alpha_C, \delta_C, \alpha_\odot, \delta_\odot, R_C, R_\odot, \ell, h, g, \theta_g).$$

Note that the basis $\underline{\hat{x}}_0 \equiv [\hat{x}_x, \hat{x}_y, \hat{x}_z]$, $\underline{\hat{y}}_0, \underline{\hat{z}}_0$ is adopted from the a priori values in the manner defined and held fixed forevermore; therefore $\underline{\hat{x}}_0, \underline{\hat{y}}_0, \underline{\hat{z}}_0$ are constant vectors possessed of no error terms. The solution is carried out in this basis and the transformation back into the geographic frame (if it is desired) uses these same numbers. With this understanding

$$\Delta \underline{R}_i \equiv (\Delta \underline{R}_{Gi} - \Delta \underline{R}_{G1})$$

so that

$$\begin{aligned}X_i &= X_{0i} + \Delta \underline{R}_i \cdot \underline{\hat{x}}_0 \\ Y_i &= Y_{0i} + \Delta \underline{R}_i \cdot \underline{\hat{y}}_0 \\ Z_i &= Z_{0i} + \Delta \underline{R}_i \cdot \underline{\hat{z}}_0.\end{aligned}\quad (27)$$

In essence, the Earth tide model has permitted the time varying station coordinates X_i, Y_i, Z_i to be written in terms of X_{0i}, Y_{0i}, Z_{0i} , namely, in terms of the station coordinates at a fixed epoch. This implies that X_{0i}, Y_{0i}, Z_{0i} are nontime varying parameters, i.e., they are the leading constants of the tidal function and represent the station coordinates only in the absence of tidal motion. This is important because if equations of the form

$$M(X_i, Y_i, Z_i, d, t^*) = 0 \quad (28)$$

are written for t_n^* distinct times, a solution is not possible because at each t^* the sought for values of X_i, Y_i, Z_i are different. However if the equations are written as

$$M(X_{0i}, Y_{0i}, Z_{0i}, \bar{\xi}, d, t^*) = 0, \quad (29)$$

where

$$\bar{\xi} \equiv [\alpha, \delta, \dots, \ell, h, g]$$

then for t_n^* distinct times a system of equations for X_{0i}, Y_{0i}, Z_{0i} where the coordinates are constant at each t^* becomes available and a solution is possible. Once M is solved for X_{0i}, Y_{0i}, Z_{0i} and perhaps for some of the $\bar{\xi}$, call the solutions $X_{0i}^s, Y_{0i}^s, Z_{0i}^s$, the geographic coordinates are recovered as:

$$\Delta \underline{R}_{G0i} = \begin{bmatrix} \Delta X_{G0} \\ \Delta Y_{G0} \\ \Delta Z_{G0} \end{bmatrix} = \begin{bmatrix} x_x & y_x & z_x \\ x_y & y_y & z_y \\ x_z & y_z & z_z \end{bmatrix} \begin{bmatrix} X_{0i}^s \\ Y_{0i}^s \\ Z_{0i}^s \end{bmatrix}$$

so that

$$\underline{R}_{G0i} = \underline{R}_{G01} + \Delta \underline{R}_{G0i}, \quad (30)$$

from which the polar coordinates at $t = t_0$ may be computed using Eq. (23).

Note that the time variation of the coordinates is obtained from Eq. (27) where X_{0i}^s replaces X_{0i} , etc.

A3.6 TRANSFORMATION OF VARIATIONS

The variation in $M(X_1, Y_1, Z_1, X_2, \dots, d)$, namely

$$\delta M = \frac{\partial M}{\partial X_1} \delta X_1 + \frac{\partial M}{\partial Y_1} \delta Y_1 + \dots + \frac{\partial M}{\partial d} \delta d$$

transforms in terms of $X_{01}, Y_{01}, Z_{01}, X_{02}, \dots, d$, as

$$\begin{aligned} \delta M = & \sum_1^I \left\{ \left(1 + \hat{x}_0 \cdot \frac{\partial \Delta R_i}{\partial X_{0i}} \right) \frac{\partial M}{\partial X_i} + \left(\hat{y}_0 \cdot \frac{\partial \Delta R_i}{\partial X_{0i}} \right) \frac{\partial M}{\partial Y_i} + \left(\hat{z}_0 \cdot \frac{\partial \Delta R_i}{\partial X_{0i}} \right) \frac{\partial M}{\partial Z_i} \right\} \delta X_{0i} \\ & + \sum_1^I \left\{ \left(\hat{y}_0 \cdot \frac{\partial \Delta R_i}{\partial Y_{0i}} \right) \frac{\partial M}{\partial X_i} + \left(1 + \hat{y}_0 \cdot \frac{\partial \Delta R_i}{\partial Y_{0i}} \right) \frac{\partial M}{\partial Y_i} + \left(\hat{z}_0 \cdot \frac{\partial \Delta R_i}{\partial Y_{0i}} \right) \frac{\partial M}{\partial Z_i} \right\} \delta Y_{0i} \\ & + \sum_1^I \left\{ \left(\hat{z}_0 \cdot \frac{\partial \Delta R_i}{\partial Z_{0i}} \right) \frac{\partial M}{\partial X_i} + \left(\hat{z}_0 \cdot \frac{\partial \Delta R_i}{\partial Z_{0i}} \right) \frac{\partial M}{\partial Y_i} + \left(1 + \hat{z}_0 \cdot \frac{\partial \Delta R_i}{\partial Z_{0i}} \right) \frac{\partial M}{\partial Z_i} \right\} \delta Z_{0i} \\ & + \left\{ \sum_1^I \left(\hat{x}_0 \cdot \frac{\partial \Delta R_i}{\partial \alpha_{\mathcal{C}}} \frac{\partial M}{\partial X_i} + \hat{y}_0 \cdot \frac{\partial \Delta R_i}{\partial \alpha_{\mathcal{C}}} \frac{\partial M}{\partial Y_i} + \hat{z}_0 \cdot \frac{\partial \Delta R_i}{\partial \alpha_{\mathcal{C}}} \frac{\partial M}{\partial Z_i} \right) \right\} \delta \alpha_{\mathcal{C}} \\ & + \left\{ \sum_1^I \left(\hat{x}_0 \cdot \frac{\partial \Delta R_i}{\partial \delta_{\mathcal{C}}} \frac{\partial M}{\partial X_i} + \hat{y}_0 \cdot \frac{\partial \Delta R_i}{\partial \delta_{\mathcal{C}}} \frac{\partial M}{\partial Y_i} + \hat{z}_0 \cdot \frac{\partial \Delta R_i}{\partial \delta_{\mathcal{C}}} \frac{\partial M}{\partial Z_i} \right) \right\} \delta (\delta_{\mathcal{C}}) \\ & + \left\{ \sum_1^I (\cdot) \right\} \delta R_{\mathcal{C}} + \left\{ \sum_1^I (\cdot) \right\} \delta \alpha_{\odot} + \dots + \left\{ \sum_1^I (\cdot) \right\} \delta \theta_g \\ & + \frac{\partial M}{\partial d} \delta d, \end{aligned} \tag{31}$$

where I is the total number of stations contained in M and

$$\frac{\partial \Delta R_i}{\partial (\cdot)} = \frac{\partial R_{Gi}}{\partial (\cdot)} - \frac{\partial R_{G1}}{\partial (\cdot)}.$$

Hence

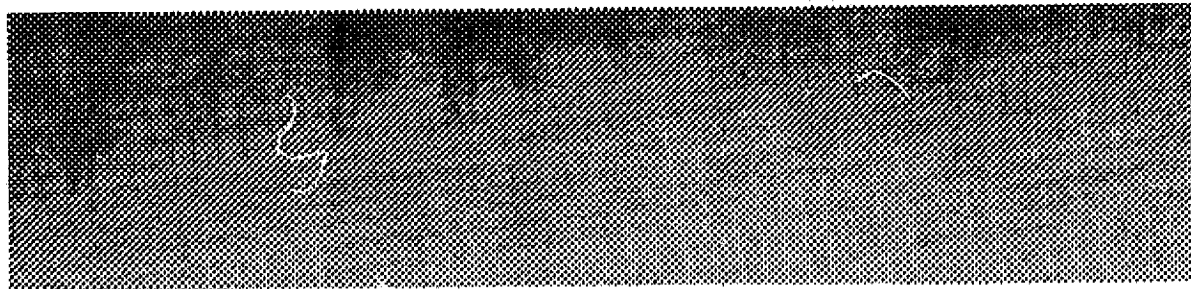
$$\delta M = \sum_1^I \left\{ \frac{\partial M}{\partial X_{0i}} \right\} \delta X_{0i} + \sum_1^I \left\{ \frac{\partial M}{\partial Y_{0i}} \right\} \delta Y_{0i} + \sum_1^I \left\{ \frac{\partial M}{\partial Z_{0i}} \right\} \delta Z_{0i} \\ + \dots + \frac{\partial M}{\partial d} \delta d \quad (32)$$

where $\partial M / \partial X_{0i}$, etc., are defined by the brackets in Eq. (31). In essence the point herein is that if the partial derivatives of Eq. (28) are available, namely $\partial M / \partial X_i$, etc., the partial derivatives of Eq. (29), namely $\partial M / \partial X_{0i}$ are obtained from the brackets in Eq. (32).

A3.7 REFERENCES

- [3.1] Knopoff, L., Private Communication.
- [3.2] Garland, G.D., Introduction To Geophysics, W.B. Saunders Co., London 1971.
- [3.3] Takeuchi, H., Theory of the Earth's Interior, Blaisdell Publishing Co., London 1966.
- [3.4] Escobal, P.R., Methods of Orbit Determination, John Wiley and Sons, New York 1965; Second Edition, Krieger Publishing, N.Y. 1976.
- [3.5] Escobal, P.R., et al., 3-D Laser Multilateration: A Precision Geodetic Measurement System (Section IX, M. S. Shumate), JPL TM 33-605, March 15, 1973.
- [3.6] Melbourne, W.G., et al., Constants and Related Information for Astrodynamic Calculations, JPL TR 32-1306, July 1968.
- [3.7] Escobal, P.R., "Explicit Analytic Model for Earth Tide Station Coordinate Deflections," JPL EM, 6 January 1975 (JPL internal document).

A4. Ground Station Deflections Due to Ocean Tides



Abstract

Equilibrium theory is used to develop the shape of the sea envelope engendered by the gravitational, centrifugal and Moon/Sun potentials. The ocean surface is then subdivided into a finite number of sea water mascons and the potential at a given ground station due to the mascons is developed. Lifting of the ocean bottom due to the solid Earth tides is included in the potential calculation. Calibration of this approximate and incorrect potential (due to the equilibrium assumption) is then performed via gravimeter data. Elastic theory is then used to predict the deflection at the station occasioned by the loading sea water potential. (This deflection is not to be confused with the deflection due to the Earth tides.) The model for the ocean tide discussed in this Appendix is simpler than other proposed models. The only aim of the present model is to reduce the error in ground station movement vis-a-vis the accuracy achieved by considering only the Earth tides. The inadequacy of present analytic techniques prompted the development of this engineering model.

PRECEDING PAGE BLANK NOT FILMED

A4.1 INTRODUCTION

The problem of predicting the three-dimensional deflections of a station located on dry ground due to the oceanic tides is difficult, to say the least. The difficulty of prediction arises from the fact that the Moon/Sun potentials cause an instantaneous deformation of the Earth's elastic surface (including the ocean floor). Simultaneously, oceanic tidal bulges are created such that the sea water loading varies over a given point within the ocean, and to make further complications the sea water mass is redistributed due to the instantaneous deformation of the ocean floor thus causing the potentials to be disturbed. The previous chain of events can be segregated into the following components which ultimately will enable a solution to be obtained:

- a) Development of an equilibrium surface for the ocean using the Earth's gravitational potential and the centrifugal potential.
- b) Development of an equilibrium surface for the ocean using the two previous potentials along with the induced Moon/Sun external non-loading potentials.
- c) Subtraction of the above two surfaces to obtain an undulating layer of sea water over the Earth's surface which represents the variation of the ocean surface from mean sea level (as defined herein).
- d) Subdivision of the ocean surface into sea water mascons of small volume.
- e) Computation of the loading potential at a given ground station occasioned by all the sea water mascons.
- f) Calibration of the loading potential using gravimeter measurements.
- g) Employment of elastic theory to predict the ground station deflection due to ocean tides.
- h) Iteration with the previous items to refine the computation, if so desired.

It is acknowledged that the analysis herein makes several assumptions which simplify the solution to the ocean tide problem [4.19]. However since the object herein is to reduce the 3 to 4 centimeter accuracy achieved from the Earth tide deflection model by only a factor of 3, in order to achieve 1 cm accuracies, these assumptions were deemed acceptable. The most stringent assumption is item c, listed on the preceding page, which establishes the ocean surface free of the disturbed potentials caused by the mass redistributions occasioned by the deflections. This assumption can be eliminated by the process of iteration. The model developed herein needs further testing and verification. It is substantially different from those discussed in [4.2 - 4.18].

A4.2 OCEAN SURFACE EQUATIONS

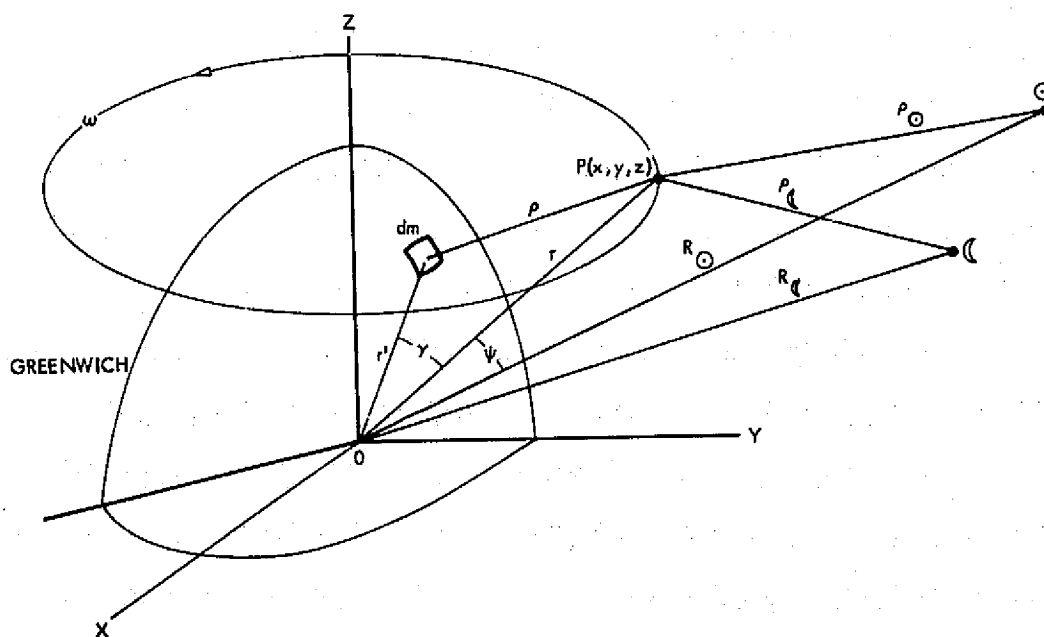


Figure A4.1. Geometry for Development of Potential

Consider an observer at point P rotating about the Z axis of Figure A4.1 with angular velocity ω . The potential at point P can be written in terms of the gravitational, centrifugal and perturbative potentials as:

$$U = G \int \frac{dm}{\rho} + \frac{1}{2} (x^2 + y^2) \omega^2 + U_{\text{C}} + U_{\text{O}}, \quad (1)$$

where G is the universal gravitational constant, dm is the mass element at distance r' from the mass center O, and $U_{\text{C}}, U_{\text{O}}$ are the potentials occasioned at P by the Moon and Sun. As previously developed, (Appendix A3) in terms of the Moon/Sun masses $M_{\text{C}}, M_{\text{O}}$:

$$\begin{aligned} U_{\text{C}} &= GM_{\text{C}} \left(\frac{1}{\rho_{\text{C}}} - \frac{1}{R_{\text{C}}} - \frac{r \cos \psi_{\text{C}}}{R_{\text{C}}^2} \right) \\ U_{\text{O}} &= GM_{\text{O}} \left(\frac{1}{\rho_{\text{O}}} - \frac{1}{R_{\text{O}}} - \frac{r \cos \psi_{\text{O}}}{R_{\text{O}}^2} \right), \end{aligned} \quad (2)$$

where the elongation angle $\psi_{\text{C/O}}$ is given by the respective dot products of \underline{r} with \underline{R}_{C} and \underline{R}_{O} . Via the law of cosines the slant range from dm to P can be written in terms of $\cos \gamma \equiv (xx' + yy' + zz')/rr'$ as

$$\frac{1}{\rho} = \frac{1}{r} \left[1 - 2 \frac{r'}{r} \cos \gamma + \frac{r'^2}{r^2} \right]^{-1/2}$$

and since r' ranges from 0 to the surface of the Earth, for the most part the last two terms in the bracket are < 1 so that a binomial expansion yields:

$$\frac{1}{\rho} = \frac{1}{r} \left[P_0(\cos \gamma) + \frac{r'}{r} P_1(\cos \gamma) + \left(\frac{r'}{r} \right)^2 P_2(\cos \gamma) + \dots \right] \quad (3)$$

where P_0, P_1, P_2 are the Legendre polynomials. By the same reasoning

$$\frac{1}{r_{C/\odot}} = \frac{1}{R_{C/\odot}} \left[P_0(\cos \psi_{C/\odot}) + \frac{r}{R_{C/\odot}} P_1(\cos \psi_{C/\odot}) + \dots \right] \quad (4)$$

Substitution of Eqs. (3) and (4) into Eq. (1) yields:

$$\begin{aligned} U = \frac{G}{r} & \left[\int dm + \frac{1}{r} \int P_1(\cos \gamma) r' dm + \frac{1}{r^2} \int P_2(\cos \gamma) r'^2 dm + \dots \right] \\ & + \frac{1}{2} (x^2 + y^2) \omega^2 + \frac{GM_C r^2}{R_C^3} \left[P_2(\cos \psi_C) + \frac{r}{R_C} P_3(\cos \psi_C) + \dots \right] \\ & + \frac{GM_\odot r^2}{R_\odot^2} \left[P_2(\cos \psi_\odot) + \frac{r}{R_\odot} P_3(\cos \psi_\odot) + \dots \right]. \end{aligned} \quad (5)$$

The Z axis is the principal axis of greatest inertia. By choosing the X and Y axes (located at λ_p from the Greenwich meridian) as the principal axes of inertia, Eq. (5) can be simplified. Obviously, the first integral is the mass of the Earth, M_\oplus . The second integral reduces to taking first moments about the mass center and therefore vanishes. The cross products of inertia in the third integral also vanish so that after integration

$$\begin{aligned} \int P_2(\cos \gamma) r'^2 dm &= \frac{3}{2} \left(\frac{A+B}{2} - C \right) \left(\sin^2 \phi - \frac{1}{3} \right) \\ &+ \frac{3}{4} (B - A) \cos^2 \phi \cos 2(\lambda - \lambda_p), \end{aligned} \quad (6)$$

where

$A \equiv$ Moment of inertia about the X axis,

$B \equiv$ Moment of inertia about the Y axis,

$C \equiv$ Moment of inertia about the Z axis,

$\lambda_p =$ longitude of principal axis (X) from Greenwich.

Introducing the definitions $J_{20} = [C - (A + B)/2]/M_{\oplus}$, $J_{22} = [B - A]/4M_{\oplus}$, etc., and noting that

$$\begin{aligned}\frac{1}{2}(x^2 + y^2)\omega^2 &= \frac{1}{2} \left\{ \left[r \cos \phi \cos(\lambda - \lambda_p) \right]^2 + \left[r \cos \phi \sin(\lambda - \lambda_p) \right]^2 \right\} \\ &= \frac{1}{2} \omega^2 r^2 \cos^2 \phi\end{aligned}$$

reduces U (including a few higher order terms [4.1] to:

$$\begin{aligned}U &= \frac{GM_{\oplus}}{r} \left[1 - \frac{J_{20}}{2r^2}(1 - 3 \sin^2 \phi) + 3 \frac{J_{22}}{r^2} \cos^2 \phi \cos 2(\lambda - \lambda_{22}) \right. \\ &\quad - \frac{J_{30}}{2r^3}(3 - 5 \sin^2 \phi) \sin \phi + \frac{3J_{31}}{4r^3} \cos \phi \cos(\lambda - \lambda_{31}) \\ &\quad \left. + \frac{J_{40}}{8r^4}(3 - 30 \sin^2 \phi + 35 \sin^4 \phi) + \frac{r^3 \omega^2}{2GM_{\oplus}} \cos^2 \phi \right] + U_{\odot+\oplus},\end{aligned}\quad (7)$$

where $U_{\odot+\oplus}$ is the combined Moon/Sun potential.

The numerical values of the coefficients are listed in Table A4.1.

Table A4.1. Harmonic Constants [4.1]

J_{20}	$= -1082.645 \times 10^{-6}$	
J_{30}	$= + 2.546 \times 10^{-6}$	
J_{40}	$= + 1.649 \times 10^{-6}$	
J_{22}	$= + 1.766 \times 10^{-6}$,	$\lambda_{22} = -14^{\circ}.79$
J_{31}	$= + 2.111 \times 10^{-6}$,	$\lambda_{31} = + 7^{\circ}.818$

By inserting the values of Table A4.1 into expression (7), neglecting the Moon/Sun contribution, and putting $r = a_p$, the polar Earth radius, then setting $\phi = 90^\circ$, U can be numerically evaluated, i. e.,

$$U_p = \frac{GM_\oplus}{a_p} \left[1 + \frac{J_{20}}{a_p^2} + \frac{J_{30}}{a_p^3} + \frac{J_{40}}{a_p^4} \right].$$

Hence, the equation for an equipotential surface, the ocean, is given by:

$$\begin{aligned} r_0 = \frac{GM_\oplus}{U_p} & \left[1 - \frac{J_{20}}{2a_p^2} (1 - 3 \sin^2 \phi) + 3 \frac{J_{22}}{a_p^2} \cos^2 \phi \cos 2(\lambda - \lambda_{22}) \right. \\ & - \frac{J_{30}}{2a_p^3} (3 - 5 \sin^2 \phi) \sin \phi + \frac{3}{4} \frac{J_{31}}{a_p^3} \cos \phi \cos (\lambda - \lambda_{31}) \\ & \left. + \frac{J_{40}}{8a_p^4} (3 - 30 \sin^2 \phi + 35 \sin^4 \phi) + \frac{a_p^3 \omega^2}{2GM_\oplus} \cos^2 \phi \right], \end{aligned} \quad (8)$$

or

$$r_0 \equiv \frac{GM}{U_p} \Delta_\oplus,$$

where, in the small terms, r has been set equal to a_p . Obviously Eq. (8) does not have the lunisolar contribution to the potential. Proceeding from Eq. (5), i. e.,

$$\begin{aligned} U_{\odot+\oplus} = \frac{GM_\odot}{R_\odot^3} r^2 & \left[P_2(\cos \psi_\odot) + \frac{r}{R_\odot} P_3(\cos \psi_\odot) + \dots \right] \\ & + \frac{GM_\oplus}{R_\oplus^2} r^2 \left[P_2(\cos \psi_\oplus) + \frac{r}{R_\oplus} P_3(\cos \psi_\oplus) + \dots \right] \end{aligned}$$

a direct expansion using

$$\cos \psi_{\zeta/\odot} = \sin \delta_{\zeta/\odot} \sin \phi + \cos \delta_{\zeta/\odot} \cos \phi \cos \overline{HA}_{\zeta/\odot}$$

where, in terms of the Greenwich sidereal time, θ_g and right ascensions, $\overline{HA}_{\zeta/\odot} = \theta_g - \alpha_{\zeta/\odot} + \lambda$, yields:

$$\begin{aligned} U_{\zeta+\odot} = & -\frac{GM_{\zeta}r^2}{2R_{\zeta}^3} \left[1 - 3 \sin^2 \delta_{\zeta} \sin^2 \phi - 3 \cos^2 \delta_{\zeta} \cos^2 \overline{HA}_{\zeta} \cos^2 \phi \right. \\ & - 6 \sin \delta_{\zeta} \cos \delta_{\zeta} \sin \phi \cos \phi \cos \overline{HA}_{\zeta} - \frac{r}{R_{\zeta}} (5 \sin^3 \delta_{\zeta} \sin^3 \phi \\ & + 15 \cos^2 \delta_{\zeta} \sin \delta_{\zeta} \cos^2 \overline{HA}_{\zeta} \cos^2 \phi \sin \phi \\ & + 15 \sin^2 \delta_{\zeta} \cos \delta_{\zeta} \cos \overline{HA}_{\zeta} \sin^2 \phi \cos \phi \\ & \left. - 3 \sin \delta_{\zeta} \sin \phi - 3 \cos \delta_{\zeta} \cos \overline{HA}_{\zeta} \cos \phi) \right] \\ & - \frac{GM_{\odot}r^2}{2R_{\odot}^3} \left[1 - 3 \sin^2 \delta_{\odot} \sin^2 \phi - 3 \cos^2 \delta_{\odot} \cos^2 \overline{HA}_{\odot} \cos^2 \phi \right. \\ & - 6 \sin \delta_{\odot} \cos \delta_{\odot} \sin \phi \cos \phi \cos \overline{HA}_{\odot} - \frac{r}{R_{\odot}} (5 \sin^3 \delta_{\odot} \sin^3 \phi \\ & + 15 \cos^2 \delta_{\odot} \sin \delta_{\odot} \cos^2 \overline{HA}_{\odot} \cos^2 \phi \sin \phi \\ & + 15 \sin^2 \delta_{\odot} \cos \delta_{\odot} \cos \overline{HA}_{\odot} \sin^2 \phi \cos \phi \\ & \left. - 3 \sin \delta_{\odot} \sin \phi - 3 \cos \delta_{\odot} \cos \overline{HA}_{\odot} \cos \phi) \right], \quad (9) \end{aligned}$$

For convenience the brackets in the previous expression are defined as

$$U_{\zeta+\odot} = -\frac{GM_{\zeta}r^2}{2R_{\zeta}^3} \Delta_{\zeta} - \frac{GM_{\odot}r^2}{2R_{\odot}^3} \Delta_{\odot}. \quad (10)$$

Obviously for $\phi = 90^\circ$, $r = a_p$ the value of this potential is:

$$U_{(\odot+\oplus)_p} = -\frac{GM_{\odot}a_p^2}{2R_{\odot}^3} \left[1 - 3 \sin^2 \delta_{\odot} - \frac{a_p}{R_{\odot}} (5 \sin^3 \delta_{\odot} - 3 \sin \delta_{\odot}) \right] - \frac{GM_{\oplus}a_p^2}{2R_{\oplus}^3} \left[1 - 3 \sin^2 \delta_{\oplus} - \frac{a_p}{R_{\oplus}} (5 \sin^2 \delta_{\oplus} - 3 \sin \delta_{\oplus}) \right] \quad (11)$$

and use of Eq. (7) yields the equation for an equipotential surface (including the Sun and Moon), namely,

$$r_e = \frac{GM_{\oplus}}{\bar{U}} \Delta_{\oplus} - \frac{GM_{\odot}a_p^2}{2\bar{U}R_{\odot}^3} \Delta_{\odot} - \frac{GM_{\oplus}a_p^2}{2\bar{U}R_{\oplus}^3} \Delta_{\oplus} \quad (12)$$

where $\bar{U} \equiv U_p + U_{(\odot+\oplus)_p}$. Subtraction of Eqs. (8) and (12) yields the radial difference between the two equipotential surfaces, i. e., between the gravitational plus centripetal and gravitational plus centripetal plus Moon-Sun equipotential as:

$$\Delta r = \left(\frac{1}{\bar{U}} - \frac{1}{U_p} \right) GM_{\oplus} \Delta_{\oplus} - \frac{GM_{\odot}a_p^2}{2\bar{U}R_{\odot}^3} \Delta_{\odot} - \frac{GM_{\oplus}a_p^2}{2\bar{U}R_{\oplus}^3} \Delta_{\oplus} \quad (13)$$

This difference is geometrically displayed in Figure A4.2.

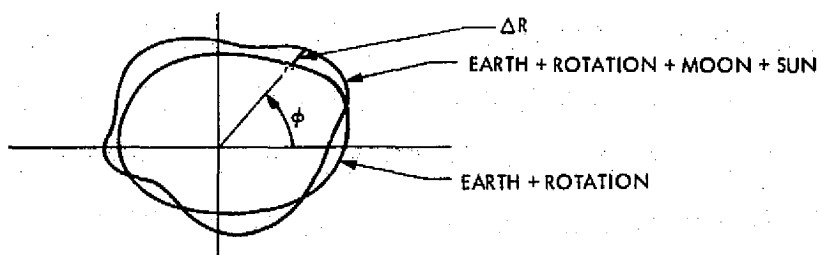


Figure A4.2. Difference in Equipotential Surfaces

A4.3 INTEGRATION LIMITS OVER THE OCEAN SURFACE

Consider Figure A4.3 which shows a continental land mass.

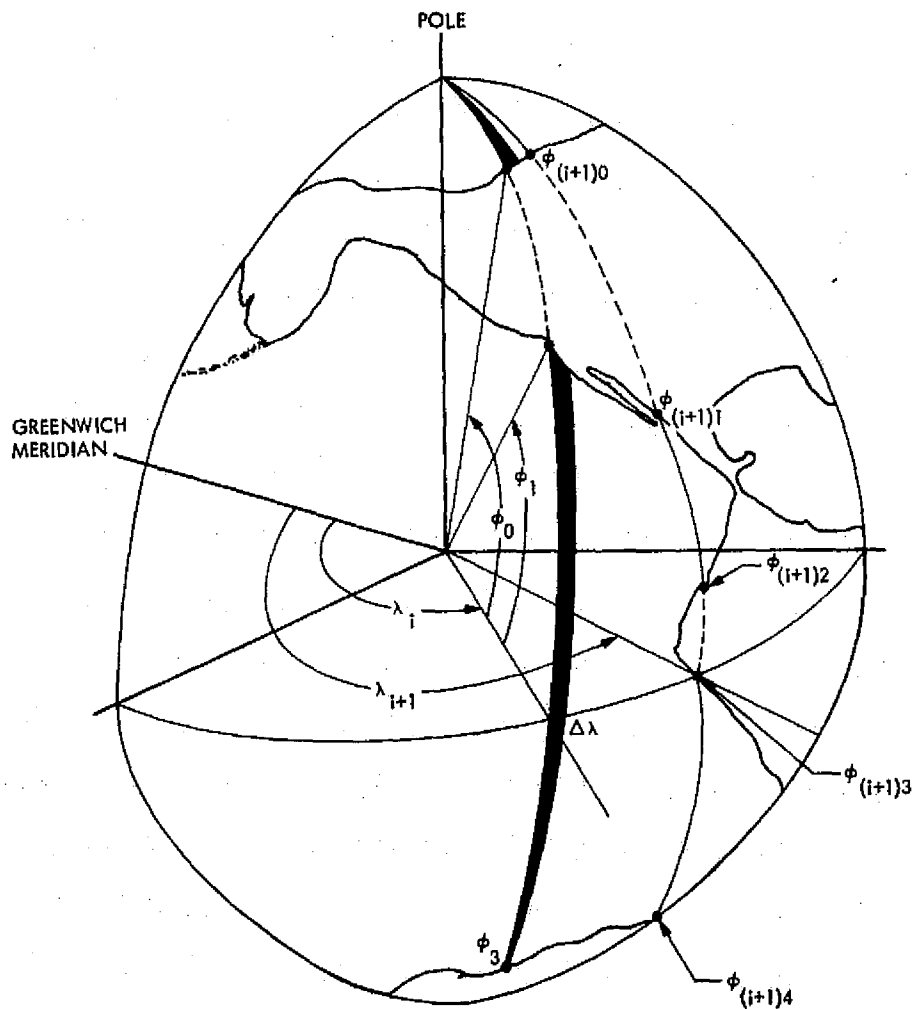


Figure A4.3. Subdivision of Land/Sea Surfaces

From Figure A4.3 it is easy to see that for a sequence of adopted latitudes (starting from the Greenwich meridian), namely

$$\lambda_0, \lambda_1, \dots, \lambda_i, \lambda_{i+1}, \dots, \lambda_\ell$$

there exists for each element of this sequence, say, λ_i , a second sequence

$$\phi_{i0}, \phi_{i1}, \dots, \phi_{ij}, \dots, \phi_{ik}$$

which in a latitudinal direction separates ocean/sea areas from land areas in the meridian of λ_i . Hence in the simplified illustration for λ_i an Earth/ocean vector E can be defined as

$$E_i \equiv [\lambda_i, \phi_{i0}, \phi_{i1}, \phi_{i2}]$$

while for longitude λ_{i+1} , e. g.,

$$E_{i+1} = [\lambda_{i+1}, \phi_{(i+1)0}, \phi_{(i+1)1}, \phi_{(i+1)2}, \phi_{(i+1)3}, \phi_{(i+1)4}].$$

The convention is adopted that ϕ_0 denotes the first land area encountered in the North to South direction. Evidently then, to the degree of accuracy desired, from available cartographic maps, the vector sequence

$$E_0, E_1, E_2, \dots, E_\ell \tag{14}$$

can be constructed and stored as data internal to the computer. Consider now a longitude difference such that the black swath in Figure A4.1 with width $\Delta\lambda$ is numerically defined. A latitudinal increment can also be obtained, call it $\Delta\phi$, by division of all swath segments by an adopted factor, i. e., a $3^\circ \times 3^\circ$ grid. In accordance with the previous definition, the potential of each grid subdivision mass can now be computed.

A4.4 NUMERICAL DEVELOPMENT OF LOADING POTENTIAL

From Figure A4.4, which depicts a differential sea water mascon (subscript l), the potential at station S is given by:

$$dU_l = Gdm \left(\frac{1}{\rho_s} - \frac{1}{r'} - \frac{r_s}{r'^2} \cos \psi_m \right) \quad (15)$$

where

$$\rho_s = \left(r'^2 + r_s^2 - 2r_s r' \cos \psi_m \right)^{1/2}$$

and

$$\cos \psi_m = \sin \phi' \sin \phi_s + \cos \phi' \cos \phi_s \cos (\lambda' - \lambda_s),$$

with the understanding that the primed parameters denote the variables of integration.*

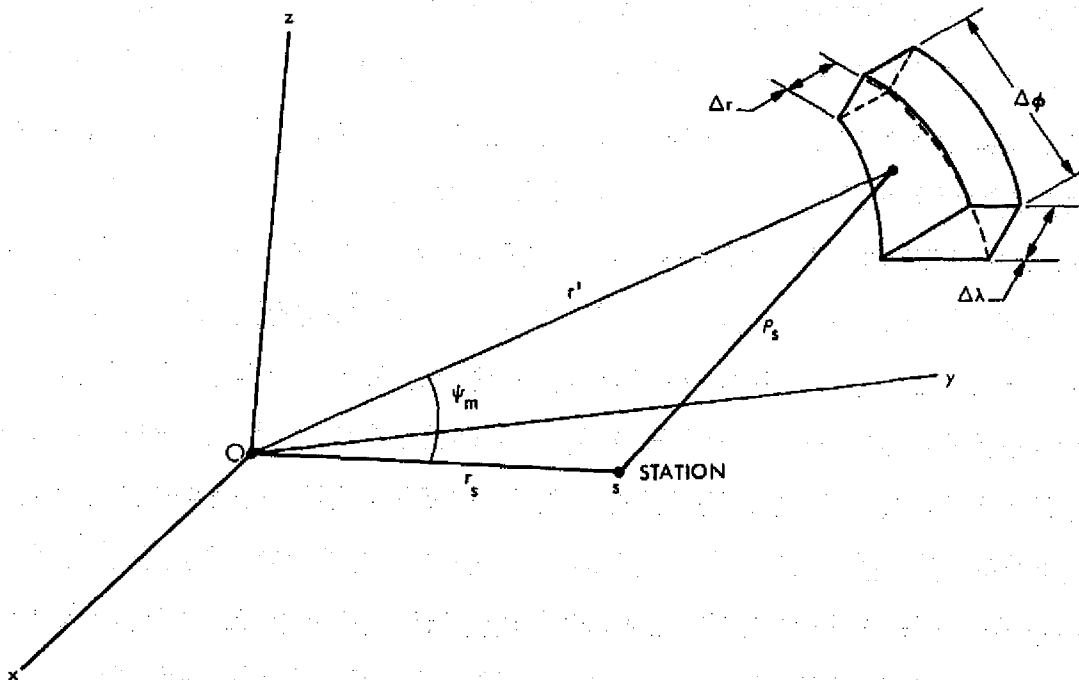


Figure A4.4. Sea Water Mascon

*Note that Eq. (15) is similar in structure to Eq. (2) except that the sea water mascon replaces either the Moon or Sun.

Using σ to denote the density of sea water, Eq. (15) can be written as:

$$dU_{\ell} = G\sigma \left(\frac{1}{\rho_s} - \frac{1}{r'} - \frac{r_s}{r'^2} \cos \psi_m \right) dV,$$

where the volume element $dV = r'^2 \cos \phi' d\phi' d\lambda' dr'$.

In order to obtain the total potential an integration over the whole sea volume is necessary. To accomplish this it has to be borne in mind that the sea bottom has been lifted upward by the Moon/Sun potential Φ_t . From Appendix A3 it is seen that:

$$\Delta R = \frac{h}{g} \Phi_t \quad (16)$$

represents the radial deformation of the elastic Earth with equilibrium radius r_o (Eq. 8). The total potential now becomes:

$$U_{\ell} = \iiint dU_{\ell} = G\sigma \int_{\Delta\phi} \int_{\Delta\lambda} \cos \phi' d\phi' d\lambda' \int_{r_o + \Delta R}^{r_o + \Delta r} r'^2 dr' \left(\frac{1}{\rho_s} - \frac{1}{r'} - \frac{r_s}{r'^2} \cos \psi_m \right), \quad (17)$$

where due account has been taken of the fact that the sea bottom is located at $r_o + \Delta R$ and the sea surface at $r_o + \Delta r$, the latter being uninfluenced by the Earth tide of Appendix A3. Because both ΔR and Δr are small compared to r_o , the radial integration can be performed immediately, to yield:

$$U_{\ell} = G\sigma \int_{\Delta\phi} \int_{\Delta\lambda} \cos \phi' (\Delta r - \Delta R) r_o^2 \left(\frac{1}{\rho_{so}} - \frac{1}{r_o} - \frac{r_s}{r_o^2} \cos \psi_m \right) d\phi' d\lambda', \quad (18)$$

where

$$\rho_{so} = \left(r_o^2 + r_s^2 - 2 r_s r_o \cos \psi_m \right)^{1/2}$$

Numerical integration of Eq. (18) over the Earth's oceans with the limits set by the E_i vectors, Eq. (14), obviously yields the ocean tide potential.

A4.5 CALIBRATION VIA GRAVIMETER DATA

The potential presently engendered, due to the use of equilibrium theory, is incorrect. The modeling of the correct potential function is an immense undertaking and to date no true satisfactory model has been derived. However, local gravity, g , at the station can be measured with a gravimeter to high precision. From the value of g , via Eq. (7) of Appendix A3 it is now possible to compute the residual ocean tide acceleration, g_s , as

$$g_s(t) = g_m(t) - g - g_t(t), \quad (19)$$

where $g_m(t)$ is the gravimeter acceleration time variation and g_t is the solid Earth tide acceleration given by (See Appendix A3):

$$g_t = -(2 + 2h - 3k) \frac{\Phi}{r_s}, \quad (20)$$

where $k \cong 0.27$.

The partial derivative $\partial U_\ell / \partial r_s$ can also be obtained numerically as:

$$\frac{\partial U_\ell}{\partial r_s} \cong \frac{U_\ell(r_s) - U_\ell(r_s + \Delta r_s)}{\Delta r_s}. \quad (21)$$

However, since

$$g_s = - \frac{\partial U_\ell}{\partial r_s} \quad (22)$$

it is possible to write

$$\kappa \left| U_\ell(r_s) - U_\ell(r_s + \Delta r_s) \right| = g_s \Delta r_s \quad (23)$$

and to solve for $\kappa(t)$ at a discrete number of times during the day. The ocean loading deflection is now given directly by:

$$\Delta R_o = \frac{h'}{g} \kappa(t) U_\ell(t), \quad (24)$$

where the Love number h' for a loading potential is given in terms of the non-loading Love number by $-\frac{2}{3}h$ or $h' = -0.4$. The negative value shows that the sea bottom is depressed by a positive tide. If the $\partial U_\ell / \partial \phi_s$, $\partial U_\ell / \partial \lambda_s$ are also obtained numerically the deformations in the latitude and longitude directions will be determined as in Appendix A3.

A4.6 INVESTIGATION OF SINGULARITY POINT

Note that if the station is located very close to the coast or on the surface of the ocean (ships radar) a singularity in ρ_s appears which is difficult to handle numerically. Therefore an analytic investigation of this singularity is indicated. The troublesome term is:

$$I = \int_{\phi_s - \Delta\phi}^{\phi_s + \Delta\phi} \cos \phi' d\phi' \int_{\lambda_s - \Delta\lambda}^{\lambda_s + \Delta\lambda} d\lambda' \int_{r_o + \Delta R}^{r_o + \Delta r} r'^2 \left(r_s^2 + r'^2 - 2 r_s r' \cos \psi_m \right)^{-1/2} dr' \quad (25)$$

If $r_s = r_o + \Delta r$ (the station being on the surface of the ocean) then with the substitution:

$$r' = r_o + \Delta r + r \text{ and } r \ll r_o:$$

it follows that

$$I = r_o^2 \int_{\Delta R - \Delta r}^0 dr \int_{\phi_s - \Delta \phi}^{\phi_s + \Delta \phi} \cos \phi' d\phi' \int_{\lambda_s - \Delta \lambda}^{\lambda_s + \Delta \lambda} \left(4 r_s^2 \sin^2 \frac{\psi_m}{2} + r^2 \right)^{-1/2} d\lambda'. \quad (26)$$

From the definition of ψ_m , Eq. (15), and the fact that the angular integration is extended only over a small area ($4 \Delta \phi \Delta \lambda \ll 1$), it follows that for

$$\cos \psi_m = 1 - \frac{1}{2} \phi'^2, \quad \begin{cases} -\Delta \phi \leq \phi' \leq \Delta \phi \\ \Delta \lambda \ll \Delta \phi \end{cases}$$

or

$$\psi_m = \phi' \ll 1$$

that

$$I = 2\Delta \lambda r_o \int_{\Delta R - \Delta r}^0 dr \int_{\phi_s - \Delta \phi}^{\phi_s + \Delta \phi} d\phi' [\phi'^2 + (r/r_s)^2]^{-1/2}, \quad (27)$$

or

$$\begin{aligned}
 I &= 2 r_o \Delta \lambda \int_{\Delta R - \Delta r}^0 dr \left\{ \sinh^{-1} \left[\frac{(\phi_s + \Delta \phi) r}{r_s} \right] - \right. \\
 &\quad \left. \sinh^{-1} \left[\frac{(\phi_s - \Delta \phi) r}{r_s} \right] \right\} \\
 &= -2 \Delta \lambda \Delta \phi (\Delta R - \Delta r)^2 \rightarrow 0.
 \end{aligned} \tag{28}$$

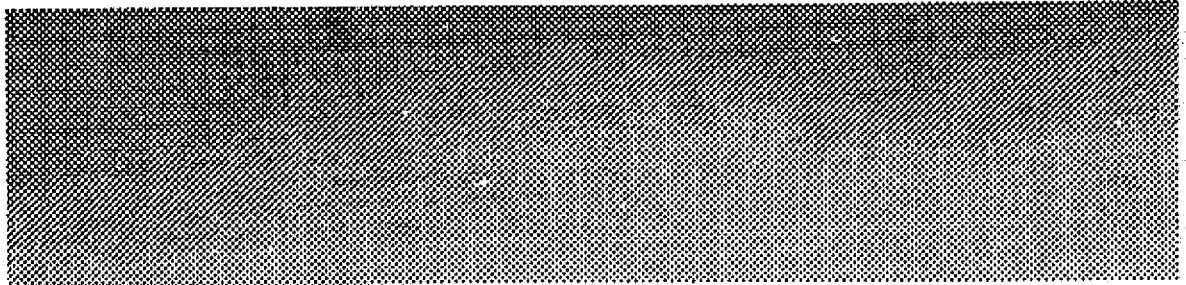
Namely disregarding a small area of integration about the singularity contributes nothing to the value of the potential.

A4.7 REFERENCES

- [4.1] Escobal, P.R., Methods of Astrodynamics, Appendix 2, John Wiley and Sons, New York, 1969.
- [4.2] Munk, W.H., and MacDonald, G.J.F., The Rotation of the Earth, Cambridge University Press, 1960.
- [4.3] Kopal, Z., Physics and Astronomy of the Moon, Academic Press, New York, 1962.
- [4.4] Landsberg, H.E., and Van Mieghem, J., Advances in Geophysics (A.T. Dodson, Vol. 5), Academic Press, New York, 1958.
- [4.5] Lambeck, K., Cayenave, A., and Balmino, G., "Solid Earth and Ocean Tides Estimated from Satellite Orbit Analyses," Reviews of Geophysics and Space Physics, Vol. 12, No. 3, Aug. 1974.
- [4.6] Newton, R. R., "An Observation of the Satellite Perturbation Produced by the Solar Tide", J. Geophys. Res., 70, 5983-5989, 1965.
- [4.7] Newton, R.R., "A Satellite Determination of Tidal Parameters and Earth Deceleration", Geophys. J. Roy. Astron. Soc., 14, 505-539, 1968.
- [4.8] Pekeris, C.L., and Y. Accad, "Solution of Laplace's Equations for M_2 Tide in the World Oceans", Phil. Trans. Roy. Soc. London, Ser. A, 265, 413-436, 1969.
- [4.9] Pertsev, B. P., "The Effect of Ocean Tides upon Earth Tide Observations", Comm. A-9 Ser. Geophys. Observ. Roy. Belgique, 96, 113-115, 1969.
- [4.10] Prothero, W.A., and J.M. Goodkind, "Earth Tide Measurements with the Superconducting Gravimeter," J. Geophys. Res. 77, 926, 1972.

- [4.11] Reigber, C., "Generalized Fourier Analysis of Resonant Orbits," Space Res., 13, 3-10, 1973.
- [4.12] Slichter, L.B., "Earth Tides", in The Nature of the Solid Earth, edited by E. C. Robertson, pp. 285-320, McGraw-Hill, New York, 1972.
- [4.13] Smith, D.E., P.J. Dunn, and R. Kolenkiewicz, "Earth Tidal Amplitude and Phase," Nature, 244, 498, 1973.
- [4.14] Stacey, F.D., Physics of the Earth, p. 324, John Wiley and Sons, New York, 1970.
- [4.15] Takeuchi, M., M. Saito, and N. Kobayashi, "Statical Deformations and Free Oscillations of a Model Earth," J. Geophys. Res., 67, 1141-1154, 1962.
- [4.16] Wagner, C.A., "Zonal Gravity Harmonics from Long Satellite Arcs by a Seminumeric Method," J. Geophys. Res., 78, 3271, 3280, 1973.
- [4.17] Wunsch, C., "Bermuda Sea Level in Relation to Tides, Weather and Baroclinic Fluctuation," Rev. Geophys. Space Phys., 10, 1-49, 1972.
- [4.18] Hendershott, M.C., "The Effects of Solid Earth Deformation on Global Ocean Tides," Geophysical Journal of Royal Astronomical Society, pp. 389-402, 29, 1972.
- [4.19] Escobal, P.R., and Von Roos, O.H., "Ground Station Deflections Due to Ocean Tides," JPL EM 391-629, 29 March 1976 (JPL internal document).

A5. Generalized Tropospheric Calibration and Error Analysis



Abstract

A second order analytic tropospheric calibration technique is developed herein which permits ground station-to-satellite, airplane-to-satellite, airplane-to-airplane, and ground-to-airplane range corrections to be determined. Standard deviations of the atmospheric modeling constants are cited. Every parameter included in the model is varied to obtain the error contribution peculiar to the parameter. The total random error in the calibration range increment is determined to be 1.3 cm. Bias errors of 0.25 cm are also determined. The model has been verified and compared to a numerically integrated counterpart. Accuracies in the calibration as quoted above are expected to zenith angles $\leq 50^\circ$. Beyond this range of zenith angles, an additional correction, also developed herein, is required. The pertinent covariance matrix of the model is developed.

PRECEDING PAGE BLANK NOT FILMED

A5.1 INTRODUCTION

The evolution of multilateration theory, capable of centimeter level interstation coordinate determination, clearly places stringent requirements on all components of an operational multilateration system. In essence, no system is better from an accuracy point of view than its weakest link. To this end, the accuracy to which the basic data observables can be corrected for atmospheric attenuation is central to the operational multilateration system. Further constraints imposed on a multilateration system are those of system flexibility, i.e., the analytic calibration theory should be capable of handling ground-to-satellite, airplane-to-satellite, ground-to-airplane, and airplane-to-airplane multilateration systems. Finally, the calibration equations should be valid over as large a viewing arc as possible in order to achieve maximum statistical improvement.

The analysis performed herein considers and includes the aforementioned components in the detail demanded by the sought for multilateration objectives [5.6]. The ionospheric corrections are discussed in Appendix A6.

A5.2 ERROR BUDGET ANALYSIS

Table A5.1 lists the atmospheric parameters, nomenclature, nominal value, units, and standard deviation of the parameters used in the calibration model. A distinction is made between parameters which are true random variables (possessed of slow or fast jitter) and those parameters which are bias like. The bias like variables are enclosed by a box. These parameters have a standard deviation, but for purposes of processing a batch of data, have fixed (non-jittering) errors. The standard deviations (wherever possible) were obtained from literature surveys and represent realistic values required to meet the multilateration objectives.

Since the atmospheric effects will be largest for the ground-to-satellite calibration analysis, the analytic calibration algorithm was exercised for this worst case with various zenith angles (angle between station vertical and vehicle position vector as viewed at the station; see Figure A5.1) extending to the limits of applicability of the analytic expansions peculiar to the model. Typical results for random error type parameters are displayed in Table A5.2.

The results in this table show the finite difference partial derivatives of the atmospheric correction Δp with respect to a typical parameter, p , i.e., $\partial \Delta p / \partial p$.

The partial derivatives in Table A5.2 permit a quick evaluation of the errors induced by these parameters. This evaluation can then serve as a basis for segregating the major error sources (for analytic partial considerations) and bounding the errors of all the minor error sources. Hence, extracting average partials from Table A5.2 and using the standard deviations in Table A5.1, the minor error contributors are given by Σ_1 , namely,

$$\Sigma_1 \equiv \Sigma \left(\frac{\partial \Delta p}{\partial p} \sigma_p \right)^2 :$$

$$\begin{aligned} \Sigma_1 = & (1.0 \times 10^4 \times 0.5 \times 10^{-5})^2 = 25.0 \times 10^{-4}, & \alpha \\ & + (0.06 \times 1.0)^2 = 36.0 \times 10^{-4}, & T^* \\ & + (0.30 \times 10^{-5} \times 5.0 \times 10^3)^2 = 2.25 \times 10^{-4}, & h_0 \\ & + (0.2 \times 10^{-6} \times 2.5 \times 10^4)^2 = 4.0 \times 10^{-4}, & h_1 \\ & + (0.07 \times 1.0)^2 = 49.0 \times 10^{-4}, & t \\ & + (50.0 \times 0.25 \times 10^{-3})^2 = 1.56 \times 10^{-4}, & g \\ & + (0.6 \times 10^{-3} \times 1.0 \times 10^2)^2 = 36.0 \times 10^{-4}, & H_0 \\ & + \text{Negligible terms} \approx 245.0 \times 10^{-4}. \end{aligned}$$

Denoting the major contributions by:

$$\Sigma_2 = \Sigma \left(\frac{\partial \Delta p}{\partial p} \sigma_p \right)^2$$

$$\begin{aligned} \Sigma_2 = & (1.5 \times 0.1)^2 = 225.0 \times 10^{-4}, & T_0 \\ & + (0.4 \times 10^{-4} \times 1.0 \times 10^4)^2 = 1,600.0 \times 10^{-4}, & h_w \\ & + (3.5 \times 10^5 \times 0.25 \times 10^{-6})^2 = 76.0 \times 10^{-4}, & \rho_0 \\ & + (700.0 \times 0.1 \times \pi/180)^2 = 15,000.0 \times 10^{-4}, & z \\ & \approx 16,900 \times 10^{-4}. \end{aligned}$$

Therefore an estimate to the random error of the atmospheric calibration is given by:

$$\sigma_{\Delta\rho} = (\Sigma_1 + \Sigma_2)^{1/2} \cong 1.35 \text{ cm.}$$

Performing a similar error analysis for the bias like error sources (see Table A5.2), it follows that

$$\Sigma_3 = \Sigma \left| \frac{\partial \Delta\rho}{\partial p} \Delta p \right|$$

is given by:

$$\begin{aligned} \Sigma_3 = & \left| 1.0 \times 10^{-2} \times 2.0 \right| = 2.0 \times 10^{-2}, \bar{R} \\ & + \left| 32.0 \times 3.0 \times 10^{-3} \right| = 9.6 \times 10^{-2}, M \\ & + \left| 25.0 \times 3.0 \times 10^{-3} \right| = 7.5 \times 10^{-2}, K_3 \\ & + \left| 1.5 \times 10^{-2} \right| = 1.5 \times 10^{-2}, e_1 \\ & \hline & \approx 21 \times 10^{-2}. \end{aligned}$$

The bias like estimate, $\Delta_{\rho B}$, (always in a fixed direction) is therefore determined for the worst case as:

$$\Delta_{\rho B} = \Sigma_3 \cong 0.25 \text{ cm.}$$

It must be realized that the above estimates for the pertinent error bounds do not account for deviations of the analytic model from the exact theoretical expression defining the atmospheric correction (Eq. 18). Hence, in order to ascertain the accuracy of the analytic model, the residual error between the correction computed via the analytic model and expression (18) was determined using double precision integration. This residual is displayed graphically in Figure A5.1 as a function of increasing zenith angle. As can

be seen for all system configurations (ground-to-satellite, etc.) the error is less than 1 cm for zenith angles less than 50° . For purposes other than multilateration this level of numerical accuracy would suffice, however to reduce the threshold accuracy the analytic model used herein must be supplemented via a hybrid technique. This technique consist of performing a numerical integration for a limited number of zenith angles and curve fitting the residual error as a function of zenith angle. This provides an analytic polynomial which can be used to erradicate the modeling error. This hybrid technique is adopted for all multilateration studies discussed herein.

Table A5.1. Atmospheric Parameters

Definition	Symbol	Value	Units	Error σ *
Universal Gas Constant	\bar{R}	$8.3142 \cdot 10^4$	mbar cm^3 ($^\circ\text{K}$) $^{-1}$	$0.0002 \cdot 10^4$
Molecular Weight of Air	M	28.966	g	0.003
Vertical Temperature Lapse Rate	α	6.8	$^\circ\text{K}/\text{km}$	0.5
Inversion Layer Altitude	h_0	depending on season and time of day	m	50
Tropopause Altitude	h_1	11000	m	1000
1st Refractivity Constant	K_1			
Microwave:		77.624	$^\circ\text{K}$ (mbar) $^{-1}$	0.1
Laser: (Ruby)		80.34	$^\circ\text{K}$ (mbar) $^{-1}$	0.01
2nd Refractivity Constant	K_2			
Microwave:		12.92	$^\circ\text{K}$ (mbar) $^{-1}$	9.0
Laser: (Ruby)		-11.3		
3rd Refractivity Constant	K_3			
Microwave:		0.3719	($^\circ\text{K}$) 2 (mbar) $^{-1}$	0.003
Laser:		0.0		
Zenith Angle	z		deg	0.1
Ground Temperature	T_0		$^\circ\text{K}$	0.1
Water Vapor Scale Height	h_w	2	km	0.1
Surface Gravity	g_R	978.0495 at sealevel, equator	cm sec^{-2}	0.25×10^{-3}
Water Vapor Constants of Eq. (30):	k_1	7.567		0.001
	k_2	2066.92	$^\circ\text{K}$	1.0
	k_3	33.45	$^\circ\text{K}$	0.01
	e_1	6.11	mbar	0.01
Ground air mass density at Station 1	ρ_0	1.5×10^{-3}	gm/cm^3	$2.5 \cdot 10^{-5}$
Temperature of Inversion layer	T^*		$^\circ\text{K}$	1
Dew Point Temperature of H_2O	t		K	1
Lower Station Altitude	H_0		cm	100
Upper Station Altitude	H_1		cm	1000

(Boxed Parameters Denote Bias-like Error Sources)

(*Errors Taken Purposely Large)

Table A5.2 Pertinent Partial Derivatives

Parameter	$\partial(\text{correction})/\partial p$	
p	z = 40°	z = 60°
$\alpha \text{ } ^\circ\text{K}^{-1} \text{ cm}^2$	7933	15,000
$\bar{R} \text{ cm}^{-2} \text{ } ^\circ\text{K/mbar}$	0.009	0.014
$T^* \text{ cm/}^\circ\text{K}$	-0.045	-0.072
h_0	-0.3×10^{-5}	0.3×10^{-5}
h_w	0.37×10^{-4}	$+0.56 \times 10^{-4}$
h_1	-0.3×10^{-6}	-0.1×10^{-5}
$t \text{ cm/}^\circ\text{C}$	0.058	0.088
$z \text{ cm/rad}$	221	1069
$M \text{ cm/gm}$	-26	-39.7
$gr \text{ sec}^2$	-38	-58
$\rho_0 \text{ cm}^4/\text{gm}$	2.8×10^5	3.9×10^5
$T_0 \text{ cm/}^\circ\text{K}$	1.31	2.00
$K_1 \text{ cm-mbar/}^\circ\text{K}$	4.87	7.5
$K_2 \text{ cm-mbar/}^\circ\text{K}$	-0.01	-0.01
$K_3 \text{ cm-mbar/}^\circ\text{K}^2$	17.74	28.3
$R_{\text{earth}} \equiv a_e$	-0.1×10^{-8}	$+0.3 \times 10^{-8}$
H_0	-0.5×10^{-3}	-0.7×10^{-3}
H_1	0.7×10^{-7}	$+0.1 \times 10^{-7}$
$k_1 \text{ cm}$	-0.026	-0.040
$k_2 \text{ cm/}^\circ\text{K}$	1.9×10^{-4}	2.9×10^{-4}
$k_3 \text{ cm/}^\circ\text{K}$	-8.97×10^{-3}	-11.96×10^{-3}
$e_1 \text{ cm/mbar}$	1.705	1.115

ORIGINAL PAGE IS
OF POOR QUALITY

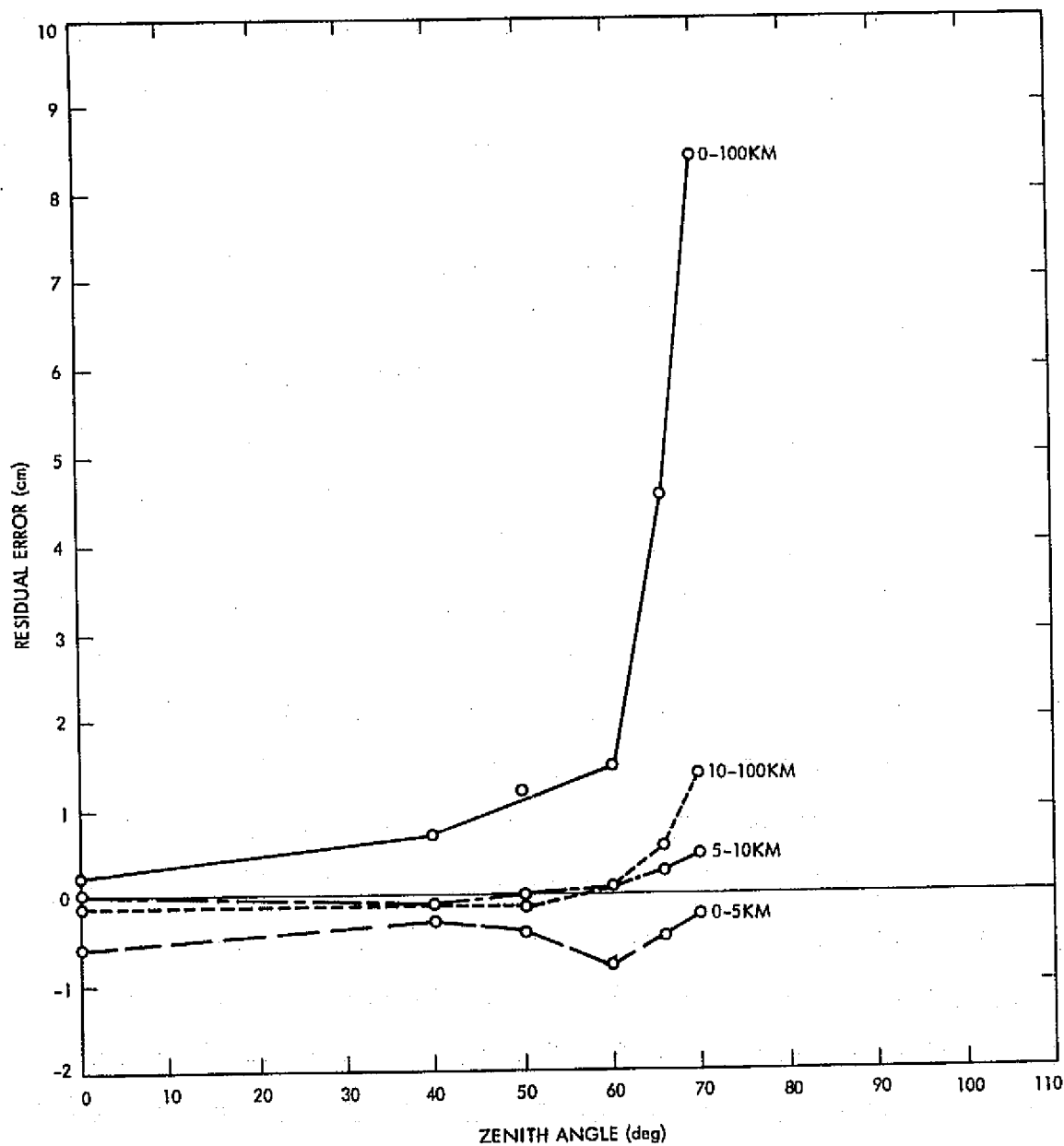


Figure A5.1. Plot of Exact versus Analytic Range Correction Residuals

A5.3 TROPOSPHERIC RANGE CORRECTION DERIVATION

Let the raypath between an observing station on the surface of the Earth and the receiving satellite be given analytically by:*

$$\theta_p = \theta_p(r). \quad (1)$$

From Fig. A5.2 the end point conditions can be obtained as

$$\theta_p(R) = \theta_s \quad (2)$$

and

$$\theta_p(r_1) = \theta_1 = \theta_s - z + \sin^{-1} \left(\frac{R}{r_1} \sin z \right),$$

where z is the zenith angle of the geometrical raypath between station and satellite, θ_s the latitude of the station, R the radius of the Earth, and r_1 the distance of the satellite from the center of the Earth. The range correction $\Delta \rho$ due to the troposphere is then given by:

$$\Delta \rho = \int_R^{r_1} n(r) dr \left(1 + r^2 \theta_p'^2 \right)^{1/2} - \int_R^{r_1} \left(dr \left(1 + r^2 \theta_o'^2 \right) \right)^{1/2}. \quad (3)$$

In Eq. (3) the prime signifies the derivative with respect to r , and $\theta_o(r)$ is the geometric (straight line) path in the absence of the troposphere. Both $\theta_p(r)$ and $\theta_o(r)$ are subject to conditions (2). The refractive index n is assume to be stratified radially. The actual raypath θ_p , i. e., θ_p as a function of r is determined by Euler's equations which in this case reduce to just one equation.

* Later we will consider the general case of two stations immersed in the atmosphere at arbitrary positions.

$$\frac{d}{dr} \left\{ n(r) \left(1 + r^2 \theta_p'^2 \right)^{-1/2} r^2 \theta_p' \right\} = 0, \quad (4)$$

which yields with the integration constant c

$$\theta_p' = \frac{c}{r} (n^2 r^2 - c^2)^{-1/2} \quad (5)$$

and

$$\theta_p(r) = \theta_s + \int_R^r \frac{c}{x} dx (n^2 x^2 - c^2)^{-1/2}. \quad (6)$$

Equation (6) already satisfies one of the conditions (2). The second condition (2) determines the integration constant c and reads:

$$\int_R^{r_1} \frac{c}{x} dx (n^2 x^2 - c^2)^{-1/2} = -z + \sin^{-1} \left(\frac{R}{r_1} \sin z \right). \quad (7)$$

Advantage will now be taken of the fact that $n - 1 \ll 1$ so that an expansion of Eq. (7) to 1st order in $n - 1$ is possible. Therefore putting $n = 1 + \chi$ and $c = c_0 + c_1$ where $c_0 \equiv 0(1)$ and $c_1 \equiv 0(\chi)$ and expanding the integrand of Eq. (7) to order χ after a little algebra gives:

$$\begin{aligned} -z + \sin^{-1} \left(\frac{R}{r_1} \sin z \right) &= \int_R^{r_1} \frac{c_0}{x} dx (x^2 - c_0^2)^{-1/2} \\ &+ \int_R^{r_1} x dx (c_1 - c_0 \chi) (x^2 - c_0^2)^{-3/2}. \end{aligned} \quad (8)$$

Equation (8) is satisfied by demanding that:

$$\begin{aligned} \int_R^{r_1} \frac{c_o}{x} (x^2 - c_o^2)^{-1/2} dx &= \cos^{-1}\left(\frac{c_o}{r_1}\right) - \cos^{-1}\left(\frac{c_o}{R}\right) \\ &= -z + \sin^{-1}\left(\frac{R}{r_1} \sin z\right) \end{aligned} \quad (9a)$$

and

$$\int_R^{r_1} dx x (x^2 - c_o^2)^{-3/2} [c_1 - c_o \chi(x)] = 0. \quad (9b)$$

Before solving Eq. (9a) for c_o Eq. (3) is evaluated to first order in $n - 1 = \chi$. From Eq. (5) it follows that:

$$\theta_p' = \frac{c_o}{r} (r^2 - c_o^2)^{-1/2} + r \frac{c_1 - c_o \chi}{(r^2 - c_o^2)^{3/2}} \equiv \theta_o' + \theta_1'. \quad (10)$$

Inserting therefore Eq. (10) into Eq. (3) gives

$$\begin{aligned} \Delta \rho &= \int_R^{r_1} dr \left[(1 + \chi) \left(1 + r^2 \theta_o'^2 + 2 r^2 \theta_o' \theta_1' \right)^{1/2} \right. \\ &\quad \left. - \left(1 - r^2 \theta_o'^2 \right)^{1/2} \right], \end{aligned} \quad (11)$$

where θ_o' and θ_1' are given by Eq. (10). Hence expanding the square roots in Eq. (11) to first order in χ yields:

$$\Delta \rho = \int_R^{r_1} dr \chi(r) \left(1 + r^2 \theta_o'^2\right)^{1/2} + \int_R^{r_1} dr \frac{r^2 \theta_o' \theta_1'}{\left(1 + r^2 \theta_o'^2\right)^{1/2}}. \quad (12)$$

The second integral in Eq. (12) vanishes identically because of Eq. (9b). Expressing θ_o' by:

$$\theta_o' = \frac{c_o}{r} \left(r^2 - c_o^2\right)^{-1/2} \quad (13)$$

it follows from Eq. (12) that:

$$\Delta \rho = \int_R^{r_1} dr (n(r) - 1) r \left(r^2 - c_o^2\right)^{-1/2}, \quad (14)$$

and it remains to determine c_o^2 from Eq. (9a). This is easily done using an addition theorem for the inverse cosine function. It is:

$$\cos^{-1}\left(\frac{c_o}{r_1}\right) - \cos^{-1}\left(\frac{c_o}{R}\right) = \cos^{-1}\left\{\frac{c_o^2}{r_1 R} + \left(1 - \frac{c_o^2}{r_1^2}\right)^{1/2} \left(1 - \frac{c_o^2}{R^2}\right)^{1/2}\right\}, \quad (15)$$

and therefore:*

$$c_o^2 = r_1^2 r_o^2 \sin^2 \alpha \left(r_1^2 + r_o^2 - 2 r_1 r_o \cos \alpha\right)^{-1}, \quad (16)$$

with (see Figure A5.1)

$$\alpha \equiv z - \sin^{-1}\left(\frac{r_o}{r_1} \sin z\right), \quad (16b)$$

* $R = r_o$ allowing for the 1st station to be above ground.

C.3

so that finally

$$c_o^2 = r_o^2 \sin^2 z \quad . \quad (17)$$

This is just the expression used before [5.1].

A5.4 DEVELOPMENT OF ANALYTIC EXPRESSIONS FOR TROPOSPHERIC RANGE CORRECTIONS

The expression for the range correction derived in Section A5.3, may be written as

$$\Delta \rho = \int_{r_o}^{r_1} dr (n(r) - 1) \left(1 - \frac{c_o^2}{r^2} \right)^{-1/2} \quad (18)$$

with c_o given by Eq. (17). Before discussing the details concerning the refractive index $n(r)$, the square root occurring in Eq. (18) must be expanded, otherwise expression (18) could only be treated numerically. The fact that the troposphere consists only of a thin layer of an extent much smaller than the radius of the Earth, R , suggests a change of variables, viz.

$$r = R(1+x), \quad (19)$$

where x is dimensionless and $x \ll 1$ throughout the range of integration. Hence the square root of Eq. (18) can be written as:

$$\left(1 - \frac{c_o^2}{r^2} \right)^{-1/2} = \left\{ 1 - \frac{c_o^2}{R^2} (1+x)^{-2} \right\}^{-1/2} \quad (20)$$

and an expansion in powers of x carried out. It is sufficient to expand up to the second order in x (since x is the tropospheric altitude divided by R which is always small). Therefore upon expansion:

$$\begin{aligned}
\left(1 - \frac{c_o^2}{r^2}\right)^{-1/2} &= (1+x) \left((1+x)^2 - \frac{c_o^2}{R^2}\right)^{-1/2} \\
&= \left(1 - c_o^2/R^2\right)^{-1/2} (1+x) \left(1 + \frac{2x + x^2}{1 - c_o^2/R^2}\right)^{-1/2} \\
&= \left(1 - c_o^2/R^2\right)^{-1/2} \left\{ 1 + \left[1 - \left(1 - c_o^2/R^2\right)^{-1} \right] x \right. \\
&\quad \left. + \frac{3}{2} \left(1 - c_o^2/R^2\right)^{-1} \left[\left(1 - c_o^2/R^2\right)^{-1} - 1 \right] x^2 \right\}. \quad (21)
\end{aligned}$$

Considering two stations at position r_o and r_1 , the range correction applicable between the two stations can be obtained from Eqs. (18) and (21) (with R replaced by r_o in expression (21)):

$$\begin{aligned}
\Delta\rho = R (\cos z)^{-1} \int_{\frac{r_o - R}{R}}^{\frac{r_1 - R}{R}} dx (n(x) - 1) \left\{ 1 - x \tan^2 z \right. \\
\left. + \frac{3}{2} x^2 (\cos z)^{-2} \tan^2 z \right\}. \quad (22)
\end{aligned}$$

The expansion (21) breaks down if $c_o \approx r_o$. This is for instance true if $z \approx 90^\circ$ (near horizon tracking). If the allowable zenith angles are less or equal to 80° then $1 - c_o^2/R^2 \approx 0.03$ if $r_1 \gg R$ and $z = 80^\circ$; whereas x is at most equal to 0.02 (assuming a vastly overestimated tropospheric height of 100 km) so that $x^2 (1 - c_o^2/R^2)^{-1} \ll 1$, and the series in the bracket of expression (22) is rapidly convergent. For $z \leq 80^\circ$ the retention of terms up to order x^2 is amply sufficient. With these understandings it is possible to turn to the determination of $\chi(x) = n(x) - 1$.

A5.5 THE REFRACTIVE INDEX AS A FUNCTION OF ALTITUDE

The foundations of this analysis rely on previous work. Reference [5, 2] gives some reviews of previous work. It turns out that an excellent expression for χ in the microwave region is the following (adopted from Ref. [5, 3]):

$$\chi \cdot 10^6 = K_1 \frac{P}{T} - K_2 \frac{e_w}{T} + K_3 \frac{e_w}{T^2}, \quad (23)$$

where P is the total air pressure in mbar, e_w the partial pressure of water vapor also in mbar, and T the temperature in °K. The constants occurring in Eq. (23) are displayed in Table 5.1. For visible light (laser) K_3 is essentially zero and K_1 differs somewhat from the microwave case (see Table A5.1). In order to evaluate the integral (22) we have to know the pressure and temperature variations with altitude. To take account of an inversion layer near ground the following model for the temperature as a function of altitude h is adopted:

$$\left. \begin{aligned} T &= T_0 - (\alpha - 2h_0^{-1} \Delta) h - h_0^{-2} \Delta h^2 & \text{for } h < h_0 \\ T &= T_1 - \alpha h & \text{for } h > h_0 \end{aligned} \right\} \quad (24)$$

This temperature profile is depicted in Fig. A5.3. Note that T and its first derivative are continuous at $h = h_0$. The parameters introduced in Eq. (24) are the lapse rate α , the height h_0 of the inversion layer, and $\Delta = T_1 - T_0$ which is given by $\Delta = T^* - T_0 + \alpha h_0$. Therefore only three parameters are involved the lapse rate α , the height h_0 of the inversion layer and the temperature T^* at which the inversion layer goes over into the linear regime. The linear regime extends just to the border of the stratosphere (the tropopause). Adopting the I. C. A. O. standard atmosphere (see Fig. A5.4) it can be seen that at an altitude of $h_1 = 11$ km the temperature becomes constant, viz.:

$$T = T_1 - \alpha h_1, \quad \text{for } h > h_1. \quad (24b)$$

Equations (24) and (24b) give the phenomenological expressions for the altitude dependence of the atmospheric temperature below 25 km. Above 25 km the I. C. A. O. model suggests an altitude dependence of the form

$$T = T_1 - \alpha h_1 + \beta h, \quad \text{for } h > 25 \text{ km.} \quad (24c)$$

Since the air pressure drops down to insignificant values at altitudes greater than 45 km there is no need to extend the temperature model any further. The dry air pressure and density are now determined by:

$$P = \rho \frac{\bar{R}}{M} T \quad (25)$$

$$dP = -10^{-3} \rho \bar{g} dh. \quad (26)$$

In Eqs. (25) and (26) M is the molecular weight in grams of air and \bar{g} is the average gravitational acceleration (see Table A5.1 and Ref. [5.3]). The molecular weight and gas constant R are found in Table A5.1.

The water vapor pressure e_w on the other hand may sometimes be given by the equation:

$$e_w = e_{ow} 10^{-\left(\frac{h}{\gamma} - \frac{h^2}{\delta}\right)} \quad (27)$$

with $\gamma = 8 \text{ km}$, $\delta = 48 \text{ km}^2$ [5.4]. Equation (27) is an empirical expression. Values for γ and δ have been found during a time period of 2 years in the Moscow area to be $\gamma = 11.8 \text{ km}$ and $\delta = 62.1 \text{ km}^2$. Obviously the empirical values γ and δ are subject to considerable variations depending on the climate and the seasons. Reference [5.4] has proposed (for the altitude dependence of the water vapor pressure):

$$e_w = e_{ow} \exp \left\{ - (h / h_w) \right\} \quad (28)$$

with h_w ranging from 2 to 2.5 km. Yet still other authors [5.3, 5.5] use

$$e_w = e_{ow} (T / T_o)^{-n}, \quad (29)$$

where $n \approx 20$ or 4 or 1.3 a choice apparently motivated by the whim of the investigator. In the further analysis the empirical expression (28) shall be used, where the scale height h_w of the water vapor pressure must be determined by measurements prior to an application of Eq. (22). In all these equations e_{ow} signifies the ground water vapor pressure and is given by:

$$e_{ow} = e_1 \cdot 10^{\{(7.567t - 2066.92)/(t - 33.45)\}}, \quad (30)$$

again an empirical formula. The values of the various constants occurring in Eq. (30) are listed in Table A5.1.

Use of Eqs. (24), (24b), and (24c) for the temperature, Eqs. (25) and (26) for dry air in hydrostatic equilibrium and finally Eqs. (28) and (30) for the water vapor pressure determines ultimately the range correction (Eq. (22)).

A5.6 DETERMINATION OF THE RANGE CORRECTION

Equation (22) is repeated here for ease of reference (considering only terms up to the second order in x and expressing the dimensionless variable x in terms of the altitude in cm. From Eq. (19) it is clear that $x = h/r_o$ and so:

$$\Delta P = (\cos z)^{-1} \int_{H_0}^{H_1} dh \times (h) \left\{ 1 - \tan^2 z \left(\frac{h}{r_o} - \frac{3}{2} (\cos z)^{-2} \frac{h^2}{r_o^2} \right) \right\}. \quad (31)$$

In the further analysis it is convenient to split the contributions to the range correction (31) into dry and wet components according to Eq. (23).

a. The Dry Component

For the dry air component, from Eq. (23)

$$\chi_{\text{dry}} = 10^{-6} K_1 \frac{P}{T} \quad (32)$$

which gives together with Eqs. (25) and (26)

$$\Delta p_{\text{dry}} = (\cos z)^{-1} 10^{-3} \frac{K_1 \bar{R}}{M \bar{g}} \int_{P_1}^{P_0} dP \left\{ 1 - \tan^2 z \left(\frac{h}{r_0} - \frac{3}{2} (\cos z)^{-2} \frac{h^2}{r_0^2} \right) \right\}, \quad (33)$$

where P_0 and P_1 are the pressures at their respective altitudes H_0 and H_1 . The first term on the RHS of Eq. (33) makes the largest contribution to the range correction and can be evaluated immediately to give the 1st term of Eq. (33):

$$\Delta p_{\text{dry}} = (\cos z)^{-1} 10^{-3} K_1 \frac{\bar{R} (P_0 - P_1)}{M \bar{g}}. \quad (34)$$

The 2nd term of Eq. (33) is somewhat more difficult to evaluate. First Eqs. (25) and (26) yield for ρ as a function of altitude:

$$\rho(h) = \rho_0 \frac{T_0}{T(h)} \exp \left\{ -10^{-3} \frac{g M}{\bar{R}} \int_0^h \frac{dh'}{T(h')} \right\}, \quad (35)$$

so that

$$A_1 = \int_{P_1}^{P_0} dP h = 10^{-3} \bar{g} \int_{H_0}^{H_1} h dh \frac{\rho_0 T_0}{T(h)} \exp \left\{ -10^{-3} \frac{\bar{g} M}{R} \int_0^h \frac{dh'}{T(h')} \right\} \quad (36a)$$

and the third integral of Eq. (33) becomes:

$$A_2 = \int_{P_1}^{P_0} dP h^2 = 10^{-3} \bar{g} \int_{H_0}^{H_1} h^2 dh \frac{\rho_0 T_0}{T(h)} \exp \left\{ -10^{-3} \frac{\bar{g} M}{R} \int_0^h \frac{dh'}{T(h')} \right\}. \quad (36b)$$

The substitution

$$\int_0^h \frac{dh'}{T(h')} = x \quad (37)$$

yields

$$\left. \begin{matrix} A_1 \\ A_2 \end{matrix} \right\} = 10^{-3} \rho_0 T_0 \bar{g} \int_{X_0}^{X_1} \left\{ \begin{matrix} h \\ h^2 \end{matrix} \right\} dx e^{-10^{-3} \frac{\bar{g} M}{R} x} \quad (38)$$

It is now necessary to determine h as a function of x . The temperature profiles as given in Eqs. (24) must be used in conjunction with Eq. (37). It follows that if an inversion layer exists ($h < h_o$; $\Delta \neq 0$) then the computations proceed with Eq. (39); otherwise they proceed to Eq. 44b. Hence for the inversion layer ($h < h_o$) introducing the definition:

$$a \equiv \left[\left(\alpha - 2 h_o^{-1} \Delta \right)^2 + 4 T_o \Delta h_o^{-2} \right]^{1/2} \quad (39)$$

it follows that:

$$x = a^{-1} \left[\ln \left(\frac{2 \Delta h_o^{-2} h + \alpha - 2 h_o^{-1} \Delta + a}{2 \Delta h_o^{-2} h + \alpha - 2 h_o^{-1} \Delta - a} \right) - \ln \left(\frac{\alpha - 2 h_o^{-1} \Delta + a}{\alpha - 2 h_o^{-1} \Delta - \alpha} \right) \right], \quad h < h_o. \quad (40a)$$

However for $h_o < h < h_1$:

$$x = a^{-1} \ln \left(\frac{\alpha + a}{\alpha - a} \right) - a^{-1} \ln \left(\frac{\alpha - 2 h_o^{-1} \Delta + a}{\alpha - 2 h_o^{-1} \Delta - a} \right) + \frac{1}{\alpha} \ln \left(\frac{T_1 - \alpha h_o}{T_1 - \alpha h} \right), \quad h_o < h < h_1 \quad (40b)$$

and for $h > h_1$

$$x = a^{-1} \ln \frac{(\alpha + a)(\alpha - 2h_o^{-1}\Delta - a)}{(\alpha - a)(\alpha - 2h_o^{-1}\Delta + a)} + \frac{1}{\alpha} \ln \frac{T_1 - \alpha h_o}{T_1 - \alpha h_1} + \frac{h - h_1}{T_1 - \alpha h_1}, \quad h > h_1. \quad (40c)$$

It follows now that inversion of Eqs. (40) yields

$$h = h_{\text{inv}} = 2T_o \frac{1 - e^{-ax}}{\alpha - 2h_o^{-1}\Delta + a - (\alpha - 2h_o^{-1}\Delta - a)e^{-ax}}, \quad h < h_o, \quad (41a)$$

and

$$h = h_{\text{lapse}} = \frac{1}{\alpha} \left\{ T_1 - (T_1 - \alpha h_o) \left(\frac{(\alpha - 2h_o^{-1}\Delta - a)(\alpha + a)}{(a - 2h_o^{-1}\Delta + a)(\alpha - a)} \right)^{\alpha/a} e^{-\alpha x} \right\}, \quad h_o < h < h_1 \quad (41b)$$

and

$$h = h_{\text{strato}} = h_1 + (T_1 - \alpha h_1) \left[x - \frac{1}{\alpha} \ln \left(\frac{T_1 - \alpha h_0}{T_1 - \alpha h_1} \right) - \frac{1}{a} \ln \left(\frac{(\alpha + a)(\alpha + 2h_1^{-1}\Delta - a)}{(\alpha - a)(\alpha + 2h_1^{-1}\Delta + a)} \right) \right] \text{ for } h > h_1. \quad (41c)$$

The integration of Eqs. (38) can now be performed. Hence with $b \equiv 10^{-3} \bar{g} M/\bar{R}$ (from Eq. (38)):

$$\left(10^{-3} \bar{g} \rho_0 T_0 \right)^{-1} A_1 = \int_{X_0}^{x_0} dx e^{-bx} h_{\text{inv}} + \int_{x_0}^{x_1} dx e^{-bx} h_{\text{lapse}} + \int_{x_1}^{\infty} dx e^{-bx} h_{\text{strato}}, \quad (42)$$

where X_1 corresponds to the vehicle altitude. Hence defining the previous integrals by:

$$A'_1 = A'_{11} + A'_{12} + A'_{13} \quad (43)$$

the corresponding values are:

$$A'_{11} = 2\lambda_1 T_0 \int_{X_0}^{x_0} dx e^{-bx} \frac{1 - e^{-ax}}{\alpha - 2h_0^{-1}\Delta + a - (\alpha - 2h_0^{-1}\Delta - a)e^{-ax}},$$

$$\lambda_1 = \begin{cases} 1 & \text{if } X_0 \leq x_0 \\ 0 & \text{if } X_0 > x_0 \end{cases} \quad (44)$$

With the substitution $e^{-ax} = y$, A'_{11} is given by

$$A'_{11} = -2\lambda_1 T_o a^{-1} \int_{Y_o}^{y_o} dy y^{\frac{b}{a}-1} (A - By)^{-1} (1 - y) , \quad (44a)$$

where

$$y_o = e^{-ax_o} = \frac{(\alpha - a)(\alpha - 2h_o^{-1}\Delta + a)}{(\alpha + a)(\alpha - 2h_o^{-1}\Delta - a)} . \quad (44b)$$

Noting that

$$Y_o = \frac{(2\Delta h_o^{-2} H_o + \alpha - 2h_o^{-1}\Delta - a)(\alpha - 2h_o^{-1}\Delta + a)}{(2\Delta h_o^{-2} H_o + \alpha - 2h_o^{-1}\Delta + a)(\alpha - 2h_o^{-1}\Delta - a)} \quad (44c)$$

$$y_o - 1 \ll 1, \quad Y_o - 1 \ll 1$$

and using prevalent values of the parameters ($\alpha \approx 6$ [$^{\circ}\text{K}/\text{km}$], $a \approx 6$ to 60 [$^{\circ}\text{K}/\text{km}$], $\Delta \approx 10^{\circ}\text{K}$, $h_o \approx 0.5$ km), A'_{11} is obtained by expanding about $y = 1$ and keeping only the lowest order in $y_o - 1$ as:

$$A'_{11} = \lambda_1 \frac{T_o}{2a^2} \left[(y_o - 1)^2 - (Y_o - 1)^2 \right] . \quad (44c)$$

Similarly:

$$A'_{12} = \lambda_2 \frac{T_1}{a b} y_o^{b/a} \left(1 - \left(\frac{T_1 - \alpha H_1}{T_1 - \alpha h_o} \right)^{b/a} \right) - \lambda_2 \frac{T_1 - \alpha h_o}{a(\alpha + b)} y_o^{(\alpha+b)/a} \left(1 - \left(\frac{T_1 - \alpha H_1}{T_1 - \alpha h_o} \right)^{(\alpha+b)/a} \right) \quad (44d)$$

$$\begin{aligned}
A'_{13} = & \frac{\lambda_3}{b} \left(h_1 - \frac{T_1 - \alpha h_1}{\alpha} \ln \frac{T_1 - \alpha h_o}{T_1 - \alpha h_1} \right. \\
& + \left. \frac{T_1 - \alpha h_1}{a} \ln y_o \right) y_o^{b/a} \left(\frac{T_1 - \alpha h_1}{T_1 - \alpha h_o} \right)^{b/\alpha} \\
& + \frac{T_1 - \alpha h_1}{b^2} y_o^{b/a} \left(\frac{T_1 - \alpha h_1}{T_1 - \alpha h_o} \right)^{b/\alpha} \\
& + \frac{T_1 - \alpha h_1}{b} y_o^{b/a} \left(\frac{T_1 - \alpha h_1}{T_1 - \alpha h_o} \right)^{b/\alpha} \left(-a^{-1} \ln y_o \right. \\
& + \left. \frac{1}{\alpha} \ln \left(\frac{T_1 - \alpha h_o}{T_1 - \alpha h_1} \right) \right) \quad X_o < x_o
\end{aligned}$$

or

$$\begin{aligned}
A'_{13} = & \lambda_3 \left(\frac{h_1}{b} + \frac{T_1 - \alpha h_1}{b^2} \right) y_o^{b/a} \left(\frac{T_1 - \alpha h_1}{T_1 - \alpha h_o} \right)^{b/\alpha}, \\
\lambda_3 = & \begin{cases} = 1 & \text{if } x_1 \geq X_1 \\ \text{otherwise } 0 \end{cases} \quad (44e)
\end{aligned}$$

Introducing

$$\frac{T_1 - \alpha h_1}{T_1 - \alpha h_o} = y_1 \quad (45)$$

it follows that:

$$\begin{aligned}
 (10^{-3} \bar{g} \rho_o T_o)^{-1} A_1 = & \lambda_1 \frac{T_o}{2a^2} \left\{ (y_o - 1)^2 - (y_o - 1)^2 \right\} \\
 & + \lambda_2 \frac{T_1}{\alpha b} y_o^{b/a} \left(1 - y_1^{b/\alpha} \right) \\
 & - \lambda_2 \frac{T_1 - \alpha h_o}{\alpha (\alpha + b)} y_o^{(\alpha+b)/\alpha} \left(1 - y_1^{(\alpha+b)/\alpha} \right) \\
 & + \lambda_3 \left(\frac{h_1}{b} + \frac{T_1 - \alpha h_1}{b^2} \right) y_o^{b/a} y_1^{b/\alpha}
 \end{aligned} \tag{46}$$

Turning now to the 2nd integral A_2 , the contribution from the inversion layer can be neglected with the result:

$$(10^{-3} \rho_o \bar{g} T_o)^{-1} A_2 = \int_{X_o}^{X_1} dx e^{-bx} h_{\text{lapse}}^2 + \int_{x_1}^{X_1} dx e^{-bx} h_{\text{strato}}^2 \tag{47}$$

$$A'_2 = A'_{21} + A'_{22}$$

$$h_{\text{lapse}}^2 = \frac{T_1^2}{\alpha^2} \left(1 - y_o^{a/\alpha} e^{-\alpha x} \right)^2$$

$$\begin{aligned}
A'_{21} = & \lambda_2 \frac{T_1^2}{\alpha^2 b} \left(y_o^{b/a} - 2 \frac{b}{b+\alpha} y_o^{(b+\alpha)/\alpha} + \frac{b}{b+2\alpha} y_o^{2(b+2\alpha)/\alpha} \right. \\
& - \lambda_2 \frac{T_1^2}{\alpha^2 b} \left(y_o^{b/a} y_1^{b/\alpha} - 2 \frac{b}{b+\alpha} y_o^{(b+\alpha)/\alpha} y_1^{(b+\alpha)/\alpha} \right. \\
& \left. \left. + \frac{b}{b+2\alpha} y_o^{2(b+2\alpha)/\alpha} y_1^{(b+2\alpha)/\alpha} \right) \right. \quad (48a)
\end{aligned}$$

$\lambda_2 = 1$ if $X_o < x_o$, otherwise 0.

Similarly:

$$\begin{aligned}
A'_{22} = & \lambda_3 b^{-1} \left\{ \left[h_1 + b^{-1} (T_1 - \alpha h_1) \right]^2 + b^{-2} (T_1 - \alpha h_1)^2 \right. \\
& \left. \left(1 - 4 \frac{b}{\alpha} \ln y_1 - 4 \frac{b}{a} \ln y_o \right) \right\} y_o^{b/a} y_1^{b/\alpha} \quad (48b)
\end{aligned}$$

Hence for A_2 :

$$\begin{aligned}
(10^{-3} \bar{g} \rho_o T_o)^{-1} A_2 = & \lambda_2 \frac{T_1^2}{b \alpha^2} \left\{ y_o^{b/a} (1 - y_1^{b/\alpha}) \right. \\
& - 2 \frac{b}{b+\alpha} y_o^{(b+\alpha)/\alpha} (1 - y_1^{(b+\alpha)/\alpha}) \\
& \left. + \frac{b}{b+2\alpha} y_o^{2(b+2\alpha)/\alpha} (1 - y_1^{b+2\alpha/\alpha}) \right\} \\
& + \lambda_3 b^{-1} \left\{ \left[h_1 + b^{-1} (T_1 - \alpha h_1) \right]^2 \right. \\
& + b^{-2} (T_1 - \alpha h_1)^2 \\
& \left. \left(1 - 4 \ln (y_o^{b/a} y_1^{b/\alpha}) \right) \right\} y_o^{b/a} y_1^{b/\alpha} \quad (49)
\end{aligned}$$

Therefore the final range correction $\Delta \rho$ is given by:

$$\begin{aligned} \Delta \rho_{\text{dry}} = & (\cos z)^{-1} 10^{-3} K_1 \bar{R}/(M \bar{g}) \left\{ (P_o - P_1) \right. \\ & - 10^{-3} \bar{g} \rho_o T_o r_o^{-1} \tan^2 z \left\{ \frac{\lambda T_o}{2a^2} [(y_o - 1)^2 - (Y_o - 1)^2] \right. \\ & + \frac{T_1}{\alpha b} y_o^{b/a} (1 - U^{b/\alpha}) - \frac{T_1 - \alpha h_o}{\alpha (\alpha + b)} y_o^{(\alpha+b)/\alpha} (1 - U^{(\alpha+b)/\alpha}) \\ & + \lambda_2 \left(\frac{h_1}{b} + \frac{T_1 - \alpha h_1}{b^2} \right) y_o^{b/a} Y_1^{b/\alpha} \left. \right\} \\ & + \frac{3}{2} r_o^{-2} \tan^2 z (\cos z)^{-2} 10^{-3} \bar{g} \rho_o T_o \left\{ \frac{T_1^2}{b \alpha^2} \left[y_o^{b/a} (1 - U^{b/a}) \right. \right. \\ & - 2 \frac{b}{b + \alpha} y_o^{(b+\alpha)/\alpha} (1 - U^{(b+\alpha)/\alpha}) \\ & + \frac{b}{b + 2\alpha} y_o^{2(b+2\alpha)/\alpha} (1 - U^{(b+2\alpha)/\alpha}) \left. \right] \\ & + \lambda_3 b^{-1} \left[\left(b^{-1} (T_1 - \alpha H_1) + h_1 \right)^2 \right. \\ & + b^{-2} (T_1 - \alpha h_1)^2 (1 - 4 \ln (y_o^{b/a} Y_1^{b/\alpha})) \left. \right] y_o^{b/a} Y_1^{b/\alpha} \left. \right\}, \end{aligned} \quad (50)$$

where

$$U = Y_1 \text{ if } Y_1 < y_1 \text{ and } U = y_1, \text{ if } Y_1 > y_1.$$

b. The Wet Component

This component consists of two parts (Eq. (23)). Hence

$$10^6 \Delta p_{\text{wet}} = (\cos z)^{-1} \int_0^{\infty} dh \left(-K_2 \frac{e_{\omega}}{T} + 10^6 K_3 \frac{e_{\omega}}{T^2} \right) \left(1 - \tan^2 z \frac{h}{R} \right). \quad (51)$$

Since water vapor rapidly decreases with altitude ($h_{\omega} \approx 2$ km in Eq. (30)) it is not necessary to consider the last term in the bracket of Eq. (22). Adopting expression (30) for e_{ω} , the integrations indicated in Eq. (51) can be carried out by noting the fact that the water vapor contents is prevalent at low altitudes and thus the temperature profiles as given by Eq. (24) may be used in the form:

$$T^{-1} = T_0^{-1} \left(1 + \left(\alpha - 2 h_0^{-1} \Delta \right) T_0^{-1} h + h_0^{-2} \Delta T_0^{-1} h^2 \right), \quad h < h_0, \quad (52)$$

in the inversion layer, and

$$T^{-1} = T_1^{-1} \left(1 + \alpha T_1^{-1} h \right), \quad h > h_0.$$

It is now possible to obtain an analytic expression for the K_2 part of Eq. (51). After some algebra it is found that the K_2 part is given by:

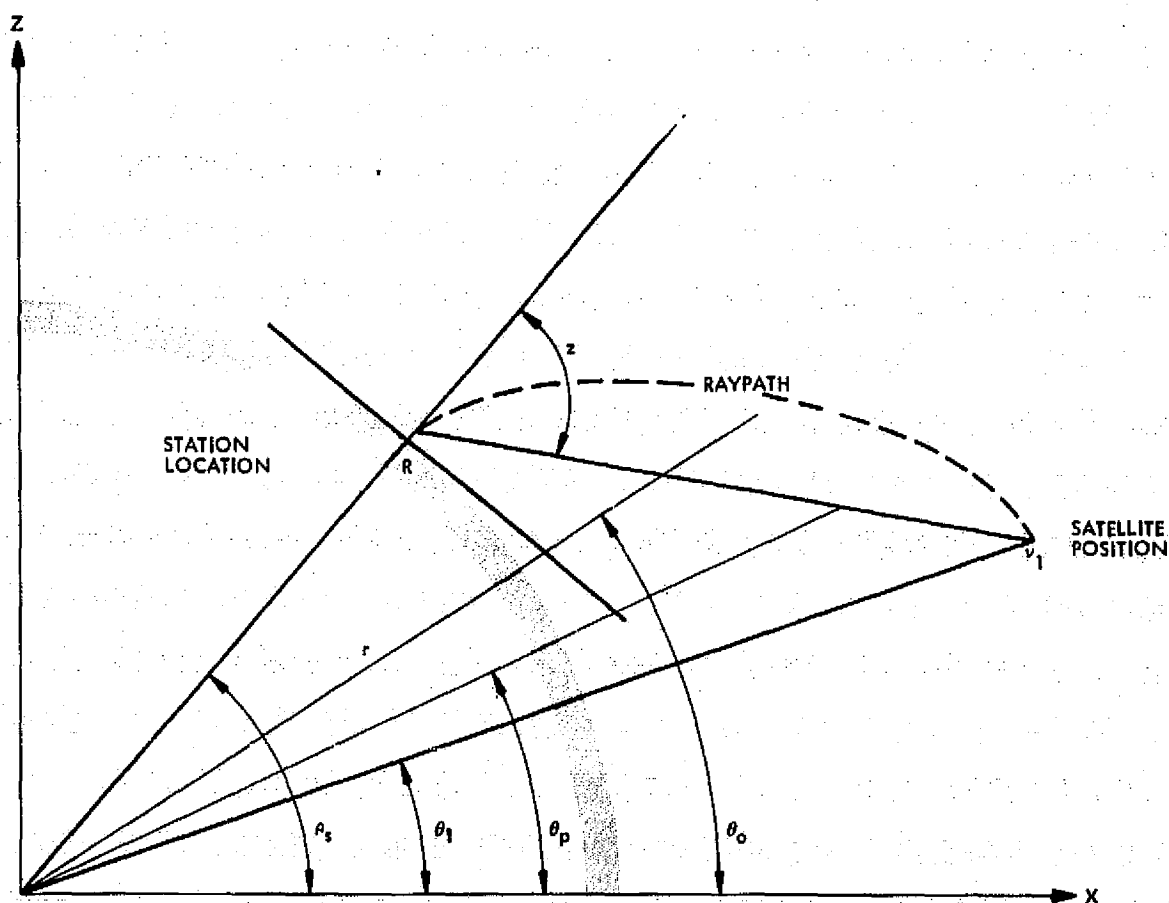
$$\begin{aligned}
\Delta \rho_{\text{wet}}(K_2) = & -\lambda_4 \cdot 10^{-6} \frac{K_2 e_{ow}}{T_o} (\cos z)^{-1} \left\{ h_\omega \left(e^{-H_o/h_\omega} - e^{-h_o/h_\omega} \right) \right. \\
& + \left[\left(\alpha - 2 h_o^{-1} \Delta \right) T_o^{-1} - r_o^{-1} \tan^2 z \right] \\
& h_\omega^2 \left[\left(1 + H_o/h_\omega \right) e^{-H_o/h_\omega} - \left(1 + h_o/h_\omega \right) e^{-h_o/h_\omega} \right] \\
& - 6 h_o^{-2} \Delta T_o^{-1} r_o^{-1} \tan^2 z \\
& h_\omega^4 \left[\left(1 + H_o/h_\omega + \frac{1}{2} H_o^2/h_\omega^2 + \frac{1}{6} H_o^3/h_\omega^3 \right) e^{-H_o/h_\omega} \right. \\
& \left. - \left(1 + h_o/h_\omega + \frac{1}{2} h_o^2/h_\omega^2 + \frac{1}{6} h_o^3/h_\omega^3 \right) e^{-h_o/h_\omega} \right] \left. \right\} \\
& -\lambda_5 \cdot 10^{-6} \frac{K_2 e_{ow}}{T_1} (\cos z)^{-1} \left\{ h_\omega \left(e^{-h_o/h_\omega} - e^{-H_1/h_\omega} \right) \right. \\
& + \left[\alpha T_1^{-1} - r_o^{-1} \tan^2 z \right] \\
& h_\omega^2 \left[\left(1 + h_o/h_\omega \right) e^{-h_o/h_\omega} - \left(1 + H_1/h_\omega \right) e^{-H_1/h_\omega} \right] \\
& - \alpha T_1^{-1} r_o^{-1} \tan^2 z h_\omega^3 \left[\left(2 + 2 h_o/h_\omega + h_o^2/h_\omega^2 \right) \right. \\
& \left. e^{-h_o/h_\omega} - \left(2 + 2 H_1/h_\omega + H_1^2/h_\omega^2 \right) e^{-H_1/h_\omega} \right] \left. \right\}. \tag{53}
\end{aligned}$$

$$\lambda_4 \equiv \begin{pmatrix} 1 & \text{if } H_o < h_o \\ 0 & \text{otherwise} \end{pmatrix}, \quad \lambda_5 \equiv \begin{pmatrix} 1 & \text{if } H_1 > h_o \\ 0 & \text{otherwise} \end{pmatrix}$$

For the K_3 part of the wet component, by analogy, using a similar expansion to Eq. (52):

$$\begin{aligned}
 \Delta p_{\text{wet}}(K_3) = & \lambda_4 \cdot \frac{K_3 e_{ow}}{T_o^2} (\cos z)^{-1} \left\{ h_\omega \left(e^{-H_o/h_\omega} - e^{-h_o/h_\omega} \right) \right. \\
 & + \left[2 \left(\alpha - 2 h_o^{-1} \Delta \right) T_o^{-1} - r_o^{-1} \tan^2 z \right] \\
 & h_\omega^2 \left[\left(1 + H_o/h_\omega \right) e^{-H_o/h_\omega} - \left(1 + h_o/h_\omega \right) e^{-h_o/h_\omega} \right] \\
 & + 4 h_\omega^3 \left[h_o^{-2} T_o^{-1} \Delta - \left(\alpha - 2 h_o^{-1} \Delta \right) T_o^{-1} r_o^{-1} \tan^2 z \right] \\
 & \left[\left(1 + H_o/h_\omega + \frac{1}{2} H_o^2/h_\omega^2 \right) e^{-H_o/h_\omega} - \left(1 + h_o/h_\omega + \frac{1}{2} h_o^2/h_\omega^2 \right) e^{-h_o/h_\omega} \right] \\
 & - 12 h_o^{-2} \Delta T_o^{-1} r_o^{-1} \tan^2 z h_\omega^4 \left[\left(1 + H_o/h_\omega + \frac{1}{2} H_o^2/h_\omega^2 \right. \right. \\
 & \left. \left. + \frac{1}{6} H_o^3/h_\omega^3 \right) e^{-H_o/h_\omega} - \left(1 + h_o/h_\omega + \frac{1}{2} h_o^2/h_\omega^2 + \frac{1}{6} h_o^3/h_\omega^3 \right) e^{-h_o/h_\omega} \right] \Big\} \\
 & + \lambda_5 \cdot \frac{K_3 e_{ow}}{T_o^2} (\cos z)^{-1} \left\{ h_\omega \left(e^{-h_o/h_\omega} - e^{-H_1/h_\omega} \right) \right. \\
 & + \left[2 \alpha T_1^{-1} - \tan^2 z r_o^{-1} \right] h_\omega^2 \left[\left(1 + h_o/h_\omega \right) e^{-h_o/h_\omega} \right. \\
 & \left. - \left(1 + H_1/h_\omega \right) e^{-H_1/h_\omega} \right] - 2 \alpha T_1^{-1} r_o^{-1} \tan^2 z \\
 & h_\omega^3 \left[\left(2 + 2 h_o/h_\omega + h_o^2/h_\omega^2 \right) e^{-h_o/h_\omega} \right. \\
 & \left. - \left(2 + 2 H_1/h_\omega + H_1^2/h_\omega^2 \right) e^{-H_1/h_\omega} \right] \Big\}.
 \end{aligned} \tag{54}$$

Equations (50), (53), and (54) give the desired result.



$$\theta_1 = \theta_s - z + \sin^{-1}\left(\frac{R}{r_1} \sin z\right) = \theta_s - \alpha$$

Figure A5.2. Geometry Considered

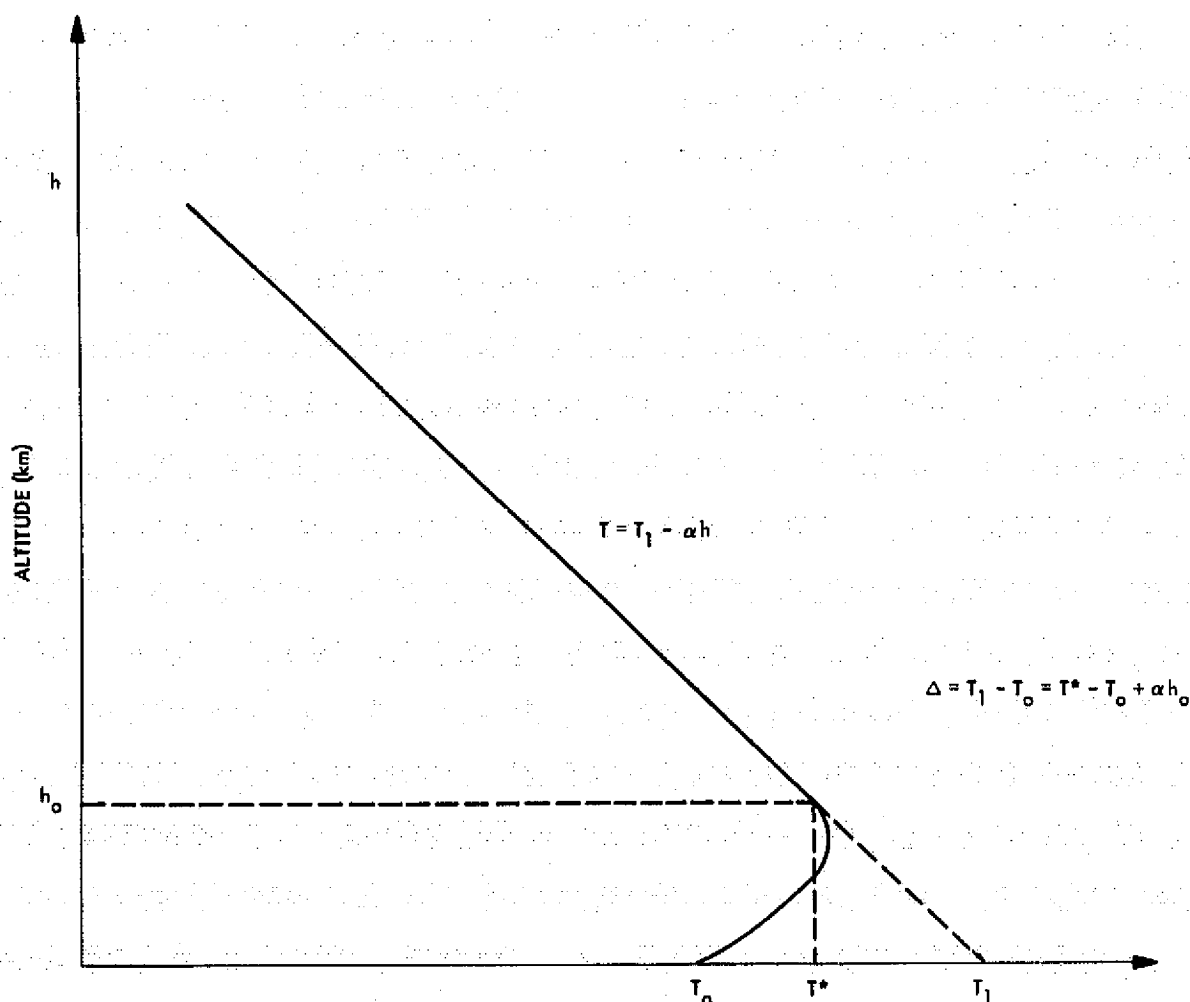


Figure A5.3. Temperature Profile versus Altitude

ORIGINAL PAGE IS
OF POOR QUALITY

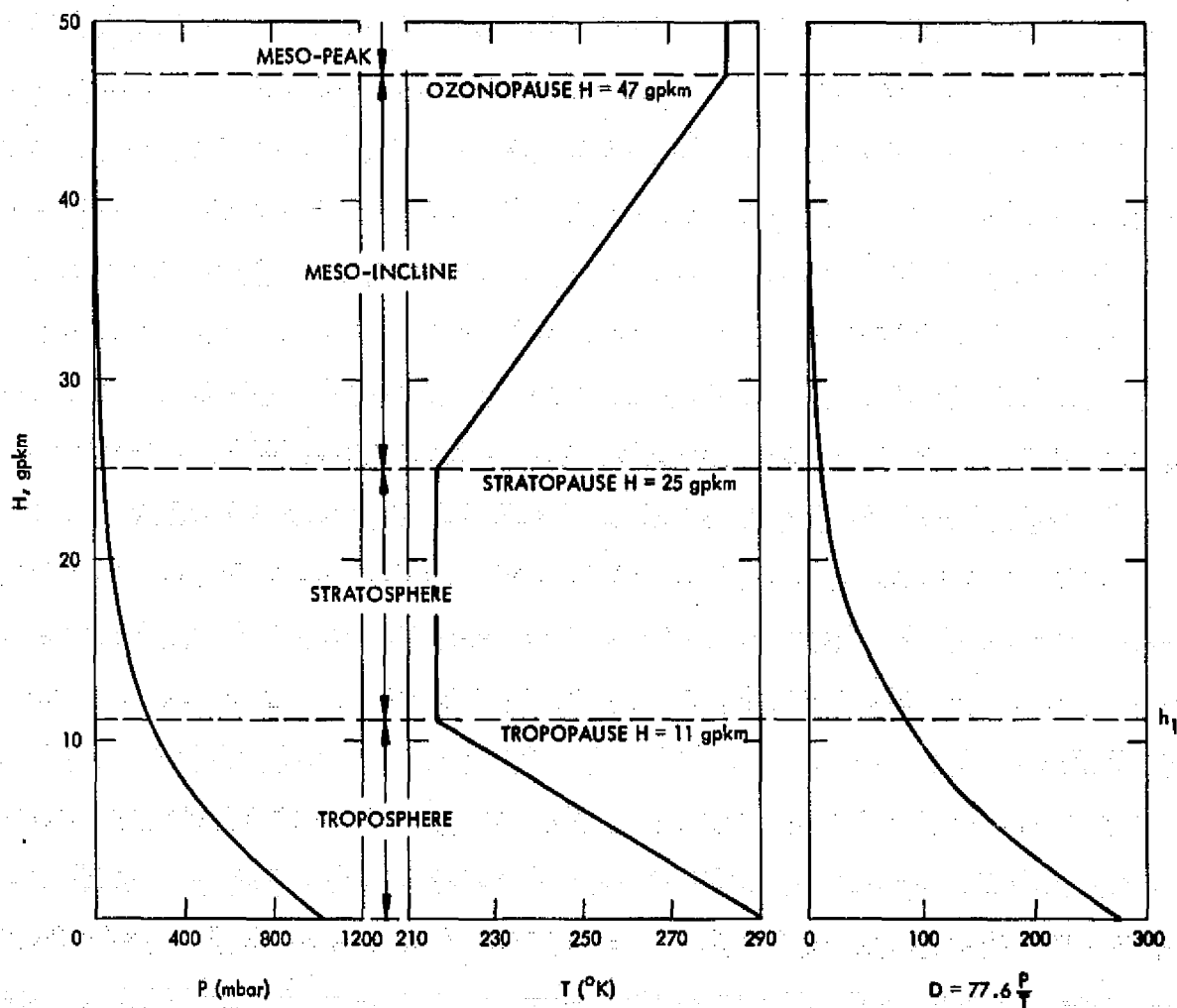


Figure A5.4. The U. S. Extension to the I. C. A. O. Standard Atmosphere

A5.7 COMPUTATIONAL ALGORITHM

Given the following input:

$\beta_1 \equiv$ Control flag; = 1 if airplane 0 monitors temperature and pressure;
= 2 otherwise,

$\beta_2 \equiv$ Control flag; = 1 if airplane 1 monitors temperature and pressure;
= 2 otherwise,

$z \equiv$ Zenith angle (rads),

$a_e \equiv$ Mean Radius of Earth (cm),

$H_0 \equiv$ Height of station 0; lower station (cm),

$H_1 \equiv$ Height of station 1; upper station (cm),

and if $\beta_1 = 1$:

$\bar{P}_0 \equiv$ Pressure at station 0 (airplane 0 or lower station) (mbar),

$\bar{T}_0 \equiv$ Temperature at station 0 (airplane 0 or lower station ($^{\circ}\text{K}$),

and if $\beta_2 = 1$:

$\bar{P}_1 \equiv$ Pressure at station 1 (airplane 1 or upper station) (mbar),

$\bar{T}_1 \equiv$ Temperature at station 1 (airplane 1 or upper station) ($^{\circ}\text{K}$),

along with:

$P_0 \equiv$ Average ground pressure (mbar)

$T_0 \equiv$ Average ground temperature ($^{\circ}\text{K}$),

$T^* \equiv$ Temperature at inversion layer height ($^{\circ}\text{K}$),

$t \equiv$ Ground dew point temperature (K),

$h_0 \equiv$ Inversion layer height (cm),

$h_1 \equiv$ Tropopause height (cm),

$h_w \equiv$ Water vapor scale height (cm),

$\alpha \equiv$ Atmospheric lapse rate ($^{\circ}\text{K}/\text{cm}$),

$\bar{R} \equiv$ Gas constant (mbar $\text{cm}^3 \text{ } ^{\circ}\text{K}^{-1}$),

$g_R \equiv$ Acceleration of Gravity at surface (cm/sec^2),

$M \equiv$ Molecular weight of air (g),

$K_1 \equiv$ First refraction constant ($^{\circ}\text{K}/\text{mbar}$),

$K_2 \equiv$ Second refraction constant ($^{\circ}\text{K}/\text{mbar}$),

$K_3 \equiv$ Third refraction constant ($^{\circ}\text{K}/\text{mbar}$),

$k_1 \equiv$ Constant in water vapor equation,

$k_2 \equiv$ Constant in water vapor equation ($^{\circ}\text{K}$),

$k_3 \equiv$ Constant in water vapor equation ($^{\circ}\text{K}$),

$e_1 \equiv$ Base water vapor pressure (mbar),

test to see if $\beta_1 = \beta_2 = 1$ and $H_0 > h_0$ then compute:

$$\alpha = (\bar{T}_0 - \bar{T}_1) / (H_1 - H_0).$$

Continue calculating with

$$T_1 = T^* + \alpha h_0$$

$$\Delta = T^* + \alpha h_0 - T_0$$

$$r_0 = a_e + H_0$$

$$r_1 = a_e + H_1$$

$$e_{0w} = e_1 \cdot 10^{[(k_1 t - k_2) / (t - k_3)]}.$$

If $H_1 \leq 25$ km compute:

$$\bar{g} = g_R \left[\left(\frac{a_e}{r_0} \right)^2 + \left(\frac{a_e}{r_1} \right)^2 \right] / 2$$

otherwise

$$\bar{g} = g_R \left[\left(\frac{a_e}{r_0} \right)^2 + \left(\frac{a_e}{R + 25} \right)^2 \right] / 2.$$

Compute:

$$a = \left[(\alpha - 2h_0^{-1}\Delta)^2 + 4T_0h_0^{-2}\Delta \right]^{1/2}$$

$$b = 10^{-3}\bar{g}M/\bar{R}.$$

If $\Delta \neq 0$ proceed to Eq. (55a); otherwise go to Eq. (55b); hence

$$y_0 = \left| \frac{(\alpha - a)(\alpha - 2h_0^{-1}\Delta + a)}{(\alpha + a)(\alpha - 2h_0^{-1}\Delta - a)} \right| \quad (55a)$$

$$Y_0 = \left| y_0 \frac{(\alpha + a)(2\Delta h_0^{-2}H_0 + \alpha - 2h_0^{-1}\Delta - a)}{(\alpha - a)(2\Delta h_0^{-2}H_0 + \alpha - 2h_0^{-1}\Delta + a)} \right|$$

and if $Y_0 < y_0$ set $\lambda_1 = 1$, otherwise $\lambda_1 = 0$. Continue computing with:

$$Y_1 = \left| y_0 \frac{(\alpha + a)(2\Delta h_0^{-2}H_1 + \alpha - 2h_0^{-1}\Delta - a)}{(\alpha - a)(2\Delta h_0^{-2}H_1 + \alpha - 2h_0^{-1}\Delta + a)} \right|$$

$$y_1 = \left| y_0 \frac{(\alpha + a)(2\Delta h_0^{-2}h_1 + \alpha - 2h_0^{-1}\Delta - a)}{(\alpha - a)(2\Delta h_0^{-2}h_1 + \alpha - 2h_0^{-1}\Delta + a)} \right|,$$

and test y_1 against Y_1 such that: if $y_1 > Y_1$; $U = Y_1$; $\lambda_2 = 0$, or if $y_1 < Y_1$; $U = y_1$; $\lambda_2 = 1$, but if $H_1 > h_1$ set $Y_1 = y_1$.

Continue calculating with

$$\lambda_1 = 0 \quad (55b)$$

$$y_0 = 1$$

$$Y_0 = 1$$

$$y_1 = (T_0 - \alpha h_1)/T_0$$

$$Y_1 = (T_0 - \alpha H_1)/T_0$$

$$\bar{\alpha} = \alpha + b, \alpha^* = b/a$$

$$A = \cos^2 z, \quad A^* = 1 - A^{-1}, \quad A_r = (1 - A^{-1})/r_0$$

$$C_1 = y_0^{\bar{\alpha}/a} \quad C_2 = y_0^{\frac{2(b+2\alpha)}{a}}, \quad C_3 = y_0^{\alpha^*}$$

$$D = Y_1^{b/\alpha}$$

If $\beta_1 = 1$ go to Eq. (55c); otherwise proceed to Eq. (55d).

$$T_0 = \bar{T}_0$$

$$P_0 = \bar{P}_0. \quad (55c)$$

Compute

$$\rho_0 = (P_0/T_0) (M/\bar{R}) \quad (55d)$$

$$E = \bar{g} \rho_0 T_0 \cdot 10^{-3}$$

$$F = (K_1 \bar{R}/M\bar{g}) \cdot 10^{-3}.$$

If $\beta_1 = 2$ and $H_0 > 10^3$ compute:

$$Y_3 = (T_1 - \alpha H_0)/(T_1 - \alpha h_0).$$

Continue with:

$$B = a^{-1} \log_e |Y_0| - (1 - \lambda_1) a^{-1} \log_e |Y_3|$$

$$P_0^* = P_0 e^{-bB},$$

however if $H_0 > h_0$ set $Y_0 = y_0$ before computing B , then set $P_0^* = P_0$ and continue:

If $H_1 \geq 1 \times 10^7$ set $P_1 = 0$ and proceed to Eq. (55e); if $\beta_2 = 1$ set $P_1 = \bar{P}_1$ and proceed to Eq. (55e); if $\beta_2 = 2$ then test H_1 against h_1 , if $H_1 > h_1$ set $\lambda_5 = 1$, otherwise set $\lambda_5 = 0$ and compute:

$$Y_2 = (T_1 - \alpha H_1) / (T_1 - \alpha h_0); \quad H_1 < h_1 \text{ and } H_0 < h_0,$$

or

$$Y_2 = (T_1 - \alpha h_1) / (T_1 - \alpha h_0); \quad H_1 > h_1 \text{ and } H_0 < h_0,$$

or

$$Y_2 = (T_1 - \alpha H_1) / (T_1 - \alpha H_0); \quad H_1 < h_1 \text{ and } H_0 > h_0,$$

or

$$Y_2 = (T_1 - \alpha h_1) / (T_1 - \alpha H_0); \quad H_1 > h_1 \text{ and } H_0 > h_0.$$

Continue calculating:

$$B = \lambda_1 a^{-1} \log_e |Y_0| - \alpha^{-1} \log_e |Y_2| + \lambda_5 (T_1 - \alpha h_1)^{-1} (H_1 - h_1).$$

$$P_1 = P_0 e^{-bB}$$

$$\begin{aligned} G_0 &= T_1 - \alpha h_0, & G_1 &= T_1 - \alpha h_1, & G_3 &= T_1 - \alpha H_1 \\ I_1 &= 1 - U^{\alpha^*}, & I_2 &= 1 - U^{\bar{\alpha}/a}, & I_3 &= 1 - U^{(b+2\alpha)/a}. \end{aligned} \quad (55e)$$

Compute

$$\begin{aligned} \omega_1 &= P_0 - P_1 + EA_r \left[\lambda_1 T_0 (2a^2)^{-1} \left\{ (y_0 - 1)^2 - (Y_0 - 1)^2 \right\} \right. \\ &\quad \left. + I_1 T_1 C_3 (\alpha b)^{-1} - G_0 C_1 I_2 (\alpha \bar{\alpha})^{-1} + \lambda_2 (h_1 b^{-1} + G_1 b^{-2}) C_3 D \right] \end{aligned}$$

$$\omega_2 = T_1^2 (b\alpha^2)^{-1} \left[C_3 I_1 - 2C_1 I_2 b\bar{\alpha}^{-1} + C_2 I_3 b(b + 2\alpha)^{-1} \right] \\ + \lambda_2 C_3 D b^{-1} \left[(b^{-1} G_3 + h_1)^2 + b^{-2} G_1^2 (1 - 4 \log_e \{C_3 D\}) \right]$$

$$\Delta p_{\text{dry}} = F A^{-1/2} \left\{ \omega_1 - 1.5 A^{-1} A^* E \omega_2 r_0^{-2} \right\}.$$

Test H_0 against h_0 and if $H_0 < h_0$; $\lambda_3 = 1$, otherwise $\lambda_3 = 0$; however if $H_1 > h_0$; $\lambda_4 = 1$, otherwise $\lambda_4 = 0$. Test H_0 against h_0 and if $H_0 > h_0$ set $h_0 = H_0$.

Compute:

$$d_1 = K_2 e_{0\omega}, \quad d_2 = K_3 e_{0\omega}$$

$$a_1 = H_0/h_\omega, \quad a_2 = h_0/h_\omega, \quad a_3 = H_1/h_\omega$$

$$b_1 = e^{-a_1}, \quad b_2 = e^{-a_2}, \quad b_3 = e^{-a_1}$$

$$c_1 = (\alpha - 2h_0^{-1}\Delta)T_0^{-1}, \quad c_2 = h_0^{-2}\Delta T_0^{-1}, \quad c_3 = \alpha T_1^{-1}$$

$$D_1 = 1 + a_1 + \frac{1}{2}a_1^2 + \frac{1}{6}a_1^3$$

$$D_2 = 1 + a_2 + \frac{1}{2}a_2^2 + \frac{1}{6}a_2^3$$

$$D_3 = 2 + 2a_2 + a_2^2$$

$$D_4 = 2 + 2a_3 + a_3^2$$

$$\omega_3 = h_\omega(b_1 - b_2) + h_\omega^2 [c_1 + A_r] [(1 + a_1)b_1 - (1 + a_2)b_2] \\ + 6h_\omega^4 c_2 A_r \{D_1 b_1 - D_2 b_2\}$$

$$\omega_4 = h_\omega(b_2 - b_3) + h_\omega^2[c_3 + A_r][(1 + a_2)b_2 - (1 + a_3)b_3] \\ + h_\omega^3 c_3 A_r \{D_3 b_2 - D_4 b_3\}$$

$$\Delta \rho'_{WET} = -d_1 A^{-1/2} [\lambda_3 \omega_3 T_0^{-1} + \omega_4 T_1^{-1}]$$

$$\omega_5 = h_\omega(b_1 - b_2) + h_\omega^2[2c_1 + A_r][(1 + a_1)b_1 - (1 + a_2)b_2] \\ + 4h_\omega^3[c_2 + c_1 A_r][(D_1 - \frac{1}{6}a_1^3)b_1 - (D_2 - \frac{1}{6}a_2^3)b_2] \\ + 12h_\omega^4 c_2 A_r [D_1 b_1 - D_2 b_2]$$

$$\omega_6 = h_\omega(b_2 - b_3) + h_\omega^2[2c_3 + A_r][(1 + a_2)b_2 - (1 + a_3)b_3] \\ + 2h_\omega^3 c_3 A_r [D_3 b_2 - D_4 b_3]$$

$$\Delta \rho''_{WET} = d_2 A^{-1/2} (\lambda_3 \omega_5 T_0^{-2} + \lambda_4 \omega_6 T_1^{-2})$$

$$\Delta \rho = \Delta \rho_{DRY} + \Delta \rho'_{WET} + \Delta \rho''_{WET},$$

and exit calculations.

A5.8 COVARIANCE MATRIX

In order to determine a viable covariance matrix for purposes of weighting the data certain parameters must be examined (see Table A5.2). The uncertainties of the parameters: z , the zenith angle; h_w , the water vapor scale height; T_0 , the ground temperature, and; P_0 , the ground air density, are definitely a major corrupting influence on the determination of the tropospheric range correction. Accordingly, the covariance matrix is determined by only taking the above mentioned four variables into account. The four parameters are assumed to be measured independently. However, the ground pressure P_0 is measured rather than the density ρ_0 . This implies simplification. It signifies that the partial derivative with respect to T_0 , which contributed to the error budget significantly, may be neglected. The reason for this is the following. Formerly ρ_0 and T_0 were considered independent variables. In this case P_0 , the ground pressure, is a derived quantity $P_0 = (\bar{R}/M) \rho_0 T_0$. A perusal of Eq. (50) shows that the temperature dependence of ΔP_{dry} is quite pronounced. It shows up in the leading term $\sim (P_0 - P_1)$, and in the coefficient $\sim \rho_0 T_0$ of the other terms (since ρ_0 is treated as an independent variable). It is true that y_0 , y_1 , Y_0 and Y_1 contain T_0 but their dependence on T_0 is very tenuous and derivatives with respect to T_0 are small. Hence in a system in which the four parameters z , h_w , T_0 and P_0 are independently measured, as far as the determination of the covariance matrix for the dry part of the tropospheric range correction is concerned, only z and P_0 have to be considered. For the wet part of the range correction z , h_w and T_0 have to be considered. The analysis proceeds as follows.

In this section the range correction is designated by Δd rather than ΔP to conform with Appendix A2 of this report. The range then can be expressed in the following way:

$$\begin{aligned} d_T = d_N + \delta d_N - \Delta d + \frac{\partial \Delta d}{\partial z} \delta z + \frac{\partial \Delta d}{\partial z} \dot{z} \delta t + \frac{\partial \Delta d}{\partial z_0} \dot{z}_0 \delta t_0 \\ + \frac{\partial \Delta d}{\partial h_w} \delta h_w + \frac{\partial \Delta d}{\partial T_0} \delta T_0 + \frac{\partial \Delta d}{\partial P_0} \delta P_0 \equiv d_N + \Delta d + v_N, \end{aligned} \quad (56)$$

where the meaning of the various terms in Eq. (56) are specified as: d_T is the true range at any instant of time as determined from the raw data, d_N , and the statistical errors. These errors in turn are listed as: δd_N , the hardware noise; Δd , the tropospheric range correction which is large at low elevation angles (large zenith angle z); δz , the error in the determination of the zenith angle at any given time throughout the multilateration pass; δt , the clock jitter; δt_0 , the error in the epoch, and finally δh_ω , δT_0 and δP_0 which have been amply explained previously. The errors ν_N give rise to a weighting matrix of dimension $k \times k$ if k different measurements are made during a fitting period. The form of this matrix is:*

$$W = U \sigma_{d_n}^2 + Z \Lambda_z Z^T + Z_t Z_t^T \sigma_t^2 + U \left(\frac{\partial \Delta d}{\partial z_0} \dot{z}_0 \sigma_{t_0} \right)^2 + K \Lambda_\omega K^T + W_I. \quad (57)$$

In expression (57) U is the unit matrix, Z^T the row vector:

$$Z^T = \left[\frac{\partial \Delta d_1}{\partial z_1}, \quad \frac{\partial \Delta d_2}{\partial z_2}, \quad \dots \quad \dots, \quad \frac{\partial \Delta d_k}{\partial z_k} \right] \quad (58)$$

and Z_t^T the row vector

$$Z_t^T = \left[\frac{\partial \Delta d_1}{\partial z_1} \dot{z}_1, \quad \dots \quad \dots \quad \frac{\partial \Delta d_k}{\partial z_k} \dot{z}_k \right]. \quad (59)$$

Finally the matrices Λ_z and Λ_ω are diagonal because the measurements are independent so that:

* W_I is the ionospheric contribution to the weight matrix (see Appendix A6).

$$\Lambda_z = \begin{bmatrix} \sigma_{z_1}^2 & & & 0 \\ & \sigma_{z_2}^2 & & \\ & & \ddots & \\ & & & \ddots & \\ 0 & & & & \sigma_{z_k}^2 \end{bmatrix}, \quad (60)$$

is a $k \times k$ matrix and

$$\Lambda_\omega = \begin{bmatrix} \sigma_{h_\omega}^2 & & 0 \\ & \sigma_{T_0}^2 & \\ 0 & & \sigma_{P_0}^2 \end{bmatrix}, \quad (61)$$

is a 3×3 matrix. With the $k \times (M + 1)$ matrix:

$$A = \begin{bmatrix} 1 & t_1 - t_0 & (t_1 - t_0)^2 & \dots & (t_1 - t_0)^M \\ \vdots & & & & \\ 1 & t_k - t_0 & (t_k - t_0)^2 & \dots & (t_k - t_0)^M \end{bmatrix} \quad (62)$$

and the matrix W defined by Eq. (57), the least square minimum variance range data fit is given by:

$$d = [A^T W^{-1} A]^{-1} A^T W^{-1} (d_N - \Delta d). \quad (63)$$

The partial derivatives of Δd with respect to the three parameters given at the beginning of this section (at k different times) determine the part of the covariance matrix expressed by Eq. (57) (see also Appendix A2) as:

$$K \equiv \frac{\partial \Delta d}{\partial \omega} = \begin{bmatrix} \frac{\partial \Delta d_1}{\partial h_\omega} & \frac{\partial \Delta d_1}{\partial T_0} & \frac{\partial \Delta d_1}{\partial P_0} \\ & & \vdots \\ & & \vdots \\ \frac{\partial \Delta d_k}{\partial h_\omega} & \frac{\partial \Delta d_k}{\partial T_0} & \frac{\partial \Delta d_k}{\partial P_0} \end{bmatrix}; \quad \omega \equiv [h, T, P] \quad (64)$$

of dimension $k \times 3$.

What remains to be done is to evaluate the partial derivatives. The range correction is given by Eqs. (50), (53) and (54) of this Appendix. Equation (53) can be completely neglected in this analysis since the contribution of this term is at the millimeter level throughout the ranges of the pertinent parameters and its errors are therefore negligible. The dry part, Eq. (50), and the wet part, Eq. (54) will be treated separately. The results of the lengthy but straightforward calculations, using as much as possible the nomenclature introduced in the algorithm of Section A5.7, follow:

1) Zenith Angle

$$\frac{\partial}{\partial z} (\Delta d) = \frac{\partial}{\partial z} (\Delta d_{\text{dry}}) + \frac{\partial}{\partial z} (\Delta d_{\text{wet}}) \quad (65)$$

$$\begin{aligned} \frac{\partial}{\partial z} (\Delta d_{\text{dry}}) = & \tan z (\cos z)^{-1} \Delta d_{\text{dry}} - 2 \cdot 10^{-3} \tan z (\cos z)^{-3} E F r_0^{-1} H_1 \\ & + 3 \cdot 10^{-3} \sin z (\cos z)^{-3} (1 + 2 \tan^2 z) E F r_0^{-2} H_2, \end{aligned} \quad (66)$$

where

$$H_1 = \frac{\lambda_1 T_0}{2a^2} \left[(y_0 - 1)^2 - (Y_0 - 1)^2 \right] + \frac{T_1}{\alpha b} C_3 I_1 - \frac{G_0}{\alpha(\alpha + b)} C_1 I_2 + \lambda_2 \left(\frac{h_1}{b} + \frac{G_1}{b^2} \right) C_3 D \quad (67a)$$

$$H_2 = \frac{T_1^2}{b\alpha^2} \left[C_3 I_1 - 2 \frac{b}{b + \alpha} C_1 I_2 + \frac{b}{b + 2\alpha} C_2 I_3 \right] + \lambda_3 b^{-1} \left[(b^{-1} G_3 + h_1)^2 + b^{-2} G_1^2 \left[1 - 4 \ln(C_3 D) \right] \right] C_3 D \quad (67b)$$

and

$$\frac{\partial}{\partial z} (\Delta d_{\text{wet}}) = \tan z (\cos z)^{-1} \Delta d_{\text{wet}} - 2 \frac{K_3 e_{ow}}{T_0^2 r_0} \tan z (\cos z)^{-3} H_3, \quad (68)$$

where

$$H_3 = 12 \lambda_4 \frac{\Delta}{T_0} h_\omega^4 h_0^{-2} (D_1 b_1 - D_2 b_2) + \lambda_5 h_\omega^2 \left[(1 + a_2) b_2 - (1 + a_3) b_3 \right] + 2 \alpha T_1^{-1} h_\omega^3 (D_3 b_2 - D_4 b_3). \quad (69)$$

2) Water Vapor Scale Height

$$\begin{aligned} \frac{\partial}{\partial h} (\Delta d) &= \frac{\partial}{\partial h_\omega} (\Delta d_{\text{wet}}) = \lambda_4 \frac{K_3 e_{ow}}{T_0^2} (\cos z)^{-1} \left\{ (1 + a_1) b_1 - (1 + a_2) b_2 \right. \\ &\quad + \left[2(\alpha - 2h_0^{-1} \Delta) T_0 - r_0^{-1} \tan^2 z \right] h_\omega \left[(2 + 2 a_1 + a_1^2) b_1 \right. \\ &\quad \left. \left. - (2 + 2 a_2 + a_2^2) b_2 \right] + 12 h_\omega^2 \left[h_0^{-2} \Delta T_0^{-1} - (\alpha - 2h_0^{-1} \Delta) \right. \right. \\ &\quad \left. \left. \times T_0^{-1} r_0^{-1} \tan^2 z \right] (D_1 b_1 - D_2 b_2) - 48 h_0^{-2} r_0^{-1} h_\omega^3 \Delta T_0^{-1} \tan^2 z \right\} \end{aligned}$$

$$\begin{aligned}
& \times \left[(1 + a_1 + \frac{1}{2} a_1^2 + \frac{1}{8} a_1^3) b_1 - (1 + a_2 + \frac{1}{2} a_2^2 + \frac{1}{8} a_2^3) b_2 \right] \Bigg\} \\
& + \lambda_5 \frac{K_3 e_{o\omega}}{T_0^2} (\cos z)^{-1} \left\{ (1 + a_2) b_2 - (1 + a_3) b_3 \right. \\
& + \left[2 \alpha T_1^{-1} - r_0^{-1} \tan^2 z \right] 2h_\omega \left[(1 + a_2 + \frac{1}{2} a_2^2) b_2 - (1 + a_3 + \frac{1}{2} a_3^2) b_3 \right] \\
& \left. - 12 \alpha T_1^{-1} r_0^{-1} \tan^2 z h_\omega^2 \left[D_2 b_2 - (1 + a_3 + \frac{1}{2} a_3^2 + \frac{1}{6} a_3^3) b_3 \right] \right\}. \quad (70)
\end{aligned}$$

3) Ground Temperature

As has been determined previously the partial derivative of the dry part of the troposphere with respect to T_0 is negligible. However, the wet part contributes and is found quickly from Eq. (54) to be:

$$\frac{\partial}{\partial T_0} (\Delta d) = \frac{\partial}{\partial T_0} (\Delta d)_{\text{wet}} = - \frac{2}{T_0} \Delta d_{\text{wet}}, \quad (71)$$

since the remainder of the T_0 dependence comes in via the inversion layer and is therefore far smaller than the main term of Eq. (71). Even the expression (71) is usually negligible for small zenith angles. Typically in summer at Goldstone $\Delta d_{\text{wet}} \approx 20$ cm at zenith, $T_0 \approx 300^\circ\text{K}$ so that $\partial/\partial T_0 (\Delta d_{\text{wet}}) \approx 0.13$ cm/ $^\circ\text{K}$, and an uncertainty in T_0 of 1°K just yields an uncertainty in Δd_{wet} of 0.13 cm. However at large zenith angles the uncertainty in Δd_{wet} is not negligible.

4) Pressure

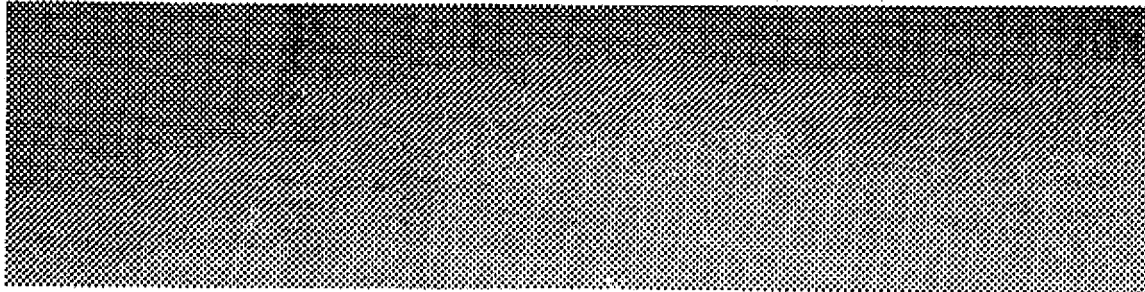
$$\frac{\partial}{\partial P_0} (\Delta d) = \frac{\partial}{\partial P_0} (\Delta d_{\text{dry}}) = P_0^{-1} \left(\Delta d_{\text{dry}} + A^{-1/2} F P_1 \right). \quad (72)$$

In summary then Eqs. (66), (69), (70) and (72) give the desired partials which are to be entered into the matrix (64) to ultimately obtain the matrix K, Eq. (64).

A5.9 REFERENCES

- [5.1] von Roos, O.H., DSN Progress Report, TR 32-1526, Vol. VI, p. 99, December 1971.
- [5.2] Bean, B.R. and Dutton, E.J., Radio Meteorology, N.B.S. Monograph 92, March 1, 1966; H.S. Hopfield, Radio Science 6, 357, 1971.
- [5.3] Saastamoinen, J. (Henriksen, S.W., Mancini A. and Chavitz B.H. ed.) The Use of Artificial Satellites for Geodesy, Am Geophys. Union Washington, D.C., 1972.
- [5.4] Tverskoi, P.N., Physics of the Atmosphere, Translated from Russian, Israel Program for Scientific Translations, 1965; NASA and NSF Publications.
- [5.5] Chao, C.C., DSN Progress Report, JPL TR 32-1526, Vol. XIV, p. 33, April 1973.
- [5.6] von Roos, O.H., Escobal, P.R., Gallagher, J.F., Hylkema, R.K., "Generalized Tropospheric Calibration and Error Analysis", JPL EM 391-637, 28 March 1974 (JPL internal document).

A6. Ionospheric Calibration and Error Analysis



Abstract

Analysis of ionospheric calibration requirements for radio ranging systems at microwave frequencies is undertaken. The interaction of the electromagnetic waves with the electron ion plasma is analyzed using approximations valid at frequencies near 10^{10} Hz. By evaluating the error budget of the pertinent physical parameters it is shown that a single carrier frequency system (S, C or X band) is not capable of ascertaining range corrections to the one centimeter accuracy level. However, by taking advantage of dispersion and use of a dual frequency system (preferably S and C band) the achievement of the one centimeter goal is possible. The analysis performed herein has been used to develop a calibration routine which not only yields the correction but also the appropriate weighting matrix of the corrections. Various entry points are used in the routine in order to minimize computing time and to permit closely spaced corrections to be obtained without performing the costly numerical integrations required to obtain the corrections.

PRECEDING PAGE BLANK NOT FILMED

A6.1 INTRODUCTION

As will be presently shown, the problem in ionospheric calibration arises from the uncertainty of the various physical parameters which are used in the calibration model. Most of the uncertainty can be removed by use of dual frequencies, are discussed and developed in this Appendix, with single frequency mode must be used in order to reach accuracies of 1 centimeter in the data observables. Nevertheless both calibration techniques, i. e., single and dual frequency, are discussed and developed in this Appendix, with single frequency calibration being placed in a position of a backup operating technique [6.3].

A6.2 ERROR BUDGET ANALYSIS

Table A6.1 lists the ionospheric parameters, nomenclature, nominal values, units, and errors of the parameters used in the calibration model. A distinction is made between parameters which are true random variables (possessed of slow or fast jitter) and those parameters which are bias like. The bias like variables are enclosed by a box. These parameters have a standard deviation, but for purposes of processing a batch of data, have fixed non-jittering errors. The standard deviations (wherever possible) were obtained from literature surveys and represent realistic values required to meet the multilateration objectives.

Since the atmospheric effects will be largest for large zenith angles the analytic calibration algorithm was exercised for the worst case zenith angle (angle between station vertical and vehicle position vector as viewed at the station). Typical results for random error type parameters are displayed in Table A6.2. The results in this table show the finite difference partial derivatives of the atmospheric correction Δp with respect to a typical parameter, p , i. e., $\partial \Delta p / \partial p$.

The partial derivatives in Table A6.2 permit a quick evaluation of the errors induced by these parameters. This evaluation can then serve as a basis for segregating the major error sources (for analytic partial considerations) and bounding the errors of all the minor error sources. Hence, using worst case partials from Table A6.2 and using the errors listed in Table A6.1, the error contributors are given by Σ , namely, Σ_s , Σ_x , Σ_c where S, X, C denote the respective radio band. Hence for S-Band during daytime

Table A6.1. Atmospheric Parameters (F-Layer)

Definition	Symbol	Value	Units	Error
Maximum Electron Density	N_{\max}	$\approx (0.1 - 2.0) \cdot 10^6$	cm^{-3}	10%
Scale Height	H	$\approx (30 - 45)$	km	5 km
Altitude of Maximum Electron Concentration	h_{\max}	$\approx (250 - 450)$	km	10 km
Zenith Angle	z		deg	0.1
Diffusion Constant [*] (at h_{\max})	α	$2 \cdot 10^{-8}$	sec^{-1}	10%
Attachment Coefficient (at h_{\max})	β	1	sec^{-1}	200%
Declination of Sun	δ_{\odot}	$+23^\circ - 23^\circ$	deg	1°
Radar Frequency (S-Band)	ω_S	$\approx 1.445 \cdot 10^{10}$	Hz	$5 \cdot 10^6$
Radar Frequency (X-Band)	ω_X	$\approx 5.78 \cdot 10^{10}$	Hz	10^7
Radar Frequency (C-Band)	ω_C	$\approx 2.890 \cdot 10^{10}$	Hz	10^7
Station Co-Latitude	β_G		deg	1°
Station East Longitude	λ_G		deg	1°
Line of Sight Azimuth	α_G		deg	1°
Earth Sidereal Rate	$\dot{\theta}$	$4.3752695 \cdot 10^{-3}$	rad/min	
Range Correction Constant	K	$1.591 \cdot 10^9$	cm^3/sec^2	10^4
Earth Radius	a_e	6378.	km	
Station Height Above Geoid	H_{\odot}		km	1
Satellite Altitude	H_1		km	0.1

^{*}Note that α can be computed as discussed in Section A6.5 if it is so desired.

ORIGINAL PAGE IS
OF POOR QUALITY

Table A6.2, Worst Case Pertinent Partial Derivatives

$z = 60^\circ, N_{\max} = 2.10^6 \text{ cm}^{-3}, \delta_\odot = 20^\circ, \beta_G = 55^\circ, \lambda_G = 240^\circ$ $\alpha_G = 270^\circ, H = 30 \text{ km}, h_{\max} = 300 \text{ km}, \sigma = 2.10^{-8}, \beta = 1 \text{ sec}^{-1}$		
Parameter (p)	$\partial(\text{Correction})/\partial p$ 4 P.M. Local	$\partial(\text{Correction})/\partial p$ 7 P.M. Local
$N_{\max} \text{ cm}^{-4}$	$3.4 \cdot 10^{-4}$	$3.7 \cdot 10^{-4}$
$H \text{ cm/km}$	22	18.6
$h_{\max} \text{ cm/km}$	- 0.15	-0.58
$z \text{ cm/deg}$	19.2	19.3
$\alpha \text{ cm sec}$	--	-48.10^8
$\beta \text{ cm sec}$	--	- 0.05

the following expression results

$$\sum_S^2 = \sum \left(\frac{\partial \Delta p}{\partial p} \sigma_p \right)^2 = \begin{matrix} 68^2, & N_{\max} \\ +44^2, & H \\ +0.6^2, & h_{\max} \\ +0.8^2, & z \end{matrix}$$

so that $\Sigma_S \cong 81$ cm. During nighttime

$$\begin{aligned} \sum_S^2 = \sum \left(\frac{\partial \Delta \rho}{\partial p} \sigma_p \right)^2 = & 72^2, \quad N_{\max} \\ & +37^2, \quad H \\ & +2.3^2, \quad h_{\max} \\ & +0.8^2, \quad z \\ & +3.8^2, \quad \alpha \\ & +0^2, \quad \beta \end{aligned}$$

and $\Sigma_S \cong 82$ cm. Similar calculations yield the summary results (on the average):

$$\sum_S = 80 \text{ cm}, \quad \sum_C = 20 \text{ cm}, \quad \sum_X = 5 \text{ cm}$$

Note that these values are for $z = 60^\circ$. At $z = 0^\circ$ these errors are about half as great. It must also be remembered that the maximal electron density varies by an order of magnitude depending on the solar cycle. The errors Σ_S etc., just quoted are for an active Sun condition. For a quiet Sun, taking $N_{\max} = 0.2 \cdot 10^6 \text{ cm}^{-3}$ as a typical value, they are:

$$\sum_S = 8 \text{ cm}, \quad \sum_C = 2 \text{ cm}, \quad \sum_X = 0.5 \text{ cm}.$$

Note that for zenith ranging these values are about half as great. These results indicate that a satellite ranging system accurate to the subcentimeter level is difficult, if not impossible to implement for a single frequency system. However, a dual frequency system using both S and C band (or S and X) is capable of such accuracy because the major error contributing parameters,

as will be presently demonstrated, do not enter into the analysis. The S-C band combination would be preferable for such dual frequency calibration because C band is less affected than X band by noise due to atmospheric disturbances (fog, clouds, etc.).

A6.3 THE IONOSPHERIC RANGE CORRECTION

In Reference [6.1] it has been shown that the range correction, $\Delta\rho$, for an electro-magnetic signal at microwave frequencies is given by:

$$\Delta\rho = \pm \frac{2\pi e^2}{m\omega^2} \int_{r_0}^{r_1} dr N\{S(r)\} \left(1 - c_0^2/r^2\right)^{-1/2}. \quad (1)$$

Here c_0 is determined by the relationship:

$$c_0^2 = r_0^2 \sin^2 z, \quad (2)$$

where z is the zenith angle from the zenith to the line of sight between the two tracking stations. Note that $S(r)$ is the line of sight path as a function of the radial distance from the center of the Earth with the endpoints r_0 and r_1 , $N(s)$ is the electron number density in cm^{-3} , ω the tracking frequency and m and e the mass and the charge of the electron. The $+$ sign is valid for the propagation of the modulation (group velocity) and the $-$ sign for the phase velocity. Since a ranging system uses modulated carriers only the plus sign is applicable. The correction $\Delta\rho$ therefore is associated with a time delay and has to be subtracted from the measured transit time.

As discussed in the previous section the only hope for 1 centimeter ranging accuracy lies rooted in the use of a dual frequency calibration technique. This technique is very simple, and the calibration formula is obtained by writing Eq. (1) for two frequencies, e.g., S and C bands, and differencing the respective equations to yield

$$\Delta \rho_S - \Delta \rho_C = \frac{2\pi e^2}{m} \left[\frac{1}{\omega_S^2} - \frac{1}{\omega_C^2} \right] \int_{r_j}^{r_1} dr N\{S(r)\} \left(1 - c_o^2/r^2 \right)^{-1/2}.$$

However, since $\Delta \rho_S - \Delta \rho_C \cong \rho_S - \rho_C$ is a known measured quantity, the integral in the previous equation can be determined at once and use of Eq. (1) yields the desired ionospheric range corrections.

If only one frequency is available then the only recourse is to develop the calibration equations as follows.* It has been shown in [6.2] that the electron density profile during daytime is given by:

$$N = N_{\max} \exp \left\{ \frac{1}{2} \left[1 - Z + \int_{\infty}^Z dx e^{-x} \left[1 - \left(y_o^2 + z_o^2 \right) / (Hx + R + h_{\max})^2 \right]^{-1/2} \right] \right\} \quad (3)$$

with

$$Z = (r - R - h_{\max})/H \quad (4a)$$

$$y_o = r \sin \beta_o \sin \lambda_o, \quad z_o = r \cos \beta_o. \quad (4b)$$

Figures A6.1 and A6.2 show the geometry involved. The coordinate system used is Earth fixed and Sun oriented. The x-axis is directed toward the Sun and the x, y plane lies in the ecliptic. Later a transformation to the geographical coordinate system will be required. There are three important parameters involved in Eq. (3). They are: N_{\max} the maximum electron density of the F layer ($\approx 10^6$ electrons per cm^3), H the scale height of the F layer which is a measure of the tapering off of the electronic density profile at high

*Here only the F-layer of the ionosphere, i. e., the layer with the largest electron density is contemplated. For an accuracy of 1 cm in the range determination the E-layer must also be calibrated for a single frequency system. But because of the large uncertainties in the pertinent parameters a 1 cm accuracy cannot be achieved.

altitudes and finally the altitude at which the maximum electron density occurs h_{\max} . Numerical studies have shown that the range correction Eq. (1) is not very sensitive to changes in the parameters H and h_{\max} . Typical values are $H \approx 35 \text{ km}$, $h_{\max} \approx 350 \text{ km}$.

Equation (3) depicts a model of the daytime ionosphere. In Reference [6.1] a model of the nighttime ionosphere has been given. The details can be found in [6.2] and only the resulting profile is quoted here.

$$N = \sum_{n=0}^{n=1} c_n \exp \left\{ -\gamma_n t - h - (\beta/\alpha)^{1/2} e^{-h} \right\} L_n^{1/2} \left(2 (\beta/\alpha)^{1/2} e^{-h} \right), \quad (5)$$

where the various terms are as follows:

$$\gamma_n = \sqrt{\alpha\beta} \left(2n + \frac{3}{2} \right)$$

where α is the diffusion coefficient for heavy ions in sec^{-1} and β is the electron attachment coefficient in sec^{-1} (electrons closely follow heavy ions in order not to build up a space charge); $L_n^{1/2}(x)$ is the Laguerre polynomial defined by:

$$L_n^{1/2}(x) = \frac{(-1)^n x^{-1/2}}{n! 2^{2n+1}} H_{2n+1}(\sqrt{x}), \quad (6)$$

where $H_n(x)$ is a Hermite polynomial. From [6.2] it can be ascertained that $\sqrt{\beta/\alpha} \approx 10^{-4} \text{ sec}^{-1}$ and $\sqrt{\beta/\alpha} \approx 2 \cdot 10^4$. Unfortunately the series, Eq. (5), is slowly converging and thus many terms of the series have to be taken into account. From [6.2] it is easy to see that the coefficients c_n are given by:

$$\Gamma(3/2) \binom{n+1/2}{n} c_n = 2 \beta/\alpha \int_0^\infty dx L_n^{1/2}(x) e^{-Ax} N_{\max} e^{1/2 \left(1 + \frac{h_{\max}}{H} \right)}, \quad (7)$$

where

$$A = \frac{1}{2} \left\{ 1 + \left(\frac{\pi R \alpha}{2 H \beta} \right)^{1/2} e^{\frac{h_{\max}}{H}} \right\} \quad (8)$$

Noting that

$$\binom{n+1/2}{n} = \frac{\Gamma(n+1+1/2)}{n! \Gamma(1/2)} \quad (9)$$

the series defined via Eq. (5) can be expressed as:

$$\begin{aligned} \sum_{n=0}^{\infty} c_n e^{-\gamma_n t} L_n^{1/2} \left(2 \sqrt{\beta/\alpha} e^{-h} \right) &= 2 \frac{\beta \Gamma(1/2)}{\alpha \Gamma(3/2)} N_{\max} e^{(1+h_{\max}/H)/2} \\ &\times \int_0^{\infty} dx e^{-Ax} e^{-3/2 \sqrt{\alpha\beta} t} \sum_n e^{-2 \sqrt{\alpha\beta} t n} L_n^{1/2}(x) L_n^{1/2} \left(2 \sqrt{\beta/\alpha} e^{-h} \right) \quad (10) \\ &\times \frac{n!}{\Gamma(n+3/2)} e^{-h - \sqrt{\beta/\alpha} e^{-h}}. \end{aligned}$$

The sum over n can be performed rather easily with contour integral representations of the Laguerre polynomials. It suffices to say that:

$$\sum_{n=0}^{\infty} \frac{n!}{\Gamma(n+3/2)} L_n^{1/2}(x) L_n^{1/2}(y) z^n = \frac{(xyz)^{-1/4}}{1-z} e^{-z(x+y)/(1-z)} I_{1/2} \left(2 \sqrt{\frac{xyz}{1-z}} \right), \quad (11)$$

where x is the integration variable of Eq. (10)* and

$$y = 2 \sqrt{\beta/\alpha} e^{-h}, \quad z = e^{-2 \sqrt{\alpha\beta} t}. \quad (12)$$

The modified Bessel function appearing in Eq. (11) is defined by:

$$I_{1/2}(t) = \left(\frac{2}{\pi t} \right)^{1/2} \sinh t. \quad (13)$$

Inserting expression (11) into Eq. (10) yields, for the nighttime ionosphere, a rather complicated, but nevertheless analytic expression, namely:

$$N(h, t) = \frac{1}{\sqrt{2}} N_{\max} \left(\frac{\beta}{\alpha} \right)^{-1/4} e^{(1+h_{\max}/H)/2} \times \\ e^{-3/2 \sqrt{\alpha\beta} t} e^{-1/2 y} \left[(1-z) y^{-1} z \right]^{-1/2} \times \\ e^{-yz(1-z)^{-1}} \left[A + z(1-z)^{-1} \right]^{1/2} e^D \operatorname{erf}(\sqrt{D}), \quad (14)$$

where y and z are given by Eq. (12) and D is given by:

$$D = y z \left[(1-z)^2 A + z(1-z) \right]^{-1}. \quad (15)$$

Expression (14) represents the nighttime ionosphere. The troublesome slow convergence of Eq. (7) has been overcome. The fact that Eq. (15) is very sensitive to $\sqrt{\alpha\beta}$ and $\sqrt{\beta/\alpha}$ makes it necessary to carefully evaluate both the diffusion coefficient and the attachment coefficient for electrons in the F layer. It also should be noted that near $t = 0$ or $z = 1$ expression (14) goes over into the day time ionospheric density profile. The range correction, Eq. (1), will now be determined in detail:

* If $z=1$ expression (11) becomes a delta function in $(\sqrt{x} - \sqrt{y})$ thus leading to the result Eq. (38) of [A6.1].

Typically $\sqrt{\alpha\beta} = 10^{-4} \text{ sec}^{-1}$; h is of course the altitude in units of H . The time t is the hour angle (in sec) in the Sun fixed coordinate system normalized such that $\lambda_0 = \pi/2$ represents $t = 0$. Later it will be shown how the parameter t is linked to the geographical coordinates of a point on Earth. For the present, operations will be carried out only in a Sun fixed coordinate system with λ_0 ranging from 0 to 2π and the colatitude β_0 ranging from 0 (z axis of Fig. A6.1) to π (negative z direction of Fig. A6.1). The subsolar point is then defined by $\lambda_0 = 0$ $\beta_0 = \frac{\pi}{2}$.

In addition to the three parameters N_{max} , H and h_{max} two new parameters have been introduced: α the diffusion coefficient and β the attachment coefficient. So far then the five parameters determining the ionosphere are considered to be empirical.

The slow decay of the ionosphere during the night as indicated in Eq. (5) will be overcome by ionization when the Sun rises.

The duration of twilight is given by (again from [6.2]) as:

$$\tau_D = \dot{\theta}^{-1} \sin^{-1} \left\{ \frac{\cos \delta_{\odot}}{\sin \beta_G} \left[\left(2 \frac{h_{\text{max}} + H}{R} \right)^{1/2} - \left(2 \frac{h_{\text{max}}}{R} \right)^{1/2} \right] \right\}, \quad (16)$$

where δ_{\odot} is the declination of the Sun and β_G the colatitude of the station in question. Using $\beta_G = 60^\circ$, $\delta_{\odot} = 10^\circ$, $h_{\text{max}} = 350 \text{ km}$, $H = 35 \text{ km}$, $R = 6370 \text{ km}$ for the radius of the Earth and for the spin rate of the Earth $\dot{\theta} = 7.3 \cdot 10^{-5} \text{ rad/sec}$ one obtains:

$$\tau_D = 4.3 \text{ min.} \quad (17)$$

which is quite a short duration. The dawn transition as can be seen is negligible. Therefore calling the electron density profile for the day time (Eq. (3)) by N_D and the night time electron density profile (Eq. (14)) by N_N then, in the Sun-centered coordinate system an expression for the zenith electron density is given by:

$$N = N_D + (N_N - N_D) S(\lambda_o - \frac{\pi}{2}) + (N_D - N_N) S(\lambda_o - \frac{3\pi}{2}) , \quad (18)$$

where λ_o is the longitude in the Sun centered coordinate system $0 \leq \lambda \leq 2\pi$ and $S(x)$ is the step function: $S(x) = 1$ if $x > 0$, $S(x) = 0$ if $x < 0$. The parameter t (the time) is given by

$$t = \frac{1}{\theta} (\lambda_o - \frac{\pi}{2}) . \quad (19)$$

If β_G is the colatitude and λ_G the longitude of a station in a geographical coordinate system corresponding to β_o and λ_o in the Sun fixed system and if the angle between the X-axis and projection of the X-axis on the XY plane is called T , the connection between the two coordinate systems is given by [6.2].

$$\sin \beta_o \sin \lambda_o = \sin \beta_G \sin (\lambda_G - T) \quad (20a)$$

$$\sin \beta_o \cos \lambda_o = \sin \delta_o \cos \beta_G + \cos \delta_o \sin \beta_G \cos (\lambda_G - T) \quad (20b)$$

$$\cos \beta_o = \cos \delta_o \cos \beta_G - \sin \delta_o \sin \beta_G \cos (\lambda_G - T) . \quad (20c)$$

41

As can be seen from Figure A6.3 the angle T is related to the universal time U. T. by

$$T = \pi - U. T. \quad (21)$$

From Eq. (20) the Sun fixed coordinates β_o and λ_o can be determined and the zenith electron distribution expressed in geographical coordinates.

The range correction Eq. (1) can now be obtained from [6.2] without any further elaboration. The prescription to be used follows. Define

$$S = -r_o \cos z + (r^2 - r_o^2 \sin^2 z)^{1/2} \quad (22)$$

where z is the zenith angle of the ray path between the two stations (station/satellite) performing a range determination and r_o is the distance of the lower station from the center of the Earth. Instead of Eq. (4b) use the following equations:

$$y_o = S (\cos z \sin \beta_o \sin \lambda_o - \sin z \cos \alpha \cos \beta_o \sin \lambda_o + \sin z \sin \alpha \cos \lambda_o) + r_o \sin \beta_o \sin \lambda_o \quad (23a)$$

and

$$z_o = S (\cos z \cos \beta_o + \sin z \cos \alpha \sin \beta_o) + r_o \cos \beta_o. \quad (23b)$$

in the expression for the electron density profile Eq. (3). This will completely take care of the daytime ionosphere. Equation (10) however takes the day-night transition into account automatically. It is therefore a fairly simple matter to obtain the ionospheric range correction by using Eqs. (1), (3), (11), (18), and (19) in that order.

One final point has to be made. The angle α in Eqs. (23) is the azimuth of the line of sight between the two stations in the Sun fixed coordinate system (Figure A6.1). If α_G , that is, the azimuth given in a geographical coordinate system, is known, a determination of α can be made via the following equation:

$$\begin{aligned} \cos z \cos \beta_G + \sin z \cos \alpha_G \sin \beta_G &= \sin \delta_\odot (\cos z \sin \beta_o \cos \lambda_o \\ &- \sin z \cos \alpha \cos \beta_o \cos \lambda_o - \sin z \sin \alpha \sin \beta_o) \\ &+ \cos \delta_\odot (\cos z \cos \beta_o + \sin z \cos \alpha \sin \beta_o) \end{aligned} \quad (24)$$

once β_o and λ_o are determined from Eqs. (20).

6.4 COMPUTATIONAL ALGORITHM

Given the following input:

$\mu = 1$, First entry into routine,

2, Second entry into routine,

3, Third entry; proceed directly to Eq. (32)

$\alpha_G \equiv$ Azimuth of the line of sight between station 0 and station 1 (satellite) (rad),

$z \equiv$ Zenith angle of the line of sight between station 0 and station 1 (satellite) (rad),

$T \equiv$ Time in sec after midnight Greenwich. (U. T.)

$\delta_{\odot} \equiv$ Declination of the Sun at time T (rad),

$\lambda_G \equiv$ East geographical longitude (rad), $0 \leq \lambda_G \leq 2\pi$,

$\beta_G \equiv$ Geographical colatitude (rad), $0 \leq \beta_G \leq \pi$

$\dot{\theta} \equiv$ Spinrate of the Earth (rad/sec),

$K = 2\pi e^2/m \equiv$ Range correction constant (cm^3/sec^2),

$H_0 \equiv$ Height of station 0 above geoid (cm),

$H_1 \equiv$ Height of station 1 (cm),

$\omega \equiv$ Operating microwave angular frequency (sec^{-1}),

$N_{\text{max}} \equiv$ Peak electron density (cm^{-3}),

$h_{\text{max}} \equiv$ Altitude above ground of peak electron density (cm),

$H \equiv$ Scale height of the electron density profile (cm),

$a_e \equiv$ radius of the Earth (cm),

$\alpha = \alpha^* \equiv$ Diffusion coefficient for electrons (sec^{-1}),

$\beta \equiv$ Attachment coefficient for electrons (sec^{-1}),

define (Tol 1 = 100 cm, Tol 2 \equiv 0.2) and

$r \equiv$ 1st integration variable; and Δr (step size)

$x \equiv$ 2nd integration variable; and Δx (step size).

Start by computing:

$$r_0 = H_0 + a_e$$

$$r_1 = H_1 + a_e$$

$$\Delta\theta = \dot{\theta}T,$$

and determine λ_0 from the equations:

$$\cos \beta_0 = \cos \delta_0 \cos \beta_G + \sin \delta_0 \sin \beta_G \cos (\lambda_G + \Delta\theta), \quad 0 \leq \beta_0 \leq \pi \quad (25a)$$

$$\sin \beta_0 \cos \lambda_0 = \sin \delta_0 \cos \beta_G - \cos \delta_0 \sin \beta_G \cos (\lambda_G + \Delta\theta), \quad 0 \leq \lambda_0 \leq 2\pi \quad (25b)$$

$$\sin \beta_0 \sin \lambda_0 = -\sin \beta_G \sin (\lambda_G + \Delta\theta). \quad (25c)$$

Set

$$J = 0$$

$$I = 0$$

$$r = r_0.$$

If $\pi/2 \leq \lambda_0 \leq 3\pi/2$ proceed to Eq. (28) otherwise continue by computing:
 $\cos \beta_0$, $\sin \beta_0$, $\cos \lambda_0$ and $\sin \lambda_0$ as well as

$$a_1 = \cos z \cos \beta_G + \sin z \cos \alpha_G \sin \beta_G - \sin \delta_\odot \cos z \sin \beta_0 \cos \lambda_0 \\ - \cos \delta_\odot \cos z \cos \beta_0$$

$$a_2 = \cos z \sin \beta_G \cos \lambda_G - \sin z \cos \alpha_G \cos \beta_G \cos \lambda_G - \sin z \sin \alpha_G \sin \lambda_G \\ + \cos \Delta_\theta \cos \delta_\odot \cos z \sin \beta_0 \cos \lambda_0 + \sin \Delta_\theta \cos z \sin \beta_0 \sin \lambda_0 \\ - \cos \Delta_\theta \sin \delta_\odot \cos z \cos \beta_0$$

$$b_1 = -\sin \delta_\odot \sin z \cos \beta_0 \cos \lambda_0 + \cos \delta_\odot \sin z \sin \beta_0$$

$$b_2 = -\sin \delta_\odot \sin z \sin \lambda_0$$

$$b_3 = \cos \Delta_\theta \cos \delta_\odot \sin z \cos \beta_0 \cos \lambda_0 + \sin \Delta_\theta \sin z \cos \beta_0 \sin \lambda_0 \\ + \cos \Delta_\theta \sin \delta_\odot \sin z \sin \beta_0$$

$$b_4 = \cos \Delta_\theta \sin z \sin \lambda_0 - \sin \Delta_\theta \sin z \cos \lambda_0.$$

Determine α from:

$$\cos \alpha = (b_1 b_4 - b_2 b_3)^{-1} (a_1 b_4 - a_2 b_2)$$

$$\sin \alpha = (b_1 b_4 - b_2 b_3)^{-1} (a_2 b_1 - a_1 b_3).$$

and continue to compute:

$$c_1 = \cos z \sin \beta_o \sin \lambda_o - \sin z \cos \alpha \cos \beta_o \sin \lambda_o + \sin z \sin \alpha \cos \lambda_o$$

$$c_2 = \sin \beta_o \sin \lambda_o$$

$$c_3 = \cos z \cos \beta_o + \sin z \cos \alpha \sin \beta_o$$

$$x = x_1 = 6 \cdot 10^7 / H$$

$$S = -r_o \cos z + (r^2 - r_o^2 \sin^2 z)^{1/2}$$

(26)

$$y_o = S c_1 + r_o c_2$$

$$z_o = S c_3 + r_o \cos \beta_o$$

$$A = y_o^2 + z_o^2$$

$$B = Hx + a_e + h_{\max}$$

$$c = (1 - A/B)^{-1/2}$$

$$Z = (r - a_e - h_{\max})/H$$

Compute the integral:

$$I = I + e^{-x} c \Delta x \longrightarrow \left\{ I = \int_{x_1}^Z e^{-x} c dx . \right.$$

If $x = z$ (Tol 2 = 0.2) proceed to Eq. (27); otherwise $x = x_1 - \Delta x$ and return to Eq. (26).

$$D = \frac{1}{2} (1 - z + I)$$

(27)

$$N_D = N_{\max} e^D,$$

and go to Eq. (29). Continue to compute:

$$h = (r - a_e)/H$$

(28)

$$\alpha_1 = 2 \sqrt{\beta/\alpha^*} e^{-h}$$

$$t = \frac{1}{\theta} (\lambda_0 - \pi/2)$$

$$\alpha_2 = e^{-2\sqrt{\alpha^* \beta} t}$$

$$\alpha_3 = \frac{1}{2} \left[1 + \left(\frac{\pi a_e \alpha^*}{2H \beta} \right)^{1/2} \exp(h_{\max}/H) \right]$$

$$\alpha_4 = \frac{3}{2} \sqrt{\alpha^* \beta} t$$

$$\beta_1 = \frac{1}{2} (1 + h_{\max}/H)$$

$$\beta_2 = \frac{1}{2} \alpha_1$$

$$\beta_3 = \left\{ [\alpha_3 (1 - \alpha_2) + \alpha_2] \alpha_1^{-1} \alpha_2 \right\}^{-1/2}$$

$$\beta_4 = \alpha_1 \alpha_2 [\alpha_3 (1 - \alpha_2)^2 + \alpha_2 (1 - \alpha_2)]^{-1}$$

$$\beta_5 = \alpha_1 \alpha_2 (1 - \alpha_3) [\alpha_3 (1 - \alpha_2) + \alpha_2]^{-1}$$

$$\operatorname{erf}(t) = \frac{2}{\sqrt{\pi}} \int_0^t e^{-v^2} dv.$$

$$N_N = \frac{1}{\sqrt{2}} (\beta/\alpha^*)^{-1/4} N_{\max} \beta_3 \exp(\beta_1 - \beta_2 + \beta_5 - \alpha_4) \operatorname{erf}(\beta_4^{1/2}).$$

$$N = N_N.$$

Compute

$$\lambda_1 = K \omega^{-2}$$

$$c_o = r_o \sin z$$

$$\lambda_2 = \left(1 - c_o^2/r^2\right)^{-1/2} \quad (29)$$

$$J = J + \lambda_2 N \Delta r \longrightarrow \left\{ \int_{r_o}^{r_1} \lambda_2 N dr. \right.$$

If $r = r_1$ (Tol 1) proceed to Eq. 30; otherwise set $r = r + \Delta r$, and $x = x_1$, $I = 0$, and return to Eq. (26).

First entry (if $\mu = 1$ proceed to Eq. (30))

$$\begin{aligned}\Delta\rho &= \lambda_1 J \\ J_1 &= J \\ z_1 &= z\end{aligned}\tag{30}$$

$$\Delta\rho_1 = \Delta\rho$$

$$\mu = 2$$

and exit calculations.

Second entry (if $\mu = 2$ proceed to Eq. (31))

$$\begin{aligned}J_2 &= J \\ z_2 &= z\end{aligned}\tag{31}$$

$$\frac{\partial J}{\partial z} = (J_2 - J_1)/(z_2 - z_1)$$

$$\mu = 3$$

and exit calculations.

Third and subsequent entries ($\mu = 3$)

$$\Delta z = z - z_1\tag{32}$$

$$\Delta\rho = \Delta\rho_1 + \lambda_1 \frac{\partial J}{\partial z} \Delta z$$

ORIGINAL PAGE IS
OF POOR QUALITY

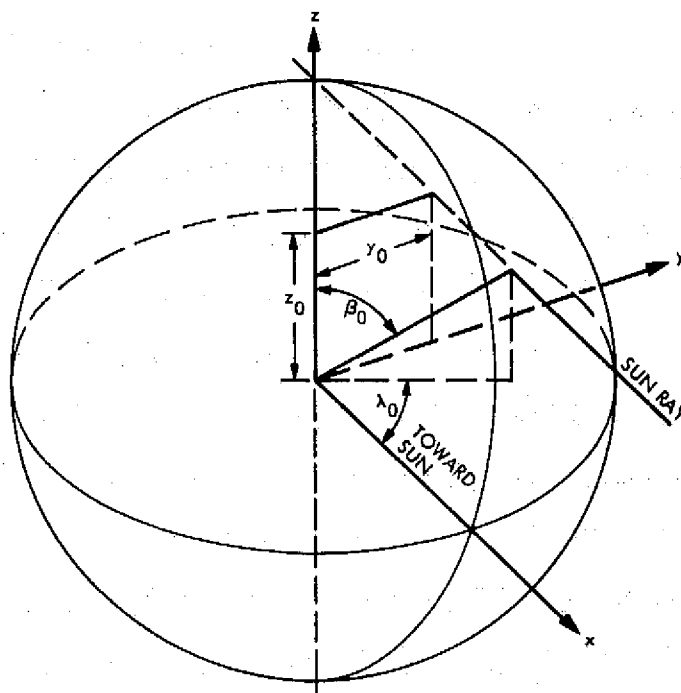


Fig. A6.1. Geometry of the System

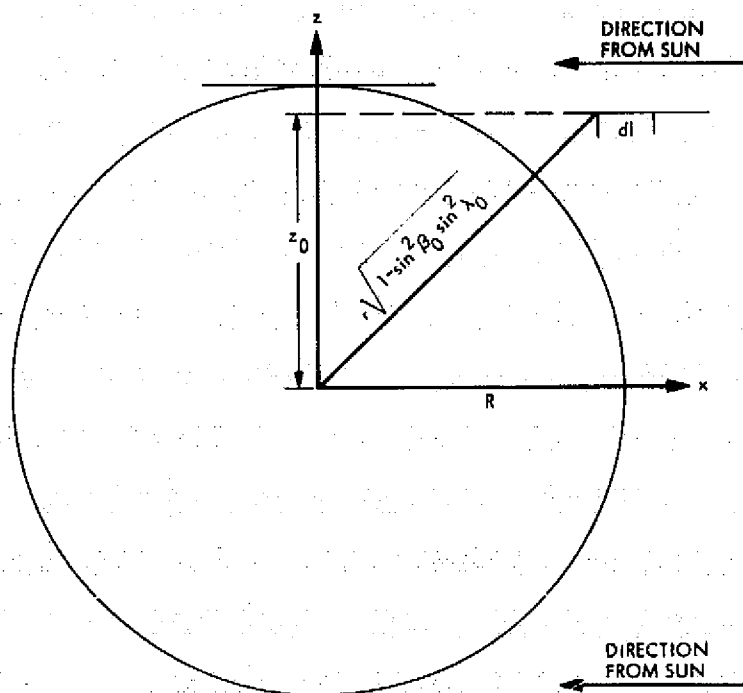


Fig. A6.2a. Cross-section Through the X-Z Plane of Fig. A6.1

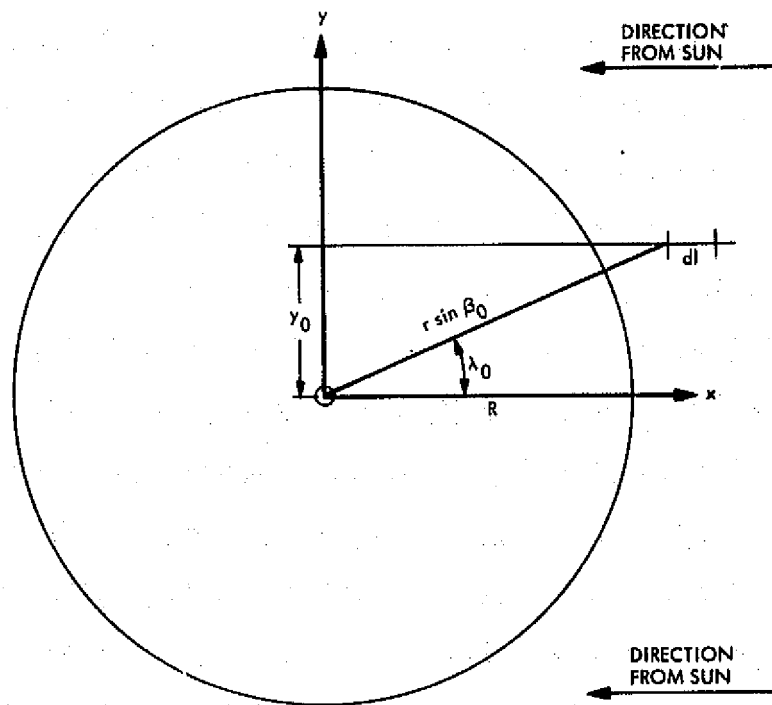


Fig. A6.2b. Cross-section Through the X-Y Plane of Fig. A6.1

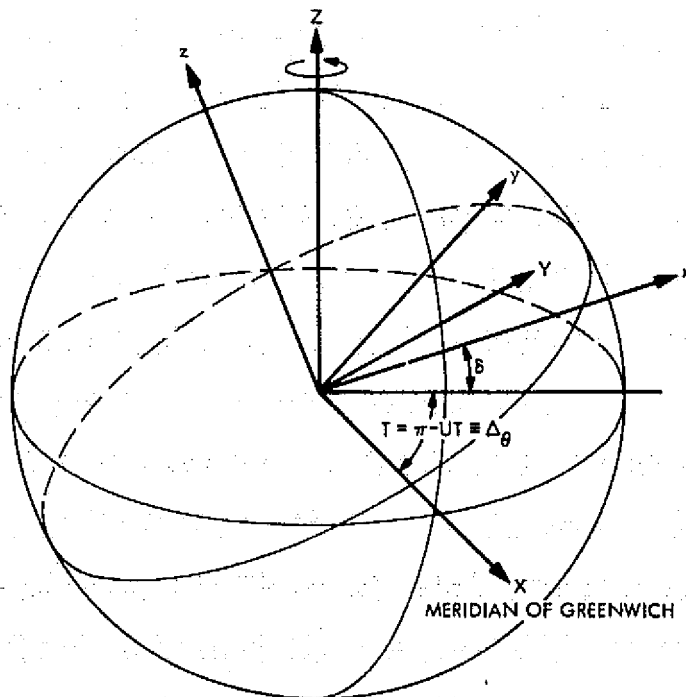


Fig. A6.3. Transformation from the Sun Oriented to the Geographical Coordinate System

A6.5 COVARIANCE MATRIX

As mentioned before (A6.3) the one way range correction Δp can only be determined to an accuracy of some 10 cm with a single frequency system at S-band. A glance at Table A6.2 reveals that the only important parameters for the covariance matrix are N_{\max} and H (during daytime). Added to these parameters is α , the diffusion coefficient (during nighttime). The analysis proceeds as follows.

In this section, as in Section A5.8, the range correction is again designated by Δd to conform with Appendices A1 and A2 of this work. The range can now be expressed as

$$d_T = d_N - \Delta d_t + v_N - \Delta d_i + \mu_N, \quad (33)$$

where Δd_t is the tropospheric range correction of Appendix A5 denoted therein by Δd , v_N is defined in Section A5.8 by Eq. (56), Δd_i is the ionospheric range correction analyzed in this Appendix and μ_N is given by:

$$\mu_N = \frac{\partial \Delta d_i}{\partial N_{\max}} \delta N_{\max} + \frac{\partial \Delta d_i}{\partial H} \delta H + \left[\frac{\partial \Delta d_i}{\partial \alpha} \delta \alpha \right] \quad (34)$$

where the errors in N_{\max} , H and α are δN_{\max} , δH and $\delta \alpha$ respectively. The bracket in Eq. (34) signifies that this term occurs only at nighttime. That part of the covariance matrix engendered by μ_N called W_I in Section A5.8 (Eq. 57), is now given by

$$W_I = Z \Lambda_z Z^T + Z_t Z_t^T \sigma_t^2 + U \left(\frac{\partial \Delta d}{\partial z_o} z_o \sigma_{t_o} \right)^2 + K_I \Lambda_i K_I^T \quad (35)$$

where the Z , Z_t , etc. are the same matrices as in Appendix A5. Note that in Appendix A5 the Z matrix (Eq. 58) should now read $Z^T = \left[\frac{\partial \Delta d_{t1}}{\partial z_1}, \frac{\partial \Delta d_{t2}}{\partial z_2} \dots \right]$ while the Z matrix here reads $\left[\frac{\partial \Delta d_{i1}}{\partial z_1}, \frac{\partial \Delta d_{i2}}{\partial z_2} \dots \right]$ etc. The other matrices here are as follows:

$$\Lambda_i = \begin{pmatrix} \sigma_{N_{\max}}^2 & 0 \\ 0 & \sigma_H^2 \\ 0 & [\sigma_\alpha^2] \end{pmatrix} \quad (36)$$

and

$$K_I = \begin{bmatrix} \frac{\partial \Delta d_{i1}}{\partial N_{\max}} & \frac{\partial \Delta d_{i1}}{\partial H} & \left[\frac{\partial \Delta d_{i1}}{\partial \alpha} \right] \\ \vdots & \vdots & \vdots \\ \frac{\partial \Delta d_{ik}}{\partial N_{\max}} & \frac{\partial \Delta d_{ik}}{\partial H} & \left[\frac{\partial \Delta d_{ik}}{\partial \alpha} \right] \end{bmatrix} \quad (37)$$

Note that K_I is of dimension $k \times 3$. This structuring is in complete analogy to the derivation given in A5.8. What remains to be done is the evaluation of the partial derivatives. This is particularly simple for $\partial \Delta d_i / \partial N_{\max}$, i.e.,

$$\partial \Delta d_i / \partial N_{\max} = \Delta d_i (N_{\max})^{-1}. \quad (38)$$

The remaining derivatives can be obtained from the pertinent expressions given earlier in this appendix. But it turns out that the ensuing formulae are expressed by integrals with different integrands than those used in the

expressions for the range correction itself. Since these integrals can only be computed numerically it certainly seems preferable to compute the partials from the range correction directly. Accordingly we have

$$\frac{\partial \Delta d_1}{H} = \frac{\Delta d_1 (H + 1 \text{ km}) - \Delta d_1 (H)}{1 \text{ km}} \quad (39)$$

where all other inputs are the prevailing values of N_{max} , h_{max} , z , α and β during the fitting interval. Furthermore for a single frequency system which cannot be calibrated to better than 10 cm (at S-band) the uncertainty in the diffusion coefficient α may be completely ignored. Nominal values for both α and β may be used throughout. The suggested values are

$$\alpha = 2g \frac{\sin^2 I}{H\nu} \quad (40)$$

$$\beta = 1 \text{ sec}^{-1}$$

Here H is the scale height, ν the ion collision frequency at h_{max} , g the Earth's gravitational acceleration and finally I is the magnetic dip angle. The parameters N_{max} , h_{max} , H , ν and I can be obtained for various areas in the U.S.A. from ESSA in Boulder Colorado.

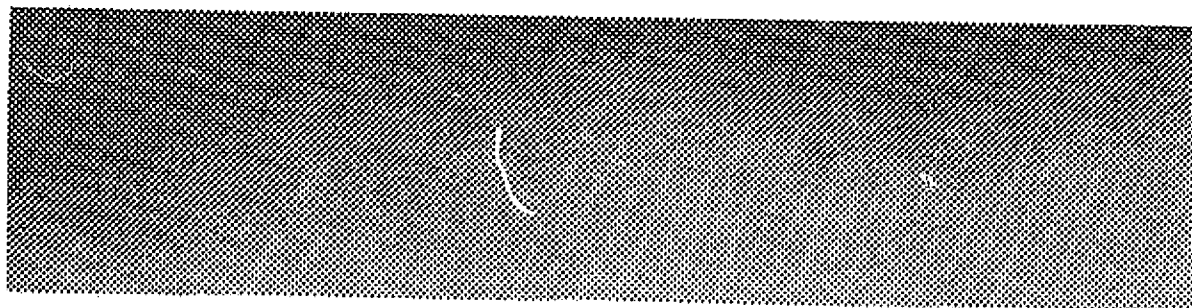
A6.6 REFERENCES

[6.1] von Roos, O.H., and Yip, K.W., "Derivation of a General Expression for Ionospheric Range Corrections Valid for Arbitrary Solar Zenith Angles, Azimuths, Elevation Angles and Station Locations," in The Deep Space Network Progress Report, Technical Report 32-1526, Vol. XI, pp. 53-61. Jet Propulsion Laboratory, Pasadena, Calif., Oct. 15. 1972.

[6.2] von Roos, O.H., Yip, K.B.W., and Escobal, P.R., "A Global Model of the Earth's Ionosphere for Use in Space Applications," Astronautica Acta, Vol. 18 (Supplement) p. 215 (1974).

[6.3] von Roos, O.H. and Escobal, P.R. "Ionospheric Range Correction for Multilateration", JPL EM 391-740, 6 May 1976 (JPL internal document).

A7. Coordinate Transformation and Covariance Mappings for High Precision Orbital State Estimation



Abstract

The coordinate transformations necessary for high precision orbital state estimation are developed. These transformations include the effect of the rate of change of the transformation matrices. The transformation mappings are used to develop the differential of the state vector. This differential is used to extract the covariance of the state vector in the coordinate systems of interest. Every error source of the sidereal time and polar motion, nutation and precession matrix is included. Cross correlations in the parameters are taken into account. The effects of tidal motion are included in the geographic system. Transformations from the geographic system to the geometric system used in multilateration studies are also derived.

PRECEDING PAGE BLANK NOT FILMED

A7.1 INTRODUCTION

Multilateration systems analysis makes use of three different coordinate reference frames [A7. 1]. These coordinate frames are: the geometric, geographic, and the inertial rectangular coordinate frames. The three coordinate systems are illustrated in Fig. A7. 1. The first of these systems is depicted in more detail in Fig. A7. 2.

As is evident from the figure, the first station defines the origin of the coordinate system, $[0, 0, 0]$ the second station $[X_2, 0, 0]$ fixes the principal axis of the coordinate system, and station 3, located at $[X_3, Y_3, 0]$ is used to define the basis fundamental plane.

The geometric system is linked to the geographic system via the geographic coordinates of the first three stations. In the geographic system, the fundamental axis is taken to pass through the Greenwich meridian and the equator is the fundamental plane. Stations are located in this system by the East longitude, λ_E , geodetic latitude, ϕ , and elevation, H , above and measured normal to the adopted ellipsoid.

Finally, through the sidereal time linkage, including precession, nutation and polar motion, the geographic system can be linked to the various inertial systems. The principal axis of the inertial system is the equinox and the fundamental plane is the equator.

In passing it is worthwhile to note that the process of multilateration is usually undertaken in a topocentric geometric frame, as denoted by T in Fig. A7. 1. The basis $\hat{x}_0, \hat{y}_0, \hat{z}_0$ is constructed from the position vectors $\underline{R}_{G1}, \underline{R}_{G2}, \underline{R}_{G3}$ of stations 1, 2 and 3 by a procedure which will be described shortly.* The T basis is convenient as a working datum and has been adopted for use in all multilateration studies. As time proceeds the station coordinates change due to Earth tides, etc. The right handed orthogonal basis T is determined from values of the station coordinates in basis G and adopted as a convenient reference frame. The values of $\underline{R}_{G1}, \underline{R}_{G2}, \underline{R}_{G3}$ used to determine T do not induce any uncertainty in T to an observer in T except for small tidal coupling. Hence for important applications such as fault monitoring, etc.,

*See also A3.

ORIGINAL PAGE IS
OF POOR QUALITY

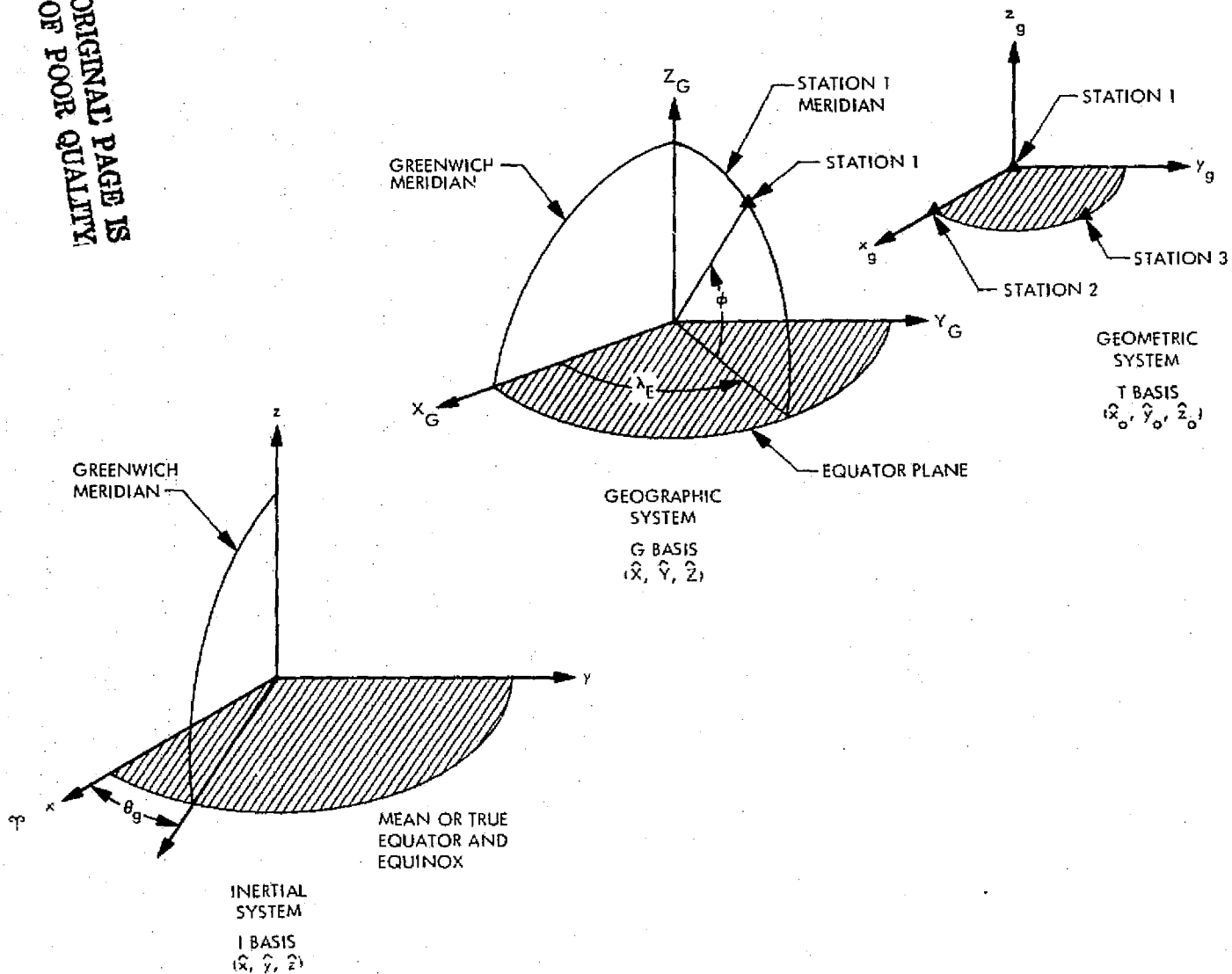


Fig. A7.1. Coordinate Systems

measurements would be made in T and accurate interstation distances would be obtained free of uncertainties in the vectors taken from G to define the T basis.*

To an observer in T, however, the uncertainty of the translation and rotation become evident as the observer moves from T to G. By the same token as the observer moves into the true of date basis, denoted by I, errors in the right ascension in nutation, or in θ_T and movement in the pole (x_p, y_p) also materialize. The true of date (TOD) basis is of importance because it is in this inertial system that satellite observables are obtained. Further errors are introduced as orbital positions and velocities are referred to the mean of date (MOD) basis via the nutation matrix N used to effect the coordinate transformation. Finally precession errors come into play via the matrix P used in transforming from the MOD basis into the mean of epoch (MOE) basis (usually 1950.0) wherein most orbital element comparisons are undertaken.

A7.2 TRANSFORMATION FROM GEODETIC TO GEOMETRIC COORDINATES

Consider Fig. A7.2 which illustrates the two basic coordinate systems of this study. In the figure the numbers 1, 2 and 3 refer respectively to the three primary stations which define the geometric coordinate system.

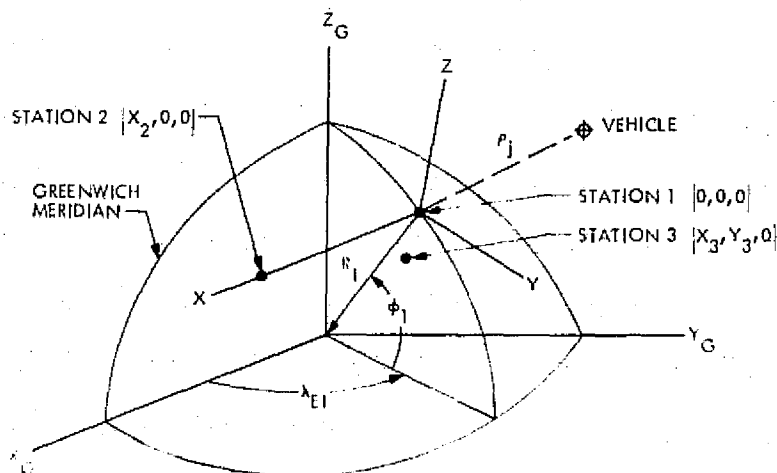


Fig. A7.2. Geographic and Geometric Coordinate Systems

* It is assumed that the small uncertainty in R_{G1} , R_{G2} , R_{G3} as it affects the prediction of station movement via the tidal model is of second order.

Figure A7.2 has displayed the basic relationships of the station geocentric coordinate vectors \underline{R}_{Gi} , namely

$$\underline{R}_{Gi} = \begin{bmatrix} X_G \\ Y_G \\ Z_G \end{bmatrix}_i = \begin{bmatrix} -G_1 \cos \phi \cos \lambda_E \\ -G_1 \cos \phi \sin \lambda_E \\ -G_2 \sin \phi \end{bmatrix}_i, \quad (1)$$

where i is the station number and

$$G_1 \equiv \frac{a_e}{[1 - (2f - f^2) \sin^2 \phi]^{1/2}} + H$$

$$G_2 \equiv \frac{(1 - f)^2 a_e}{[1 - (2f - f^2) \sin^2 \phi]^{1/2}} + H \quad (2)$$

with

$\phi \equiv$ geodetic latitude,

$H \equiv$ elevation of station measured normal to and above the adopted ellipsoid,

$\lambda_E \equiv$ east longitude of station,

$a_e \equiv$ equatorial radius of Earth,

$f \equiv$ geometric flattening of Earth.

As can be seen from Fig. A7.2, \underline{R}_1 is the vector from station 1 to the dynamical origin.* The vector from the dynamical origin to station 2 is denoted by $-\underline{R}_2$. Subtracting these vectors and normalizing results in

$$\hat{x}_o = -\frac{\underline{R}_2 - \underline{R}_1}{|\underline{R}_2 - \underline{R}_1|} = -\frac{(X_2 - X_1)\underline{I} + (Y_2 - Y_1)\underline{J} + (Z_2 - Z_1)\underline{K}}{[(X_2 - X_1)^2 + (Y_2 - Y_1)^2 + (Z_2 - Z_1)^2]^{1/2}}, \quad (3)$$

*The subscript G is dropped for convenience.

where \underline{I} , \underline{J} , \underline{K} are the unit vectors in the geocentric coordinate system, in this case, along the x-axis of the geographic system. Similarly, the vector subtraction of the third and origin station yields:

$$\hat{s}_o = -\frac{\underline{R}_3 - \underline{R}_1}{|\underline{R}_3 - \underline{R}_1|} = -\frac{(X_3 - X_1)\underline{I} + (Y_3 - Y_1)\underline{J} + (Z_3 - Z_1)\underline{K}}{[(X_3 - X_1)^2 + (Y_3 - Y_1)^2 + (Z_3 - Z_1)^2]^{1/2}}, \quad (4)$$

a unit vector toward station 3 in the geometric system. Taking the cross product of these vectors produces a unit vector in the geometric Z-direction:

$$\begin{aligned} \hat{x}_o \times \hat{x}_s = & \left\{ [(Y_2 - Y_1)(Z_3 - Z_1) - (Y_3 - Y_1)(Z_2 - Z_1)] \underline{I} \right. \\ & + [(Z_2 - Z_1)(X_3 - X_1) - (Z_3 - Z_1)(X_2 - X_1)] \underline{J} \\ & \left. + [(X_2 - X_1)(Y_3 - Y_1) - (X_3 - X_1)(Y_2 - Y_1)] \underline{K} \right\} / |\hat{x}_o \times \hat{x}_s|. \end{aligned} \quad (5)$$

Hence using the definition of the cross product

$$\hat{z}_o = s \hat{x}_o \times \hat{x}_s / [1 - (\hat{x}_o \cdot \hat{s}_o)^2]^{1/2},$$

where s is taken $= \pm 1$ such that \hat{z}_o has an adopted orientation.

Finally taking the cross product of the two orthogonal unit vectors yields

$$\hat{y}_o = \hat{z}_o \times \hat{x}_o, \quad (6)$$

which completes the determination of the \hat{x}_o , \hat{y}_o , \hat{z}_o basis.

In terms of these unit vectors, the coordinates of the stations relative to the geometric system are now given simply by

$$\begin{aligned}
X_i &= (\underline{R}_i - \underline{R}_1) \cdot \hat{x}_o \\
Y_i &= (\underline{R}_i - \underline{R}_1) \cdot \hat{y}_o \\
Z_i &= (\underline{R}_i - \underline{R}_1) \cdot \hat{z}_o.
\end{aligned}
\tag{7}$$

The transformation is now complete and can be expressed symbolically as:

$$\begin{array}{ccccc}
\text{Polar Geodetic} & & \text{Rectangular Geodetic} & & \text{Adopted Rectangular Geometric} \\
\phi_i, \lambda_i, H_i & \longrightarrow & X_{Gi}, Y_{Gi}, Z_{Gi} & \longrightarrow & X_i, Y_i, Z_i.
\end{array}$$

A7.3 TRANSFORMATION FROM TOPOCENTRIC TO GEOGRAPHIC FRAME INCLUDING EARTH/OCEAN TIDE EFFECTS

The previous section discussed the procedure for computing a basis $\hat{x}_o, \hat{y}_o, \hat{z}_o$ in which the actual multilateration analysis would be performed. The basis $\hat{x}_o, \hat{y}_o, \hat{z}_o$ was computed using the geographic a priori values of nine station coordinates $\underline{R}_{G1}, \underline{R}_{G2},$ and \underline{R}_{G3} . The transformation developed previously follows in vector notation as

$$\underline{R}_{Gi} = X_i \hat{x}_o + Y_i \hat{y}_o + Z_i \hat{z}_o + \underline{R}_{G0i}, \quad i = 1, 2, \dots, I \tag{8}$$

This is a general mapping from the geometric (topocentric) frame into the geographic (Greenwich) frame. Due to Earth/ocean tides the coordinates X_i, Y_i, Z_i vary as a function of time (Appendix A3). More specifically the set $\bar{\xi}$, i.e., the list of modeling parameters required to model the Earth/ocean tides, can be defined as

$$\bar{\xi} \equiv \left[X_{Gi}, Y_{Gi}, Z_{Gi}, \alpha_c, \delta_c, \alpha_o, \delta_o, R_c, R_o, l, h, q, \theta_g \right], \tag{9}$$

where the symbols peculiar to the tidal model are defined in Appendix A3. The parameter list in $\bar{\xi}$ can be modified via Eq. (8) to read

$$\bar{\xi} \equiv [X_{G01}, Y_{G01}, Z_{G01}, \hat{x}_o, \hat{y}_o, \hat{z}_o, X_i, Y_i, Z_i, \alpha_c, \dots, \theta_g]. \quad (10)$$

In essence Eq. (8) has been used to make the tidal model depend on a limited number of geographic stations. Note that $\hat{x}_o, \hat{y}_o, \hat{z}_o$ are functions of $R_{G01}, R_{G02},$ and R_{G03} via Eqs. (7). Hence $\bar{\xi}$ can again be expressed functionally as

$$\bar{\xi} \equiv [X_{G01}, Y_{G01}, Z_{G01}, X_{G02}, Y_{G02}, \dots, Z_{G03}, X_i, Y_i, Z_i, \alpha_c, \dots, \theta_g]. \quad (11)$$

This states that the arguments of the tidal correction are dependent on the positions of the first three stations and the rectangular positions of the stations in the adopted geometric frame, along with the modeling parameters $\alpha_c, \dots, \theta_g$. Furthermore since the tidal correction is small, the time variations in X_i, Y_i, Z_i are of second order in the correction. For example, variations of 30 cm will not affect the perturbing acceleration of the Moon and Sun to any appreciable degree. With this understanding the final functional representation of $\bar{\xi}$ is:

$$\bar{\xi} = [X_{G01}, Y_{G01}, \dots, Z_{G03}, X_{oi}, Y_{oi}, Z_{oi}, \alpha_c, \dots, \theta_g]. \quad (12)$$

The rectangular coordinates in the geometric frame, $\underline{R} \equiv [X_i, Y_i, Z_i]$ can now be modeled via the tidal functions and represented as

$$\underline{R}(t) = \underline{R}_o + F(\bar{\xi}, t), \quad (13)$$

where \underline{R}_o is a constant which can only be interpreted physically as the station location in the absence of tidal movement and $F(\bar{\xi}, t)$ is the analytic function which when added to \underline{R}_o yields the rectangular station location at time t .

When the tidal model is included it is only possible to estimate \underline{R}_0 , and perhaps some of the $\underline{\xi}$ via the multilateration procedure. The generalized transformation inclusive of tidal movement is now given by:

$$\underline{R}_{Gi} = X_i(t) \underline{\hat{x}}_0 + Y_i(t) \underline{\hat{y}}_0 + Z_i(t) \underline{\hat{z}}_0 + \underline{R}_{G1} \quad (14)$$

$$= (X_{oi} + \underline{f}_i \cdot \underline{\hat{x}}_0) \underline{\hat{x}}_0 + (Y_{oi} + \underline{f}_i \cdot \underline{\hat{y}}_0) \underline{\hat{y}}_0 + (Z_{oi} + \underline{f}_i \cdot \underline{\hat{z}}_0) \underline{\hat{z}}_0 + \underline{R}_{G01} + \Delta \underline{R}_{G1}(t), \quad (15)$$

where the $\Delta \underline{R}$ functions are defined in Appendix A3 and $\underline{f} \equiv \Delta \underline{R}_{Gi} - \Delta \underline{R}_{G1}$. Note that the tidal station velocities are

$$\dot{\underline{R}}_{Gi} = (\dot{\underline{f}}_i \cdot \underline{\hat{x}}_0) \underline{\hat{x}}_0 + (\dot{\underline{f}}_i \cdot \underline{\hat{y}}_0) \underline{\hat{y}}_0 + (\dot{\underline{f}}_i \cdot \underline{\hat{z}}_0) \underline{\hat{z}}_0 \equiv \dot{\underline{f}}_i. \quad (16)$$

A7.4 STATION POSITIONS/VELOCITIES AND COVARIANCES IN GEOMETRIC FRAME

Within the T basis, it is evident that by letting

$$\underline{\xi}_i \equiv \begin{bmatrix} X \\ Y \\ Z \end{bmatrix}_i ; \quad \dot{\underline{\xi}} \equiv \begin{bmatrix} \dot{X} \\ \dot{Y} \\ \dot{Z} \end{bmatrix}_i \quad (17)$$

one has

$$\begin{aligned} \underline{\xi} &= \underline{\xi}_0 + \underline{f}_\xi(t) \\ \dot{\underline{\xi}} &= \underline{0} + \dot{\underline{f}}_\xi(t), \end{aligned} \quad (18)$$

where

$$\underline{f}_\xi(t) \equiv \begin{bmatrix} \underline{f}_i \cdot \underline{\hat{x}}_0 \\ \underline{f}_i \cdot \underline{\hat{y}}_0 \\ \underline{f}_i \cdot \underline{\hat{z}}_0 \end{bmatrix} ; \quad \dot{\underline{f}}_\xi(t) \equiv \begin{bmatrix} \dot{\underline{f}}_i \cdot \underline{\hat{x}}_0 \\ \dot{\underline{f}}_i \cdot \underline{\hat{y}}_0 \\ \dot{\underline{f}}_i \cdot \underline{\hat{z}}_0 \end{bmatrix}.$$

The errors in the set $\xi, \bar{\xi}$ are given directly as

$$\begin{aligned}\delta \xi &= \delta \xi_o + \frac{\partial f_{\xi}}{\partial \bar{\xi}} \delta \bar{\xi} \\ \delta \dot{\xi} &= 0 + \frac{\partial \dot{f}_{\xi}}{\partial \bar{\xi}} \delta \bar{\xi}\end{aligned}\tag{19}$$

and hence a direct computation yields the covariance matrix

$$\Lambda_{\xi \dot{\xi}}^{ij} = \begin{bmatrix} \Lambda_{aa}^{ij} & \Lambda_{ab}^{ij} \\ \left[\Lambda_{ab}^{ij} \right]^T & \Lambda_{bb}^{ij} \end{bmatrix} = E \left[\begin{bmatrix} -\delta \xi \\ \delta \dot{\xi} \end{bmatrix} \begin{bmatrix} \delta \xi^T & \delta \dot{\xi}^T \end{bmatrix} \right], \tag{20}$$

where since $\delta \xi = \left[\partial \xi / \partial \bar{\xi} \right] \delta \bar{\xi}$

$$\begin{aligned}\Lambda_{aa}^{ij} &= \Lambda_{\xi_o}^{ij} + \left[\frac{\partial \xi_o^i}{\partial \bar{\xi}} \right] \Lambda_{\bar{\xi}} \left[\frac{\partial f_{\xi}^j}{\partial \bar{\xi}} \right]^T + \left[\frac{\partial f_{\xi}^i}{\partial \bar{\xi}} \right] \Lambda_{\bar{\xi}} \left[\frac{\partial \xi_o^j}{\partial \bar{\xi}} \right]^T \\ &\quad + \left[\frac{\partial f_{\xi}^i}{\partial \bar{\xi}} \right] \Lambda_{\bar{\xi}} \left[\frac{\partial f_{\xi}^j}{\partial \bar{\xi}} \right]^T\end{aligned}$$

$$\Lambda_{ab}^{ij} = \left[\frac{\partial f_{\xi}^i}{\partial \bar{\xi}} \right] \Lambda_{\bar{\xi}} \left[\frac{\partial \xi_o^j}{\partial \bar{\xi}} \right]^T + \left[\frac{\partial f_{\xi}^i}{\partial \bar{\xi}} \right] \Lambda_{\bar{\xi}} \left[\frac{\partial f_{\xi}^j}{\partial \bar{\xi}} \right]^T$$

$$\Lambda_{bb}^{ij} = \left[\frac{\partial f_{\xi}^i}{\partial \bar{\xi}} \right] \Lambda_{\bar{\xi}} \left[\frac{\partial f_{\xi}^j}{\partial \bar{\xi}} \right]^T$$

with the understanding that if $i = j$ the submatrices of auto correlations are determined while $i \neq j$ determines all the cross correlations between station i and j . Note that in more detail the previous notation implies

$$\frac{\partial \xi_o}{\partial \xi} \equiv \begin{bmatrix} \frac{\partial \xi_{o1}}{\partial \xi_1} & \frac{\partial \xi_{o1}}{\partial \xi_2} & \dots & \frac{\partial \xi_{o1}}{\partial \xi_\ell} \\ \frac{\partial \xi_{o2}}{\partial \xi_1} & & \dots & . \\ & & & . \\ \frac{\partial \xi_{ok}}{\partial \xi_1} & \dots & \dots & \frac{\partial \xi_{ok}}{\partial \xi_\ell} \end{bmatrix} ; \quad \delta \bar{\xi} = \begin{bmatrix} \delta \bar{\xi}_1 \\ \delta \bar{\xi}_2 \\ \vdots \\ \delta \bar{\xi}_\ell \end{bmatrix} \quad (21)$$

$$\frac{\partial f_\xi}{\partial \xi} \equiv \begin{bmatrix} \frac{\partial f_{\xi 1}}{\partial \xi_1} & \frac{\partial f_{\xi 1}}{\partial \xi_2} & \dots & \frac{\partial f_{\xi 1}}{\partial \xi_\ell} \\ . & . & & . \\ . & & & . \\ . & & & \frac{\partial f_{\xi k}}{\partial \xi_\ell} \end{bmatrix} \quad (22)$$

etc. Hence the complete covariance of all estimated parameters at time t can be computed by repeated application of the previous formulas which in essence determine all the necessary submatrices. The parameters themselves are obtained (at time t) from Eqs. (18).

A7.5 TRANSFORMATION OF ANY GEOGRAPHIC POSITION AND VELOCITY VECTOR INTO THE TRUE SIDEREAL SYSTEM (TOD) AND DEVELOPMENT OF ERROR DIFFERENTIAL OF THE TRANSFORMATION

The analysis of this section is lengthy but can be summarized simply as that of obtaining formulas for the transformation of positions and velocities from a geographic (G) to a true of date (TOD) sidereal system. It will be shown that the results are:

$$\begin{bmatrix} \underline{r} \\ \underline{\dot{r}} \end{bmatrix}_{\text{TOD}} = [\bar{S}] \begin{bmatrix} \underline{r} \\ \underline{\dot{r}} \end{bmatrix}_G \quad (23)$$

$$\begin{bmatrix} \delta \underline{r} \\ \delta \underline{\dot{r}} \end{bmatrix}_{\text{TOD}} = [\bar{S}] \begin{bmatrix} \delta \underline{r} \\ \delta \underline{\dot{r}} \end{bmatrix}_G + [\bar{V}] \begin{bmatrix} \delta \theta_{\text{GM}} \\ \delta d\psi \\ \delta \Delta\psi \\ \vdots \\ \delta \dot{y}_p \end{bmatrix} \quad (24)$$

where \underline{r} , $\underline{\dot{r}}$ represent any position and velocity vector, e. g., station or satellite vectors; the matrices $[\bar{S}]$ and $[\bar{V}]$ will be presently defined; and $\delta \theta_{\text{GM}}$, ..., $\delta \dot{y}_p$ are the errors peculiar to the transformation parameters, i. e., nutation in right ascension and obliquity, and polar motion.

To accomplish these objectives, the standard position matrix is taken as

$$\begin{bmatrix} x \\ y \\ z \end{bmatrix}_{\text{TOD}} = \begin{bmatrix} \cos \theta_T & -\sin \theta_T & -(x_p \cos \theta_T + y_p \sin \theta_T) \\ \sin \theta_T & \cos \theta_T & -(x_p \sin \theta_T - y_p \cos \theta_T) \\ x_p & -y_p & 1 \end{bmatrix} \begin{bmatrix} x_G \\ y_G \\ z_G \end{bmatrix} \quad (25)$$

where

$$\theta_T = \theta_{\text{GM}} + (d\psi + \Delta\psi) \cos(\epsilon_M + d\epsilon + \Delta\epsilon)$$

with x_p, y_p taken as the instantaneous coordinates of the pole; θ_{GM} is the mean sidereal time; $(d\psi, \Delta\psi)$ are the short and long period nutation in right ascension; $(d\epsilon, \Delta\epsilon)$ are the short and long period nutation in obliquity, and ϵ_M is the mean obliquity of the ecliptic. Hence in more compact notation:

$$\underline{r}_{TOD} = [S] \underline{r}_G \quad (26)$$

and by differentiation

$$\dot{\underline{r}}_{TOD} = [S] \dot{\underline{r}}_G + [\dot{S}] \underline{r}_G, \quad (27)$$

where

$$[\dot{S}] = \begin{bmatrix} -\dot{\theta}_T \sin \theta_T & -\dot{\theta}_T \cos \theta_T \\ +\dot{\theta}_T \cos \theta_T & -\dot{\theta}_T \sin \theta_T \\ \dot{x}_p & -\dot{y}_p \end{bmatrix}$$

$$\begin{bmatrix} \left\{ (x_p \sin \theta_T - y_p \cos \theta_T) \dot{\theta}_T - \dot{x}_p \cos \theta_T - \dot{y}_p \sin \theta_T \right\} \\ \left\{ -(x_p \cos \theta_T + y_p \sin \theta_T) \dot{\theta}_T - \dot{x}_p \sin \theta_T + \dot{y}_p \cos \theta_T \right\} \\ 0 \end{bmatrix}$$

so that the complete state is given by:

$$\begin{bmatrix} \underline{r} \\ \dot{\underline{r}} \end{bmatrix}_{TOD} \equiv [\bar{S}] \begin{bmatrix} \underline{r} \\ \dot{\underline{r}} \end{bmatrix}_G \quad (28)$$

with

$$[\overline{S}] = \begin{bmatrix} [S] & [0] \\ [\dot{S}] & [S] \end{bmatrix}.$$

Now since $\overline{S} = \overline{S}(\theta_{GM}, d\psi, \Delta\psi, d\epsilon, \Delta\epsilon, \epsilon_M, x_p, y_p, \dot{\theta}_{GM}, d\dot{\psi}, \Delta\dot{\psi}, d\dot{\epsilon}, \Delta\dot{\epsilon}, \dot{\epsilon}_M, \dot{x}_p, \dot{y}_p)$ it follows that by using matrix tensor analysis

$$\delta[\overline{S}] = \frac{\partial[\overline{S}]}{\partial\theta_{GM}} \delta\theta_{GM} + \frac{\partial[\overline{S}]}{\partial d\psi} \delta d\psi + \dots + \frac{\partial[\overline{S}]}{\partial \dot{y}_p} \delta \dot{y}_p \quad (29)$$

or

$$\delta[\overline{S}] = s_1 \delta\theta_{GM} + s_2 \delta d\psi + \dots + s_{16} \delta \dot{y}_p, \quad (30)$$

where

$$s_i = \begin{bmatrix} \frac{\partial[S]}{\partial u} & [0] \\ \frac{\partial[\dot{S}]}{\partial u} & \frac{\partial[S]}{\partial u} \end{bmatrix}$$

for $u = [\theta_{GM}, d\psi, \dots, \dot{y}_p]$. The explicit matrices are given by:

$$s_1 = \begin{bmatrix} -\sin \theta_T & -\cos \theta_T & +(x_p \sin \theta_T - y_p \cos \theta_T) \\ \cos \theta_T & -\sin \theta_T & -(x_p \cos \theta_T + y_p \sin \theta_T) \\ 0 & 0 & 0 \end{bmatrix} \quad (31)$$

$$s_2 = s_1 \cos(\epsilon_M + d\epsilon + \Delta\epsilon) = s_3 \quad (32)$$

$$s_4 = -s_1(d\psi + \Delta\psi) \sin(\epsilon_M + d\epsilon + \Delta\epsilon) = s_5 = s_6 \quad (33)$$

$$s_7 = \begin{bmatrix} 0 & 0 & -\cos \theta_T \\ 0 & 0 & -\sin \theta_T \\ 1 & 0 & 0 \end{bmatrix} \quad (34)$$

$$s_8 = \begin{bmatrix} 0 & 0 & -\sin \theta_T \\ 0 & 0 & +\cos \theta_T \\ 0 & -1 & 0 \end{bmatrix} \quad (35)$$

$$s_9 = \begin{bmatrix} -\sin \theta_T & -\cos \theta_T & \{x_p \sin \theta_T - y_p \cos \theta_T\} \\ \cos \theta_T & -\sin \theta_T & -\{x_p \cos \theta_T + y_p \sin \theta_T\} \\ 0 & 0 & 0 \end{bmatrix} \quad (36)$$

$$s_{10} = -s_9 \cos(\epsilon_M + d\epsilon + \Delta\epsilon) = s_{11} \quad (37)$$

$$s_{12} = -s_9(d\psi + \Delta\psi) \sin(\epsilon_M + d\epsilon + \Delta\epsilon) = s_{13} = s_{14} \quad (38)$$

$$s_{15} = s_7 \quad (39)$$

$$s_{16} = s_8. \quad (40)$$

Use of these matrices permits the station errors to be written as

$$\begin{bmatrix} \delta \underline{r} \\ \delta \dot{\underline{r}} \end{bmatrix}_{\text{TOB}} = [\tilde{S}] \begin{bmatrix} \delta \underline{r} \\ \delta \dot{\underline{r}} \end{bmatrix}_G + \delta[\tilde{S}] \begin{bmatrix} \underline{r} \\ \dot{\underline{r}} \end{bmatrix}_G. \quad (41)$$

However

$$\delta[\bar{S}] \begin{bmatrix} \underline{r} \\ \underline{\dot{r}} \end{bmatrix}_G = \begin{bmatrix} \delta[S] & \delta[0] \\ \delta[\dot{S}] & \delta[S] \end{bmatrix} \begin{bmatrix} \underline{r} \\ \underline{\dot{r}} \end{bmatrix} = \begin{bmatrix} \delta[S]\underline{r} + [0]\underline{\dot{r}} \\ \delta[\dot{S}]\underline{r} + \delta[S]\underline{\dot{r}} \end{bmatrix} \quad (42)$$

so that use of the differentials $\delta[S]$, $\delta[\dot{S}]$ yields:

$$\begin{aligned} \begin{bmatrix} \delta[S]\underline{r} + [0]\underline{\dot{r}} \\ \delta[\dot{S}]\underline{r} + \delta[S]\underline{\dot{r}} \end{bmatrix} &= \begin{bmatrix} \frac{\partial[S]}{\partial\theta_{GM}} \underline{r}, & \frac{\partial[S]}{\partial d\psi} \underline{r}, & \dots, & \frac{\partial[S]}{\partial y_p} \underline{r}, & 0, & \dots, & 0 \\ \frac{\partial[\dot{S}]}{\partial\theta_{GM}} \underline{r}, & \frac{\partial[\dot{S}]}{\partial d\psi} \underline{r}, & \dots, & \dots, & \dots, & \dots, & \frac{\partial[\dot{S}]}{\partial y_p} \underline{r} \end{bmatrix} + \\ &\quad \begin{bmatrix} 0 \dots \dots \dots 0 \\ \frac{\partial[S]}{\partial\theta_{GM}} \underline{\dot{r}}, & \frac{\partial[S]}{\partial d\psi} \underline{\dot{r}}, & \dots, & \frac{\partial[S]}{\partial y_p} \underline{\dot{r}}, & 0, & \dots, & 0 \end{bmatrix} \begin{bmatrix} \delta\theta_{GM} \\ \delta d\psi \\ \vdots \\ \delta y_p \end{bmatrix} \\ &= \begin{bmatrix} [s_1] \begin{bmatrix} \underline{r} \\ \underline{\dot{r}} \end{bmatrix}_G, & [s_2] \begin{bmatrix} \underline{r} \\ \underline{\dot{r}} \end{bmatrix}_G, & \dots, & [s_{16}] \begin{bmatrix} \underline{r} \\ \underline{\dot{r}} \end{bmatrix}_G \end{bmatrix} \begin{bmatrix} \delta\theta_{GM} \\ \delta d\psi \\ \vdots \\ \delta y_p \end{bmatrix}. \end{aligned}$$

Hence

$$\begin{bmatrix} \delta\underline{r} \\ \delta\underline{\dot{r}} \end{bmatrix}_{TOD} = [\bar{S}] \begin{bmatrix} \delta\underline{r} \\ \delta\underline{\dot{r}} \end{bmatrix}_G + [\bar{V}] \begin{bmatrix} \delta\theta_{GM} \\ \delta d\psi \\ \vdots \\ \delta y_p \end{bmatrix}, \quad (43)$$

where

ORIGINAL PAGE IS
OF POOR QUALITY

$$\bar{V} \equiv \left[[s_1] \begin{bmatrix} \underline{r} \\ \underline{\dot{r}} \end{bmatrix}_G, [s_2] \begin{bmatrix} \underline{r} \\ \underline{\dot{r}} \end{bmatrix}_G, \dots, [s_{16}] \begin{bmatrix} \underline{r} \\ \underline{\dot{r}} \end{bmatrix}_G \right] \quad (44)$$

Note that the matrix $[\bar{V}]$ must be formed first to permit the previous matrix representation of the errors $\delta \underline{r}$, $\delta \underline{\dot{r}}$ in the TOD system.

A7.6 TRANSFORMATION OF ANY TRUE OF DATE POSITION AND VELOCITY VECTOR INTO THE MEAN OF DATE (MOD) SYSTEM AND DEVELOPMENT OF THE ERROR DIFFERENTIAL OF THE TRANSFORMATION

Bearing in mind the same objectives as those of the previous section, the transformation to the mean of date coordinate system is accomplished by using the standard nutation matrices, i. e.,

$$[N] = \begin{bmatrix} 1 & +\Delta\psi \cos \epsilon & \Delta\psi \sin \epsilon \\ -\Delta\psi \cos \epsilon & 1 & +\Delta\epsilon \\ -\Delta\psi \sin \epsilon & -\Delta\epsilon & 1 \end{bmatrix} \quad (45)$$

$$[\dot{N}] = \begin{bmatrix} 0 & -(\Delta\psi \dot{\epsilon} \sin \epsilon - \Delta\dot{\psi} \cos \epsilon)(\Delta\psi \dot{\epsilon} \cos \epsilon + \Delta\dot{\psi} \sin \epsilon) \\ (\Delta\psi \dot{\epsilon} \sin \epsilon - \Delta\dot{\psi} \cos \epsilon) & 0 & \Delta\dot{\epsilon} \\ -(\Delta\psi \dot{\epsilon} \cos \epsilon + \Delta\dot{\psi} \sin \epsilon) & -\Delta\dot{\epsilon} & 0 \end{bmatrix} \quad (46)$$

so that the transformation is given as

$$\begin{bmatrix} \underline{r} \\ \underline{\dot{r}} \end{bmatrix}_{\text{MOD}} = \begin{bmatrix} [N] & [0] \\ [\dot{N}] & [N] \end{bmatrix} \begin{bmatrix} \underline{r} \\ \underline{\dot{r}} \end{bmatrix}_{\text{TOD}} \quad (47)$$

Therefore by direct differentiation

$$\begin{bmatrix} \delta \underline{r} \\ \delta \underline{\dot{r}} \end{bmatrix}_{\text{MOD}} = \begin{bmatrix} \dot{N} & 0 \\ \dot{N} & N \end{bmatrix} \begin{bmatrix} \delta \underline{r} \\ \delta \underline{\dot{r}} \end{bmatrix}_{\text{TOD}} + \begin{bmatrix} \delta N & 0 \\ \delta \dot{N} & \delta N \end{bmatrix} \begin{bmatrix} \underline{r} \\ \underline{\dot{r}} \end{bmatrix}_{\text{TOD}}. \quad (48)$$

Now from the previous equations it is simple to verify that:

$$N_1 \equiv \frac{\partial[N]}{\partial \Delta \psi} = \begin{bmatrix} 0 & \cos \epsilon & \sin \epsilon \\ -\cos \epsilon & 0 & 0 \\ -\sin \epsilon & 0 & 0 \end{bmatrix} \quad (49)$$

$$N_2 \equiv \frac{\partial[N]}{\partial \epsilon} = \begin{bmatrix} 0 & -\Delta \psi \sin \epsilon & \Delta \psi \cos \epsilon \\ \Delta \psi \sin \epsilon & 0 & 0 \\ -\Delta \psi \cos \epsilon & 0 & 0 \end{bmatrix} \quad (50)$$

$$N_3 \equiv \frac{\partial[N]}{\partial \Delta \epsilon} = \begin{bmatrix} 0 & 0 & 0 \\ 0 & 0 & 1 \\ 0 & -1 & 0 \end{bmatrix} \quad (51)$$

$$N_4 \equiv \frac{\partial[\dot{N}]}{\partial \Delta \psi} = \begin{bmatrix} 0 & -\dot{\epsilon} \sin \epsilon & \dot{\epsilon} \cos \epsilon \\ \dot{\epsilon} \sin \epsilon & 0 & 0 \\ -\dot{\epsilon} \cos \epsilon & 0 & 0 \end{bmatrix} \quad (52)$$

$$N_5 \equiv \frac{\partial[\dot{N}]}{\partial \epsilon} = \begin{bmatrix} 0 & -(\Delta \psi \dot{\epsilon} \cos \epsilon + \Delta \dot{\psi} \sin \epsilon) & -(\Delta \psi \dot{\epsilon} \sin \epsilon - \Delta \dot{\psi} \cos \epsilon) \\ (\Delta \psi \dot{\epsilon} \cos \epsilon + \Delta \dot{\psi} \sin \epsilon) & 0 & 0 \\ (\Delta \psi \dot{\epsilon} \sin \epsilon - \Delta \dot{\psi} \cos \epsilon) & 0 & 0 \end{bmatrix} \quad (53)$$

$$N_6 \equiv \frac{\partial[\dot{N}]}{\partial \Delta \epsilon} = \begin{bmatrix} 0 & 0 & 0 \\ 0 & 0 & 1 \\ 0 & -1 & 0 \end{bmatrix} = \frac{\partial[N]}{\partial \Delta \epsilon} = N_3 \quad (54)$$

$$N_7 \equiv \frac{\partial[\dot{N}]}{\partial \epsilon} = \begin{bmatrix} 0 & -\Delta \psi \sin \epsilon & \Delta \psi \cos \epsilon \\ \Delta \psi \sin \epsilon & 0 & 0 \\ -\Delta \psi \cos \epsilon & 0 & 0 \end{bmatrix} = \frac{\partial[N]}{\partial \epsilon} = N_2 \quad (55)$$

$$N_8 \equiv \frac{\partial[\dot{N}]}{\partial \Delta \dot{\epsilon}} = \begin{bmatrix} 0 & 0 & 0 \\ 0 & 0 & 1 \\ 0 & -1 & 0 \end{bmatrix} = \frac{\partial[N]}{\partial \Delta \dot{\epsilon}} = N_3 \quad (56)$$

$$N_9 \equiv \frac{\partial[\dot{N}]}{\partial \Delta \dot{\psi}} = \begin{bmatrix} 0 & \cos \epsilon & \sin \epsilon \\ -\cos \epsilon & 0 & 0 \\ -\sin \epsilon & 0 & 0 \end{bmatrix} = \frac{\partial[N]}{\partial \Delta \dot{\psi}} = N_1 \quad (57)$$

The five previous matrices permit δN and $\delta \dot{N}$ to be written as

$$\delta N = N_1 \delta \Delta \psi + N_2 \delta \epsilon + N_3 \delta \Delta \epsilon \quad (58)$$

$$\delta \dot{N} = N_4 \delta \Delta \psi + N_5 \delta \epsilon + N_6 \delta \Delta \epsilon + N_7 \delta \dot{\epsilon} + N_8 \delta \Delta \dot{\epsilon} + N_9 \delta \Delta \dot{\psi} \quad (59)$$

so that explicitly performing the multiplication indicated by the second matrix on the right hand side of Eq. (48) yields

$$\begin{bmatrix} \delta N & 0 \\ \delta \dot{N} & \delta N \end{bmatrix} \begin{bmatrix} \underline{r} \\ \underline{\dot{r}} \end{bmatrix}_{\text{TOD}} = \begin{bmatrix} \delta N \underline{r} + 0 \cdot \underline{\dot{r}} \\ \delta \dot{N} \underline{r} + \delta N \underline{\dot{r}} \end{bmatrix} \quad (60)$$

Then by use of the differentials δN , $\delta \dot{N}$

$$\begin{bmatrix} \delta N \underline{r} + 0 \cdot \underline{\dot{r}} \\ \delta \dot{N} \underline{r} + \delta N \underline{\dot{r}} \end{bmatrix} = \begin{bmatrix} N_1 \underline{r} & N_2 \underline{r} & N_3 \underline{r} & 0 \cdot \underline{r} & 0 \cdot \underline{r} & 0 \cdot \underline{r} \\ N_4 \underline{r} & N_5 \underline{r} & N_6 \underline{r} & N_7 \underline{r} & N_8 \underline{r} & N_9 \underline{r} \end{bmatrix} \begin{bmatrix} \delta \Delta \psi \\ \delta \epsilon \\ \vdots \\ \delta \Delta \psi \end{bmatrix} \\ + \begin{bmatrix} 0 & \dots & \dots & \dots & \dots & 0 \\ N_1 \underline{\dot{r}} & N_2 \underline{\dot{r}} & N_3 \underline{\dot{r}} & 0 & 0 & 0 \end{bmatrix} \begin{bmatrix} \delta \Delta \psi \\ \delta \epsilon \\ \vdots \\ \delta \Delta \psi \end{bmatrix}$$

and the error differential in terms of the constituent errors becomes:

$$\begin{bmatrix} \delta \underline{r} \\ \delta \underline{\dot{r}} \end{bmatrix}_{\text{MOD}} = [\underline{N}] \begin{bmatrix} \delta \underline{r} \\ \delta \underline{\dot{r}} \end{bmatrix}_{\text{TOD}} + [\underline{W}] \begin{bmatrix} \delta \psi \\ \delta \epsilon \\ \vdots \\ \delta \Delta \psi \end{bmatrix} \quad (61)$$

where

$$[\underline{W}] \equiv \begin{bmatrix} \begin{bmatrix} N_1 & 0 \\ N_4 & N_1 \end{bmatrix} \begin{bmatrix} \underline{r} \\ \underline{\dot{r}} \end{bmatrix}_{\text{TOD}}, & \begin{bmatrix} N_2 & 0 \\ N_5 & N_2 \end{bmatrix} \begin{bmatrix} \underline{r} \\ \underline{\dot{r}} \end{bmatrix}_{\text{TOD}}, & \begin{bmatrix} N_3 & 0 \\ N_6 & N_3 \end{bmatrix} \begin{bmatrix} \underline{r} \\ \underline{\dot{r}} \end{bmatrix}_{\text{TOD}}, \\ \begin{bmatrix} 0 & 0 \\ N_7 & 0 \end{bmatrix} \begin{bmatrix} \underline{r} \\ \underline{\dot{r}} \end{bmatrix}_{\text{TOD}}, & \begin{bmatrix} 0 & 0 \\ N_8 & 0 \end{bmatrix} \begin{bmatrix} \underline{r} \\ \underline{\dot{r}} \end{bmatrix}_{\text{TOD}}, & \begin{bmatrix} 0 & 0 \\ N_9 & 0 \end{bmatrix} \begin{bmatrix} \underline{r} \\ \underline{\dot{r}} \end{bmatrix}_{\text{TOD}} \end{bmatrix}.$$

A7.7 TRANSFORMATION OF ANY MEAN OF DATE POSITION AND VELOCITY VECTOR INTO THE MEAN OF EPOCH (MOE) SYSTEM AND DEVELOPMENT OF THE ERROR DIFFERENTIAL OF THE TRANSFORMATION

The standard precession transformation to the Mean of Epoch (MOE) coordinate system is given by:

$$\begin{bmatrix} x \\ y \\ z \end{bmatrix}_{\text{MOE}} = \begin{bmatrix} a_{11} & a_{21} & a_{31} \\ a_{12} & a_{22} & a_{32} \\ a_{13} & a_{23} & a_{33} \end{bmatrix} \begin{bmatrix} x \\ y \\ z \end{bmatrix}_{\text{MOD}} \quad (62)$$

or more compactly as

$$\underline{r}_{\text{MOE}} = [P] \underline{r}_{\text{MOD}} \quad (63)$$

from which

$$\dot{\underline{r}}_{\text{MOE}} = [\dot{P}] \underline{r}_{\text{MOD}} + [P] \dot{\underline{r}}_{\text{MOD}} \quad (64)$$

Hence

$$\begin{bmatrix} \underline{r} \\ \dot{\underline{r}} \end{bmatrix}_{\text{MOE}} = \begin{bmatrix} [P] & [0] \\ [\dot{P}] & [P] \end{bmatrix} \quad (65)$$

The parameters contained in $[P]$ are ζ_o, θ_p, Z_p , namely $\zeta_o + Z_p \equiv$ general precession in right ascension, $\theta_p \equiv$ precession in declination, $\pi/2 - \zeta_o \equiv$ angle from mean equinox of epoch to the ascending node of mean equator of date; the elements of $[P]$ are:

$$\begin{aligned} a_{11} &= \cos \zeta_o \cos \theta_p \cos Z_p - \sin \zeta_o \sin Z \\ a_{12} &= -\sin \zeta_o \cos \theta_p \cos Z_p - \cos \zeta_o \sin Z \\ a_{13} &= -\sin \theta_p \cos Z_p \end{aligned}$$

$$\begin{aligned}
a_{21} &= \cos \zeta_o \cos \theta_p \sin Z_p + \sin \zeta_o \cos Z_p \\
a_{22} &= -\sin \zeta_o \cos \theta_p \sin Z_p + \cos \zeta_o \cos Z_p \\
a_{23} &= -\sin \theta_p \sin Z_p \\
a_{31} &= \cos \zeta_o \sin \theta \\
a_{32} &= -\sin \zeta_o \sin \theta_p \\
a_{33} &= \cos \theta_p.
\end{aligned} \tag{66}$$

Hence by direct differentiation

$$\begin{bmatrix} \delta \underline{r} \\ \delta \underline{\dot{r}} \end{bmatrix}_{\text{MOE}} = \begin{bmatrix} P & 0 \\ \dot{P} & P \end{bmatrix} \begin{bmatrix} \delta \underline{r} \\ \delta \underline{\dot{r}} \end{bmatrix}_{\text{MOD}} + \begin{bmatrix} \delta P & 0 \\ \delta \dot{P} & \delta P \end{bmatrix} \begin{bmatrix} \underline{r} \\ \underline{\dot{r}} \end{bmatrix}_{\text{MOD}}. \tag{67}$$

The partial derivatives of $[P]$ and $[\dot{P}]$ with respect to $\zeta_o, \theta_p, Z_p, \dot{\zeta}_o, \dot{\theta}_p, \dot{Z}_p$ are easily obtained, e. g.,

$$\Gamma_1 \equiv \frac{\partial [P]}{\partial \zeta_o} = \begin{bmatrix} \frac{\partial a_{11}}{\partial \zeta_o} & \frac{\partial a_{21}}{\partial \zeta_o} & \frac{\partial a_{31}}{\partial \zeta_o} \\ \frac{\partial a_{12}}{\partial \zeta_o} & \frac{\partial a_{22}}{\partial \zeta_o} & \frac{\partial a_{32}}{\partial \zeta_o} \\ 0 & 0 & 0 \end{bmatrix}. \tag{68}$$

Hence defining

$$\begin{aligned}
P_2 &\equiv \frac{\partial [P]}{\partial \theta_p}, & P_3 &\equiv \frac{\partial [P]}{\partial Z_p}, & P_4 &\equiv \frac{\partial [\dot{P}]}{\partial \zeta_o} \\
P_5 &\equiv \frac{\partial [\dot{P}]}{\partial \theta_p}, & P_6 &\equiv \frac{\partial [\dot{P}]}{\partial Z_p}, & P_7 &\equiv \frac{\partial [\dot{P}]}{\partial \zeta_o} \\
P_8 &\equiv \frac{\partial [\dot{P}]}{\partial \dot{\theta}_p}, & P_9 &\equiv \frac{\partial [\dot{P}]}{\partial \dot{Z}_p},
\end{aligned} \tag{69}$$

and using the same approach as in the previous sections

$$\begin{bmatrix} \delta \underline{r} \\ \delta \dot{\underline{r}} \end{bmatrix}_{\text{MOE}} = [\underline{P}] \begin{bmatrix} \delta \underline{r} \\ \delta \dot{\underline{r}} \end{bmatrix}_{\text{MOD}} + [\underline{T}] \begin{bmatrix} \delta \underline{z}_o \\ \delta \theta_p \\ \vdots \\ \delta \dot{\underline{z}}_p \end{bmatrix}, \quad (70)$$

where

$$\underline{T} \equiv \begin{bmatrix} \begin{bmatrix} P_1 & 0 \\ P_4 & P_1 \end{bmatrix} \begin{bmatrix} \underline{r} \\ \dot{\underline{r}} \end{bmatrix}_{\text{TOD}}, & \begin{bmatrix} P_2 & 0 \\ P_5 & P_2 \end{bmatrix} \begin{bmatrix} \underline{r} \\ \dot{\underline{r}} \end{bmatrix}_{\text{TOD}}, & \begin{bmatrix} P_3 & 0 \\ P_6 & P_3 \end{bmatrix} \begin{bmatrix} \underline{r} \\ \dot{\underline{r}} \end{bmatrix}_{\text{TOD}}, \\ \begin{bmatrix} 0 & 0 \\ P_7 & 0 \end{bmatrix} \begin{bmatrix} \underline{r} \\ \dot{\underline{r}} \end{bmatrix}_{\text{TOD}}, & \begin{bmatrix} 0 & 0 \\ P_8 & 0 \end{bmatrix} \begin{bmatrix} \underline{r} \\ \dot{\underline{r}} \end{bmatrix}_{\text{TOD}}, & \begin{bmatrix} 0 & 0 \\ P_9 & 0 \end{bmatrix} \begin{bmatrix} \underline{r} \\ \dot{\underline{r}} \end{bmatrix}_{\text{TOD}} \end{bmatrix}.$$

A7.8 COMPOUND COORDINATE ROTATIONS AND COVARIANCE TRANSFORMATIONS

The previous discussions can now be codified and the complete error mappings can be developed depending on which particular transformations are to be performed. For example the compound rotation from the geographic to the mean of epoch coordinate system becomes

$$\begin{bmatrix} \underline{r} \\ \dot{\underline{r}} \end{bmatrix}_{\text{MOE}} = [\underline{P}] [\underline{N}] [\underline{S}] \begin{bmatrix} \underline{r} \\ \dot{\underline{r}} \end{bmatrix}_{\text{G}} \quad (71)$$

while

$$\begin{aligned}
 \begin{bmatrix} \delta \underline{r} \\ \delta \dot{\underline{r}} \end{bmatrix}_{\text{MOE}} &= [\bar{P}] \begin{bmatrix} \delta \underline{r} \\ \delta \dot{\underline{r}} \end{bmatrix}_{\text{MOD}} + [\bar{T}] \begin{bmatrix} \delta \zeta_o \\ \vdots \\ \delta \dot{Z}_p \end{bmatrix} \\
 &= [\bar{P}][\bar{N}] \begin{bmatrix} \delta \underline{r} \\ \delta \dot{\underline{r}} \end{bmatrix}_{\text{TOD}} + [\bar{P}][\bar{W}] \begin{bmatrix} \delta \psi \\ \vdots \\ \delta \Delta \dot{\psi} \end{bmatrix} + [\bar{T}] \begin{bmatrix} \delta \zeta_o \\ \vdots \\ \delta \dot{Z}_p \end{bmatrix} \\
 &= [\bar{P}][\bar{N}][\bar{S}] \begin{bmatrix} \delta \underline{r} \\ \delta \dot{\underline{r}} \end{bmatrix}_G + [\bar{P}][\bar{N}][\bar{V}] \begin{bmatrix} \delta \theta_{GM} \\ \vdots \\ \delta \dot{y}_p \end{bmatrix} + [\bar{P}][\bar{W}] \begin{bmatrix} \delta \psi \\ \vdots \\ \delta \Delta \dot{\psi} \end{bmatrix} \\
 &\quad + [\bar{T}] \begin{bmatrix} \zeta_o \\ \vdots \\ \delta \dot{Z}_p \end{bmatrix}. \tag{72}
 \end{aligned}$$

The covariances of the error sources are assumed to be known and are taken as

$$\Lambda_{(\underline{r}\dot{\underline{r}})_G}, \quad \Lambda_{\theta_{GM}}, \dots, \dot{y}_p, \quad \Lambda_{\delta\psi, \dots, \delta\Delta\dot{\psi}}, \quad \Lambda_{\zeta_o, \dots, \dot{Z}_p},$$

while the cross correlation between the second and third column matrices of the right hand side of Eq. (72) is easily evaluated by inspection and defined to be

$$\Lambda_{\delta\theta_{GM}, \dots, \delta\Delta\dot{\psi}}.$$

The notation used is somewhat cumbersome and thus the previous five matrices (covariances) are numbered 1 through five respectively. The state covariance can now be computed as:

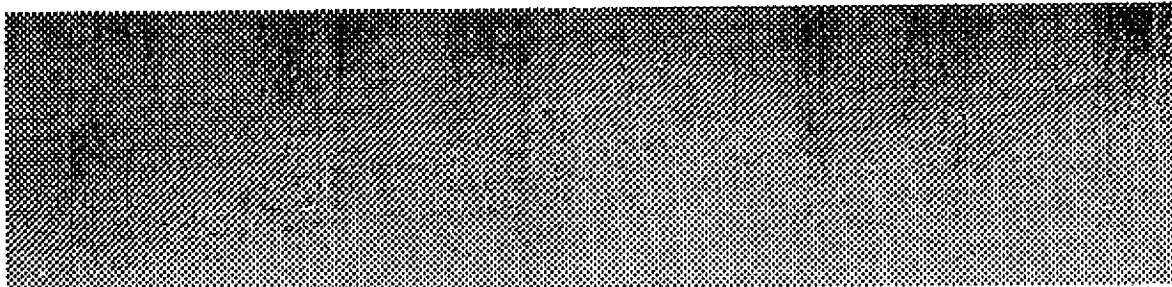
$$\begin{aligned} \Lambda_{(\underline{r}, \dot{\underline{r}})_{\text{MOE}}} = & [\bar{\mathbf{P}}] [\bar{\mathbf{N}}] [\bar{\mathbf{S}}] \Lambda_1 [\bar{\mathbf{S}}]^T [\bar{\mathbf{N}}]^T [\bar{\mathbf{P}}]^T + \\ & [\bar{\mathbf{P}}] [\bar{\mathbf{N}}] [\bar{\mathbf{V}}] \Lambda_2 [\bar{\mathbf{V}}]^T [\bar{\mathbf{N}}]^T [\bar{\mathbf{P}}]^T + \\ & [\bar{\mathbf{P}}] [\bar{\mathbf{W}}] \Lambda_3 [\bar{\mathbf{W}}]^T [\bar{\mathbf{P}}]^T + [\bar{\mathbf{T}}] \Lambda_4 [\bar{\mathbf{T}}]^T + \\ & [\bar{\mathbf{P}}] [\bar{\mathbf{N}}] [\bar{\mathbf{V}}] \Lambda_5 [\bar{\mathbf{W}}]^T [\bar{\mathbf{P}}]^T. \end{aligned} \quad (73)$$

The previous formulas are easily changed for different transformations [7.1, 7.2, 7.3].

A7.9 REFERENCES

- [7.1] Escobal, P.R., Methods of Astrodynamics, John Wiley and Sons, New York, 1968
- [7.2] Lundquist, C.A. and Veis, G., "Geodetic Parameters for a 1966 Smithsonian Institution Standard Earth," Vol. 1, SAQ Special Report 200, 1966.
- [7.3] Escobal, P.R., "Coordinate and Covariance Transformations for High Precision Orbital State Estimation," JPL EM 391-748, 29 May 1976 (JPL internal document).

A8. Short and Long-Arc Orbit Determination Using Multilateration



Abstract

The equations necessary for trilaterating a vehicle after station coordinate reduction has been achieved via multilateration are stated. Orbit determination functions for position and velocity determination are developed. Estimation equations to obtain vehicle state with a system of N stations, with and without statistical correlation are derived in a geographic Earth-fixed coordinate system. Earth/ocean tide effects are included in the estimation equations. The estimated satellite ephemeris, within the multilateration viewing window, is then used as derived data to determine the constants of integration required for long-arc orbital prediction as based on a series of short-arc solutions. The performance functional of the long-arc prediction problem is minimized with the aid of the variational or the differential equations adjoint to those of the vehicle motion using the principle of equating geometric to dynamic estimates.

PRECEDING PAGE BLANK NOT FILMED

A8.1 INTRODUCTION

Multilateration provides a method wherein interstation coordinates determined in a geometric coordinate frame are used to construct baseline constraints of high precision.* These baseline constraints are used, along with a priori geographic station coordinates to estimate the geographic coordinates to higher levels of precision than were previously possible. The details of this technique can be found in Appendix A14.

Hence it is evident that after sufficient data filtering an improved set of station coordinates will be available which are obtained strictly by means of geometric as opposed to dynamic principles.

For purposes of geophysical applications, e.g., geoid definition, etc., the trajectory of the vehicle is always of paramount importance, with a definite stress on the accuracy to which the state can be predicted on a global basis. For most applications, the coordinate system of interest is the geographic system, and therefore it seems appropriate to determine the state of the vehicle relative to this system directly. To this end the geographic station coordinates, including the 30 cm variations occasioned by Earth/ocean tides can be used as the starting point for orbital or trajectory reconstruction via trilateration over the common viewing window afforded by various ground station constellations, i.e., by several station clusters capable of multilaterating to the vehicle. It seems reasonable to assume that geographic coordinates, after sufficient data gathering and imposition of baseline constraints will be obtained with accuracies of 30 to 50 cm. Hence, these coordinates can be employed as medium precision data types to generate the state of the satellite during the viewing window, i.e., to reconstruct the satellite ephemeris [8.3].

These short arc ephemerides (for low satellites) will be available each time the satellite passes over the station constellations involved in a given experiment.

*In the geometric frame the first station is taken as the origin, the second station defines the principal axis, and the third station fixes the fundamental plane.

The short arc ephemerides so derived are strictly of a geometric nature. With this in mind it becomes interesting to inquire what would happen if the short arc geometric state is equated to the short arc dynamic state, i. e., can a set of constants to the dynamic equations of motion be found that minimizes a performance functional containing the geometric and dynamic states. The answer, of course, is yes, and it would appear that since the accuracy will certainly not degrade, only an increase in orbital prediction accuracy will result.

The idea of equating geometrically determined parameters to their equivalent dynamic counterparts, as generated from an assumed state vector at an adopted epoch, is explored herein. The objective is that of improving the assumed state vector and the dynamic constants required in the differential equations of motion.

A8.2 TRILATERATION EQUATIONS

Reference [8.1] shows that in the standard geographic coordinate system (Earth fixed) the spacecraft position vector at epoch, t_0 , is given by:

$$\underline{r}_0 = \begin{bmatrix} x_0 \\ y_0 \\ z_0 \end{bmatrix} = \begin{bmatrix} \left(-\epsilon_2 + s \left[\epsilon_2^2 - 4\epsilon_1\epsilon_3 \right]^{1/2} \right) / 2\epsilon_1 \\ Cx_0 + D \\ Ax_0 + B \end{bmatrix}, \quad (1)$$

where

$$\epsilon_1 \equiv A^2 + C^2 + 1$$

$$\epsilon_2 \equiv 2(AB + CD + X_1 + CY_1 + AZ_1)$$

$$\epsilon_3 \equiv B^2 + D^2 + 2DY_1 + 2BZ_1 + R_1^2 - \rho_1^2$$

$$A \equiv \left[(X_{G2} - X_{G1})(Y_{G3} - Y_{G1}) - (X_{G3} - X_{G1})(Y_{G2} - Y_{G1}) \right] / \Delta_1$$

$$B \equiv \left[\zeta_{31}(Y_{G2} - Y_{G1}) - \zeta_{21}(Y_{G3} - Y_{G1}) \right] / \Delta_1$$

$$C \equiv - \left[(X_{G2} - X_{G1})(Z_3 - Z_1) - (X_{G3} - X_{G1})(Z_{G2} - Z_{G1}) \right] / \Delta_1$$

$$D \equiv - \left[\zeta_{31}(Z_{G2} - Z_{G1}) - \zeta_{21}(Z_{G3} - Z_{G1}) \right] / \Delta_1$$

$$\Delta_1 \equiv (Z_{G3} - Z_{G1})(Y_{G2} - Y_{G1}) - (Z_{G2} - Z_{G1})(Y_{G3} - Y_{G1})$$

$$\zeta_{21} = \frac{1}{2} \left[\rho_2^2 - \rho_1^2 - R_2^2 + R_1^2 \right]$$

$$\zeta_{31} = \frac{1}{2} \left[\rho_3^2 - \rho_1^2 - R_3^2 + R_1^2 \right]$$

with \underline{R}_{Gi} denoting the position vector* of the trio of stations performing the trilateration and ρ_i denoting the slant range measurements from each of the stations to the spacecraft; $s = \pm 1$, and is chosen in accordance with the physically acceptable trajectory position.

The velocity in the geographic (Earth fixed) system is given directly by:

$$\begin{bmatrix} \dot{x}_0 \\ \dot{y}_0 \\ \dot{z}_0 \end{bmatrix} = [M_s]^{-1} \begin{bmatrix} E_1 \\ E_2 \\ E_3 \end{bmatrix}, \quad (2)$$

*Note that $\underline{\rho} \equiv \underline{r}_0 + \underline{R}_{Gi}$.

where

$$M_s \equiv \begin{bmatrix} x_0 + X_{G1} & y_0 + Y_{G1} & z_0 + Z_{G1} \\ x_0 + X_{G2} & y_0 + Y_{G2} & z_0 + Z_{G2} \\ x_0 + X_{G3} & y_0 + Y_{G3} & z_0 + Z_{G3} \end{bmatrix}$$

with

$$E_i \equiv \rho_i \dot{\rho}_i - \dot{\underline{R}}_{Gi} \cdot \underline{\rho}_i$$

Note that $\dot{\underline{R}}_{Gi} = \underline{0}$ if Earth tide variations are ignored.

A8.3 DEVELOPMENT OF ORBIT DETERMINATION FUNCTIONS

For a system of three stations it follows that a trilateration position function, \underline{P} , can be written as:

$$\underline{P} = \begin{bmatrix} x_0 \\ y_0 \\ z_0 \end{bmatrix} - \begin{bmatrix} \left(-\epsilon_2 + s[\epsilon_2^2 - 4\epsilon_1\epsilon_3]^{1/2} \right) / 2\epsilon_1 \\ C \left(-\epsilon_2 + s[\epsilon_2^2 - 4\epsilon_1\epsilon_3]^{1/2} \right) / 2\epsilon_1 + D \\ A \left(-\epsilon_2 + s[\epsilon_2^2 - 4\epsilon_1\epsilon_3]^{1/2} \right) / 2\epsilon_1 + B \end{bmatrix}, \quad (3)$$

while the velocity function \underline{V} takes the form:

$$\underline{V} = \begin{bmatrix} (x_0 + X_{G1})(\dot{x}_0 + \dot{X}_{G1}) + (y_0 + Y_{G1})(\dot{y}_0 + \dot{Y}_{G1}) + (z_0 + Z_{G1})(\dot{z}_0 + \dot{Z}_{G1}) - \rho_1 \dot{\rho}_1 \\ (x_0 + X_{G2})(\dot{x}_0 + \dot{X}_{G2}) + (y_0 + Y_{G2})(\dot{y}_0 + \dot{Y}_{G2}) + (z_0 + Z_{G2})(\dot{z}_0 + \dot{Z}_{G2}) - \rho_2 \dot{\rho}_2 \\ (x_0 + X_{G3})(\dot{x}_0 + \dot{X}_{G3}) + (y_0 + Y_{G3})(\dot{y}_0 + \dot{Y}_{G3}) + (z_0 + Z_{G3})(\dot{z}_0 + \dot{Z}_{G3}) - \rho_3 \dot{\rho}_3 \end{bmatrix} \quad (4)$$

Examination of \underline{P} and \underline{V} quickly reveals the following functional dependence on the parameters of the problem. In the geographic basis of Figure A8.1 which is adopted herein for the orbit determination process, attention is drawn to the geographic rectangular coordinates of any given station.

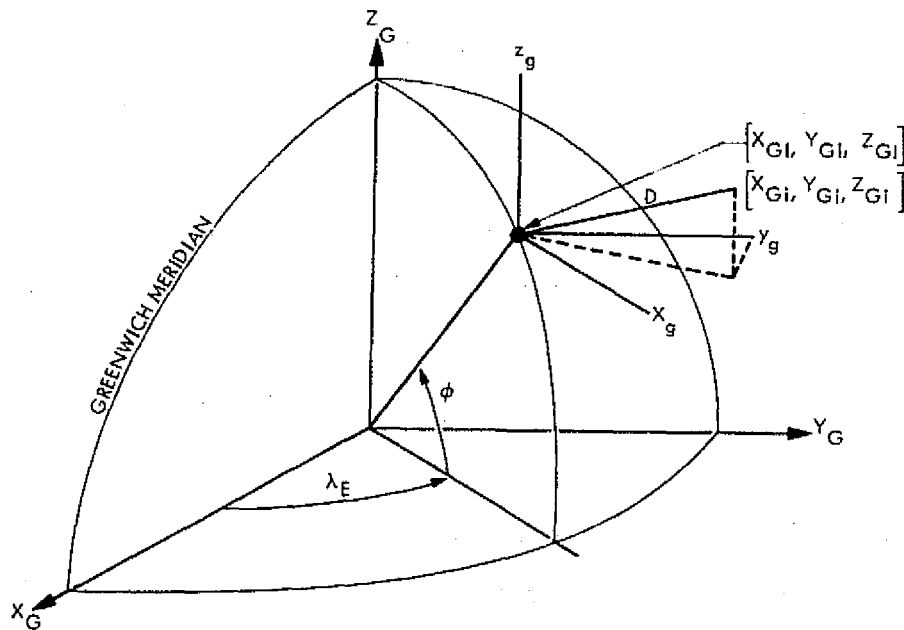


Fig. A8.1. Geographic Coordinate Basis

These geographic coordinates are obtained through the process of multilateration by means of the technique described in Appendix A14. Specifically, the generation of these geographic, so called absolute, coordinates is accomplished by an estimation procedure. This estimation procedure takes the interstation coordinates determined via multilateration in the geometric basis, $[x_g, y_g, z_g]$, of Figure A8.1, constructs the interstation baselines D , and combines these baselines with the given a priori station coordinates in the geographic basis in order to yield improved station coordinates. Hence it is obvious that any given station coordinate in the geographic basis can be written as $\underline{R}_G = \underline{R}_G(\underline{R}_{Ga}, D)$, where \underline{R}_{Ga} are the a priori station coordinates and D are the invariant station baselines obtained from the process

of multilateration. The baselines D are in turn obtained from the data coefficients c , of the synchronization polynomials, i. e., $d = c_0 + c_1 t + c_2 t^2 + \dots$, the modeling parameters of the tidal model $\bar{\xi}$, and the time, t . Hence $D = D(c, \bar{\xi}, t)$. Finally, \underline{P} and \underline{V} are also functions of c , $\bar{\xi}$, and t .

These preliminary discussions are the background for the next section wherein it is desired to determine the functional form of the error vector which must be used to uncorrelate the equations peculiar to the geometric trajectory state estimation. In the next section this error vector will be developed inclusive of all correlations and all error sources within the geographic coordinate frame.

A8.4 ESTIMATION EQUATIONS WITH NO CORRELATION

The system of equations (3) and (4) is statistically correlated and solution is most easily effected by means of a Newton-Raphson minimum variance estimation technique. The position and velocity equations can be combined in the vector \underline{T} , where

$$\underline{T} \equiv \begin{bmatrix} \underline{P} \\ \underline{V} \end{bmatrix} = \underline{0} \quad (5)$$

and functionally written in terms of the input estimates ($\hat{\cdot}$) as:

$$\underline{T} = \underline{T}(q, \hat{\xi}_G, \hat{\xi}, \hat{d}, \hat{\dot{d}}, \hat{t}, \hat{t}_0) \quad (6)$$

with the understanding that, $q \equiv [x_0, y_0, \dots, z_0]$; $\hat{\xi}_G$ are the set of geographic station coordinates improved by the multilateration process; $\hat{\xi}$ are the modeling constants of the tidal models, \hat{d} and $\hat{\dot{d}}$ are the data and data-rate, e. g., ρ and $\dot{\rho}$; and \hat{t} is the time at which the state of the orbit is desired as measured from \hat{t}_0 . Linearization of \underline{T} now yields

$$\begin{aligned} \frac{\partial \underline{T}}{\partial \underline{q}} \Delta \underline{q} = & -\underline{T} - \frac{\partial \underline{T}}{\partial \xi_G} \hat{\xi}_G - \frac{\partial \underline{T}}{\partial \xi} \hat{\xi} - \frac{\partial \underline{T}}{\partial d} \hat{d} - \frac{\partial \underline{T}}{\partial d} \hat{d} \\ & - \frac{\partial \underline{T}}{\partial t} \hat{t} - \frac{\partial \underline{T}}{\partial t_0} \hat{t}_0 \end{aligned} \quad (7)$$

or

$$[\underline{T}_q] \Delta \underline{q} = -\underline{T} + \underline{\beta} \quad , \quad (8)$$

where

$$[\underline{T}_q] \equiv \partial \underline{T} / \partial \underline{q}$$

and

$$\underline{\beta} \equiv -\frac{\partial \underline{T}}{\partial \xi_G} \hat{\xi}_G - \frac{\partial \underline{T}}{\partial \xi} \hat{\xi} - \dots - \frac{\partial \underline{T}}{\partial t} \hat{t} - \frac{\partial \underline{T}}{\partial t_0} \hat{t}_0 \quad . \quad (9)$$

If cross correlations are neglected it is not necessary to consider that $\hat{\xi}_G$ is actually obtained as a function of the same data, modeling constants, etc., and a direct computation of $\beta \beta^T$ leads to $W_u = E(\beta \beta^T)$ or

$$\begin{aligned} [W_u] = & \left[\frac{\partial \underline{T}}{\partial \xi_G} \right] \Lambda_{\hat{\xi}_G} \left[\frac{\partial \underline{T}}{\partial \xi_G} \right]^T + \left[\frac{\partial \underline{T}}{\partial \xi} \right] \Lambda_{\hat{\xi}} \left[\frac{\partial \underline{T}}{\partial \xi} \right]^T + \dots \\ & + \left[\frac{\partial \underline{T}}{\partial t_0} \right] \left[\frac{\partial \underline{T}}{\partial t_0} \right]^T \sigma_{\hat{t}_0}^2 \end{aligned} \quad (10)$$

where $\hat{\Lambda}_{\xi_G}$, $\hat{\Lambda}_{\xi_d}$, $\hat{\Lambda}_d$, $\hat{\Lambda}_d$, are the respective covariance matrices of the error sources, and σ_t^2 is the variance of time variable. The estimate of q is now given directly as:

$$\hat{q}_{n+1} = \hat{q}_n - \left[[T_q]^T [W_u]^{-1} [T_q] \right]^{-1} [T_q]^T W_u^{-1} \hat{T} \quad (11)$$

for Newton iterations $n = 1, 2, \dots N$.

A8.5 EXTENSION OF MATRIX SYSTEM FOR ADDITIONAL STATIONS

Obviously for additional stations, Eq. (8) can be partitioned to read:

$$\begin{bmatrix} [T_q]_1 \\ \vdots \\ [T_q]_{I-2} \end{bmatrix} \Delta q = - \begin{bmatrix} T_1 \\ T_2 \\ \vdots \\ T_{I-2} \end{bmatrix} + \begin{bmatrix} \beta_1 \\ \beta_2 \\ \vdots \\ \beta_{I-2} \end{bmatrix}, \quad (12)$$

where I is the total number of stations, and the solution proceeds as before.

A8.6 ESTIMATION EQUATIONS WITH CORRELATION

On the other hand, consideration of cross correlations requires that the relationships used to estimate the geographic coordinates be known. By Appendix A14, Eq. (7) this is given by:

$$\overline{G}(X_{G1}, \dots, Z_{GI}, X_{G1a}, \dots, Z_{G1a}, D_{12}, \dots, D_{I-1,I}) = 0 \quad (13)$$

or, in effect, the geographic coordinates, ξ_G , are estimated from \bar{G} , i. e.,

$$\bar{G}(\xi_G, \hat{\xi}_{Ga}, \hat{D}) = 0, \quad (14)$$

which in itself has been statistically decoupled. Following the notation of Appendix A14 it follows that

$$\bar{G} = V^{-1} \bar{H}, \quad (15)$$

where \bar{H} is the matrix defined by Eq. (6) of Appendix A14, and V is the square root of the weight matrix, W , of system \bar{H} . It is evident that:

$$\frac{\partial \bar{G}}{\partial \xi_G} \delta \hat{\xi}_G + \frac{\partial \bar{G}}{\partial \xi_{Ga}} \delta \hat{\xi}_{Ga} + \frac{\partial \bar{G}}{\partial \hat{D}} \delta \hat{D} = 0 \quad (16)$$

so that taking $\partial \bar{G} / \partial(\cdot) = V^{-1} \partial \bar{H} / \partial(\cdot)$

$$\begin{aligned} \delta \hat{\xi}_G = & - \left[\frac{\partial \bar{H}^T}{\partial \xi_G} W^{-1} \frac{\partial \bar{H}}{\partial \xi_G} \right]^{-1} \frac{\partial \bar{H}^T}{\partial \xi_G} W^{-1} \frac{\partial \bar{H}}{\partial \xi_{Ga}} \delta \hat{\xi}_{Ga} \\ & - \left[\frac{\partial \bar{H}^T}{\partial \xi_G} W^{-1} \frac{\partial \bar{H}}{\partial \xi_G} \right]^{-1} \frac{\partial \bar{H}^T}{\partial \xi_G} W^{-1} \frac{\partial \bar{H}}{\partial \hat{D}} \delta \hat{D}. \end{aligned} \quad (17)$$

Note further that the interstation baselines D are a function of d , ξ and $t - t_0$, so that the error in the baseline estimate is given by

$$\delta \hat{D} = \frac{\partial D}{\partial d} \delta \hat{d} + \frac{\partial D}{\partial \xi} \delta \hat{\xi} + \frac{\partial D}{\partial t} \delta \hat{t} + \frac{\partial D}{\partial t_0} \delta \hat{t}_0. \quad (18)$$

By collecting and equating coefficients:

$$\delta \hat{\xi}_G = [\alpha_1] \delta \hat{\xi}_{Ga} + [\alpha_2] \delta \hat{d} + [\alpha_3] \delta \hat{\xi} + [\alpha_4] \delta \hat{t} + [\alpha_5] \delta \hat{t}_0, \quad (19)$$

where the explicit formulas for the α matrices are:

$$\begin{bmatrix} \alpha_1 \end{bmatrix} \equiv - \begin{bmatrix} H^* \end{bmatrix} \begin{bmatrix} \frac{\partial \bar{H}}{\partial \xi_G} \end{bmatrix}^T \begin{bmatrix} W \end{bmatrix}^{-1} \begin{bmatrix} \frac{\partial \bar{H}}{\partial \xi_{Ga}} \end{bmatrix}$$

$$\begin{bmatrix} \alpha_2 \end{bmatrix} \equiv - \begin{bmatrix} H^* \end{bmatrix} \begin{bmatrix} \frac{\partial \bar{H}}{\partial \xi_G} \end{bmatrix}^T \begin{bmatrix} W \end{bmatrix}^{-1} \begin{bmatrix} \frac{\partial \bar{H}}{\partial D} \end{bmatrix} \begin{bmatrix} \frac{\partial D}{\partial d} \end{bmatrix} \equiv - \begin{bmatrix} H^* \end{bmatrix} \begin{bmatrix} L^* \end{bmatrix} \begin{bmatrix} \frac{\partial D}{\partial d} \end{bmatrix}$$

$$\begin{bmatrix} \alpha_3 \end{bmatrix} \equiv - \begin{bmatrix} H^* \end{bmatrix} \begin{bmatrix} L^* \end{bmatrix} \begin{bmatrix} \frac{\partial D}{\partial \xi} \end{bmatrix}$$

$$\begin{bmatrix} \alpha_4 \end{bmatrix} \equiv - \begin{bmatrix} H^* \end{bmatrix} \begin{bmatrix} L^* \end{bmatrix} \begin{bmatrix} \frac{\partial D}{\partial t} \end{bmatrix}$$

$$\begin{bmatrix} \alpha_5 \end{bmatrix} \equiv - \begin{bmatrix} H^* \end{bmatrix} \begin{bmatrix} L^* \end{bmatrix} \begin{bmatrix} \frac{\partial D}{\partial t_0} \end{bmatrix}$$

$$\begin{bmatrix} H^* \end{bmatrix} \equiv \begin{bmatrix} \frac{\partial \bar{H}}{\partial \xi_G} \end{bmatrix}^T \begin{bmatrix} W \end{bmatrix}^{-1} \begin{bmatrix} \frac{\partial \bar{H}}{\partial \xi_G} \end{bmatrix} .$$

Since the error $\hat{\delta \xi}_G$ is now explicitly expressed in terms of its constituent errors, the error in the total system of equations $\begin{bmatrix} T_q \end{bmatrix}$, i. e., $\underline{\beta}$, can now be computed by means of Eq. (19). The result of this computation is

$$\begin{aligned} \underline{\beta} \equiv & [\omega_1] \hat{\delta \xi}_{Ga} + [\omega_2] \hat{\delta \xi} + [\omega_3] \hat{\delta t} + [\omega_4] \hat{\delta t}_0 + [\omega_5] \hat{\delta d} \\ & + [\omega_6] \hat{\delta d} , \end{aligned} \quad (20)$$

where

$$[\omega_1] \equiv - \left[\frac{\partial T}{\partial \xi_G} \right] [\alpha_1]$$

$$[\omega_2] \equiv - \left[\frac{\partial T}{\partial \xi_G} \right] [\alpha_3] - \left[\frac{\partial T}{\partial \xi} \right]$$

$$[\omega_3] \equiv - \left[\frac{\partial T}{\partial \xi_G} \right] [\alpha_4] - \left[\frac{\partial T}{\partial t} \right]$$

$$[\omega_4] \equiv - \left[\frac{\partial T}{\partial \xi_G} \right] [\alpha_5] - \left[\frac{\partial T}{\partial t_0} \right]$$

$$[\omega_5] \equiv - \left[\frac{\partial T}{\partial \xi_G} \right] [\alpha_2] - \left[\frac{\partial T}{\partial d} \right]$$

$$[\omega_6] \equiv - \left[\frac{\partial T}{\partial d} \right]$$

Finally, the data, \hat{d} , is obtained from the data compression coefficients \hat{c} of Appendix A1 as

$$\hat{d} = [A] \hat{c}, \quad (21)$$

where

$$[A] = [1, \hat{t} - \hat{t}_0, (\hat{t} - \hat{t}_0)^2, \dots, (\hat{t} - \hat{t}_0)^M]$$

$$\hat{c} = [\hat{c}_0, \hat{c}_1, \dots, \hat{c}_{M+1}]$$

This enables the data errors to be evaluated in the following manner:

$$\delta d = \dot{d} \delta t - \dot{d}_0 \delta t_0 + A \delta c \quad (22)$$

$$\delta \ddot{d} = \ddot{d} \delta t - \ddot{d}_0 \delta t_0 + \dot{A} \delta c ,$$

so that by defining

$$\begin{aligned} [\omega_3^*] &\equiv [\omega_3] + [\omega_5] \dot{d} + [\omega_6] \ddot{d} \\ [\omega_4^*] &\equiv [\omega_4] - [\omega_5] \dot{d}_0 - [\omega_6] \ddot{d}_0 \end{aligned} \quad (23)$$

$$[\omega_5^*] \equiv [\omega_5] [A] + [\omega_6] [\dot{A}]$$

the error vector $\underline{\beta}$ becomes

$$\underline{\beta} \equiv [\omega_1] \delta \hat{\xi}_{Ga} + [\omega_2] \delta \hat{\xi} + [\omega_3^*] \delta \hat{t} + [\omega_4^*] \delta \hat{t}_0 + [\omega_5^*] \delta \hat{c} . \quad (24)$$

The correlated weight matrix of the system can now be directly computed, namely:

$$\begin{aligned} [W_c] &= [\omega_1] \Lambda_{\hat{\xi}_{Ga}} [\omega_1]^T + [\omega_2] \Lambda_{\hat{\xi}} [\omega_2]^T + [\omega_3^*] [\omega_3^*]^T \sigma_t^2 \\ &\quad + [\omega_4^*] [\omega_4^*]^T \sigma_{t_0}^2 + [\omega_5^*] \Lambda_{\hat{c}} [\omega_5^*]^T \end{aligned} \quad (25)$$

and the estimate of the orbital state can be obtained as

$$\begin{aligned} \hat{q}_{n+1} &= \hat{q}_n - \left[[T_q]^T [W_c]^{-1} [T_q] \right]^{-1} [T_q]^T W_u^{-1} \underline{\hat{I}} \\ &= \hat{q}_n - \Lambda_q [T_q]^T W_u^{-1} \underline{\hat{I}} \end{aligned} \quad (26)$$

for Newton iterations $n = 1, 2, \dots, N$; where Λ_q is the covariance of the state vector q . The above estimation equations account for all possible error sources.

A8.7 A NEW APPROACH TO REPETITIVE SHORT-ARC ORBIT DETERMINATION

The previous sections addressed themselves to the problem of high accuracy trajectory reconstruction, i. e., generation of the state of the vehicle undergoing multilateration in a window of common viewing by a station constellation. In summary, the best possible estimate of the station coordinates, inclusive of tidal motions, was used to obtain the state q , where $q \equiv [x, y, z, \dot{x}, \dot{y}, \dot{z}]$ at a discrete number of points: $t = t_1, t_2, t_3, \dots, t_K$, within the period of common station visibility. This was accomplished using only geometric principles, except of course for the tidal model adopted to represent the Earth's plasticity.

The short viewing window (for low satellites) permits this type of orbital reconstruction to be performed every time the satellite passes over the station constellation participating in the orbit determination process. Obviously one or more station constellations located in the adopted Earth-rotating (non-inertial) coordinate system can be used to construct a sequence of short arcs q_{ij} , where the subscript i denotes discrete times and the subscript j denotes various station constellations.

The state q_{ij} , estimated as previously described, is an osculating state and represents the movement of the satellite as occasioned by all accelerations. These accelerations are felt by the satellite at every instant of time (within the one-or-two minutes data compression arc used by the synchronization polynomials).

Suppose that the estimates q_{ij} are now taken as the derived observables from which the integration constants, q_0 , of the dynamic equations of motion are to be determined. It is exactly this device which will be used to determine the starting conditions for long-arc orbital propagation. The solution is outlined in the next section. Note that analysis is carried out in a rotating frame of reference. The transformation of the state into the standard inertial system is discussed in Appendix A7.

A8.8 OUTLINE OF ORBIT DETERMINATION ESTIMATION PROCEDURE FOR LONG-ARC PROPAGATION

The equations of motion of a satellite in a rotating geographic system are easily written as:

$$\ddot{\underline{r}}_G = [M]\ddot{\underline{r}}_I + 2[\dot{M}]\dot{\underline{r}}_I + [\ddot{M}]\underline{r}_I, \quad (27)$$

where $[M]$ is the adopted time dependent transformation matrix from the inertial to the topocentric system (See Appendix A7), and $\ddot{\underline{r}}_I$, $\dot{\underline{r}}_I$, \underline{r}_I are the accelerations, velocities, and positions in the inertial frame.³ The expression for $\ddot{\underline{r}}_I$ inclusive of Sun/Moon, tesseral and zonal harmonics, drag, lift, radiation pressure, etc. is listed in many references, e. g., [8.1], and will not be discussed further.

Direct integration of these accelerations via numerical techniques is usually symbolized as

$$\underline{r}(t) = \underline{r}_0 + \iint_0^t \ddot{\underline{r}}_G dt^2 \quad (28)$$

$$\dot{\underline{r}}(t) = \dot{\underline{r}}_0 + \int_0^t \ddot{\underline{r}}_G dt.$$

These equations can be written equivalently in the following manner, with the objective of finding \underline{r}_0 , $\dot{\underline{r}}_0$.

$$\underline{u} \equiv \begin{bmatrix} \underline{r}(t) - \iint_0^t \ddot{\underline{r}}_G dt^2 - \underline{r}_0 \\ \dot{\underline{r}}(t) - \int_0^t \ddot{\underline{r}}_G dt - \dot{\underline{r}}_0 \end{bmatrix} = \underline{0}. \quad (29)$$

³Unmodeled accelerations can be easily incorporated by adding $\sum a \sin bt + \sum c \cos dt$ to the previous expression. Solution for the constants a , b , etc. and the state can then be handled simultaneously.

As can be seen, by picking t and the corresponding \underline{r} and $\dot{\underline{r}}$ at a multilateration point and integrating from the a priori values $(\underline{r}_0, \dot{\underline{r}}_0)$ at $t = t_0$ to time $t = t_1, t_2, t_3 \dots t_K$ a performance functional J where, e.g.,

$$J \equiv \sum_{j=1}^K \sum_{i=1}^6 u_{ij}^2$$

can be defined. This implies that, J , which is the sum of squares of each individual residual, can be written as:

$$J = J(\underline{r}_0, \dot{\underline{r}}_0, k, \underline{r}_j(t), \dot{\underline{r}}_j(t))$$

where $\underline{r}_0, \dot{\underline{r}}_0$ are the sought for values which minimize this functional, k are modeling constants peculiar to the process, e.g., sidereal spin rate of the Earth, etc., and $\underline{r}(t), \dot{\underline{r}}(t)$ are the derived observables. The a priori values $\hat{\underline{r}}_{0a}, \hat{\dot{\underline{r}}}_{0a}, \hat{k}_a$ can be incorporated into this system as follows. Define

$$\hat{\underline{S}} \equiv \begin{bmatrix} \underline{r}_0 - \hat{\underline{r}}_{0a} \\ \dot{\underline{r}}_0 - \hat{\dot{\underline{r}}}_{0a} \\ k - \hat{k}_a \end{bmatrix} = \begin{bmatrix} \mu_1 \\ \mu_2 \\ \mu_3 \end{bmatrix} \quad (31)$$

with the understanding that μ is the uncertainty in the a priori values. The performance functional can now be linearized with respect to the error sources, i. e.,

$$J = J(\underline{r}_0, \dot{\underline{r}}_0, k, \underline{r}(t), \dot{\underline{r}}(t)) + \frac{\partial J}{\partial \underline{r}} \delta \underline{r} + \frac{\partial J}{\partial \dot{\underline{r}}} \delta \dot{\underline{r}} = 0$$

and the augmented estimation system written as:

$$J^* = \begin{bmatrix} \hat{\underline{S}} \\ \hat{\underline{J}} \end{bmatrix} = \begin{bmatrix} \mu \\ \nu \end{bmatrix}, \quad (32)$$

where

$$v \equiv - \frac{\partial J}{\partial \underline{r}} \delta \underline{\hat{r}} - \frac{\partial J}{\partial \underline{r}} \delta \underline{\hat{r}}.$$

The weighting matrix of system (32) can now be determined for as many short arcs of data as are to be analyzed, namely,

$$W_d = E \left(\begin{bmatrix} \underline{\mu} \\ v \end{bmatrix} \begin{bmatrix} \underline{\mu}^T & v^T \end{bmatrix} \right) \quad (33)$$

inclusive of all desired correlations. The square root of W_d , call it R_a , where $R_a R_a^T = W_d$ can also be extracted and J^* premultiplied by R_a to uncorrelate the equations. Hence:

$$R_a J^* \equiv F$$

defines the system of equations whose solution is to be obtained. Since F is a statistically uncorrelated system the standard method of least squares can now be applied. Proceeding formally:

$$F = F + \frac{\partial F}{\partial \underline{r}_0} \Delta \underline{r}_0 + \frac{\partial F}{\partial \underline{r}_0} \Delta \underline{\hat{r}}_0 + \frac{\partial F}{\partial k} \Delta k = 0 \quad (34)$$

Noting that $\partial F / \partial (\cdot) = R_a \partial (J^*) / \partial (\cdot)$ along with the definition of J^* via Eq. (32) with the q_a denoting the vector $\underline{\hat{r}}_{0a}, \underline{\hat{r}}_{0a}, \underline{\hat{k}}_a$, the final estimation equations can be written as

$$\begin{aligned} \underline{\hat{q}}_{n+1} = \underline{\hat{q}}_n - & \left[[W_a]^{-1} + \left[\frac{\partial J}{\partial q} \right]^T [W_d]^{-1} \left[\frac{\partial J}{\partial q} \right] \right]^{-1} \left[[W_a]^{-1} (q_n - q_a) \right. \\ & \left. + \left[\frac{\partial J}{\partial q} \right]^T [W_d]^{-1} J \right] \quad (35) \end{aligned}$$

where $[W_a]$ is the a priori weight matrix and $q \equiv [\underline{r}_0, \dot{\underline{r}}_0, k]$. For more details relating to the estimation equations the reader is directed to Appendix A2.

A8.9 USE OF VARIATIONAL EQUATIONS FOR PARTIAL DERIVATIVE GENERATION

In closing, it should be mentioned that the estimation equations of the previous section require partial derivatives of J with respect to the estimated and non-estimated parameters. As can be noticed from Eqs. (29). The partial derivatives of J , as defined by Eq. (30), with respect to the data, i. e., \underline{r} , $\dot{\underline{r}}$ are trivial and are given by:

$$\begin{aligned} \frac{\partial J}{\partial \underline{r}_{ij}} &= 2u_{ij} \quad , \quad i = 1, 2, 3; \quad j = 1, 2, \dots, K \\ \frac{\partial J}{\partial \dot{\underline{r}}_{ij}} &= 2u_{ij} \quad , \quad i = 4, 5, 6, \quad j = 1, 2, \dots, K \end{aligned} \quad (36)$$

The partial derivatives with respect to the estimated parameters are more complicated, and can only be obtained by integration of the variational equations, i. e., the differential equations adjoint to the differential equations of motion. This is true because $\partial J / \partial \underline{r}_0$, $\partial J / \partial \dot{\underline{r}}_0$ and $\partial J / \partial k$ involve differentiation under the integral sign. For example

$$\frac{\partial J}{\partial \underline{r}_0} = \sum_1^K u_{1j} \frac{\partial u_{1j}}{\partial \underline{r}_0} \quad , \quad (37)$$

where

$$\begin{aligned} \frac{\partial u_{1k}}{\partial \underline{r}_0} &= - \frac{\partial}{\partial \underline{r}_0} \int_0^t \ddot{\underline{r}}_G dt^2 - \begin{bmatrix} 1 \\ 1 \\ 1 \end{bmatrix} \\ &= - \int_0^t \frac{\partial \ddot{\underline{r}}_G}{\partial \underline{r}_G} \frac{\partial \underline{r}_G}{\partial \underline{r}_0} dt^2 - \begin{bmatrix} 1 \\ 1 \\ 1 \end{bmatrix} \end{aligned} \quad (38)$$

The introduction of

$$[\Gamma] \equiv \begin{bmatrix} \frac{\partial \underline{r}_G}{\partial \underline{r}_0} & \frac{\partial \underline{r}_G}{\partial \underline{\dot{r}}_0} \\ \frac{\partial \underline{\dot{r}}_G}{\partial \underline{r}_0} & \frac{\partial \underline{\dot{r}}_G}{\partial \underline{\dot{r}}_0} \end{bmatrix} \quad (39)$$

with initial condition $[\Gamma]_0 = [I]$, $[I]$ being the identity matrix and solution of

$$[\dot{\Gamma}] = [A(t)][\Gamma] \quad (40)$$

directly yields $[\Gamma]$ as a function of time. In the variational equations, e.g.,

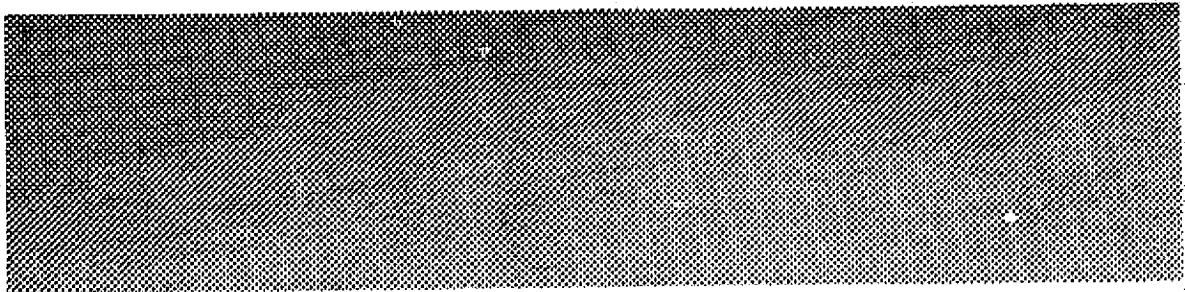
$$A(t) \equiv \begin{bmatrix} [0] & [I] \\ \frac{\partial \ddot{\underline{r}}_G}{\partial \underline{r}} & \frac{\partial \ddot{\underline{r}}_G}{\partial \underline{\dot{r}}} \end{bmatrix}. \quad (41)$$

Hence the matrix $\partial \underline{r}_G / \partial \underline{r}_0$ in Eq. (38) and all its counterparts, including the variation of the constants, k , can be obtained through solution of the adjoint system. The details are given in [8.2].

A8.10 REFERENCES

- [8.1] Escobal, P. R., Methods of Orbit Determination, John Wiley and Sons 1965 (First Edition); Krieger Publications 1976 (Revised Second Edition), New York
- [8.2] Escobal, P. R., Methods of Astrodynamics, John Wiley and Sons, New York, 1969.
- [8.3] Escobal, P. R., "Short and Long-Arc Orbit Determination Using Multilateration," JPL EM 391-736, 23 April 1976 (JPL internal document).

A9. Fast Algorithm for Complete Nutation and Nutation Rate Calculations



Abstract

The one hundred and nine sine and cosine terms of Woolards expressions for the nutation expansions are replaced by equivalent sums and products of the sines and cosines of the five fundamental mean longitudes. This transformation of the Woolard equations requires only ten trigonometric evaluations by a computer. Hence at every time point a manyfold increase in computational efficiency is obtained. The analytic nutation time derivatives are computed by a similar process. The constants listed in the *Connaissance des Temps* are adopted herein. The checked-out routine is exhumed from previous work performed by the first author (1965) during the now defunct but glorious Apollo project. The routine will be used in the GEOS-3 multilateration project but may be useful elsewhere.

PRECEDING PAGE BLANK NOT FILMED

A9.1 INTRODUCTION

The expressions by E. W. Woolard[9.1][9.3] for the nutation expansions contain a total of 109 sine and cosine terms. The lack of speed of computers in the evaluation of trigonometric functions would appear to dictate a transformation of Woolard's expressions wherein the multiple angle trigonometric expressions are expanded by brute force using the identities:

$$\cos (\alpha \pm \beta) = \cos \alpha \cos \beta \mp \sin \alpha \sin \beta$$

$$\sin (\alpha \pm \beta) = \sin \alpha \cos \beta \pm \cos \alpha \sin \beta.$$

The effect of this is the replacement of 109 trigonometric evaluations by the extraction of the sines and cosines of the five fundamental mean longitudes peculiar to the Woolard theory. Once these mean longitudes are extracted for a given time, and the trigonometric functions are evaluated, then the nutations and the derivatives are obtained by a chain of multiplications and additions. This approach was adopted on the Apollo project for both the nutations and the nutation time rates. A full documentation of this effort and the associated selenographic transformations can be found in [9.2], [9.4].

A9.2 NUTATION AND NUTATION RATE ALGORITHM

Define:

$\Gamma \equiv$ mean longitude of the Sun's perigee measured in the ecliptic plane from the mean equinox of date,

$\Gamma' \equiv$ mean longitude of the Moon's perigee measured in the ecliptic plane from the mean equinox of date to the mean ascending node of the lunar orbit and then along the orbit,

$L \equiv$ mean longitude of the Sun measured in the ecliptic plane from the mean equinox of date,

$\Omega \equiv$ longitude of the mean ascending node of the lunar orbit measured in the ecliptic plane from the mean equinox of date,

$\epsilon \equiv$ geocentric mean longitude of the Moon measured in the ecliptic plane from the mean equinox of date to the mean ascending node of the lunar orbit, and then along the orbit,

$\epsilon \equiv$ angle between the mean celestial equator and the ecliptic (mean obliquity),

$d\epsilon \equiv$ short period terms of the nutation in obliquity,

$\Delta\epsilon \equiv$ long period terms of the nutation in obliquity,

$d\psi \equiv$ short period terms of the nutation in longitude,

$\Delta\psi \equiv$ long period terms of the nutation in longitude,

$\delta\epsilon \equiv$ nutations in obliquity,

$\delta\psi \equiv$ nutations in longitude,

$\delta\dot{\epsilon} \equiv$ the time derivative of the nutation in obliquity (total) $= \frac{d}{d\tau} (\delta\epsilon)$,

$\delta\dot{\psi} \equiv$ the time derivative of the nutation in longitude (total) $= \frac{d}{d\tau} (\delta\psi)$,

$$\tau \equiv k_r (32525.0 \times 1440.0) T_u,$$

$$k_r \equiv 0.07436574 (\text{e.r.})^{1/2} / \text{min.}$$

ORIGINAL PAGE IS
OF POOR QUALITY

Compute:

$$\lambda = 0,$$

$$K = \frac{\pi}{180 \times 3600},$$

$$(J.D.)_{Jan 0.5, 1900} = 2415020.0,$$

$$T_u = \frac{J.D. - (J.D.)_{Jan 0.5, 1900}}{36525.0},$$

$$\begin{aligned} \dot{T}_u &\equiv \frac{dT_u}{d\tau} = (36,525.0 \times 24 \times 60 \times 0.07436574)^{-1} \\ &\simeq 0.255666824 \times 10^{-6}, \end{aligned}$$

$$\begin{aligned} \Gamma &= 281^{\circ}.2208333 + 1^{\circ}.7191750 T_u + 0^{\circ}.4527778 \\ &\quad \times 10^{-3} T_u^2 + 0^{\circ}.3333333 \times 10^{-5} T_u^3, \end{aligned}$$

$$\begin{aligned} \Gamma' &= 334^{\circ}.3295556 + 4069^{\circ}.0340333 T_u - 0^{\circ}.1032500 \\ &\quad \times 10^{-1} T_u^2 - 0^{\circ}.1250000 \times 10^{-4} T_u^3, \end{aligned}$$

$$L = 279^{\circ}.6966778 + 36,000^{\circ}.7689250 T_u + 0^{\circ}.3025000 \times 10^{-3} T_u^2,$$

$$\begin{aligned} \Omega &= 259^{\circ}.1832750 - 1,934^{\circ}.1420083 T_u + 0^{\circ}.2077778 \\ &\quad \times 10^{-2} T_u^2 + 0^{\circ}.2222222 \times 10^{-5} T_u^3, \end{aligned}$$

$$\begin{aligned} \zeta &= 270^{\circ}.4341639 + 481,267^{\circ}.8831417 T_u - 0^{\circ}.1133333 \\ &\quad \times 10^{-2} T_u^2 + 0^{\circ}.1888889 \times 10^{-5} T_u^3, \end{aligned}$$

$$\begin{aligned} \epsilon &= 23^{\circ}.4522944 - 0^{\circ}.1301250 \times 10^{-1} T_u - 0^{\circ}.1638889 \\ &\quad \times 10^{-3} T_u^2 + 0^{\circ}.5027778 \times 10^{-6} T_u^3, \end{aligned}$$

$$\begin{aligned} \dot{\Gamma} &\equiv \frac{d\Gamma}{d\tau} = \frac{d\Gamma}{dT_u} \dot{T}_u = [1^{\circ}.7191750 + 0^{\circ}.9055556 \times 10^{-3} T_u \\ &\quad + 1^{\circ}.0000000 \times 10^{-5} T_u^2] \frac{\pi}{180} \dot{T}_u, \end{aligned}$$

$$\begin{aligned} \dot{\Gamma}' &\equiv \frac{d\Gamma'}{d\tau} = \frac{d\Gamma'}{dT_u} \dot{T}_u = [4069^{\circ}.0340333 - 0^{\circ}.2065000 \times 10^{-1} T_u \\ &\quad - 0^{\circ}.3750000 \times 10^{-4} T_u^2] \frac{\pi}{180} \dot{T}_u, \end{aligned}$$

$$L \equiv \frac{dL}{d\tau} = \frac{dL}{dT_u} \dot{T}_u = [36,000^{\circ}.7689250 + 0^{\circ}.6050000 \times 10^{-3} T_u] \frac{\pi}{180} \dot{T}_u,$$

$$\begin{aligned} \dot{\Omega} &\equiv \frac{d\Omega}{d\tau} = \frac{d\Omega}{dT_u} \dot{T}_u = [-1,934^{\circ}.1420083 + 0^{\circ}.4155556 \times 10^{-2} T_u \\ &\quad + 0^{\circ}.6566667 \times 10^{-5} T_u^2] \frac{\pi}{180} \dot{T}_u, \end{aligned}$$

$$\dot{\epsilon} \equiv \frac{d\epsilon}{d\tau} = \frac{d\epsilon}{dT_u} \dot{T}_u = [481,267,883,1417 - 0.226,6667 \times 10^{-3} T_u,$$

$$+ 0.566,6667 \times 10^{-5} T_u^2] \frac{\pi}{180} \dot{T}_u,$$

$$\dot{\epsilon} \equiv \frac{d\epsilon}{d\tau} = \frac{d\epsilon}{dT_u} \dot{T}_u = [-0.130,1250 \times 10^{-1} - 0.327,7778 \times 10^{-5} T_u,$$

$$+ 1.508,3333 \times 10^{-8} T_u^2] \frac{\pi}{180} \dot{T}_u,$$

$$g' \equiv \zeta - l'', \quad g \equiv L - l', \quad \omega \equiv \Gamma - \Omega, \quad \text{and} \quad \omega' \equiv l'' - \Omega;$$

$$X_1 = \cos 2\zeta = 1 - 2 \sin^2 \zeta,$$

$$\sin 2\zeta = 2 \sin \zeta \cos \zeta,$$

$$X_2 = \cos (2\zeta - \Omega) = X_1 \cos \Omega + \sin 2\zeta \sin \Omega,$$

$$\sin (2\zeta - \Omega) = \sin 2\zeta \cos \Omega - X_1 \sin \Omega,$$

$$\cos g' = \cos \zeta \cos l'' + \sin \zeta \sin l'',$$

$$\sin g' = \sin \zeta \cos l'' - \cos \zeta \sin l'',$$

$$X_3 = \cos (2\zeta + g') = X_1 \cos g' - \sin 2\zeta \sin g',$$

$$\sin (2\zeta + g') = \sin 2\zeta \cos g' + X_1 \sin g',$$

$$X_4 = \cos (\zeta + l'') = \cos \zeta \cos l'' - \sin \zeta \sin l'',$$

$$X_5 = \cos (g' + \Omega) = \cos g' \cos \Omega - \sin g' \sin \Omega,$$

$$X_6 = \cos (g' - \Omega) = \cos g' \cos \Omega + \sin g' \sin \Omega,$$

$$\sin (g' - \Omega) = \sin g' \cos \Omega - \cos g' \sin \Omega,$$

$$X_7 = \cos [2\zeta + (g' - \Omega)]$$

$$= X_1 X_6 - \sin 2\zeta \sin (g' - \Omega),$$

$$\cos 4\zeta = 1 - 2 \sin^2 2\zeta,$$

$$\sin 4\zeta = 2 X_1 \sin 2\zeta,$$

$$\cos 2L = 1 - 2 \sin^2 L,$$

$$\sin 2L = 2 \sin L \cos L,$$

$$X_9 = \cos (4\zeta - 2L) = \cos 4\zeta \cos 2L + \sin 4\zeta \sin 2L,$$

$$\sin (4\zeta - 2L) = \sin 4\zeta \cos 2L - \cos 4\zeta \sin 2L,$$

$$X_{10} = \cos [(4\zeta - 2L) - g']$$

$$= X_9 \cos g' + \sin (4\zeta - 2L) \sin g',$$

$$\sin [(4\zeta - 2L) - g'] = \sin (4\zeta - 2L) \cos g' - X_9 \sin g',$$

$$X_{11} = \cos [(2\zeta + g') + g']$$

$$= X_3 \cos g' - \sin (2\zeta + g') \sin g',$$

$$X_{12} = \cos (2L + g') = \cos 2L \cos g' - \sin 2L \sin g',$$

$$\sin (2L + g') = \sin 2L \cos g' + \cos 2L \sin g'.$$

ORIGINAL PAGE IS
OF POOR QUALITY

$$\begin{aligned}
\cos \omega' &= \cos \Gamma' \cos \Omega + \sin \Gamma' \sin \Omega, \\
\sin \omega' &= \sin \Gamma' \cos \Omega - \cos \Gamma' \sin \Omega, \\
X_{12} &= \cos (\varphi + \omega') = \cos \varphi \cos \omega' - \sin \varphi \sin \omega', \\
\cos (2L - \varphi) &= \cos 2L \cos \varphi + \sin 2L \sin \varphi, \\
\sin (2L - \varphi) &= \sin 2L \cos \varphi - \cos 2L \sin \varphi, \\
X_{13} &= \cos [(2L - \varphi) - \omega'] = \cos (2L - \varphi) \cos \omega' + \sin (2L - \varphi) \sin \omega', \\
\sin [(2L - \varphi) - \omega'] &= \sin (2L - \varphi) \cos \omega' - \cos (2L - \varphi) \sin \omega', \\
\cos 2\Omega &= 1 - 2 \sin^2 \Omega, \\
\sin 2\Omega &= 2 \sin \Omega \cos \Omega, \\
X_{14} &= \cos (2L - \varphi - \omega' - 2\Omega) \\
&= X_{13} \cos 2\Omega + \sin (2L - \varphi - \omega') \sin 2\Omega, \\
X_{15} &= \cos [(4\varphi - 2L - g') - \Omega] \\
&= X_8 \cos \Omega + \sin (4\varphi - 2L - g') \sin \Omega, \\
\cos g &= \cos L \cos \Gamma' + \sin L \sin \Gamma', \\
\sin g &= \sin L \cos \Gamma' - \cos L \sin \Gamma', \\
X_{16} &= \cos (2\varphi - g) = X_1 \cos g + \sin 2\varphi \sin g, \\
X_{17} &= \cos [(4\varphi - 2L) + g'] \\
&= X_9 \cos g' - \sin (4\varphi - 2L) \sin g', \\
X_{18} &= \cos [(2\varphi - \Omega) - 2L] \\
&= X_2 \cos 2L + \sin (2\varphi - \Omega) \sin 2L, \\
\sin [(2\varphi - \Omega) - 2L] &= \sin (2\varphi - \Omega) \cos 2L - X_2 \sin 2L, \\
X_{19} &= \cos (2\varphi - 2L + \Omega) \\
&= \cos [(2\varphi - \Omega - 2L) + 2\Omega] \\
&= X_{18} \cos 2\Omega - \sin (2\varphi - \Omega - 2L) \sin 2\Omega, \\
X_{20} &= \cos [(4\varphi - 2L) - \Omega] \\
&= X_9 \cos \Omega + \sin (4\varphi - 2L) \sin \Omega, \\
X_{21} &= \cos (2\varphi + g) = X_1 \cos g - \sin 2\varphi \sin g, \\
X_{22} &= \cos [2L + (g' - \Omega)] \\
&= X_8 \cos 2L - \sin (g' - \Omega) \sin 2L, \\
X_{23} &= \cos (2\varphi - \Omega + 2g') \\
&= \cos [(2\varphi + g') + (g' - \Omega)] \\
&= X_9 X_8 - \sin (2\varphi + g') \sin (g' - \Omega), \\
X_{24} &= \cos (2L + 2g') = \cos [(2L + g') + g'] \\
&= X_{11} \cos g' - \sin (2L + g') \sin g', \\
Y_1 &= \cos \Omega, \\
Y_2 &= \cos 2L, \\
Y_3 &= \cos 2\Omega, \\
Y_4 &= \cos (2L + g) = \cos 2L \cos g - \sin 2L \sin g, \\
\sin (2L + g) &= \sin 2L \cos g + \cos 2L \sin g, \\
Y_5 &= \cos (L + \Gamma') = \cos L \cos \Gamma' - \sin L \sin \Gamma',
\end{aligned}$$

$$Y_4 = \cos (2L - \Omega) = \cos 2L \cos \Omega + \sin 2L \sin \Omega,$$

$$\sin (2L - \Omega) = \sin 2L \cos \Omega - \cos 2L \sin \Omega,$$

$$Y_7 = \cos (\Gamma' + \omega') = \cos \Gamma' \cos \omega' - \sin \Gamma' \sin \omega',$$

$$\sin (\omega' + \Gamma') = \sin \omega' \cos \Gamma' + \cos \omega' \sin \Gamma',$$

$$Y_8 = \cos (\Omega + g) = \cos \Omega \cos g - \sin \Omega \sin g,$$

$$Y_9 = \cos (2L + 2g) = \cos [(2L + g) + g]$$

$$= Y_4 \cos g - \sin (2L + g) \sin g,$$

$$Y_{10} = \cos (\Omega - g) = \cos \Omega \cos g + \sin \Omega \sin g,$$

$$\cos 2\Gamma' = 1 - 2 \sin^2 \Gamma',$$

$$\sin 2\Gamma' = 2 \sin \Gamma' \cos \Gamma',$$

$$Y_{11} = \cos (2\Gamma' - 2L + \Omega)$$

$$= Y_8 \cos 2\Gamma' + \sin (2L - \Omega) \sin 2\Gamma',$$

$$\cos 2\Gamma = 1 - 2 \sin^2 \Gamma,$$

$$\sin 2\Gamma = 2 \sin \Gamma \cos \Gamma,$$

$$Y_{12} = \cos (2\Gamma - \Omega) = \cos 2\Gamma \cos \Omega + \sin 2\Gamma \sin \Omega,$$

$$\sin (2\Gamma - \Omega) = \sin 2\Gamma \cos \Omega - \cos 2\Gamma \sin \Omega,$$

$$Y_{13} = \cos (2\Gamma - \Omega + g) = \cos [(2\Gamma - \Omega) + g],$$

$$= Y_{12} \cos g - \sin (2\Gamma - \Omega) \sin g,$$

$$Y_{14} = \cos 2\Gamma',$$

$$Y_{15} = \cos (2L - \omega' - \Gamma') = \cos [2L - (\omega' + \Gamma')]$$

$$= Y_7 \cos 2L + \sin 2L \sin (\omega' + \Gamma'),$$

$$Y_{16} = \cos [(2L - \Omega) + g]$$

$$= Y_4 \cos g - \sin (2L - \Omega) \sin g,$$

$$Z_1 = \sin 2\epsilon,$$

$$Z_2 = \sin g',$$

$$Z_3 = \sin (2\epsilon - \Omega),$$

$$Z_4 = \sin (2\epsilon + g'),$$

$$Z_5 = \sin [(2L - \epsilon) - \Gamma']$$

$$= \sin (2L - \epsilon) \cos \Gamma' - \cos (2L - \epsilon) \sin \Gamma',$$

$$Z_6 = \sin (\epsilon + \Gamma') = \sin \epsilon \cos \Gamma' + \cos \epsilon \sin \Gamma',$$

$$\cos (\epsilon + \Gamma') = \cos \epsilon \cos \Gamma' - \sin \epsilon \sin \Gamma',$$

$$Z_7 = \sin (2\epsilon - 2L) = \sin 2\epsilon \cos 2L - X_1 \sin 2L,$$

$$Z_8 = \sin (\Omega + g') = \sin \Omega \cos g' + \cos \Omega \sin g',$$

$$Z_9 = -\sin (g' - \Omega),$$

$$Z_{10} = \sin (4\epsilon - 2L - g'),$$

$$Z_{11} = \sin [(2\epsilon - \Omega) + g'] = Z_3 \cos g' + X_2 \sin g',$$

$$Z_{12} = \sin 2g' = 2 \sin g' \cos g',$$

$$Z_{13} = \sin (4\epsilon - 2L),$$

$$Z_{14} = \sin (2L + g'),$$

$$Z_{15} = \sin (2\epsilon + 2g') = \sin [(2\epsilon + g') + g']$$

$$= Z_4 \cos g' + X_3 \sin g',$$

$$Z_{16} = \sin (2\epsilon - 2\Omega) = \sin [(2\epsilon - \Omega) - \Omega]$$

$$= Z_3 \cos \Omega - X_2 \sin \Omega,$$

ORIGINAL PAGE IS
OF POOR QUALITY

$$\begin{aligned}
Z_{17} &= \sin (\varphi + \omega') = \sin \varphi \cos \omega' + \cos \varphi \sin \omega', \\
Z_{18} &= \sin (2L - \varphi - \omega'), \\
Z_{19} &= \sin (\varphi - 2L + \Omega + \Gamma') \\
&= \sin [(\varphi + \Gamma') - (2L - \Omega)] \\
&= Z_8 Y_8 - \cos (\varphi + \Gamma') \sin (2L - \Omega), \\
Z_{20} &= \sin (4\varphi - 2L - \Omega - g') \\
&= \sin [(4\varphi - 2L - g') - \Omega] \\
&= \sin (4\varphi - 2L - g') \cos \Omega - X_8 \sin \Omega, \\
Z_{21} &= \sin (2\varphi + g) = Z_1 \cos g + X_1 \sin g, \\
Z_{22} &= \sin (2L + g - \varphi - \Gamma') \\
&= \sin [(2L + g) - (\varphi + \Gamma')] \\
&= \sin (2L + g) \cos (\varphi + \Gamma') - Y_4 Z_8, \\
Z_{23} &= \sin (2L + 2g') = \sin [(2L + g') + g'] \\
&= \sin (2L + g') \cos g' + X_{11} \sin g', \\
Z_{24} &= \sin (2\varphi - 2L + g') = \sin [(2\varphi + g') - 2L] \\
&= \sin (2\varphi + g') \cos 2L - X_3 \sin 2L, \\
Z_{25} &= \sin (2\varphi - g) = Z_1 \cos g - X_1 \sin g, \\
Z_{26} &= \sin (4\varphi - 2L + g') = \sin [(4\varphi - 2L) + g'] \\
&= Z_{13} \cos g' + X_9 \sin g', \\
Z_{27} &= \sin (2\varphi - 2L + \Omega) = \sin [2\varphi - (2L - \Omega)] \\
&= Y_8 \sin 2\varphi - X_1 \sin (2L - \Omega), \\
Z_{28} &= \sin (2L + g' - \Omega) = \sin [(2L + g') - \Omega] \\
&= \sin (2L + g') \cos \Omega - X_{11} \sin \Omega, \\
Z_{29} &= \sin (2L - 2\varphi + \Omega) = \sin [2L - (2\varphi - \Omega)] \\
&= X_2 \sin 2L - \sin (2\varphi - \Omega) \cos 2L, \\
Z_{30} &= \sin (4\varphi - 2L - \Omega) = \sin [(4\varphi - 2L) - \Omega] \\
&= \sin (4\varphi - 2L) \cos \Omega - X_9 \sin \Omega, \\
Z_{31} &= \sin (g' - g) = \sin g' \cos g - \cos g' \sin g, \\
\cos (\varphi + \omega') &= \cos \varphi \cos \omega' - \sin \varphi \sin \omega', \\
Z_{32} &= \sin (\Omega - \varphi - \omega') = \sin [\Omega - (\varphi + \omega')] \\
&= \sin \Omega \cos (\varphi + \omega') - Z_{17} \cos \Omega, \\
Z_{33} &= \sin (2\varphi - \Omega + 2g') \\
&= \sin [(2\varphi + g') + (g' - \Omega)] \\
&= X_8 \sin (2\varphi + g') + X_3 \sin (g' - \Omega), \\
Z_{34} &= \sin (2L + g - 2\varphi) = \sin [(2L + g) - 2\varphi] \\
&= X_1 \sin (2L + g) - Y_4 \sin 2\varphi, \\
Z_{35} &= \sin (\varphi - L) = \sin \varphi \cos L - \cos \varphi \sin L, \\
Z_{36} &= \sin (2\varphi + g' - 2\Omega) = \sin [(2\varphi + g') - 2\Omega] \\
&= \sin (2\varphi + g') \cos 2\Omega - X_3 \sin 2\Omega, \\
Z_{37} &= \sin (g + g') = \sin g \cos g' + \cos g \sin g', \\
Z_{38} &= \sin (2\varphi + g' - g) = \sin [(2\varphi + g') - g] \\
&= \sin (2\varphi + g') \cos g - X_3 \sin g, \\
Z_{39} &= \sin (\Omega + 2g') = \sin [(\Omega + g') + g'] \\
&= Z_8 \cos g' + X_5 \sin g',
\end{aligned}$$

$$Z_{40} = \sin (2\epsilon + g' + g) = \sin [(2\epsilon + g') + g]$$

$$= \sin (2\epsilon + g') \cos g + X_3 \sin g,$$

$$Z_{41} = \sin (2g' - \Omega) = \sin [g' + (g' - \Omega)]$$

$$= X_6 \sin g' - Z_9 \cos g',$$

$$Z_{42} = \sin (2L - \Omega - g') = \sin [(2L - \Omega) - g']$$

$$= \sin (2L - \Omega) \cos g' - Y_6 \sin g',$$

$$Z_{43} = \sin (4\epsilon - 2L - g' - g)$$

$$= \sin [(4\epsilon - 2L - g') - g]$$

$$= \sin (4\epsilon - 2L - g') \cos g - X_8 \sin g,$$

$$Z_{44} = \sin (4\epsilon - 2L - g) = \sin [(4\epsilon - 2L) - g]$$

$$= \sin (4\epsilon - 2L) \cos g - X_6 \sin g,$$

$$Z_{45} = \sin (2\Omega + g') = \sin 2\Omega \cos g' + \cos 2\Omega \sin g',$$

$$Z_{46} = \sin (2\epsilon + 3g') = \sin [(2\epsilon + 2g') + g']$$

$$= Z_{16} \cos g' + X_{10} \sin g',$$

$$W_1 = \sin \Omega,$$

$$W_2 = \sin 2L,$$

$$W_3 = \sin 2\Omega,$$

$$W_4 = \sin g,$$

$$W_5 = \sin (2L + g),$$

$$W_6 = \sin (L + \Gamma) = \sin L \cos \Gamma + \cos L \sin \Gamma,$$

$$W_7 = \sin (2L - \Omega),$$

$$W_8 = \sin (\omega' + \Gamma'),$$

$$W_9 = \sin (2L - 2\Gamma')$$

$$= \sin 2L \cos 2\Gamma' - \cos 2L \sin 2\Gamma',$$

$$W_{10} = \sin (2L - 2\Omega)$$

$$= \sin 2L \cos 2\Omega - \cos 2L \sin 2\Omega,$$

$$W_{11} = \sin 2g = 2 \sin g \cos g,$$

$$W_{12} = \sin (2L + 2g) = \sin \{(2L + g) + g\}$$

$$= \sin (2L + g) \cos g + Y_4 \sin g,$$

$$W_{13} = \sin (g + \Omega) = \sin g \cos \Omega + \sin \Omega \cos g,$$

$$W_{14} = \sin 2\omega' = 2 \sin \omega' \cos \omega',$$

$$W_{15} = \sin (\Omega - g) = \sin \Omega \cos g - \cos \Omega \sin g,$$

$$W_{16} = \sin (2\Gamma' - 2L + \Omega)$$

$$= Y_8 \sin 2\Gamma' - \cos 2\Gamma' \sin (2L - \Omega),$$

$$W_{17} = \sin (L + \Gamma - \Omega) = \sin \{(L + \Gamma) - \Omega\}$$

$$= W_8 \cos \Omega - Y_8 \sin \Omega,$$

$$\cos (2L + \Omega) = \cos 2L \cos \Omega - \sin 2L \sin \Omega,$$

$$\sin (2L + \Omega) = \sin 2L \cos \Omega + \cos 2L \sin \Omega,$$

$$W_{18} = \sin (2L + \Omega - 2\Gamma')$$

$$= \sin (2L + \Omega) \cos 2\Gamma' - \cos (2L + \Omega) \sin 2\Gamma',$$

$$\begin{aligned}
W_{19} &= \sin (2\Gamma - \Omega), \\
W_{20} &= \sin (2L - \Omega + g) \\
&= \sin (2L - \Omega) \cos g + Y_6 \sin g, \\
W_{21} &= \sin 2\Gamma', \\
W_{22} &= \sin (L - \Gamma') = \sin L \cos \Gamma' - \cos L \sin \Gamma', \\
W_{23} &= \sin (\Gamma - \Gamma') = \sin \Gamma \cos \Gamma' - \cos \Gamma \sin \Gamma',
\end{aligned}$$

$A_1 = 0''.0884 - 0''.00005T_u$	$A_9 = 0''.0014$	$A_{17} = A_{18}$
$A_2 = 0''.0183$	$A_{10} = 0''.0011$	$A_{18} = A_{19}$
$A_3 = 0''.0113 - 0''.00001T_u$	$A_{11} = -0''.0011$	$A_{19} = A_{20}$
$A_4 = -0''.0050$	$A_{12} = -0''.0010$	$A_{20} = A_{21}$
$A_5 = -0''.0031$	$A_{13} = 0''.0007$	$A_{21} = -A_{18}$
$A_6 = 0''.0030$	$A_{14} = -0''.0007$	$A_{22} = -A_{18}$
$A_7 = 0''.0023$	$A_{26} = 0''.0005$	$A_{23} = 0''.0002$
$A_8 = 0''.0022$	$A_{16} = 0''.0003$	$A_{24} = -A_{23}$
$B_1 = 9''.2100 + 0''.00091T_u$	$B_9 = 0''.0007$	
$B_2 = 0''.5522 - 0''.00029T_u$	$B_{10} = 0''.0005$	
$B_3 = -0''.0904 + 0''.00004T_u$	$B_{11} = 0''.0003$	
$B_4 = 0''.0216 - 0''.00006T_u$	$B_{12} = B_{11}$	
$B_5 = -0''.0093 + 0''.00003T_u$	$B_{13} = 0''.0002$	
$B_6 = -0''.0066$	$B_{14} = B_{13}$	
$B_7 = -0''.0024$	$B_{15} = -B_{14}$	
$B_8 = 0''.0008$	$B_{16} = -B_{14}$	
$C_1 = -0''.2037 - 0''.00002T_u$	$C_{24} = C_{23}$	
$C_2 = 0''.0675 + 0''.00001T_u$	$C_{25} = -C_{23}$	
$C_3 = -0''.0342 - 0''.00004T_u$	$C_{26} = -C_{23}$	
$C_4 = -0''.0261$	$C_{27} = -C_{23}$	
$C_5 = -0''.0149$	$C_{28} = 0''.0005$	
$C_6 = 0''.0114$	$C_{29} = -C_{28}$	
$C_7 = 0''.0060$	$C_{30} = -C_{28}$	
$C_8 = 0''.0058$	$C_{31} = 0''.0004$	
$C_9 = -0''.0057$	$C_{32} = C_{31}$	
$C_{10} = -0''.0052$	$C_{33} = -C_{31}$	
$C_{11} = -0''.0044$	$C_{34} = -C_{31}$	
$C_{12} = 0''.0028$	$C_{35} = -C_{31}$	
$C_{13} = -0''.0032$	$C_{36} = 0''.0003$	
$C_{14} = 0''.0026$	$C_{37} = -C_{34}$	
$C_{15} = -C_{14}$	$C_{38} = -C_{36}$	
$C_{16} = 0''.0025$	$C_{39} = 0''.0002$	
$C_{17} = 0''.0019$	$C_{40} = C_{39}$	
$C_{18} = -0''.0013$	$C_{41} = C_{39}$	
$C_{19} = 0''.0014$	$C_{42} = -C_{39}$	
$C_{20} = -0''.0009$	$C_{43} = -C_{39}$	
$C_{21} = 0''.0007$	$C_{44} = -C_{39}$	
$C_{22} = -C_{21}$	$C_{45} = -C_{39}$	
$C_{23} = 0''.0006$	$C_{46} = -C_{39}$	
$D_1 = -17''.2327 - 0''.01737T_u$	$D_{13} = -0''.0015$	
$D_2 = -1''.2729 - 0''.00013T_u$	$D_{14} = -0''.0010$	
$D_3 = 0''.2088 + 0''.00002T_u$	$D_{15} = D_{14}$	
$D_4 = 0''.1261 - 0''.000317T_u$	$D_{16} = -0''.0005$	
$D_5 = -0''.0497 + 0''.000127T_u$	$D_{17} = D_{16}$	
$D_6 = 0''.0214 - 0''.000057T_u$	$D_{18} = 0''.0004$	
$D_7 = 0''.0124 + 0''.000017T_u$	$D_{19} = -D_{18}$	
$D_8 = 0''.0045$	$D_{20} = 0''.0003$	
$D_9 = D_8$	$D_{21} = -D_{20}$	
$D_{10} = -0''.0021$	$D_{22} = -D_{20}$	
$D_{11} = 0''.0016 - 0''.000017T_u$	$D_{23} = -0''.0002$	
$D_{12} = -0''.0015 + 0''.000017T_u$		

ORIGINAL PAGE IS
OF POOR QUALITY

$$d\epsilon = \sum_{i=1}^8 A_i X_i + (1 - \lambda) \sum_{i=9}^{24} A_i X_i,$$

$$\Delta\epsilon = \sum_{i=1}^7 B_i Y_i + (1 - \lambda) \sum_{i=8}^{16} B_i Y_i,$$

$$d\psi = \sum_{i=1}^{12} C_i Z_i + (1 - \lambda) \sum_{i=13}^{28} C_i Z_i,$$

$$\Delta\psi = \sum_{i=1}^9 D_i W_i + (1 - \lambda) \sum_{i=10}^{23} D_i W_i,$$

$$\delta\epsilon = d\epsilon + \Delta\epsilon,$$

$$\delta\psi = d\psi + \Delta\psi.$$

If rates are desired compute:

$$\dot{g} = L - \dot{\Gamma},$$

$$\dot{g}' = \dot{\Gamma} - \dot{\Gamma}',$$

$$\dot{\omega}' = \dot{\Gamma} - \dot{\Omega},$$

$$A_1 = -0''.00005 \dot{T}_u,$$

$$A_2 = -0''.00001 \dot{T}_u;$$

$$\dot{X}_1 = -Z_1(2\dot{\Gamma}),$$

$$\dot{X}_2 = -Z_3(2\dot{\Gamma} - \dot{\Omega}),$$

$$\dot{X}_3 = -Z_4(2\dot{\Gamma} + \dot{g}'),$$

$$\dot{X}_4 = -Z_6(\dot{\Gamma} + \dot{\Gamma}'),$$

$$\dot{X}_5 = -Z_8(\dot{\Omega} + \dot{g}'),$$

$$\dot{X}_6 = Z_9(\dot{g}' - \dot{\Omega}),$$

$$\dot{X}_7 = -Z_{11}(2\dot{\Gamma} + \dot{g}' - \dot{\Omega}),$$

$$\dot{X}_8 = -Z_{10}(4\dot{\Gamma} - 2\dot{L} - \dot{g}'),$$

$$\dot{X}_9 = -Z_{13}(4\dot{\Gamma} - 2\dot{L}),$$

$$\dot{X}_{10} = -Z_{15}(2\dot{\Gamma} + 2\dot{g}'),$$

$$\dot{X}_{11} = -Z_{14}(2\dot{L} + \dot{g}'),$$

$$\dot{X}_{12} = -Z_{17}(\dot{\Gamma} + \dot{\omega}'),$$

$$\dot{X}_{13} = -Z_{18}(2\dot{L} - \dot{\Gamma} - \dot{\omega}'),$$

$$\dot{X}_{14} = [X_{13} \sin 2\Omega - Z_{18} \cos 2\Omega](2\dot{L} - \dot{\Gamma} - \dot{\omega}' - 2\dot{\Omega}),$$

$$\dot{X}_{15} = -Z_{20}(4\dot{\Gamma} - 2\dot{L} - \dot{g}' - \dot{\Omega}),$$

$$\dot{X}_{16} = -Z_{25}(2\dot{\Gamma} - \dot{g}'),$$

$$\dot{X}_{17} = -Z_{26}(4\dot{\Gamma} - 2\dot{L} + \dot{g}'),$$

$$\dot{X}_{18} = -\sin(2\dot{\Gamma} - \dot{\Omega} - 2\dot{L})[2\dot{\Gamma} - \dot{\Omega} - 2\dot{L}],$$

$$\dot{X}_{19} = -Z_{27}(2\dot{\Gamma} - 2\dot{L} + \dot{\Omega}),$$

$$\dot{X}_{20} = -Z_{30}(4\dot{\Gamma} - 2\dot{L} - \dot{\Omega}),$$

$$\dot{X}_{21} = -Z_{21}(2\dot{\Gamma} + \dot{g}'),$$

$$\dot{X}_{22} = -Z_{28}(2\dot{L} + \dot{g}' - \dot{\Omega}),$$

$$\dot{X}_{23} = -Z_{33}(2\dot{\Gamma} - \dot{\Omega} + 2\dot{g}'),$$

$$\dot{X}_{24} = -Z_{43}(2\dot{L} + 2\dot{g}');$$

$$\dot{B}_1 = 0''.00091 \dot{T}_u,$$

$$\dot{B}_2 = -0''.00029 \dot{T}_u,$$

$$\dot{B}_3 = 0''.00004 \dot{T}_u,$$

$$\dot{B}_4 = -0''.00006 \dot{T}_u,$$

$$\dot{B}_5 = 0''.00003 \dot{T}_u;$$

$$\dot{Y}_1 = -W_1(\dot{\Omega}),$$

$$\dot{Y}_2 = -W_2(2\dot{L}),$$

$$\dot{Y}_3 = -W_3(2\dot{\Omega}),$$

$$\dot{Y}_4 = -W_4(2\dot{L} + \dot{g}),$$

$$\dot{Y}_5 = -W_5(\dot{L} + \dot{\Gamma}),$$

$$\dot{Y}_6 = -W_7(2\dot{L} - \dot{\Omega}),$$

$$\dot{Y}_7 = -W_8(\dot{\Gamma}'' + \dot{\omega}'),$$

$$\dot{Y}_8 = -W_{13}(\dot{\Omega} + \dot{g}),$$

$$\dot{Y}_9 = -W_{12}(2\dot{L} + 2\dot{g}),$$

$$\dot{Y}_{10} = -W_{15}(\dot{\Omega} - \dot{g}),$$

$$\dot{Y}_{11} = W_{16}(2\dot{L} - \dot{\Omega} - 2\dot{\Gamma}''),$$

$$\dot{Y}_{12} = -[W_{18} \cos g + Y_{13} W_4](2\dot{\Gamma}' - \dot{\Omega} + \dot{g}),$$

$$\dot{Y}_{13} = -W_{19}(2\dot{\Gamma}' - \dot{\Omega}),$$

$$\dot{Y}_{14} = -W_{21}(2\dot{\Gamma}''),$$

$$\dot{Y}_{15} = -W_{18}(2\dot{L} - \dot{\omega}' - \dot{\Gamma}'),$$

$$\dot{Y}_{16} = -W_{20}(2\dot{L} - \dot{\Omega} + \dot{g});$$

$$\dot{C}_1 = -0''.00002 \dot{T}_u,$$

$$\dot{C}_2 = 0''.00001 \dot{T}_u,$$

$$\dot{C}_3 = -0''.00004 \dot{T}_u;$$

$$\dot{Z}_1 = X_1(2\dot{\Gamma}),$$

$$\dot{Z}_2 = \cos g'(\dot{g}'),$$

$$\dot{Z}_3 = X_2(2\dot{\Gamma} - \dot{\Omega}),$$

$$\dot{Z}_4 = X_3(2\dot{\Gamma} + \dot{g}'),$$

$$\dot{Z}_5 = [\cos(2L - \Gamma) \cos \Gamma'' + \sin(2L - \Gamma) \sin \Gamma''](2\dot{L} - \dot{\Gamma} - \dot{\Gamma}'),$$

$$\dot{Z}_6 = X_4(\dot{\Gamma} + \dot{\Gamma}''),$$

$$\dot{Z}_7 = [X_1 Y_2 + Z_1 W_2](2\dot{\Gamma} - 2\dot{L}),$$

$$\dot{Z}_8 = X_5(\dot{\Omega} + \dot{g}'),$$

$$\dot{Z}_9 = X_6(\dot{\Omega} - \dot{g}'),$$

$$\dot{Z}_{10} = X_8(4\dot{\Gamma} - 2\dot{L} - \dot{g}'),$$

$$\dot{Z}_{11} = X_7(2\dot{\Gamma} - \dot{\Omega} + \dot{g}'),$$

$$\dot{Z}_{12} = [1 - 2 \sin^2 g'](2\dot{g}'),$$

$$\dot{Z}_{13} = X_9(4\dot{\Gamma} - 2\dot{L}),$$

$$\dot{Z}_{14} = X_{11}(2\dot{L} + \dot{g}'),$$

$$\dot{Z}_{15} = X_{10}(2\dot{\Gamma} + 2\dot{g}'),$$

$$\dot{Z}_{16} = [X_2 \cos \Omega + Z_3 \sin \Omega](2\dot{\Gamma} - 2\dot{\Omega}),$$

$$\dot{Z}_{17} = X_{12}(\dot{\Gamma} + \dot{\omega}'),$$

$$\begin{aligned}
\dot{Z}_{10} &= X_{13}(2L - \dot{\ell} - \dot{\omega}'), \\
\dot{Z}_{11} &= X_{14}(\dot{\ell} - 2L + \dot{\Omega} + \dot{\Gamma}'), \\
\dot{Z}_{20} &= X_{15}(4\dot{\ell} - 2L - \dot{\Omega} - \dot{g}'), \\
\dot{Z}_{21} &= X_{21}(2\dot{\ell} + \dot{g}), \\
\dot{Z}_{22} &= [X_4 Y_4 + Z_4 W_3](2L + \dot{g} - \dot{\ell} - \dot{\Gamma}'), \\
\dot{Z}_{23} &= X_{24}(2L + 2\dot{g}'), \\
\dot{Z}_{24} &= [X_3 Y_2 + Z_4 W_2](2\dot{\ell} - 2L + \dot{g}'), \\
\dot{Z}_{25} &= X_{16}(2\dot{\ell} - \dot{g}), \\
\dot{Z}_{26} &= X_{17}(4\dot{\ell} - 2L + \dot{g}'), \\
\dot{Z}_{27} &= X_{18}(2\dot{\ell} - 2L + \dot{\Omega}), \\
\dot{Z}_{28} &= X_{22}(2L + \dot{g}' - \dot{\Omega}), \\
\dot{Z}_{29} &= X_{19}(2L - 2\dot{\ell} + \dot{\Omega}), \\
\dot{Z}_{30} &= X_{20}(4\dot{\ell} - 2L - \dot{\Omega}), \\
\dot{Z}_{31} &= [\cos g' \cos g + Z_4 W_4](\dot{g}' - \dot{g}), \\
\dot{Z}_{32} &= [Y_1 \cos(\dot{\ell} + \dot{\omega}') + Z_{17} W_1](\dot{\Omega} - \dot{\ell} - \dot{\omega}'), \\
\dot{Z}_{33} &= X_{23}(2\dot{\ell} - \dot{\Omega} + 2\dot{g}'), \\
\dot{Z}_{34} &= [X_1 Y_4 + Z_1 W_3](2L + \dot{g} - 2\dot{\ell}), \\
\dot{Z}_{35} &= [\cos \dot{\ell} \cos L + \sin \dot{\ell} \sin L](\dot{\ell} - L), \\
\dot{Z}_{36} &= [X_3 Y_3 + Z_4 W_3](2\dot{\ell} + \dot{g}' - 2\dot{\Omega}), \\
\dot{Z}_{37} &= [\cos g \cos g' - Z_2 W_4](\dot{g} + \dot{g}'), \\
\dot{Z}_{38} &= [X_3 \cos g + Z_4 W_4](2\dot{\ell} + \dot{g}' - \dot{g}), \\
\dot{Z}_{39} &= [X_3 \cos g' - Z_2 Z_8](\dot{\Omega} + 2\dot{g}'), \\
\dot{Z}_{40} &= [X_3 \cos g - Z_4 W_4](2\dot{\ell} + \dot{g}' + \dot{g}), \\
\dot{Z}_{41} &= [X_8 \cos g' + Z_2 Z_9](2\dot{g}' - \dot{\Omega}), \\
\dot{Z}_{42} &= [Y_8 \cos g' + Z_2 W_7](2L - \dot{\Omega} - \dot{g}'), \\
\dot{Z}_{43} &= [X_8 \cos g + Z_{10} \sin g](4\dot{\ell} - 2L - \dot{g}' - \dot{g}), \\
\dot{Z}_{44} &= [X_9 \cos g + Z_{13} W_4](4\dot{\ell} - 2L - \dot{g}), \\
\dot{Z}_{45} &= [Y_3 \cos g' - Z_2 W_3](2\dot{\Omega} + \dot{g}'), \\
\dot{Z}_{46} &= [X_{10} \cos g' - Z_2 Z_{15}](2\dot{\ell} + 3\dot{g}');
\end{aligned}$$

$$\dot{D}_1 = -0''.01737 \dot{T}_u,$$

$$\dot{D}_2 = -0''.00013 \dot{T}_u,$$

$$\dot{D}_3 = 0''.00002 \dot{T}_u,$$

$$\dot{D}_4 = -0''.00031 \dot{T}_u,$$

$$\dot{D}_5 = 0''.00012 \dot{T}_u,$$

$$\dot{D}_6 = -0''.00005 \dot{T}_u,$$

$$\dot{D}_7 = 0''.00001 \dot{T}_u, \quad \dot{D}_8 = \dot{D}_9 = \dot{D}_{10} = 0,$$

$$\dot{D}_{11} = -0''.00001 \dot{T}_u,$$

$$\dot{D}_{12} = 0''.00001 \dot{T}_u;$$

$$W_1 = Y_1(\dot{\Omega}),$$

$$W_2 = Y_2(2L),$$

$$W_3 = Y_3(2\dot{\Omega}),$$

$$W_4 = \cos g(\dot{g}).$$

$$\begin{aligned}
W_5 &= Y_4(2L + g), \\
W_6 &= Y_5(L + \Gamma'), \\
W_7 &= Y_6(2L - \Omega), \\
W_8 &= Y_7(\dot{\omega}' + \Gamma''), \\
W_9 &= [Y_2 \cos 2\Gamma' + W_2 \sin 2\Gamma'](2L - 2\Gamma''), \\
W_{10} &= [Y_2 Y_3 + W_2 W_3](2L - 2\Omega), \\
W_{11} &= [1 - 2 \sin^2 g](2g), \\
W_{12} &= Y_9(2L + 2g), \\
W_{13} &= Y_8(\dot{g} + \Omega), \\
W_{14} &= [1 - 2 \sin^2 \omega'](2\dot{\omega}'), \\
W_{15} &= Y_{10}(\Omega - g), \\
W_{16} &= Y_{11}(2\Gamma' - 2L + \Omega), \\
W_{17} &= [Y_1 Y_5 + W_1 W_5](L + \Gamma' - \Omega), \\
W_{18} &= Y_{15}(2L + \Omega - 2\Gamma''), \\
W_{19} &= Y_{13}(2\Gamma' - \Omega), \\
W_{20} &= Y_{10}(2L - \Omega + g), \\
W_{21} &= Y_{14}(2\Gamma''), \\
W_{22} &= [\cos L \cos \Gamma' + \sin L \sin \Gamma'](L - \Gamma''), \\
W_{23} &= [\cos \Gamma' \cos \Gamma'' + \sin \Gamma' \sin \Gamma''](\Gamma' - \Gamma''),
\end{aligned}$$

$$d\epsilon = \left[A_1 X_1 + A_2 X_2 + \sum_{i=1}^8 A_i \dot{X}_i + (1 - \lambda) \sum_{i=9}^{24} A_i \dot{X}_i \right] K,$$

$$\Delta\epsilon = \left[\sum_{i=1}^5 B_i Y_i + \sum_{i=1}^7 B_i \dot{Y}_i + (1 - \lambda) \sum_{i=8}^{18} B_i \dot{Y}_i \right] K,$$

$$d\psi = \left[\sum_{i=1}^3 C_i Z_i + \sum_{i=1}^{12} C_i \dot{Z}_i + (1 - \lambda) \sum_{i=13}^{46} C_i \dot{Z}_i \right] K,$$

$$\Delta\psi = \left[\sum_{i=1}^7 D_i W_i + (1 - \lambda) \sum_{i=8}^{12} D_i \dot{W}_i + \sum_{i=1}^9 D_i W_i + (1 - \lambda) \sum_{i=10}^{23} D_i \dot{W}_i \right] K,$$

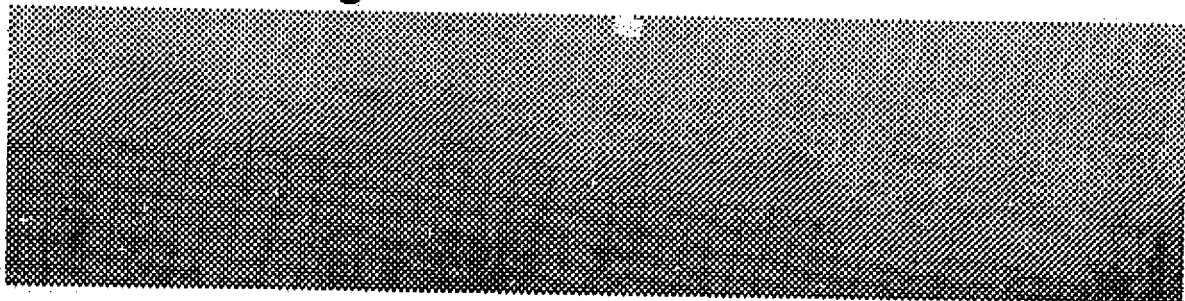
$$\delta\epsilon = d\epsilon + \Delta\epsilon,$$

$$\delta\psi = d\psi + \Delta\psi.$$

A9.3 REFERENCES

- [9.1] Woolard, E. W., "A Redevelopment of the Theory of Nutation," The Astronomical Journal Vol. 58 No. 1, February 1953.
- [9.2] Escobal, P. R., Methods of Astrodynamics, John Wiley and Sons, New York, 1969.
- [9.3] Connaissance des Temps, Bureau des Longitudes, France, 1965.
- [9.4] Escobal, P. R., "Fast Algorithm for Complete Nutation and Nutation Rate Calculations," JPL EM 391-615, 21 January 1975 (JPL internal document).

A10. Precession Algorithm



Abstract

The algorithm for evaluation of the precession of the equinox is stated.

Second order terms not listed in the Explanatory Supplement [10.2] are included along with the precession derivatives.

PRECEDING PAGE BLANK NOT FILMED

A10.1 INTRODUCTION

Development of the precession algorithm can be found in [10.1]; this Appendix is directly abstracted from the reference. The Explanatory Supplement presents expressions for the determination of the three terms ζ_0 , z_p , and θ_p , illustrated in Figure A10.1. These three terms determine the general precession of the equinox between two dates. However, the equations for ζ_0 , z_p , and θ_p listed in [10.2] neglect certain second-order terms. A complete set of equations, including these second-order terms, is given in Connaissance des Temps [10.3]. These equations are based on the work of H. Andoyer [10.4].

The more complete expressions in [10.3] are adopted in this chapter. Each of the equations for the components of the total precession is expressed in terms of the quantities

$T_0 \equiv$ time from 1900.0 to the selected reference epoch in tropical centuries,

$T \equiv$ elapsed time since the reference epoch in tropical centuries.

The quantity T_0 is a constant determined by the particular reference epoch chosen. The reference epoch chosen in [10.1], [10.3], [10.2], because of

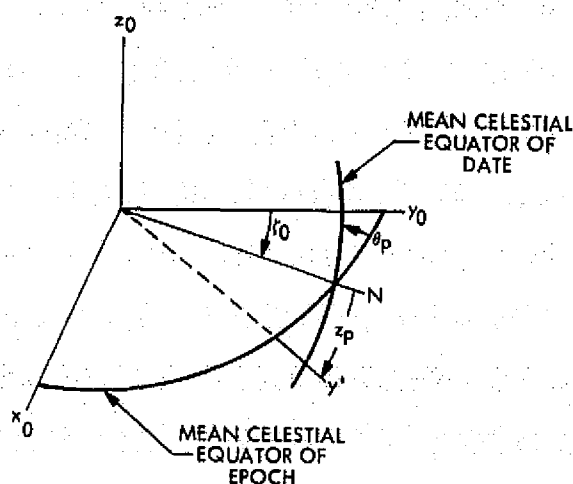


Fig. A10.1. Coordinate Rotations Induced By the Precession of the Equinox.

the ready accessibility of data relative to this epoch, is the reference epoch = 1950.0, for which

$$T_0 = 0.5. \quad (1)$$

A change in reference epoch therefore entails a change of the constant and a corresponding change in the expression for T.

A more convenient form for T is the following expression which is a function of the constant in Eq. (1):

$$T = \frac{J.D. - [(J.D.)_{1900.0} + 36524.220 T_0]}{36524.219879}. \quad (2)$$

where the denominator is an 11 significant figure representation of the number of ephemeris days in a tropical century (neglecting the very small secular variation). The reference Julian date $(J.D.)_{1900.0}$ is

$$(J.D.)_{1900.0} = 2415020.313. \quad (3)$$

One additional constant is required. It is the derivative \dot{T} of T with respect to the modified time variable τ ,

$$\dot{T} = \frac{d}{d\tau}(T) = (36524.219879 \times 24 \times 60 \times 0.07436574)^{-1}. \quad (4)$$

where $\tau = k(t - t_0)$, k being the Gaussian constant.

A10.2 PRECESSION AND PRECESSION RATE ALGORITHM

With the previous understandings it is possible to consider three general precession terms which are defined as follows:

$\zeta_0 + Z_p \equiv$ general precession in right ascension,

$\theta_p \equiv$ precession in declination,

$\frac{\pi}{2} - \zeta_0 \equiv$ angle from mean equinox of epoch to the ascending node of mean equator of date.

The precession equations to be developed require the values of Z_p , θ_p , ζ_0 , and the corresponding derivatives

$$\dot{Z}_p = \frac{dZ_p}{d\tau}, \quad \dot{\theta}_p = \frac{d\theta_p}{d\tau}, \quad \dot{\zeta}_0 = \frac{d\zeta_0}{d\tau}.$$

Values of these six variables above are determined from the following equations* [10.3]:

$$C_1 = 2304''.253 + 13''.973 \times 10^{-1} T_0 + 0''.006 \times 10^{-2} T_0^2,$$

$$C_2 = (3''.023 - 0''.027 \times 10^{-1} T_0) \times 10^{-1},$$

$$D_1 = 2004''.685 - 8''.533 \times 10^{-1} T_0 - 0''.037 \times 10^{-2} T_0^2,$$

$$D_2 = (4''.267 + 0''.037 \times 10^{-1} T_0) \times 10^{-1},$$

$$E_1 = C_1 - 0''.001 \times 10^{-1} T_0,$$

$$E_2 = (10''.950 + 0''.039 \times 10^{-1} T_0) \times 10^{-1},$$

$$\zeta_0 = C_1 T + C_2 T^2 + 1''.800 \times 10^{-2} T^3,$$

*Multiplication by $\pi/(3600 \times 180)$ will convert from seconds of arc to radians.

$$\theta_p = D_1 T - D_2 T^2 - 4''.180 \times 10^{-2} T^3,$$

$$Z_p = E_1 T + E_2 T^2 + 1''.832 \times 10^{-2} T^3,$$

$$\dot{\zeta}_0 = [C_1 + 2C_2 T + 5''.400 \times 10^{-2} T^2] \dot{T},$$

$$\dot{\theta}_p = [D_1 - 2D_2 T - 12''.540 \times 10^{-2} T^2] \dot{T},$$

$$\dot{Z}_p = [E_1 + 2E_2 T + 5''.496 \times 10^{-2} T^2] \dot{T}, \quad (5)$$

$$a_{11} = \cos \zeta_0 \cos \theta_p \cos Z_p - \sin \zeta_0 \sin Z_p$$

$$a_{12} = -\sin \zeta_0 \cos \theta_p \cos Z_p - \cos \zeta_0 \sin Z_p$$

$$a_{13} = -\sin \theta_p \cos Z_p$$

$$a_{21} = \cos \zeta_0 \cos \theta_p \sin Z_p + \sin \zeta_0 \cos Z_p$$

$$a_{22} = -\sin \zeta_0 \cos \theta_p \sin Z_p + \cos \zeta_0 \cos Z_p$$

$$a_{23} = -\sin \theta_p \sin Z_p$$

$$a_{31} = \cos \zeta_0 \sin \theta_p$$

$$a_{32} = -\sin \zeta_0 \sin \theta_p$$

$$a_{33} = \cos \theta_p$$

$$P = \begin{bmatrix} a_{11} & a_{21} & a_{31} \\ a_{12} & a_{22} & a_{32} \\ a_{13} & a_{23} & a_{33} \end{bmatrix}$$

$$\underline{r}_0 = [P] \underline{r}_t$$

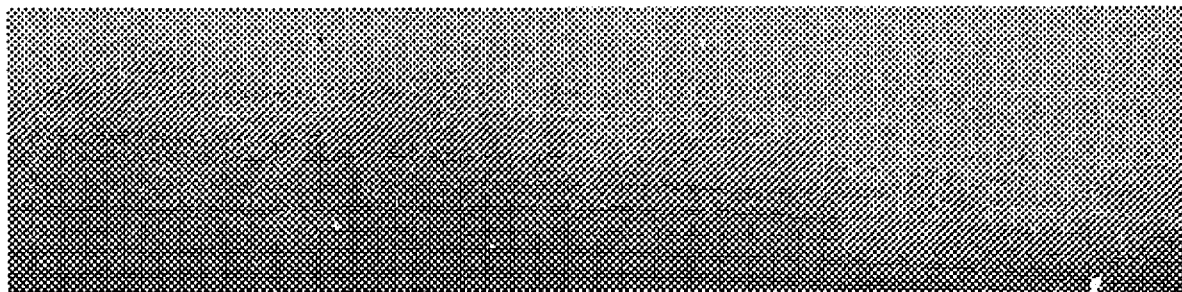
$$\dot{\underline{r}}_0 = [P] \dot{\underline{r}}_t + [\dot{P}] \underline{r}_t$$

The transformation is now complete. Note that position and velocity vectors at time t are transformed to earlier times. For inverse transformations $[P]^T$ should be used.

A10.3 REFERENCES

- [10.1] Escobal, P. R., Methods of Astrodynamics, John Wiley and Sons, New York, 1968.
- [10.2] Explanatory Supplement to the Astronomical Ephemeris and the American Ephemeris and Nautical Almanac, H.M.S. Nautical Almanac Office, London 1961.
- [10.3] Connaissance des Temps, Bureau des Longitudes, France 1965.
- [10.4] Andoyer, H., Bulletin Astronomique, Vol. 28, 1911.

A11. Automatic Generation of Multilateration Functions for SST and Range Only Data Types with Identical Algebraic Structures



Abstract

A generalized quadratic equation is developed. Manipulation of this quadratic equation in specified sequences generates all the multilateration functions peculiar to a specified geometry. Both range and satellite-to-satellite, or airplane-to-airplane, etc., are handled by the generalized equations.

A11.1 INTRODUCTION

Multilateration can be performed using different data types. The two most common data types are range data and satellite-to-satellite (SST) range data.* Solution to the multilateration equations using range only data was originally effected in a specialized coordinate system, which used the stations themselves to define the coordinate system within which the multilateration procedure was exercised. This technique gave rise to a simpler set of equations than if a general coordinate system were used but at the expense of destroying the inherent symmetry of the equations. Symmetry of the equations is of paramount importance for the process of extracting partial derivatives used in the Newton iteration required to solve the equations and for error mapping considerations. The GEOS-3 project added other considerations which favored symmetric multilateration functions, especially for ease in machine implementation and operational software development.

Under the previous constraints, e. g., use of range and SST data types a new solution to the equations was sought. The new solution had to have certain properties, namely: symmetry of the solution ought to be maintained, the SST multilateration equations ought to contain the simpler range multilateration equations as a subset or special case, and the addition of stations in any combination should keep giving rise to Multilateration functions of identical algebraic structure. In essence, a unified multilateration theory was sought.

To accomplish the above objectives the geometry and notation in Figure A11.1 is introduced. Figure A11.1 displays a topocentric coordinate system with the principal axis taken due south; the fundamental plane of this coordinate system is taken to be tangent to the adopted ellipsoid[†] of revolution at arbitrary origin $[X_o, Y_o, Z_o]$ which, for example could be the Greenwich or Naval Observatory. Two separate orbits or airplane trajectories are depicted on which the vehicles track each other with SST data, c. A subset of stations C, called cluster 1, is shown making slant range measurements to the vehicle in orbit 1 at the same time that a subset of stations C,* called cluster 2, makes slant

*Or airplane-to-airplane (AAT) range data.

[†]Without adopting the standard ellipsoid, the computation of geodetic latitude is not possible.

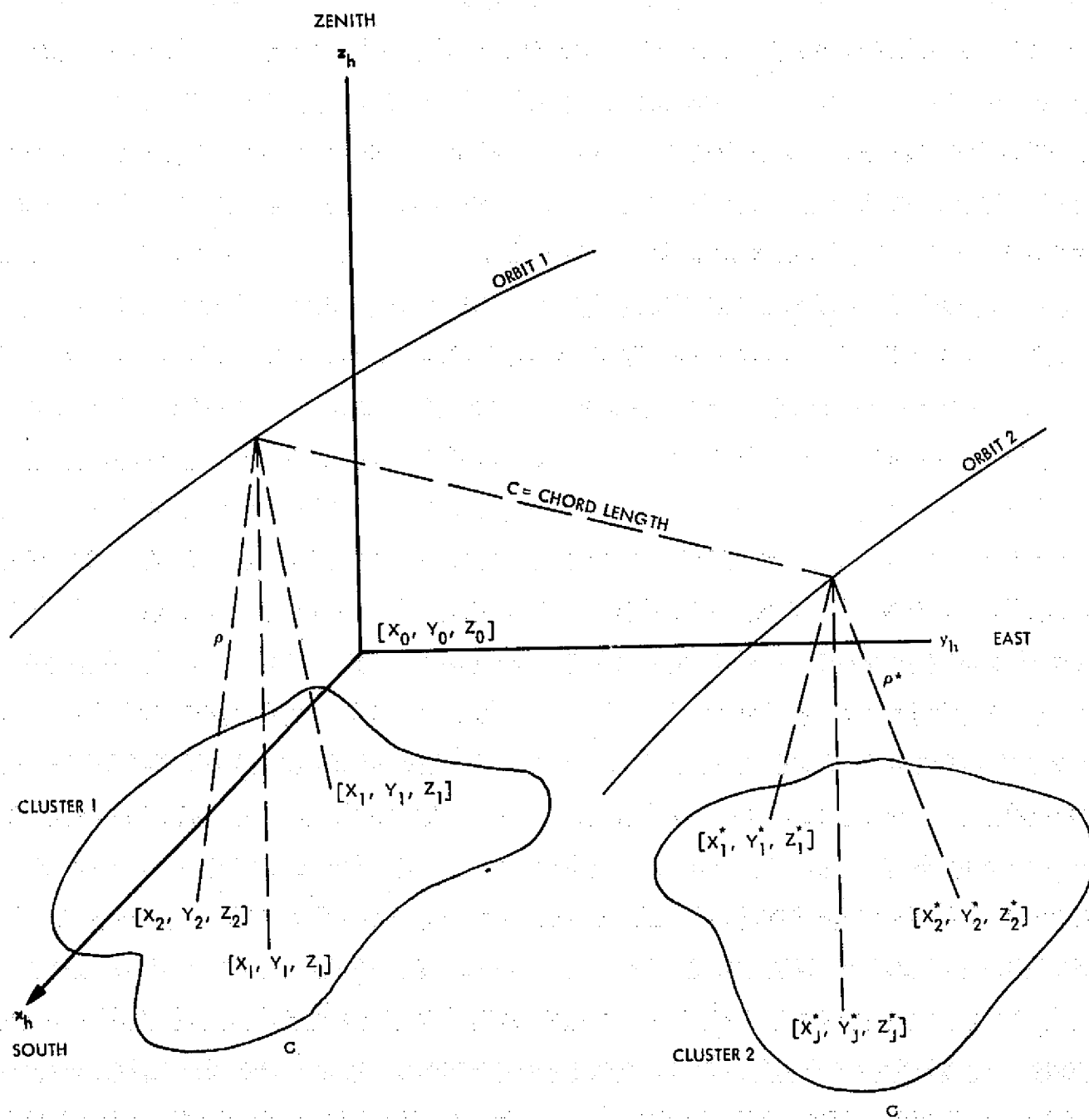


Figure A11.1. Topocentric Multilateration Coordinate System Using or Not Using SST Data Types

range measurements to the vehicle in orbit 2. Configurations in which the coordinates in cluster 1 and 2 are identical were examined in [11.2], i. e., $C = C^*$. This technique called Dual Trilateration was expanded in [11.1] to include the case where $C \neq C^*$, which is the geometry presently under investigation with the SST data, i. e., with the chord length, c , taken as equal or not equal to zero.

The first step in the unification process was to note that if at least three stations are available in each cluster, a quadratic equation in the zenith coordinate, z , of the satellite peculiar to that cluster could be obtained wherein the coefficients of the quadratic are functions of the slant range data ρ from each station to the vehicle and of the coordinates of all three stations (See A11.5). Symbolically, letting:

$$C_I \equiv [X_I, Y_I, Z_I, X_2, Y_2, Z_2, X_I, Y_I, Z_I, \rho_1, \rho_2, \rho_I],$$

where I denotes a specific station out of p stations in C , then

$$H_0(C_I) z_1^2 + H_1(C_I) z_1 + H_2(C_I) = 0. \quad (1)$$

The next step was to note that if X_I, Y_I, Z_I , e. g., X_3, Y_3, Z_3 is replaced by the coordinates of another station, e. g., X_7, Y_7, Z_7 a new independent equation similar to (1) would be generated wherein, of course, the new range measurement ρ_7 would replace ρ_3 in C . Now, since the necessary and sufficient condition that two quadratic equations have a root in common is the vanishing of the resultant, M , of these equations, it was trivial to write:*

$$M_v(H_0[C_I], H_1[C_I], H_2[C_I]) = 0, \quad (2)$$

where I has two values between 3 and p , i. e., there are 6 coefficients in Eq. (2).

Equation (2) is the sought for Multilateration function for stations with coordinates C_I , i. e., for four (4) stations and is a function of only the

*In practice the two quadratics are solved for z and equated to define M_v .

station coordinates and the slant range data. Obviously, if a fifth station is introduced, say, X_9, Y_9, Z_9 , a third independent quadratic can be generated and the resultant of the first and third quadratic equations can be obtained, namely, M_2 . As can be seen the pattern now evolves for the generation of the set of multilateration functions M_v with

$$v = 1, \dots, (p-3), \quad (3)$$

where p is the number of stations in the first cluster and wherein each equation is coupled to the other by the coordinates of the first two stations. Simultaneous solutions via a sequential algorithm is discussed in Appendix A2.

Up to this point only ordinary multilateration has been discussed and the solution to the equations arranged in a sequential mechanical manner. Consider Figure A11.1 and the geometry peculiar to the second cluster. From the previous discussion it is evident that using at least three stations from this cluster, C^* , will lead to:

$$H_0^*(C_J^*) z_2^2 + H_1^*(C_J^*) z_2 + H_2^*(C_J^*) = 0 \quad (4)$$

with

$$C_J^* \equiv [X_1^*, Y_1^*, Z_1^*, X_2^*, Y_2^*, Z_2^*, X_J^*, Y_J^*, Z_J^*, \rho_1^*, \rho_2^*, \rho_J^*]$$

and where z_2 now refers to the zenith coordinate of the second vehicle. There is no way to obtain the resultant of Eqs. (4) and (1) to obtain a new M_v because one equation is a quadratic in z_1 and the other is a quadratic in z_2 ; however the linkage between vehicles 1 and 2 is given by:

$$(x_2 - x_1)^2 + (y_2 - y_1)^2 + (z_2 - z_1)^2 = c^2. \quad (5)$$

It will be shown that use of Eq. (5) permits Eq. (4) to be transformed so that it reads:

$$\bar{H}_0(C_I, C_J, c) z_1^2 + \bar{H}_1(C_I, C_J, c) z_1 + \bar{H}_2(C_I, C_J, c) = 0 \quad (6)$$

Equation (6) is what is defined herein as the generalized quadratic of the multilateration process. At this point abandon the thought of all previous equations and consider how M_v can be generated using only Eq. (6).

By mechanically setting

$$C_J^* = C_I, \quad c = 0$$

prior to entering Eq. (6), all knowledge of the second cluster stations, range data and SST data is annihilated and Eq. (1) is recovered from Eq. (6). Hence as I runs through its range from 3 to p , the sought for M_v functions are generated.

Suppose now that at least three stations exist in each cluster and c data is available. In this case the first three stations in cluster 1 would give rise to a quadratic in z_1 (obtained just as before by letting $C_J^* = C_J$, $c = 0$), while use of Eq. (6) directly with $c \neq 0$ would give rise to a second independent quadratic and the multilateration function M_v would be obtained where $v = I + J = 6$, i.e., for three stations in C , $I = 3$ and for three stations in C^* , $J = 3$.

Suppose now that there are more than three stations in each cluster (or in at least one cluster); then by repeating the previous six station analysis for each new index of I or J independently, a sequence of M_v will be generated where the total number of M_v generated is:

$$v = p + q - 5,$$

where q is the number of stations in the second cluster.

From the previous discussion it can be seen that the mechanical generation of M_v is a function of the number of stations and whether the SST data is to be incorporated into the overall solution. The logic flow for the M_v generation process is outlined in Section A11.3.

A11.2 ANALYSIS

It is demonstrated in A11.5 that given at least three ground stations in a standard inertial coordinate system, the following equation can be developed:

$$H_0 z^2 + H_1 z + H_2 = 0,$$

where H_0 , H_1 , H_2 are coefficients which depend on the station coordinates X_i , Y_i , Z_i , $i = 1, 2, 3$ and the simultaneously measured range data p_i ; the coordinate z is the z component of the satellite position vector relative to the origin of the coordinate system.

Consider a cluster of three stations ranging to a satellite with coordinates x_1, y_1, z_1 and a separate station cluster ranging to a different satellite with coordinates x_2, y_2, z_2 . Obviously for the first cluster:

$$H_0 z_1^2 + H_1 z_1 + H_2 = 0 \quad (7)$$

and for the second cluster:

$$H_0^* z_2^2 + H_1^* z_2 + H_2^* = 0, \quad (8)$$

where the H_0^* , H_1^* , H_2^* are now functions of the coordinate of the three stations in the second cluster and of the range data to the second satellite. The algebraic structure of the H and H^* coefficients is identical.]

If satellite-to-satellite data is available then an additional constraint is given by:

$$(x_2 - x_1)^2 + (y_2 - y_1)^2 + (z_2 - z_1)^2 - c^2 = 0, \quad (9)$$

where c is the chord length between both satellites (SST range).

From the analysis performed in All. 5 it follows that the satellite x and y coordinates for both satellites can be expressed as:

$$\begin{aligned} x_1 &= D_1^{-1}(F_1 + G_1 z_1), & y_1 &= D_1^{-1}(F_2 + G_2 z_1) \\ x_2 &= D_1^{*-1}(F_1^* + G_1^* z_2), & y_2 &= D_1^{*-1}(F_2^* + G_2^* z_2), \end{aligned}$$

where D, F , and G are functions of the station coordinates and range data, therefore:

$$D_1 D_1^*(x_2 - x_1) = D_1 F_1^* - D_1^* F_1 - D_1^* G_1 z_1 + D_1 G_1^* z_2$$

$$D_1 D_1^*(y_2 - y_1) = D_1 F_2^* - D_1^* F_2 - D_1^* G_2 z_1 + D_1 G_2^* z_2$$

while from Eq. (8)

$$z_2 = \frac{-H_1^* + s [H_1^{*2} - 4H_0^* H_2^*]^{1/2}}{2H_0^*},$$

where $s = \pm 1$, the sign ambiguity being resolved by a special procedure*. With this understanding the previous equations can be written as:

$$\begin{aligned}\Delta (x_2 - x_1) &= K + Lz_1 \\ \Delta (y_2 - y_1) &= K^* + L^*z_1\end{aligned}\tag{10}$$

where

$$\begin{aligned}\Delta &\equiv D_1 D_1^* \\ K &\equiv D_1 F_1^* - D_1^* F_1 + D_1 G_1^* M^* \\ L &\equiv -D_1^* G_1 \\ K^* &\equiv D_1 F_2^* - D_1^* F_2 + D_1 G_2^* M^* \\ L^* &\equiv -D_1^* G_2 \\ M^* &\equiv \left(-H_1^* + s \left[H_1^{*2} - 4H_0^* H_2^* \right]^{1/2} \right) / 2H_0^*\end{aligned}$$

The individual x , y , and z coordinate differences between the satellites can now be formed with the previous parameters utilized to obtain each particular difference. Hence a direct computation now yields:

*When an orbit is trilaterated (three station cluster equations) two solutions exist, one on each side of the plane formed by the stations. The elimination is actually much more complicated but has no bearing on the present discussion.

$$\Delta^2(x_2 - x_1)^2 = K^2 + 2KL z_1 + L^2 z_1^2$$

$$\Delta^2(y_2 - y_1)^2 = K^{*2} + 2K^*L^* z_1 + L^{*2} z_1^2$$

$$\Delta^2(z_2 - z_1)^2 = \Delta^2 M^{*2} - 2\Delta^2 M^* z_1 + \Delta^2 z_1^2$$

$$-\Delta^2 c^2 = -\Delta^2 c^2$$

and upon addition of the left hand side of the previous equations the new quadratic results:

$$\begin{aligned} (L^2 + L^{*2} + \Delta^2) z_1^2 + 2(KL + K^*L^* - \Delta^2 M^*) z_1 \\ + K^2 + K^{*2} + \Delta^2 M^{*2} - \Delta^2 c^2 = 0 \end{aligned} \quad (11)$$

Equation (11) is the transformed second cluster equation (Eq. (8)) derived via the SST constraint defined by Eq. (9). The following question is now asked: What happens to Eq. (11) if there is no SST data, i.e., if $c = 0$? Obviously, the last term of Eq. (11) vanishes while Eqs. (10) imply that:

$$z_1 = -\frac{K}{L}, \quad z_1 = -\frac{K^*}{L^*}, \quad KL^* = LK^*.$$

Direct substitution into Eq. (11) yields

$$LL^* M^{*2} + 2KL^* M^* + KK^* = 0$$

or the trivial solution $\Delta = 0$. Therefore

$$M^{*2} + 2\frac{K}{L} M^* + \frac{KK^*}{LL^*} = 0$$

or

$$M^* = -\frac{K}{L} \pm \left[\frac{K^2}{L^2} - \frac{KK^*}{LL^*} \right]^{1/2} = -\frac{K}{L}$$

$$z_1 = M^*.$$

Hence using the definition of M^*

$$z_1 = \frac{-H_1^* + s \left[H_1^{*2} - 4 H_0^* H_2^* \right]^{1/2}}{2H_0^*}$$

which is really the solution of Eq. (8) if z_2 is replaced by z_1 . The proof is now evident that if c is set equal to zero, solution of Eq. (11) reduces to the solution of Eq. (8). Furthermore if one calls the station coordinates of the second cluster the coordinates of the first cluster then it is evident that Eq. (7) results. In essence the conclusion is drawn that Eq. (11) is the generalized quadratic resolvent of the multilateration process. It is this equation which will be used to develop the necessary multilateration functions. This will be accomplished by generating independent quadratic equations and solving them simultaneously.

The generalized H coefficients of Eq. (11) can now be directly computed via K, L, K^* , etc. as:

$$\bar{H}_0 = D_1^{*2} \left[G_1^2 + G_2^2 + D_1^2 \right]$$

$$\begin{aligned} \bar{H}_1 = & 2D_1^* \left[D_1^* (F_1 G_1 + F_2 G_2) - D_1 (F_1^* G_1 + F_2^* G_2) \right. \\ & \left. - D_1 M^* (G_1^* G_1 + G_2^* G_2 + D_1 D_1^*) \right] \end{aligned}$$

$$\begin{aligned}
\bar{H}_2 = & D_1^2 \left[F_1^{*2} + F_2^{*2} + M^{*2} \begin{pmatrix} G_1^{*2} & G_2^{*2} \end{pmatrix} \right] + D_1^{*2} \left[F_1^2 + F_2^2 \right] \\
& - 2D_1 D_1^* \left[F_1^* F_1 + F_2^* F_2 + M^* \begin{pmatrix} F_1 G_1^* + F_2 G_2^* \end{pmatrix} \right] + \left(D_1 D_1^* \right)^2 [M^{*2} - c^2] \\
& + 2D_1^2 \left[F_1^* G_1^* + F_2^* G_2^* \right] M^*
\end{aligned}$$

Using these coefficients it is possible to write

$$\bar{H}_0 z_1^2 + \bar{H}_1 z_1 + H_2 = 0 \quad (12)$$

as the generalized resolvent of the multilateration process.

A11.3 CONSTRUCTION OF MULTILATERATION FUNCTIONS

Section A11.1 outlined the procedure to be followed in the generation of the necessary Multilateration functions. The outline is delineated further herein.

The SST Multilateration Functions

If $c \neq 0$ and there are at least six stations (three in each cluster) the procedure is as follows:

Step 1:

Set: $c = 0$,

Set: $C = C^*$,

Obtain: $\bar{H}_{03} z_1^2 + \bar{H}_{13} z_1 + \bar{H}_{23} = 0$.

Step 2:

Set: $c \neq 0$,

Set: $C = C, \quad C^* = C^*,$

Obtain: $\bar{H}_{06} z_1^2 + \bar{H}_{16} z_1 + \bar{H}_{26} = 0.$

Step 3:

Obtain: resultant of quadratics from step 1 and 2, * namely, M_1 ,
i.e.,

$$M_1(\bar{H}_{03}, \bar{H}_{13}, \bar{H}_{23}, \bar{H}_{06}, \bar{H}_{16}, \bar{H}_{26}) = 0.$$

Step 4:

If additional stations are available, e.g., station I in cluster 1,
 $I > 3$ and/or station J in cluster 2, $J > 3$, return to Step 2 and for
each I and J,

Obtain: $\bar{H}_{0K} z_1^2 + \bar{H}_{1K} z_1 + \bar{H}_{2K} = 0, \quad K = \begin{Bmatrix} I \\ J \end{Bmatrix}.$

Step 5:

Obtain: resultant of quadratics from step 1 and 4, namely, M_ν ,
i.e.,

$$M_\nu(\bar{H}_{03}, \bar{H}_{13}, \bar{H}_{23}, \bar{H}_{0K}, \bar{H}_{1K}, \bar{H}_{2K}) = 0.$$

Therefore obtain: $M_\nu, \quad \nu = 6, 7, \dots$

* See Section A11.4.

Range Only Multilateration Functions

In this case return to Step 1 and,

Step 6:

Set: $c = 0$,

Set: $C = C(I) = C^*(J)$,

Obtain: $\bar{H}_{0I}z_1^2 + \bar{H}_{1I}z_1 + \bar{H}_{2I} = 0$, $I > 3$.

Step 7:

Obtain: resultant of quadratics from steps 1 and 6, namely, M_v ,
i.e.,

$$M_v = M_v(\bar{H}_{0I}, \bar{H}_{1I}, \bar{H}_{2I}, \bar{H}_{0I}, \bar{H}_{1I}, \bar{H}_{2I}) = 0 .$$

Therefore obtain: M_v , $v = 4, 5, 6, \dots$

Step 8:

In the event that the error in c is greater than the error in ρ but at least 4 stations in each cluster have overlapping data, then both the SST multilateration functions and the range only functions should be generated.

All.4 EXPLICIT FORMULA FOR RESULTANT OF TWO QUADRATIC EQUATIONS

The necessary and sufficient condition that two quadratic equations have a root in common is:

$$M \equiv (a_0b_2 - a_2b_0)^2 - (a_0b_1 - a_1b_0)(a_1b_2 - a_2b_1) = 0 , \quad (13)$$

where the two quadratics in question are:*

$$a_0 z^2 + a_1 z + a_2 = 0$$

$$b_0 z^2 + b_1 z + b_2 = 0.$$

Hence, M_v becomes a function of the station coordinates only and can be determined numerically directly as a function of the initial estimates of the station coordinates. Specifically, letting the to-be-solved-for parameters be denoted by ξ , e.g. station coordinates, etc.

$$M_v = M_v(\xi_1, \xi_2, \xi_3, \dots, \xi_l) = 0$$

is the defining multilateration function. In practice it suffices to set the values of z from the previous equations equal to each other; numerically this is a better procedure.

A11.5 QUADRATIC RESOLVENTS IN MULTILATERATION

Consider the relationship

$$(x - X_i)^2 + (y - Y_i)^2 + (z - Z_i)^2 = \rho_i^2,$$

where $x y z$ is the satellite position and X_i, Y_i, Z_i are the station coordinates corresponding to measurements ρ_i . Subtracting the previous equation written for station i and l gives rise to

$$(X_2 - X_1)x + (Y_2 - Y_1)y + (Z_2 - Z_1)z = \omega_{21}$$

$$(X_i - X_1)x + (Y_i - Y_1)y + (Z_i - Z_1)z = \omega_{i1}, \quad i = 3, 4, 5, 6, \quad (14)$$

*It can be proved that solving each equation for z and equating each z yields a valid M function which is numerically better behaved.

where

$$\omega_{i1} = + \left\{ \rho_i^2 - \rho_1^2 - (R_i^2 - R_1^2) \right\} / 2$$

$$R_i^2 = x_i^2 + y_i^2 + z_i^2.$$

Considering Eqs. (14) as a linear system in x and y it follows that

$$x_i = D_{1i}^{-1} \left\{ (Y_2 - Y_1)(\omega_{i1} + [Z_i - Z_1] z_i) - (Y_i - Y_1)(\omega_{21} + [Z_2 - Z_1] z_i) \right\} \quad (15)$$

$$y_i = D_{1i}^{-1} \left\{ (X_i - X_1)(\omega_{21} + [Z_2 - Z_1] z_i) - (X_2 - X_1)(\omega_{i1} + [Z_i - Z_1] z_i) \right\}, \quad (16)$$

where

$$D_{1i} = (X_2 - X_1)(Y_i - Y_1) - (X_i - X_1)(Y_2 - Y_1).$$

The equation peculiar to the first station is given by

$$(z - Z_1)^2 = \rho_1^2 - (x - X_1)^2 - (y - Y_1)^2. \quad (17)$$

Equations (15) and (16) will be substituted directly into Eq. (17) in order to eliminate x and y . To simplify the analysis let Eqs. (15) and (16) be written as:

$$x_i = D_{1i}^{-1}(F_{1i} + G_{1i}z), \quad y_i = D_{1i}^{-1}(F_{2i} + G_{2i}z), \quad (18)$$

where

$$F_{1i} \equiv -\omega_{11}(Y_2 - Y_1) + \omega_{21}(Y_i - Y_1)$$

$$G_{1i} \equiv (Y_2 - Y_1)(Z_i - Z_1) - (Y_i - Y_1)(Z_2 - Z_1)$$

$$F_{2i} \equiv -\omega_{21}(X_i - X_1) + \omega_{11}(X_2 - X_1)$$

$$G_{2i} \equiv (X_i - X_1)(Z_2 - Z_1) - (X_2 - X_1)(Z_i - Z_1).$$

Explicitly performing the substitution of Eqs. (18) into Eq. (17) yields

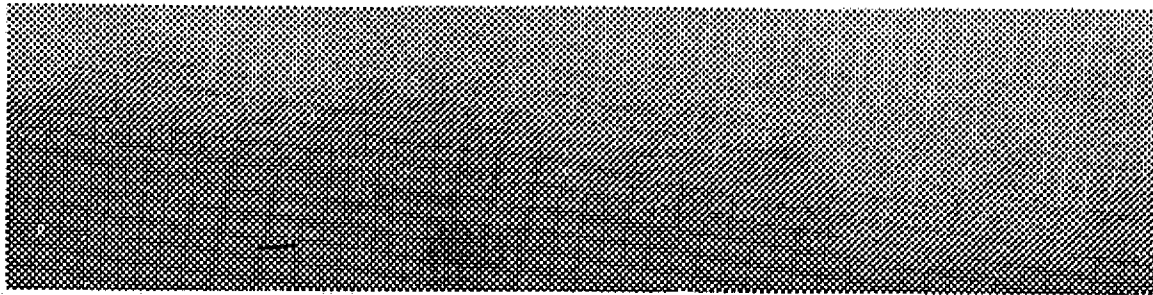
$$\begin{aligned} & \left[1 + D_{1i}^{-2} (G_{1i}^2 + G_{2i}^2) \right] z^2 - 2 \left[Z_1 + D_{1i}^{-1} (X_1 G_{1i} + Y_1 G_{2i}) \right. \\ & \quad \left. - D_{1i}^{-2} (F_{1i} G_{1i} + F_{2i} G_{2i}) \right] z + \left[R_1^2 - \rho_1^2 - 2D_{1i}^{-1} (X_1 F_{1i} + Y_1 F_{2i}) \right. \\ & \quad \left. + D_{1i}^{-2} (F_{1i}^2 + F_{2i}^2) \right] = 0, \quad i = 3, 4, 5, 6. \end{aligned} \quad (19)$$

A11.6 REFERENCES

- [11.1] Escobal, P. R., "Automatic Generation of Multilateration Functions for SST and Range Only Data Types with Identical Algebraic Structures," JPL IOM 391.6-426, 4 April 1974.*
- [11.2] Escobal, P. R., "Dual Trilateration With Vehicle-to-Vehicle Tracking: An Inexpensive Multilateration System," JPL TM 391-393, 4 December 1972.*

*JPL internal document.

A12. Obtaining Slant Range Between Station and Satellite or Satellite-to-Satellite From Turnaround Timing Pulses



Abstract

Closed form expressions for determination of the slant range magnitude between a satellite and ground station, and between two satellites at pulse emit time are derived. The correction equations require no knowledge of the satellite dynamics. An algorithm for the required computations is provided.

PRECEDING PAGE BLANK NOT FILMED

A12.1 INTRODUCTION

Since the transit times between the stations and the satellites are the only measure of the various ranges and since the Earth as well as the satellites are moving with respect to each other a correction to the ranges as inferred from the transit times has to be applied [12.2]. To be specific the SST link (ρ_{sst} in Fig. A12.1) is measured by means of the pulse originating at station 1 which is received at satellite 1 and transmitted to satellite 2 with a delay time Δ_1 . Subsequently satellite 2 transponds by emitting a signal (with a delay time Δ_2) which is received by the transponder of satellite 1 which in turn retransmits this signal (with a delay time Δ_1) to station 1. By this means the ranges ρ_1 and ρ_{sst} (Fig. A12.1) are ascertained. The range ρ_2 is measured independently from station 2 to satellite 2.

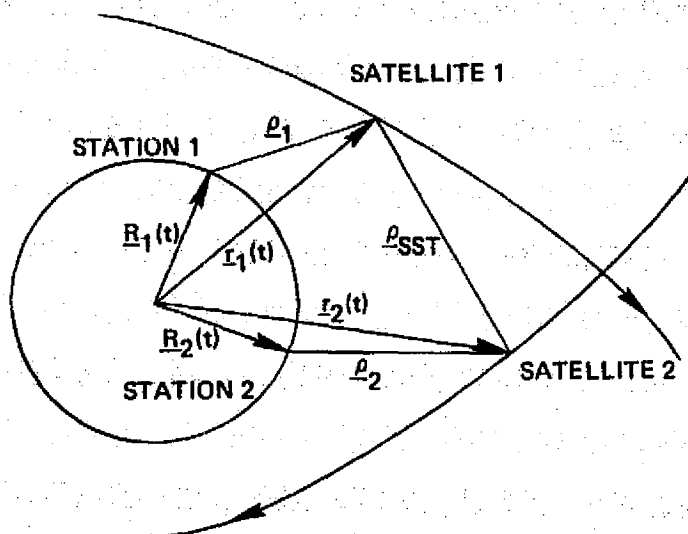


Fig. A12.1 Geometry of the System

A12.2 TIMING CONSIDERATIONS FOR TWO-SATELLITE RANGING WITH AND WITHOUT AN SST LINK

In order to find out how the time delay measurements reflect the true ranges, the vector distances of the stations and the satellites in an Earth fixed inertial frame are introduced, viz:

$\underline{R}_1(t') \equiv$ distance from the center of the Earth to station 1

$\underline{R}_2(t') \equiv$ same to station 2

$\underline{r}_1(t') \equiv$ distance from the center of the Earth to satellite 1

$\underline{r}_2(t') \equiv$ same to satellite 2

The following notation is also adopted herein:

$t' \equiv$ universal time

$\Delta_1 \equiv$ transponder delay of satellite 1

$\Delta_2 \equiv$ transponder delay of satellite 2

$t_1 \equiv$ time of initiation pulse transmitted from station 1.

$t_2 \equiv$ time of initiation pulse transmitted from station 2.

Using these definitions it follows that:

$$\rho_1 = \underline{r}_1 - \underline{R}_1 \quad \rho_2 = \underline{r}_2 - \underline{R}_2 \quad \rho_{sst} = \underline{r}_2 - \underline{r}_1 \quad (1)$$

For the range measurements ρ_1 and ρ_2 which are independent, the analysis follows the same lines, therefore the index (1 or 2) can be omitted. Let a pulse be transmitted at time t from a ground station to a satellite. It will arrive at a time $t + T^{(1)}$ such that

$$c T^{(1)} = \left| \underline{r}(t + T^{(1)}) - \underline{R}(t) \right|. \quad (2)$$

The signal will subsequently be retransmitted with the addition of the transponders delay time Δ (if any). The return time must therefore obey the equation

$$c T^{(2)} = \left| \underline{r}(t + T^{(1)} + \Delta) - \underline{R}(t + \Delta + T^{(1)} + T^{(2)}) \right|. \quad (3)$$

Equations (2) and (3) can be solved for $T^{(1)}$ and $T^{(2)}$, at least to order v/c . Any higher order effects are extremely small and can safely be neglected [1]. Accordingly we have in terms of the upleg transmit time $T^{(1)}$ sent out at time t :

$$c T^{(1)} = \left| \underline{r}(t) + T^{(1)} \dot{\underline{r}}(t) - \underline{R}(t) \right| = \rho(t) + T^{(1)} \dot{\underline{r}} \cdot \underline{\rho} \rho^{-1} \quad (4)$$

and in terms of the downleg transit time $T^{(2)}$

$$\begin{aligned} c T^{(2)} &= \left| \underline{r}(t) + (T^{(1)} + \Delta) \dot{\underline{r}}(t) - \underline{R}(t) - (T^{(1)} + T^{(2)} + \Delta) \dot{\underline{R}}(t) \right| \\ &= \rho(t) + (T^{(1)} + \Delta) \dot{\underline{r}} \cdot \underline{\rho} \rho^{-1} - (T^{(1)} + T^{(2)} + \Delta) \dot{\underline{R}} \cdot \underline{\rho} \rho^{-1}. \end{aligned} \quad (5)$$

From Eq. (4) we find (again to 1st order);

$$c T^{(1)} = \rho + (1/c) \dot{\underline{r}} \cdot \underline{\rho}. \quad (6)$$

Using this equation and remembering that only first order corrections are considered, it follows from Eq. (5) that

$$c T^{(2)} = \rho + \frac{1}{c} \dot{\underline{r}} \cdot \underline{\rho} \left(1 + \frac{c\Delta}{\rho} \right) - \frac{1}{c} \dot{\underline{R}} \cdot \underline{\rho}. \quad (7)$$

The total time delay therefore is

$$T^{(1)} + T^{(2)} = \frac{2}{c} \left(\rho + \frac{1}{c} \dot{\underline{r}} \cdot \underline{r} \right) + \frac{\Delta}{c} \underline{r} \cdot \dot{\underline{r}} \rho^{-1} , \quad (8)$$

but since

$$\underline{r} \cdot \dot{\underline{r}} = \rho \dot{\rho} , \quad (9)$$

the range in terms of the total time delay $T^{(1)} + T^{(2)}$ is given by:

$$\rho = \frac{c}{2} (1 - c^{-1} \dot{\rho}) (T^{(1)} + T^{(2)}) - \frac{1}{2} \Delta \dot{\rho} . \quad (10)$$

which expresses the range in terms of the measured time delay and the measured range rate. Expression (10) is identical with an expression derived previously in [12.1] if the transponder delay Δ is neglected. Equation (10) is valid for both stations 1 and 2 and satellites 1 and 2, giving the direct range at the initial time, i. e., at the time the first identifying pulse was transmitted.

The investigation of the SST link will now be undertaken. Again let the identifying pulse be transmitted at time t from station 1 to satellite 1, then transmitted to satellite 2, then transponded back to satellite 1, then transmitted back to station 1. All this is done coherently (in a locked in mode). In this case the various arrival times are given by:

Arrival at satellite 1:

$$c T^{(1)} = \left| \underline{r}_1 (t + T^{(1)}) - \underline{R}_1 (t) \right| . \quad (11a)$$

Arrival at satellite 2:

$$c T^{(2)} = \left| \underline{r}_2 (t + T^{(1)} + \Delta_1 + T^{(2)}) - \underline{r}_1 (t + T^{(1)} + \Delta_1) \right| . \quad (11b)$$

Arrival at satellite 1:

$$c T^{(3)} = \left| \underline{r}_2 (t + T^{(1)} + \Delta_1 + T^{(2)} + \Delta_2) - \underline{r}_1 (t + T^{(1)} + \Delta_1 + T^{(2)} + \Delta_2 + T^{(3)}) \right|. \quad (11c)$$

Arrival at station 1:

$$c T^{(4)} = \left| \underline{r}_1 (t + T^{(1)} + 2\Delta_1 + T^{(2)} + \Delta_2 + T^{(3)}) - \underline{R}_1 (t + T^{(1)} + 2\Delta_1 + T^{(2)} + \Delta_2 + T^{(3)} + T^{(4)}) \right|. \quad (11d)$$

Due account has been taken of the transponder delay times Δ_1 and Δ_2 . It is again sufficient to solve for the transit times $T^{(1)}$, $T^{(2)}$, $T^{(3)}$ and $T^{(4)}$ to 1st order. Therefore:

$$c T^{(1)} = \rho_1 + c^{-1} \underline{p}_1 \cdot \dot{\underline{r}}_1 \quad (12)$$

$$c T^{(2)} = \rho_{sst} + \frac{1}{c} \underline{p}_{sst} \cdot \dot{\underline{r}}_2 + \frac{1}{c} \rho_1 \dot{\rho}_{sst} + \Delta_1 \dot{\rho}_{sst}, \quad (13)$$

where $\rho_{sst} = \left| \underline{r}_2(t) - \underline{r}_1(t) \right|$ is the SST range. Furthermore:

$$c T^{(3)} = \rho_{sst} - \frac{1}{c} \underline{p}_{sst} \cdot \dot{\underline{r}}_1 + \frac{1}{c} (\rho_1 + \rho_{sst}) \dot{\rho}_{sst} + (\Delta_1 + \Delta_2) \dot{\rho}_{sst} \quad (14)$$

$$c T^{(4)} = \rho_1 - \frac{1}{c} \underline{p}_1 \cdot \dot{\underline{R}}_1 + (2\Delta_1 + \Delta_2) \dot{\rho}_1 + \frac{1}{c} (\rho_1 + 2\rho_{sst}) \dot{\rho}_1. \quad (15)$$

The total transit time therefore is given by:

$$\begin{aligned}
 T = T^{(1)} + T^{(2)} + T^{(3)} + T^{(4)} &= 2/c (\rho_1 + \rho_{sst}) \\
 &+ \frac{2}{c} \rho_{sst} \dot{\rho}_{sst} + \frac{2}{c} \rho_1 \dot{\rho}_1 \\
 &+ \frac{2}{c} (\rho_1 \dot{\rho}_{sst} + \dot{\rho}_1 \rho_{sst}) + \frac{1}{c} (2\Delta_1 + \Delta_2) (\dot{\rho}_1 + \dot{\rho}_{sst}) . \quad (16)
 \end{aligned}$$

Note that $T = T^{(1)} + T^{(2)} + T^{(3)} + T^{(4)}$ is observed, and that ρ_1 and $\dot{\rho}_1$ are known independently from Eq. (10). It is therefore possible to obtain ρ_{sst} from Eq. (16) if the range rate $\dot{\rho}_{sst}$ is known. But the range rate is simply given using 1st order theory by:

$$d/dt (T^{(1)} + T^{(2)} + T^{(3)} + T^{(4)}) = 2/c (\dot{\rho}_1 + \dot{\rho}_{sst}) . \quad (17)$$

Therefore the correct range ρ_{sst} can be inferred from Eq. (16). The final result for the SST range follows from Eq. (16) and is given by:

$$\begin{aligned}
 \rho_{sst} = \frac{c}{2} \left[1 - c^{-1} (\dot{\rho}_1 + \dot{\rho}_{sst}) \right] T - \rho_1 \\
 - \left(\Delta_1 + \frac{1}{2} \Delta_2 \right) (\dot{\rho}_1 + \dot{\rho}_{sst}) . \quad (18)
 \end{aligned}$$

If $\rho_1 \equiv 0$, station 1 and satellite 1 are equivalent, and Eq. (18) goes over into Eq. (10) as it must. It should be remembered that Eqs. (10) and (18) have been derived to first order via the Taylor series expansions of ρ .

In the second order approximation, correction terms of the order of $(\dot{\rho}^2/c^2) \rho$ and $(\ddot{\rho}/c^2) \rho^2$ will appear. For typical range-rates of 1 km/sec and accelerations of 10^{-3} km/sec², $\dot{\rho}^2/c^2 \approx 10^{-11}$ and $\rho \ddot{\rho}/c^2 \approx 10^{-12}$ (for ranges $\rho \approx 10^4$ km), so that the corrections to the range only amount to fractions of a mm and can therefore be totally neglected. Note that $\dot{\rho}$ is positive when the range ρ increases and negative when ρ decreases.

A12.3 COMPUTATIONAL ALGORITHM

Given the input:

c \equiv Speed of light (cm/sec),

$T_{1,2} \equiv$ Total measured transit time of a pulse between a ground station and satellite 1 or 2 (sec),

$\Delta_1 \equiv$ Transponder delay time of satellite 1 (sec),

$\Delta_2 \equiv$ Transponder delay time of satellite 2 (sec),

$T \equiv$ Total measured transit time of a pulse between a ground station and satellite 2 via satellite 1,

calculate uncorrected (u) slant range ρ_{iu} at station i from

$$\rho_{iuj} = \frac{c}{2} T_{ij}, \quad j = 1, 2, 3, \dots, J \quad (19)$$

for all measured transit times, j , in the adopted fitting interval. Fit range data over the adopted fitting interval and obtain

$$\rho_{iu} = f_i(t) \quad (20)$$

where, e.g., $f_i(t) = a_{0i} + a_{1i}t + a_{2i}t^2 \dots$ Differentiate f_i to obtain

$$\dot{\rho}_{iu} = \dot{f}_i(t). \quad (21)$$

If SST data is to be used calculate uncorrected SST range ρ_{sstu} from

$$\rho_{sstu} = \frac{1}{2} c T_j - \rho_{iu_j} \quad , \quad j = 1, 2, 3, \dots, J, i = 1, \quad (22)$$

for all measured SST transit times T_j in adopted fitting interval. Fit SST range data over the fitting interval and obtain

$$\rho_{sstu} = g(t). \quad (23)$$

Differentiate g to obtain

$$\dot{\rho}_{sstu} = \dot{g}(t). \quad (24)$$

Compute corrected ranges at station signal emit time, t_e , from

$$\rho_i = \frac{c}{2} \left[1 - c^{-1} \dot{f}_i(t_e) \right] T_{ij} - \frac{1}{2} \Delta_l \dot{f}_i(t_e), \quad (25)$$

where Δ_l signifies the satellite transponder delay time.

If signal emit time for SST measurement T does not correspond to t_e but rather to t_e^* go to Eq. (27), otherwise proceed to (26):

$$\rho_{sst} = \frac{1}{2} c T - f_i(t_e) - \left\{ \frac{1}{2} T + \Delta_1 + \frac{1}{2} \Delta_2 \right\} \left\{ \dot{f}_i(t_e) + \dot{g}(t_e) \right\}. \quad (26)$$

Compute

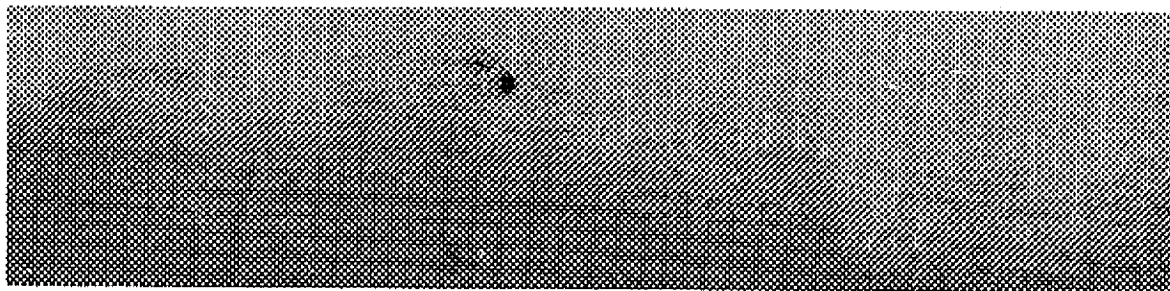
$$\begin{aligned} p_{sst} = & \frac{1}{2} c T - f_i(t_e^*) \\ & - \left\{ \frac{1}{2} T + \Delta_1 + \frac{1}{2} \Delta_2 \right\} \left\{ \dot{f}_i(t_e^*) + \dot{g}(t_e^*) \right\}. \end{aligned} \quad (27)$$

Exit Calculations.

A12.4 REFERENCES

- [12.1] Escobal, P.R., et al, 3-D Multilaterations: A Precision Geodetic Measurement System, JPL TM 33-605, March 15, 1973.
- [12.2] von Roos, O.H., and Escobal, P.R., "Obtaining Slant Range Between Station and Satellite or Satellite-to-Satellite From Turnaround Timing Pluses," JPL EM 391-704, 14 November 1975 (JPL internal document).

A13. Center of Mass Corrections



Abstract

A brief outline of spacecraft attitude determination procedures is presented. Accepting the spacecraft attitude as known, data corrections to laser measurements can be made to ensure that all the data types are referred to the spacecraft center of mass. When accurate radiofrequency data is available, and it is to be combined with, e. g. laser data, correction equations to make the data types consistent are required. These correction equations are developed both for the straight slant range and the vehicle-to-vehicle slant range data types.

A13.1 INTRODUCTION

When ranging a satellite from several stations via laser or radio pulses a correction must be made so that each range measurement is related to a common center. This is necessary because the attitude of the satellite changes in time and depending on the station location different corner reflectors will be active in reflecting the signal. The common center to which ranges have to be referred is the center of mass, since it does not depend on the attitude of the satellite [13.2].

A13.2 ATTITUDE DETERMINATION

Use of an Earth/Sun or star sensor located at S as depicted in Figure A13.2 permits small angular separations to be measured about the cone angle swept out by the sensor as it rotates about the satellite spin axis A. These small excursions, i. e., the associated leading and trailing pulses can be used to fix the spacecraft attitude in a coarse (Earth/Sun references) and fine (star references) mode. The attitude determination equations give rise to quadratic equations in the declination of the spin axis. Other equations can be used to determine the right ascension of the spin axis. The analysis is lengthy and is discussed in [13.1]. If the satellite is boom stabilized, then the attitude vector is taken to be approximately along the satellite radius vector. This latter case is typical of the GEOS-3 satellite where, e. g., the attitude is taken to be $\pm 1^\circ$ from the satellite radius vector. In the subsequent analysis it will be assumed that the satellite attitude is known.

A13.3 LASER SLANT RANGE CORRECTION

Figure A13.1 is indicative of the geometry involved. The satellite is typical of GEOS-3 configurations and as far as laser ranging is concerned it has cylindrical symmetry. An array of corner reflectors is mounted in a ring like fashion perpendicular to the symmetry axis. The radius of this ring of corner reflectors is called B. The distance between the center of mass, CM, and the plane of the reflectors is called A. In order to be able to correct for the variation in range due to the activation of different corner reflectors dependence on station location, satellite attitude and ephemeris have to be known. Specifically let:

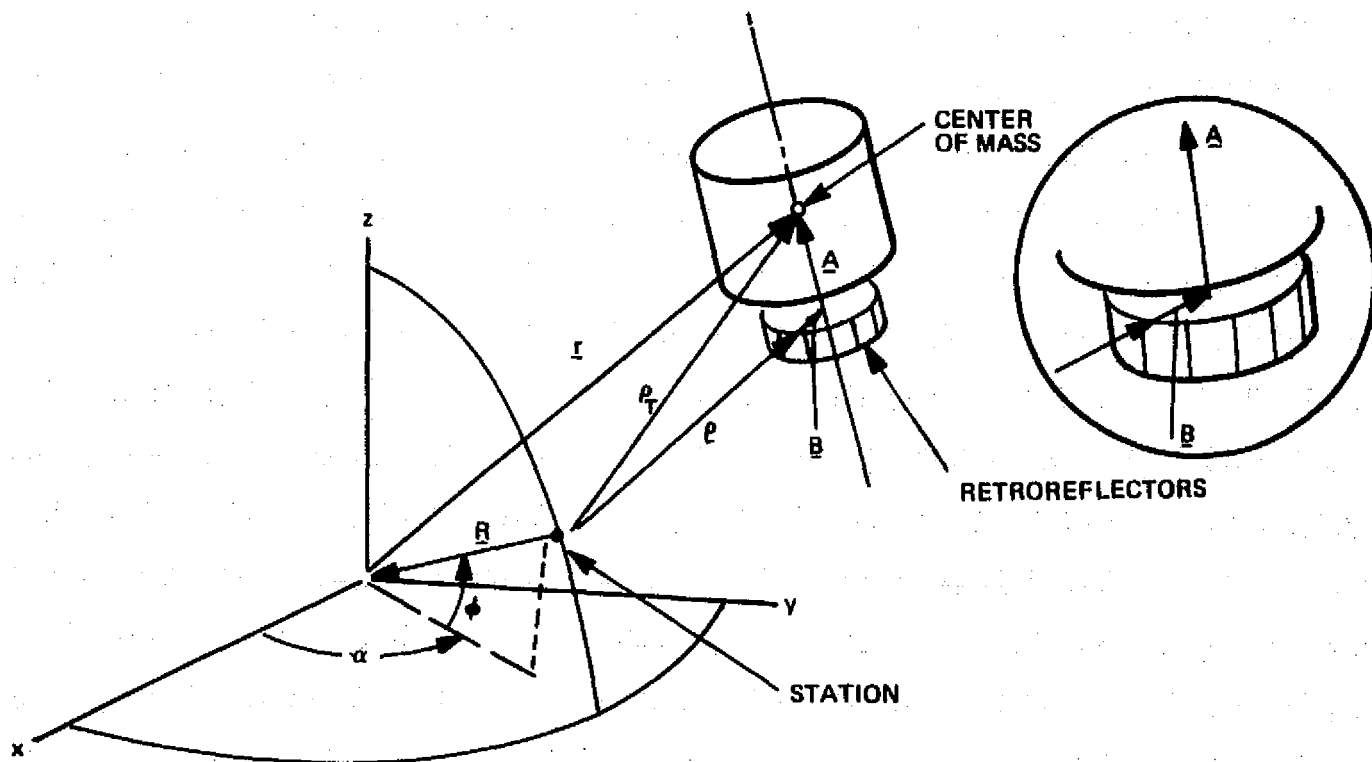


Figure A13.1. Laser Retroreflector Geometry

\underline{r} \equiv the vector from the center of the Earth to the CM of the satellite (at epoch t)

\underline{R} \equiv the vector from the ranging station to the center of the Earth (same epoch)

\underline{A} \equiv the attitude vector of the satellite (magnitude A). For GEOS-C this vector has usually a direction aligned with \underline{r} but may deviate by a few degrees.

Now then, from Figure A13.1 it is clear that:

$$\underline{R} + \underline{r} = \underline{\rho}_T, \quad (1)$$

where $\underline{\rho}_T$ is the true range from the station to the center of mass of the satellite. It must be emphasized that neither \underline{R} nor \underline{r} is well known. Their magnitude for instance is only known to 50 m. Therefore Eq. (1) cannot be used to determine ρ_T to the cm level. However the measurement of ρ , that

is, the distance between the station and the active corner reflector is known to this accuracy. Use has to be made of this fact.

From Figure A13.1 there results another relationship:

$$\underline{\rho}_T = \underline{\rho} + \underline{A} + \underline{B} , \quad (2)$$

where \underline{B} is a vector in the plane of the ring of corner reflectors perpendicular to \underline{A} of magnitude B and obviously coplanar with $\underline{\rho}$ and $\underline{\rho}_T$.

Since \underline{A} is known, by use of vector analysis, it is found by crossing $\underline{\rho}$ into \underline{A} and crossing $\underline{\rho} \times \underline{A}$ into \underline{A} that:

$$\underline{B} = (\underline{\rho} \times \underline{A}) \times \underline{A} B A^{-2} \rho^{-1} . \quad (3)$$

Dotting Eq. (2) with the as yet unknown vector $\underline{\rho}_T$, there results:

$$\rho_T^2 = \underline{\rho} \cdot \underline{\rho}_T + (\underline{A} + \underline{B}) \cdot \underline{\rho}_T . \quad (4)$$

The dot product between $\underline{\rho}$ and $\underline{\rho}_T$ can safely be replaced by the direct product of the magnitudes, i. e.:

$$\underline{\rho} \cdot \underline{\rho}_T = \rho \rho_T \cos (\angle \underline{\rho}, \underline{\rho}_T) \approx \rho \rho_T . \quad (5)$$

This is because the angle between $\underline{\rho}$ and $\underline{\rho}_T$ is very small. Typically for $\rho \sim 500$ km and $A \sim 10$ m the angle is only $2 \cdot 10^{-5}$ rad and this implies for worst case analysis that the error occasioned in $\rho_T \approx 0.1$ mm. With this approximation there results a quadratic equation for ρ_T (Eq. (4)). In the correction term, clearly given by $(\underline{A} + \underline{B}) \cdot \underline{\rho}_T$, it is now safe to replace $\underline{\rho}_T$ by its not so well known counterpart from Eq. (1). Accordingly, from Eq. (4), using Eq. (1) and approximation (5) the following equation is obtained:

$$\rho_T = \frac{1}{2} \rho + \left\{ \frac{1}{4} \rho^2 + \underline{A} \cdot (\underline{R} + \underline{r}) + B \rho^{-1} A^{-2} \left[(\underline{R} + \underline{r}) \times \underline{A} \right]^2 \right\}^{1/2} . \quad (6)$$

Equation (6) can be simplified to read:

$$\rho_T = \rho + \rho^{-1} \underline{A} \cdot (\underline{R} + \underline{r}) + B(\rho A)^{-2} \left[(\underline{R} + \underline{r}) \times \underline{A} \right]^2 \quad (7)$$

which is the desired result. This equation will correct the measured range with modeling errors and parameter uncertainty to the order of

$$\sigma = \frac{A}{\rho} \left[\sigma_{\rho x}^2 + \sigma_{\rho y}^2 + \sigma_{\rho z}^2 \right]^{1/2}$$

$$\approx 2 \text{ mm}$$

for $\sigma(\underline{R} + \underline{r}) \approx 50 \text{ m}$, $A = 10 \text{ m}$ and $\rho \approx 800 \text{ km}$.

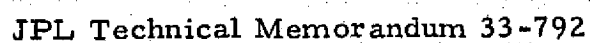
A13.4 RADIO FREQUENCY ANTENNA SLANT RANGE CORRECTION

Ranging with C or S band microwave frequencies entails another correction similar to that determined for the laser ranging data type discussed in A13.3. The range, ρ , from the focal point of the station's antenna to the focal point of the receiving transponder on the satellite is determined by a radio ranging system. The true range from the station to the center of mass of the satellite, in order to have a common reference point for all modes of ranging be it by laser, S band or C band etc., must be determined. This is so because retroreflectors, S band antennas, C band antennas etc. are all located at different places on the satellite, and for processing accurate range data from various sources a common point of reference must be chosen. This is taken to be the center of mass. For an antenna horn located as in Figure A13.2 it is clear that the range vectors satisfy the equations:

$$\underline{\rho} = \underline{r} + \underline{R} - \underline{B} - \underline{A} , \quad (8)$$

$$\underline{\rho}_T = \underline{\rho} + \underline{A} + \underline{B} , \quad (9)$$

$$\frac{\mathbf{e}_y}{\mathbf{y}} = \frac{\mathbf{e}_z}{z} \times \frac{\mathbf{e}_x}{x} = \begin{bmatrix} -\sin \alpha \\ +\cos \alpha \\ 0 \end{bmatrix}$$



where $\underline{\rho}$ is the slant range vector from the station to the transponder, $\underline{\rho}_T$ is the slant range vector from the station to the satellite's center of mass, \underline{A} is the satellite attitude vector with magnitude equal to the distance from the transponder horn to the satellite center of mass, \underline{r} is the satellite geocentric position vector, \underline{R} is the station position vector, and \underline{B} is a vector at right angles to \underline{A} with magnitude equal to the distance from the centerline to the transponder horn. Note that the vector \underline{B} has an undetermined direction unless an Earth/Sun or star sensor, \underline{S} , is employed to determine the spacecraft attitude.* In this case it may be possible to obtain the orientation of \underline{B} directly without using the following analysis.

The correction scheme proposed herein is as follows.

From Figure A13.2 the \underline{e}_x , \underline{e}_y , \underline{e}_z basis is obtained from the known values of the right ascension, α , and declination, δ , of the satellite spin or centerline axis. Therefore in this basis \underline{B} is given by

$$\underline{B} = B \left\{ \cos(\omega t + \psi) \underline{e}_x + \sin(\omega t + \psi) \underline{e}_y \right\}, \quad (10)$$

where $|\underline{B}|$ is known, ω is the satellite spin rate, if any, and ψ is the unknown phase angle. The object herein is to determine ψ .

From Eq. (8) it follows that

$$\rho^2 = \Delta + a_1 \cos(\omega t + \psi) + a_2 \sin(\omega t + \psi), \quad (11)$$

where

$$\Delta(t) \equiv (\underline{r} + \underline{R}) \cdot (\underline{r} + \underline{R}) - 2(\underline{r} + \underline{R}) \cdot \underline{A}$$

$$a_1(t) \equiv -2B(\underline{r} + \underline{R}) \cdot \underline{e}_x$$

$$a_2(t) \equiv -2B(\underline{r} + \underline{R}) \cdot \underline{e}_y$$

It should be evident that to a fair degree of precision $\Delta(t)$, $a_1(t)$, and $a_2(t)$ can be modeled and are thus accepted as known functions of time. Equation (11) will be employed to determine ψ in two different cases from values of the raw data ρ .

*Gravity gradient stabilized satellites may not necessarily have such sensors.

The first case involves fast spinning satellites where ω is much greater than the inverse of the fitting interval and a_1 , a_2 , Δ are slowly varying functions of time. Hence by differentiating Eq. (11)

$$\frac{d\rho}{d\psi} = -a_1 \sin(\omega t_i^* + \psi) + a_2 \cos(\omega t_i^* + \psi) = 0, \quad (12)$$

where t_i^* are the observed times of the occurrence of maxima and minima of ρ . The problem now is to minimize J with respect to ψ , where J is defined by:

$$J = \sum_i \left[-a_1 \sin(\omega t_i^* + \psi) + a_2 \cos(\omega t_i^* + \psi) \right]^2. \quad (13)$$

Thus using trigonometric relationships a quartic in $\cos \psi$ can be obtained and solved for the sought for phase angles and spurious roots eliminated by substitution of the ψ angles into Eq. (12).

The second case involves slow to negligible satellite spin rates. Hence from Eq. (11) the functional G , where

$$G = \sum_i \left[\rho_i^2 - \Delta_i - a_{1i} \cos(\omega t_i + \psi) - a_{2i} \sin(\omega t_i + \psi) \right]^2 \quad (14)$$

needs to be minimized with respect to ψ . Note that the i subscript refers to the data point. The solution proceeds as before.

In summary then the angle ψ is determined as well as possible, either by direct sensor measurement or by means of Eq. (13) or (14) subject to a minimization criterion. Hence having obtained ψ the vector \underline{B} , Eq. (10), becomes known, and the correction equation for the true range can be obtained from Eq. (9) written as:

$$\rho_T^2 = \rho^2 + A^2 + B^2 + 2\rho \cdot \underline{A} + 2\rho \cdot \underline{B}, \quad (15)$$

where ρ is the measured data but $\underline{\rho}$ is taken as the modeled slant range vector, i.e., \underline{A} and \underline{B} in Eq. (8) are neglected. Thus expanding Eq. (15) and neglecting higher order terms

$$\rho_T = \rho + \rho^{-1} \left[(\underline{r} + \underline{R}) \cdot (\underline{A} + \underline{B}) \right] \quad (16)$$

where \underline{B} is given by Eq. (10). Numerical studies indicate that if the range accuracy is to the meter level, the unknown correction containing the unknown spin angle can be disregarded, i.e., $\underline{B} = 0$ for elevation angles ranging from 40° to 90° .

A13.5 RADIO FREQUENCY SATELLITE-TO-SATELLITE RANGE CORRECTION

To conclude this appendix a brief description of the center of mass correction for the SST link (the range between two satellites) is in order. A look at Figure A13.2 will convince the reader that the true SST range $\rho_{sst}^{(T)}$ is given by:

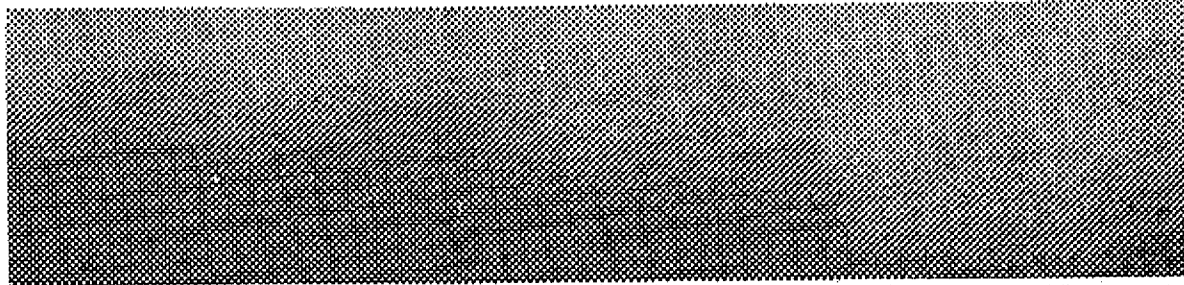
$$\rho_{sst}^{(T)} = \rho_{sst} + \rho_{sst}^{-1} (\underline{r}_2 - \underline{r}_1) \cdot (\underline{A}_2 - \underline{A}_1 + \underline{B}_2 - \underline{B}_1) , \quad (17)$$

where $\underline{A}_1, \underline{B}_1$ as well as $\underline{A}_2, \underline{B}_2$ are defined exactly as before, but now pertain to the two satellites. Again, as before, \underline{r}_1 and \underline{r}_2 are the trajectory vectors for the two satellites as determined by trilateration to the (sufficient) accuracy of 100 m. The determination of the vectors \underline{B}_1 and \underline{B}_2 follows the same lines as described in the body of the paper.

A13.6 REFERENCES

- [13.1] Escobal, P.R., "Dynamics of Spacecraft Attitude Determination," Hughes Aircraft Company, Orbiting Solar Observatory Proposal to NASA, 1971.
- [13.2] von Roos, O.H. and Escobal, P.R., "Center of Mass Corrections to Slant Range Data," JPL EM391-708, 2 December 1975 (JPL internal document).

A14. Estimation of Geographic Coordinates from Multilateration Constraints: the N-Dimensional Case



Abstract

The equations required to estimate geographic coordinates from coordinates determined by multilateration are developed for the N-station, three-dimensional case. The equations are solved and the covariance matrix of the solution is obtained. From the general solution, the one-dimensional case is extracted and the results are found to agree with the results obtained by others.

PRECEDING PAGE BLANK NOT FILMED

A14.1 INTRODUCTION

The method by which multilateration improves geographic coordinates is statistical in nature. Multilateration, by the construction of the equations, can only determine the interstation three-dimensional coordinates relative to a basis, call it T_0 , which for all intents and purposes is detached from the standard latitude-longitude geographic basis.* This implies that the origin of the T_0 basis and its orientation relative to the geographic basis is unknown to an observer within the T_0 basis. Construction of the T_0 basis and application of multilateration theory provides a method of resolving the three-dimensional interstation coordinates within the T_0 basis. From these coordinates the interstation baselines can be determined to high precision. Since these baselines are invariant under a coordinate rotation and translation, it follows that the multilateration information content can be used in the geographic frame in the form of baseline constraints, which when combined with the a priori geographic coordinate information will result in a statistical improvement in the geographic coordinates [14.3].

A14.2 COMPUTATION OF BASELINE DISTANCE AND COVARIANCE

Once measurements have been taken in the T_0 basis it is evident that the interstation coordinates can be determined via the multilateration equations derived in Appendix A2. These interstation coordinates, due to the manner in which the T_0 basis is defined, are free of any errors which are in the vectors used to define T_0 . However, as soon as the coordinates are desired in the geographic basis, then the uncertainties of the basis vectors relative to the origin of the geographic system become important if a coordinate rotation and translation is attempted. Actually, from the structure of the multilateration equations the only accurately determined parameters are the interstation distances, i.e., the invariants, D_{ij} :

$$(X_{Gi} - X_{Gj})^2 + (Y_{Gi} - Y_{Gj})^2 + (Z_{Gi} - Z_{Gj})^2 = D_{ij}^2, \quad (1)$$

where the subscript G implies geographic coordinates.

*Some slight linkage occurs due to the Earth/Ocean tidal models.

Selection of the geometric invariants of the multilateration procedure can best be understood from Figures A14.1, A14.2 and A14.3.

Consider Figure A14.1 which shows three stations located in the geometric basis which is usually adopted for multilateration coordinate reduction. The first station (1) is at the origin of the basis, the second station (2) defines the X axis and station (3) defines the XY plane. Obviously the square of the difference between the station coordinates is invariant under any rotation and translation. Hence for the first three stations there is a one-to-one correspondence between the coordinates $(X_2, 0, 0)$ and d_{12}^2 ; those of station three $(X_3, Y_3, 0)$ and d_{13}^2 and the invariant $d_{23}^2 = (X_2 - X_3)^2 + Y_3^2$, in the sense that if the d distances are known, the X and Y coordinates can be determined. The inverse process is also possible. Consider the addition of station 4 as illustrated in Figure A14.2. If d_{14} is specified then knowledge of d_{34} defines plane 1, 3, 4. Hence to fix the dihedral angle between planes 1, 2, 3 and 1, 3, 4 one can elect to specify the distance d_{24} . In summary then for rigidity of the d or rod superstructure one must specify $d_{12}^2, d_{13}^2, d_{23}^2, d_{41}^2, d_{24}^2, d_{34}^2$, namely six invariants. Continuing the process as illustrated in Figure A14.3 one would specify d_{15}, d_{45} and d_{35} . The general rule for invariant specifications is given in Table A14.1

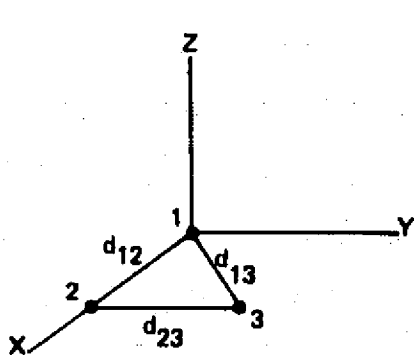


Figure A14.1.
3 Stations

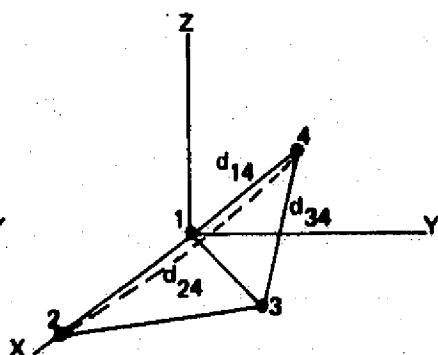


Figure A14.2.
4 Stations

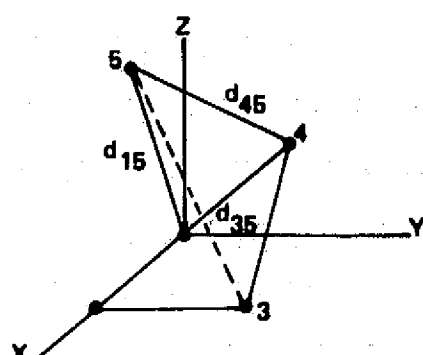


Figure A14.3.
5 Stations

Table A14.1. Multilateration Invariants

Stations	Invariants
3	$d_{12}^2, d_{13}^2, d_{23}^2$
4	$d_{14}^2, d_{24}^2, d_{34}^2$
5	$d_{15}^2, d_{35}^2, d_{45}^2$
.	
.	
.	
I	$d_{1I}^2, d_{I-2, I}^2, d_{I-1, I}^2$

Functionally in the T_0 basis the invariants are written as

$$X_{ij}^2 + Y_{ij}^2 + Z_{ij}^2 = D_{ij}^2. \quad (2)$$

Obviously at time t , given X_{ij} , Y_{ij} and Z_{ij} and the associated covariance of the rectangular components, D_{ij}^2 , from multilateration coordinate reduction, D_{ij}^2 and its covariance is determined as

ORIGINAL PAGE IS
OF POOR QUALITY

$$\delta D_{ij}^2 = \begin{bmatrix} \delta D_{12}^2 \\ \delta D_{13}^2 \\ \vdots \\ \delta D_{1I}^2 \\ \hline \delta D_{23}^2 \\ \delta D_{24}^2 \\ \hline \delta D_{34}^2 \\ \delta D_{35}^2 \\ \hline \vdots \\ \hline \delta D_{I-2, I-1}^2 \\ \delta D_{I-2, I}^2 \\ \hline \delta D_{I-1, I}^2 \end{bmatrix} = \begin{bmatrix} \omega \end{bmatrix} \begin{bmatrix} \delta X_2 \\ \delta Y_2 \\ \delta Z_2 \\ \vdots \\ \delta Z_I \end{bmatrix},$$

where the matrix $[\omega]$ of dimension $(3I-6) \times (3I-6)$ given by:

$$[\omega] \equiv \begin{bmatrix} x_2 & y_2 & z_2 & 0 & 0 & 0 & 0 & \cdot & \cdot & \cdot & 0 & 0 \\ 0 & 0 & 0 & x_3 & y_3 & z_3 & 0 & \cdot & \cdot & \cdot & \cdot & 0 \\ \cdot & & & & & & \cdot & & & & & \\ \cdot & & & & & & \cdot & & & & & \\ \cdot & & & & & & \cdot & & & & & \\ 0 & \cdot & \cdot & \cdot & \cdot & \cdot & \cdot & \cdot & \cdot & \cdot & x_I & y_I & z_I \\ \hline \Delta X_{23} & \Delta Y_{23} & \Delta Z_{23} & -\Delta X_{23} & -\Delta Y_{23} & -\Delta Z_{23} & 0 & 0 & \cdot & \cdot & \cdot & 0 \\ 0 & 0 & 0 & \Delta X_{24} & \Delta Y_{24} & \Delta Z_{24} & -\Delta X_{24} & -\Delta Y_{24} & -\Delta Z_{24} & 0 & \cdot & 0 \\ \hline \cdot & & & & & & & & & & & \\ \hline 0 & \cdot & \cdot & 0 & 0 & 0 & 0 & \Delta X_{I-1, I} & \Delta Y_{I-1, I} & \Delta Z_{I-1, I} & -\Delta X_{I-1, I} & -\Delta Y_{I-1, I} & -\Delta Z_{I-1, I} \end{bmatrix}$$

Hence it follows after taking expected values that the interstation baseline covariance is given by:

$$\Lambda_{D_i}^2 = [\omega] \Lambda_{\underline{R}} [\omega]^T, \quad (3)$$

where $\Lambda_{\underline{R}}$ is the covariance matrix of the station coordinates in the T_0 basis as determined via the multilateration equations.

A14.3 SOLUTION OF THE EQUATIONS IN GEOGRAPHIC BASIS

The system of equations defining the interstation baselines can be written as:

$$F = \begin{bmatrix} (X_{G2} - X_{G1})^2 + (Y_{G2} - Y_{G1})^2 + (Z_{G2} - Z_{G1})^2 - D_{12}^2 \\ \vdots \\ (X_{GI} - X_{G1})^2 + (Y_{GI} - Y_{G1})^2 + (Z_{GI} - Z_{G1})^2 - D_{1I}^2 \\ \hline (X_{G2} - X_{G3})^2 + (Y_{G2} - Y_{G3})^2 + (Z_{G2} - Z_{G1})^2 - D_{23}^2 \\ (X_{G2} - X_{G4})^2 + (Y_{G2} - Y_{G4})^2 + (Z_{G2} - Z_{G4})^2 - D_{24}^2 \\ \hline \vdots \\ (X_{G(I-1)} - X_{GI})^2 + (Y_{G(I-1)} - Y_{GI})^2 + (Z_{G(I-1)} - Z_{GI})^2 - D_{I-1,I}^2 \end{bmatrix} = 0. \quad (4)$$

Hence

$$F = F(X_{G1}, Y_{G1}, \dots, Z_{GI}, D_2^2, \dots, D_I^2, D_{23}^2, \dots, D_{I-1,I}^2).$$

Note that F would be identically equal to zero if the D_i were in fact errorless. This not being the case it follows that

$$F = \bar{F} + \frac{\partial \bar{F}}{\partial D^2} \delta D^2 = \bar{F} + \gamma, \quad (5)$$

where \bar{F} is the value of F obtained by using corrupted D_i . With this understanding the combined system of equations, i. e., the baseline constraints and a priori equations take the form:

$$\bar{H}(X_{G1}, Y_{G1}, \dots, Z_{GI}) = \begin{bmatrix} X_{G1} - X_{G1a} \\ Y_{G1} - Y_{G1a} \\ Z_{G1} - Z_{G1a} \\ \vdots \\ Z_{GI} - Z_{GIa} \\ \hline (X_{G2} - X_{G1})^2 + (Y_{G2} - Y_{G1})^2 + (Z_{G2} - Z_{G1})^2 - D_{12}^2 \\ \vdots \\ (X_{G(I-1)} - X_{GI})^2 + (Y_{G(I-1)} - Y_{GI})^2 + (Z_{G(I-1)} - Z_{GI})^2 - D_{I-1,I}^2 \end{bmatrix} = \begin{bmatrix} \beta \\ \vdots \\ \gamma \end{bmatrix} \quad (6)$$

where β and γ are the uncertainties in the a priori and F functions and the subscript a denotes a priori values. The previous system of equations is correlated and thus premultiplication by the matrix V^{-1} where $VV^T = W$ is the covariance matrix of the error sources will permit the previous equations to be statistically conditioned. Note that the numerical value of V need not be computed.* The new function G is now formed as

$$\bar{G}(X_{G1}, Y_{G1}, \dots, Z_{GI}) \equiv \bar{G}(\xi) = V^{-1} \bar{H} = V^{-1} \begin{bmatrix} \beta \\ \gamma \end{bmatrix} \equiv \mu \quad (7)$$

* Unless a square root algorithm is to be employed.

which as required has uncorrelated components, i.e.,

$$E \begin{bmatrix} \mu & \mu^T \end{bmatrix} = I,$$

where I is the identity matrix. Now G can be set equal to zero to solve the decorrelated set of equations using the method of ordinary least squares.

Hence, to apply the Newton procedure G is expanded as

$$\bar{G} + \frac{\partial \bar{G}}{\partial X_{G1}} \Delta X_{G1} + \frac{\partial \bar{G}}{\partial Y_{G1}} \Delta Y_{G1} + \dots + \frac{\partial \bar{G}}{\partial Z_{G1}} \Delta Z_{G1} = 0$$

or more compactly as

$$\bar{G} + \frac{\partial \bar{G}}{\partial \xi} \Delta \xi,$$

where as before

$$\xi = \begin{bmatrix} X_{G1}, & Y_{G1}, & \dots & Z_{G1} \end{bmatrix}.$$

The least squares solution to the previous system is now given by:

$$\Delta \xi = - \left\{ \begin{bmatrix} \frac{\partial \bar{G}}{\partial \xi} \end{bmatrix}^T \begin{bmatrix} \frac{\partial \bar{G}}{\partial \xi} \end{bmatrix} \right\}^{-1} \begin{bmatrix} \frac{\partial \bar{G}}{\partial \xi} \end{bmatrix}^T \bar{G}(\xi) \quad (8)$$

or since

$$\partial \bar{G} / \partial \xi = V^{-1} \partial \bar{H} / \partial \xi$$

it is possible to write

$$\hat{\xi}_{q+1} = \hat{\xi}_q - \left\{ \left[\frac{\partial \bar{H}}{\partial \xi} \right]^T W^{-1} \left[\frac{\partial \bar{H}}{\partial \xi} \right] \right\}^{-1} \left[\frac{\partial \bar{H}}{\partial \xi} \right]^T W^{-1} \bar{H}(\xi) \quad (9)$$

where q is the Newton iteration index. However, from the structure of H , the matrix $\partial H / \partial \xi$ can be written directly as:

$$\frac{\partial H}{\partial \xi} = \begin{bmatrix} U \\ \frac{\partial F}{\partial \xi} \end{bmatrix}, \quad d \longrightarrow (4I-6) \times (4I-6),$$

where

$$U = \begin{bmatrix} 1 & 0 & 0 & 0 & . & . & . & 0 \\ 0 & 1 & 0 & . & . & . & . & 0 \\ 0 & 0 & 1 & . & . & . & . & 0 \\ . & 0 & . & 1 & . & . & . & 0 \\ . & . & . & . & . & . & . & . \\ . & . & . & . & . & . & . & . \\ 0 & . & . & . & . & . & . & 1 \end{bmatrix}, \quad d \longrightarrow I \times I$$

and $\partial F / \partial \xi \xrightarrow{d} (3I-6) \times (3I-6)$ is given by

$$\frac{\partial F}{\partial \xi} = \begin{bmatrix} -2(X_{G2} - X_{G1}) & -2(Y_{G2} - Y_{G1}) & -2(Z_{G2} - Z_{G1}) & 2(X_{G2} - X_{G1}) & . & . & 2(Z_{G2} - Z_{G1}) & 0 & . & . & 0 \\ . & . & . & 0 & . & . & . & . & . & . & . \\ . & . & . & . & . & . & . & . & . & . & . \\ . & . & . & . & . & . & . & . & . & . & . \\ 0 & . & . & 0 & -2(X_{G(I-1)} - X_{G1}) & -2(Y_{G(I-1)} - Y_{G1}) & -2(Z_{G(I-1)} - Z_{G1}) & . & . & 2(Z_{G(I-1)} - Z_{G1}) & . \end{bmatrix} \quad (10)$$

Hence assuming no correlation between the a priori and multilateration uncertainty W can be taken as*

$$W = \begin{bmatrix} W_\beta & 0 \\ 0 & W_\gamma \end{bmatrix} = \begin{bmatrix} \Lambda_{Ra} & 0 \\ 0 & \Lambda_{Di}^2 \end{bmatrix}, \quad (11)$$

and multiplication of the partitioned matrices yields

$$\begin{aligned} \hat{\xi}_{q+1} = \hat{\xi}_q - & \left\{ \Lambda_{Ra}^{-1} + \left[\frac{\partial \bar{F}}{\partial \xi} \right]^T \Lambda_{Di}^{-1} \left[\frac{\partial \bar{F}}{\partial \xi} \right] \right\}^{-1} \\ & \times \left\{ \Lambda_{Ra}^{-1} (\hat{\xi}_q - \xi_a) + \left[\frac{\partial \bar{F}}{\partial \xi} \right]^T \Lambda_{Di}^{-1} \bar{F}_q \right\}, \end{aligned} \quad (12)$$

where

$$\Lambda_{Di}^2 = [\omega] \Lambda_R [\omega]^T.$$

Note that the covariance of ξ is given by

$$\Lambda_\xi = \left\{ \Lambda_{Ra}^{-1} + \left[\frac{\partial \bar{F}}{\partial \xi} \right]^T \Lambda_{Di}^{-1} \left[\frac{\partial \bar{F}}{\partial \xi} \right] \right\}^{-1}. \quad (13)$$

* Obviously if W is correlated, i. e., if new baseline information is obtained via multilateration, then Eq. (9) provides the final coordinate estimations.

A14.4 REDUCTION OF SOLUTION TO THE ONE-DIMENSIONAL CASE

If the multilateration constraint is taken as

$$X_{G2} - X_{G1} - D = \gamma$$

and the a priori values

$$X_{G2} - X_{G2a} = \beta_2$$

$$X_{G1} - X_{G1a} = \beta_1$$

are specified, it follows at once that

$$\frac{\partial F}{\partial \xi} = \begin{bmatrix} -1 & , & 1 \end{bmatrix}$$

and the covariance formula, Eq. (13) yields:

$$\begin{bmatrix} \sigma_{XG1}^2 & \sigma_{XG1} \sigma_{XG2} \\ \sigma_{XG2} \sigma_{XG1} & \sigma_{XG2}^2 \end{bmatrix} = \left\{ \begin{bmatrix} \sigma_{XG1a}^2 & 0 \\ 0 & \sigma_{XG2a}^2 \end{bmatrix}^{-1} + \begin{bmatrix} -1 \\ 1 \end{bmatrix} \sigma_D^{-2} \begin{bmatrix} -1 & , & 1 \end{bmatrix} \right\}^{-1}$$

or

$$\Lambda_{\underline{RG}} = \begin{pmatrix} \frac{1}{\sigma_{\text{XG1a}}^2} + \frac{1}{\sigma_D^2} & -\frac{1}{\sigma_D^2} \\ -\frac{1}{\sigma_D^2} & \frac{1}{\sigma_{\text{XG2a}}^2} + \frac{1}{\sigma_D^2} \end{pmatrix}^{-1}.$$

Extracting the inverse results in

$$\Lambda_{\underline{RG}} = \begin{pmatrix} \left(\frac{1}{\sigma_{\text{XG2a}}^2} + \frac{1}{\sigma_D^2} \right) / \Delta & \left(\frac{1}{\sigma_D^2} \right) / \Delta \\ \frac{1}{\sigma_D^2} / \Delta & \left(\frac{1}{\sigma_{\text{XG1a}}^2} + \frac{1}{\sigma_D^2} \right) / \Delta \end{pmatrix}.$$

so that, e. g.,

$$\begin{aligned} \sigma_{\text{XG1}}^2 &= \left(\frac{1}{\sigma_{\text{XG2a}}^2} + \frac{1}{\sigma_D^2} \right) / \Delta \\ &= \frac{\frac{1}{\sigma_{\text{XG2a}}^2} + \frac{1}{\sigma_D^2}}{\left(\frac{1}{\sigma_{\text{XG2a}}^2} + \frac{1}{\sigma_D^2} \right) \left(\frac{1}{\sigma_{\text{XG1a}}^2} + \frac{1}{\sigma_D^2} \right) - \frac{1}{\sigma_D^4}} \end{aligned}$$

or multiplying top and bottom by σ_D^4

$$\begin{aligned}\sigma_{\text{XG1}}^2 &= \sigma_D^2 \left(\frac{\sigma_D^2}{\sigma_{\text{XG2a}}^2} + 1 \right) / \left\{ \left(1 + \frac{\sigma_D^2}{\sigma_{\text{XG2a}}^2} \right) \left(1 + \frac{\sigma_D^2}{\sigma_{\text{XG1a}}^2} \right) - 1 \right\} \\ &= \left(1 + \frac{\sigma_D^2}{\sigma_{\text{XG2a}}^2} \right) / \left\{ \left(\frac{\sigma_D^2}{\sigma_{\text{XG1a}}^2 \sigma_{\text{XG2a}}^2} \right) + \frac{1}{\sigma_{\text{XG1a}}^2} + \frac{1}{\sigma_{\text{XG2a}}^2} \right\},\end{aligned}$$

so that as the multilateration constraint becomes more and more accurate, i. e., as $\sigma_D^2 \rightarrow 0$

$$\sigma_{\text{XG1}}^2 = \frac{1}{\frac{1}{\sigma_{\text{XG1a}}^2} + \frac{1}{\sigma_{\text{XG2a}}^2}}$$

and if

$$\sigma_{\text{XG1a}} \cong \sigma_{\text{XG2a}}$$

$$\sigma_{\text{XG1}} = \sigma_{\text{XG1a}} / \sqrt{2}. \quad (14)$$

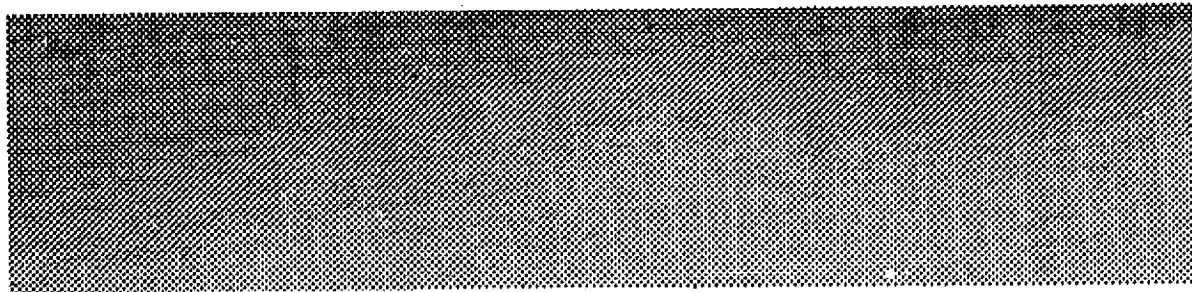
The previous analysis shows that the multilateration constraints will have the effect of improving the absolute geographic coordinates by $1/\sqrt{2}$. This is the result obtained by Lass [14.1] and later verified by Bierman [14.2]. In the general case an improvement of about $1/\sqrt{N}$ where N are the number of baselines would be expected.

A14.5 REFERENCES

- [14.1] Lass, H., "The Effect of Multilateration on the Improvement of Station Location Coordinates," JPL EM 391-553, April 1974. *
- [14.2] Bierman, G. J., personal communication.
- [14.3] Escobal, P. R., "Estimation of Geographic Coordinates from Multilateration Constraints; The N-Dimensional Case," JPL EM 391-691, 1 October 1975. *

*JPL internal document.

A15. Data Stream Definition for Calibration



Abstract

The parameters required as input in order to perform data calibration are specified and the frequency of the input is estimated. The parameter input data or data streams are defined with the goal in mind of attaining calibrations accurate to the one centimeter level.

A15.1 INTRODUCTION

Reduction of raw data to usable form requires calibration. For purposes of multilateration and orbit determination to centimeter level accuracy four distinct data categories can be identified [15.1]:

- Measurement Data Type (range, range-rate, SST range)
- Atmospheric Data Type (pressure, temperature, etc.)
- Earth/Ocean Data Type (local gravity)
- Vehicle Data Type (attitude, etc.)

The purpose of this Appendix is to set down the data types and the frequency or density of the data types as a function of time such that the individual data types (as supplied from various sources) can be reduced into a single continuous data stream valid over a finite time interval.

To this end I individual ground stations, J airborne stations, and K satellites are identified. Limits on I and J are: $1 \leq I \leq 15$, $1 \leq J \leq 3$, $1 \leq K \leq 3$.

A15.2 MEASUREMENT DATA TYPE

It will be assumed that range and range-rate will be supplied on tape.

- Frequency: 1 Data Type or point/Sec
- Amount: $2(I+J) + K$ streams

A15.3 ATMOSPHERIC DATA TYPE (TROPOSPHERE)

This data will be supplied on tape, table, or graph.

H_0 : Height of vehicle (lower station); cm

H_1 : Height of vehicle (upper station); cm

- Frequency: 1 Data Type or point/10 Sec
- Amount: J streams

\bar{P}_0 : Pressure at vehicle (lower station); mbar
 \bar{P}_1 : Pressure at vehicle (lower station); mbar
 • Frequency: 1 Data Type/10 Sec
 • Amount: J streams
 \bar{T}_0 : Temperature at vehicle (lower station); °K
 \bar{T}_1 : Temperature at vehicle (upper station); °K
 • Frequency: 1 Data Type/10 Sec
 • Amount: J streams
 P_0 : Average ground pressure (ground station); mbar
 T_0 : Average ground temperature (ground station); °K
 t : Dew point temperature (ground station); °K
 h_w : Water vapor scale height (ground station); cm
 • Frequency: 1 Data Type/3600 Sec
 • Amount: 4I streams
 T^* : Temperature at inversion layer height; °K
 h_0 : Inversion layer height; cm
 • Frequency: 1 Data Type/21600 Sec
 • Amount: 2I streams
 h_1 : Troposphere height; cm
 α : Atmospheric lapse rate; °K/cm
 • Frequency: 1 Data Type/86400 Sec
 • Amount: 2I streams

A15.4 ATMOSPHERIC DATA TYPE (IONOSPHERE)

This data to be supplied as in above.

N_{MAX} : Peak electron Density at station; cm^{-3}

- Frequency: 1 Data Type/1000 Sec
- Amount: 1 streams

h_{MAX} : Altitude above ground of peak electron; cm

α^* : Diffusion coefficient for electrons; Sec^{-1}

β : Attachment coefficient for electrons; Sec^{-1}

- Frequency: 1 Data Type/3600 Sec
- Amount: 31 streams

H: Scale height of the electron density profile; cm

- Frequency: 1 Data Type/86400 Sec
- Amount: 1 streams

A15.5 EARTH/OCEAN DATA TYPE

This data will be supplied on tape or on graphical roll.

g: Local gravity at station; cm/Sec^2

- Frequency: 1 Data Type/3600 Sec
- Amount: 1 streams

A15.6 VEHICLE DATA TYPE

This data will be supplied on tape.

a: Accelerometer data; cm/Sec^2

- Frequency: 1 Data Type/10 Sec
- Amount: J streams

- A: Attitude vector; rads
- r: Vehicle position; meters
- r: Vehicle velocity; meters/Sec
 - Frequency: 1 Data Type/10 Sec
 - Amount: 9K streams

A15.7 TOTAL NUMBER OF DATA STREAMS

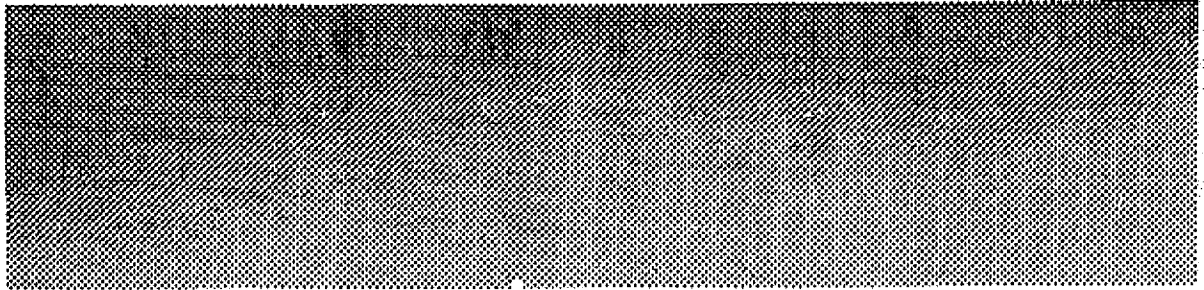
Adding up all previous data streams yields:

$$\text{streams} = 6J + 16I + 10K = 285 \cong 300_{\text{MAX}}$$

A15.8 REFERENCE

- [15.1] Escobal, P.R., "Identification of Data Streams Required for Precision Multilateration and Orbit Determination," JPL IOM 391, 5-562, 29 April 1975 (JPL internal document).

A16. Partial Derivatives of Estimated Parameters With Respect to Non-Estimated Parameters



Abstract

Formulas are developed for the partial derivatives of multilateration estimated parameters $\hat{\xi}$ with respect to modeling constants $\bar{\xi}$. The sensitivity partials of the data c and time t are also developed. The analysis is general and may have many other applications.

PRECEDING PAGE BLANK NOT FILMED

A16.1 INTRODUCTION

For purposes of orbit determination the assessment of the effects of non-estimated parameters, $\bar{\xi}$, on estimated parameters is of primary importance. Determination of the manner in which data, c , and time, t , uncertainties affect the estimated parameters is also of importance. This Appendix develops the explicit partial derivatives of the pertinent parameters.

A16.2 THE MULTILATERATION FUNCTION

As introduced previously in Appendix A2 the multilateration function can be written as:

$$M \equiv M(\xi, \bar{\xi}, c, t) = 0, \quad (1)$$

where ξ are the estimated parameters, $\bar{\xi}$ are the non-estimated parameters, c are the data compression coefficients, and t are the interrogation times. If the vector system denoted respectively by Eq. (1) is to be solved for estimates of ξ , call then $\hat{\xi}$, with estimates $\hat{\xi}$, \hat{c} , \hat{t} then M evaluated with these parameters can be written as

$$M = M(\hat{\xi}, \bar{\xi}, \hat{c}, \hat{t}) + \frac{\partial M}{\partial \bar{\xi}} \delta \bar{\xi} + \frac{\partial M}{\partial c} \delta c + \frac{\partial M}{\partial t} \delta t = 0 \quad (2)$$

or

$$M(\hat{\xi}, \bar{\xi}, \hat{c}, \hat{t}) = v, \quad (3)$$

where

$$v = - Q \delta \bar{\xi} - S \delta c - R \delta t$$

with

$$Q \equiv \partial M / \partial \bar{\xi}, S \equiv \partial M / \partial c, R \equiv \partial M / \partial t$$

The previous nonlinear system of equations is statistically coupled but is usually uncoupled by computing

$$W = \text{cov}(\nu \nu^T),$$

extracting the square root of W and premultiplying Eq. (3) by the square root so that

$$VM(\hat{\xi}, \hat{\xi}, \hat{c}, \hat{t}) = V\nu.$$

It is this uncoupled system that can now be set equal to zero and solved to yield the estimates $\hat{\xi}$ by the standard least squares Newton-Raphson procedure.

A16.3 PARTIAL DERIVATIVE COMPUTATION

Assuming that the equations have been solved for values of $\hat{\xi}$ it is evident from the chain rule of differential calculus that

$$V \frac{\partial M}{\partial \xi} \frac{\partial \xi}{\partial \xi} \equiv -VQ$$

$$V \frac{\partial M}{\partial \xi} \frac{\partial \xi}{\partial c} \equiv -VS$$

$$V \frac{\partial M}{\partial \xi} \frac{\partial \xi}{\partial t} \equiv -VR$$

Letting $\partial M / \partial \xi \equiv P$, the previous equations can be squared up to yield

$$P^T V^T V P \frac{\partial \xi}{\partial \xi} = -P^T V^T V Q$$

$$P^T V^T V P \frac{\partial \xi}{\partial c} = -P^T V^T V S$$

$$P^T V^T V P \frac{\partial \xi}{\partial t} = -P^T V^T V R$$

Hence letting $C \equiv P^T V^T V P = P^T W^{-1} P$

$$\frac{\partial \xi}{\partial \bar{\xi}} = -C^{-1} P^T W^{-1} Q$$

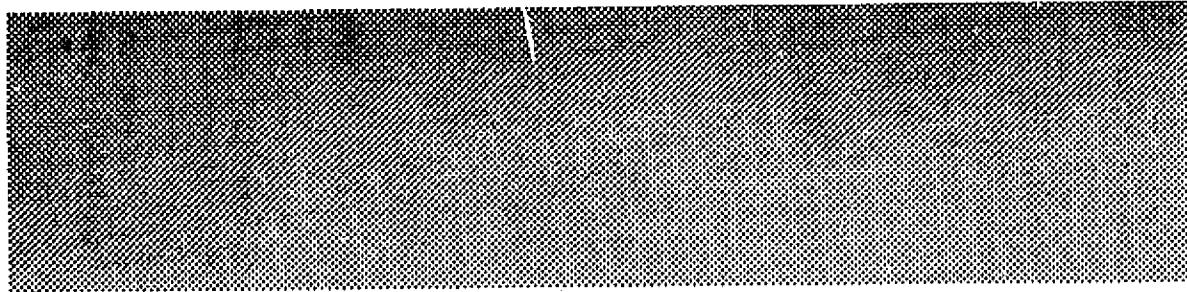
$$\frac{\partial \xi}{\partial c} = -C^{-1} P^T W^{-1} S$$

$$\frac{\partial \xi}{\partial t} = -C^{-1} P^T W^{-1} R$$

These formulas give the sensitivity of the estimated to the nonestimated parameters in the multilateration solutions. Note that the matrix $\partial \xi / \partial \bar{\xi}$ is usually bounded in size, while $\partial \xi / \partial c$ and $\partial \xi / \partial t$ continue to increase in dimension for increasing amounts of data.

The partial derivative $\partial \xi / \partial \bar{\xi}$ is of interest in determining the sensitivity of estimated parameters with respect to consider modeling parameters and is always a useful output. The partial derivative $\partial \xi / \partial c$ has value in the geometric trilateration procedure (See Appendix A8). The same can be said of $\partial \xi / \partial t$. These last two partial derivatives are usually computed for only a small batch of data.

A17. Analytic Partial Derivative Generation



Abstract

The method of partial derivative extraction using symbolic Jacobian notation is discussed from a general point of view. A simple example to illustrate the technique is included. The method described herein, to a great extent, avoids long chain differentiation.

A17.1 INTRODUCTION

This Appendix describes the manner in which the analytic partial derivatives required for multilateration were derived and coded.

The method is illustrated using one of the smaller sets or "chains" of equations of the MICRODOT software for which partial derivatives are required. The other sets or chains of equations are handled in the very same way, therefore nothing more will be said of them here.

A17.2 METHOD OF DERIVATION

The method of derivation can be described as follows:

- 1) The set, chain or sequence of equations to be differentiated is clearly laid out, from the original independent variables, through a sequence of well chosen intermediate variables, to the ultimate set of dependent variables.
- 2) Groups of variables that tend to occur together are identified so that efficient use of Jacobian matrices of partial derivatives can be achieved.
- 3) Symbolic differentiation is then done, level by level, taking the derivatives of a set of variables with respect to only the set on which they explicitly depend, as formulated in the chain of equations.
- 4) A back substitution phase is then carried out in which, by continual regrouping, matrix formulas for the partial derivatives of any set of variables with respect to the original independent variables are derived. The back substitution is continued until the partial derivatives of the ultimate dependent variables with respect to the original independent variables are arrived at.
- 5) Lastly, actual differentiation at each level is done so that later, in the computer program, numerical values of the matrix elements can be computed. Actual differentiation is not required for the derivation of the matrix formulas for the partials themselves.

A17.3 DERIVATION OF THE PARTIAL DERIVATIVES OF THE BASIS UNIT VECTORS WITH RESPECT TO THE GEOGRAPHIC CARTESIAN COORDINATES OF THE THREE BASIS STATIONS

For this derivation the geographic cartesian coordinates of the basis stations, denominated \underline{R}_{G1} , \underline{R}_{G2} , \underline{R}_{G3} are the original independent variables. The ultimate dependent variables are the unit vectors $\hat{\underline{x}}$, $\hat{\underline{y}}$, $\hat{\underline{z}}$. The chain of equations connecting these is as follows:

$$\hat{\underline{x}} = \frac{\underline{R}_{G2} - \underline{R}_{G1}}{d_{12}}, \quad (1)$$

where

$$d_{12} = \left| \underline{R}_{G2} - \underline{R}_{G1} \right|.$$

This is followed by the unit vector

$$\hat{\underline{s}} = \frac{\underline{R}_{G3} - \underline{R}_{G1}}{d_{13}}, \quad (2)$$

where

$$d_{13} = \left| \underline{R}_{G3} - \underline{R}_{G1} \right|.$$

The next unit vector is given by

$$\hat{\underline{z}} = S \frac{\hat{\underline{x}} \times \hat{\underline{s}}}{\sin \phi}, \quad (3)$$

where

$$s = +1 \text{ or } -1$$

and

$$\sin \phi = \left[1 - \hat{\underline{x}} \cdot \hat{\underline{s}} \right]^{1/2}.$$

Finally the relationship

$$\hat{\underline{y}} = \hat{\underline{z}} \times \hat{\underline{x}} \quad (4)$$

is employed.

The derivation then begins with Eq. (4), the very last link in the chain.

Writing Eq. (4) in component form and naming the functions we have

$$\begin{aligned}\hat{y}_X &= F_1(\hat{x}_X, \hat{x}_Y, \hat{x}_Z, \hat{z}_X, \hat{z}_Y, \hat{z}_Z) \\ \hat{y}_Y &= F_2(\quad \cdot \quad) \\ \hat{y}_Z &= F_3(\quad \cdot \quad) .\end{aligned}\tag{5}$$

Direct differentiation yields:

$$\delta \hat{y} = M_1 \delta \hat{x} + M_2 \delta \hat{z} ,\tag{6}$$

where the matrices M_1 and M_2 are the Jacobians:

$$\begin{aligned}M_1 &= \frac{\partial F_1, F_2, F_3}{\partial \hat{x}_X, \hat{x}_Y, \hat{x}_Z} \\ M_2 &= \frac{\partial F_1, F_2, F_3}{\partial \hat{z}_X, \hat{z}_Y, \hat{z}_Z} .\end{aligned}\tag{7}$$

Next, consider Eq. (3). In component form these equations can be written as:

$$\begin{aligned}\hat{z}_X &= F_4(\hat{x}_X, \hat{x}_Y, \hat{x}_Z, \hat{s}_X, \hat{s}_Y, \hat{s}_Z) \\ \hat{z}_Y &= F_5(\quad \cdot \quad) \\ \hat{z}_Z &= F_6(\quad \cdot \quad) .\end{aligned}\tag{8}$$

Hence by differentiation

$$\delta \hat{\underline{z}} = M_3 \delta \hat{\underline{x}} + M_4 \delta \hat{\underline{s}} \quad , \quad (9)$$

where

$$M_3 = \frac{\partial F_4, F_5, F_6}{\partial \hat{x}_X, \hat{x}_Y, \hat{x}_Z}$$

$$M_4 = \frac{\partial F_4, F_5, F_6}{\partial \hat{s}_X, \hat{s}_Y, \hat{s}_Z} \quad . \quad (10)$$

Next consider Eq. (1) in component form; i. e.,

$$\hat{x}_X = F_7(X_{G1}, Y_{G1}, Z_{G1}, X_{G2}, Y_{G2}, Z_{G2})$$

$$\hat{x}_Y = F_8(\quad \quad \quad)$$

$$\hat{x}_Z = F_9(\quad \quad \quad) \quad . \quad (11)$$

By differentiation it follows that

$$\delta \hat{\underline{x}} = M_5 \delta \underline{R}_{G1} + M_6 \delta \underline{R}_{G2} \quad , \quad (12)$$

where

$$M_5 = \frac{\partial F_7, F_8, F_9}{\partial X_{G1}, Y_{G1}, Z_{G1}}$$

$$M_6 = \frac{\partial F_7, F_8, F_9}{\partial X_{G2}, Y_{G2}, Z_{G2}} \quad . \quad (13)$$

Lastly, consider Eq. (2). In component form these equations can be written as:

$$\begin{aligned}\hat{s}_X &= F_{10}(X_{G1}, Y_{G1}, Z_{G1}, X_{G3}, Y_{G3}, Z_{G3}) \\ \hat{s}_Y &= F_{11}(\quad \quad \quad) \\ \hat{s}_Z &= F_{12}(\quad \quad \quad) \quad \quad \quad (14)\end{aligned}$$

By differentiation it follows that:

$$\delta \hat{s} = M_7 \delta R_{G1} + M_8 \delta R_{G3} \quad , \quad (15)$$

where

$$\begin{aligned}M_7 &= \frac{\partial F_{10}, F_{11}, F_{12}}{\partial X_{G1}, Y_{G1}, Z_{G1}} \\ M_8 &= \frac{\partial F_{10}, F_{11}, F_{12}}{\partial X_{G3}, Y_{G3}, Z_{G3}} \quad . \quad (16)\end{aligned}$$

At this point the back substitution phase begins. This phase produces matrix equations for partials with respect to the original independent variables, R_{G1} , R_{G2} and R_{G3} .

Referring to Eq. (12) it is evident that M_5 and M_6 provide the required partials

$$\frac{\partial \hat{x}_X, \hat{x}_Y, \hat{x}_Z}{\partial X_{G1}, Y_{G1}, Z_{G1}} \quad \text{and} \quad \frac{\partial \hat{x}_X, \hat{x}_Y, \hat{x}_Z}{\partial X_{G2}, Y_{G2}, Z_{G2}} \quad . \quad (17)$$

Substituting Eq. (12) for $\delta \hat{\underline{x}}$ and Eq. (15) for $\delta \hat{\underline{g}}$ into Eq. (9) and regrouping yields:

$$\begin{aligned} \delta \hat{\underline{z}} = & (M_3 M_5 + M_4 M_7) \delta \underline{R}_{G_1} \\ & + (M_3 M_6) \delta \underline{R}_{G_2} + (M_4 M_8) \delta \underline{R}_{G_3} . \end{aligned} \quad (18)$$

It will be convenient to rename the coefficients of Eq. (18). Thus

$$\delta \hat{\underline{z}} = N_1 \delta \underline{R}_{G_1} + N_2 \delta \underline{R}_{G_2} + N_3 \delta \underline{R}_{G_3} . \quad (19)$$

Obviously, the matrices N_1 , N_2 and N_3 provide the required partials

$$\frac{\partial \hat{z}_X, \hat{z}_Y, \hat{z}_Z}{\partial x_{G_1}, y_{G_1}, z_{G_1}} , \quad \frac{\partial \hat{z}_X, \hat{z}_Y, \hat{z}_Z}{\partial x_{G_2}, y_{G_2}, z_{G_2}} , \quad \frac{\partial \hat{z}_X, \hat{z}_Y, \hat{z}_Z}{\partial x_{G_3}, y_{G_3}, z_{G_3}} . \quad (20)$$

Finally, substituting Eq. (12) for $\delta \hat{\underline{x}}$ and Eq. (19) for $\delta \hat{\underline{z}}$ into Eq. (6) and regrouping yields:

$$\begin{aligned} \delta \hat{\underline{y}} = & (M_1 M_5 + M_2 N_1) \delta \underline{R}_{G_1} \\ & + (M_1 M_6 + M_2 N_2) \delta \underline{R}_{G_2} \\ & + (M_2 N_3) \delta \underline{R}_{G_3} . \end{aligned} \quad (21)$$

Renaming the coefficients results in

$$\delta \hat{\underline{y}} = N_4 \delta \underline{R}_{G_1} + N_5 \delta \underline{R}_{G_2} + N_6 \delta \underline{R}_{G_3} . \quad (22)$$

Obviously, the matrices N_4 , N_5 and N_6 provide the last of the required partials

$$\frac{\partial \hat{y}_X, \hat{y}_Y, \hat{y}_Z}{\partial X_{G_1}, Y_{G_1}, Z_{G_1}}, \quad \frac{\partial \hat{y}_X, \hat{y}_Y, \hat{y}_Z}{\partial X_{G_2}, Y_{G_2}, Z_{G_2}} \quad \text{and} \quad \frac{\partial \hat{y}_X, \hat{y}_Y, \hat{y}_Z}{\partial X_{G_3}, Y_{G_3}, Z_{G_3}} \quad (23)$$

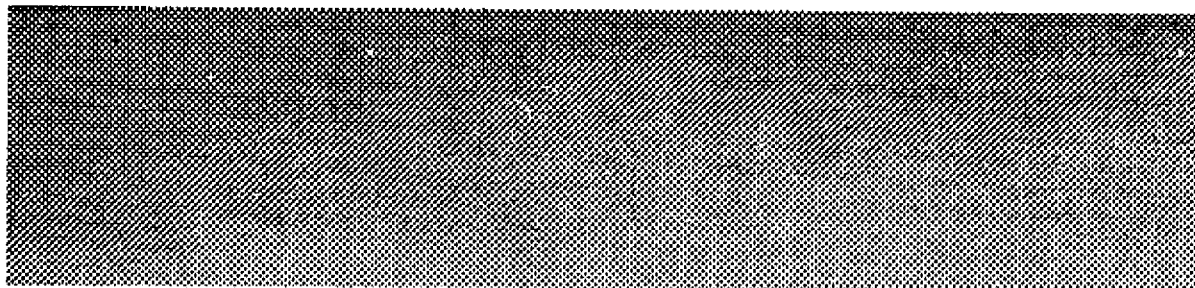
This completes the derivation of the formulas for the partials.

A17.4 MACHINE IMPLEMENTATION OF THE FORMULAS FOR THE PARTIAL DERIVATIVES

The coding of the formulas for the partials is a simple matter. One merely follows the sequence of matrix formulas developed in the back substitution phase, computing as required the M-matrices from formulas derived from actual differentiation of the F-functions with respect to their explicitly appearing arguments. In the example of the foregoing section the steps would be:

- 1) Compute M_5 and M_6 .
- 2) Compute M_7 , M_8 and M_3 , M_4 and combine these with M_5 , M_6 as indicated in Eq. (18) to get the matrices N_1 , N_2 , N_3 .
- 3) Compute the matrices M_1 , M_2 and combine them with M_5 , M_6 and N_1 , N_2 , N_3 as indicated in Eq. (21) to get the matrices N_4 , N_5 , N_6 .

A18. Signal Strength Fluctuations in a Laser Ranging System Due to Optical Interference Between the Many Reflectors on a Vehicle



Abstract

The dynamic range parameter used in pulsed laser ranging systems is discussed with the objective of fixing this parameter for a reflecting system of a large number of individual corner reflectors.

A18.1 INTRODUCTION

An important parameter used in pulsed laser ranging systems is called the dynamic range. Leaving details aside for the present, the dynamic range in a sequence of M pulses emitted by a laser and returned to the receiving system, is simply given by:

$$\text{dynamic range} = \frac{\text{power of strongest returned pulse}}{\text{power of weakest returned pulse}}. \quad (1)$$

Because of interference effects, the pulses reflected from corner reflectors mounted on a satellite will vary in magnitude. In this Appendix the expected variation of pulse size will be calculated. The raison d'etre for performing this calculation is the simple fact that the receiving system, as it is conceived, consists of a photomultiplier (PMT) and a constant fraction timing discriminator (CFTD), and these components experience such variations. In this system the CFTD searches electronically for the complete pulse as generated by the PM.* This search is performed in order to determine at which time the leading edge of the incoming pulse was received. In order to determine this time the dynamic range must be known because when the dynamic range is large, many of the received pulses cannot be handled by the receiving system, i.e., they are lost for use in the process of range determination.

In the following analysis the aim will be to determine the dynamic range for a reflecting system consisting of a large number of individual corner

*The PM becomes saturated, i.e., overloads, at an input level of about 5V.

reflectors [18.1]. The reason is twofold: first, the mathematical complexity is enormously simplified, and second, a large number of corner reflectors signifies a large return signal and therefore weaker laser pulses might be employed. The obvious advantages are: considerably reducing any safety hazards and also reducing the net cost per station. However it will turn out that the dynamic range is too large when the number of corner reflectors is large. Realizing that the dynamic range is just a measure of the interference effects caused by the interplay of the multitude of corner reflectors it is clear that a small number of corner reflectors will bring the dynamic range to acceptable levels.

A18.2 DERIVATION OF THE PROBABILITY DENSITY OF THE RECEIVED POWER

The net signal received at the ground station will be the sum of the signals returned from the ensemble of retroreflectors. Since each retroreflector is at a slightly different distance from the ground station, the signals returned from the ensemble of retroreflectors will all have different phases.* Consequently, the signals from the retroreflectors will constructively and destructively interfere.

In an actual system, the laser transmitter emits a sequence of pulses at a rate of 10 pulses/minute. Since each pulse is extremely short ($<10^{-9}$ seconds), the relative positions of the retroreflectors (and consequently, the relative phases of the reflected signals) will not vary appreciably within the duration of a single pulse. However, the satellite will move a vast number of optical wavelengths between successive pulses. Consequently, the relative phases of the reflected signals will vary drastically from pulse to pulse, and the resulting

*At the light frequency (approximately 10^{14} cycles/sec).

variation in interference effects will cause significant fluctuations in the net received power from pulse to pulse.

A18.3 ANALYSIS

The linearly polarized electric field, E , of the light transmitted from the ground station can be represented as*

$$E_T(t) = k \cos(\omega t), \quad (2)$$

where k is a gain constant and ω is the light frequency. Now consider the light reflected from the i^{th} reflector on the satellite. The E -vector of the light, when received at the ground station, can be represented as

$$E_i(t) = a_i E_T \left(t - \frac{2\rho_i}{c} \right), \quad (3)$$

where a_i is a gain constant, ρ_i is the range between the station and the i^{th} reflector, and c is the speed of light. ** Combining Eqs. (2) and (3) yields

$$E_i(t) = k a_i \cos \omega \left(t - \frac{2\rho_i}{c} \right). \quad (4)$$

*Only the magnitude (not the direction) of the E -vectors in these equations will be considered.

**Throughout this analysis, the following effects are ignored: 1) atmospheric effects upon propagation, and 2) the variation of a_i with range. Since both of these effects will tend to increase the fluctuations of the received signal (as measured over a large number of pulses), the estimate of fluctuations will be conservative.

Since the argument of the cosine can be varied by any integral multiple of 2π without changing the value of the cosine, the value of $2\omega\rho_i/c$ can be replaced by

$$\phi_i = \left[\frac{2\omega\rho_i}{c} \right] \bmod 2\pi. \quad (5)$$

Combining Eqs. (4) and (5) yields the final equation for the E-vector of the light which is reflected from the i^{th} reflector and received at the ground station:

$$E_i(t) = k a_i \cos(\omega t - \phi_i). \quad (6)$$

Since all E-vectors will add algebraically*, if there are N contributing reflectors on the satellite, the net E-vector of the light received at the ground station will be given by

$$\begin{aligned} E_R(t) &= \sum_{i=1}^N E_i(t) \\ &= k \sum_{i=1}^N a_i \cos(\omega t - \phi_i). \end{aligned} \quad (7)$$

*The aperture of the ground station's receiving telescope subtends a miniscule angle as seen from the satellite. Consequently, the light rays which are received from the ensemble of reflectors must be essentially parallel in order to be received. Therefore, all of the E-vectors will lie in the same plane i.e., in the plane perpendicular to the direction of propagation, and the net received light will constitute a plane wave. If all reflected signals are linearly polarized the net received E-vector will be the algebraic sum of the individual E-vectors, and Eq. (7) will be strictly valid. However, since mode-locked ruby lasers emit linearly-polarized light, and since all of the extant satellites employ metal-coated, e.g., aluminized, reflectors which do not appreciably distort the polarization of the incident light, it is reasonable to assume that all reflected signals will be linearly polarized and that Eq. (7) is valid.

The assumption is now made that each reflected signal has the same amplitude (this will be essentially true if all reflectors have the same size and are mounted in the same plane), and therefore Eq. (7) simplifies to

$$E_R(t) = ka \sum_{i=1}^N \cos(\omega t - \phi_i), \quad (8)$$

where each of the various a_i 's have been replaced by the single parameter, a .

In order to determine the probability densities of the amplitude and power of the net received signal, it will be necessary to specify the probability densities of the ϕ_i 's. First note that Eq. (5) can be rewritten as:

$$\phi_i = \left[\frac{4\pi\rho_i}{\lambda} \right]_{\text{mod } 2\pi}, \quad (9)$$

where λ is the wavelength of the light. Since λ will have a typical value of about 7×10^{-5} centimeters, i.e., about 7000 Å, even slight changes in ρ_i (the range between the station and the i^{th} reflector) can cause large changes in $4\pi\rho_i/\lambda$. Since ϕ_i is equal to the value of $4\pi\rho_i/\lambda$ taken mod 2π , the various ϕ_i 's will assume essentially random values from pulse to pulse.* In particular:

- a) the value of ϕ_j during one pulse will be independent of the value of ϕ_j during all preceding pulses (where j is any integer from 1 to N), and
- b) the values of all ϕ_i 's will be independent of each other during any one pulse.

*The relationship between ρ_i and ϕ_i is analogous to the relationship between x and y , where y is the 10th significant figure of $\log x$. In general, even if a succession of x values has a definite pattern, the corresponding succession of y values will be essentially random.

Now consider the random process which consists of a large number of successive received pulses. In this process, each of the ϕ_i 's will represent a random variable, i.e., each ϕ_i will assume random values from pulse to pulse. Since each ϕ_i is equally likely to have any value from 0 to 2π , the probability density of each ϕ_i will be:

$$p(\phi_i) = \frac{1}{2\pi} ; 0 \leq \phi_i \leq 2\pi .$$

Furthermore, since the various ϕ_i 's are independent, the joint probability density of the ϕ_i 's will equal the product of the individual probability densities, viz.,

$$p(\phi_1, \phi_2, \dots, \phi_N) = p(\phi_1) p(\phi_2), \dots, p(\phi_N) .$$

Equation (8) shows that the net received E-vector is proportional to the sum of N sinusoids which have the same amplitude and frequency but different phases. The remaining problem consists in determining the probability distribution of the electric field Eq. (8) and that of its power. According to the foregoing assumptions the probability of $E_R(t)$ having the value E is given by the phase space available to all random variables ϕ_i subject to the condition:*

$$E = \frac{1}{\sqrt{N}} \sum_{i=1}^N \cos(\omega t - \phi_i) . \quad (10)$$

*Equation (10) is conveniently normalized by the number N of corner reflectors to ease a subsequent passage to a large number of such reflectors. Note that E is a normalized electric field.

Taking into account condition (10), the probability density of $E_R(t)$, can then be written as

$$P(E, t) = (2\pi)^{-N} \int_0^{2\pi} \prod_n d\phi_n \delta \left[E - \frac{1}{\sqrt{N}} \sum_1^N \cos(\omega t - \phi_i) \right], \quad (11)$$

where $\delta(x)$ is the Dirac δ -function.*

The integral (11) can be evaluated with the help of the integral representations of the δ -function and the Bessel function**, yielding:

$$P(E, t) = \frac{1}{2\pi} \int_{-\infty}^{\infty} e^{iEy} \left[J_0 \left(\frac{y}{\sqrt{N}} \right) \right]^N dy, \quad (12)$$

*The δ -functions in Eq. (11) may be thought of as the conditional probability density that $E_R(t)$ will have the value of E , given the values of $\phi_1, \phi_2, \dots, \phi_N$. Hence, the probability that $E_R(t)$ will have any value is given by

$$\int_{-\infty}^{\infty} \delta \left[E - \frac{1}{\sqrt{N}} \sum \cos(\omega t - \phi_i) \right] dE = 1,$$

which is consistent with the definition of the δ -function.

**These integral representations are as follows:

$$\delta(y) = \frac{1}{2\pi} \int_{-\infty}^{\infty} dx e^{ixy}$$

and

$$J_0(y) = \frac{1}{2\pi} \int_0^{2\pi} d\theta e^{iy \cos \theta}$$

These formulas can be looked up in any handbook, e. g., [18.3]

where J_0 is the Bessel function of zero order. Equation (12) determines the instantaneous probability density of expression (11) and is seen to be time independent. The determination of the probability for the instantaneous electric field given in Eq. (12) is not yet quite what is needed. The PM tube responds to the average power* W rather than to the instantaneous electric field. The derivation for the probability density of the average power W is somewhat more involved but follows strictly along the same lines as the derivation given above. This is amply explained in [18.2] and [18.3]. For the sake of brevity and for the simple reason that essentially no additional physical insight is gained from a straightforward but tedious derivation, the result will merely be quoted, namely, the probability density for the average power W is given by:

$$P(W) = \int_0^\infty J_0(y\sqrt{2W}) \left[J_0\left(\frac{y}{\sqrt{N}}\right) \right]^N y \, dy \quad (13)$$

for a large number of corner reflectors, N . Expanding the Bessel function, results in

$$P(W) \sim 2e^{-2W} \quad (14)$$

This equation shall be used in the subsequent analysis.

A18.4 PROBABILITY DISTRIBUTION OF THE DYNAMIC RANGE

The probability distribution of the dynamic range of a sequence of M pulses will now be derived.

Let the following definitions be introduced:

$v \equiv$ power of the strongest pulse in a sequence of M pulses, **

*Averaged over the period of the carrier wave.

**Throughout this analysis, we will assume that $M > 2$.

$u \equiv$ power of the weakest pulse in a sequence of M pulses.

$g_M(u, v) \equiv$ joint probability density of u and v .

Since the power of each pulse in the sequence has a probability density of $P(W)$, then:

$P(u) du =$ probability that any one pulse will have a power between u and $u + du$,

$P(v) dv =$ probability that any one pulse will have a power between v and $v + dv$,

$\int_u^v P(W) dW =$ probability that any one pulse will have a power between u and v ,

There are M possible choices for the weakest pulse, $M-1$ possible choices for the strongest pulse (after the weakest pulse has been chosen), and $M-2$ pulses whose powers have to lie between u and v in order for u and v to respectively correspond to the powers of the weakest and strongest pulses. Thus.

$M P(u) du =$ probability that the weakest pulse will have a power between u and $u + du$,

$(M-1)P(v) dv =$ probability that the strongest pulse will have a power between v and $v + dv$ (after the weakest pulse has been chosen),

$\left[\int_u^v P(W) dW \right]^{M-2} =$ probability that $M-2$ pulses have power between u and v (assuming that the pulses are statistically independent).

Since the definition of $g_M(u, v)$ shows that,

$g_M(u, v) du dv$ = probability that, in a sequence of M pulses, the power of the weakest pulse lies between u and $u + du$, while the power of the strongest pulse lies between v and $v + dv$, and since the pulses are statistically independent, it therefore follows that:

$$g_M(u, v) du dv = [MP(u) du] [(M-1)P(v) dv] \left[\int_u^v P(W) dW \right]^{M-2}. \quad (15)$$

Combining Eqs. (14) and (15) shows that, when the probability density of power in a single pulse is given by (14), the joint probability density described by $g_M(u, v)$ becomes:

$$g_M(u, v) = 4M(M-1) \exp \left\{ -2[(M-1)u + v] \right\} \left\{ 1 - \exp[-2(v-u)] \right\}^{M-2}. \quad (16)$$

A18.5 PROBABILITY THAT THE DYNAMIC RANGE OF THE SEQUENCE OF M PULSES WILL BE $\geq k$.

Let $P_M(k)$ be the probability that the dynamic range of a sequence of M pulses will be $\geq k$. Then, using the definition of $g_M(u, v)$ given above:

$$P_M(k) = \text{Prob}(v \geq ku) = \int_0^\infty \int_{ku}^\infty g_M(u, v) dv du \quad ; \quad k \geq 1^*. \quad (17)$$

*Note that k must be ≥ 1 since we have assumed in the derivation of $g_M(u, v)$ that v is $\geq u$. Specifically, it is assumed that v is the power of the strongest pulse and u is the power of the weakest pulse.

The integral (17) can be evaluated and after some admittedly tedious algebra and yields the result:

$$P_M(k) = 1 - \frac{1}{\underbrace{\left(1 + \frac{M}{M-1} \Delta\right) \left(1 + \frac{M}{M-2} \Delta\right) \dots (1 + M\Delta)}_{M-1 \text{ Terms}}}, \quad (18)$$

where $\Delta = (k-1)^{-1}$. Equation (18) is displayed in Fig. A18.1 with M as a parameter.

A18.6 CONCLUSIONS

The receiving system can handle a ratio $k = 50$ efficiently. However, as seen from Fig. 18.1 for a series of 100 pulses, the dynamic range k is twice as much with essentially unit probability.* This of course means that the pulse rejection rate is high. It must be remembered however that Fig. A18.1 is based on the simplifying premise of assuming a large number of corner reflectors. This assumption is tantamount to saying that interference effects are particularly severe. The use of a minimum number of corner reflectors is therefore a logical conclusion.

*This is just the dynamic range of Beethoven's 5th Symphony during the transition from the second to the third movement.

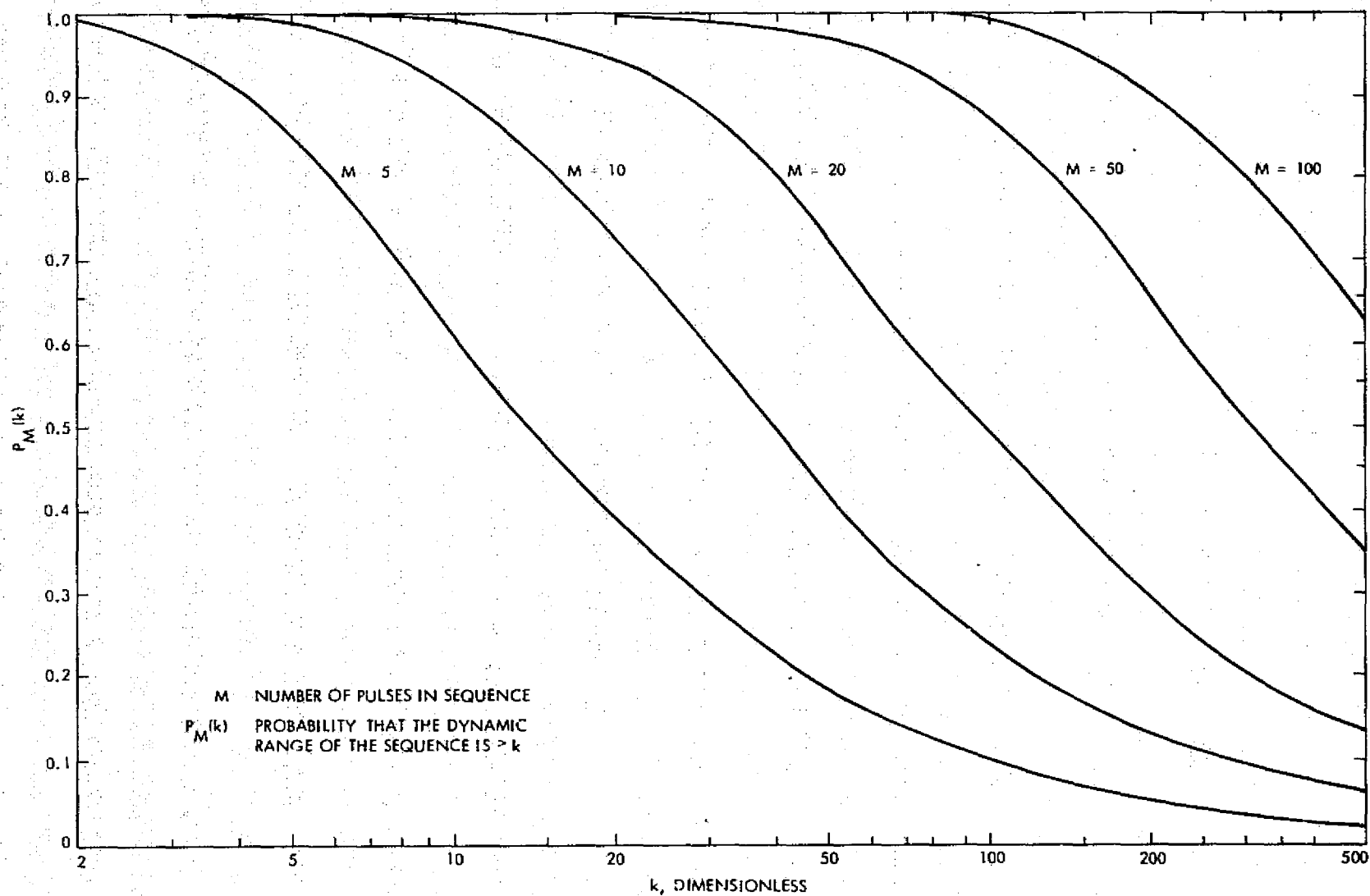
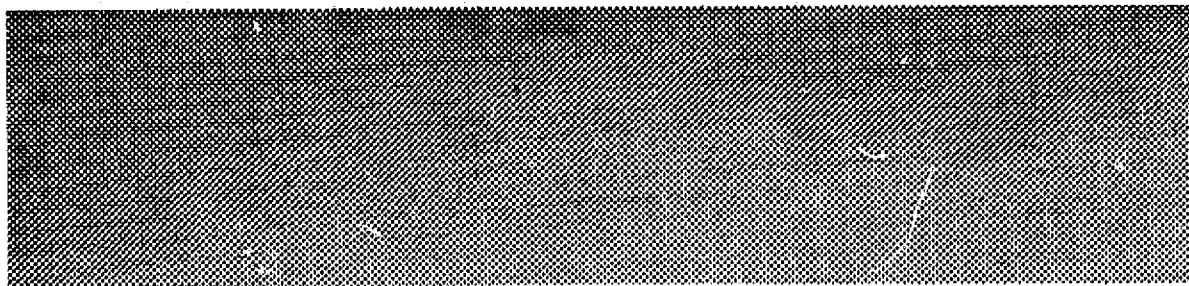


Fig. A18.1. Probability Distribution of Dynamic Range

A18.7 REFERENCES

- [18.1] Jaffe, R. M., "Signal Strength Fluctuation in a Laser Ranging System Due to Optical Interference Between the Many Reflectors on a Satellite," JPL TM 391-218, 28 July 1971 (JPL internal document).
- [18.2] Slack, M., "The Probability Distributions of Sinusoidal Oscillations Combined in Random Phase," Journal of the Institution of Electrical Engineers, Vol. 93, No. 22 (England), pp. 76-86.
- [18.3] Magnus, A. W., Oberhettinger, F., and Soni, R. P., Formulas and Theory for the Special Functions of Mathematical Physics, Springer Verlag, New York, 1966.

A19. Laser Pulse Shape Degradation By Multiple Reflection From Corner Reflectors Mounted On A Satellite



Abstract

The change of a rectangular laser pulse upon reflection from an array of retroreflectors is analyzed by means of a simplified model. It is demonstrated that interference effects will degrade returned pulses and that the use of a small number of corner reflectors will be required to overcome such inherent difficulties.

A19.1 INTRODUCTION

Appendices A19 and A18 consider pulse shape degradation and pulse height degradation due to interference effects from multiple retroreflectors. It will be shown that for a large number of reflectors the interference effects will degrade the returned pulse, both in dynamic range (See Appendix A18) and in pulse shape (Appendix A19) to unacceptable levels. The analysis will indicate the need to use a small number of corner reflectors.

In this Appendix the change of a rectangular laser pulse upon reflection from an array of retroreflectors will be analyzed via a simplified model. A numerical calculation for a typical set of parameters will also be presented.

A19.2 ANALYSIS

Suppose the corner reflectors are mounted uniformly and radially on a spherical satellite; i.e., the reflectors are positioned equidistantly along a circle facing radially outward so that the angle subtended by the two lines emerging from the center of any two adjacent reflectors joining the center of the spherical satellite is a constant angle θ_0 (See Figure A19.1).

Next consider a ruby laser light pulse of frequency $\nu = 4.3 \cdot 10^{14} \text{ sec}^{-1}$ which is conveniently expressed analytically in an arbitrary coordinate system as:

$$A(t) = [S(\underline{k} \cdot \underline{r} - \omega t) - S(\underline{k} \cdot \underline{r} - \omega t - T)] \cos (\underline{k} \cdot \underline{r} - \omega t), \quad (1)$$

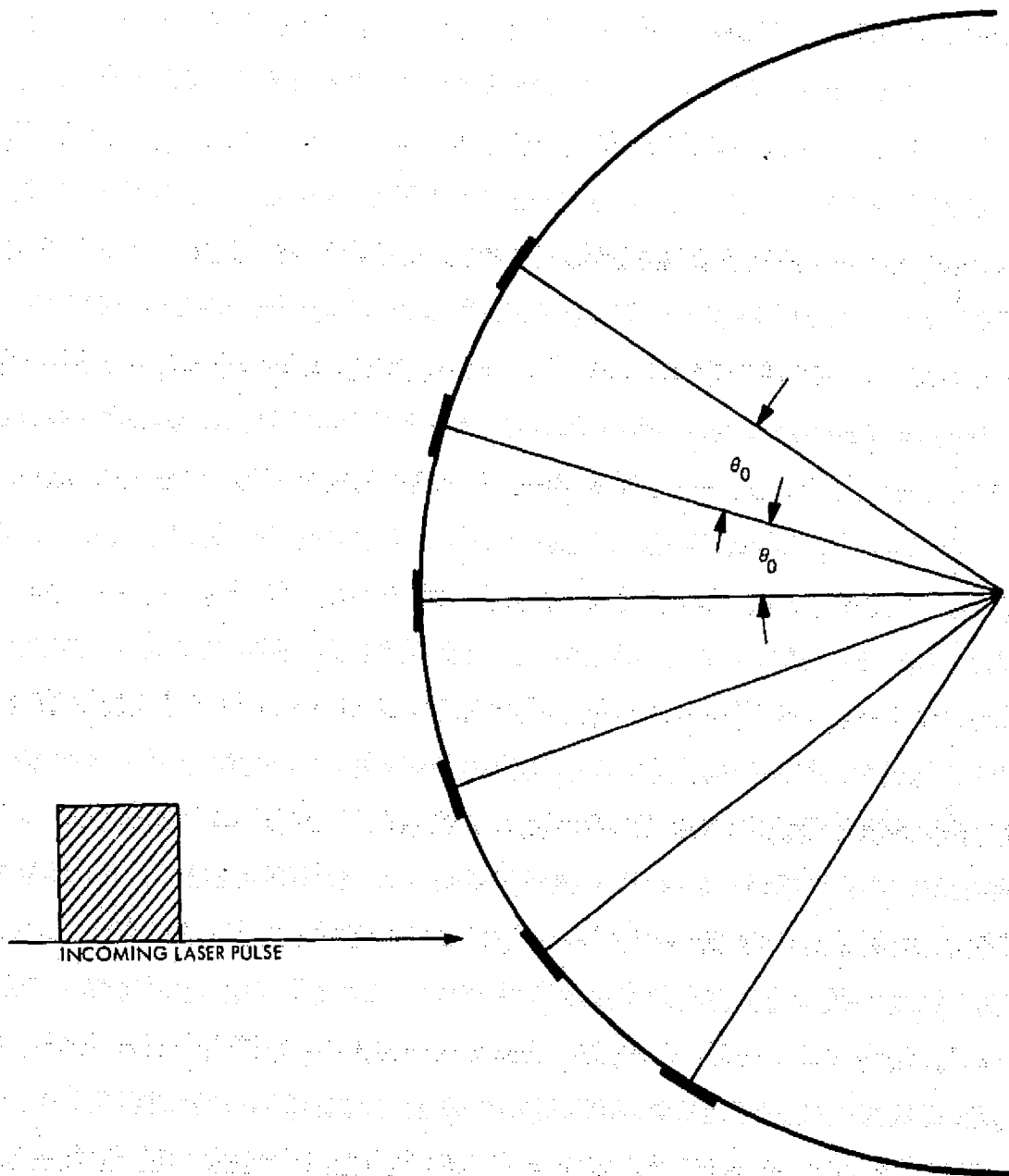


Fig. A19.1. Reflectors Mounted on Spherical Satellite

where A is the amplitude of the electric field, \underline{k} is the propagation vector, T is the pulse duration (assumed equal to $2 \cdot 10^{-9}$ sec), and S is the step function defined by:

$$S(x) = \begin{cases} 1 & \text{if } x > 0 \\ 0 & \text{if } x < 0 \end{cases} \quad (2)$$

The light pulse (Eq. (1)) subject to the previously described reflector model, will therefore be reflected by the arrangement of mirrors. Assuming that the incoming light strikes one reflector normally, all the other reflectors will receive the light under a slant angle governed by θ_0 . The intensity of the back scattered light is sensitive to the angle θ between the axis of the reflector and the direction of the incoming light beam.

It can be shown that, for reflectors currently in use, the amplitude of the reflected light may be expressed by:

$$A = e^{-\frac{\theta_0}{\alpha}} \quad (3)$$

with $\alpha = 16^\circ$. The reflected light may now be expressed easily in a coordinate system centered at the center of the spherical satellite, viz:

$$A(t) = \sum_{n=0}^N \left[S\left(t + \frac{r}{c} \cos n\theta_0\right) - S\left(t + \frac{r}{c} \cos n\theta_0 - T\right) \right] \cdot \cos\left(\omega \frac{r}{c} \cos n\theta_0 - \omega t\right) e^{-\frac{n\theta_0}{\alpha}} \quad (4)$$

where r is the radius of the sphere and the summation index runs over all corner reflectors.

Since the receiving photo multiplier is sensitive only to power, and since the inverse frequency ν^{-1} is much smaller than the pulse length, a time averaging can be performed over the period of the carrier wave, i.e., over the high frequency component. Hence, from Eq. (4)

$$2P(t) = \left\{ \sum_n \left[S\left(t + \frac{r}{c} \cos n\theta_o\right) - S\left(t + \frac{r}{c} \cos n\theta_o - T\right) \right] e^{-\frac{n\theta_o}{\alpha}} \cos\left(\omega \frac{r}{c} \cos n\theta_o\right) \right\}^2 + \left\{ \sum_n \left[S\left(t + \frac{r}{c} \cos n\theta_o\right) - S\left(t + \frac{r}{c} \cos n\theta_o - T\right) \right] e^{-\frac{n\theta_o}{\alpha}} \cdot \sin\left(\omega \frac{r}{c} \cos n\theta_o\right) \right\}^2 \quad (5)$$

where $P(t)$ is the instantaneous power in the received signal.

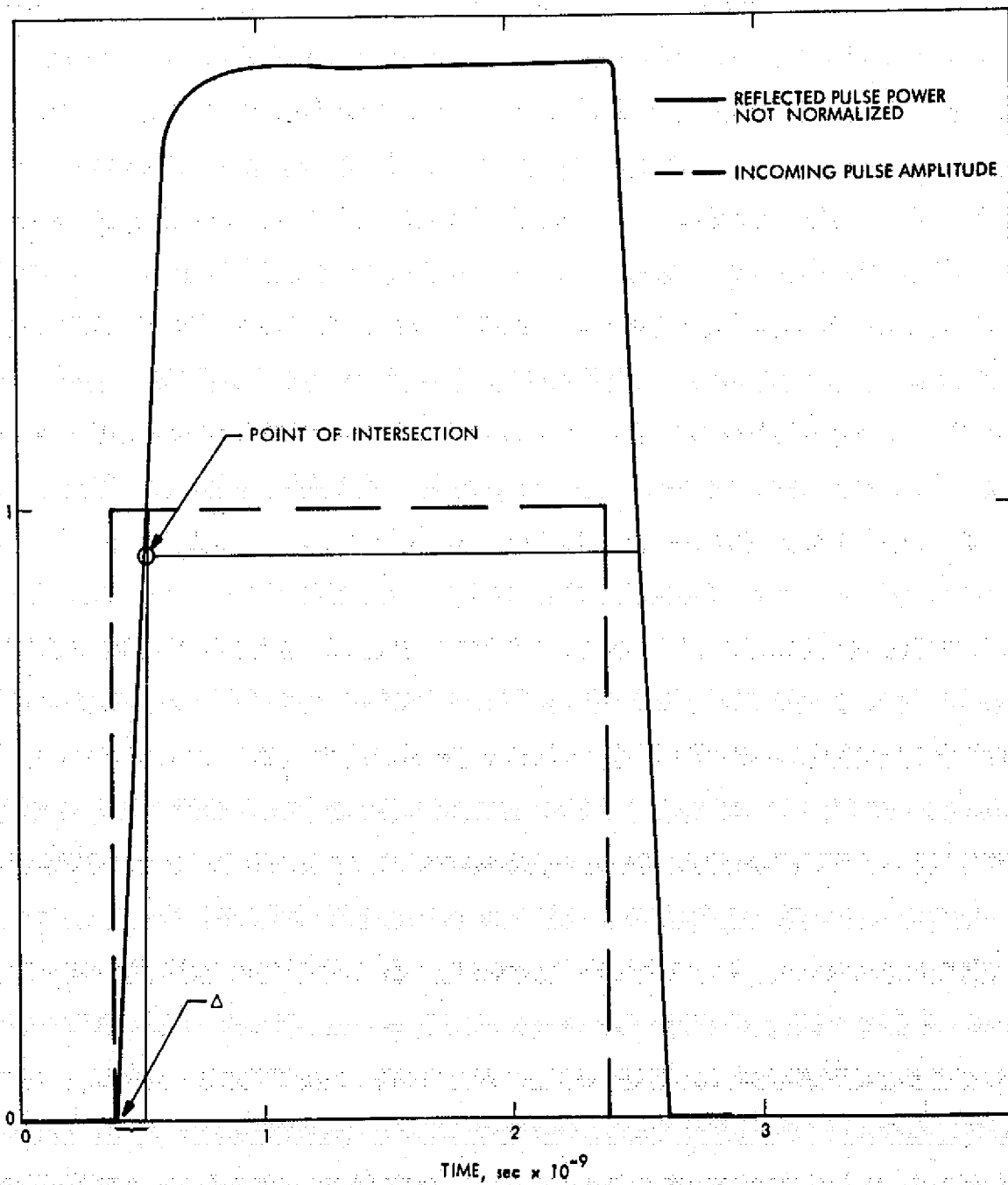
A19.3 TYPICAL RESULTS

Figure A19.2 displays a graph of Eq. (5) for the following set of parameters: $T = 2 \cdot 10^{-9}$ sec, $r = 1$ m, $\omega = 2.84 \cdot 10^{15}$ sec $^{-1}$ and $\theta_o = 5^\circ$. Although only one set of parameters was used, albeit a typical one, it is clearly seen that the pulse shape degradation is significant. As is seen from Fig. A19.2 the leading edge of the reflected pulse is shifted somewhat in time. The constant fraction timing discriminator employed in the receiving electronics integrates the pulse, determines the half width, and decides on the arrival time by selecting the particular point on the leading edge which corresponds to the half width. For the parameters chosen, it is clearly seen from

Fig. A19.2 that the arrival time determined in this manner is late by $1/8 \times 10^{-9}$ sec; this corresponds to about 4 cm.* This of course is unacceptable for a system which purports to be accurate to the centimeter level.

On the other hand, a shortening of the pulse would eventually create a separate return from each reflector, and therefore a series of individual but weaker pulses would be obtained. Again this is unacceptable since it would confuse the receiving electronics. Here, as well as in Appendix A18, the necessity of a small number of corner reflectors is demonstrated.

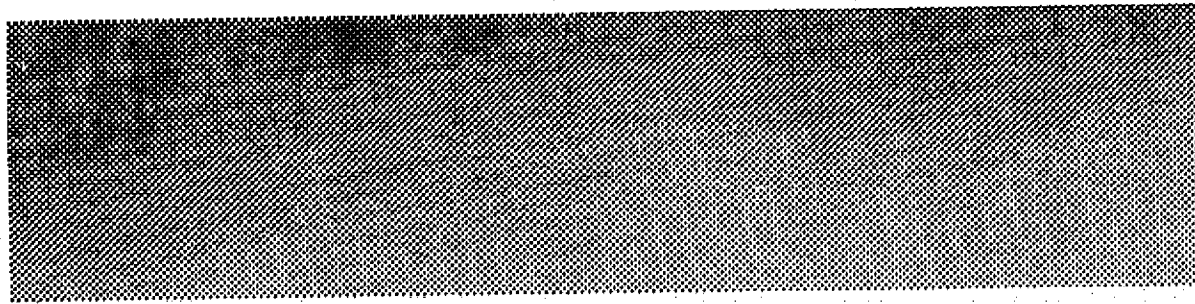
*See Δ in Fig. A19.2



ORIGINAL PAGE IS
OF POOR QUALITY

Figure A19.2. Pulse Shapes

A20. Aberration and Fresnel Diffraction



Abstract

The angular shift experienced by a reflected laser beam is analyzed in this Appendix. Increases in beam-width of the corner reflector required such that reflected light returns to the ground station are examined.

PRECEDING PAGE BLANK NOT FILMED

A20.1 INTRODUCTION

The need for a compact corner reflector has been demonstrated in Appendices A18 and A19. Accordingly, the reflected light will consist of a narrow (~5 cm) diffraction limited beam. Furthermore, it is well known that the reflected beam will also suffer an angular shift due to the motion of the satellite. This angular shift is called aberration and its value, α , is:

$$\alpha = 2 \frac{v}{c}, \quad (1)$$

where α is in radians and v is the velocity component of the satellite perpendicular to the line of sight. The factor 2 is due to the fact that reflected light rather than emitted light is being considered.

Since satellites in circular orbits of from 500 to 1000 km have relative velocities approximately equal to 7.5 km/sec, the maximum value of angular shift when ranging to these satellites is

$$|\alpha| = \frac{2v}{c} = \frac{2 \times (7.5 \times 10^3)}{3 \times 10^8} = 50 \text{ } \mu\text{radians} = 10 \text{ arcsec} \quad (2)$$

This amount of angular shift is about 5 times the diffraction-limited beamwidth of a 5 cm corner reflector at ruby-laser wavelengths. Consequently if this size corner reflector is needed (in order to obtain sufficient capture area), the beamwidth of the corner reflector must be increased in order to cause a usable amount of reflected light to return to the ground station.

One way of ameliorating the situation is to artificially widen the beam by means of a divergent lens or by rounding off appropriately the faces of the

reflector. The following analysis is a preliminary study of this problem using cylindrically symmetric apertures.

The equation governing the diffraction pattern as depicted on Fig. A20.2 is derived in Sommerfeld's lectures on theoretical physics*. However, before going into a detailed analysis of the diffraction pattern corresponding to Fig. A20.2 a connection between Fig. A20.1 and A20.2 must be established. Figure A20.1 shows a corner reflector. A diverging lens has been placed in front of the corner reflector. The purpose of this lens is simply to make the reflected beam sufficiently divergent so that the receiving telescope, which incidentally is also the transmitting telescope, does not have to be aimed at a different angle upon receiving the returned pulse. To repeat, the aberration is an angular deviation of about $5 \cdot 10^{-5}$ radians assuming a satellite velocity of about 7 km/sec. This angular deviation is sufficient so that a telescope transmitting a laser pulse will not be able to receive the pulse back unless the telescope is aimed at the new direction. This is very difficult to accomplish. Obviously, the alternative is to widen the reflected beam sufficiently to overcome the problem.

A20.2 ANALYSIS

In order to analyze this problem proceed from Fig. A20.1 to Fig. A20.2. Figure A20.2 shows (in cross section) a circular aperture illuminated by a point source at position S. The object here is to determine the far field diffraction pattern [$R \rightarrow \infty$ in Fig. A20.2]. The light source at S (Fig. A20.2) is just a replica of the virtual focal point of Fig. A20.1. The problem as stated in Fig. A20.1 can therefore be transposed to the configuration depicted in Fig. A20.2 and it is then amenable to mathematical analysis.

*Sommerfeld A., Optik, Dieterich'sche Verlagsbuchhandlung, Germany, 1950.

The analysis starts with Kirchoff's Integral:

$$U(P) = -\frac{iA}{2} \iint dS \frac{e^{ik(r+s)}}{rs} [\cos(n, r) - \cos(n, s)] . \quad (3)$$

Most symbols are amply explained by merely scrutinizing Fig. A20.2. The other quantities are defined as follows: A is the strength of the source [the focal point of Fig. A20.1]. The wave length, λ , of the radiation which is assumed to be monochromatic. The angles (n, r) and (n, s) are clearly defined in Fig. A20.2. A number of assumptions are now made: 1) the radius of the circular aperture a is 2.5 cm, 2) the distance r_0 of the focal point from the aperture is large compared to its radius a, and 3) the distance R between the aperture and the observation plane is essentially infinite. Therefore it follows that to a high degree of accuracy:

$$\cos(n, r) = 1 \quad , \quad \cos(n, s) = -\cos \alpha . \quad (4)$$

Since the aperture of radius a is symmetrical about the z-axis it suffices to contemplate Fig. A20.2. Let ξ and η be the integration variables corresponding to x and y inside the aperture ($z = 0$). The location of S, the focus of the lens off the center axis, is

$$S = (-x_0, 0, -r_0) \quad (5)$$

The location of P is

$$P = (\tan \alpha R, 0, R) \quad (6)$$

ORIGINAL PAGE IS
OF POOR QUALITY

Therefore:

$$r = \left[r_o^2 + (\xi + x_o)^2 + \eta^2 \right]^{1/2} \doteq r_o + \frac{\eta^2 + \xi^2}{2r_o} + \frac{\xi x_o}{r_o} . \quad (7)$$

If x_o is not small, then:

$$r = r_o + \frac{\delta^2}{2r_o} + \frac{\xi x_o}{r_o} - \frac{\xi x_o \delta^2}{2r_o^3} , \quad x_o \ll r_o$$

and

$$s = \left[R^2 + \eta^2 + (R \tan \alpha - \xi)^2 \right]^{1/2} = R (\cos \alpha)^{-1} - \xi \sin \alpha , \quad (8)$$

where $R \rightarrow \infty$ (far field).

Let:

$$\xi^2 + \eta^2 = \delta^2 , \quad \xi = \delta \cos \phi \quad (9)$$

so that upon omitting all irrelevant phase factors:

$$U(P) \sim \frac{A}{2\lambda} \frac{1 + \cos \alpha}{R r_o} \cos \alpha \int ds \exp \left\{ -ik \xi \sin \alpha + ik \frac{\delta^2}{2r_o} + i \frac{x_o k}{r_o} \cos \phi \right\} . \quad (10)$$

Letting

$$\lim_{R \rightarrow \infty} \frac{A}{R} \rightarrow B$$

and omitting all factors which vary slowly with α in the neighborhood of $\alpha \approx 10^{-4}$ radians, it follows that:

$$U(P) \sim \int_0^a \delta d\delta \int_0^{2\pi} d\phi \exp \left\{ ik \frac{\delta^2}{2r_o} \right\} \exp \left\{ ik \delta \cos \phi \left(\sin \alpha - \frac{x_o}{r_o} \right) \right\}. \quad (11)$$

Equation (11) can be written immediately with the use of Bessel function representations as:

$$U(P) \sim \int_0^a \delta d\delta \exp \left(i \frac{k\delta^2}{2r_o} \right) J_0 \left[k\delta \left(\sin \alpha - \frac{x_s}{r_o} \right) \right] \quad (12)$$

Equation (12) is true for large values of r_o (the focal length of the lens).

Hence, it is seen that the diffraction pattern is just shifted by the amount x_o/r_o . This amount is a small number considering that r_o is of the order of hundreds of meters.

A20.3 TYPICAL RESULTS

For the case in point x_o/r_o therefore can be neglected.

Figure A20.3 has been computed with values of the pertinent parameters, given by

$$ka = 2 \cdot 10^5, \quad r_o = 250 \text{ m}, 500 \text{ m}, 1000 \text{ m}, \text{ and } \infty.$$

The scale is normalized to the intensity P_o of the far field center line diffraction pattern without a lens ($r_o = \infty$) and is plotted in db $\left(db = 10 \log \left[\frac{P}{P_o} \right] \right)$.

It is usual to call the case $r_o = \infty$ Fraunhofer diffraction since the incoming light is a plane wave. The other cases deal with spherical waves and are called Fresnel diffraction; hence the caption on Fig. A20.3. Figure A20.3

depicts the four cases just mentioned. Because of the rapid fluctuations and the wide spacing of the computed values, at least for the case $r_0 = \infty$, it was not possible to actually draw a curve through the black dots representing the Fraunhofer case of Fig. A20, 3. Indicated on the abscissa of Fig. A20, 3 are the first three zeros of the $r_0 = \infty$ pattern. It is seen that (at least for the aperture and wave length used here) the third zero appears in the neighborhood of 50 μ radians. This is the critical angle for aberration, so that the beam cannot be seen by the receiving telescope. The other cases shown, although there are no nulls, are down in power by at least two orders of magnitude in the critical region around 50 μ radians. This, however, constitutes sufficient intensity to be successfully processed by the receiver.

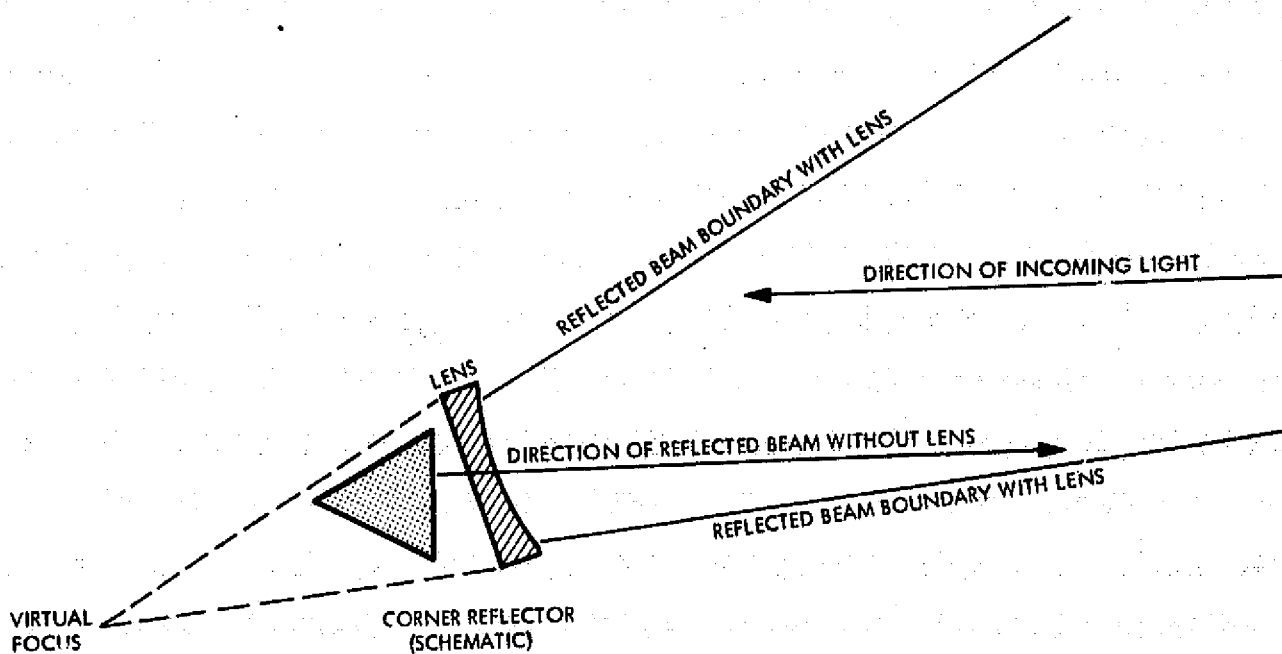


Figure A20.1. The Idealized Configuration for the Optical System Consisting of a Corner Reflector and a Beam Spreading Lens

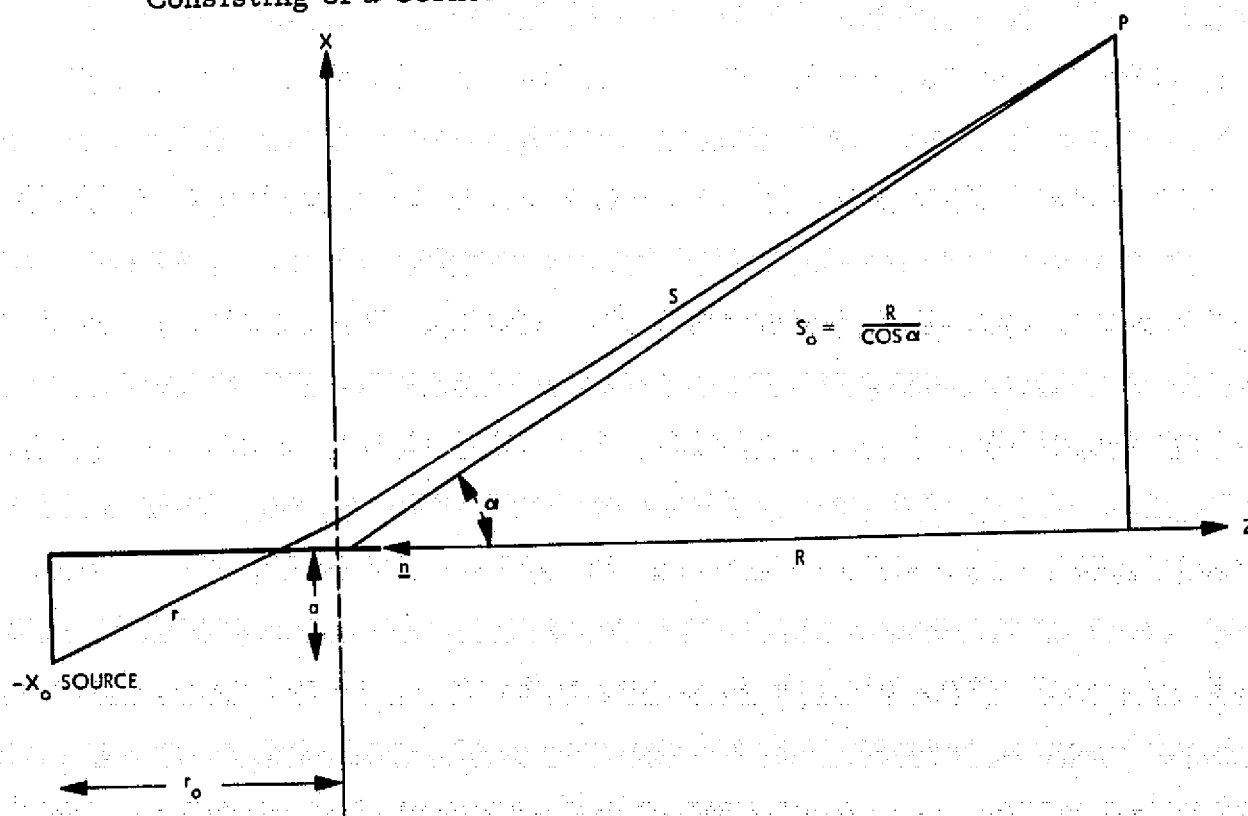
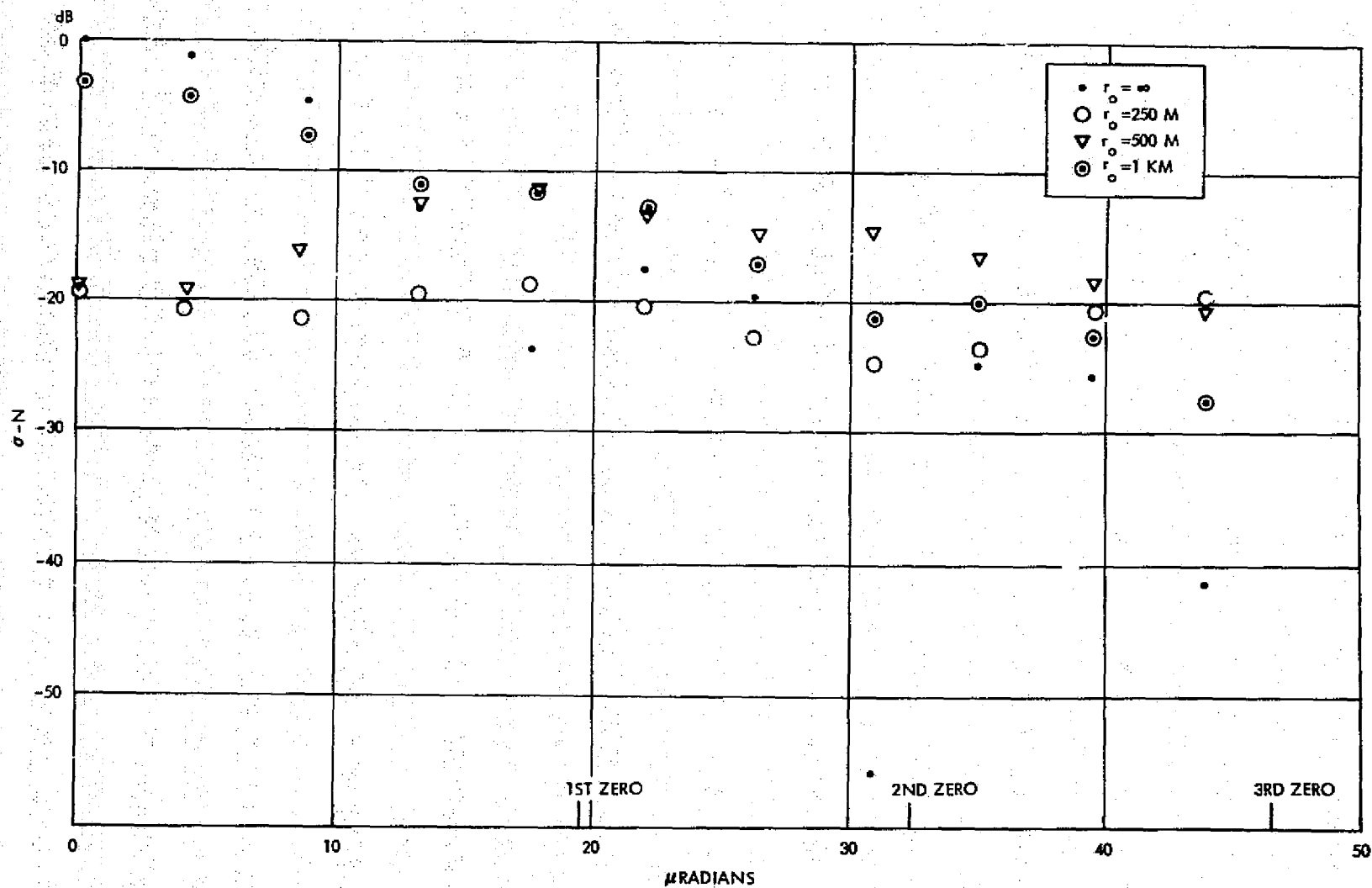
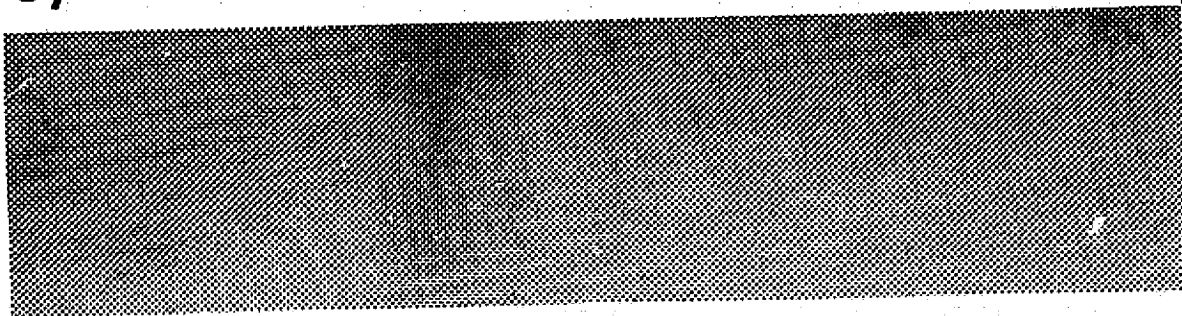


Figure A20.2. The Mathematical Model Simulating Fig. A20.1. Source is the virtual focus of the lens on Fig. A20.1. The corner reflector is simulated by a circular aperture of radius a . The far field diffraction pattern is calculated by standard means.

Figure A20.3. Fraunhofer ($r_o = \infty$) and Fresnel Diffraction. Explanations in the text

A21. Multibaseline: A Three-Dimensional Precision Geodetic Measurement System Not Using Airplanes or Data Synchronization



ORIGINAL PAGE IS
OF POOR QUALITY

Abstract

A geometric measurement system called Multibaseline is introduced. The system can be used to determine three-dimensional interstation coordinates in areas of geodetic interest. It is shown that station horizontal coordinates can always be determined to subcentimeter accuracy using one or two color geodolites as the fundamental measuring devices. For moderate topographic relief, about 75 meters, it is demonstrated that a two-color geodolite can be used to determine station out-of-plane coordinates to accuracies of one centimeter over baselines extending from 1 to 10 kilometers. It is shown that in a given station constellation only one station needs to be out of the plane in order to permit determination of the remaining out-of-plane coordinates. Next the equivalence between a static multilateration system and the multibaseline system is established. For terrain possessed of virtually no topographic relief, i.e., less than 75 meters in 10 km, the concept of hybrid multilateration is discussed as a backup system. Finally a discussion on extending local networks to wider monitoring grids is presented and the conclusions reached herein are summarized.

PRECEDING PAGE BLANK NOT FILMED

A21.1 INTRODUCTION

At the present time considerable interest exists in developing a viable measurement system capable of determining three-dimensional interstation coordinates to one centimeter accuracy. Multilateration [21.1] is certainly a system which ultimately will be able to reach these threshold accuracies. Multilateration uses the principle of simultaneous range measurements taken from an ensemble of ground stations to a vehicle, i. e., to a satellite or airplane, so that the determination of the three-dimensional coordinates can be carried out. For local or short baseline estimation an airplane system, i. e., an airplane used in the multilateration framework, can be structured along the lines of development discussed in [21.2], [21.1]. For global multilateration a satellite structured system appears to be the only viable geometric procedure. Actually, even for a local network (5 to 300 kilometer baselines), use of a satellite will probably yield the same coordinate resolution accuracies, e. g., for a six station multilateration system using satellites, capable of one centimeter coordinate resolution, it would seem that addition of new stations positioned a few kilometers distant would permit multilateration to be performed again and thus the difference between the two solutions would appear to have inherent accuracies of one centimeter.

Jet Propulsion Laboratory has been involved in these advanced multilateration studies. During these system investigations it became apparent that baseline measurements, i. e., the direct measurement of the distance between stations also could be used to obtain the three-dimensional interstation coordinates to high precision without relying on either airplanes or satellites. The process of measuring the baselines over, e. g., ten kilometer distances without imposing the constraint of data simultaneity is called multibaseline. This process, along with various extensions, is addressed in this paper.

For example consider the geometry and terrain displayed in Figure A21.1 wherein a geodolite is being used to measure the interstation baselines. Here

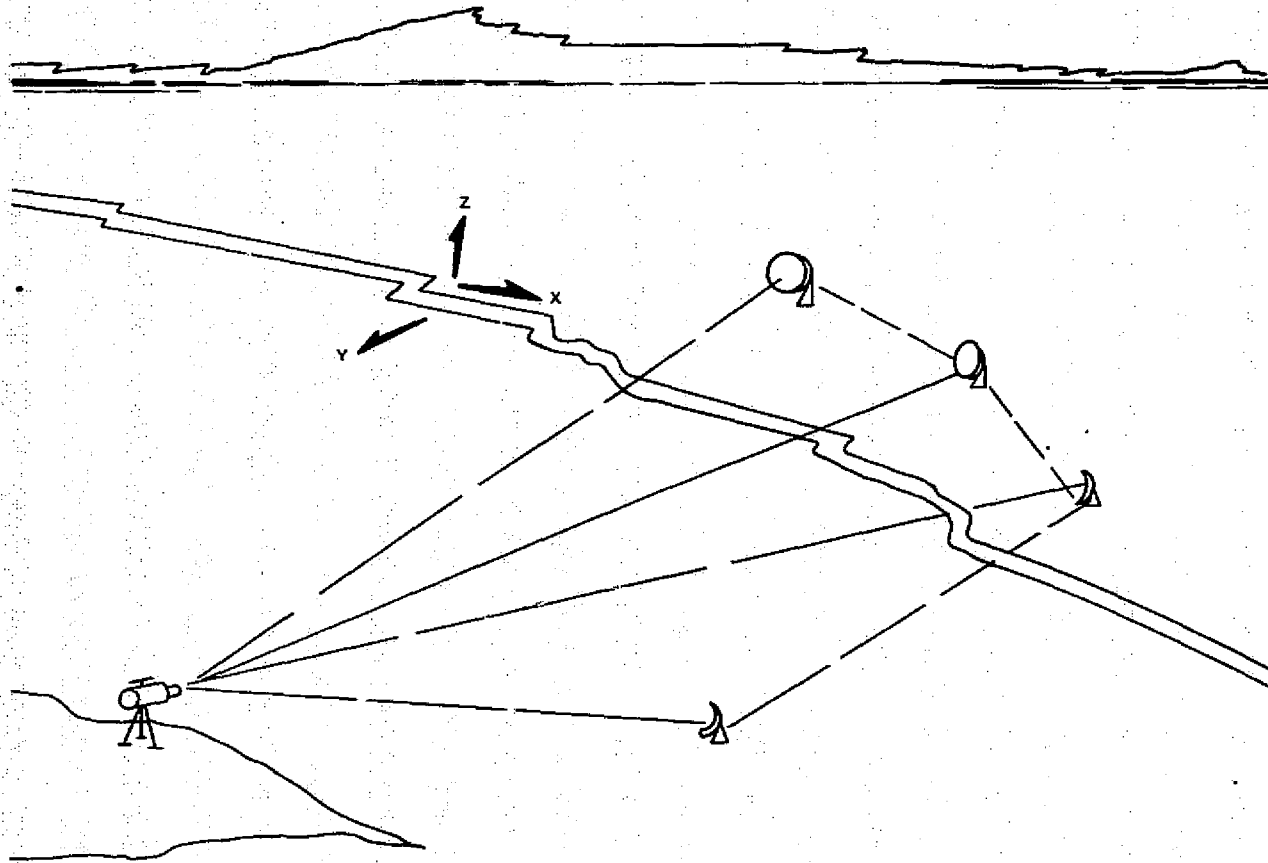


Figure A21.1 Multibaseline System

a cluster of four stations is depicted on a terrain possessed of natural topographic relief. Moderate relief is common in many areas of the world and is the key in making the multibaseline system capable of resolving the interstation three-dimensional coordinates to accuracies approaching 1 or 2 cm with presently existing range measurement tools.

These measurement tools are one- or two-color laser geodolites. Presently over short baselines (1 - 6 km) one-color geodolites are capable of 1/3 cm measurement accuracies. Two-color systems (currently in operation at places such as Hollister, California) can obtain interstation baselines (10 km) to measurement accuracies of 2-3 tenths of a millimeter [21.3].

Hence even with very modest topographic relief (10 to 100 meters) the equations defining the relative three-dimensional coordinates in terms of the measured baseline data, can be accurately solved for all the coordinates, including the controversial out-of-plane or Z component which may be of interest for earthquake hazards assessment. Specifically, the process of measuring the baselines, which yields a spider weblike network of lines can be easily used to extract these out-of-plane components [21.4].

Presently there is a debate as to the importance of these out-of-plane coordinates vis-a-vis the idea of using the out-of-plane coordinate changes as premonitors of earthquakes. However there is no question that an experiment could be performed in order to obtain these coordinates to levels of accuracy which might have impact on the earthquake problem.

The only requirement for operation of the multibaseline system is the availability of the geodolites themselves. The geodolites currently in use by the USGS are the one-color type which require a helicopter to fly along the baseline to yield atmospheric calibration data. The two-color self-calibrating geodolites are currently in field test; their modest cost and ease of implementation dictates an increase in future availability.

In any case, multibaseline or its closely related variations seem to have applications to three-dimensional coordinate resolution over local areas wherein surveying or local fault monitoring, etc., are of interest. The multibaseline variations are: static and hybrid multilateration. Multibaseline, as previously discussed requires a number of baseline measurements sufficient

to permit determination of the three-dimensional coordinates peculiar to a given station constellation and also uses any redundant baselines which can be obtained. Static Multilateration places the geodolite at a specified station and the laser retroreflector is then moved at least four times to different locations. This process is repeated for at least five other stations. It should be noted that the multilateration (not multibaseline) equations are nearly singular if less than six stations are used in a given experiment. This singularity can be avoided and fewer stations need be used if the multibaseline equations are first used to determine all the inplane coordinates, before the multilateration equations are used. Many combinations are possible. Finally hybrid multilateration [21.8], [21.10] would make use of a target retroreflector elevated on a balloon or helicopter.

It may well be that multibaseline can stand as a system on its own; however, if after indepth systems analysis this is not the case, then it is certain that multibaseline would be of assistance to present short baseline multilateration coordinate reduction. Certainly the prospect of such a system for local surveying and many other geodetic applications seems bright.

The analysis and simulation performed in this paper demonstrate that three-dimensional interstation coordinate reduction can be performed to levels of high precision over short baselines. Network propagation, i. e., expansion of the spiderweb station net along the lines discussed herein can also be carried out, if indeed network propagation is required as a necessary constraint to aid in local fault monitoring. Certainly over terrain such as exists in the California area three-dimensional crustal movement directly across and in close proximity to a fault can be determined to the centimeter level using geodolites and the multibaseline approach. Multibaseline monitoring over a very short baseline perimeter can be performed at a number of unconnected links and the relative ground movements can thus be detected. Perhaps this is sufficient to achieve extraction of meaningful geodetic data. Actually, for fault monitoring it would seem strange that suspicious ground movement in the San Francisco area would permit meaningful identification of Los Angeles earthquake premonitors. Actually Savage [21.6] suggests that a) stress accumulation and release are restricted to a few tens of kilometers from the actual fault; b) actual relative plate velocity across the California section of the San Andreas fault is related to creep in only the central section of the fault; c) the stress

level on all sections of the fault would be nearly equal to the stress level several tens of kilometers away from the fault; d) cyclic processes on the north and south locked sections would be decoupled. On the other hand Turcotte and Spence [21.7] express contrary viewpoints yet conclude by saying that rheological studies and observations of stress and shear strain adjacent to the fault could differentiate between the theories but that currently data are inadequate to provide for verification of the theory proposed by Savage.

Perhaps then a local monitoring system has as good a chance of meaningful input to any proposed warning system. However if this is not true, let it be assumed that the baseline system developed herein does indeed yield the indicated accuracies and that at least, at a set number of locations three-dimensional coordinates between stations are computed not to the centimeter but to the 1 mm level. Geodolites over 5 to 10 km baselines approach these accuracies. The question then is one of what can be done with these better micrometers.

A21.2 THE MULTIBASELINE CONCEPT

Consider an ensemble of benchmarks, Δ , set into the ground as illustrated in Figure A21.2.

Assume that geodolite distances between a presently to be defined sequence of benchmarks are known, e. g., $\Delta_2 - \Delta_1$, $\Delta_3 - \Delta_1$, etc., as depicted by the dashed lines in Figure A21.2 by d_{12} , d_{13} , d_{23} , etc.

Now let Δ_1 be the origin of a coordinate system, Δ_2 define the X axis of this system and Δ_3 define the XY plane; Z is taken perpendicular to the XY plane. The coordinate system is illustrated in Figure A21.3.

Since the baseline distances d_{ij} are given by:

$$d_{12}^2 = X_2^2$$

$$d_{13}^2 = X_3^2 + Y_3^2 \quad (1)$$

$$d_{23}^2 = (X_2 - X_3)^2 + Y_3^2,$$

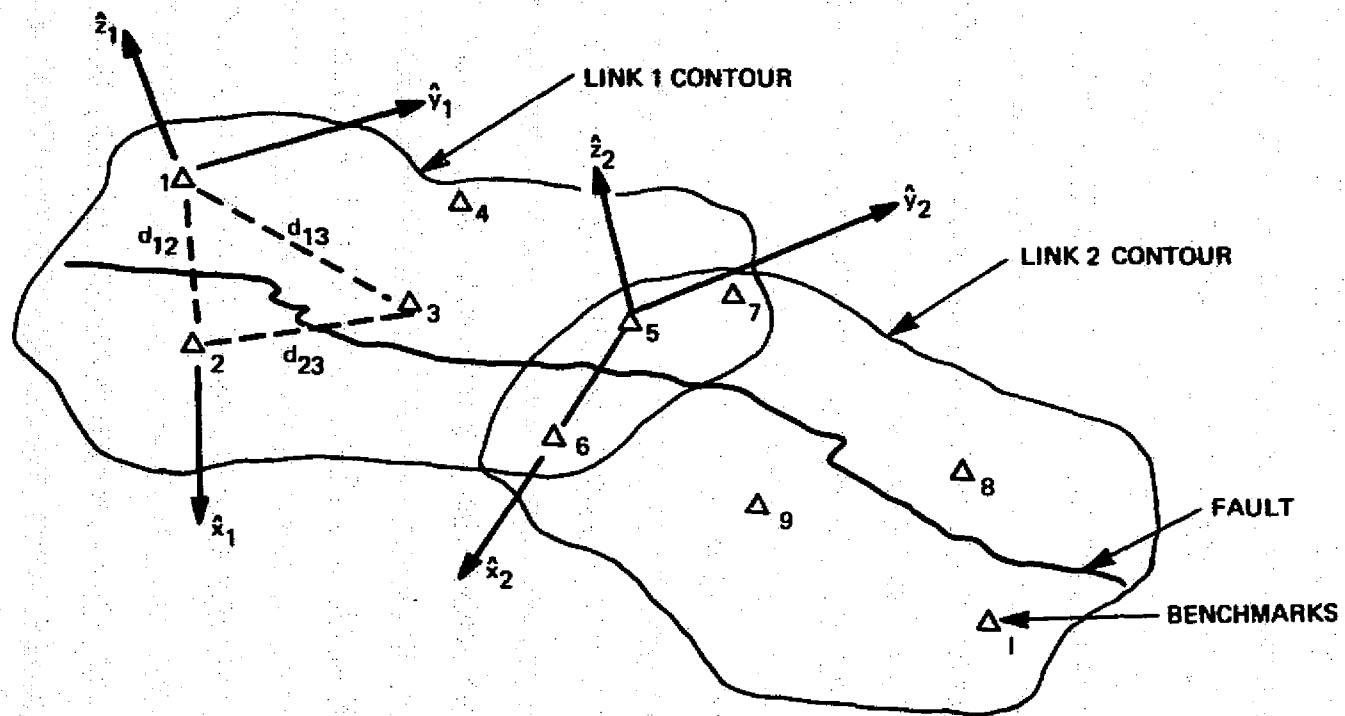


Figure A21.2. Arbitrarily Scattered Benchmarks

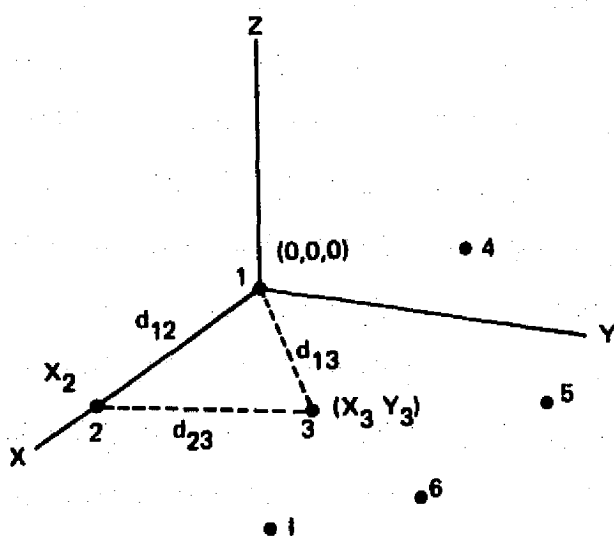


Figure A21.3. Geodolite Determined Baselines in a Geometrically Defined Basis

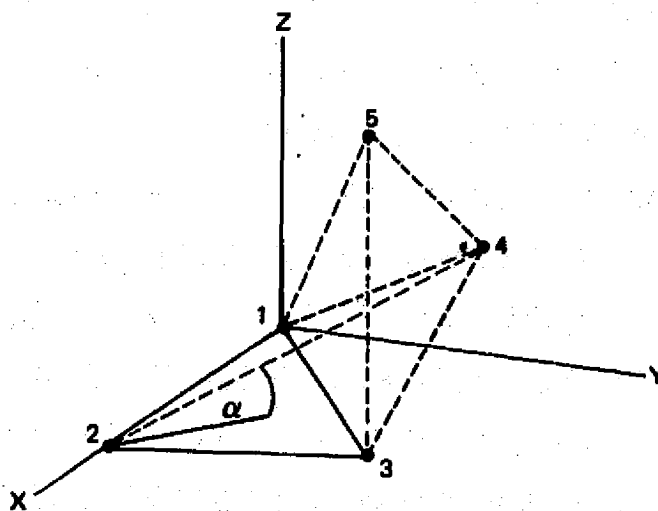


Figure A21.4. Addition of Extra Stations

a simple inversion yields:

$$X_2 = d_{12}$$

$$X_3 = \left(d_{13}^2 + d_{12}^2 - d_{23}^2 \right) / 2 d_{12} \quad (2)$$

$$Y_3 = \left[d_{13}^2 - X_3^{*2} \right]^{1/2},$$

where the star superscript implies that X_3 has already been determined previously in the computational chain. In Figure A21.4 a fourth station (4) is now added.

The geodolite now measures $\Delta_4 - \Delta_1 \equiv d_{14}$ and $\Delta_4 - \Delta_3$ as indicated by the dashed lines. This defines plane 1, 3, 4 with elevation angle α of station 4 relative to station 2. Obviously to the baseline superstructure currently being evolved, rigidity between the two planes can be achieved if a geodolite is employed to measure $\Delta_4 - \Delta_2$ or d_{24} .

Now since

$$\begin{aligned}d_{14}^2 &= X_4^2 + Y_4^2 + Z_4^2 \\d_{34}^2 &= (X_3^* - X_4)^2 + (Y_3^* - Y_4)^2 + Z_4^2 \\d_{24}^2 &= (X_2^* - X_4)^2 + Y_4^2 + Z_4^2,\end{aligned}\tag{3}$$

an inversion yields:

$$\begin{aligned}X_4 &= \left[d_{14}^2 - d_{24}^2 + X_2^{*2} \right] / 2 X_2^* \\Y_4 &= \left[d_{24}^2 - d_{34}^2 + (X_3^{*2} - X_2^{*2}) - 2 (X_3^* - X_2^*) X_4^* + Y_3^{*2} \right] / 2 Y_3^* \\Z_4 &= \pm \left[d_{14}^2 - X_4^{*2} - Y_4^{*2} \right]^{1/2},\end{aligned}\tag{4}$$

where the sign ambiguity on Z is removed by a priori knowledge, e.g., if the elevation angle of station 4 with respect to station 2 > 0 then $Z_4 > 0$. Repeating the previous scheme for station 5 implies that the geodolite measure d_{15} , d_{35} and that the new elevation angle be fixed using d_{45} . Actually for the five station case a redundant constraint d_{25} can be measured (see Figure A21.4). In general for station I

$$X_I = \left(d_{12}^2 + d_{1I}^2 - d_{2I}^2 \right) / 2 X_2^* \tag{5}$$

$$Y_I = \left[d_{13}^2 + d_{1I}^2 - d_{3I}^2 - 2 X_3^* X_I^* \right] / 2 Y_3^* \tag{6}$$

$$Z_I = \pm \left[d_{1I}^2 - X_I^{*2} - Y_I^{*2} \right]^{1/2} \tag{7}$$

with the redundant relationships

$$Z_J^* Z_I = \left[d_{1J}^2 + d_{1I}^2 - d_{JI}^2 - 2 (X_J^* X_I^* + Y_J^* Y_I^*) \right] / 2 \tag{8}$$

for $J = 4, 5, \dots, I-1$, $I = 5, 6, 7, \dots, I_{MAX}$. The number of these redundant constraints will most likely be reduced by local topography. However rigidity of the baseline superstructure can always be maintained by proper station positioning. As can be seen, the equations are exceedingly simple in algebraic structure.

A21.3 MULTIBASELINE NUMERICAL RESULTS

Reference [21.5] states that the precision in length determination using geodolites is described by a normal distribution with standard deviation given by:

$$\sigma_d = \left(a^2 + b^2 L^2 \right)^{1/2}, \quad (9)$$

where $a = 3$ mm, $b = 2 \times 10^{-7}$ (dimensionless) and L is the baseline length, i. e., $L = d$ as used in this paper.

For purposes of simulation it will be assumed that a few geodolites are placed in the immediate location of Hollister, California (used herein as a hypothetical example) such that baselines of about 5 km are obtained and where for the present a high Z_4 coordinate is assumed. Hence using the previous formula $\sigma_d \cong 3$ mm. Assuming this data type accuracy let a constellation of six stations be placed as indicated in Figure A21.5, with the actual coordinates displayed in Table A21.1.

Table A21.1. Adopted Station Coordinates (km)

	Station Number					
	1	2	3	4	5	6
X	0	+4.0	+5.0	+6.0	-1.0	2.0
Y	0	0	+3.5	4.5	+2.0	-0.5
Z	0	0	0	+1	+0.2	-0.1

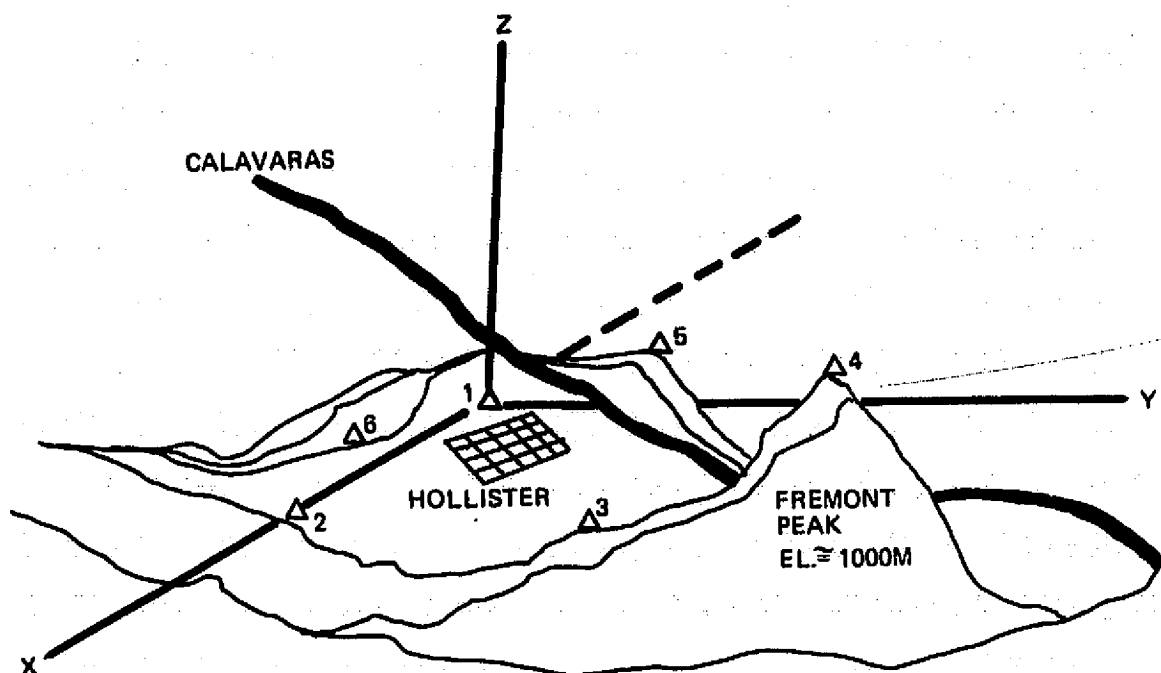


Figure A21.5. Simulation Terrain for Hollister Experiment

The coordinates adopted herein are not meant to be true representatives of the Hollister, California topography. No optimization of station placement was undertaken. For purposes of sensitivity analysis the previous coordinates were assumed as perfectly well known (God-given) and the baseline distances calculated from the coordinates. For ease of understanding and since the equations are so simple a Monte Carlo simulation was then employed to generate noisy baselines and the mean value and the standard deviation of the coordinates were computed for all the coordinates using Eqs. (2), (4), (5), (6) and (8). Note that the redundant relationship (8) was used in the form

$$Z_I = \left[d_{1J}^2 + d_{1I}^2 - d_{JI}^2 - 2 \left(X_J^* X_I + Y_J Y_I \right) \right] / 2 Z_4^* \quad (10)$$

for $I = 5, 6$. The standard deviations of the redundant Z_I , i.e., $Z_I^{(R)}$ for $I = 5, 6$ were also determined from Eq. (7); the redundant constraint $Z_5 Z_6$ and its corresponding statistics were also computed. The results are displayed in Table A21.2.

Table A21.2. Solution of Multibaseline Equations for Non-Optimum Configurations

$$\sigma_d = 1/3 \text{ cm}$$

$$N = 500$$

$$\bar{Q} = \frac{1}{N} \sum_{i=1}^N Q_i$$

$$\sigma^2 = \frac{1}{N} \sum_{i=1}^N (Q_i - \bar{Q})^2$$

Q	No Redundant Constraints		Redundant Constraints
	$\bar{Q}(\text{km})$	$\sigma \text{ (cm)}$	$\sigma \text{ (cm)}$
X ₂	4.00000000	0.29	.
X ₃	4.99999985	0.53	.
Y ₃	3.49999998	0.41	.
X ₄	6.00000014	0.72	.
Y ₄	4.49999955	0.60	.
Z ₄	1.00000054	0.89	.
X ₅	-1.00000013	0.55	.
Y ₅	1.99999996	1.21	.
Z ₅	0.20000064	6.02	5.46
X ₆	2.00000008	0.28	.
Y ₆	-0.49999986	0.63	.
Z ₆	-0.10000172	3.49	3.04

As can be seen, the inplane coordinates are very well defined. This was found to be the case even as Z_4' , whose accuracy is better than 1 cm, was decreased to any desired amount. The question then arose as to the level to which Z_4 could be decreased and yet be determined below 1 cm. To this end it was now assumed that a two-color geodolite capable of measurement accuracies of 0.3 to 0.1 of a millimeter replaced the one-color geodolite. The results are displayed in Table A21.3.

Table A21.3. Standard Deviation of Z_4 (cm) as a Function of Decreasing Z_4 (meters) for Various Geodolite Accuracies σ (mm) (N = 500)

$\sigma \backslash Z_4$	1000	500	100	50	10
0.3	0.09	0.17	0.9	1.7	9.0
0.2	0.06	0.11	0.6	1.1	6.0
0.1	0.03	0.06	0.3	0.6	3.0

For a station constellation exactly one half in horizontal extension the standard deviations in Z_4 were reduced by about 40%. Hence, it can be seen at once that with a 0.2 mm accuracy geodolite instrument, the topographic relief over baselines of 5-8 kilometers need only be about 50 meters. This constraint should be met with ease. An optimized network wherein station 4 is placed at a more centroidal location than in the present configuration will also lower the topographic relief constraint.

A21.4 STATIC MULTILATERATION EQUIVALENCE

The basic equations for multilateration, [21.1] which represent the intersection of a set of spheres positioned around each station are given in the adopted coordinate system by:

$$\begin{aligned}x^2 + y^2 + z^2 &= \rho_1^2 \\(x - X_2)^2 + y^2 + z^2 &= \rho_2^2 \\(x - X_3)^2 + (y - Y_3)^2 + z^2 &= \rho_3^2 \\(x - X_i)^2 + (y - Y_i)^2 + (z - Z_i)^2 &= \rho_i^2, \quad i = 4, 5, \dots, I,\end{aligned}\tag{11}$$

where x, y, z represent the location of the retroreflector and ρ_i are the simultaneous range distances from the station to the retroreflector. This system can be solved by letting the first three equations determine x, y, z and substitution of $\underline{r} = \underline{r}(X_2, X_3, Y_3, \rho_1, \rho_2, \rho_3)$ into the equations for $i = 4, 5, \dots, I$. This procedure results in a set of equations in terms of the station coordinates and the data which if written at j distinct times allows a solution for the coordinates to be carried forth.

To reduce these equations to the baseline form it is only necessary to place the retroreflector at each station using the $i = 4, 5, \dots, I$ equations. Hence by measuring the ranges, i.e., baselines, between stations 4, 5, \dots, I and the origin, between stations 4, 5, \dots, I and station 2, between stations 4, 5, \dots, I and station 3, etc., the following system of equations can be generated ($I=6$)

$$M_{1j} \equiv X_i^2 + Y_i^2 + Z_i^2 - d_{i1}^2 = 0, \quad i = 4, 5, 6$$

$$M_{2i} \equiv (X_2 - X_i)^2 + Y_i^2 + Z_i^2 - d_{i2}^2 = 0, \quad i = 4, 5, 6$$

$$M_{3i} \equiv (X_3 - X_i)^2 + (Y_3 - Y_i)^2 + Z_i^2 - d_{i3}^2 = 0, \quad i = 4, 5, 6,$$

$$M_{4i} \equiv (X_4 - X_i)^2 + (Y_4 - Y_i)^2 + (Z_4 - Z_i)^2 - d_{i4}^2 = 0, \quad i = 5, 6,$$

$$M_{5i} \equiv (X_5 - X_i)^2 + (Y_5 - Y_i)^2 + (Z_5 - Z_i)^2 - d_{i5}^2, \quad i = 6.$$

(12)

For the adopted six station system discussed herein, the previous system represents 12 equations in 12 unknowns. The solution in closed form can be obtained by subtracting the M_{1i} equations from the M_{2i} , M_{3i} , M_{4i} and M_{5i} equations to yield

$$X_2 X_i = -\left(d_{i2}^2 - d_{i1}^2\right)/2, \quad i = 4, 5, 6 \quad (13)$$

$$X_3 X_i + Y_3 Y_i = -\left(d_{i3}^2 - d_{i1}^2\right)/2, \quad i = 4, 5, 6 \quad (14)$$

$$X_4 X_i + Y_4 Y_i + Z_4 Z_i = -\left(d_{i4}^2 - d_{i1}^2\right)/2, \quad i = 5, 6 \quad (15)$$

$$X_5 X_i + Y_5 Y_i + Z_5 Z_i = -\left(d_{i5}^2 - d_{i1}^2\right)/2, \quad i = 6. \quad (16)$$

Now since

$$X_2 = d_{21} = d_{12},$$

$$X_3 = \left(d_{31}^2 + d_{21}^2 - d_{32}^2\right)/2 d_{21},$$

$$Y_3 = \left[d_{31}^2 - X_3^{*2}\right]^{1/2},$$

Eqs. (13) determine X_4 , X_5 , X_6 . Knowing the X coordinates Eqs. (14) now yield Y_4 , Y_5 , Y_6 , while Eqs. (15) and (16) determine Z_4 , Z_5 , Z_6 . As can be

seen the previous system is equivalent to the multibaseline system equations previously discussed. Redundant constraints can be included if desired. Obviously the reflectors can be placed at any convenient location. This mode of operation would result in a static multilateration system.

A21.5 HYBRID MULTILATERATION

The multibaseline or static multilateration options previously discussed indicate that the out-of-plane coordinate can be determined to below the 1 centimeter threshold level but only if modest topographic relief is available, i. e., for elevations of about 75 meters. If nearly flat terrain is to be monitored, then a Hybrid system [21.8] seems to be the only recourse. This hybrid system [21.9], as suggested by Muller [21.10] would use a nearly stationary vehicle such as a balloon or helicopter to carry the retroreflector. In such a system the multilateration requirement for data synchronization is minimized.

The analysis is simple and follows from Eqs. (2). Hence, accepting the X_2 , X_3 , Y_3 coordinates as known permits the hovercraft trilateration to be performed, such that the position coordinates are given by

$$\begin{aligned} x &= \left(X_2^{*2} - \left[\rho_2^2 - \rho_1^2 \right] \right) / 2X_2^* \\ y &= \left(X_3^{*2} + Y_3^{*2} - \left[\rho_3^2 - \rho_1^2 \right] - X_3^* \left(X_2^{*2} - \left[\rho_2^2 - \rho_1^2 \right] \right) / X_2^* \right) / 2Y_3^* \quad (17) \\ z &= + \left[\rho_1^2 - x^{*2} - y^{*2} \right]^{1/2} \end{aligned}$$

where ρ_i are the geodolite measured slant ranges from station $i = 1, 2, 3$.

Use of ρ_1 and d_{11} , d_{31} , d_{41} , or other suitable combinations, yields:

$$X_I^* = \left[d_{11}^2 - d_{21}^2 + d_{12}^2 \right] / 2X_2^*$$

$$Y_I = \left([d_{1I}^2 - d_{3I}^2 + d_{13}^2] - 2X_I^* X_3^* \right) / 2Y_3^*$$

$$Z_I = \left(d_{1I}^2 - (\rho_I^2 - \rho_1^2) - 2x^* X_I^* - 2y^* Y_I^* \right) / 2z^*, \quad (18)$$

so that all the coordinates of the stations contained in a given link are specified.

A21.6 HYBRID MULTILATERATION NUMERICAL RESULTS

The Hollister configuration which was previously discussed is adopted. For a nearly stationary hovercraft* at $x = 1$, $y = 1$, $z = 3$ the Monte Carlo results are summarized in Table A21.4 (stations 5 and 6 are included for completeness). Note that Z_4 in this case is determined less accurately than when using pure multibaseline theory because Z_4 is located atop Fremont peak and the out of plane hovercraft/station relative distance is thus decreased. A simulated situation with a moving vehicle drifting at about 30 km/hr produced virtually the same results. These simulations, of course, are only examples.

A21.7 DETERMINATION OF THE OUT-OF-PLANE COORDINATE FOR FLAT TOPOGRAPHY

An important conclusion extracted from the multibaseline equations is that the X , Y coordinates peculiar to the station constellation are extracted to high precision. Hence from Eqs. (11) for $i = 4, 5, \dots, I$ one can write

$$Z_i^2 - 2zZ_i + z^2 + (x - X_i)^2 + (y - Y_i)^2 - \rho_i^2 = 0, \quad (19)$$

where it is assumed that X_i , Y_i have been obtained via the multibaseline procedure. By direct differentiation one has

$$2Z_i \delta Z_i - 2z \delta Z_i - 2Z_i \delta z + 2z \delta z + 2(x - X_i)(\delta x - \delta X_i) \\ + 2(y - Y_i)(\delta y - \delta Y_i) - 2\rho_i \delta \rho_i = 0, \quad (20)$$

*Airplane, helicopter, etc.

Table A21.4. Hybrid Multilateration

$$\sigma_d = 0.3 \text{ cm}$$

$$N = 500$$

$$\bar{Q} = \frac{1}{N} \sum_{i=1}^N Q_i$$

$$\sigma^2 = \frac{1}{N} \sum_{i=1}^N (Q_i - \bar{Q})^2$$

Q	$\bar{Q}(\text{km})$	$\sigma(\text{cm})$
X ₂	3.99999985	0.29
X ₃	5.00000049	0.54
Y ₃	3.49999964	0.44
X ₄	6.00000001	0.69
Y ₄	4.49999984	0.65
Z ₄	0.99999955	1.26
X ₅	-1.00000026	0.54
Y ₅	2.00000077	1.19
Z ₅	0.19999905	1.05
X ₆	1.99999971	0.26
Y ₆	-0.49999981	0.63
Z ₆	-0.09999935	0.59

or

$$\begin{aligned} \delta Z_i = & \left[(x - X_i) \delta x + (y - Y_i) \delta y + (z - Z_i) \delta z \right. \\ & \left. + (x - X_i) \delta X_i + (y - Y_i) \delta Y_i - \rho_i \delta \rho_i \right] / (z - Z_i). \end{aligned} \quad (21)$$

so that neglecting cross term $\sigma_{Z_i}^2 = E(\delta Z_i \delta Z_i^T)$

$$\begin{aligned} \sigma_{Z_i}^2 = & \left\{ (x - X_i) / (z - Z_i) \right\}^2 \sigma_x^2 + \left\{ (y - Y_i) / (z - Z_i) \right\}^2 \sigma_y^2 \\ & + \sigma_z^2 + \left\{ (x - X_i) / (z - Z_i) \right\}^2 \sigma_{X_i}^2 + \left\{ (y - Y_i) / (z - Z_i) \right\}^2 \sigma_{Y_i}^2 \\ & + \left\{ \rho_i / (z - Z_i) \right\}^2 \sigma_{\rho_i}^2. \end{aligned} \quad (22)$$

As can be seen, the coefficients of σ_x^2 , σ_y^2 , $\sigma_{X_i}^2$, $\sigma_{Y_i}^2$ become very small and vanish if the hovercraft of the hybrid system is positioned nearly above a station positioned in the adopted coordinate system plane of reference. Note that X, Y can always be extracted via multibaseline. It follows that the uncertainty in the Z coordinate is then given by:

$$\sigma_{Z_i}^2 \approx \sigma_z^2 + \sigma_{\rho_i}^2$$

Newberry [21, 11] suggests that in such configurations, the use of a laser altimeter positioned on the hovercraft would provide an accurate determination of ρ_i and also result in a cost effective monitoring system. Additional lasers could also be used via trilateration to obtain an accurate value of z. Perhaps radio trilateration using the single laser altimeter for atmospheric calibration would also be a viable system approach. Many such configurations are presently under study.

A21.8 NETWORK DENSIFICATION

There are various schemes which can be used for network densification, i. e., expanding the interstation network. The one suggested herein is operationally simple and is as follows. In Figure A21.2 multibaseline reduction is carried out in link one (1) over a contour of approximate radius equal to, say, 10 km, with stations spaced not more than 4 - 5 km relative to a coordinate basis, B_1 , defined by stations $\Delta_1, \Delta_2, \Delta_3$. When sufficient statistical averaging has been accomplished such that accuracies of less than 1 centimeter are achieved, link 2 (approximately the same size as link 1) is considered*. Link 2 has at least three stations in common with link 1 and thus a new basis B_2 can be formed at once using the rectangular coordinates of stations $\Delta_5, \Delta_6, \Delta_7$ relative to basis B_1 . Now since the sum of squares of the coordinate differences from stations Δ_5, Δ_6 and Δ_7 and stations $\Delta_1, \Delta_2, \Delta_3, \Delta_4$ (in the Figure) is invariant it follows at once that in the second link basis $(\hat{x}_2, \hat{y}_2, \hat{z}_2)$ one can write the unique invariants e. g.,

$$d_{56}^2, d_{57}^2, d_{67}^2, d_{5k}^2, d_{6k}^2, d_{7k}^2, \quad k = 1, 2, 3, 4,$$

where the d and the associated covariance are known and by the previously developed equations rigorously obtain all the coordinates of stations in Link 1 in the B_2 or second link basis, B_2 . These coordinates are now treated as a priori inputs and are used to solve the multibaseline equations in the B_2 basis. The densification proceeds as above from link to link each time abandoning the coordinate basis of the previous link. At the end of the densification chain the procedure can be reversed so that from the $B_N, N = 1, 2, 3, \dots, k$, link one can return to the B_1 basis (if it is so desired).

Densification, as a prerequisite to local fault monitoring and to the extraction of meaningful earthquake premonitors is not an established necessity. Localized unconnected high accuracy monitoring constellations (2-4 mm accuracies) might provide equally valid geodetic input. However, these localized constellations could be linked by a few baselines of high precision if this procedure proves to be of benefit.

*Obviously with more geodolites the measurements can be carried out at the same time.

A21.9 CONCLUSIONS

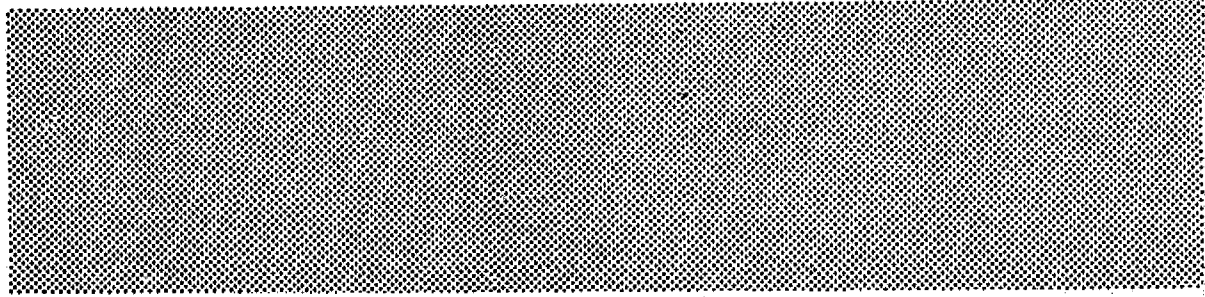
The preliminary conclusions reached herein are as follows: a) three-dimensional station coordinates can be obtained by the multibaseline procedure, without data synchronization or the use of airplanes; b) geodolite networks as listed in [21.5] are already in operation and over short baselines (9-10 km) can achieve accuracies of about 1/3 of a centimeter in all XY coordinates; c) for modest elevations (50-75 meters), the Z coordinate of one station can be determined to centimeter level accuracy using two-color geodolites; d) once the Z coordinate of one station with modest elevation is known, the Z coordinates of all other stations in a given geodolite link can be determined to centimeter level accuracy; e) use of additional stations improves the three-dimensional coordinate determination; f) network densification using a sequence of coordinate systems seems simple and feasible and necessary if its value to fault monitoring is established; and g) static and hybrid multilateration systems also appear to be viable adjuncts to the multibaseline system.

A21.10 REFERENCES

- [21.1] Escobal, P.R. et. al., 3-D Multilateration: A Precision Geodetic Measurement System, Jet Propulsion Laboratory TM 33-605, March 15, 1973.
- [21.2] Fliegel, H.F. et. al., LIBRA: An Inexpensive Geodetic Network Densification System, Jet Propulsion Laboratory TM 33-725, August 15, 1975.
- [21.3] Slatter, L., Personal Communication, Hollister Field Test Facility, 1975.
- [21.4] Escobal, P.R., "Multibaseline: A Three-Dimensional Precision Geodetic Measurement System Not Using Airplanes or Data Synchronization," Jet Propulsion Laboratory EM 391-705, November 1975.*
- [21.5] Savage, J. C., "A Possible Bias in the California State Geodimeter Data," Journal of Geophysical Research, Vol. 80, No. 29, October 1975.
- [21.6] Savage, J. C., "Comment on An Analysis of Strain Accumulation on A Slip Strike Fault," Journal of Geophysical Research, Vol. 80, No. 29, October 1975.
- [21.7] Turcotte, D.L. and Spence, D.A., "Reply," Journal of Geophysical Research, Vol. 80, No. 29, October 1975.
- [21.8] Escobal, P.R., "Hybrid Multilateration: A Method for Determination of Three Dimensional Station Coordinates Using Lasers (Geodolites) or VLBI," JPL TM 391-375, 16 October 1972.*
- [21.9] Escobal, P.R., "Hybrid Multilateration Same Numerical Results," Jet Propulsion Laboratories, EM 391-707, December 2, 1975.*
- [21.10] Muller, P.M., Personal Communication, Jet Propulsion Laboratory, 1975.
- [21.11] Newberry, A.W., Personal Communication, Jet Propulsion Laboratory, 1975.

* JPL internal document.

A22. Applications of Multilateration



Abstract

Additional multilateration applications are discussed along with a few closing remarks relative to this report.

A22.1 INTRODUCTION

The summary overview of this work touched briefly on the many applications to which an operational multilateration system can be applied. The explicit list previously introduced (Table 1) is repeated here:

Low \equiv 1-2 meter, Medium \equiv 100-10 cm, High \equiv 1-0.1 cm

Application	Accuracy Requirements
• Practical Earth Surveying	Low
• Coastal and River Erosion Monitoring	Low
• Gravity Anomaly Determination	Medium-to-High
• Measurement and Calibration of Physical Constants	Medium-to-High
• Precision Geometric Orbit Determination Over Long and Short Arcs	High
• Continental Drift Determination	High
• Solid Earth Tide Modeling Improvement	High
• Ocean Earth Tide Modeling Improvement	High
• Rapid Fault and Tectonic Plate Monitoring	High
• Earthquake/Volcano Modeling Improvement	High
• Satellite Altimeter Calibration	High

It would have been the authors' desire to simulate appropriate data and investigate some of these areas in much more detail. As it turned out the twilight hours of this effort were spent almost exclusively on the MICRODOT check-out which was required to demonstrate the feasibility of the GEOS-3 project objectives. These objectives can best be classified under the first application of the list: Practical Earth Surveying. More specifically the objectives were related to the three-dimensional determination of interstation coordinates using range and satellite-to-satellite tracking data. The results presented in the summary indicate that these objectives have been met. Indeed if high accuracy

data types are available, other applications such as Rapid Fault and Tectonic Plate Monitoring, etc., are also possible.

It may seem incomplete not to have investigated at least several other applications via the MICRODOT software, and to not include the results of these simulations in this report. Unfortunately, lack of funding and an organizational change required GEOS-3 project termination relative to this task by July of 1976. The final moments of this effort did however generate some further thoughts on future applications for which the MICRODOT system can be called forth.

A22.2 DISCUSSION

At this writing it appears that simultaneous tracking of interplanetary space probes by three or four stations can be used to determine the instantaneous state vector of these probes to high precision (data type precision) relative to a coordinate basis fixed to three of the stations. This state vector, at any point in time, can be transformed into the standard inertial coordinate basis with only the polar motion, nutation, and precession induced error degradation. The accuracy in state estimation is retained from cis-lunar space to the vicinity of Mars. With one meter data types, a probe passing Mars can be multilaterated to about 100 km accuracy. Obviously, this geometric estimate of the state of the space probe is provided instantaneously and would provide a model independent check on dynamic orbit determination software used for similar purposes.

Addition of extra stations, as is presently planned in lunar laser ranging studies provides for reduction of lunar laser ranging data by means of multilateration principles. Combination of this data with laser data reflected off a low orbiter would be an additional step of great interest in the codification and closure of Earth interstation coordinates and lunar (selenographic) positions.

The singularities in the mathematical equations used in multilateration satellite-to-satellite tracking are easily removed by letting two or more stations from the cluster of stations associated with the low satellite range to the high satellite at the same time that the cluster of stations which range to the high satellite are gathering data. The additional strength in solution engendered by the SST data link, as demonstrated in this work, can always be realized. Furthermore, it appears that choosing three stations in close proximity, so that the multibaseline technique can be used to define a geometric coordinate basis,

is a first step in establishing a ground pad of small extension which can then be used as a pivotal benchmark in conjunction with other clusters scattered at remote locations. The SST link now provides a means for station cluster unification.

The stronger the solution that can be achieved with a multilateration system, the closer will be the goals implied by the list of applications which were previously mentioned. Hence with full activation of multilateration related experiments, the estimation of physical parameters such as the Earth's plasticity parameters, e. g., the Love and Shida numbers, etc., becomes realizable.

The applications have been listed, the software exists, now the experiments need to be planned.